HYDRODYNAMIC INTERACTION OF HORIZONTAL CIRCULAR CYLINDERS WITH A FREE-SURFACE

A thesis submitted in accordance with the requirements for

the award of a degree of Doctor of Philosophy

by

Simiso Moyo

from the

Department of Mathematics and Statistics

Brunel University

Uxbridge

Middlesex

England

UB8 3PH

Declaration

Parts of chapters 4, 5 & 6 of this thesis were included in a paper submitted for publication in Philosophical Transactions of the Royal Society Series *A*, *354* by Greenhow and Moyo (1996). I declare that the work in this thesis has not been submitted for a degree to any other university or institution.

Simisto Moyo
3 June 1996

Acknowledgement

The author expresses his gratitude and thanks to Dr. M. Greenhow for help, guidance and encouragement which he has freely given me at all times. I found his approach to the subject quite inspirational. My thanks also go to Dr. J. Lawrie, my co-supervisor, for her lectures which gave me a very helpful introduction to this field. I also thank the library staff and the Mathematics & Statistics Department for providing the required facilities and enviroment which have made this work a success. Special thanks are due to Vinje T. & Brevig P., who constructed the initial version of the code for the numerical method, and Greenhow M., who further developed it to include submerged bodies, for allowing me to adopt and adjust their code according to the requirements of my problem.

The financial support of the University of Science and Technology of Zimbabwe is acknowledged. In particular, The Staff Development Committee was very supportive in the adoption of a number of crucial financial decisions without which carrying out this task would have been extremely difficult.

Lastly, my thanks go to my family for giving me the encouragement throughout the years of work.

Contents

PAGE
MISSING
IN
ORIGINAL

Abstract

The two-dimensional problem of hydrdynamic interaction of the horizontal circular cylinders with a free-surface is investigated both analytically and numerically. The fully nonlinear initial boundary-value problem is described and a numerical solution for it is presented.

The free motion of a cylinder rising towards, or moving away from the free-surface or moving horizontally is studied. The numerical calculations are compared with a simple analytic theory in which we take the low- and high-frequency limit of the added mass, and the constant added mass of the submerged cylinder in the coefficients of the equation of motion. Further numerical calculations of an initially displaced, spring-loaded cylinder undergoing slow motions are compared with a simple analytic theory in which we also take the low-frequency limit of the added mass of the submerged cylinder. The aim is to provide a useful approximate method for simulation of various offshore operations.

Fully nonlinear calculations of the free-surface deformations of the initially calm water caused by forced constant velocity motion of a totally sumerged circular cylinder are compared with small-time asymptotics due to Tyvand & Miloh (1995). Their analytic results, which are taken to third order, when gravity terms first appear in the expansion, are in excellent agreement with the numerical calculations for small times, beyond which only the numerical method will give accurate results, valid until the free-surface breaks. The breaking of the surface as a result of vertical downward motion is further investigated with the aim of establishing when and how this happens, since the phenomena causes the breakdown of the numerical calculations.

The free motion of a cylinder entering a free-surface, initially half-submerged in calm water and having specific gravity of 1.2, is also investigated. This motion is pursued beyond the complete submergence stage, giving rise to interesting free-surface deformations and body dynamics. This study is complemented by a further investigation involving impulsively started and forced constant motion of a cylinder entering a free-surface at various angles and Froude numbers, and is also taken beyond the complete engulfment stage. Hydrodynamic forces on the cylinder obtained for various angles at the same Froude number are compared. Also, the hydrodynamic forces for the motion in the same direction at various Froude numbers are compared.

Introduction

0.1 A brief history of cylinder interactions with water

The two-dimensional problem of hydrodynamic interaction of horizontal circular cylinders with a free surface is one of the most well-studied and widely applied in ocean and coastal engineering, since two-dimensional flow usually represents worst-case design loading. An engineering example might be the cross-members of an oil rig comprising horizontal circular cylinders and other cross-sections. The fluid loading and motions of such cylinders are therefore important in a wide variety of applications, for example wave loading on floating ocean structures for offshore petroleum drilling, marine operations where objects are lowered from a crane ship through the free-surface, earthquake and other extreme loading on floating bridges and dams, interaction of waves with other fixed structures such as wave energy devices, impact of waves with pipelines, impact of steep waves on breakwaters, ship slamming and extreme ship motions. For a wide variety of application, in the above situations, the offshore engineers have used and continue to use the linear theory to predict wave effects on offshore structures, but practical engineering problems remain unsolved where nonlinear effects are important. In general, we require the ability to analyse the wave conditions for the structure when submerged close to the free-surface or entering or exiting it. Accurate nonlinear theories are required for the extreme situations described above.

The usual problem for most experimental researchers in this field, is the sensitivity to the initial conditions and repeatability for the early stages, and

scaling for all stages of the fluid-structure interaction. It is well known that at infinite depth the added mass coefficients are constant and the wave damping is not present, but the body's close proximity to the fluid boundary makes it vulnerable to rapid increase in added mass and damping effects on it due to motion of the free-surface, see Bassett (1888) and Greenhow & Lin (1983). The physical and mathematical modelling of many of the situations above is complex and, involves such variables as air/water mixture compressibility effects, body elasiticity, at least in the early stages of impact, and viscous shedding causing vortex shedding in the later stages.

It is widely accepted that for an unbounded inviscid fluid with irrotational flow, the energy in the fluid can be expressed in terms of the added-mass, and hence the hydrodynamic force and moment acting on a rigid body can be represented in terms of added-mass coefficients. The derivations of these added-mass coefficients can be found in Lamb (1932) and Newman (1977). In agreement with theoretical approaches the experimental results of Chung (1976) show that the added mass and wave damping coefficients are strongly influenced by the free-surface motion. His experimental results of the added mass and wave-damping coefficients were found to be in good agreement with the analytical results by Frank (1967) and, McIver and Evans (1984) gave similar results of those coefficients. For a cylinder in the proximity of a free-surface, the energy in the fluid will strongly depend on how close to the free-surface the body is, giving rise to hydrodynamic forces proportional to the square of the body velocity, see Bassett (1888) and Greenhow and Lin (1983). These then act like viscous drag forces, and since the scaling of viscous loading and inviscid loading cannot be done at the same time, model-scale results are diffi-

cult to interpret and use. We propose here to study only the inviscid loading, meaning that the initial boundary-value problem needs to be simplified before an attempt to solve it, either analytically or numerically, is made. In principle, subject to boundary conditions on the boundary surface of the fluid, one can solve the Navier-Stokes equations for a fluid with stress relations and obtain arbitrary values of the Reynolds number and Froude number, which are respectively scales for viscous fluid loading and inviscid fluid loading. In practise, such a programme lies beyond present numerical techniques.

For simplicity, we here consider only the inviscid fluid loading due to fluid motion around a submerged horizontal circular cylinder moving in an infinite fluid. Further linearisation of the free-surface or body boundary condition is not made. In particular, we study the free-motion of the cylinder below the free-surface, the general motion of a spring-loaded cylinder below the free-surface and, water-entry and -exit of the body. In some way the exit phase is less amenable to theoretical appproaches (gravity can not be neglected for example), but is nevertheless important since it can give rise to appreciable hydrodynamic effects which may affect the body motion (and therefore the subsequent slamming forces and pressures upon re-entry in the case of ship slamming in extreme ship motions, see Barringer (1996)).

The problem of fixed and moving submerged cylinders under a free-surface has a long history. Early researchers looked at various problems of cylinder and water interactions using linear steady state theory, whereas others used the unsteady but linear theory. A theoretical approach to the solution of the problems of submerged bodies, which seems to run parallel to the one of unsteady theory discussed below, with linearised free-surface was adopted by

a number of reseachers namely, Dean (1948), Ursell (1950), Ogilvie (1963), Evans et al (1979) and many others. Dean (1948) concluded that a submerged cylinder does not reflect waves, but that the transimitted waves suffer a phase shift when they pass over a submerged cylinder. Ursell (1949) had initiated a multipole expansion method which he used to solve a linearised problem of a semi-circular cylinder floating in water. Ursell (1950), then extended his studies to the problem of a submerged cylinder and produced a solution for this linearised potential problem of water waves. This approach was then adopted and extended to other problems by Ogilvie (1963), where his basic interest was to obtain first-order oscillatory force and the second-order steady force for cylinder motions below the free-surface. Grue (1984), also studied the defraction problem of waves above the cylinder, treating the velocity potential as a distribution of vortices on the free-surface and a distribution of sources on the cylinder, and obtained Dean, Ursell and Ogilvie's results in a less tedious manner. Evans & Linton (1989) and Wu & Eatock Taylor (1990) have also used the multipole expansion technique in the investigation of the reduction of wave (profile) intensity and the second-order wave diffraction force on a submerged cylinder in finite water depth.

The first approximation of wave motion in the case of a flow past a cylinder seems to have been given by Lamb (1913, see Lamb 1932, pp. 410). Using his method, one simply replaces the cylinder by a dipole potential, which is chosen to satisfy the linearised free-surface condition (i.e equal to zero). The second approximation was obtained in 1928 by Havelock and, eight years later in 1936 he gave a complete solution to the linear problem. Following his remarkable achievements, Havelock (1948) then started on a problem of

a submerged cylinder assuming an unsteady (i.e transient) state for the free-surface of the fluid. The main thrust of his work was to present some theoretical results for the wave resistance of a submerged cylinder below a time-dependent free-surface, when it is initially given an impulsive start and made to move at that velocity. Havelock linearises the free surface and treats the cylinder as a dipole moving below the free surface, which gives rise to an image dipole above the free surface. Having obtained the velocity potential, using Fourier integral method, of the ensuing motion of the fluid, he then derived the complex potential from which the wave resistance is found. Applying Blasius's theorem he found the resistance to be the real part of

$$-\frac{1}{2}\rho i \int (\frac{dw}{dz})^2 dz \qquad (1)$$

where the contour is taken around the origin, ρ is fluid density, $z = x + iy$ is complex with x and y being horizontal and vertical dispacements from the centre of the cylinder (the origin) respectively and w the complex potential. This gives the required horizontal force on the cylinder. In a similar way Havelock (1949) derived an expression for wave resistance for a cylinder moving with linearly varying velocity. In a follow up of Havelock's work, Hepworth (1991) and Greenhow (1992) compared his results with those of a nonlinear numerical method of Vinje and Brevig (1981). Havelock's results, which showed the presence of steady forces and transient oscillatory forces on the body, were shown to be qualitatively similar to the numerical calculations, especially when a body is deeply submerged and moving slowly. Lui and Yue (1996) have also reported the presence of oscillatory forces similar to the ones discussed above.

Following Lamb and Havelock's work, Tuck (1964) also studied the unsteady theory of fluid motion due to the presence of bodies below the free-surface but

without assuming the free surface to be linear. Tuck revealed the inadequacies of Havelock's second approximation results, obtained by the dipole method (which assumes linear free-surface even for higher order approximations), arguing that the most accurate way of calculating the wave resistance is not through successive approximations in the way of Havelock, but that nonlinear second-order terms are more important. Tuck wholly agreed with Wehausen's (Wehausen & Laitone 1960, p. 574) approach which could be extended to treat the nonlinear case by adding the Wehausen & Laitone (1960, p.601) potential due to the pressure distribution on the free-surface to the part of the potential that satisfies the homogeneous free-surface condition as well as the cylinder condition. The forces were then obtained in the form of infinite series, under the conditions where the Wehausen scheme converges, giving, in the case of linear free-surface, the same result of the wave resistance force as obtained by Havelock (1936). Bessho (1957) carried out investigations of the nonlinear second-order approximations and obtained the results (for the potential) which were in good agreement with those of Tuck. However, he then used Havelock's formula, only valid in the linearised approximation, to derive the forces involving amplitude far downstream, instead of using the Blasius theorem. This forced Bessho to make wrong conclusions about the second-order nonlinearity effects on the potential and he claimed that they only contributed to the third-order term of the forces.

Haussling and Coleman (1979) use the finite-element approach to solve, numerically, the problem initiated by successive authors mentioned above, namely that of determining the wave resistance force on an accelerated submerged circular cylinder. They then considered the unsteady nonlinear free-surface prob-

lem. Comparing with their results, we see that the linear steady-state solution proves quite inaccurate, because of the approximation of both the dynamic pressure distrubution on the body and the subsequent free-surface elevations. The theories requiring the simplification of boundary conditions, have of late been a subject of criticism by some recent research studies carried out on problems similar to those discussed above, see Tuck (1964), and Brevig, Greenhow & Vinje (1981), and Lin, Newman & Yue (1984), Cointe (1989), Greenhow (1983, 1987, 1988,1993), Telste (1987), Wu (1993), Tynand & Miloh (1995) and many others.

It is common knowledge now that the above solutions, although still holding for a considerable range of applicability under normal conditions, will fail to predict accurately the hydrodynamic forces and free-surface motions for extreme situations considered here. In order to advance the study of fluid loading on offshore structures and response mechanisms of those structures for extreme situations, it is essential to account correctly for the nonlinearity of the free-surface boundary conditions, and the fact that the body condition, while appearing to be linear, must be applied not on the "mean" position of the body surface, but on its actual position (which for free motion will not be known *a priori*). This second requirement means that series expansion methods, which apply boundary conditions on the initial body surface position, will only be valid for small times after the motion has started. Peregrine (1972) developed a series expansion method valid except close to a free-surface which was then adopted by King and Needham (1994) to study the problem of an impulsively-started constant velocity or constantly accelerated motion of a vertical wavemaker. This was followed by the application of the same

approach, by Tyvand & Miloh (1995), to a problem of the forced motion with constant velocity or acceleration of a submerged cylinder under an unsteady nonlinear free-surface. Tyvand & Miloh's expansions are taken as far as the leading-order gravitational effects, with surface elevations and hydrodynamic forces calculated to each order. The results of Tyvand & Miloh are further discussed in chapter 4 of this thesis.

Tyvand & Miloh's (1995) results lay a foundation for comparison of the free-surface deflections produced by their method with those of a numerical method based on the potential theory and described in the works of Vinje & Brevig (1981a and b), followed by Brevig et al (1981), Telste (1987), Greenhow (1987), Terent'ev (1991), Hepworth (1991) and Greenhow (1993). Firstly, Brevig, Greenhow & Vinje (1981) extended the numerical work of Longuet-Higgins (1976), using a nonlinear time-stepping procedure to evaluate the hydrodynamic force on moving and fixed cylinders. Actually, their work entails solving the Cauchy's equation for the fluid in a physical plane which contains a body in the fluid. Works on completely submerged bodies include those of Hepworth (1991) who studied the forced horizontal motion of a cylinder at various depths below the free-surface using the Brevig, Greenhow & Vinje approach. Other works have concentrated on motion of bodies in the free-surface with the main aim being that of solving the intersection problem. These include Lin, Newman & Yue (1984) and Greenhow & Lin (1985). Telste (1986) avoided the problem involving the free-surface and body intersection, and used the vortex method of Baker, Meiron & Orszag (1981, 1982) to solve the unsteady state nonlinear free-surface potential flow problem about a cylinder forced to move upwards towards a free-surface. From his numerical calculations, he came to

one conclusion that the low-speed approach to a free-surface is similar to the approach to a fixed wall, whereas the high-speed approach is similar to motion in an infinite fluid.

Greenhow (1987) also utilises the method of Vinje & Brevig to simulate flows about a surface-piercing wedge and later-on about a cylinder entering a free-surface. In his work, Greenhow (1987), considers the time-dependent motions of wedges of various angles with both gravity and the nonlinearity of the boundary conditions on the body and the free-surface correctly described. To make progress, in simulating the flows when a jet has formed, Greenhow modified the numerical scheme and allowed the jet to leave the wedge. This proved very successful as the result showed good agreement with experiments by Greenhow and Lin (1983). He also discovered the appearance of negative pressures above the wetted part of the wedge around the region of jet formation when implementing the intersection point treatment method of Lin, Newman & Yue (1984). This was followed by a paper in 1989 about cylinders entering and exiting a free-surface at various Froude numbers. In this paper Greenhow, uses a modified method for surface-piercing bodies of Vinje & Brevig (1981a) for the treatment of the jet. The assumption of full nonlinearity of boundary conditions is unchanged and the resulting flow features were quite promising from the viewpoint of solving the complete engulfment problem in the case of surface entry. Some complimentary studies on free-surface entry by either blunt or sharp objects have been carried out by several authors. These include works of Garabedian (1953), Korobkin (1984), Greenhow (1987, 1988, 1993), and Howison, Ockendon & Wilson (1990) and Fraenkel (1992). Their major aim, apart from the usual problem of establishing wave resistance force and

free-surface motion, is that of the treatment of the intersection point, since the potential is known to be potentially singular there and the numerical schemes tend to fail at that point.

For wedge entry at high enough Froude numbers for gravity to be ignored, the flow is known to be self-similar, see Wagner (1932) and Howison et al (1990) who give a modern approach. The arc length between free-surface Lagrangian marker particles is conserved, see also Garabedian (1953). This provides a stringent test on the accuracy of the present numerical method, see Greenhow (1987). It was shown that the numerical method for surface-piercing bodies of Vinje & Brevig (1981a) gives accurate results if the deadrise angle (between the fluid and the immediate body surface extending away from the fluid) is not smaller than 45 degrees, and we do not violate this condition in the present calculations. In the case of small deadrise angles, see Fig. 0.1, Zhao and Faltinsen (1993) have implemented a scheme whereby the jets are cut-off and the calculations are allowed to continue. Their approach does not seem to affect the energy and fluid conservation of the system. In general, these jets are thin and have almost atmospheric pressure throughout and subsequently would only affect the stability/robustness of the numerical scheme. We therefore feel justified in adopting this approach of pursuing the numerical calculations of the surface-piercing problem beyond complete engulfment stage when otherwise the jet formation would have inhibited this.

0.2 A brief synopsis of this work

This thesis seeks to extend the above work. Our main task revolves around accurate determination of hydrodynamic forces and pressures around a hori-

zontal circular cylinder moving in or near a free surface. To be able to do that, the motion of the unsteady nonlinear free-surface has also to be determined correctly, without which the main objective can not be achieved. The method of Brevig et al (1981) is used extensively in this work, both as a check of our analytical methods and as the only means available to solve some problems lacking theoretical solutions. Their code, which has a provision for restarting previously stopped runs, could not be used in that form for calculations stopped due to complications at the free-surface. The swapping of programs, one for partially-submerged bodies and the other for fully-submerged bodies, then takes place with alterations in the latter program to accept the data generated by the former. A cylinder is initially at equilibrium position either below the free-surface completely or only half-submerged in water. The cylinder is then either forced, or is allowed to move freely in a number of specified directions. The obtained numerical results are then compared to the approximate but analytical results in order to check the accuracy of the latter.

In chapter 1 of this work we give the description of the the fully nonlinear initial boundary-value problem we wish to solve using both the analytical and numerical methods and the numerical method alone, in cases where no known theoretical approach is applicable. An outline of the numerical algorithm we use for solving our problems is also given.

The second chapter of the thesis looks at the free motion of a cylinder moving away from or towards a free-surface for different masses and initial depths of submergence of the body. The analytical methods used are based on added mass theory and to be able to obtain a solution we make a number of simplifications of the free-surface boundary condition. The problem is solved under

the assumption that the free-surface does not deflect much for a relatively large amount of time. Thus we apply a low-frequency free-surface boundary condition $\frac{\partial \phi}{\partial z} = 0$ on z=0 - a rigid wall condition, or high-frequency free-surface boundary condition $\phi = 0$ on z=0 - equivalent infinite fluid condition, for motion of the cylinder near the free-surface boundary, but not penetrating it. A case of constant added mass (equilibrium position added mass) is also included as a means of testing the importance of updating the added mass in contrast with the use of constant added mass. The impulsively started free horizontal motion with constant velocity is also investigated. A comparison of the three methods with the fully nonlinear numerical method show interesting results, with good agreement in some cases, which should prove very helpful in a number of practical situations.

The added mass approach was also appplied to the problem of a spring-loaded cylinder oscillating below a free-surface in chapter 3. The cylinder is initially held at an equilibrium position before it is displaced through one radius upwards, to the side, upwards and to the side, downwards, and downwards and to the side of the equilibrium position. It is then allowed to oscillate. Initially motion without damping is investigated in order to determine the conservation of energy and hence consistency of the system. For comparison with the fully nonlinear scheme, we then introduce damping into our analytical method. Good agreement was recorded in some cases and it is hoped that engineers will find our findings quite attractive in a number of practical ways; the method is less detailed in terms of complexity and computations using the method are quite inexpensive to handle.

Chapter 4 is mainly concerned with the limitations of the small-time as-

ymptotic expansion method of Tyvand & Miloh (1995), and in particular the case of forced motion of a cylinder below a free-surface with constant velocity. A small-time expansion method as employed by Tyvand & Miloh is compared to the fully nonlinear method, so that we can establish how small time must be for their method to be accurate. A number of tests at different Froude numbers and cylinder sizes were carried out and eventually an interval within which, we think, the method is valid was established. This should be very useful information as the method proves to be very accurate for small times, especially for people wishing to apply the method in practical situations, and may also be quite useful in determining the accuracy of numerical schemes, albeit for small times only, i.e for those time intervals we have established.

In chapter 5 we carry out some runs as a preparation for the study of a major part of this work, the motion of the cylinder beyond the stage of complete engulfment studied in chapter 6. Some preliminary work was done in order to understand the behaviour of the free-surface motion and the behaviour of pressure distribution for the motion of a cylinder started just below the free-surface. A number of new features of the free-surface were observed for a cylinder rising to, or moving away from, the free-surface at various Froude numbers.

Some of the features of the free-surface encountered in chapter 5 are repeated, though in a slightily different manner, when motion is continued beyond the total submergence stage in chapter 6 of this thesis. Some differences were expected, since in the former case the motion is initially started with the free-surface assumed flat, whereas in later problems the motion is continued with the free-surface already deformed. The problem of complete engulfment

is a difficult one and the situation is not helped by the fact that no theoretical solution exists for us to compare our findings with. There are new features appearing which we have not encountered before, including the formation of cavities, the collapse of fluid domains and jets. The flow is investigated for various angles of penetration and velocities of free and forced motion. Free-surface profiles, pressure distribution on the cylinder, and the hydrodynamic force on the cylinder are compared for different entry-angles and approach speeds. The results of a simple hydrostatic model are compared with our results.

Chapter 1

The Mathematical Problem

1.1 Problem description

A problem of a horizontal circular cylinder of radius a which is either completely submerged or surface-piercing is considered. The problem is two-dimensional and the fluid in the given domain, see Fig. 1.1, is assumed to be incompressible, inviscid, initially at rest and of infinite depth.We shall also assume that the fluid motion is irrotational and the surface tension is neglected. At $t = 0$, where t is time, everything is at rest, and the cylinder centre is at a distance d below the free surface. A Cartesian rectangular coordinate system is defined so that the x-axis lies on the undisturbed free surface and the z-axis is positive upwards. The distance, d from the origin to the centre of the cylinder is chosen arbitrarily, whereas the vertical and horizontal displacements y and x of the cylinder at time t below the free surface are given by the moving centre of the cylinder. Hence z in terms of y is given as $z = -d + y$. Initially $t = 0$, $x = 0$, $y = 0$ and $z = -d$ and there is no fluid motion. We denote the surface elevation by $z = \zeta(x, t)$. It is assumed that the free surface boundary $\partial\Omega_f$, is known at the start of the calculations and unknown immediately after that. In some cases we have used the term surface in place of a free surface,

but a complete description is given in other situations with surfaces other than the free boundary surface of the fluid. The cylinder boundary is $\partial\Omega_b$ and the position of its centre at any time t is $(x, y) = (x_c(t), y_c(t))$ and is given by the prescribed or calculated motion of the cylinder.

The variables involved in the calculations have all been non-dimensionalised. The lengths are either scaled by the radius, a, of the cylinder or the initial submergence depth of the cylinder, d. Unless otherwise specified the dimensionless Froude number is

$$Fr = \frac{U}{\sqrt{ga}} \qquad (1)$$

where g is the gravitational acceleration and U is the velocity of the body. We introduce the units of the other dimensionless variables later as they may not be standard throughout the document. This should not cause any problems in as far as the generality of the results is concerned.

The problem is formulated as an initial-value problem defined in Eulerian and Lagrangian coordinates. A velocity vector $\mathbf{V}(x, z, t)$ is defined as the velocity of the fluid particle at the point (x, z) in a Cartesian, rectangular coordinate system at any time t. u and v denote the horizontal and vertical components of this velocity in the rectangular coordinate system. Other quantities of measurement that will be used are the variable added mass of the body M_a, the specific gravity of the body M_b, the fluid density ρ (assumed constant) and the total force acting on the body F. Since the fluid is assumed incompressible and irrotational such that $\nabla \cdot \mathbf{V} = \mathbf{0}$ and $\nabla \times \mathbf{V} = \mathbf{0}$ respectively, it is possible to describe the motion of the fluid by a velocity potential $\phi(x, y; t)$ with $\mathbf{V} = \nabla\phi$ satisfying the equation of continuity which gives the

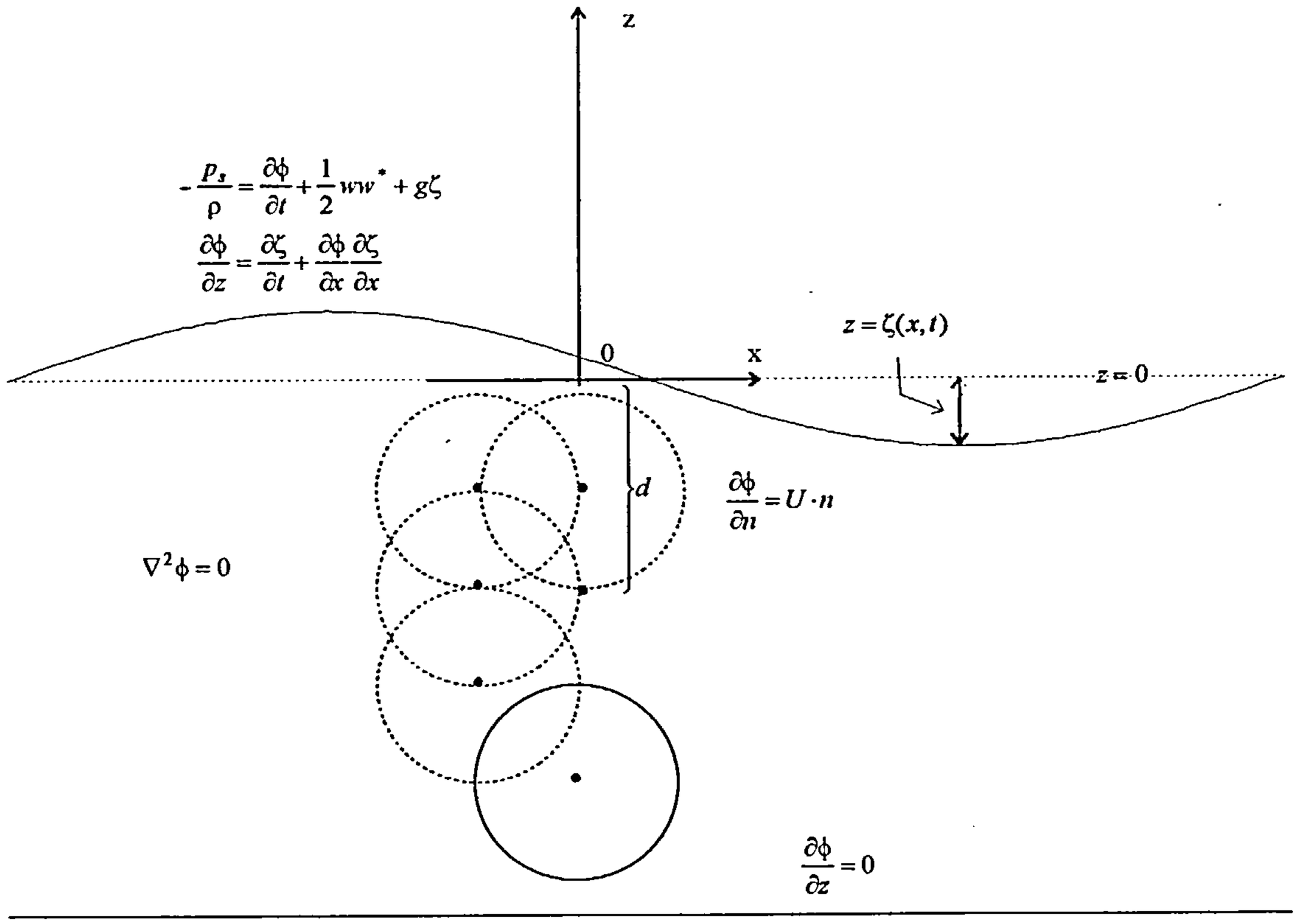

Fig 1.1 The Boundary-value problem

Laplace's equation for ϕ

$$\nabla^2\phi = 0 \qquad (2)$$

in Ω the fluid domain. $\partial\Omega$ is a closed contour consisting of the free surface $\partial\Omega_f$, the cylinder boundary $\partial\Omega_b$, the bottom where $\frac{\partial\phi}{\partial z} = 0$, and the vertical rigid walls further away from the body. The kinematic free surface boundary condition is stated as

$$\frac{Dz}{Dt} = u + iv \qquad (3)$$

where $\frac{D}{Dt}$ is the convective derivative and is given in Eulerian terms as

$$\frac{D()}{Dt} = \frac{\partial()}{\partial t} + (\nabla\phi)\cdot\nabla() \qquad (4)$$

The dynamic boundary condition at the free surface is deduced from Bernoulli's equation:

$$\frac{\partial\phi}{\partial t} = -\frac{1}{2}\mid\nabla\phi\mid^2 - gz - \frac{p_s}{\rho} \qquad (5)$$

on the surface $z = \zeta(x,t)$, where p_s is an arbitrary pressure distribution applied at the free surface. Assuming U to be the velocity of the cylinder through the fluid and n=(n_1, n_3) to be the normal unit vector drawn from any point of the surface of the cylinder, where n_1 is its horizontal component and n_3 the vertical component, we have

$$\frac{\partial\phi}{\partial n} = U\cdot\mathbf{n} \quad \textbf{on} \quad \partial\Omega_\mathbf{b} \qquad (6)$$

Thus the contact between the fluid and the cylinder is preserved.

In the calculations the vertical boundaries are positioned at distances far away, to the right and left, from the vicinity of the cylinder to avoid imposing radiation conditions which are not clear for the nonlinear problem. Alternatively, some authors e.g Cointe (1989), use an "energy sponge" of linearly

decreasing ζ and ϕ far from the body, but this is unphysical and mathematically inconsistent, thereby requiring careful checks on reflected energy from such sponges.

1.2 Method of solution of Vinje and Brevig(1981)

For the fluid described above, the flow can be fully defined by the velocity potential, ϕ, or the stream function, ψ. Taking ϕ and ψ to be the real and imaginary parts of a complex function $\beta(z)$, where $z = x + iy$, we have

$$u = \frac{\partial \phi}{\partial x} = \frac{\partial \psi}{\partial y}$$
$$v = \frac{\partial \phi}{\partial y} = -\frac{\partial \psi}{\partial x} \qquad (7)$$

the Cauchy-Riemann equations. These equations and the flow description given above imply the existence of a complex potential

$$\beta(z;t) = \phi(x,y;t) + i\psi(x,y;t) \qquad (8)$$

The velocity potential ϕ and the stream function ψ satisfy Laplace's equation and so β is analytic in the fluid region. Application of Cauchy's integral theorem gives

$$\oint_{\partial\Omega} \frac{\beta(z,t)}{z - z_0} dz = 0 \qquad (9)$$

with z_0 outside Ω.

We split the contour of integration $\partial\Omega$ to consist of $\partial\Omega_\phi$ and $\partial\Omega_\psi$, where ϕ and $\frac{\partial\phi}{\partial t}$ are prescribed on $\partial\Omega_\phi$ whereas ψ and $\frac{\partial\psi}{\partial t}$ are given on $\partial\Omega_\psi$. The free surface belongs to $\partial\Omega_\phi$ where both the velocity potential and the surface elevation are zero at $t = 0$, corresponding to no fluid flow initially. $\partial\Omega_\psi$ comprises the bottom where the stream function and its derivative are taken

to be zero and the body surface where ψ and its time derivative are specified by the body geometry and its velocity. On the vertical boundaries both ϕ and ψ and, their time derivatives are unknown. A periodicity, or rigid wall or wavemaker condition may be applied here. When periodicity is assumed we either take ϕ(and $\frac{\partial\phi}{\partial t}$) or ψ(and $\frac{\partial\psi}{\partial t}$) to be known at the left-hand side vertical control surface and vice-versa on the right-hand side vertical control surface. Periodicity then closes the problem. In this way only ψ and its time derivative or ϕ and its time derivative can be considered as unknown variables at every nodal point. The matrix equations are then formed for the calculation of the matrix coefficients, see Vinje & Brevig (1981) for details.

We introduce a moving cylinder in the flow field described without violating the description of the problem, i.e a branch cut is introduced to render the contour of integration singly connected (and closed). On the moving cylinder the exact body bondary condition gives

$$\psi(x,y;t) = U_x(y-y_c) + U_y(x-x_c) \qquad (10)$$

where U_x and U_y are respectively the horizontal and vertical velocities of the cylinder.

We take the real part of (1.9) for z_0 on $\partial\Omega_\phi$ and the imaginary part for z_0 on $\partial\Omega_\psi$ and obtain the following integral equations on $\partial\Omega$:

$$\pi\psi(x_0,y_0;t) + Re\{\oint_{\partial\Omega}\frac{\phi+i\psi}{z-z_0}dz\} = 0 \qquad (11)$$

for z_0 on $\partial\Omega_\phi$ and

$$\pi\phi(x_0,y_0;t) + Re\{i\oint_{\partial\Omega}\frac{\phi+i\psi}{z-z_0}dz\} = 0 \qquad (12)$$

for z_0 on $\partial\Omega_\psi$, where the value π in equations (1.11) and (1.12) signifies "smooth" surface. These are Fredholm's integral equations of the second kind

from which the complex potential $\beta(z,t)$ can be found on $\partial\Omega$. We also note that Fredholm integral equations of the first kind could have been easily obtained, see Vinje & Brevig (1981), but these do not, in general, have a unique solution leading to unstable numerical solutions. A similar set of equations to (1.11) and (1.12) is obtained by considering, in the same way as above, the equation

$$\oint_{\partial\Omega} \frac{\frac{\partial\phi}{\partial t} + i\frac{\partial\psi}{\partial t}}{z - z_0} dz = 0 \qquad (13)$$

In the equations derived from (1.3) the velocity potential and the stream function in equations (1.11) and (1.12) are simply replaced by their time-derivatives and the derivative of the complex potential can then be calculated. When the complex potential β and its time derivative are known on $\partial\Omega$, it is then an easy thing to find these two functions at any point of the domain Ω enabling us to calculate fluid-particle accelerations in the fluid. It is also noted that $\partial\Omega$ maybe non-smooth at corners arising from the presence of a solid boundary or due to the numerical discretisation of $\partial\Omega$. In that case the residue part of the left-hand side of equation (1.9) at $z = z_0$ is calculated and is different from π.

To step forward in time we use the free surface conditions following a free surface particle as

$$\frac{Dz}{Dt} = u + iv = w^* = \frac{\partial\beta}{\partial z} \qquad (14)$$

which is equation(1.3) and

$$\frac{D\phi}{Dt} = \frac{1}{2}ww^* - gy - \frac{p_s}{\rho} \qquad (15)$$

the form of equation (1.5) in the Lagrangian description. We note that, on the cylinder the points are not Langrangian markers, i.e they are fixed. These equations are used in the numerical (Runge Kutta) single-step method to start

the calculations to determine the subsequent position of the free surface particles and the values of ϕ corresponding to each Lagrangian free surface marker particle being followed. After three initial time steps this method is substituted by the Hamming's fourth-order predictor/corrector method.

The body forces are derived through integrating the pressure on the body surface part of the contour which is obtainable from Bernoulli's equation:

$$-\frac{p(x,z;t)}{\rho} = \frac{\partial \phi}{\partial t} + \frac{1}{2} w w^* + gz \qquad (16)$$

Thus the forces on the body are obtained from integrating (1.16) around the body and resolving in vertical, horizontal and rotational directions. From the calculated force on the body we can easily find the acceleration and hence the velocity and the new position of the body. Further details on this can be obtained from Greenhow et al (1982).

Vinje and Brevig(1981) show how to solve the integral equations(1.11) and (1.12) for β using the collocation method. Assuming β varies linearly in z between the collocation points then,

$$\beta(z) = \sum_{j=1}^{N} \bigwedge_j \beta_j \qquad (17)$$

where the influence function $\bigwedge_j$ at nodal point z_j is

$$\begin{aligned} \bigwedge_j(z) &= \frac{z - z_{j+1}}{z_j - z_{j+1}} \quad for\ z\ on\ \partial\Omega\ between\ z_j\ and\ z_{j+1} \\ &= \frac{z - z_{j-1}}{z_j - z_{j-1}} \quad for\ z\ on\ \partial\Omega\ between\ z_{j-1}\ and\ z_j \\ &= 0 \qquad\qquad elsewhere\ on\ \partial\Omega \end{aligned}$$

consistent with "smooth" surface between the nodal points and the calculated residue, as explained above, in corners.

Substituting Λ_j into equation (1.17) gives the matrix form of the integral:

$$\oint_\partial \Omega \frac{\phi + i\psi}{z - z_k} dz \simeq \sum \Gamma_{k,j}\beta_j = 0 \quad for \quad k = 1, .., N \qquad (18)$$

where z_k is the collocation point and $\Gamma_{k,j}$ is a logarithmic function arising from integrating the $\Lambda_j(z)$ function, and is hence a function of z_k. The derivation of the influence coefficients is given in detail in Vinje and Brevig(1981).

In the case of surface-piercing cylinders, we note that the complex velocity potential β and its time derivatives are known to be singular in general at the intersections of the free and body surfaces. In the formulation of the problem, we have both ϕ and ψ defined at these points which overspecifies the matrix equation. In order to step forward in time, Greenhow (1987) removes the intersection points from the matrix calculation and then treats them as ordinary regular free-surface points. Here we simply follow this approach, which has proved to be reasonably accurate for wedge entry and wavemaker problems, see Greenhow and Lin (1983) and Greenhow (1988), for initial stages of the cylinder entering the free-surface. We note nevertheless that the actual situation is more complicated in the region local to the intersection, see Roberts (1987) and King and Needham (1993) for the wavemaker problem, and Vinje (1989) for the half-submerged circular cylinder.

For the engulfment problem, see Fig. 1.2(b) for initial phase, when the free-surface closes over the top of a downwards moving cylinder, the free surface coordinates and the corresponding velocity potentials of the last reliable step from the program for surface-piercing bodies are used as initial data for continuation of the calculations using the program for totally submerged bodies. Around the region of disturbance, in the vicinity of the cylinder, an artificial boundary (a branch cut in general) is included which joins with the rest of the

free surface.

On restarting the calculations after engulfment jets will inevitably be created on the free surface, partly due to geometry of the cylinder which further complicates the already complex free surface motion. However, Zhao and Faltinsen (1991) suggest that, whenever a jet is created the problem is simplified by redefining the fluid domain $\partial\Omega$ so that it does not contain the whole jet. The part of the jet on which the pressure is almost atmospheric is truncated.

The Zhao and Faltinsen (1991) approach, together with the theoretical analysis of Best (1991) in his thesis on troidal bubbles, give the basis for the engulfment problem which is studied here. Best, in his thesis acknowledges the discontinuity of the potential and its normal derivative when the flow domain collapses and becomes doubly connected. This is the situation we have in two-dimensions when the cylinder totally submerges. Best then proved that discontinuity can not persist after impact, which paves the way for restarting the calculations after complete cylinder engulfment. The free surface condition and the cylinder position in accordance with the above description of the problem are shown in Fig. 1.2(b).

The problem of the intersection points does not arise for completely submerged bodies. In this case the integration contour involves a branch cut which may pose some problems when we integrate along it, see Fig. 1.2(a). Instead we treat the points 1 and $N3$ as neighbouring collocation points and integrate across the cut. When we integrate around the cylinder there arises a difference in the Γ functions of equation (1.18) due to the jump from one surface to another and this is equal to $2\pi i$, see Brevig, Greenhow & Vinje (1981) for further details. This value is added to Γ functions of the points of intersection between

the branch and the cylinder and subtracted from each of the Γ functions of the neighbouring points across the branch cut. In our case of moving cylinders, the variation of ψ around the cylinder from the body boundary condition to within the unknown constant value is known and this proves to be sufficient to close the problem, see Brevig, Greenhow and Vinje (1981) for details. The unknown constant can be determined after the solution is known, if required (for example as a check on the accurracy of the calculations).

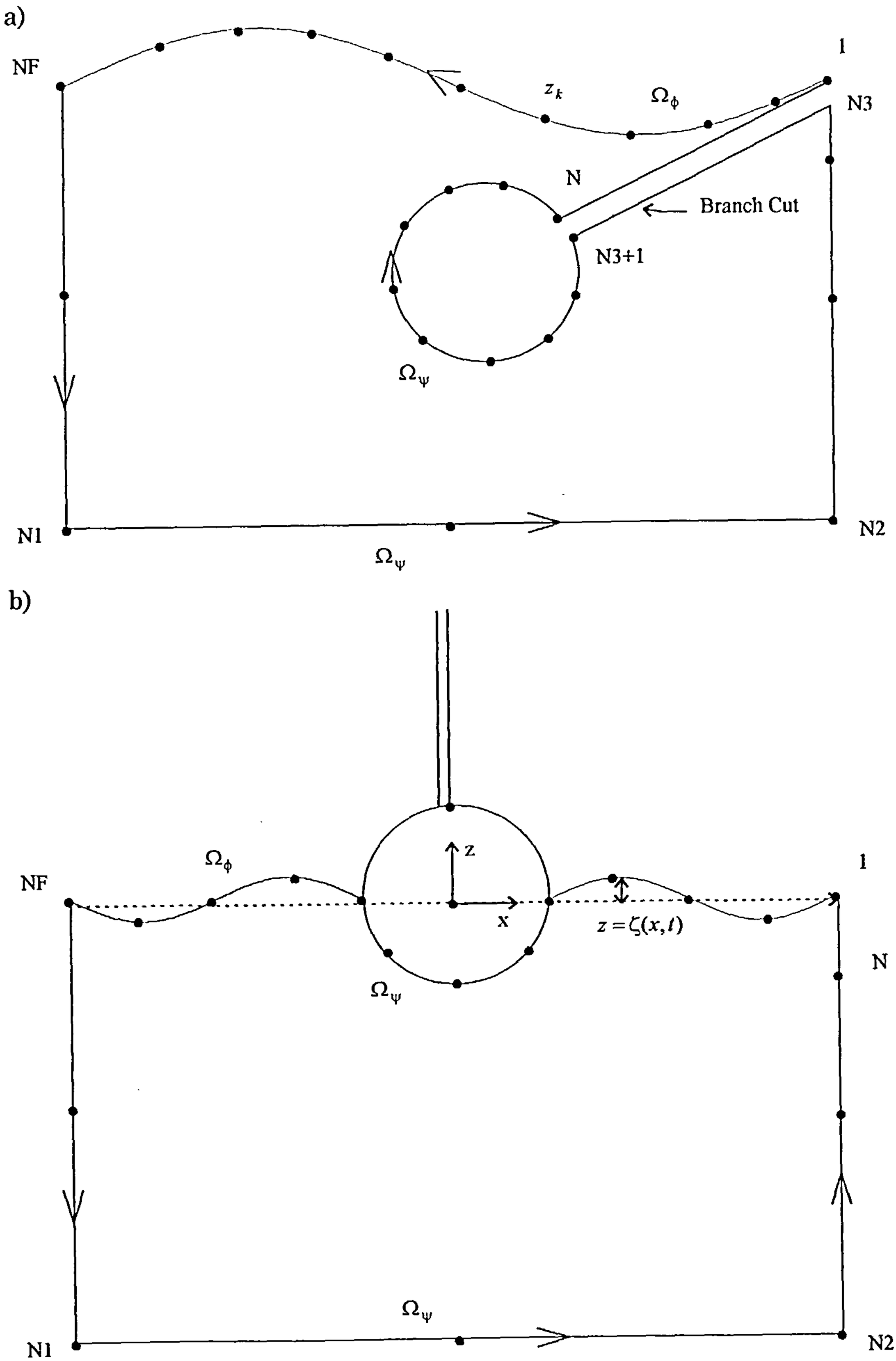

Fig. 1.2 Contours of integration

Chapter 2

Free motion of a cylinder

2.1 Introduction

The problem considered here is a result of past works which seem to have largely avoided free motion of a cylinder below a free surface. Previous experimental work on a cylinder-entry and -exit problem was carried out by Greenhow & Lin (1983). This was followed by the work by Telste (1986) for a cylinder rising to a free surface. Initially, the cylinder is located at a prescribed position below the free surface before it is accelerated to a certain uniform vertical velocity and is allowed to move up to the free surface. Further studies for impulsively started constant velocity cylinder motions were carried out by Greenhow (1987) who first recognised the occurrence of negative presssure which results in spontaneous free surface breaking. Finally, Tyvand & Miloh (1995) have used a series expansion technique to study an impulsively started motion of a cylinder with a constant velocity/acceleration moving towards a free surface. In all the above works the free surface and body interaction is discussed.

In this work we firstly consider analytically a horizontal circular cylinder which is freely but slowly rising to, or moving away from, a boundary on which

we may apply approximate boundary conditions derived from the frequency dependent free-surface boundary condition $\frac{\partial \phi}{\partial z} + K\phi = 0$, where K is related to the frequency ω by the dispersion relation $K = \frac{\omega^2}{g}$. The boundary condition $\frac{\partial \phi}{\partial z} = 0$ on $z = 0$ corresponds to a fixed boundary or to the low-frequency limit ($\omega \to 0$) of the corresponding linear oscillatory case where the body moves with time dependence $e^{i\omega t}$. The high-frequency oscillatory condition $\phi = 0$ on z=0, which is usually applied in ship slamming (high-speed entry) is also applied. The results are compared with the numerical solution of the fully-nonlinear boundary-value problem described in chapter 1. The fully-nonlinear boundary-value problem includes the effect of the free surface motion on the motion of the cylinder as well as free surface/body interactions. The situation is also discussed (incorrectly) in a paper by Greenhow and Yanbao (1988), where they used the momentum added mass instead of the energy added mass. Free and impulsively started motion of a cylinder with initial horizontal velocity is also investigated using the nonlinear numerical method.

A study of this kind has practical implications since many offshore structures, pipe-bridges and pipelines are in the form of circular cylinders. In this work we have put more effort into the analytical model's ability to predict the free motion of circular cylinders moving below a free surface. We thereby hope to provide a practical method of being able to analyse the seakeeping characteristics of submerged bodies in general, without excessive computation.

2.2 The statement of the problem

Below is a development of an analytic representation for free motion of a cylinder rising to, or moving away from a free surface. The purpose of this work is

to describe simple analytic models for a freely-moving cylinder in the vertical plane. To start the motion, a cylinder is placed at a prescribed initial depth d below the surface and freely allowed to rise to, or move away from, the surface. The predictions of these models are compared (in sections 2.4 and 2.5) with the results obtained from the numerical calculations of the fully-nonlinear boundary conditions scheme to determine the accuracy of the analytical models.

The analytic models are built on the assumption that the free surface remains fixed during the motion and hence effects such as wave damping are neglected. In formulating the problem we consider the added mass of the cylinder as it moves through the fluid. The force acting on the body is then determined as the work done in moving the cylinder through the fluid. The depth-dependent added mass coefficients are calculated in the next section. It is then a relatively simple matter to incorporate it into the equation of motion.

Generally, the motion is two-dimensional and hence the system can be specified by the generalised co-ordinates $y_i (i = 1, 2)$. We assume that $F(x, y)$ is a conservative vector force field with a potential function $f = f(x, y)$. By definition the potential energy $V = V(x, y)$ of the cylinder at $^{+1}$ is $V(x, y) = -f(x, y)$. Thus

$$F(x, y) = -\nabla V(x, y)$$

The work done by F in moving the body throu

to any point P is

$$\begin{aligned} W &= \int_O^P F \cdot d\mathbf{y} \\ &= -V(x, y)]_O^P \cdot \end{aligned}$$

since point $O(x, y) = (0, 0)$ and $P(x, y$

mass of the cylinder. The kinetic energy for vertical motion only is then given as

$$T = \frac{1}{2}(m_b + m_a(y))(\dot{y})^2 \qquad (3)$$

where m_a is the added mass and we explicitly note that it is a function of y alone. The mass $m_b + m_a(y)$ is sometimes called the virtual mass of the cylinder.

The equations of motion may be derived from Lagrange's equations, for a conservative holonomic dynamical system. Thus Langrange's equations for the generalised coordinates x_i are

$$\frac{\partial L}{\partial x_i} - \frac{d}{dt}(\frac{\partial L}{\partial \dot{x}_i}) = 0, \quad (i = 1, 2), \qquad (4)$$

where

$$\begin{aligned} L &= T - V \\ &= \frac{1}{2}(m_b + m_a(y))(\dot{y})^2 - (m_b g - \rho g \forall) y \end{aligned} \qquad (5)$$

is called the Lagrangian. Applying Lagrange's equations on (2.5) gives

$$(m_b + m_a(y))\ddot{y} + \frac{dm_a(y)}{dy}(\dot{y})^2 - \frac{1}{2}\frac{dm_a(y)}{dy}(\dot{y})^2 - gm_b + \rho g \forall = 0 \qquad (6)$$

the equation of the vertical motion of the cylinder. Forces acting horizontally are equal to zero.

The dimensionless quantities of time, mass, displacement and the fixed distance d are expressed as $T = t\sqrt{\frac{g}{a}}$, $m_b = \rho\pi a^2 M_b (m_a = \rho\pi a^2 M_a)$, $Y = \frac{y}{a}$ and $D = \frac{d}{a}$. From time, displacement and the radius of the cylinder we derive dimensionless velocity and acceleration ratios and are given as

$$\dot{Y} = \frac{\dot{y}}{\sqrt{ga}} \qquad (7)$$

and

$$\ddot{Y} = \frac{\ddot{y}}{g} \qquad (8)$$

respectively. Nondimensionalizing (3.6) gives

$$(M_b + M_a(Y))\ddot{Y} + \frac{1}{2}\frac{dM_a(Y)}{dY}(\dot{Y})^2 + 1 - M_b = 0 \qquad (9)$$

It should be noted that this apparently simple second-order ordinary differential equation has variable coefficients $M_a(Y)$ and $\frac{dM_a(Y)}{dt}$.

2.3 Calculation of the Added Mass Coefficients

For a problem of added mass calculation for a submerged circular cylinder undergoing translational or oscillatory motion below a fixed boundary we must simplify the free surface conditions rather drastically. Possibilities are $\phi = 0$ or $\frac{\partial \phi}{\partial z} = 0$ on z=0(or y=d). The second is more appropriate to the slow motion considered here, whereas ship slamming studies usually assume the former, which neglects gravity (amongst other simplifications). The accuracy of the $\frac{\partial \phi}{\partial z} = 0$ assumption will be examined by comparison with the nonlinear free-surface calculations later. We might also view the problem as the low-frequency limit of the sinusoidally oscillating cylinder below a linearised free surface. However it should be stressed that the primary motivation for this assumption is pragmatic, since the added mass of the cylinder for a fixed boundary problem is known from Greenhow and Yanbao (1987), Venkatesan (1985) and Walton (1986) who rederive Bassett's (1888) slightly incorrect expression. Thus the added mass $m_a(y)$ per unit length is (note that in our two-dimensional case the length of the cylinder is zero);

$$\frac{m_a(y)}{\rho \forall} = \frac{(1-q^2)^2}{q^2}\{\frac{1}{12} + \frac{1}{3}(1+m')\frac{K^2(m)}{\pi^2}$$

$$- \frac{E(m)K(m)}{\pi^2}\} - 1 \qquad (10)$$

where $\forall = \pi a^2$ is the displaced volume of the fluid due to the submerged cylinder, and E(m) and K(m) are complete elliptic integrals as given in Abramowitz and Stegun (1970). In addition the relation $m + m' = 1$ holds and

$$\begin{aligned} q &= exp(-\pi \frac{K(m')}{K(m)}) \\ &= exp(-\sigma_0) \end{aligned} \qquad (11)$$

where σ_0 describes the cylinder position given by

$$\begin{aligned} Y^2 - a^2 &= \frac{a^2(1-q^2)^2}{4q^2} \\ &= a^2 \sinh^2 \sigma_0 \end{aligned} \qquad (12)$$

With y and hence z, the distance of the cylinder from the fixed boundary, known at any time t, we then obtain σ_0 from (2.12) and in turn q is found from equation (2.11). Equation (2.12) assumes the form

$$K(m') + \frac{lnq}{\pi} K(m) = 0 \qquad (13)$$

To find the value of m, equation (2.13) is written in the form f(m)=0 with expressions of $K(m)$ and $K(1-m)$ taken from Abramowitz and Stegun (1970). In finding the solution of this equation the bisection algorithm was used on the interval [a,b] where f(a) and f(b) have opposite signs. With the value of m known, equation (2.13) is solved for each time step, depending on the value of q, where q changes with the depth of the cylinder below the fixed boundary. Once the values of m and q are found, the complete elliptic integrals $K(m), K(m')$ and $E(m)$ are then computed and in turn the value of the added mass is given. Since the values of m and q are updated for every time step during

the cylinder motion, the algorithm must be able to give results with updated added mass coefficient as required in our problem. In particular we must be able to account for the significant change in added mass as the body moves close to the free surface, as shown in Fig. 2.1(a). Here the full expression for added mass, $m_a(y)$, in equation (2.10) is plotted together with Walton's asymptotic expression for low-frequency limit problem

$$\frac{m_a(y)}{\rho\forall} = (2cosh2\sigma_0 - 2)(\frac{1}{12} + \frac{\pi^2}{12\sigma_0^2} - \frac{1}{2\sigma_0}) - 1 \qquad (14)$$

where

$$\sigma_0 = ln(\frac{z}{a} + \sqrt{(\frac{z}{a})^2 - 1}) \qquad (15)$$

see Greenhow and Yanbao (1987) for further details. The value of $\frac{m_a(y)}{\rho\forall}$ when $z = a$ below the surface is found to be finite and is equal to $\frac{\pi^2}{3} - 1$ whereas the gradient $\frac{dM_a(Y)}{dY}$ is infinite. Certainly as the cylinder approaches a line on which $\frac{\partial\phi}{\partial z} = 0$ i.e a wall, the more than doubling of the added mass can have a significant effect on its motion. For example, even in the absence of damping, energy considerations show that a neutrally buoyant cylinder started with initial velocity $\dot{Y}$ (towards the fixed boundary) will strike the wall with velocity $\sqrt{6}\frac{\dot{Y}}{\pi}$, as described in Greenhow and Yanbao (1987), and is similarly confirmed here by our time-stepped added mass scheme, see Fig. 2.1(c). The cylinder is started from a distance d=3a with a velocity of 5 (dimensionless) and hits the fixed boundary with a velocity of 3.9035. This underlies the fact that the cylinder decelerates as it approaches the wall and accelerates when moving in the opposite direction, see also Fig. 2.1(d) for downward motion. We note that the gradient of the added mass $\frac{dMa}{dY}$ is less than zero at all distances below the surface (wall) partially giving rise to the above observed

effects on the motion of the cylinder. In contrast with the constant added mass case where the term involving velocity squared $\frac{dMa(Y)}{dY}\dot{Y}^2$ is therefore absent in equation (2.9), the above demonstrates the importance of this term in conserving energy when added mass is position dependent.

However, it is not very clear what the appropriate boundary condition on the free surface should be, as there is significant surface deflection in the case of vertical motion near the surface i.e when the top of the cylinder is within one radius of the surface. Furthermore as the cylinder breaks such a surface the flow becomes source-like, which causes the added mass to diverge in the two-dimensional case, see eg Newman (1977). We will therefore consider applying the boundary condition at the equipotential line $\phi = 0$ in the case of vertical motion near the surface. The results may then be thought of as those of the problem of high-frequency oscillatory condition. For motion of the cylinder near the line of equipotential $\phi = 0$ on $z = 0$ Greenhow and Yanbao (1987) give the added mass per unit length as

$$\frac{m_a(y)}{\rho\forall} = \frac{(1-q^2)^2}{q^2}\{\frac{1}{12}+\frac{1}{3}(1+m')\frac{K^2(m)}{\pi^2}-\frac{E(m)K(m)}{\pi^2} - \frac{1}{6}-\frac{2}{3}(1+m_1')\frac{K^2(m_1)}{\pi^2}+2\frac{E(m_1)K(m_1)}{\pi^2}\}-1 \quad (16)$$

where the equation

$$\frac{K(m')}{K(m)} = \frac{1}{2}\frac{K(m_1')}{K(m_1)} \quad (17)$$

holds. This form of the added mass is exact but quite expensive to compute and we choose to use a polynomial approximation given as

$$\frac{m_a(y)}{\rho\forall} = 1+0.028053(\frac{a}{y})-0.65986(\frac{a}{y})^2+0.26728(\frac{a}{y})^3 \quad (18)$$

which is accurate enough for our calculations, see Greenhow and Yanbao(1987). In their work they also calculated the limiting forms of the added mass and

the gradient of the added mass as $\frac{z}{a} \to 0$ from the asymptotic expression of equation(2.16) which are respectively;

$$\frac{m_a(y)}{\rho\forall} = \frac{\pi^2}{6} - 1 \qquad (19)$$

and

$$\frac{dm_a(y)}{dy} = \rho a\pi(\frac{\pi^2}{9} - \frac{2}{3}) \qquad (20)$$

The added mass coefficients are calculated using the exact expression given by the low-frequency limit problem for, at least, $z \leq -1.44a$ below the surface plus Walton's asymptotic expression near the free surface $(-1.44a \leq z \leq -a)$. The variation of the added mass with respect to vertical displacement is shown in Fig. 2.1(a). For the high-frequency approximation, equation (2.18) is used to obtain the added masses for values of z in the range $-10a \leq z \leq -a$, see Fig. 2.1(b) for variation of the added mass with depth. With the added masses already known, (2.9) can then be treated simply as a second-order ordinary differential equation which is solved exactly at every stage of the calculations with new "constant" coefficients each time and the initial conditions given by the solution to the previous step. In other words for each time step one solves analytically a nonlinear differential equation with constant coefficients. The solution is then time stepped to give the required solutions for each distance for which added mass is calculated. The velocities and accelerations are found through differentiating the obtained solution once and twice respectively. This solution's accuracy is dependent on accurate calculation of the added mass, and serves as a check to the solution obtained numerically using the fourth-order Runge-Kutta algorithm.

Thus

$$A\ddot{Y} + B(\dot{Y})^2 + C = 0 \qquad (21)$$

where $A = M_b + M_a$, $B = \frac{1}{2}\frac{dM_a}{dY}$ and $C = 1 - M_b$. Let $U = \dot{Y}$, so that

$$A\dot{U} - B(U^2 + \frac{C}{B}) = 0. \qquad (22)$$

Solving (2.22) gives

$$U = \sqrt{\frac{C}{B}}\tan(\sqrt{\frac{BC}{A^2}}T + E\sqrt{\frac{C}{B}}) \qquad (23)$$

where E is a constant of integration and is found from the given initial conditions. Replacing U by $\dot{Y}$ in (2.23) and integrating gives

$$Y = -\frac{A}{B}\ln\{\cos(\frac{\sqrt{BC}}{A}T + E\sqrt{\frac{C}{B}})\} + G \qquad (24)$$

where G is the second constant of integration and is also determined by using the initial conditions. With initial conditions given the constants of integration are found and the motion is time stepped by assigning a value to Y, at distances for which we require solutions, in equation (2.24) so that the depth dependent added mass is calculated and in turn the velocity and acceleration, given by equations (2.23) and (2.25) respectively, are found at that time step, where the acceleration has been obtained from twice differentiating (2.24), i.e

$$\ddot{Y} = \frac{C}{A}\sec^2(\frac{\sqrt{BC}}{A}T + E\sqrt{\frac{C}{B}}) \qquad (25)$$

The solution obtained this way is not quite exact as it is dependent on the accuracy of the calculations of the added mass. In order to calculate correctly the numerical values of Y, $\dot{Y}$ and $\ddot{Y}$ we should choose M_b and the sign of B carefully i.e corresponding to the direction of motion. For a cylinder rising to the free surface, $M_b < 1$ and B is positive because Y is defined as positive upwards. The case of a sinking cylinder is the reverse of the above and the system is at equilibrium when $M_b = 1.0$.

For time-stepping the equation of motion, a fourth-order Runge-Kutta method with local truncation error of $O(h^4)$ is used. The results for complete numerical calculations using the Runge-Kutta method and the above "exact" method are compared in Fig. 2.2 for the case of M_b=0.8 starting at d=5a. The difference between the two methods is negligible and hence the results of the Runge-Kutta fourth-order algorithm are accurate. We latter on compare them with the numerical calculations of more general types of motion using the fully-nonlinear boundary conditions scheme for verification of the analytical model.

To be able to carry out comparison tests we need to ensure that the parameters in both methods are set equal. One such parameter is the mass of the cylinder. In the analytical method we use $m_b = (\rho\pi a^2 M_b)$ to represent the mass of the cylinder. In the case of the nonlinear free-surface numerical method the collocation point distribution on the cylinder contour is taken in parametric form in ϕ (the angle between the radius vector and the real axis) such that $x_{body}(t) = a\cos\phi$ and $y_{body}(t) = y_{var}(t) + a\sin\phi$, where y_{var} is the varying vertical position of the cylinder and $(x_{body}(t), y_{body}(t))$ the position of the point on the cylinder at any time t. The cylinder contour is then discretised to allow $NBODY$ (denotes number of points on the body) points on it. The initial distribution of the points on the free surface is made comparable to the distribution on the body. Assuming the cylinder contour is an $NBODY$-sided polygon, the area of that figure is then found to be

$$Area = \frac{(NBODY)a^2}{2}\sin\phi \qquad (26)$$

and approximately equal to πa^2 for large values of $NBODY$, where in our case this value coincides with the displaced volume of the fluid. In that way the buoyancy force $\rho g\frac{(NBODY)a^2}{2}$ is correctly determined.

2.4 Rising cylinder

The cylinder is located at a prescribed position, $D = \frac{d}{a}$, below the free surface and is allowed to rise freely to the surface. Firstly, we consider the results of the numerical scheme obtained under the stated conditions above. Of interest is the effect of the free surface motion on the cylinder forces. This, presumably will confirm the validity or otherwise of the simplified boundary conditions in the case of the analytical models. We shall consider below five cases of specific gravity of the cylinder, namely $M_b = 0, 0.2, 0.6, 0.8$ and 0.9.

For $M_b = 0.8$ and $d = 5a$ the surface elevations are shown in Fig. 2.3 as the cylinder is progressively approaching the free surface. In Fig. 2.3(a) we can see that at the time when the cylinder is just below the position $Z = -\frac{z}{a}$ the free surface has still not deflected much above $z = 0$. Later stages are not comparable with the analytical model since we know that in reality the free surface will move up above the line $z = 0$ together with the cylinder. In all other cases of M_b the free surface does seem to remain reasonably flat for $z < -a$, $T < 8.7$ in the case of $M_b = 0.8$, prompting us to impose the rigid wall boundary condition, $\frac{\partial \phi}{\partial z} = 0$ on $z = 0$ (the low-frequency limit). In Figs. 2.6, 7, 9, 10 we show surface profiles for cylinders of specific gravity 0, 0.2, 0.6 and 0.9. In the analytical model we then apply this simplified free-surface boundary condition for comparison with the nonlinear calculations.

We have also experimented with an equipotential boundary condition $\phi = 0$ on $Z = 0$ (the high-frequency limit for the oscillatory case usually considered), whereby the effect of gravity is ignored. In Fig. 2.5 the displacement/time and velocity/time graphs of the equipotential condition motion are compared with those of rigid wall condition motion, the numerical scheme and constant added

mass method. On comparing the equipotential motion with the other motions we see that the effect of the forces for this motion on the cylinder is opposite of that of the numerical scheme, and low-frequency motion as expected. The constant added mass (=1) motion is included as a simple check on energy conservation of the numerical system.

The imposition of the rigid wall type of the boundary condition produces results which are qualitatively in good agreement with the results of the numerical method. The difference in times for the two methods can be attributed to the fact that in reality the free surface is nonlinear and hence the assumption that we have a fixed boundary is, to some degree, a misrepresentation of the real free surface deflection. On the other hand we find that the fact that the body slows down as it approaches the free surface is inherent in both methods which shows that the choice of rigid wall boundary condition is the best of the simple models.

From the list of our chosen values of M_b it is worth noting that the agreement between the two methods is improved in the case of small values of M_b, see Fig. 2.8. In the case of a non-deformable bubble, $M_b = 0$, the agreement is excellent. The agreement is generally very good for $0 \leq M_b \leq 0.3$. The agreement gets worse for values of $M_b > 0.3$, see also Fig. 2.5, 2.11. There does not seem to be any way we can consistently improve on these results, nor others with many other values of the two parameters, M_b and D not shown here. On starting at $d = 9a$ we got similar motion, with the primary difference being a time delay. See Fig. 2.4 for surface elevations and Fig. 2.5 for body kinematics.

In conclusion we can point out the fact that the two methods are in good

agreement for values of M_b between 0 and 0.3. For values greater than 0.3 the analytical model with the rigid wall condition is qualitatively correct, and there is good agreement in the behaviour of the forces as the cylinder approaches the fixed wall/nonlinear free-surface. The cylinder slows down as it approaches the fixed wall/nonlinear free-surface in both cases, but at different rates. Calculations can only be taken to the point when $Z = -\frac{z}{a}$ for the analytical model since the added mass term has a finite value and the gradient of the added mass term tends to infinity at this point. The numerical calculations can be continued until the thin fluid layer below the body breaks causing the breakdown of the calculations. We shall see more of the features of the free surface behaviour as the rising cylinder interacts with the surface, in chapter 4 where the vertical motion of the cylinder with constant velocity is studied.

The breaking of the free surface seems to be physical and is thought to be caused by the development of negative pressures on the sides of the cylinder, see also Greenhow(1987). This causes a pressure inversion across the free surface and consequently a Rayleigh-Taylor instability. This phenomenon is depicted on a number of cases investigated above. In Figs. 2.3(e) total pressure distribution around the cylinder is shown for indicated times that correspond to some positions of the body and the surface depicted in (a) -(d). In Fig. 2.6(b) we show pressure distribution at distances $d = 3.1a, 1.1a$ and a when its centre is still below or coincides with the equipotential line and $d = -0.05a, -0.7a$ and $-3.1a$ when the centre is now above the equipotential line. At early stages, i.e $d = 3.19a$ the pressure is almost totally symmetrical about both the vertical and horizontal lines through the centre of the cylinder and is positive, see Fig. 2.6(a) . This situation changes immensely as we approach the free surface with

pressure increasing sharply at the bottom of the cylinder, decreasing slightly at the top and dropping to below zero at the sides. This kind of behaviour of the pressure is also discussed in Telste's (1986) paper for motion of a cylinder with constant velocity near the free surface. As the cylinder completely pushes its way through and above the $z = 0$ line, the pressures become positive again and still greatest at the bottom. Further similar pressure distribution plots for Mb=0.6 are shown in Fig. 2.9(g).

2.5 Sinking cylinder

For the motion of a cylinder moving away from the free surface, five cases of specific gravity $M_b = 1.1, 1.2, 1.4, 2$ and 2.4 are considered. In Fig. 2.12 we have shown the surface and cylinder positions due to the motion of a cylinder of specific gravity 1.1 as it freely moves, from a prescribed position $d = 1.2a$, away from the free surface. This motion continues for large number of time steps causing very little surface deflection. Eventually, these calculations break down immediately after a small jet has formed at the centre. Starting the motion at $d = 1.1a$ will cause the free surface to deflect and create waves of short wave length in the vicinity of a small area directly above the cylinder on the free surface. Looking closely in Fig. 2.13 one can see the features referred to above. Such jets and short waves cause numerical instability resulting in breakdown of the calculations, unless smoothed out artificially. As we increase the value of M_b the chances of the numerical calculations breaking down are also increased, see Figs. 2.16 and 2.17 for $M_b = 1.2$ and 2. In Figs. 2.16(g) and 2.17(e) we show pressure distributions around the cylinder at given times corresponding to some given free/cylinder surface positions in Figs. 2.16(a)-

(f) and 2.17(a)-(d). Initially, the pressure distribution is largely hydrostatic increasing steadily on the cylinder top and bottom. In Fig. 2.16(c), where a mound has developed, the pressure graph representing pressure at the top of the cylinder is shown to be flattening. This phenomenon is quite unclear as regards cause and effects; either the mound causes pressure variations or vice versa.

The results of the numerical calculations are then compared with the predictions of our analytical models in order to test the validity of the latter. For $M_b = 1.1$ and $d = 1.2a$ we have included four cases of the boundary condition considered in the case of a rising cylinder, namely the rigid wall with variable added mass, constant added mass, fully nonlinear and equipotential boundary conditions, see Fig. 2.14. The agreement between the case of constant added mass and the numerical results seems to be best. In the case of rigid wall with variable added mass, the agreement is poorer even though the general behaviour of the forces is comparable. At the start of the calculations ($T < 2$) the equipotential condition method is in good agreement with the numerical method. This is to be expected of course since the numerical method also starts with a flat free surface $\phi = 0$ on it. The two methods start to diverge later on the time interval $T > 2$. The cylinder seems to be moving with constant velocity in all the cases, especially at later stages of the motion where we would expect this behaviour as added mass variation becomes less important. In Fig. 2.15 we show graphs for the motion of a cylinder with $M_b = 1.1$ started from $d = 1.1a$ and $1.2a$ below the surface. The other cases of cylinders considered seem to resemble this case. For example cases for M_b =1.2, 1.4 and 2 have been considered, see Fig. 2.18. As in the case of the rising cylinder,

the delay of the motion for the rigid wall condition appears to be the main difference between the low-frequency and the numerical calculations. When comparing the numerical calculations with the equipotential calculations we notice a delay of the motion for the fully-nonlinear boundary condition.

The calculations with the equipotential boundary condition compare well with the numerical calculations for times $T < 2$ after which the cylinder starts moving faster in the former case. This maybe so, because initially the free surface is almost flat which results in very little disturbance to the motion of the body due to the free-surface motion and hence all the methods are in quite good agreement within that interval. For times $T > 2$ the high-frequency condition results in faster motion as oppossed to the low-frequency case. To a less extent, this is partly due to added mass variation near the surface which increases downward for the high-frequency condition towards the upper limiting value (=1) and upward for the low-frequency condition away from the lower limiting value (=1). At later stages the added mass plays no role and the agreement between the three methods (rigid wall, numerical and equipotential) is understood. For cases of M_b in the range $1.1 \leq M_b < 1.4$ (see Figs 2.14, 15 , 18), added mass effect is important, rigid wall condition seems to produce results which are a better approximation of the motion of the cylinder than the equipotential method. However, for large values of M_b, added mass effect is relatively less important. The constant added mass method seems to be in good agreement with the numerical calculations for all the cases of M_b considered, but can not predict the behaviour of forces near the surface where variation of the added mass is important.

To check on the divergence and convergence of the equipotential method and

the rigid wall method against the numerical method, the motion is started at a position further away from the free surface than $d = 1.2a$ to allow for better numerical calculations. The agreement between the rigid wall, equipotential and the numerical methods is improved for the motion of a cylinder started from a distance $d = 2a$ for large values of M_b. In Fig. 2.19 we contrast the results of the motion of a cylinder started from $d = 2a$ with $M_b = 1.1$ to those started from the same position, but for $M_b = 2.4$. The three methods converge as expected, since the effect of the added mass is now minimal.

The free surface does not deflect much when $1.1 \leq M_b \leq 1.4$ and hence the use of the simplified boundary condition $\frac{\partial \phi}{\partial z} = 0$ or $\phi = 0$ is justified in the case of a sinking cylinder. For $M_b > 1.4$ it is hard to justify the use of the simplified conditions, especially near the surface, since the free surface is greatly distorted when the motion is started just below the surface, $d = 1.2a$ say. Unlike in the case of a rising cylinder, the application of the equipotential condition($\phi = 0$) in the case of a cylinder moving away from the free surface has proved to be qualitatively in good agreement with the numerical method for small time for all the cases considered. This is so, because at the start of the calculations, in the case of a rising cylinder, the body is far away from the surface and hence the surface remains flat for some time before becoming quite disturbed. As a result when the body reaches the surface, the initial equipotential condition no longer apply and hence the method predicts the wrong direction of motion at the end. An improvement in predicting the motion accurately of the rigid wall and equipotential methods for a sinking cylinder can be achieved by using bigger values of M_b and starting the motion from far below the free surface, a distance below $d = 1.2a$ at least. Such results are not of any practical

significance since generally the added mass does not vary much for deeply submerged bodies and our primary need is a model of this problem near a free surface where the effect of the added masses is significant.

2.6 Free horizontal motion

In accordance with the investigations discussed in Tyvand & Miloh(1995), also to be discussed in chapter 4 of this work, we comment on some of the results obtained in their work. The main results obtained in their work are for constant velocity and acceleration, but they also conlcude that the obtained results can easily be adapted to solve the problem for free motion with initial horizontal velocity. They claim that, if a cylinder is given an initial impulsive horizontal force and is allowed to move freely then it will continue with constant velocity initially, until the free surface effects begin to act causing the horizontal motion to slow down. However, the body also experiences a downward acceleration caused by zero-order forces from their expansions, see Tyvand & Miloh(1995). Therefore, the net force causes the body to move almost parabolically during the early stages of the motion.

To check this claim, a neutrally buoyant cylinder is initially located at $d = 1.2a$ and is given an initial impulsive horizontal force before it is left to move freely. Here, we assume the dimensionless scales used in the work of Tyvand & Miloh(1995) as well as those used above, for example nondimensional time $T = t\frac{U}{d}$, distance and velocity are obtained as above, whereas the pressure and the hydrodynamic force are divided by $\rho g a$ and buoyancy respectively. We comment on those results in comparison with observed behaviour of the free motion of the cylinder produced by the nonlinear method described above.

In Fig. 2.20(a)-(b) we show free-surface deflections and cylinder positions, and (c)-(d) represent total pressure distributions around the cylinder corresponding to elevations in(a) and (b) respectively. The time in Figs. 2.20(e(i), f(i)) is nondimensionalised by $\sqrt{\frac{g}{a}}$ and by $\frac{d}{U}$ in Figs. 2.20(e(ii), f(ii), h). The path followed by the cylinder between 0 and 0.55 along the horizontal or, in terms of nondimensional time as in Fig. 2.20(e(ii)), on the interval of time from 0 to 0.085, is indeed parabolic and turns upwards immediately after that, see Fig. 2.20(g). The total hydrodynamic force on the cylinder seems to indicate that kind of behaviour, as it is almost constant at the start of the calculations and begins to rise just after a small interval of time before gradually decreasing, see Fig. 2.20(h).

2.7 Conclusion

In this chapter we have considered the free motion of the cylinder moving away or towards the free surface or horizontally. Results of low-frequency and high-frequency limit problems have been compared with those of the nonlinear numerical scheme. The low-frequency calculations with updated added mass were shown to be qualitatively in agreement with the numerical results for a cylinder moving away or towards the surface showing only a delay in time. The equipotential condition could only produce qualitatively correct results in the case of a sinking cylinder and for a rising cylinder when the body does not move near to the surface. The constant added mass model seems to be a better approximation of the numerical results than the two methods discussed above but fails to predict the direction of force at the end of the motion for a body moving towards the surface. However, for the low-frequency limit problem

the cylinder motion is retarded as it approaches the wall and accelerated as it moves away from it. This could only be achieved by the use of the variable added mass model using the low-frequency condition. An important result that has practical implications concerning offshore structures. It is essential to be able to determine correctly the size and direction of hydrodynamic forces on a structure for its safe and economic usage. In chapter 3 we investigate the effects of updating or not updating the added mass for a spring-loaded cylinder oscillating below the surface, where we also consider the effects of wave damping on the motion of the system.

The results, due to the free motion of a cylinder which is initially given a horizontal impulsive force, predicted by the small-time asymptotic method of Tyvand & Miloh are in good agreement with the nonlinear method. The early path of the cylinder is indeed parabolic and starts horizontally on the region $0 < T < 0.045$ and curves downwards in the interval $0.045 < T < 0.105$ a region where the small-time asymptotic method is known to be very accurate.

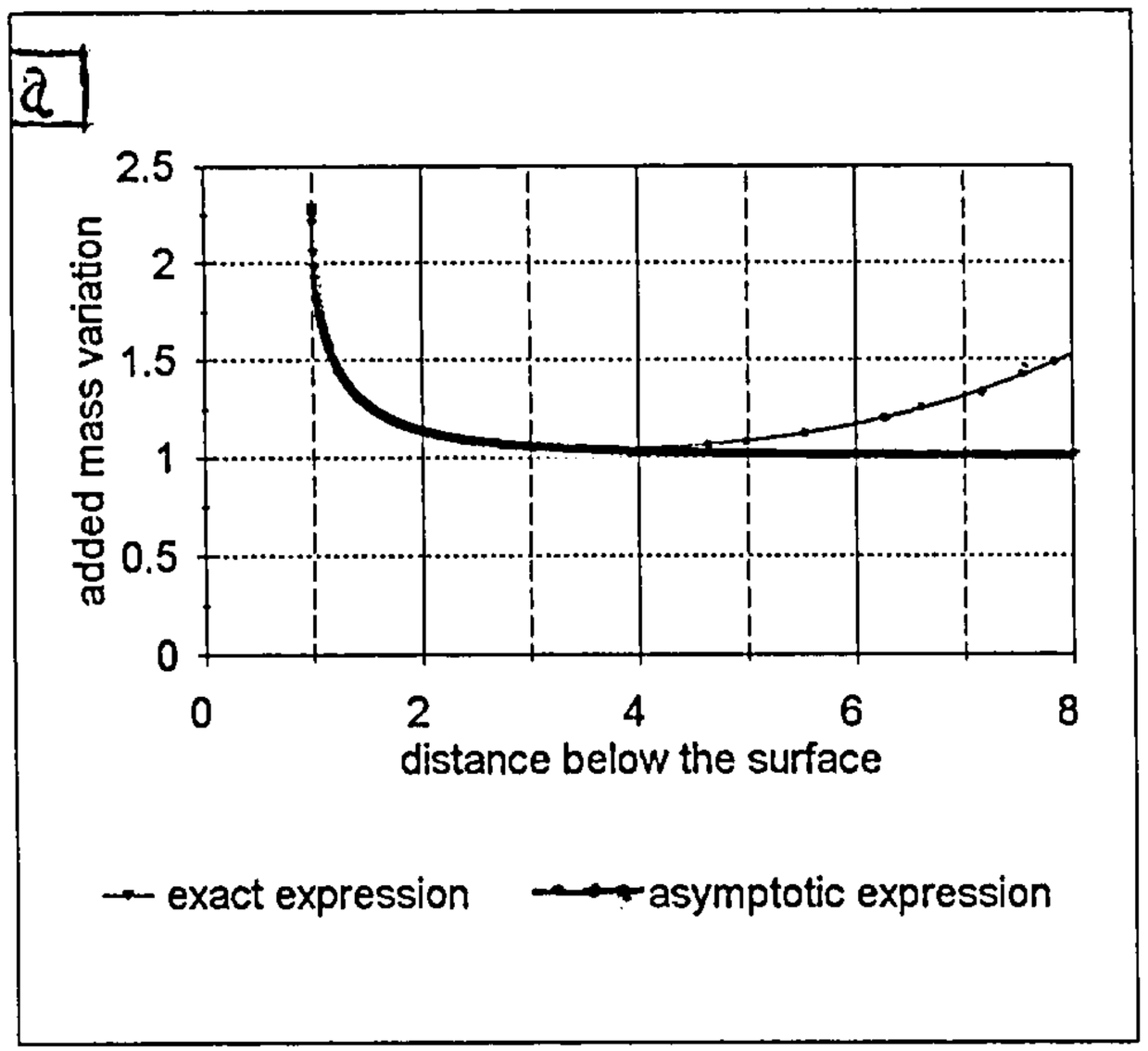

Fig. 2.1 Exact added mass expression plotted together with the asymptotic expression against distance z/a below the surface.

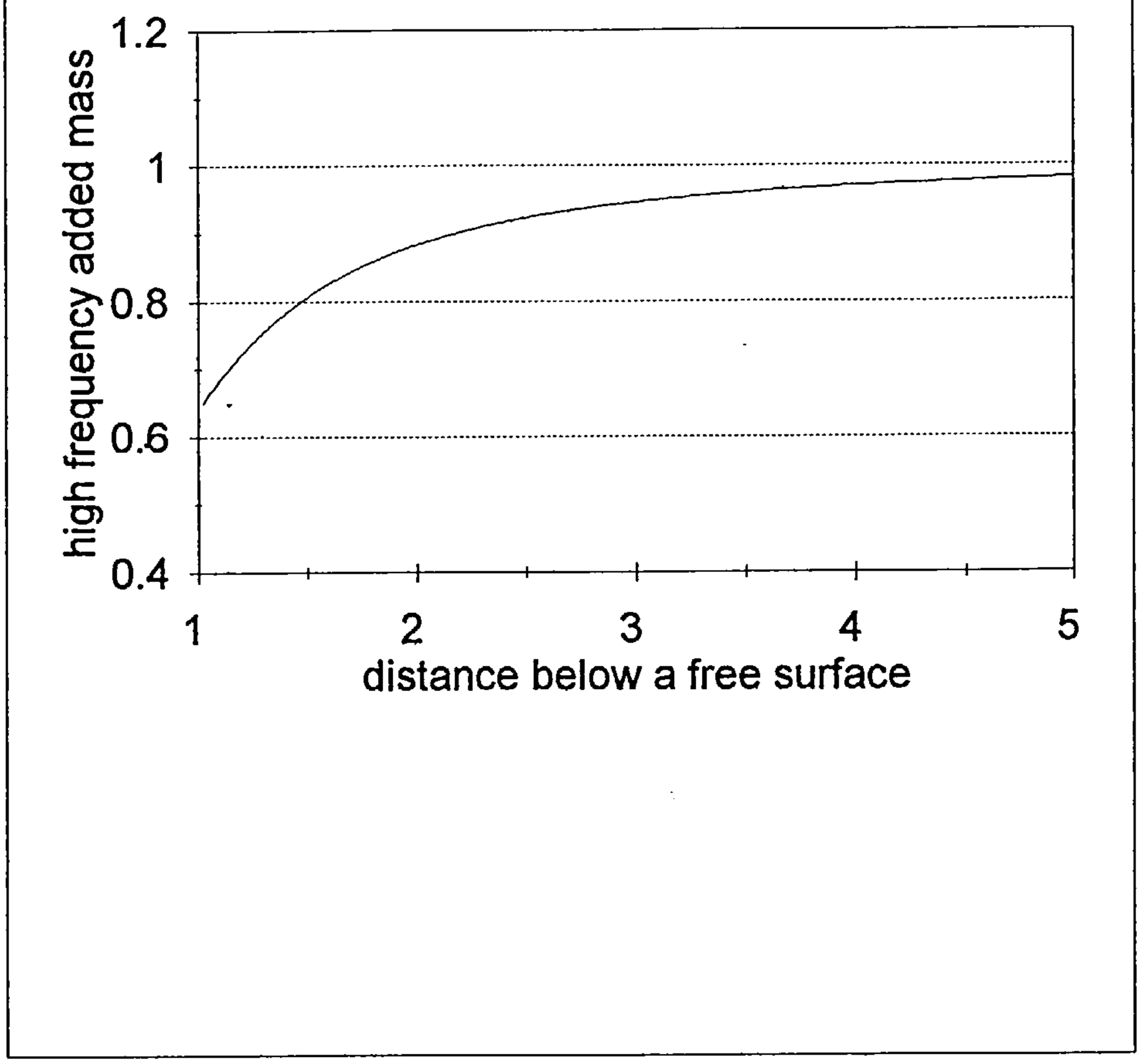

Fig. 2.1(b) Added mass variation with depth below the free surface in the case of equipotential boundary condition.

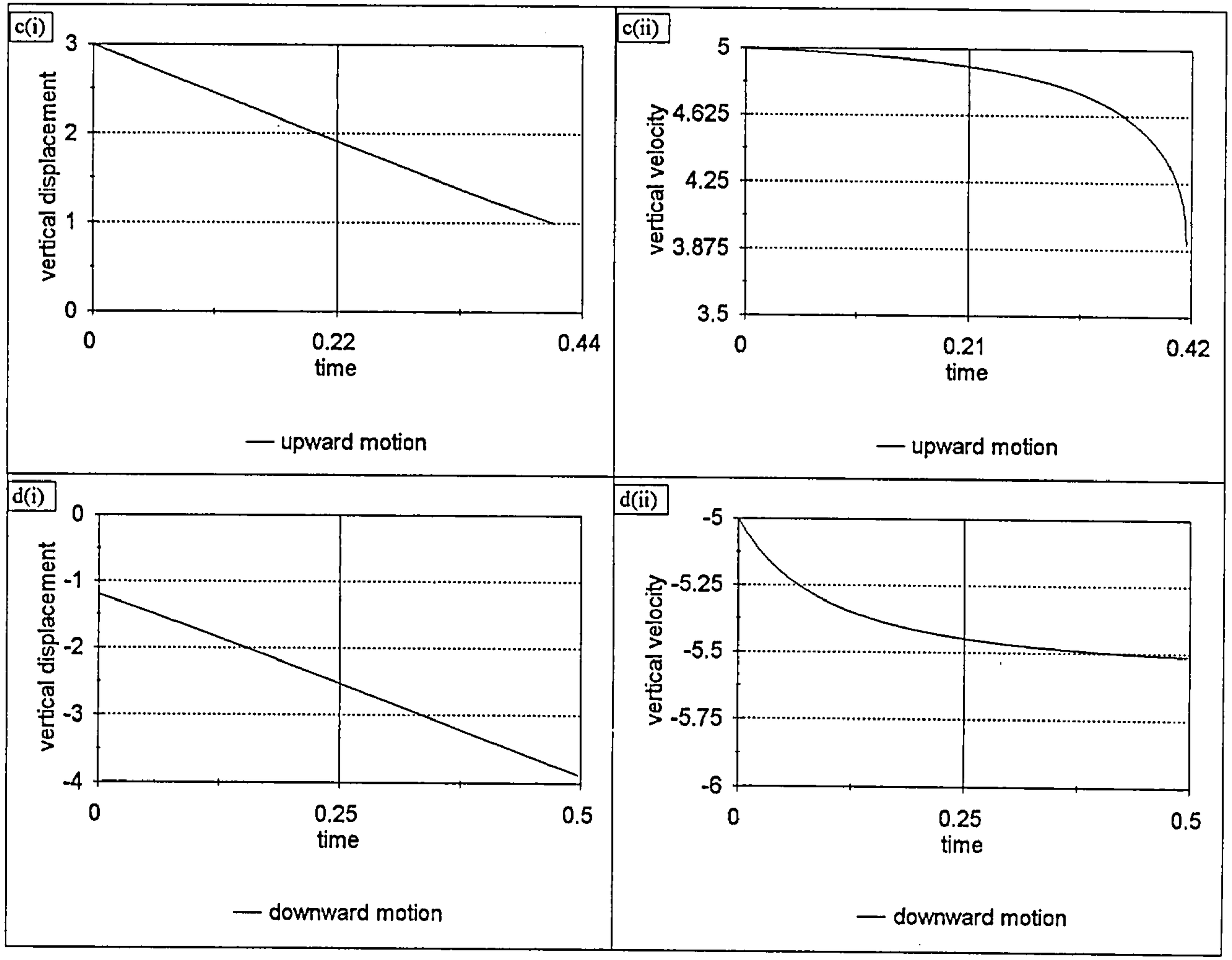

Fig. 2.1(c-d) Motion of a neutrally buoyant cylinder initially placed at c) d=3a and given an upward velocity of 5(nondimensional) and d) d=1.2a and given a downward velocity of -5(nondimensional).

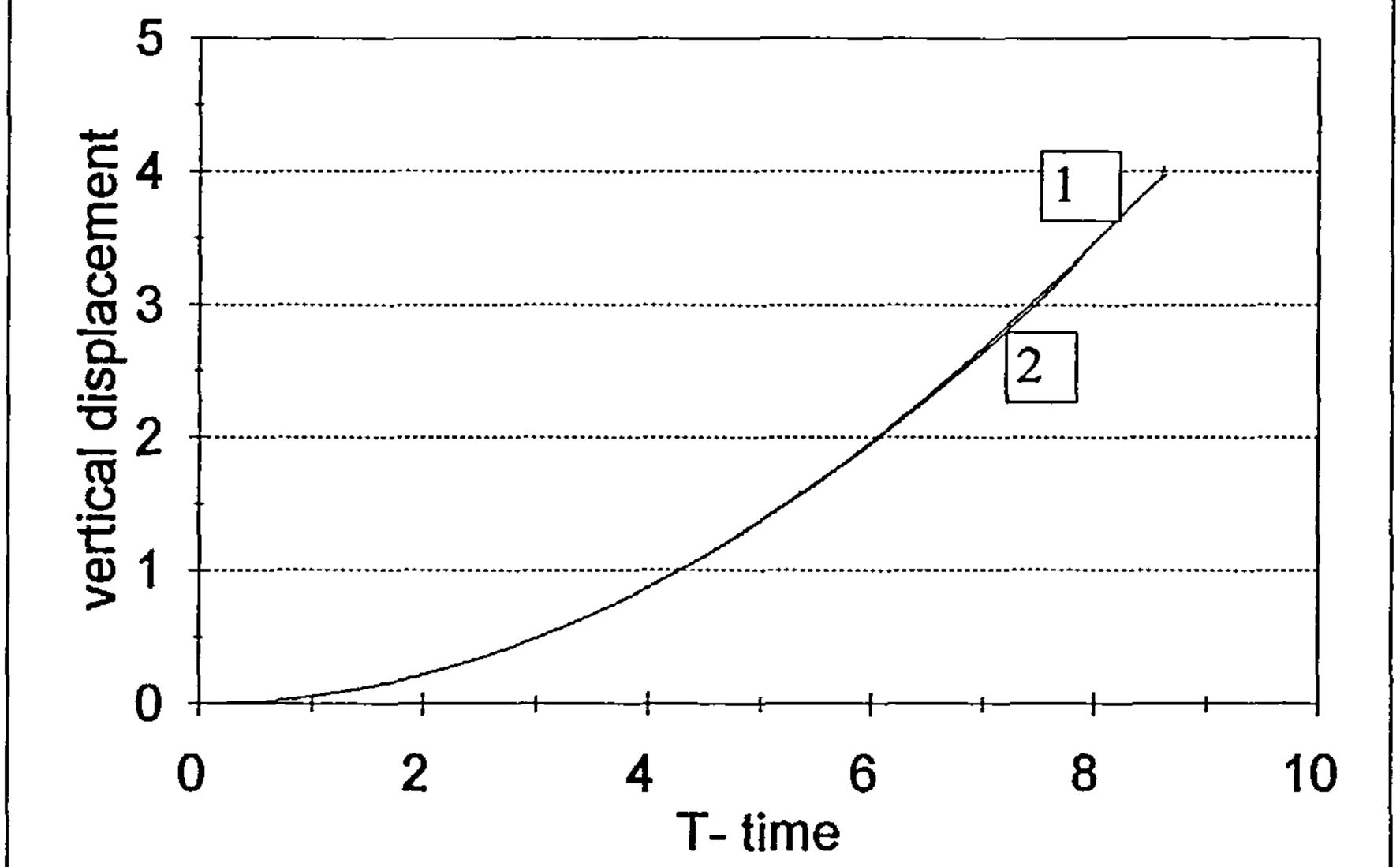

Fig. 2.2 Free motion of a cylinder rising to a free surface, d=5a and [1] represents approximation; [2]- exact solution.

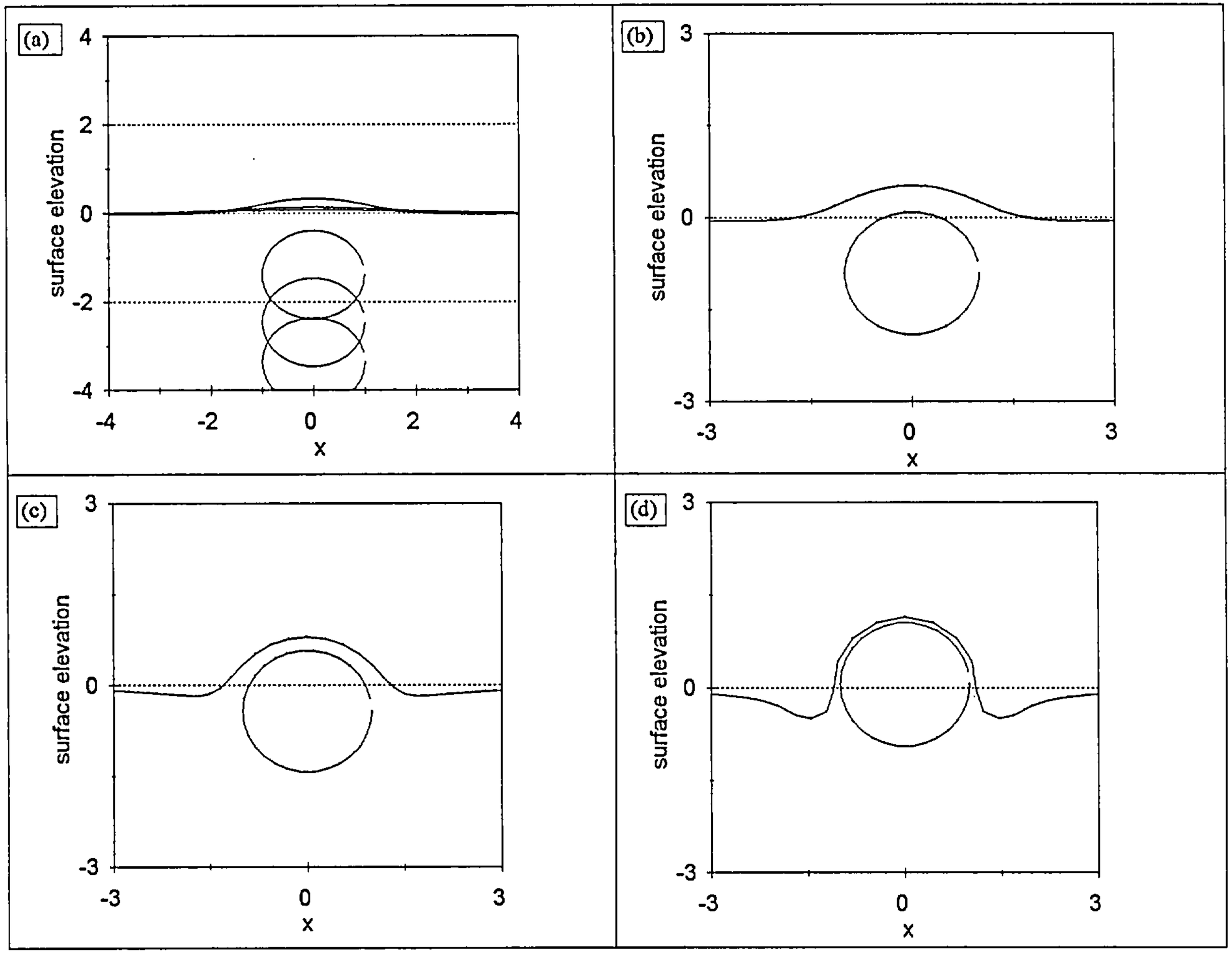

Fig. 2.3 Free-surface and cylinder positions due to the free motion of a cylinder rising to a free surface. Mb=0.8 and initially the cylinder is located at d=5a below the surface. [a] T=5.127, 6.387, 7.648; [b] T=8.194; [c] T=8.698; [d] T=9.203

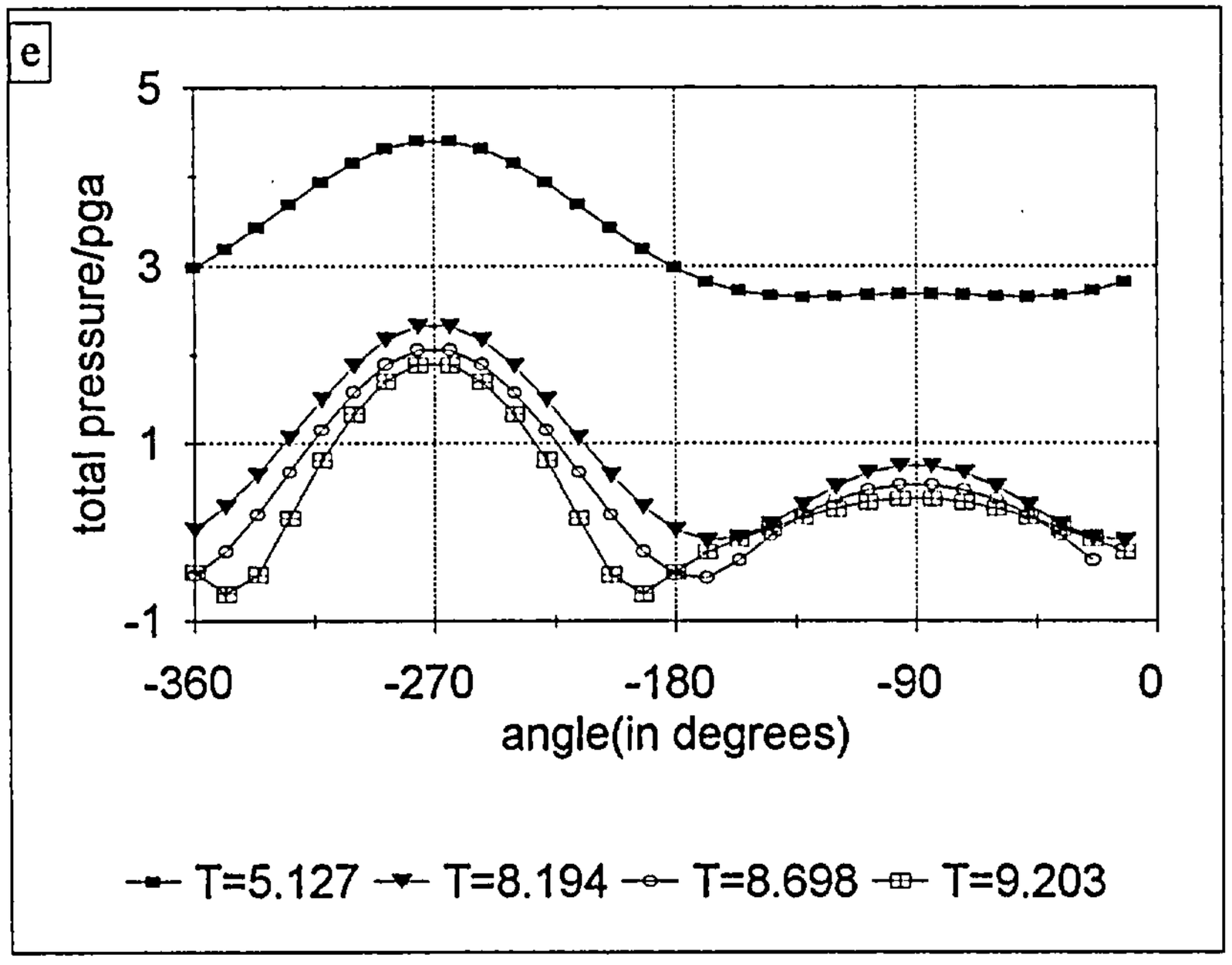
e
5
3
1
-1
total pressure/pga
-360
-270
-180
-90
0
angle(in degrees)
T=5.127
T=8.194
T=8.698
T=9.203

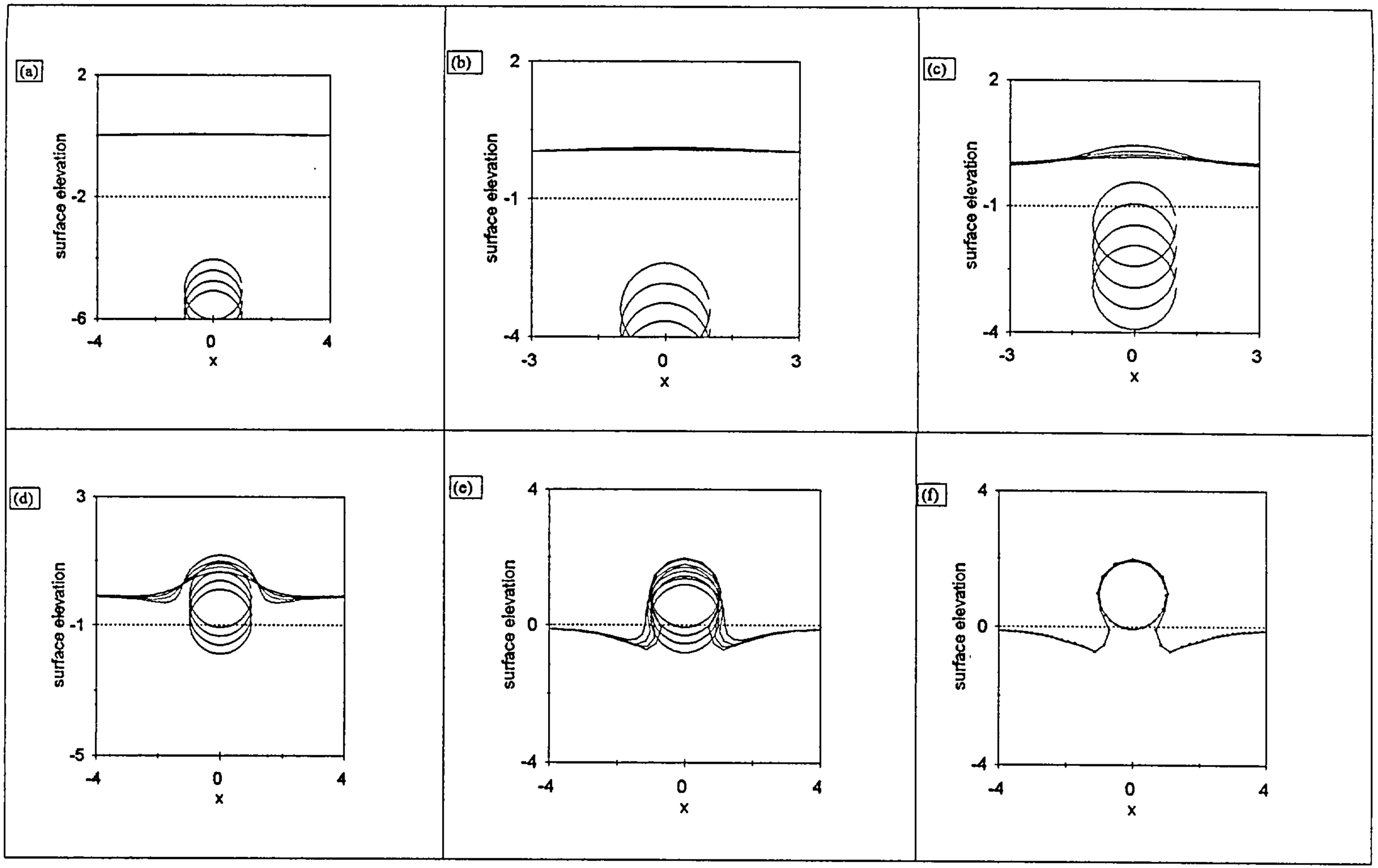

Fig. 2.4 Free-surface and cylinder positions due to the free motion of a cylinder rising to a free-surface. Mb=0.8 and initially the cylinder is located at d=9a be elow the surface. [a] T=7.564, 7.984, 8.825; [b] T=9.245, 9.665, 10.085, 10.505; [c] T=10.926, 11.346, 11.766, 12.186; [d] T=12.606, 12.817, 13.027, 13.237; [e] T= 13.447, 13.657, 13.867; [f] T=14.287

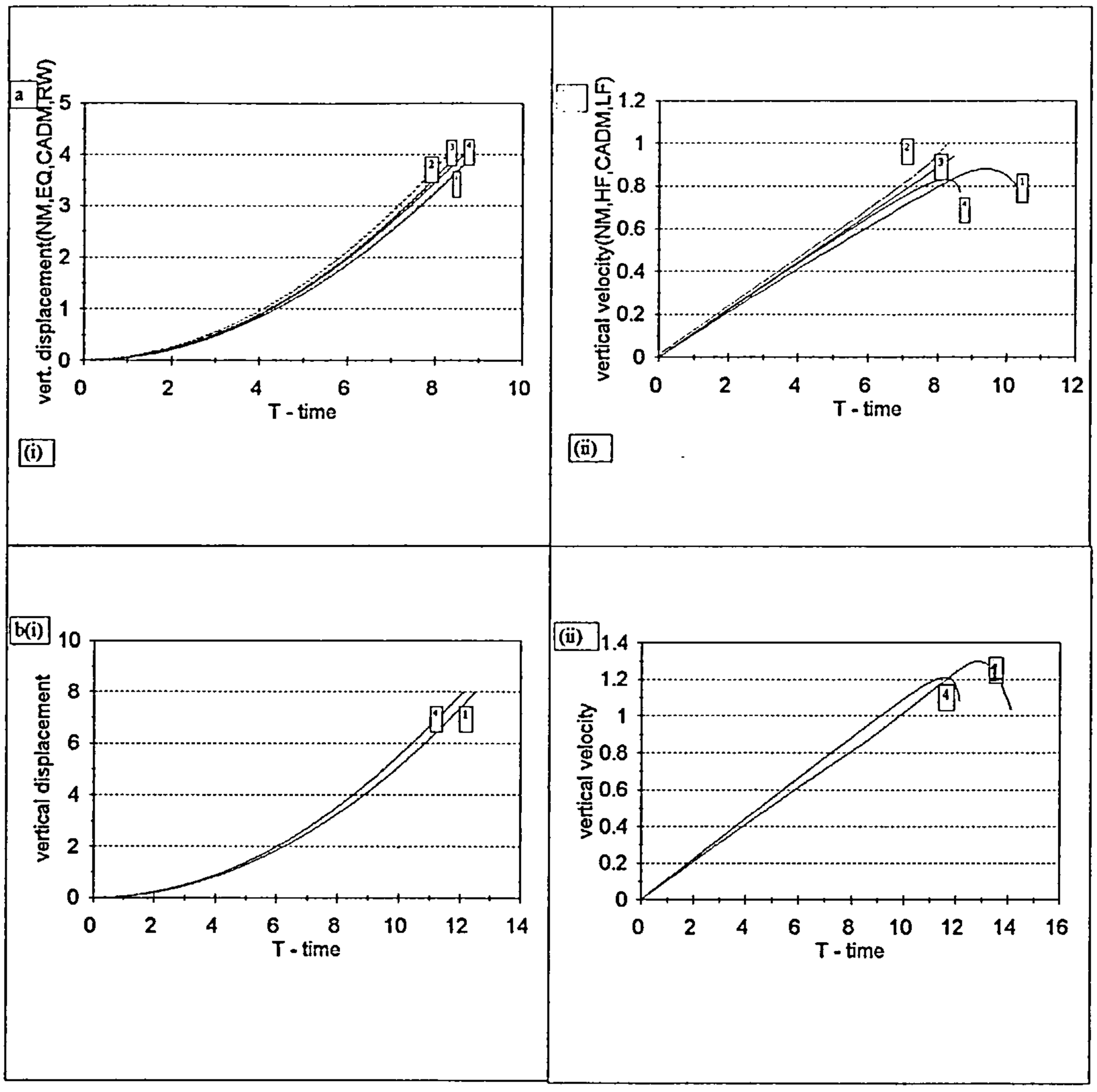

Fig. 2.5 Free motion of a cylinder rising to a free surface. a)[1] NM-numerical method, [2] EQ-equipotential condition, [3] CAMD- constant added mass(for RW) and [4] RW- rigid wall condition, Mb=0.8 and d= 5a; b) Mb=0.8 and d=9a.

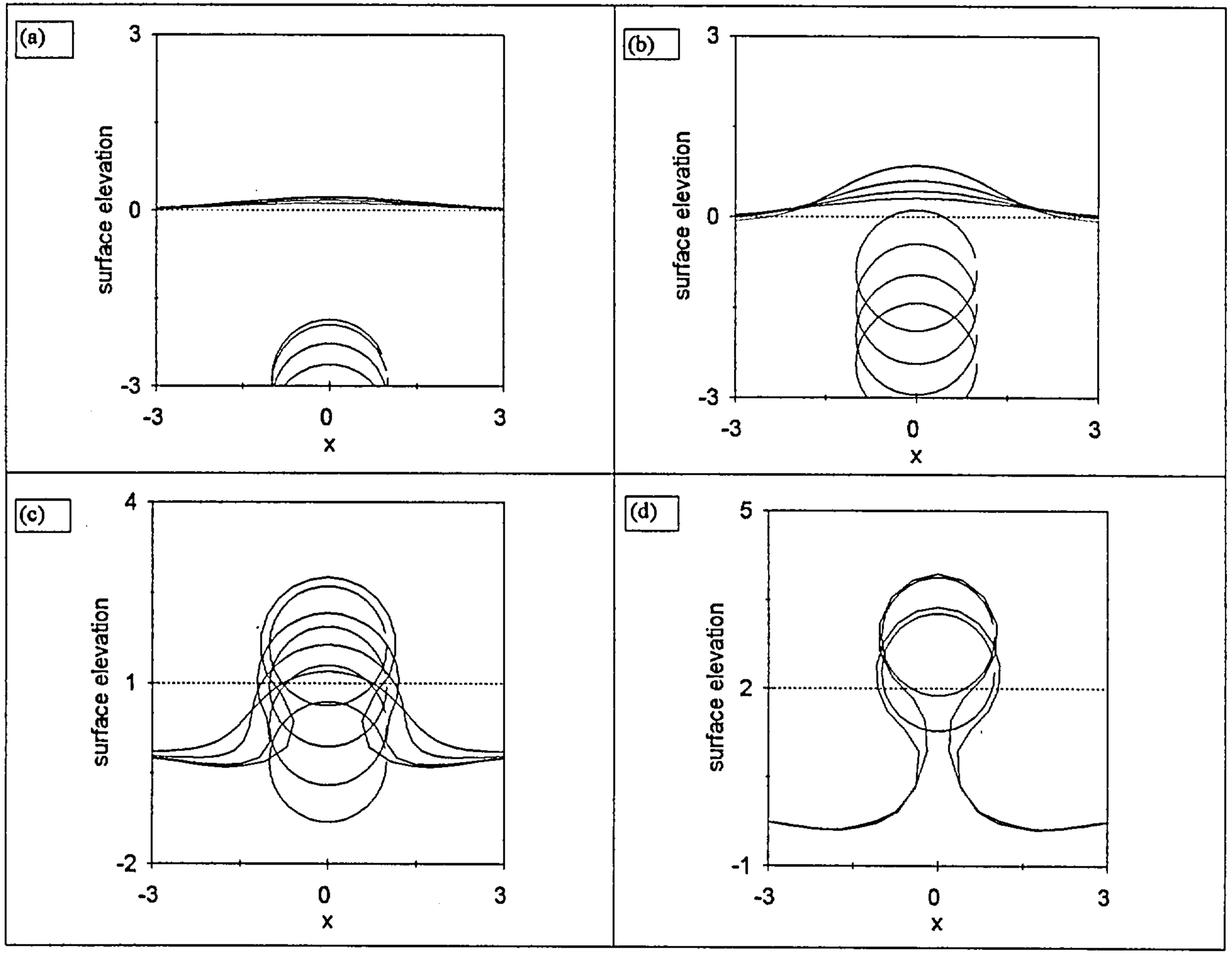

Fig. 2.6(a) Free-surface and cylinder positions due to the fre motion of a cylinder rising to a free surface. Mb=0 and initially the cylinder is located at d=5a below the surface. [a] T=1.681, 1.891, 2.059, 2.101; [b] 2.311, 2.521, 2.731, 2.942; [c] T= 3.152, 3.362, 3.572, 3.782; [d] T=3.992, 4.202, 4.412.

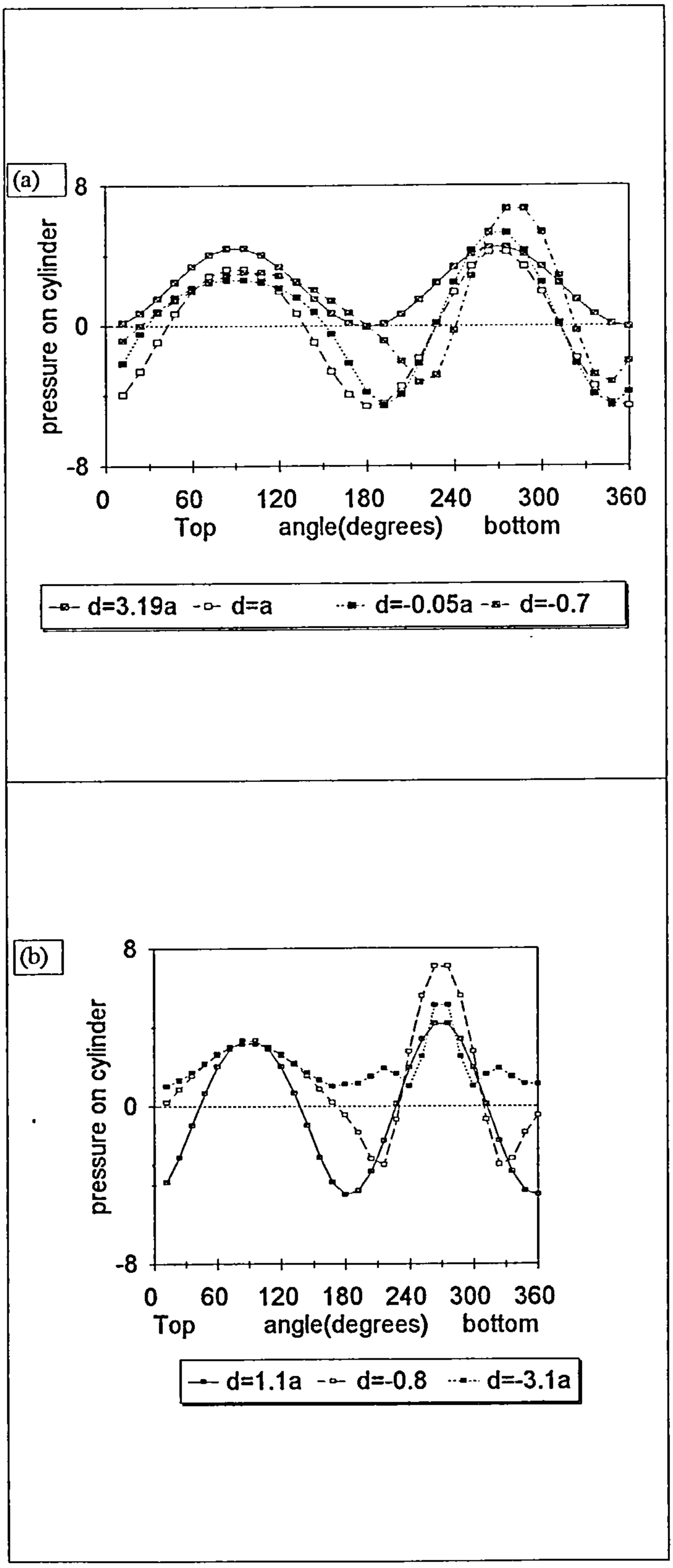

Fig. 2.6(b) total pressure distribution around the cylinder as it moves towards the surface. Negative d indicates that the cylinder is above the mean free surface position.

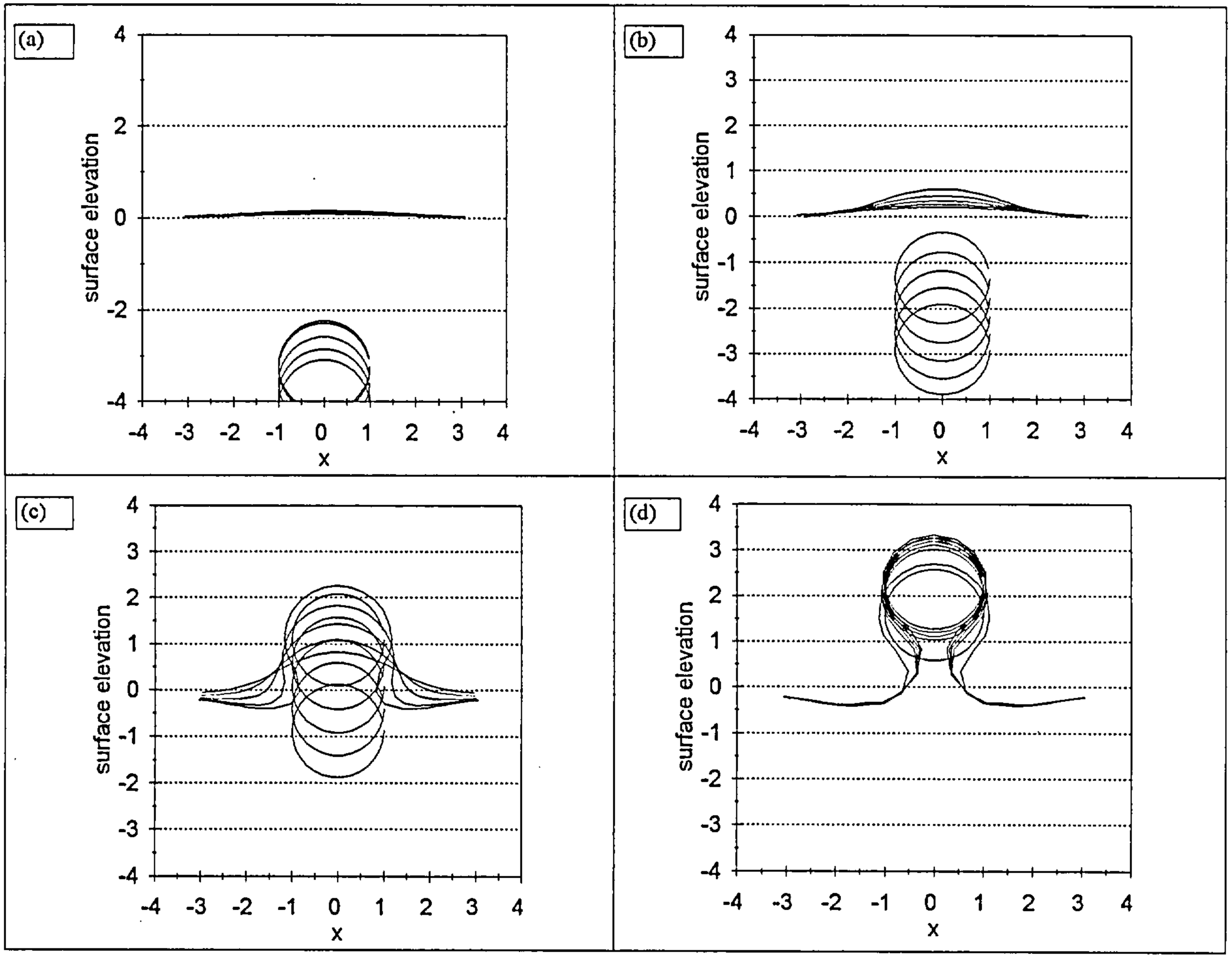

Fi. 2.7 Free-surface and cylinder positions due to the motion of a cylinder rising to a free surface. Mb=0.2 and initially the cylinder is located at d=5a below the surface. [a] T=1.681 , 1.891, 2,.101, 2.311, 2.353; [b] T=2.563, 2.773, 2.984, 3.194, 3.404; [c] T=3.614, 3.824, 4.03 , 4.244, 4.454; [d] T=4.664, 4.875, 4.917, 5.001

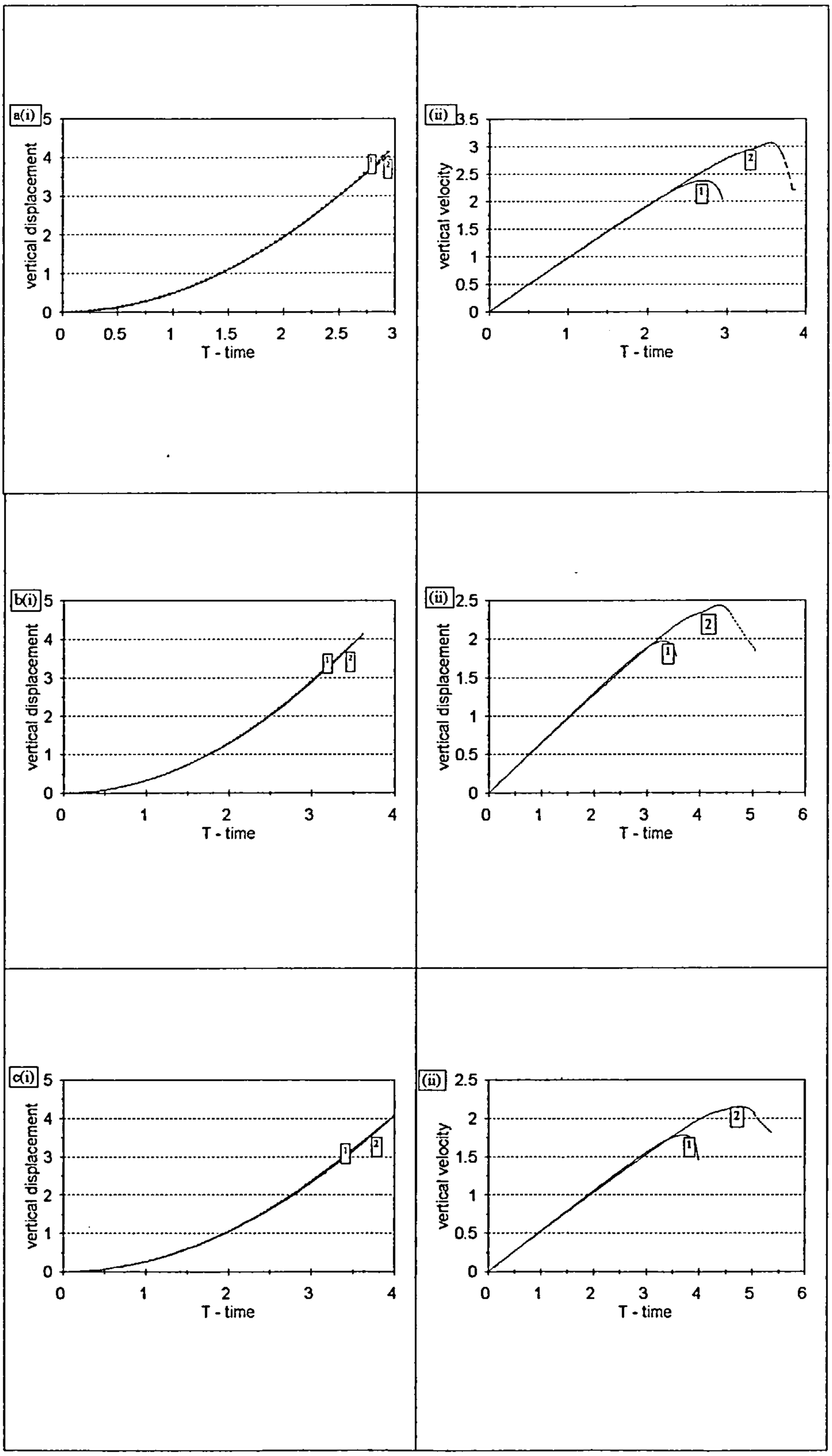

Fig. 2.8 Free motion of a cylinder rising to a free surface, d=5a, [1]- analytic method and [2]- numerical method. a) Mb=0, b) Mb=0.2 and c) Mb=0.3.

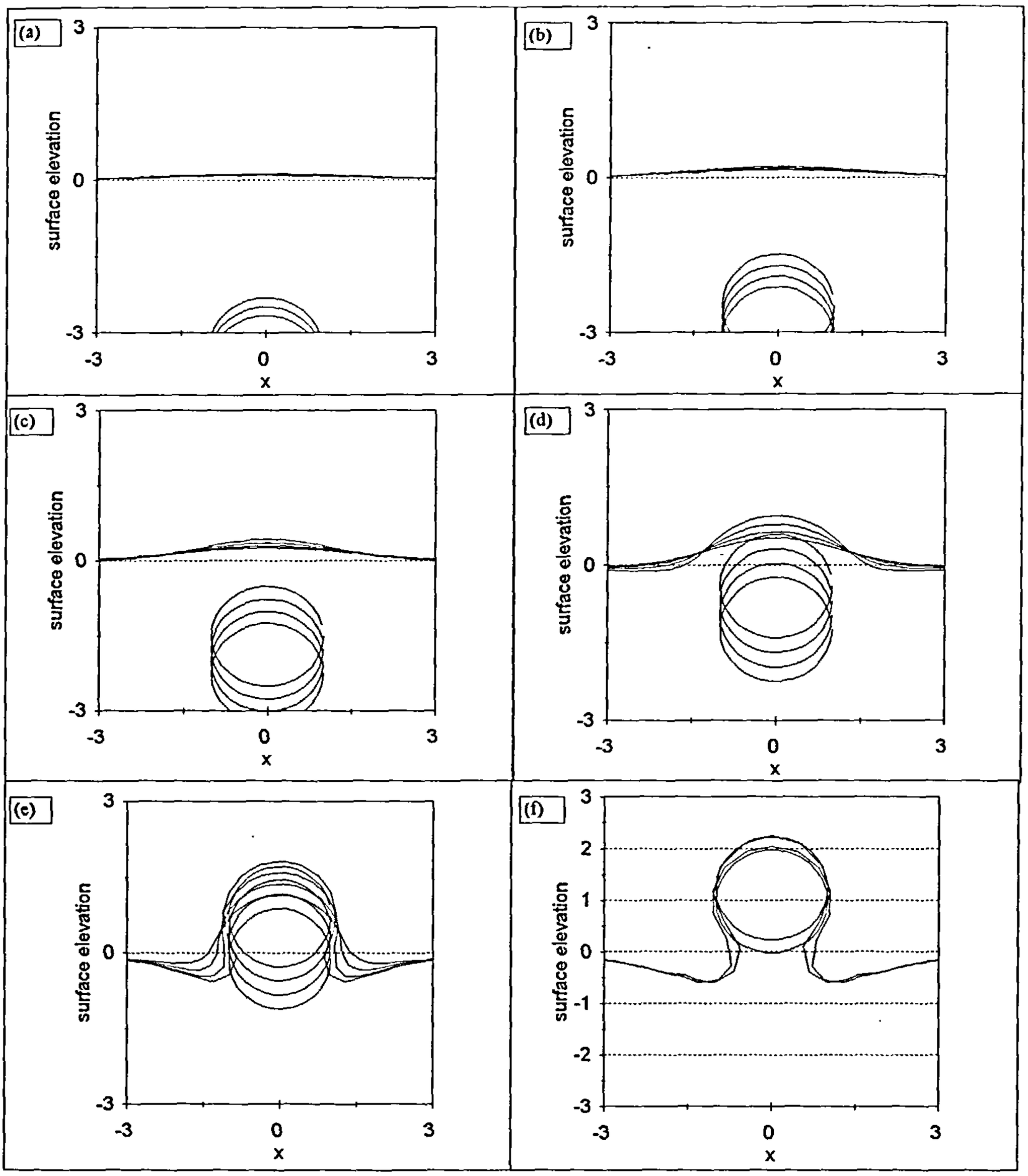

Fig. 2.9 Free-surface and cylinder positions due to the motion of a cylinder rising to a free surface. Mb=0.6 and initially the cylinder is located at d=5a below the surface. [a] T=3.362 , 3.571, 3.782; [b] T=3.992, 4.202, 4.412; [c] T=4.833, 5.043, 5.253, 5.463; [d] T=5.673, 5.883 6.093, 6.303; [e] T=6.513, 6.723, 6.9334, 7.144; [f] T=7.354, 7.564.

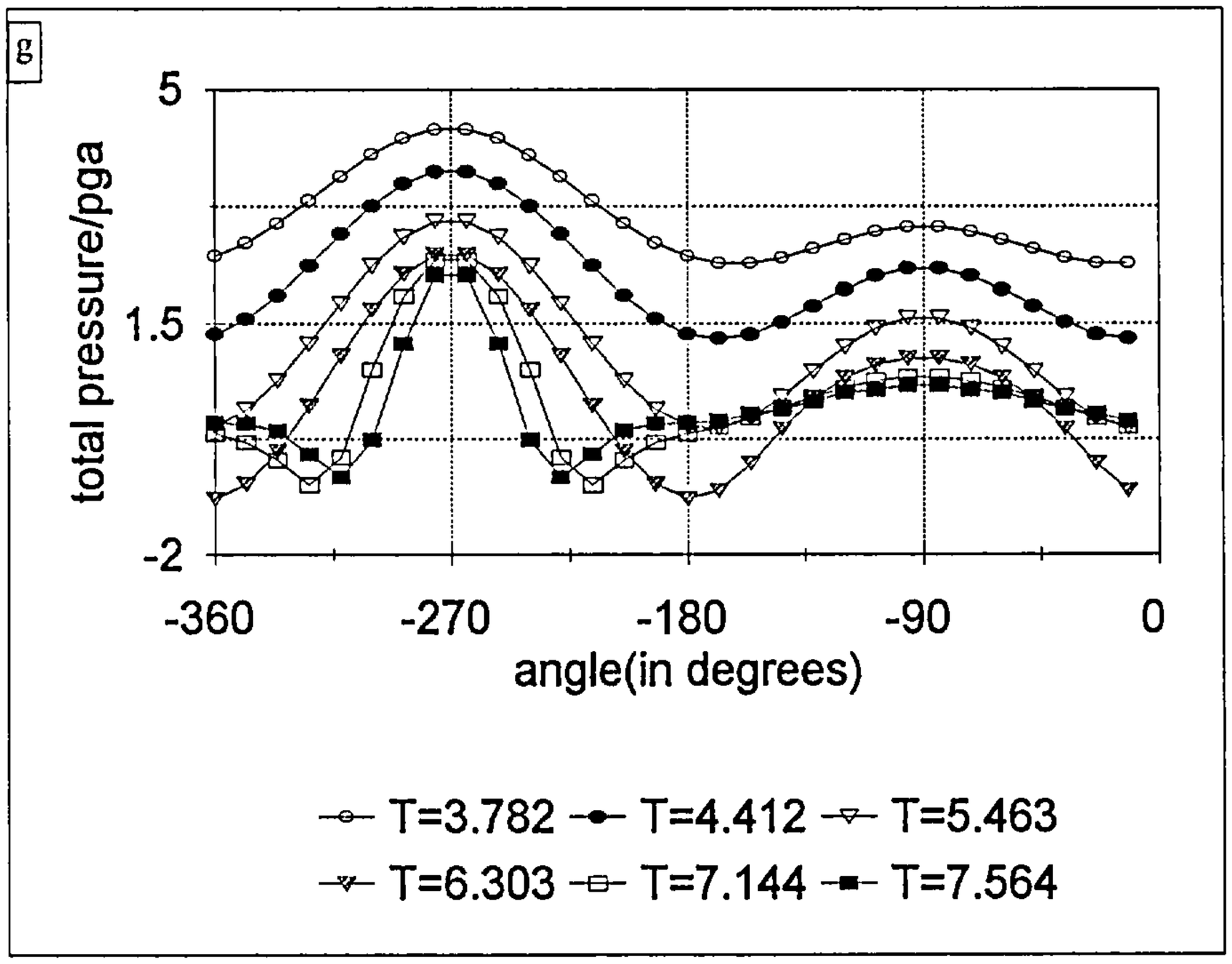
g
5
1.5
-2
total pressure/pga
-360
-270
-180
-90
0
angle(in degrees)
T=3.782
T=4.412
T=5.463
T=6.303
T=7.144
T=7.564

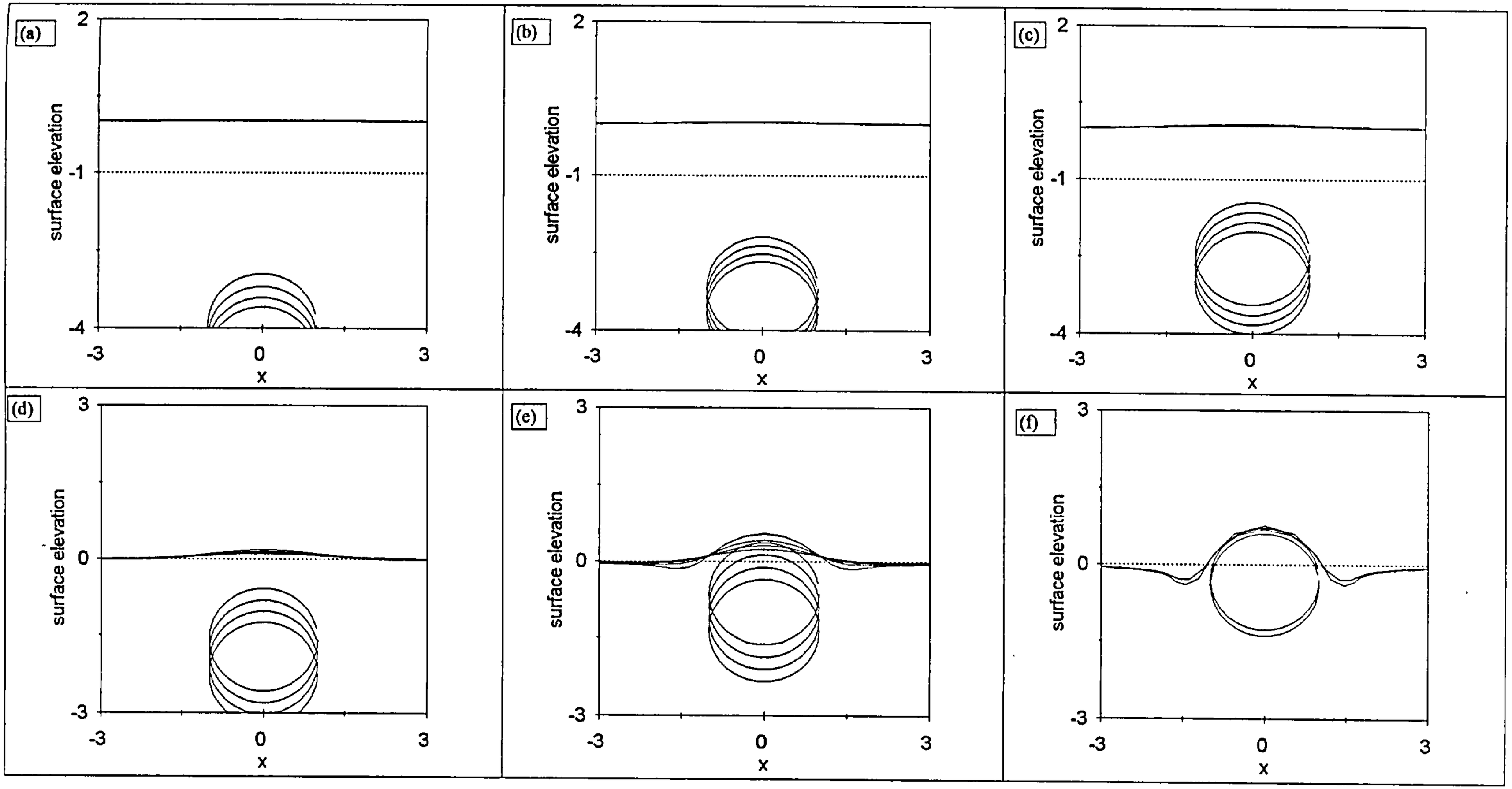

Fig. 2.10 Free-surface and cylinder positions due to the free motion of a cylindet rising to a free surface. Mb=0.9 and initially the cylinder is located at d=5a below the surface [a] T=3.222, 5.043, 5.883, 6.555; [b] T=7.564, 7.984, 8.404, 8.825; [c] T=9.245, 9.665, 10.085, 10.505; [d] T=10.926, 11.346, 11.766, 12.186; [e] T=12.606, 13.027, 13.447, 13.867; [f] T=14.287, 14.497, 14.707.

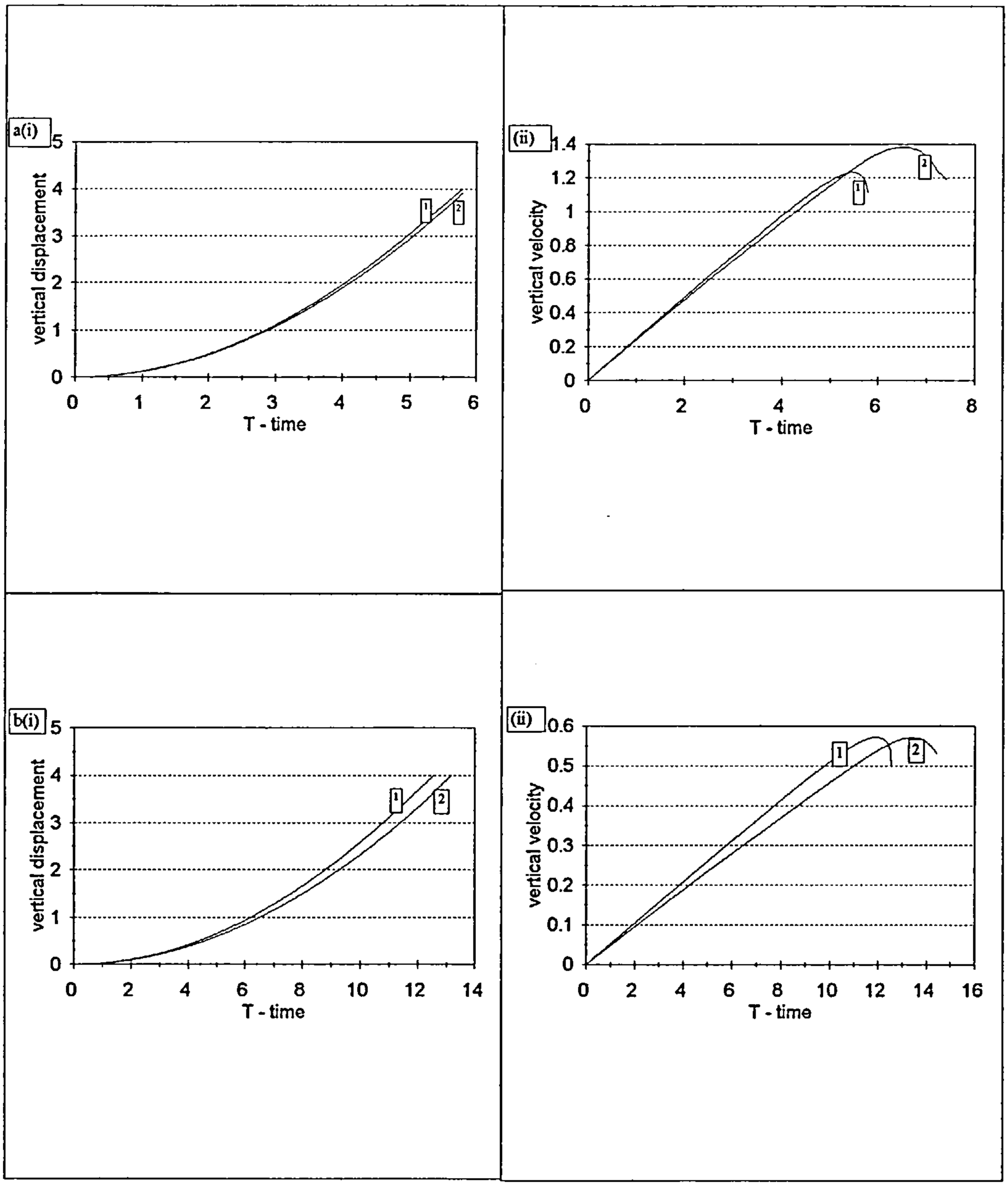

Fig. 2.11 Free motion of a cylinder rising to a free surface, d=5a. a) Mb=0.6, b) Mb=0.9, [1]- analytic method and [2]- numerical method.

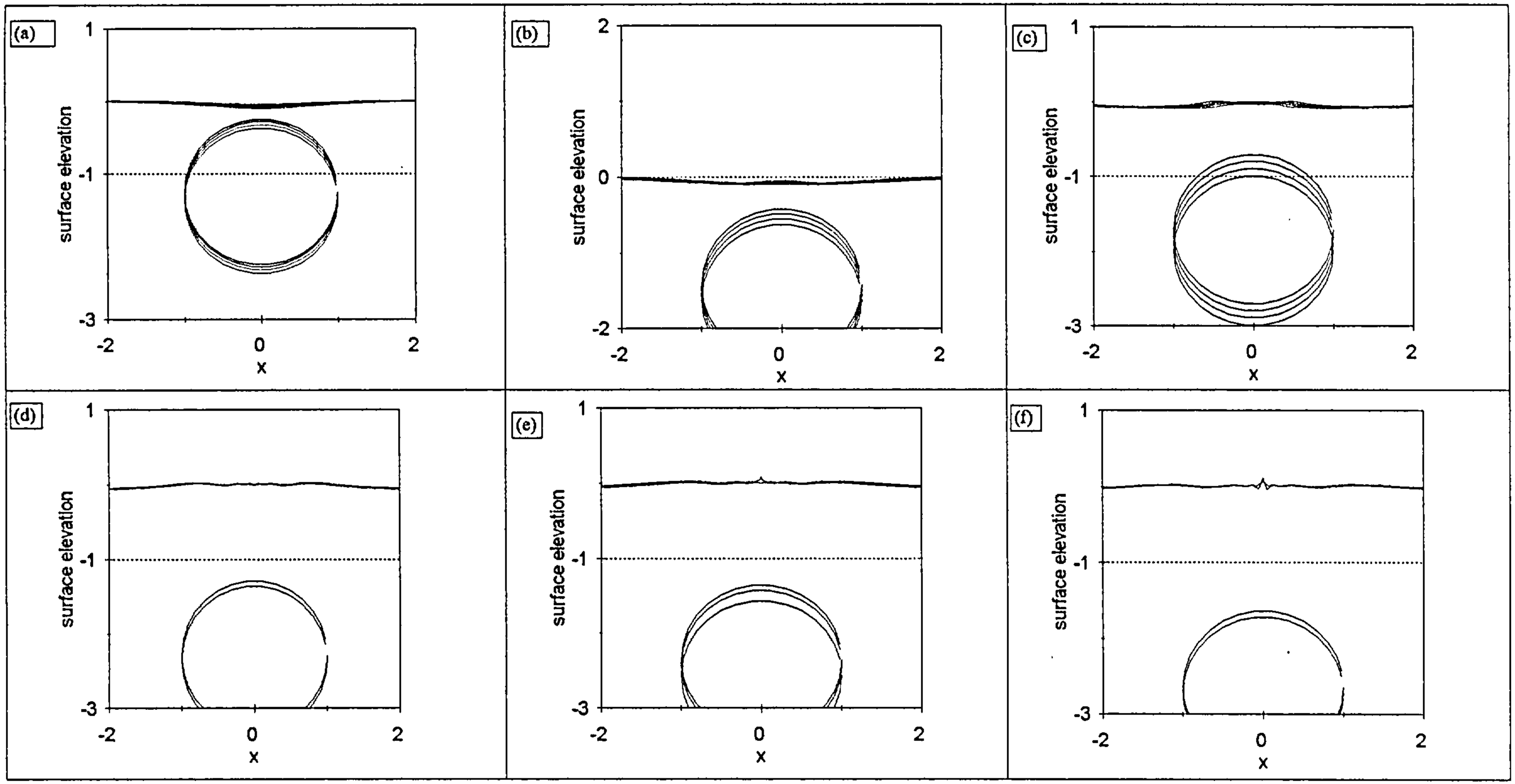

Fig. 2.12 Free-surface and cylinder positions due to the free motion of a cylinder moving away from the free surface. Mb=1.1 and initially the cylinder is located at d=5a below the surface. [a] T=1.261, 1.681, 2.101, 2.521; [b] T=2.942, 3.362, 3.782, 4.2.2; [c] T=4.622, 5.043, 5.463, 5.883; [d] T=6.934, 7.144; [e] T=7.354, 7.774; [f] T=7.984, 8.194.

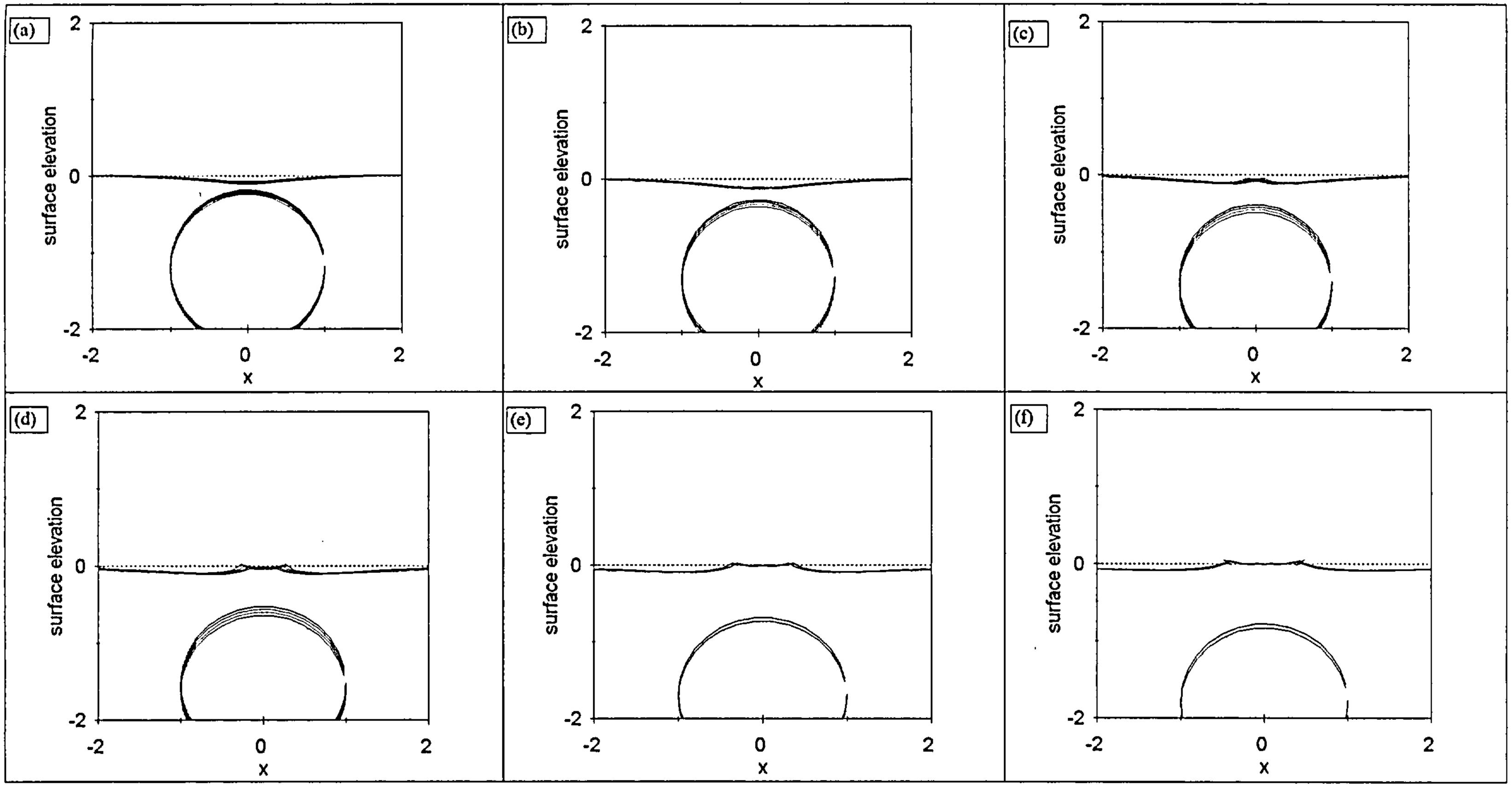

Fig. 2.13 Free-surface and cylinder positions due to the free motion of a cylinder moving away from the surface. Mb=1.1 and initially the cylinder is located at d=1.1a below the surface. [a] T=1.681, 1.891, 2.101, 2.311; [b] T= 2.521, 2.731,2.942, 3.152; [c] T=3.362, 3.489. 3.782, 3.992; [d] T=4.202, 4.412, 4.622, 4.833; [e] T=4.042, 5.253, [f] T= 5.463, 5.673.

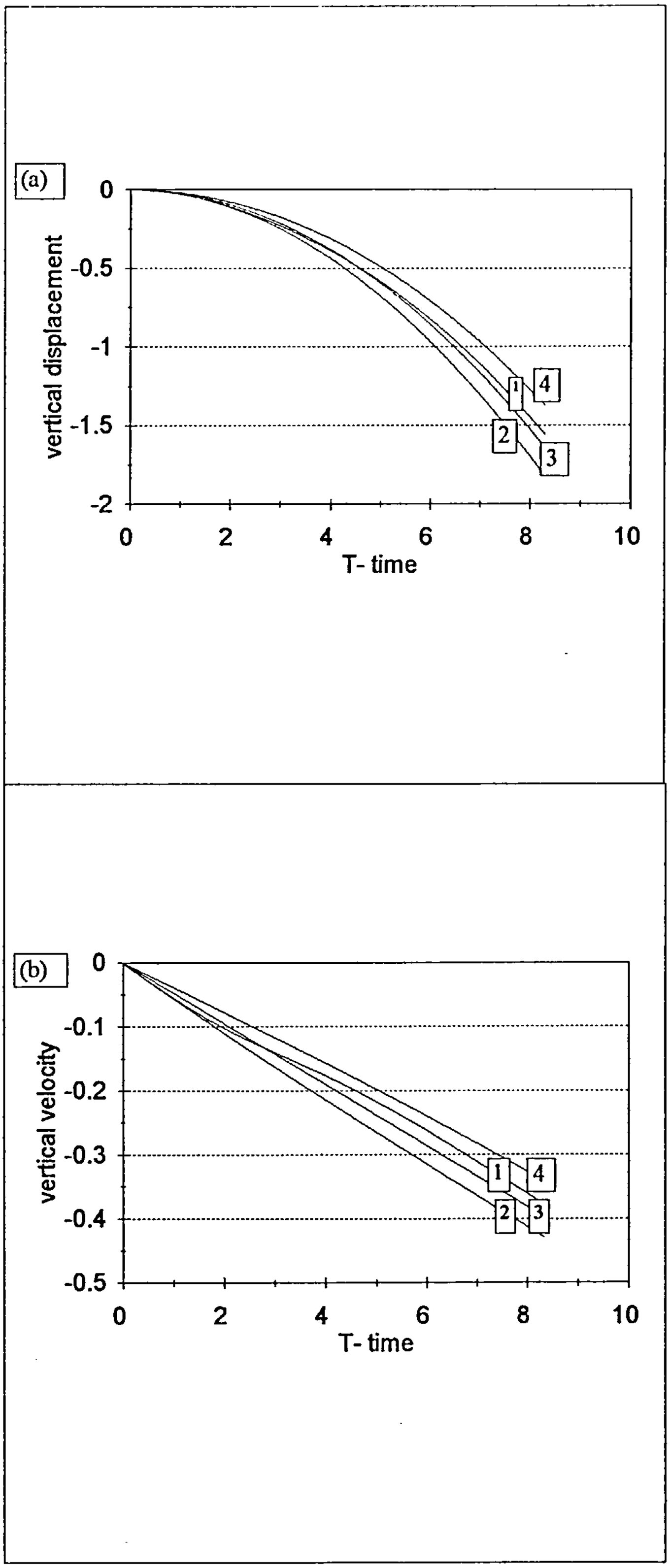

Fig. 2.14 Free motion of a cylinder moving away from the surface d=1.2a and Mb-1.1. [1]- numerical method, [2]- equipotential condition, [3] - constant added mass method and [4] - rigid wall condition.

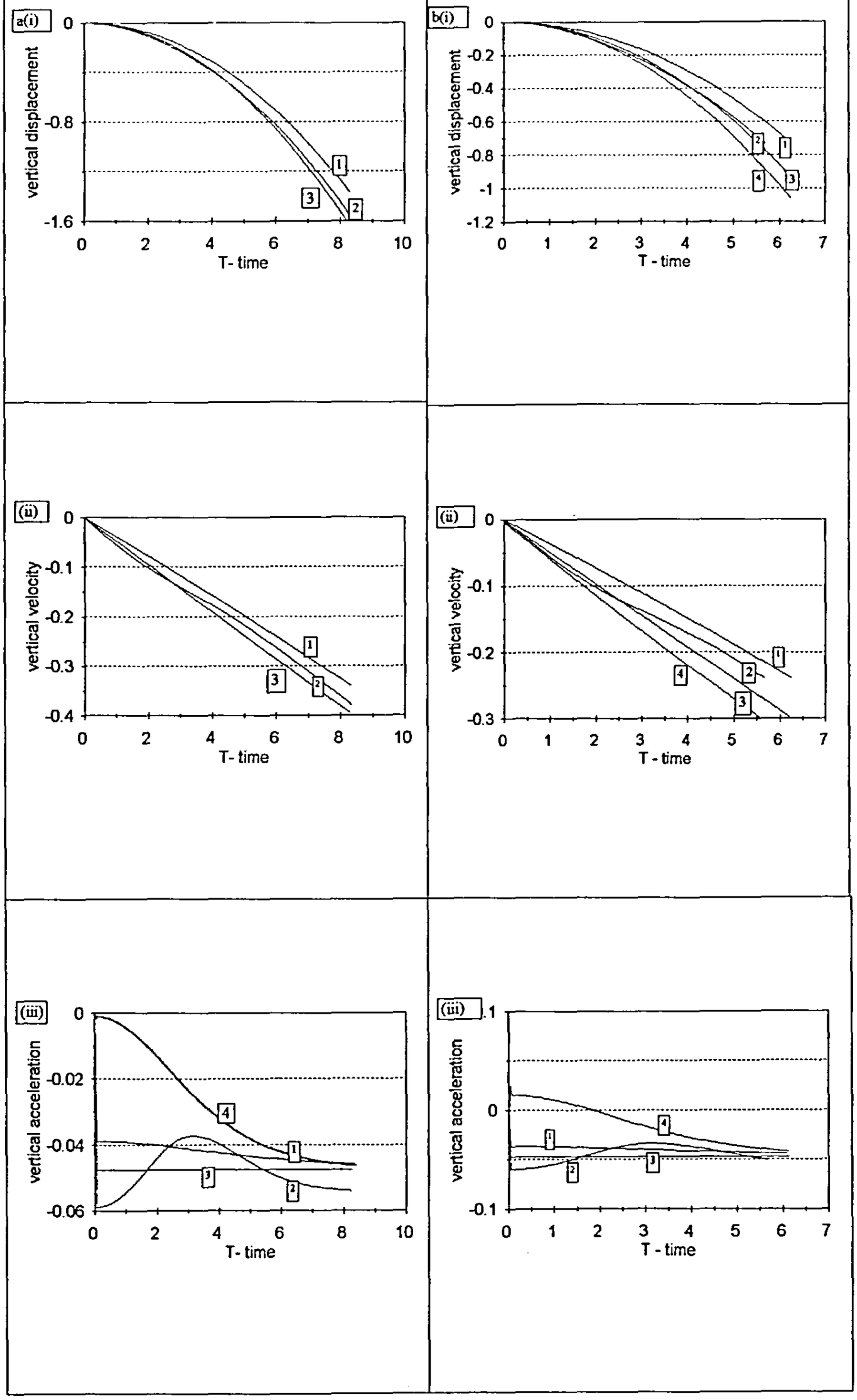

Fig. 2.15 Free motion of a cylinder moving away from the surface and initially located at a) d=1.2a and b) d=1.1a. [1] - rigid wall condition, [2] numerical method, [3] - constant added mass method and [4] - equipotential condition. Mb=1.1 for all cases.

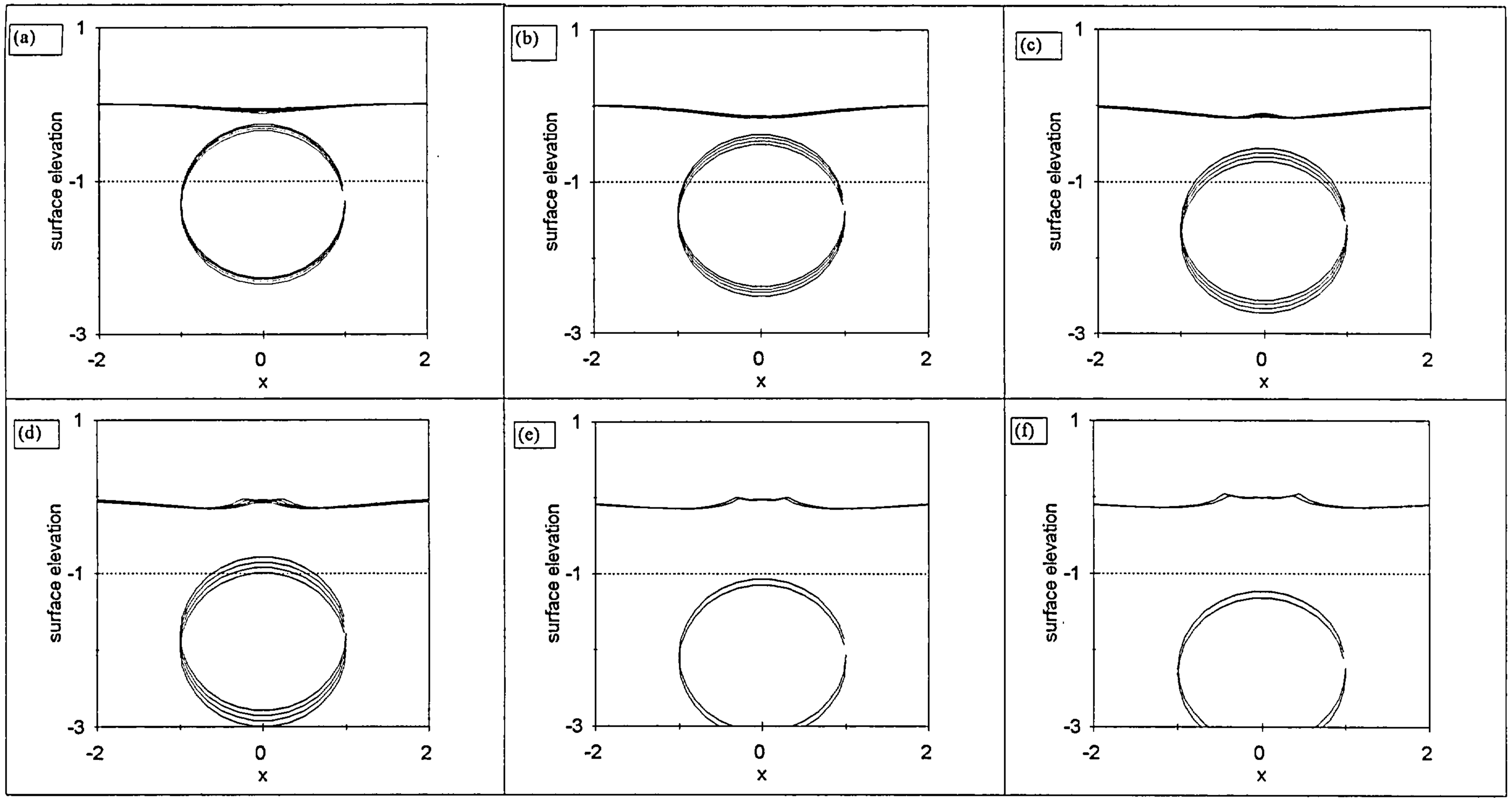

Fig. 2.16 Free-surface and cylinder positions due to the free motion of a cylinder moving away from the surface. Mb=1.2 and initially the cylinder is located at d=1.2a below the surface. [a] T=1.051, 1.261, 1.471, 1.681; [b] T= 1.891, 2.101, 2.311, 2.52; [c[T=2.773, 2.942, 3.152, 3.362; [d] T=3.572, 3.782, 3.992, 4.202; [e] T=4.412; [f] T=4.6 22, 4.833, 5.043.

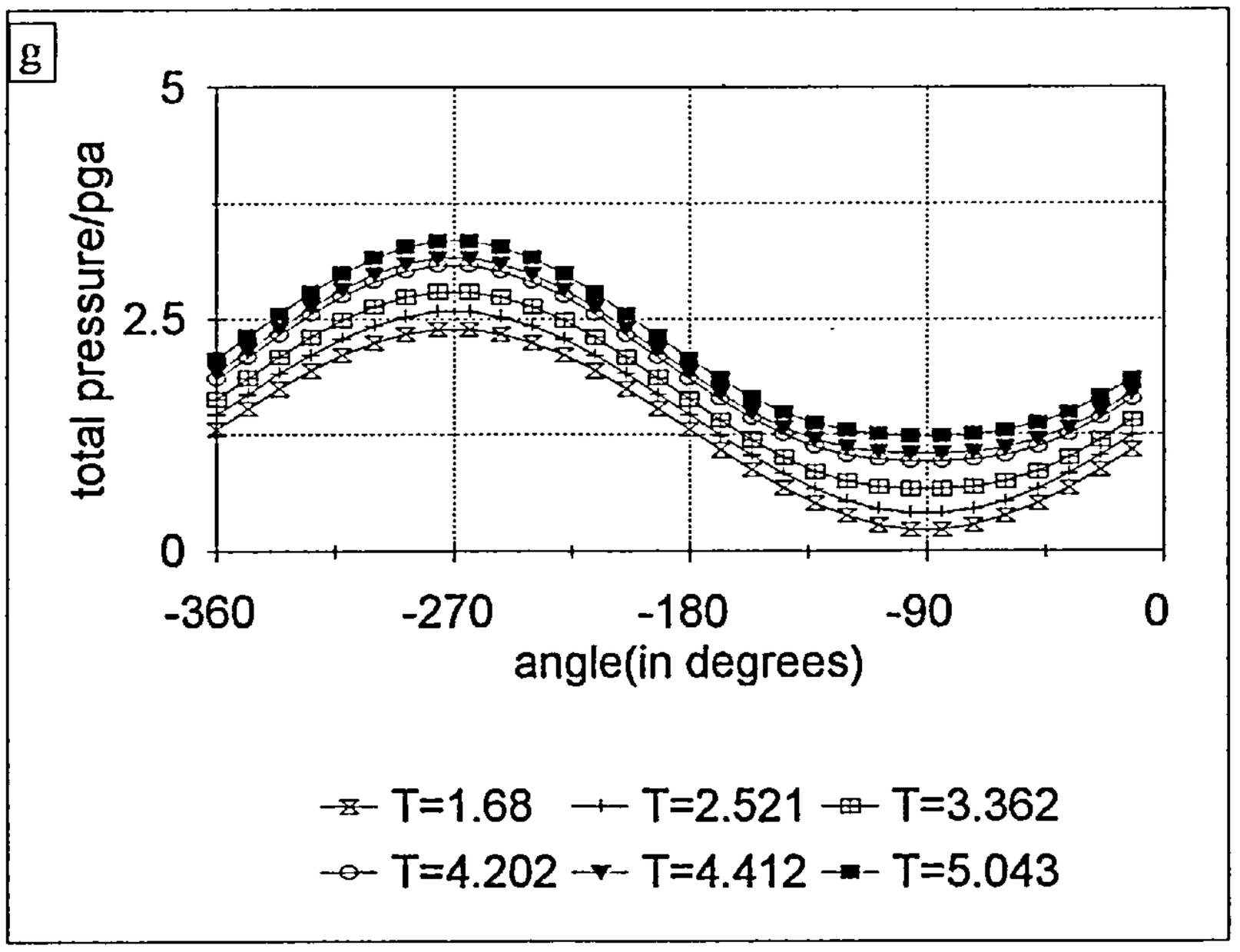
g
5
2.5
0
total pressure/pga
-360
-270
-180
-90
0
angle(in degrees)
T=1.68
T=2.521
T=3.362
T=4.202
T=4.412
T=5.043

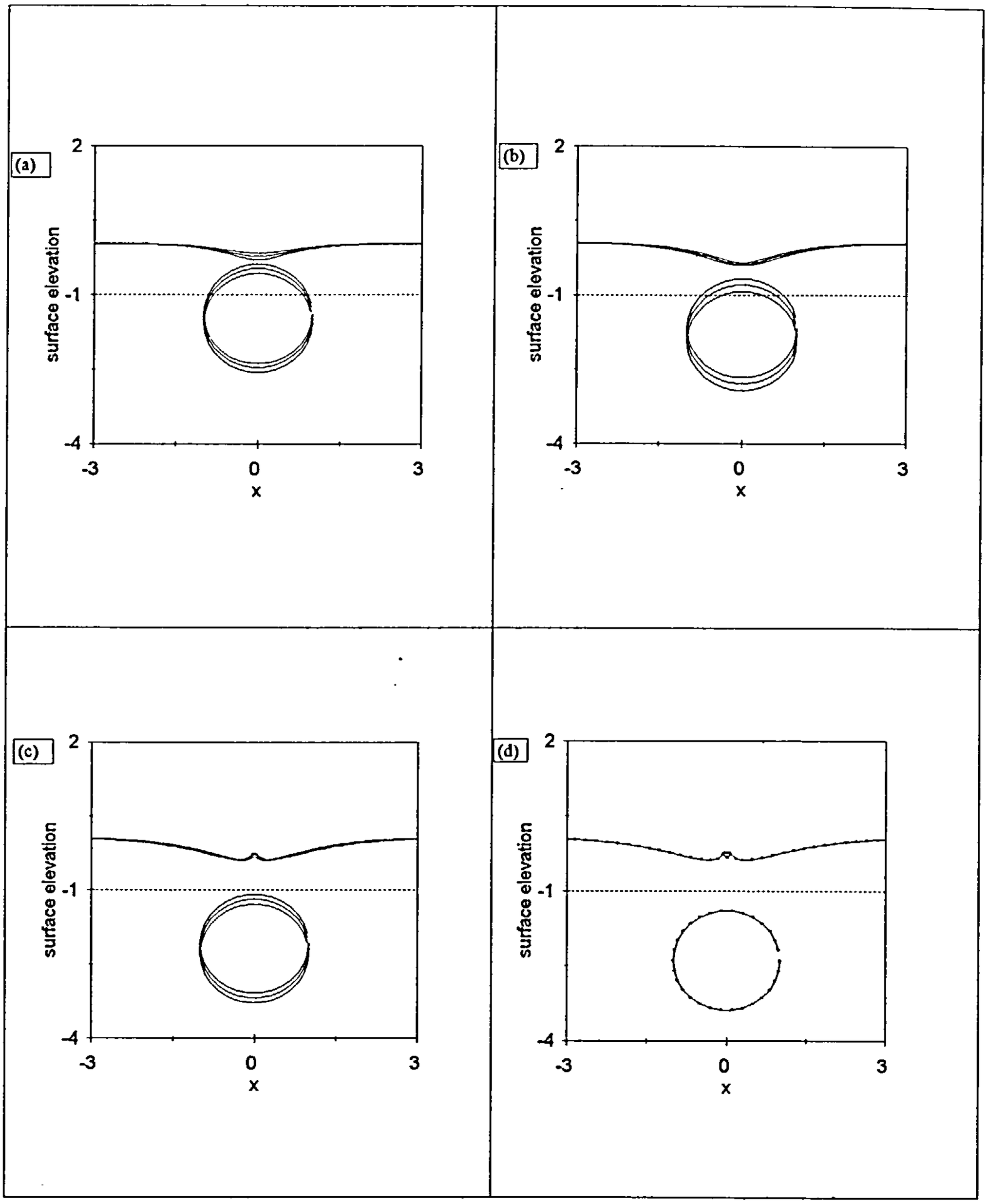

Fig. 2.17 Free-surface and cylinder positions due to the free motion of a cylinder moving away from the surface. Mb=2 and initially the cylinder is located at d=1.2a below the surface. [a] T=1.001, 1.219, 1.429; [b] T = 1.639, 1.849, 2.059; [c] T=2.269, 2.395, 2.521; [d] T=2.647.

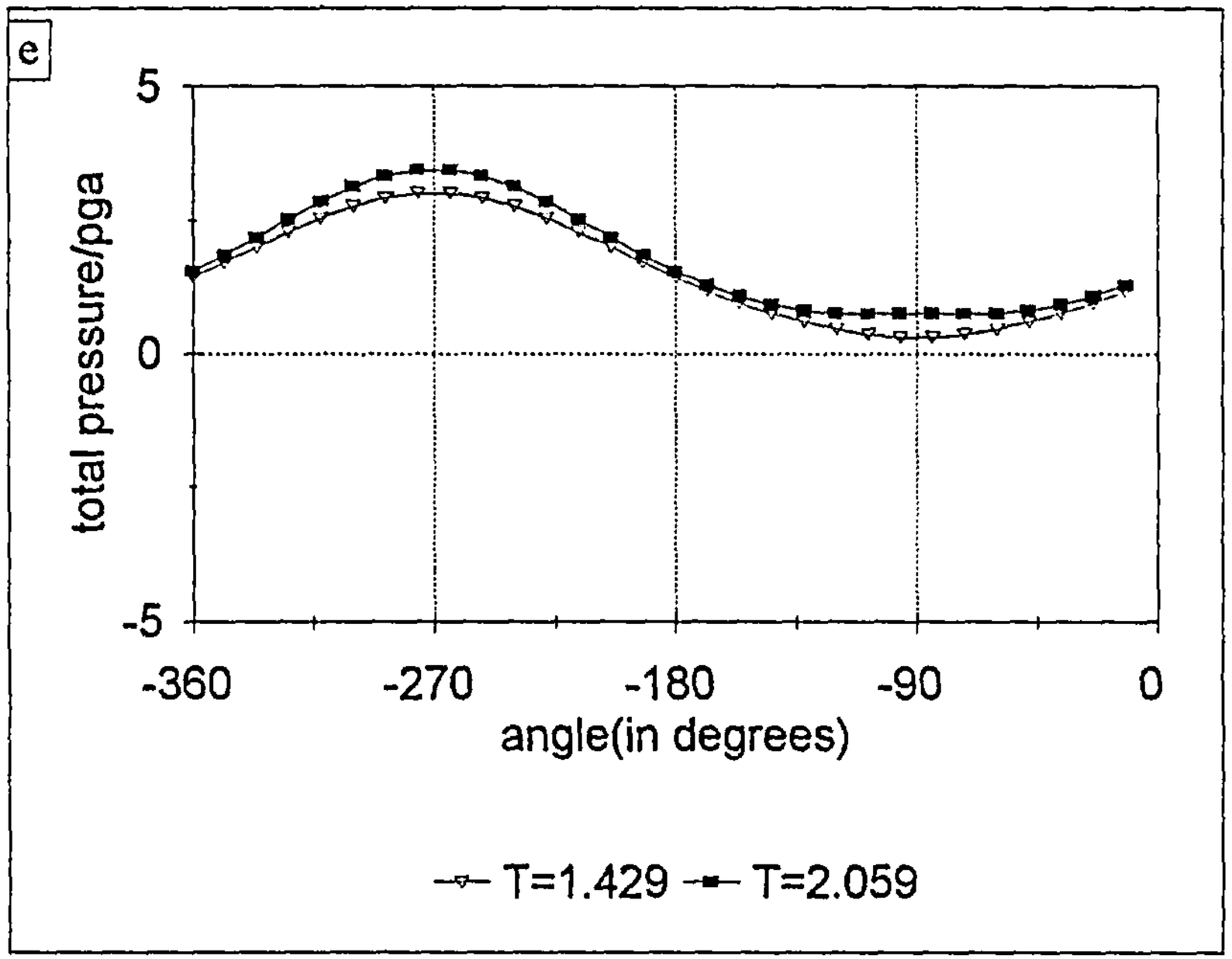
e
5
0
-5
total pressure/pga
-360
-270
-180
-90
0
angle(in degrees)
T=1.429
T=2.059

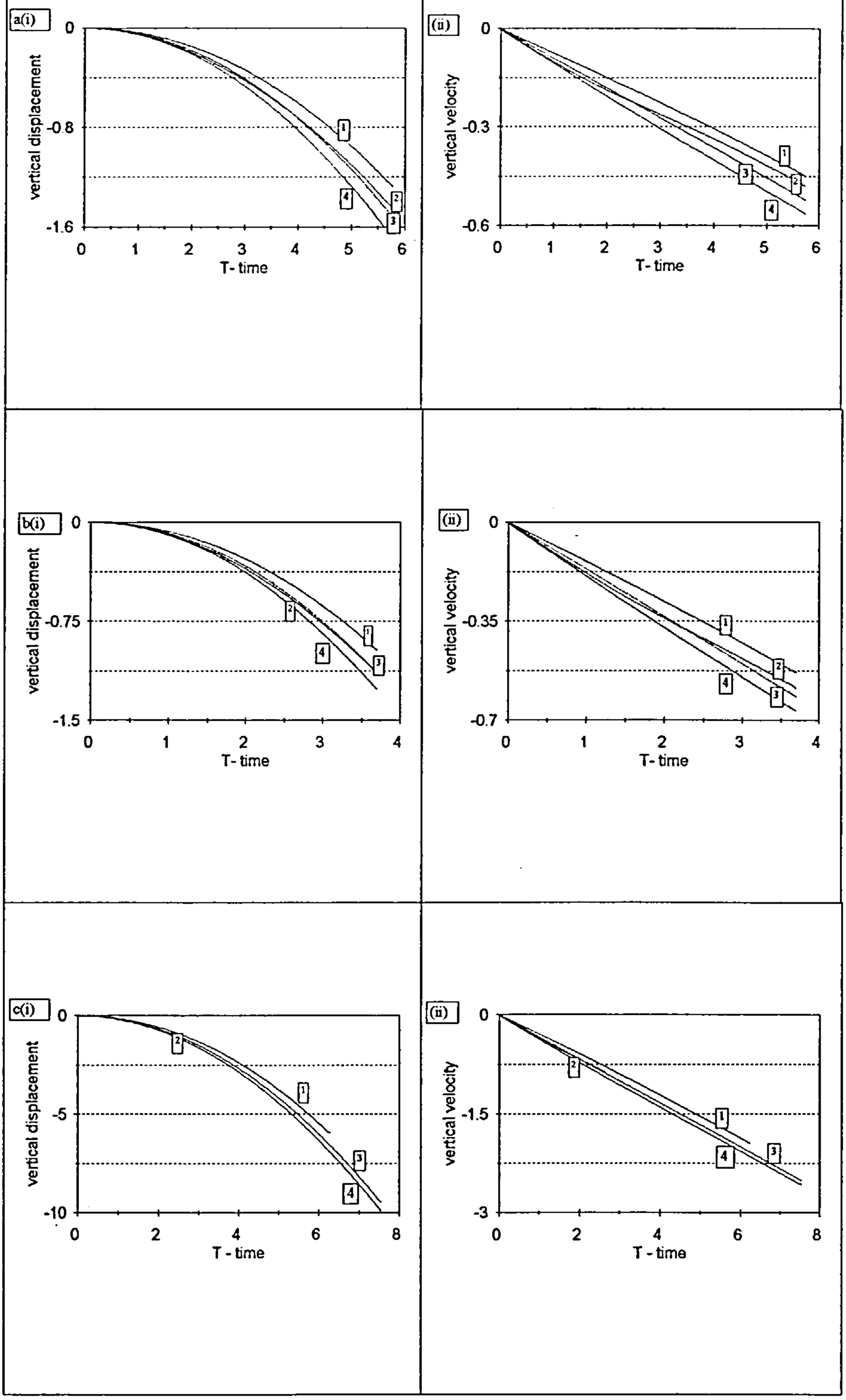

Fig. 2.18 Free motion of a cylinder moving away from the surface and initially located at d=1.2a, where a) Mb=1.2, b)Mb=1.4 and c) Mb=2. [1] - rigid wall condition, [2] - numerical method, [3] - constant added mass method and [4] - equipotential condition.

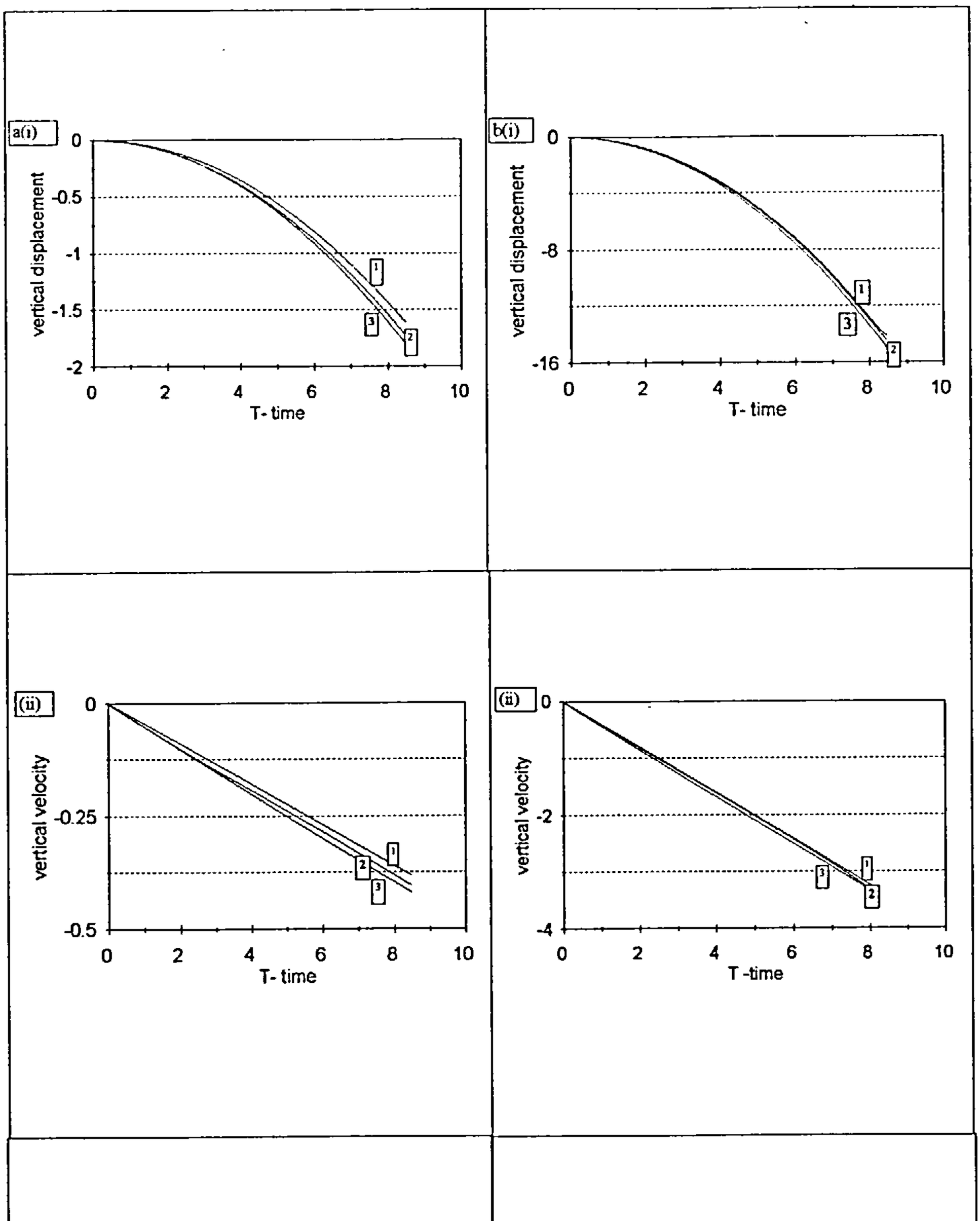

Fig. 2.19 Free motion of a cylinder moving away from the surface and initially located at d=2a. [1] - rigid wall condition, [2] - numerical method and [3] - equipotential method. a) Mb=1.1 and b) Mb=2.4.

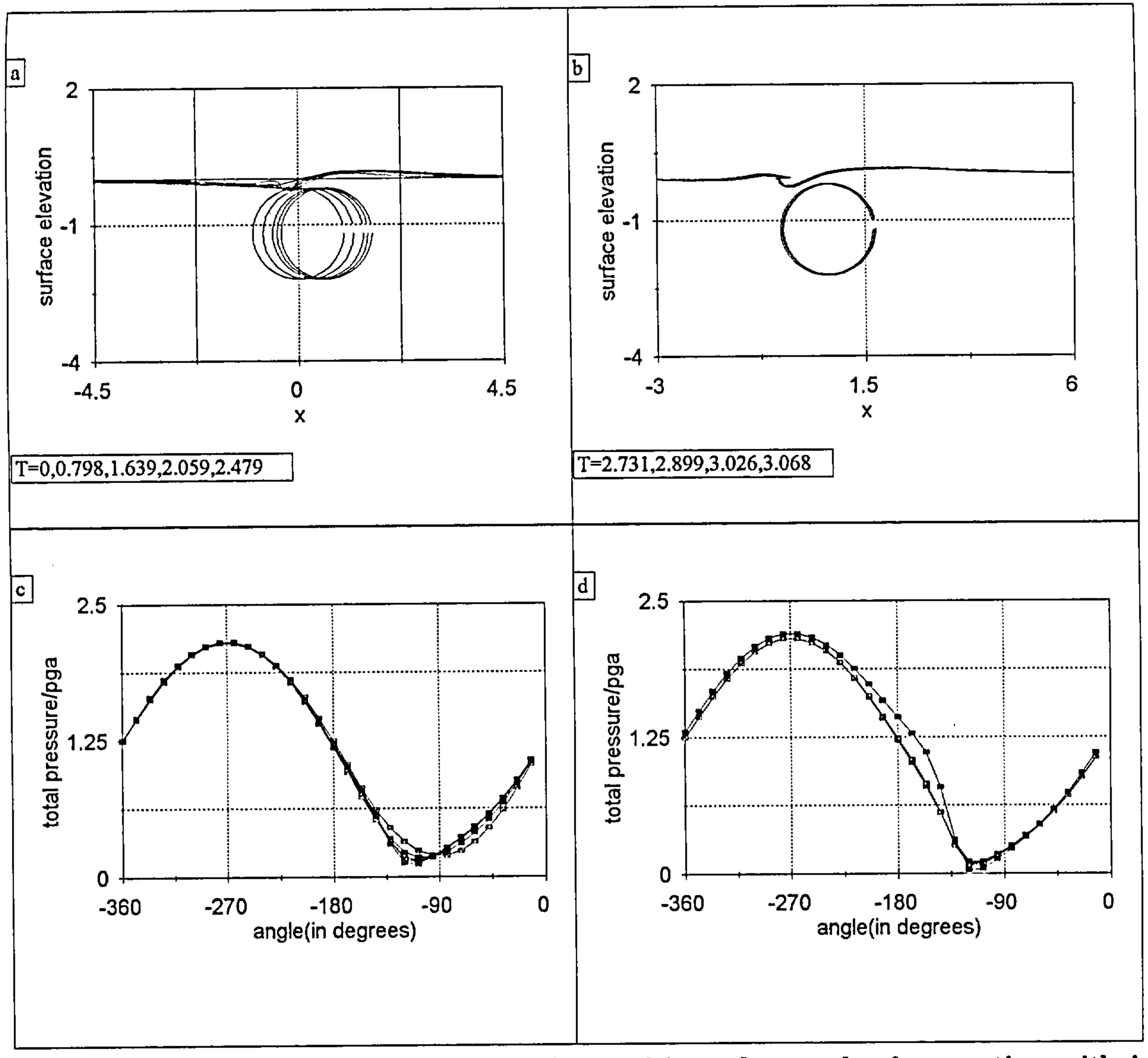

Fig. 2.20 (a)-(b) free-surface and cylinder positions due to the free motion with initial velocity in the horizontal direction, (c)-(d) are respectively corresponding pressure distributions to positions of (a)- (b), (e)- (f) represent displacement/time and velocity/time and (g)-(h) vertical/horizontal displacement and forces respectively.

e(i)

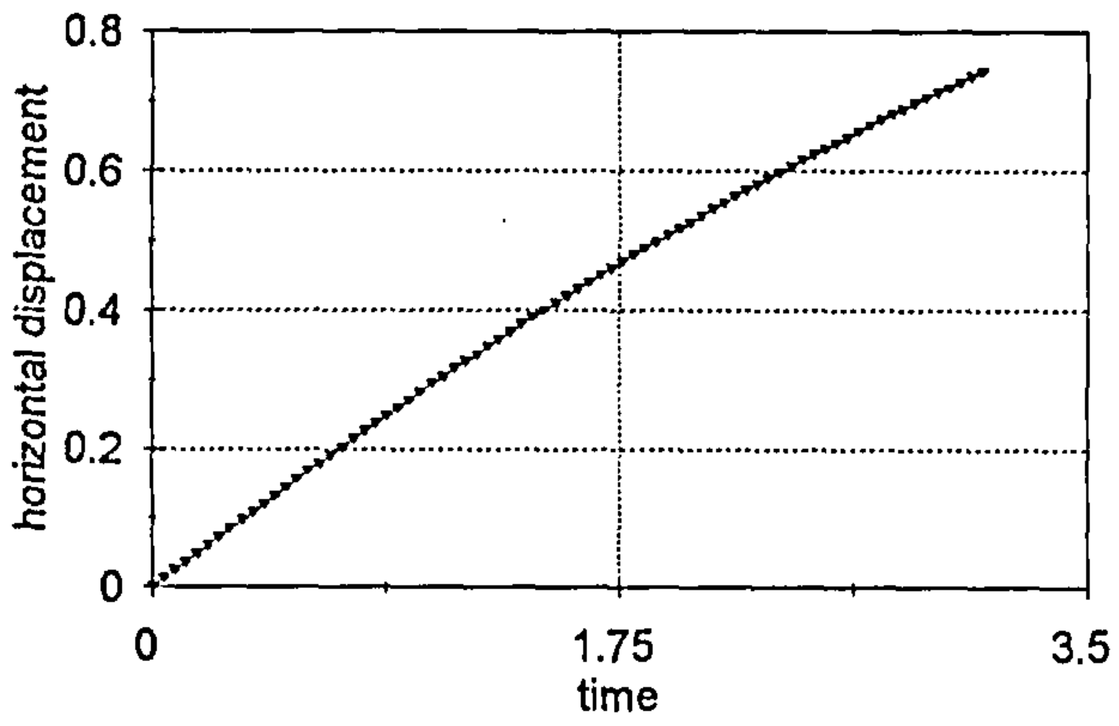
0.8
0.6
0.4
0.2
0
horizontal displacement
0
1.75
3.5
time

e(ii)

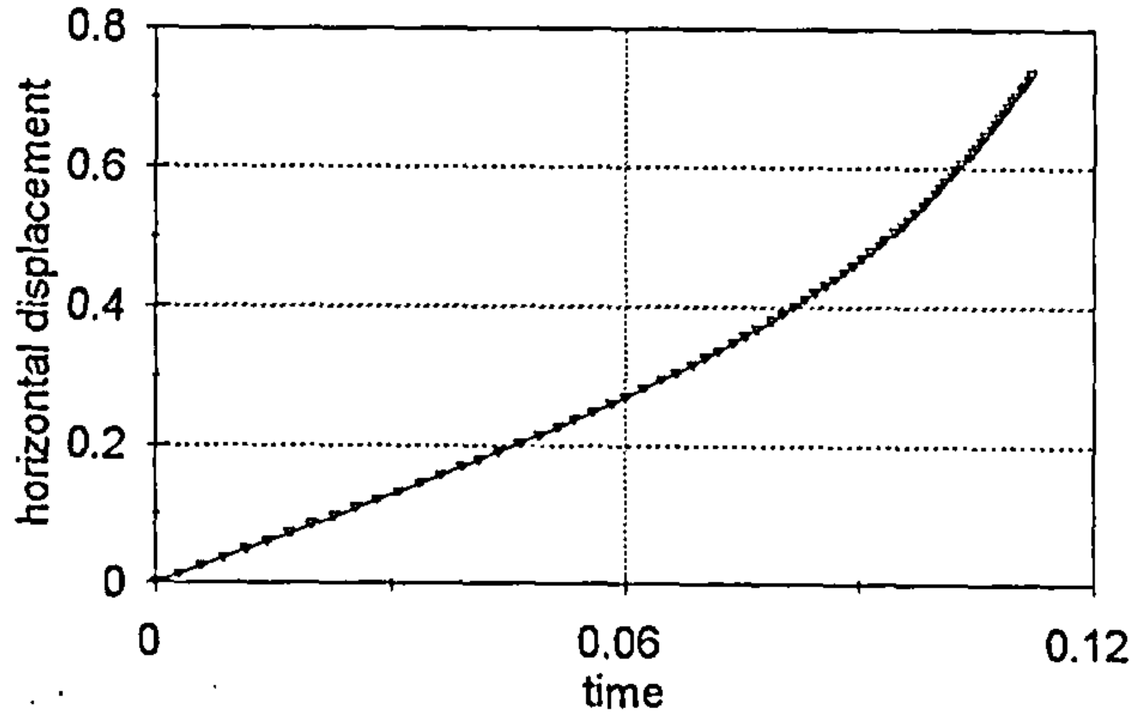
0.8
0.6
0.4
0.2
0
horizontal displacement
0
0.06
0.12
time

f(i)

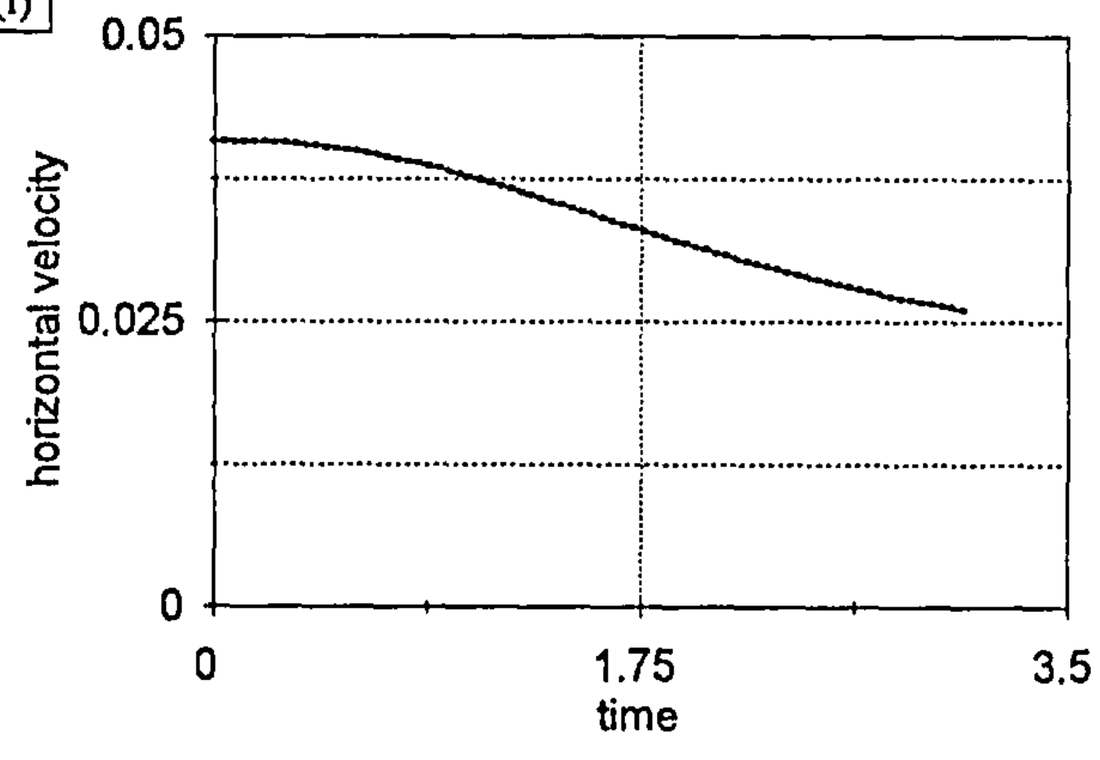
0.05
0.025
0
horizontal velocity
0
1.75
3.5
time

f(ii)

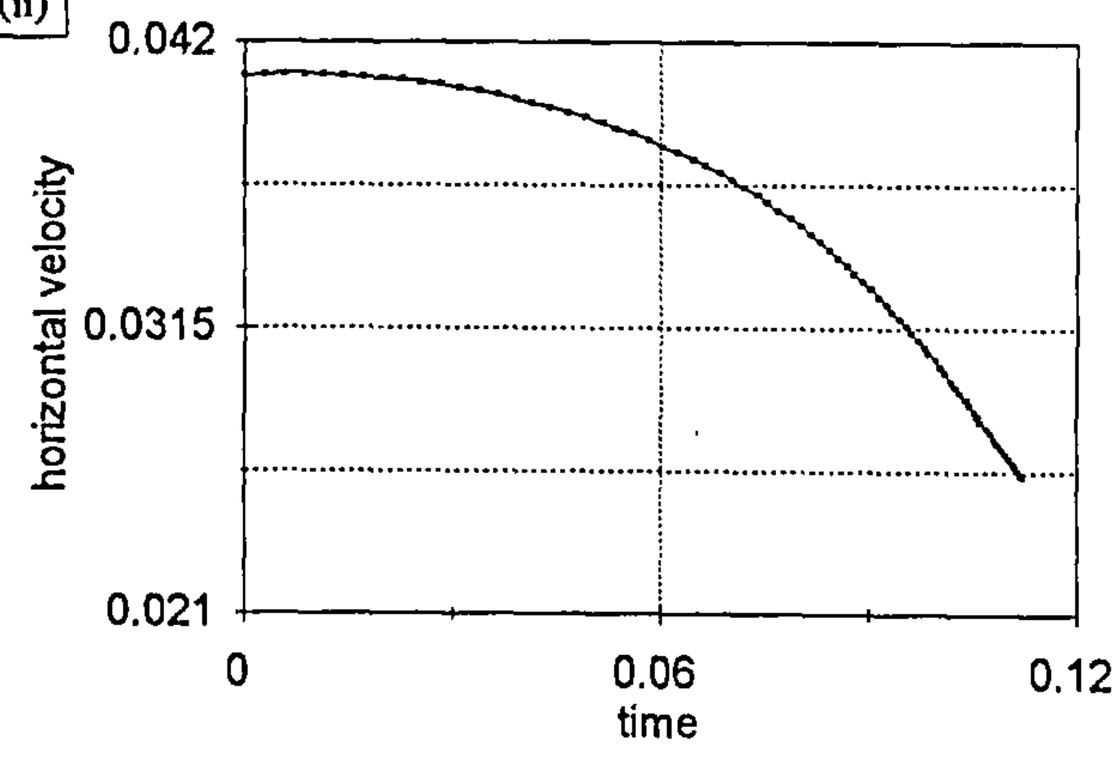
0.042
0.0315
0.021
horizontal velocity
0
0.06
0.12
time

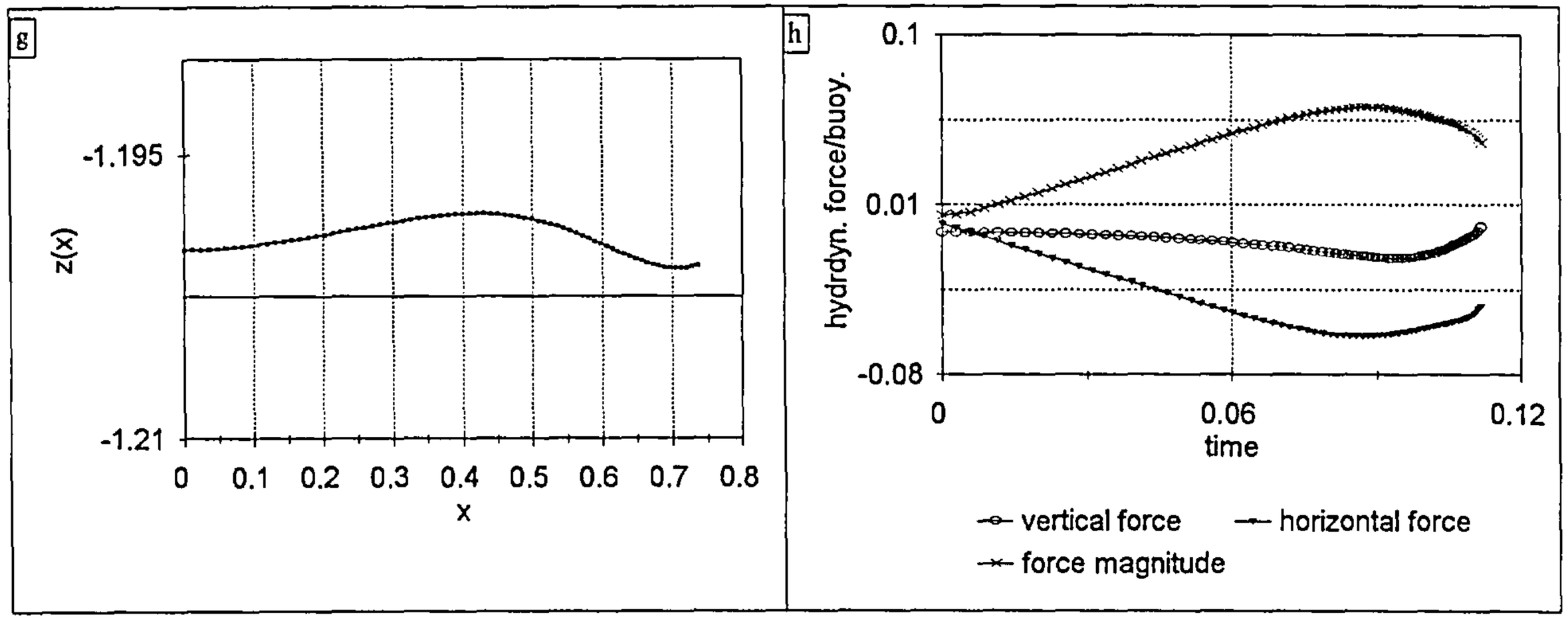
g
-1.195
-1.21
z(x)
0
0.1
0.2
0.3
0.4
0.5
0.6
0.7
0.8
x
h
0.1
0.01
-0.08
hydrdyn. force/buoy.
0
0.06
0.12
time
vertical force
horizontal force
force magnitude

Chapter 3

Constrained motion of a cylinder

3.1 Introduction

This chapter studies the constrained, but large, motions of a submerged cylinder, subject to external linear springs. Such a situation could arise for example on the pontoon of a semi-submersible oil rig, the springs being given by rig buoyancy and mooring, on a wave energy device, the springs being given by the power take-off machinery, or on a floating pipe-bridge, the springs being given by the bridge stiffness and moorings. We therefore consider a spring-loaded totally submerged horizontal circular cylinder near a free-surface which is given an initial displacement $\mathbf{r}=x\mathbf{i}+y\mathbf{j}$ from its equilibrium position and is allowed to oscillate at various fundamental frequencies depending on the spring coefficients. Constrained motion of the submerged cylinder under a fully non-linear free surface is explored by simple oscillation numerical experiments with the cylinder mounted on equal vertically- and horizontally-acting springs of modulus k. We choose initial displacement of one radius either downward, or upward, or to the side, or downward and to the side, or upward and to the side from the equilibrium position with the body remaining fully submerged. The

motion of the cylinder described with these five initial positions is considered to be fairly general, especially since they have a vertical (but not horizontal) axis of symmetry.

To make progress analytically we assume the free-surface deflections are generally small and slow enough for us to regard the free surface as a fixed line on which the low-frequency boundary condition is applicable (i.e $\frac{\partial \phi}{\partial z}=0$) and use of the added mass formula (2.10) is therefore possible. Furthermore the wave damping coefficients due to radiation are prescribed from a low-frequency asymptotic form and included in the equations of motion in the horizontal and vertical directions. The equations of motion are derived from Lagrange's equations (2.5) with the depth-depended added mass coefficient appearing in the equations. In addition, wave damping is calculated approximately from these added mass coefficients as shown in section 3.1, and then incorporated into the equations of motion. In all the results presented, the coefficients and equations used have been non-dimensionalised. For time-stepping the equations of motion, a fourth-order Runge-Kutta method with local truncation error of $O(h^4)$ was found to be suitable in approximating the difference equations of section 2.2.

In this investigation of the general motion of the submerged cylinder, a comparison of the results of the modelled nonlinear problem with those of the fully nonlinear numerical scheme of Brevig, Greenhow and Vinje (1980) is carried out. In this way, a check on the validity of the assumptions underlying the analytical model may be made.

3.2 Damping coefficient

We here follow the derivation of Greenhow and Ahn (1988), see also McIver (1994). Since low-frequency form of damping is assumed for slow oscillatory motions which are predominantly sinusoidal we shall therefore use the relative motion hypothesis which is given in Newman's (1977) notation as

$$X_1 \approx \omega B_{11} + i\omega^2(A_{11} + \rho V) \quad \text{as} \quad \omega \to 0 \qquad (1)$$

in sway and

$$X_2 \approx \rho g S + i\omega B_{22} - \omega^2(A_{22} + \rho V) \quad \text{as} \quad \omega \to 0 \qquad (2)$$

in heave correct to $O(\omega^2)$ or $O(Ka)$ since $K = \frac{\omega^2}{g}$ for deep water. In the above equations S is the waterplane area, X_1 and X_2 are sway and heave forces, A_{ii} and B_{ii} are added mass and damping coefficients and V is the displaced volume of the fluid.

An asymptotically correct low-frequency damping is obtained by considering leading order terms of equations (3.1) and (3.2) in combination with Haskind relations, see Newman (1977). The Haskind relations, in two dimensions, are expressed in the form

$$B_{ii} = \frac{\omega |\, X_i \,|^2}{\rho g^2} \qquad (3)$$

It is worth noting that this relation is valid for all frequencies of oscillation. For the circular cylinder the dimensionless added mass and damping coefficients are identical in both heave and sway at all frequencies, as proved by Ogilvie (1963) and Evans et al (1979). Since also S=0, the case of a submerged cylinder, then

$$X_1 = X_2 \approx i\omega^2(M_a(0) + \frac{V}{\forall})\rho\forall \qquad (4)$$

where $\forall = \pi a^2$ and $M_a(0)$ is dimensionless added mass at equilibrium.

Substituting (3.4) into (3.3) gives

$$B_{11} = B_{22} = \frac{\omega |\, i\omega^2 (M_a(0) + \frac{V}{\forall})\rho \forall \,|^2}{\rho g^2} \qquad (5)$$

as the dimensional damping coefficient of the low-frequency motion. In our case the cylinder is always totally submerged so that $V = \forall = \pi a^2$. This damping factor is then incorporated into the equations of motion, which are in turn nondimensionalised.

3.3 Coupled motion of a cylinder

Here we change some general definitions and adopt notations with subscripts for better presentation of the equations. x_1 and x_2 become respectively the horizontal and vertical displacements below the surface. When the mass is displaced a distance x_1 horizontally and x_2 vertically, the extension of the spring produced in either direction is proportional to the tension in the spring. If l is the natural length of the spring and x_1 or x_2 is its extension in the horizontal or vertical direction, then the force of tension in the spring is $k\frac{x_1}{l}$ horizontally or $k\frac{x_2}{l}$ vertically, where k the component of the restoring force due to the springs attached to the cylinder is the same in both directions. Thus the total energy stored in the spring is

$$W_1 = \int_0^{x_1} (k\frac{x_1}{l}) dx_1 = \frac{1}{2} k \frac{(x_1)^2}{l} \qquad (6)$$

horizontally and

$$W_2 = \int_0^{x_2} (k\frac{x_2}{l}) dx_2 = \frac{1}{2} k \frac{(x_2)^2}{l} \qquad (7)$$

vertically. The net sum of the potential energy of the system is

$$W_1 + W_2 = P.E = \frac{kx_1^2}{2} + \frac{kx_2^2}{2} \qquad (8)$$

The kinetic energy of the fluid is given from the definitions of the depth-dependent added mass and velocity U of the the body as:

$$K.E = \frac{1}{2} m_a(x_2)(\dot{x_1}^2 + \dot{x_2}^2) \qquad (9)$$

since the added mass is equal in both x_1 and x_2 directions (We here see the remarkable result that for this particular geometry, the energy of the fluid is independent of the direction of motion. This result is not true for any other known geometry or for a circular cylinder in finite depth of water).Taking into account the mass of the cylinder, the total kinetic energy of the fluid and the cylinder becomes

$$K.E = \frac{1}{2}(m_b + m_a(x_2))U^2 \qquad (10)$$

The equations of motion may be derived from Lagrange's equations (2.4), for the generalised co-ordinates x_i, where

$$\begin{aligned} L &= K.E - P.E \\ &= \frac{1}{2}(m_b + m_a(x_2))(\dot{x_1})^2 + \frac{1}{2}(m_b + m_a(x_2))(\dot{x_2})^2 \\ &\quad -\frac{1}{2}(k\frac{(x_1)^2}{l} + k\frac{(x_2)^2}{l}) \end{aligned} \qquad (11)$$

Substituting (3.11) into (2.4) gives

$$(m_b + m_a(x_2))\ddot{x_1} + \dot{x_1}\dot{x_2}\frac{dm_a(x_2)}{dx_2} + k\frac{(x_1)^2}{l} = 0 \qquad (12)$$

for motion of the body in sway and

$$(m_b + m_a(x_2))\ddot{x_2} - \frac{1}{2}\dot{x_1}^2\frac{dm_a(x_2)}{dx_2} + \frac{1}{2}\dot{x_2}^2\frac{dm_a(x_2)}{dx_2} + k\frac{(x_2)^2}{l} = 0 \qquad (13)$$

for motion of the body in heave.

3.3.1 Non-dimensionalisation of the equations

Non-dimensional quantities T, X_i, $\dot{X}_i$, $\ddot{X}_i$, M_a and M_b corresponding to, t_p-time, x_i-displacement, $\dot{x}_i$ -velocity, $\ddot{x}_i$-acceleration, m_a-added mass and m_b mass of the cylinder may be defined as

$T = \sqrt{\frac{m_a+m_b}{\rho\pi a^2 M_b}}$, $X_i = \frac{x_i}{a}$, $\dot{X}_i = \frac{2\pi\dot{x}_i}{a}\sqrt{\frac{\rho\pi a^2 l M_b}{k}}$, $\ddot{X}_i = \frac{4\rho\pi^3 a M_b l \ddot{x}_i}{k}$, $M_a = \frac{m_a}{\rho\pi a^2}$,

$M_b = \frac{m_b}{\rho\pi a^2}$

The equations of motion above are non-dimensionalised. Equations (3.12) and (3.13) then become

$$(M_b + M_a)\ddot{X}_1 + \dot{X}_1\dot{X}_2\frac{dM_a}{dX_2} + 4\pi^2 M_b X_1 = 0 \qquad (14)$$

and

$$(M_b + M_a)\ddot{X}_2 + \frac{1}{2}\frac{dM_a}{dX_2}\dot{X}_2^2 - \frac{1}{2}\frac{dM_a}{dX_2}\dot{X}_1^2 + 4\pi^2 M_b X_2 = 0 \qquad (15)$$

respectively.

This motion is not damped. By adding the nondimensional wave damping term $\delta\dot{X}_i$ given, in dimensional form, by equations (3.5), equations (3.14) and (3.15) then assume the form

$$(M_b + M_a)\ddot{X}_1 + \dot{X}_1\dot{X}_2\frac{dM_a}{dX_2} + \delta\dot{X}_1 + 4\pi^2 M_b X_1 = 0 \qquad (16)$$

and

$$(M_b + M_a)\ddot{X}_2 + \frac{1}{2}\frac{dM_a}{dX_2}\dot{X}_2^2 - \frac{1}{2}\frac{dM_a}{dX_2}\dot{X}_1^2 + \delta\dot{X}_2 + 4\pi^2 M_b X_2 = 0 \qquad (17)$$

respectively, where

$$\delta = \frac{2\pi a^2 R^2 (M_a(0)+1)^2}{l^2\sqrt{(M_b + M_a)^3}} \qquad (18)$$

and R, the coefficient of the restoring force which determines the strength of the spring, arises here because of the way the equations have been made dimensionless.

In order to compute the numerical solutions for equations (3.16) and (3.17), we need to represent each one of them in the form of a system of two first-order ordinary differential equations. Let $U_1 = X_1$ and $U_2 = \dot{X}_1$ then

$$\begin{aligned} \dot{U}_1 &= U_2 \\ \dot{U}_2 &= -\frac{U_1 V_2}{M_a + M_b}\frac{dM_a}{dV_1} - \frac{4\pi^2 M_b U_1}{M_a + M_b} - \frac{\delta U_2}{M_a + M_b} \end{aligned} \qquad (19)$$

For the second equation we take $V_1 = X_2$,$V_2 = \dot{X}_2$ so that

$$\begin{aligned} \dot{V}_1 &= V_2 \\ \dot{V}_2 &= \frac{1}{M_a + M_b}\{-\frac{1}{2}\frac{dM_a}{dV_1}V_2^2 + \frac{1}{2}\frac{dM_a}{dV_1}(U_1)^2 - 4\pi^2 M_b V_1\} \\ &\quad -\frac{\delta V_2}{M_a + M_b} \end{aligned} \qquad (20)$$

To determine the solution of the above initial-value problems, a fortran program based on the fourth-order Runge-Kutta method was used. The algorithm requires that we give the initial values i.e displacements, velocities, number of time steps, equilibrium position, length of each time step, mass of the body and the value of R, a constant which we choose to specify the spring coefficient required. Explictly R is the ratio of the spring force at one radius displacement from equilibrium to the buoyancy force. Calculations for displacements, velocities, added mass and damping (and for other parameters if neccessary) at each time step can therefore be obtained as required. The results calculated are interesting and a comparison of these results with those of the fully nonlinear model of Brevig et al (1981) will help us to determine the regions of validity of the low-frequency assumption made to calculate the added mass. The tests are discussed in section 3.5.

3.4 Added mass and damping effects on the motion

The undamped and damped motions of the cylinder are investigated in the following sections with the effect of added mass variation being highlighted. Firstly, let us consider the effect of added mass variation on the motion of the cylinder when damping is not included. Considering equation (3.20) for the vertical motion of the cylinder, since for horizontal motion the added mass coefficient is a constant, we wish to study the effects of various parameters of the system on its motion. We expect that the movement of the cylinder will depend on its mass, on changes in equilibrium position and on starting positions.

3.4.1 Undamped motion of the cylinder

The actual period t_p for the motion of a spring-loaded cylinder oscillating under a linearised free-surface is given as a function of the virtual mass of the cylinder, $m_a + m_b$, and the spring coefficient, k. For example, we may write this as $t_p = 2\pi\sqrt{\frac{m_a+m_b}{k}}l$. Here we use the equilibrium value for m_a. Non-dimensionalising the period of the cylinder by the natural period of the cylinder in air $t_n = 2\pi\sqrt{\frac{m_b l}{k}}$ gives the non dimensional period as

$$T_p = \sqrt{\frac{m_a + m_b}{m_b}} = \sqrt{\frac{M_a + M_b}{M_b}} \qquad (21)$$

The calculations that follow in this section will be for equilibrium position at $2.2a$ below the surface and all parameters used are non-dimensional.

Since M_b is a constant, the change in the period of the motion of the sytem can only be due to change in added mass. We gave a graphical illustration in Fig. 2.1, of how the added mass varies with depth below the surface. Clearly,

we can tell from (3.21) that by assuming the mass of the body $M_b > 1$, the period is increased from that of a neutrally buoyant cylinder, and vice versa. Furthermore, we let the mass of the cylinder vary, then the velocity of the cylinder changes, increasing as M_b is reduced. This leads to reduced period of the system as expected from equation (3.21), see Figs. 3.1(a)-3(a). The increasing velocity of the system is shown in Figs. 3.1(b)-3(b) for decreasing values of M_b.

Changing the position of the cylinder, to either above or below the equilibrium position, is not likely to cause any difference in the global effect of the varying added mass (see Fig. 2.1) on the motion. This is discussed in detail below. In the case of constant added mass we simply have a harmonic type of motion in a conservative force field.

In the absence of damping the forces acting on this system are conservative and hence the total energy of the body and the fluid is conserved. This is shown in Figs. 3.1(a)-3(a) (i.e displacement-time graphs) where the magnitude of the maximum upward displacement is equal to the magnitude of the maximum downward displacement. It is also important to consider and verify the neccessity of updating the added mass as opposed to using constant mass(equilibrium mass) in our computations. The phase diagrams of Figs. 3.1(c)-3.2(c)-(d) and 3.3(c) show the effect of updating or not updating the added mass. These features turn out to be more pronounced in the case of smaller values of M_b, with the phase diagrams for variable mass being symmetrical only about the horizontal line through zero and that of constant added mass being symmetrical about both the horizontal and vertical lines through zero. In the case of small values of M_b, especially $M_b = 0$, a non-deformable

bubble, the phase diagrams for both constant and variable added mass methods coincide but the actual motions around the orbit do not coincide in time, as shown in the displacement/time and velocity/time graphs.

To illustrate the importance of the term, $\frac{\partial M_a}{\partial X_2}V_2^2$, in energy conservation we include this term in the system of equations (3.20) in the case of constant added mass(knowing very well that it should equal zero rather than taking its instantaneous value from $m_a(x_2)$). From Fig. 3.3(d) observe that energy is not conserved since the displacements at zero velocity are not equal in amplitude meaning a different amount of potential energy is stored in the springs in the upward and downward strokes, whereas without that term the motion is simple harmonic with energy fully conserved. Again, if in the case of variable added mass we exclude, in system (3.20), the term $\frac{\partial M_a}{\partial X_2}V_2^2$, the system tends to gain in energy forcing the body to accelerate to a new maximum value above the equilibrium position greater than its absolute minimum value. The model is such that changing the direction of the initial displacement for a given mode of motion has no effect on the period of the system.

From the above studies we see that this model is in good agreement with the linearised (i.e no V^2 terms in the equation of motion) and equilibrium position added mass theories. The period for variable added mass is found to be almost in agreement but slightly longer. Differences exist in motion, but the variable added mass theory is consistent, a conclusion drawn from the fact that energy is conserved. Reduced M_b leads to an increased effect of the variability of M_a, as expected. We conclude that the variable added mass analytical theory is correct, and we feel justified in extending it to include damping which will be important for comparison with the numerical studies.

3.4.2 Damped motion of the cylinder

For damped motion of a cylinder dimensionless systems of equations (3.19) and (3.20) are considered. The derived damping coefficient depends on the dimensional frequency of the motion of the cylinder,

$$\begin{aligned} \omega &= \sqrt{\frac{k}{(m_a + m_b)l}} \\ &= \sqrt{\frac{Rg}{(M_a + M_b)l}} \end{aligned} \qquad (22)$$

where ω is the dimensional frequency of the cylinder in water. Since the frequency in (3.22) is small, then our damping which is depended on ω^4, see (3.5), is also going to be small. Increase in spring coefficient, k, will lead to increased damping of the motion, but this case is not desirable since it would violate the assumed low-frequency motion needed for added mass calculation. We investigate how large k can be later.

With damping it remains to be seen to what extent the added mass updating is worthwhile considering, rather than simply taking the equilibrium added mass. For undamped motion this proved to be of little significance (see Figs. 3.1(a), 3.2(a) and 3.3(a)). In section 3.6 we revisit this, with a view to comparing the variable and constant added mass cases with the fully non-linear free-surface method of Brevig et al (1981). This will give us a clear picture of the three cases put together. We shall also be looking at the question of the accuracy of the motion of the system for variable added mass case and the fully nonlinear case.

3.5 Computations using the nonlinear method

Running the nonlinear scheme for long periods, for comparison with the analytical model to be made, gives problems. When the cylinder was displaced through a distance a above the equilibrium position, of $2.2a$ below the surface so that the top of the cylinder was submerged only $0.2a$ below the free surface, disturbances were observed on the free surface which lead to break down in the calculations. A number of different combinations of Δt (small increment in time), the number of free surface points, the points around the body, the length of the control volume, the free surface point distribution ratio (which allows closer distribution of points in the region around the cylinder and wider spacing for points further away from the body towards the vertical boundaries) and the equilibrium position were tried, but the calculations always broke down. Next, the body was displaced through a below the same equilibrium position of $2.2a$ and allowed to move upward. The body could only go up to the maximum displacement above the equilibrium mark and down to a distance a little below the equilibrium position before the process broke down again. Diagrams of the above features are shown in Figs. 3.4- 5. When the cylinder is initially above the $2.2a$ mark and moving downwards, the free surface is drawn down following the body (see Fig. 3.4(a)) until it starts moving upwards into the trough created, as shown in Fig. 3.4(b) which also includes the last profile of Fig. 3.4(a), and eventually forming jets on both sides of the body as in Fig. 3.4(c). These jets appear to be physical, in which case continuing the calculations would require very fine resolution of the jet flow, and could only be continued until jet re-entry as in similar breaking wave calculations, see Longuet-Higgins and Cokelet (1976).

When the body starts from below the equilibrium position it accelerates with a volume of fluid, and as it starts to go down from its peak, some of the fluid continues to move in the upward direction. As the cylinder gains momentum in the downward direction the mound of fluid initially created above it begins to collapse following the cylinder. All this happens too quickly for the scheme to be able to correctly resolve the free surface points. The process gradually comes to an end with unphysical cracklike developments on the free surface around the centre (see Fig. 3.5(c)). The sudden slumping down of the free surface which begins in Fig. 3.5(b) and continues in Fig. 3.5(c) ensures the development of cracks responsible for the breaking down in calculations. It would, probably, be possible to continue these calculations with a finer free surface discretisation, but we have not attempted this.

As a further study we consider motion with constant velocity. A similar study was carried out by Greenhow (1988), but for bodies entering the free surface at a constant velocity. That case can be likened to ours when only considering the motion of already fully submerged cylinder. His calculations seemed not to have gone very far. We now shall consider the motion of a cylinder started impulsively with a downwards velocity at Froude number, $Fr = \frac{U}{\sqrt{dg}}$=0.082, and the resulting surface profile due to this motion is shown in Fig. 3.6. The features of this profile resemble those for variable acceleration in Fig. 3.4, indicating that for this case the breakdown of the calculations is physical rather than numerical.

It is worth mentioning that we have no problems with the numerical calculations as far as horizontal motion is concerned, since free surface deflections are much smaller (see also Hepworth, 1991). Hence most of the effort is spent

on resolving problems encountered only with the vertical and oblique motions of the cylinder.

Starting the motion from $0.8a$ above the equilibrium position of $2.2a$ below the surface changed the motion dramatically. For example, the calculations took longer to break down than in previous cases and this allowed comparisons with the analytical model to be made (see Fig. 3.7). This is primarily due to smaller amplitudes of motion. Although we cannot make general conclusions on the causes of the breakdown in numerical calculations, the results above point to physical reasons like the overturning of the free surface in the case of large amplitudes when the cylinder starts at greater than $0.8a$ above the $2.2a$-equilibrium position. Obviously the calculations for equilibrium position below $2.2a$ can be continued for a larger number of time steps, but eventually these calculations are disrupted because of radiated waves being reflected back from the distant vertical boundaries which form the far-field closure of the fluid domain. Thus Figs. 3.10-11 show sudden distortions of the oscillatory motion, when calculations are allowed to run for these longer times in the case of motion about $3a$-equilibrium position below the surface.

Numerical computations for fully non-linear free surface model have been carried out in accordance with our desire to test the results of the analytical scheme with linear damping obtained from low-frequency motion. In the section that follows we compare the results of the two models as far as possible so as to make recomendations on validity of the analytical model.

3.6 Comparison of the results between the non-linear numerical method and the analytic method

Some of these results have been outlined in Sections 3.4 and 3.5 and we here are simply presenting those predictions of the analytical model in comparison with the results of the fully nonlinear scheme. All the obtained results using the nonlinear method have been non-dimensionalised in accordance with the parameters introduced earlier on for the analytical model.

3.6.1 Example calculations of the motion of the cylinder displaced from 2.2a-equilibrium position

Consider the cylinder displaced through $0.8a$ upwards and is allowed to move downwards under the constraints described earlier, attached to springs of modulus k horizontally and vertically. The computed results of this motion are shown in Fig. 3.7 where the displacement-time and velocity-time graphs for variable and constant added mass are shown together with those of the fully-nonlinear model. Here the effect of the added mass is not very pronounced, and as a result it is difficult to say whether it is better to update the added mass or not, but nevertheless the variable added mass graph seems to be a better approximation of the fully-nonlinear model when considering the period only. The amplitudes for both variable and constant added mass models coincide and are slightly greater than that of the fully nonlinear scheme, see Fig. 3.7(a). An attempt to improve on the period and the amplitude empirically from the known numerical results and assuming that the amplitude for the fully-nonlinear scheme decreases exponentially, was abandoned since one

would need to alter parameters in the expression for period (i.e M_a) in order to reduce or increase the period and the amplitude simulteneously. Introducing a factor, calculated by comparing the two results, to increase the damping coefficient would only reduce the amplitude of the motion.

3.6.2 Example calculations of the motion of the cylinder displaced from 3a-equilibrium position

In this case we carry out further computations for a more deeply submerged cylinder and observe that the period of the motion of the analytical model has improved slightly in agreement with that of fully nonlinear model (see Figs. 3.8-12). This observation is in agreement with the fact that as the depth of submergence increases, the effect of added mass diminishes and the period becomes insensitive to the initial displacement.

For the motion of the cylinder initially displaced through a to the side and a down, the period, for the numerical calculations, of the horizontal motion seems to be in agreement with the period for vertical motion. When the two methods are compared, the amplitude for the analytical model is in closer agreement with the numerical calculations (i.e. better) for vertical motion than for horizontal motion. In all other remaining cases the amplitude for vertical motion is either better than, or the same as, the horizontal motions. In the case of the numerical scheme, the vertical motion for vertically constrained motion of the cylinder decays much slower than the vertical component of the motion for oblique case. This is also true for horizontal motion constrained in the horizontal plane compared to the horizontal component of the oblique motion. Also, for only the vertically constrained motion, the one started from below decays faster than the motion started from above. Overall observation is that

the periods for the two methods in vertical and horizontal modes of the motion differ only slightly, whereas the agreement in amplitudes is not good. Here, again we see that it is not possible to improve the amplitude for the horizontal and vertical motions at the same time as the periods, by simply changing the damping parameter empirically, or by using finite frequency damping from linear theory. However, we note that the added mass coefficient is a constant in the case of horizontal motion.

However, all the above calculations were obtained using the value of $R = \frac{1}{15}$. We conclude that the cylinder motion for the analytical model (see Figs. 3.8-12) is generally underdamped since the motion for the nonlinear model decays more rapidly than for the analytical scheme. In an effort to improve the validity of the low-frequency assumptions of the analytical model we have carried out experiments with a weaker spring, i.e reduced the value of k. In the results that follow the value of R has been halved.

3.6.3 Example calculations with $R = \frac{1}{30}$

No new features were achieved in the case of a cylinder displaced through a above $2.2a$-equilibrium position even though the calculations were extended slightly before breaking down in a similar manner as above. Similarly, displacement through $0.8a$ above the $2.2a$ did not yield any meaningful results for us to be able to carry out comparison tests with the numerical calculations. In Fig. 3.13 we show the surface elevations for this run. The calculations breakdown as the scheme fails to handle what looks like waves of short wave-length that have formed in the region above the cylinder. However, a displacement downwards through $0.8a$ produced the required results which are shown in Fig. 3.14(i).

The motion for the analytical method about $2.2a$ seems to be overdamped when considering the period only, but it is hard to draw conclusions about the amplitudes of the two methods. The initial displacements for the analytical method are greater than for the nonlinear method, but the motion seems to decay faster than for the nonlinear model. We observe that the downward displacement for the nonlinear model at $T = 3$ is now greater than that of the analytical model. Surface profiles for these results are shown in Figs. 3.14(ii). Also, the calculations were carried out for the horizontal motion about $2.2a$. The motion of the cylinder obtained in this case is depicted in Fig. 3.15 and Fig. 3.16 shows the surface elevations. The disturbance at the free surface is minimal and these calculations can be continued until the smooth flow is interupted by reflected radiated waves.

Here the period of the analytical model is about 97% of the period of the numerical scheme. However, it is not possible to determine how the amplitude of the analytical model relates to the numerical one in general since further relaxation of the spring produces an undamped motion for the analytical model and underdamped and unpredictable motion for the numerical model. In the case of the numerical scheme, we notice that the amplitude of motion varies depending on the starting positions of the motion and time for individual situations. If, for example, the motion is started from below the equilibrium position, the downward maximum displacement on the second period of the motion, is the greatest absolute displacement for the number of oscillations considered here, see Fig. 14(i(a)) and Fig. 3.18(a). The reverse is also true, as shown for the motion started from above the equilibrium position of $3a$, see Fig. 3.21(a). In general, it appears the greatest absolute displacement

is achieved on the the second period as well as on the side from where the motion was started. This includes the case of horizontal motion, see Figs. 3.15(a) and 3.19(a). This analysis seems to be insufficient in the description of the oblique motion. In this case the horizontal motion is in agreement with the above observations (see Figs. 3.17(b) and 3.20(b)) whereas the vertical motion seems to be overdamped on its downward rather than on its upward stroke. This also varies with starting positions, with the motion started from above the equilibrium position being more damped than the one started from below, see Figs. 3.17(a) and 3.20(a). Strengthening of the spring leads to increased damping, resulting in reduced amplitude. Hence this value maybe assumed to be, approximately, critical. The absolute value of the displacement, in the case of the fully-nonlinear model, seems to be greatest at around T=3 after which the motion seems to be decaying uniformly. Again, motions for variable and constant added mass in the analytical scheme seem to be in good agreement.

To be able to carry out further investigations of the motion with the new value of R we consider the cases for a deeply submerged cylinder which were discussed above for the value of R= $\frac{1}{15}$. In Figs. 3.17-21 we show the extended calculations for oblique, vertical and horizontal motions. Here, also the period of the analytical scheme appears to be less than that of the numerical scheme by about 3%. The results for the oblique, vertical and horizontal motions, when the body is started from (a,4a),(0,4a) and (a,3a) respectively away from 3a-equilibrium position appear to indicate that the respective vertical motions for the first two cases and horizontal motions for the first and the last cases attain their greatest absolute displacement values at around T=3. When the motion is started from above for the oblique and the vertical cases we notice

that the decay in motion is quite smooth. Because of non-uniformity in the decay of the motion, there is therefore hardly anything we can do to improve on the analytical results so that they can be closer to the numerical results. Also, we have no rationale for determining the change of the value of the equilibrium added mass in the analytical model, which would reduce both the amplitude and the period at the same time to give us very close results to the numerical calculations.

Summing up the above, we point out that no further reduction of the value of R produces closer numerical results to the analytical ones. Generally, the analytical model is still underdamped when compared to fully-nonlinear model, but the approximation of equation (3.5) is known to be overdamped when compared to linear time-domain theories, which makes it impossible for us to further reduce or increase the damping in any rational and consistent fashion.

3.7 Precession of the motion of the cylinder

The study of the motion of a circular cylinder, carried out above in which the acceleration is variable throughout the motion has also revealed some interesting features pertaining to the movement of the body. There seems to be something peculiar in the orientation of the motion. The results in Fig. 3.22 are for a circular cylinder oscillating about an equilibrium position below a fixed wall.

Fig. 3.22 shows the paths followed by the cylinder as it oscillates about $2.2a$-equilibrium position for an undamped motion of the analytical model. The oscillatory nature of this motion for a large time becomes unsteady, seemingly due to involvement of drag and lift forces arising from nonlinear interaction

with the free surface (rather than those due to vortex shedding which is absent in our inviscid model). The body passes below the equilibrium position as it moves obliquely downwards and passes above this position on its way upwards, see also Fig. 3.22(b-f). Because it is not clear why the path described by this motion is not a straight line we therefore further investigate the behaviour of this system for cylinder slightly displaced from the direction it is intended to follow. In Fig. 3.23 we see similar features, as above, but this time for a cylinder initial displaced to $(0.1a,1.2a)$ from $2.2a$-equilibrium position.

Since in the two above examples the motion is undamped it is worthwhile studying the damped motion. In this case also, the most visible feature of the body motion is its persitence in following two distinct paths on going through each cycle of the motion, see Figs. 3.24-26. As far as the few cases considered are concerned we observe that, generally the behaviour of the cylinder motion is the same. Thus, the problem of the motion not following a straight line remains unresolved and we attempt to further understand this problem by changing the equilibrium position.

With the equilibrium position moved to $3a$ below the surface we managed to observe some big changes in the movement of the cylinder. As illustrated in Fig. 3.27 the cylinder now moves in a straight line, as we have been expecting. Knowing that increasing the depth of the cylinder below the free surface results in reduction in added mass variation we therefore conclude that the instability is caused by the rapidly changing added mass coefficient near the free surface. In all the examples so far examined, the orientation of the motion is the same, i.e the motion of the system turns in a clockwise sense. To prove the validity of the model from the standpoint of unsteadiness of the motion, we compare our

findings through this model with the results computed from the fully-nonlinear model.

The results illustrated in Fig. 3.28 show that the motion is generally unsteady as the cylinder moves upwards and downwards to the sides of its intended path (i.e at an angle $= \frac{\pi}{4}$ to the horizontal axis). This is not due to some forces acting on the body which were not explicitly accounted for in the description of the analytical problem, but rather arise because the coefficients in the equations of motion are continuously changing, i.e horizontal period is less since the added mass coefficient is constant for motion in the horizontal direction. Results of the fully nonlinear method are fairly in good agreement with our results of then analytical model.

Similarly the velocity vector of the cylinder in the numerical scheme seems to be turning clockwise when the body is going up and anticlockwise when it is going down, see Fig. 3.28. The numerical evidence thus also points to the presence of forces which make the axis of motion precess the body clockwise, and this is a strong justification of the validity of the analytical scheme which predicts the same effect. However, the numerical results also indicate an overall downwards drift which is missing in the analytical results.

3.8 Conclusion

The problem of a cylinder oscillating about an equilibrium position below a nonlinear free surface has been solved analytically after having simplified the free surface conditions. A comparison with the calculations of the fully nonlinear free surface scheme to test the efficiency of the analytical model have also been carried out. In concluding this chapter we allude to the four major

agreements of the two models as has been described in preceding sections;

(a) the periods of the models are in close agreement, though that of the fully-nonlinear free surface scheme are slightly longer

(b) it has been, more or less, shown that with a weaker spring the two models have comparable damping, the analytical model being slightly underdamped

(c) in both models, the cylinder experiences downward force as it nears the free surface

(d) both models predict precession of the direction axis for the oblique motions.

Also, we observed a number of new features through using the nonlinear numerical scheme which we could not achieve by the simplified method. These were;

(a) the motion of the free surface resulting in formation of

(i)sharp wave breakers

(ii) waves of short wave-length

(b) breakdown of the calculations due to due to features in (a)

(c) reflected waves from the far field eventually affecting the motion of the cylinder, which might also be encountered in physical experiments in small tanks.

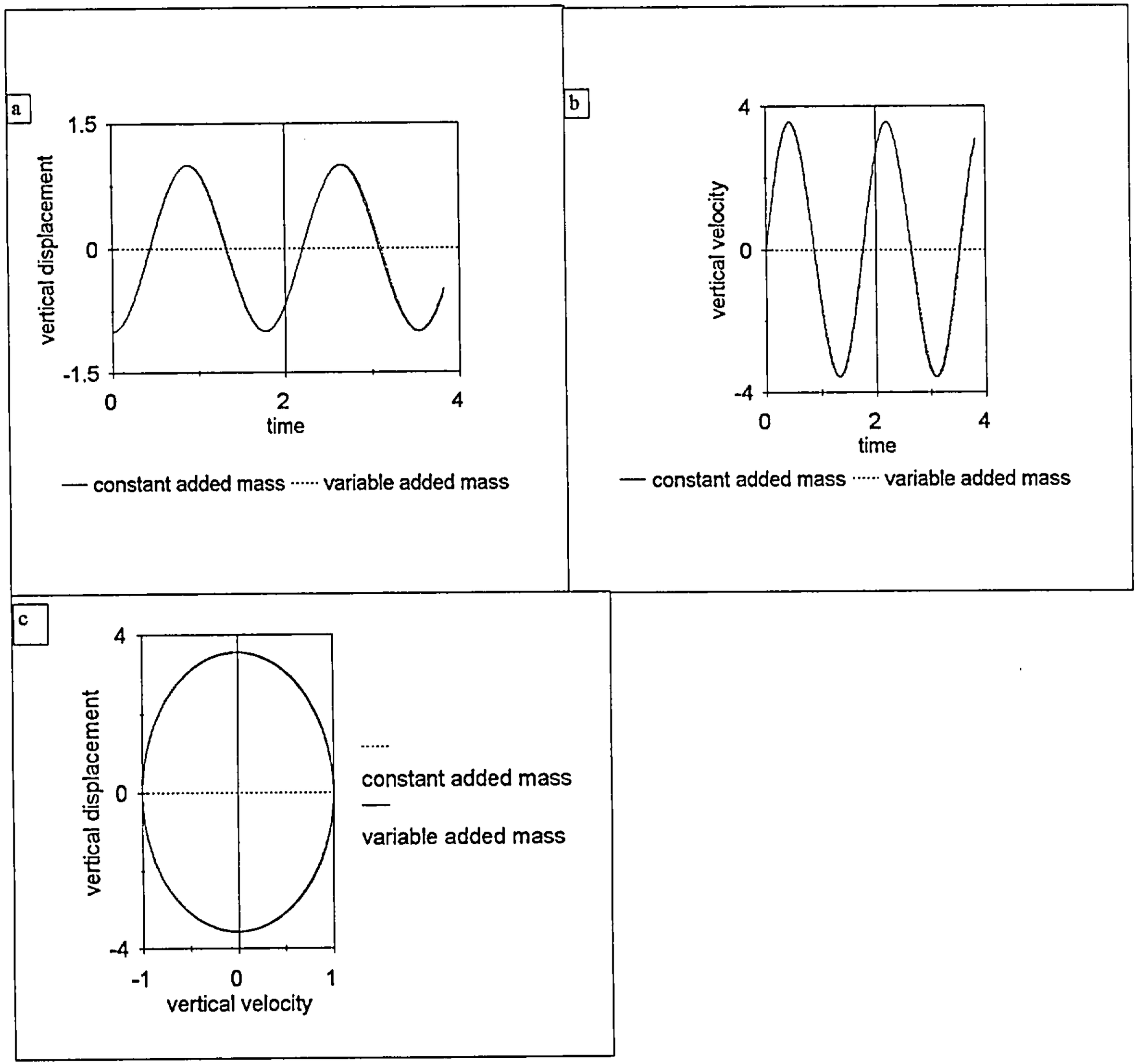

Fig. 3.1 A cylinder is initially displaced to (0,-3.2a) from (0,-2.2a) its equilibrium position. Mb=2.0 and R=1/15.

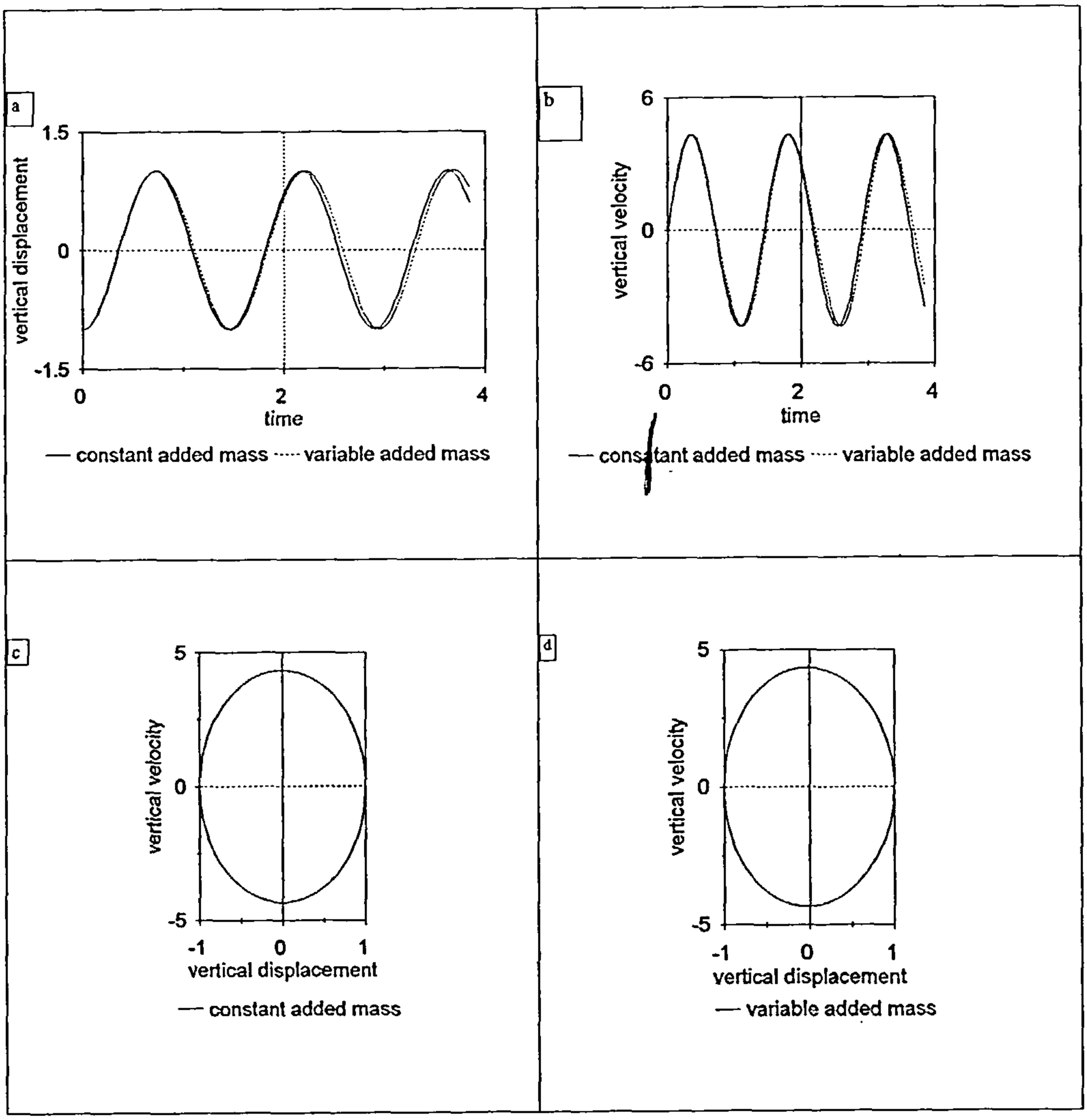

Fig. 3.2 A cylinder is initially displaced to (0,-3.2a) from (0,-2.2a) its equilibrium position. Mb=1.0 and R=1/15.

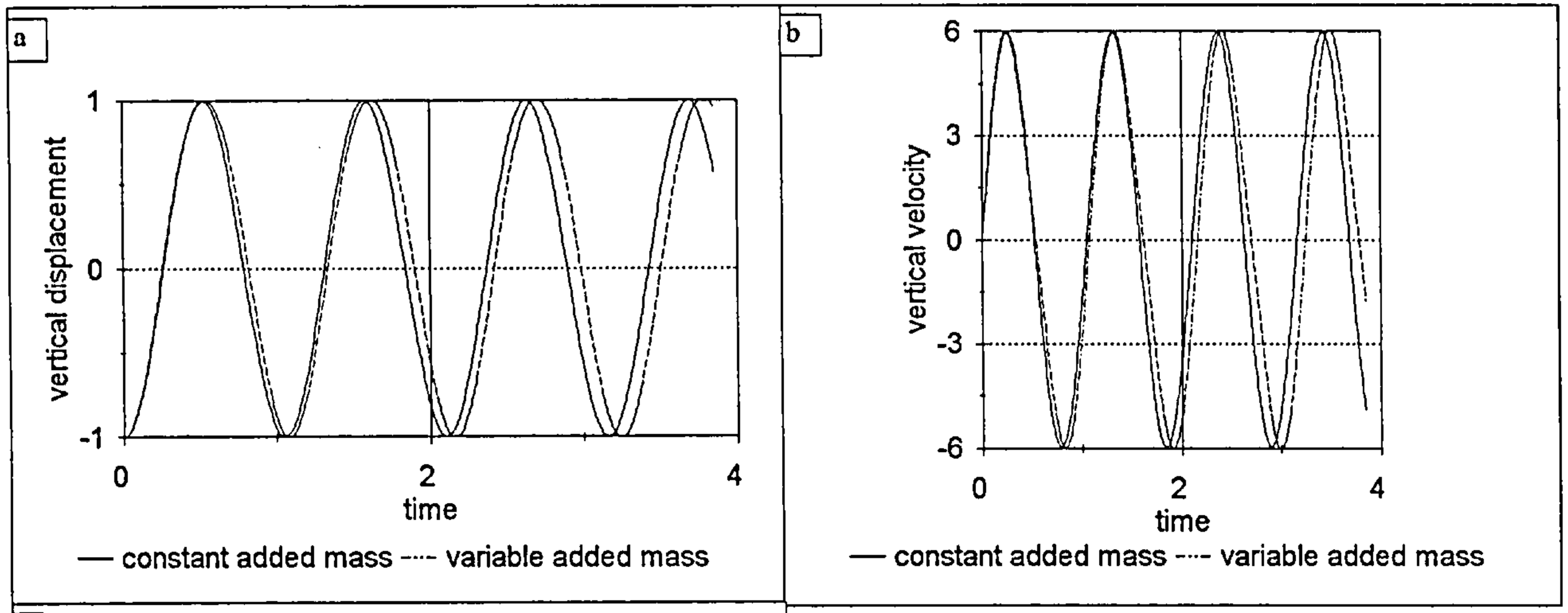

Fig. 3.3 A cylinder is initially displaced to (0,-3.2a) from (0,-2.2a) its equilibrium position. Mb=0 and R=1/15.

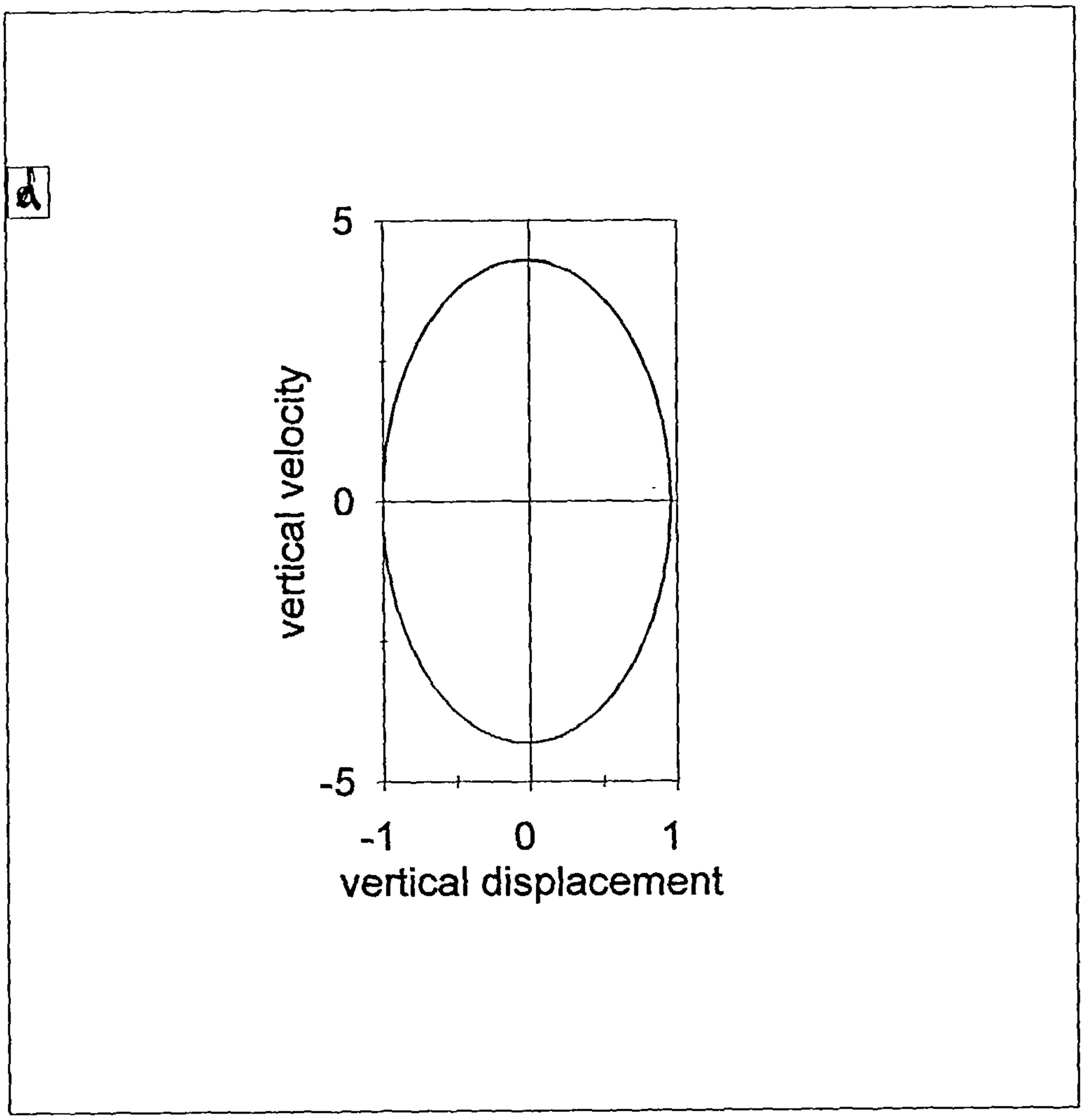

Constant added mass including the term V-squared, Mb=1.0.

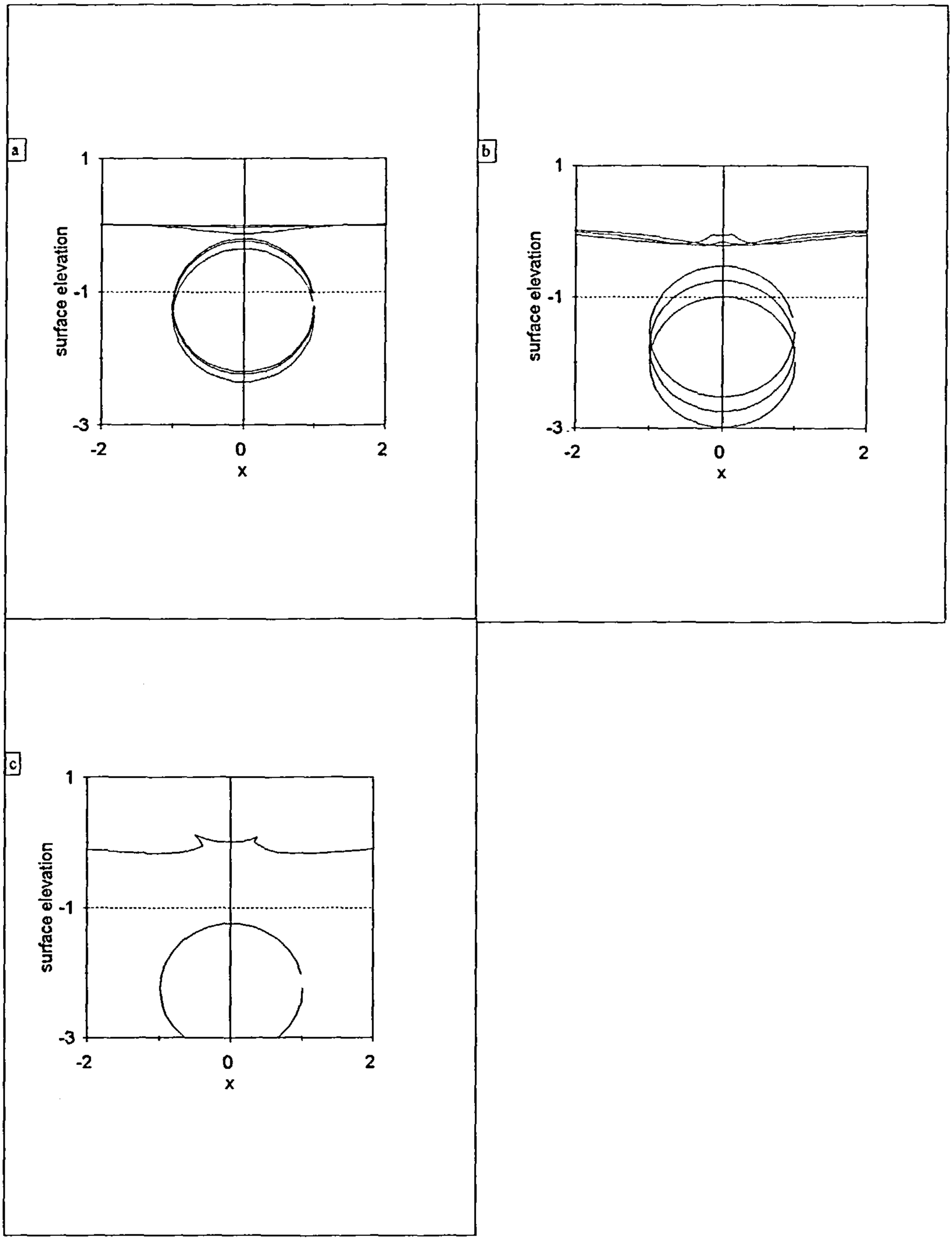

Fig. 3.4 Free-surface elevation and cylinder position due to the transient motion of a cylinder initially displaced to (0,-1.2a) from the equilibrium position (0,-2.2a) below the surface. Mb=1 and R= 1/15.

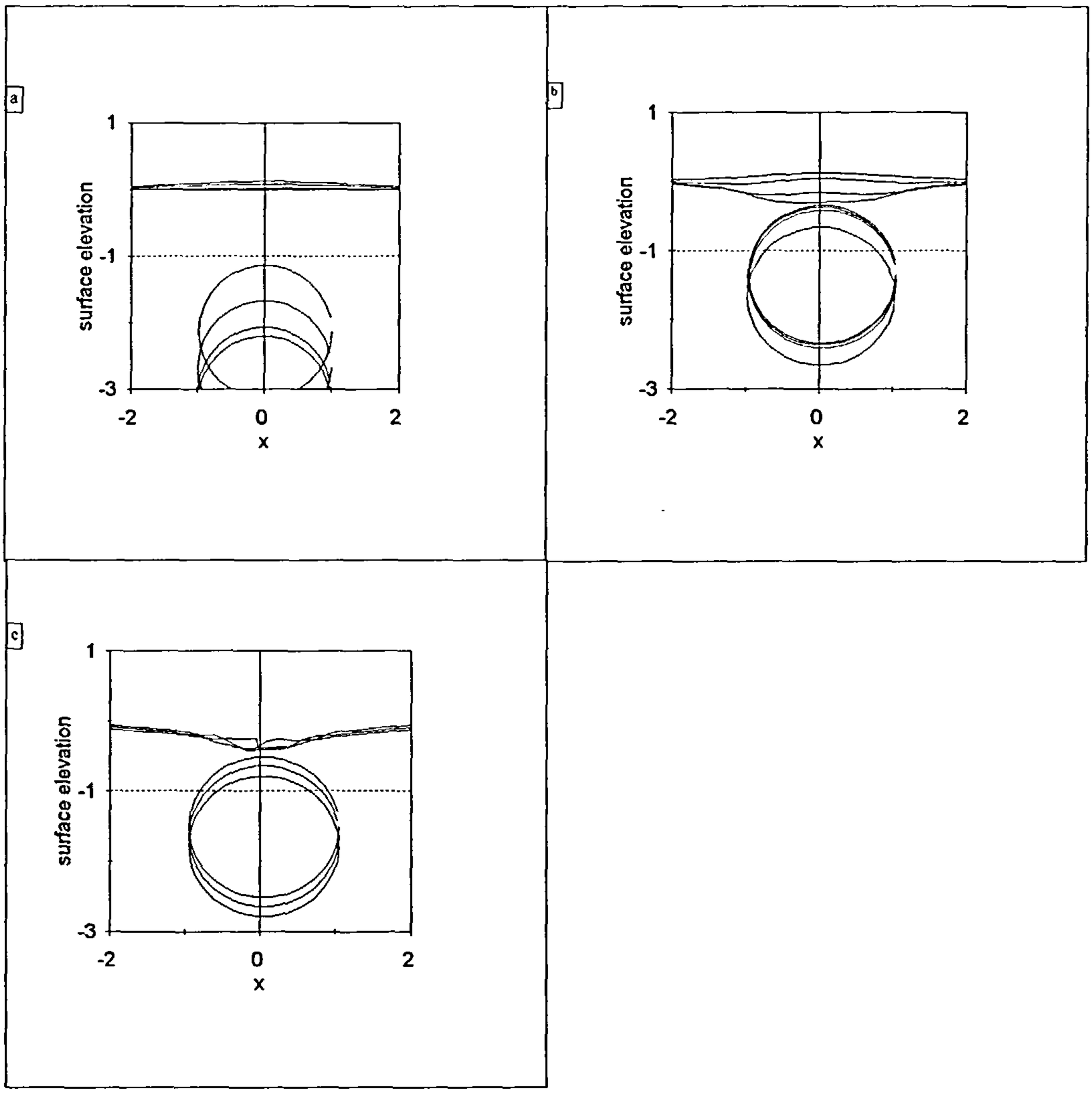

Fig. 3.5 Free-surface elevation and cylinder position due to the transient motion of a cylinder initially displaced to (0,-3.2a) from its equilibrium position (0,-2.2a) below the surface. Mb=1 and R= 1/15.

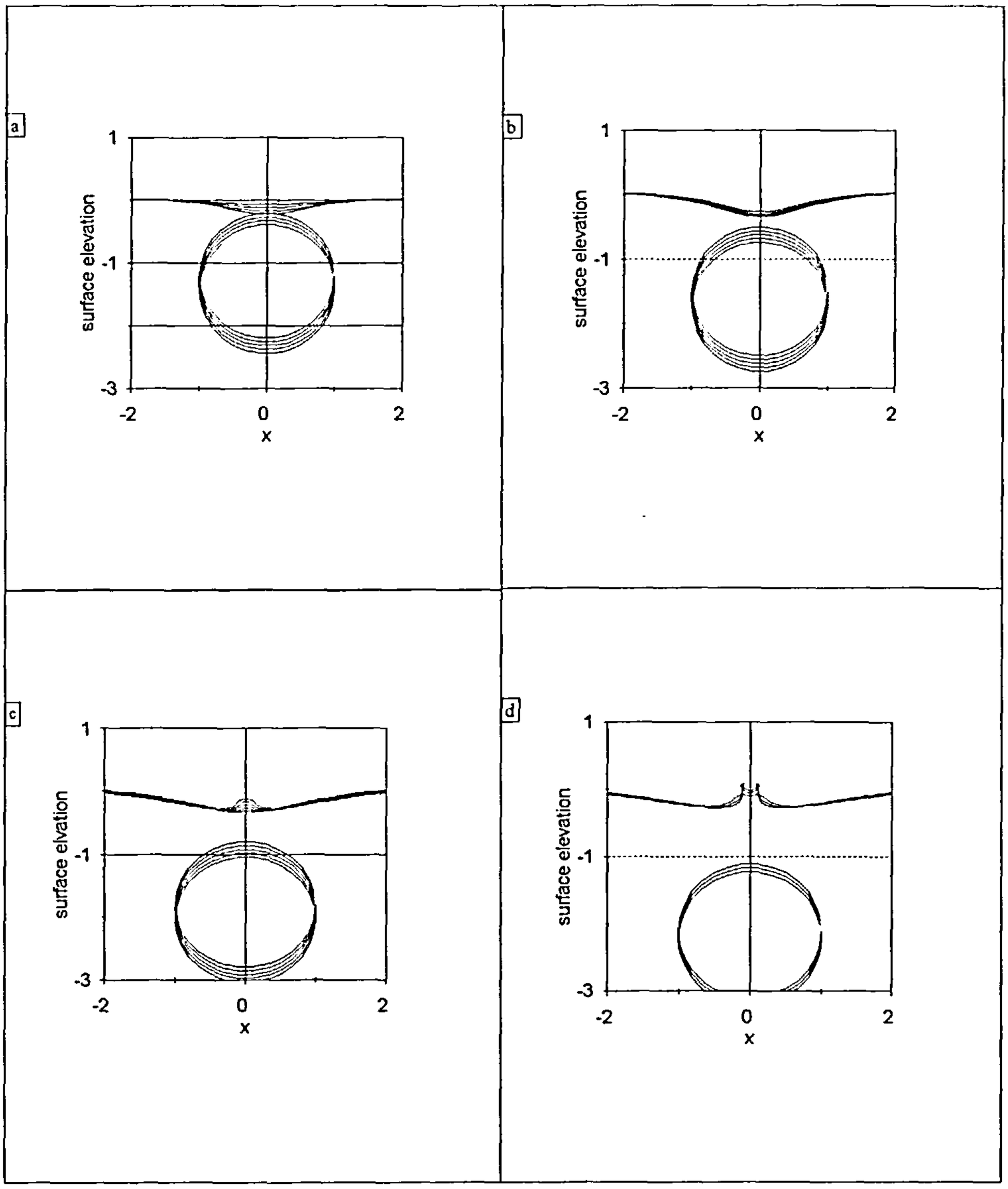

Fig. 3.6 Free-surface elevation and cylinder position due to the impulsively started motion of a cylinder at Fr=0.43 and initially displaced to (0,-1.2a) from the equilibrium position (0,-2.2a) below the surface.

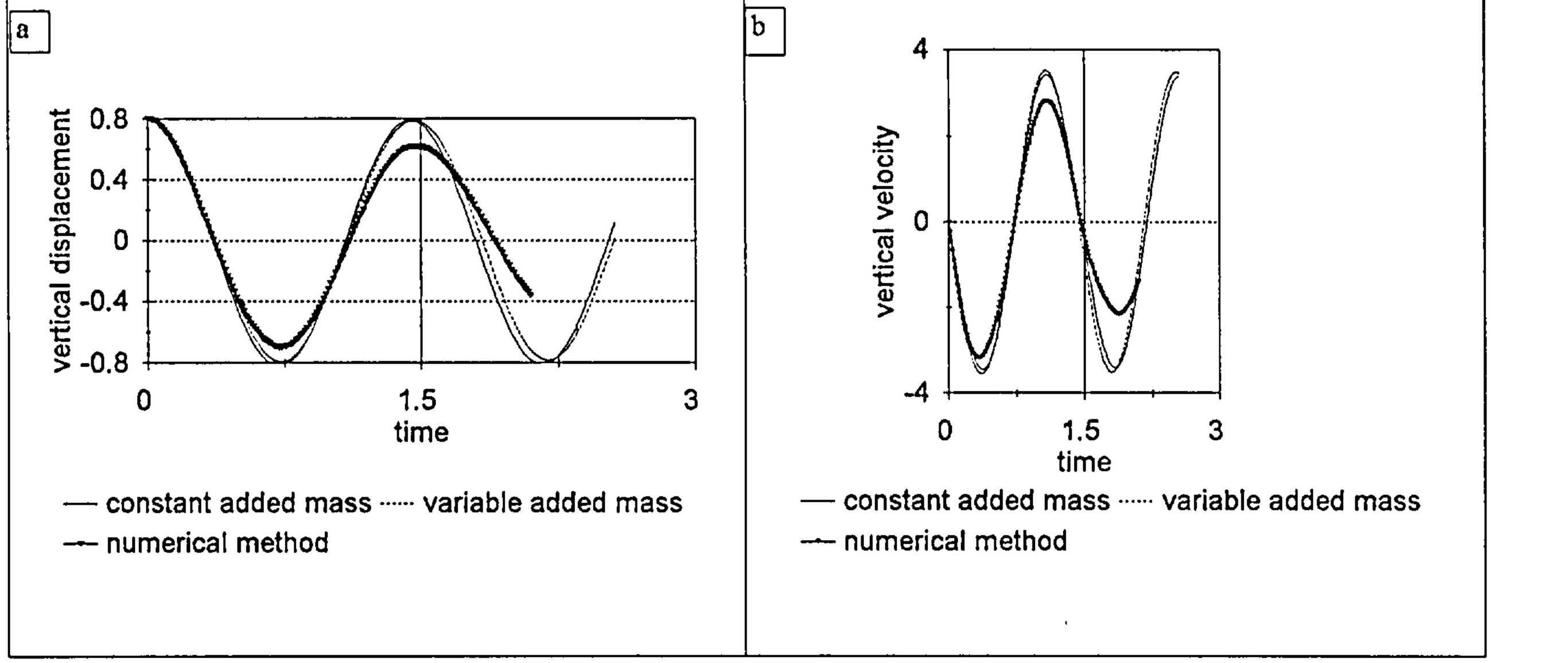

Fig. 3.7 Vertical motion of a cylinder initially displaced to (0,-1.4a) from (0,-2.2a) its equilibrium position. Mb=1.0 and R=1/15.

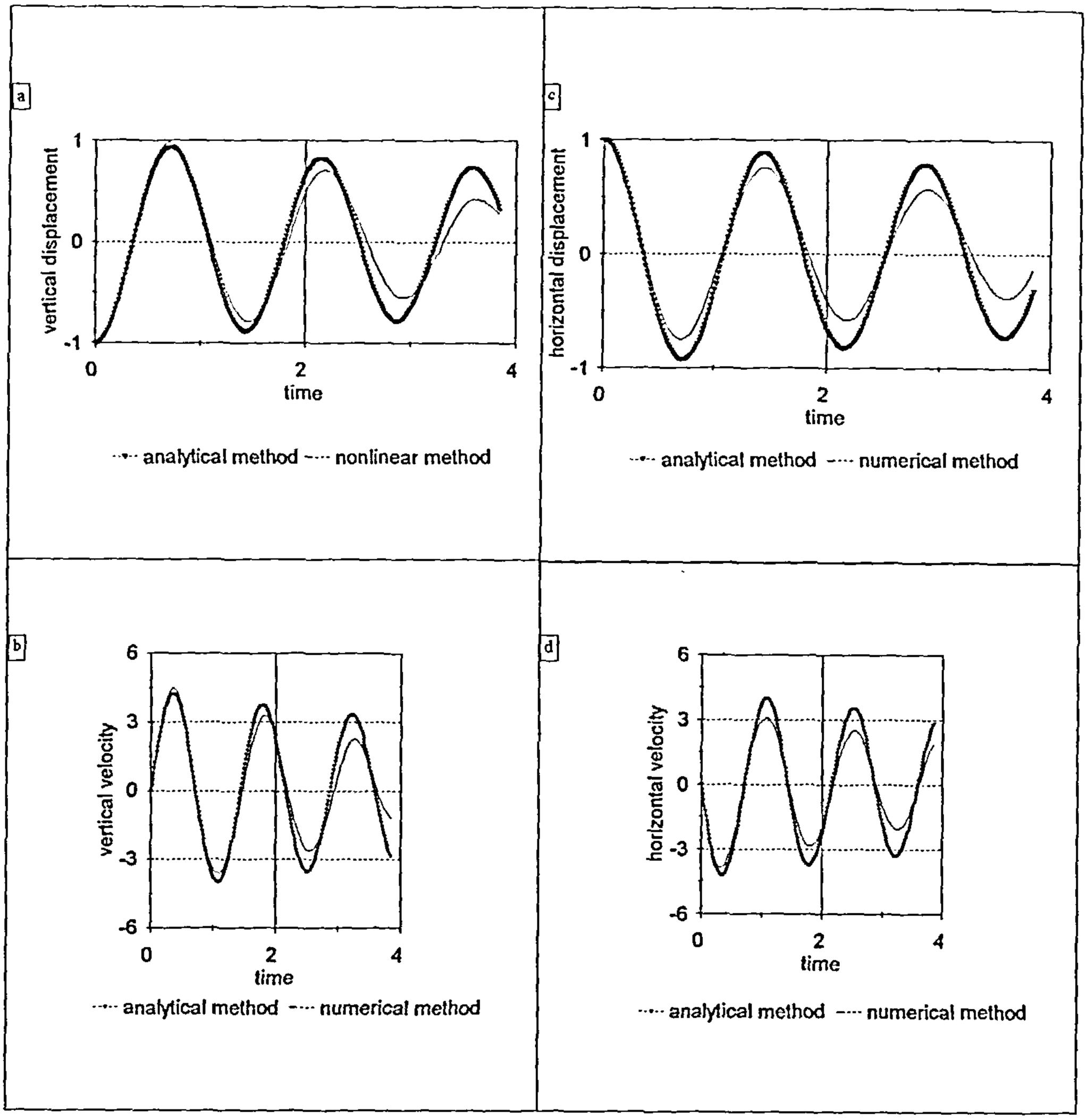

Fig. 3.8 Oblique motion of a cylinder initially displaced to (a,=4a) from its equilibrium position (0,-3a) below the surface. Mb=1 and R=1/15.

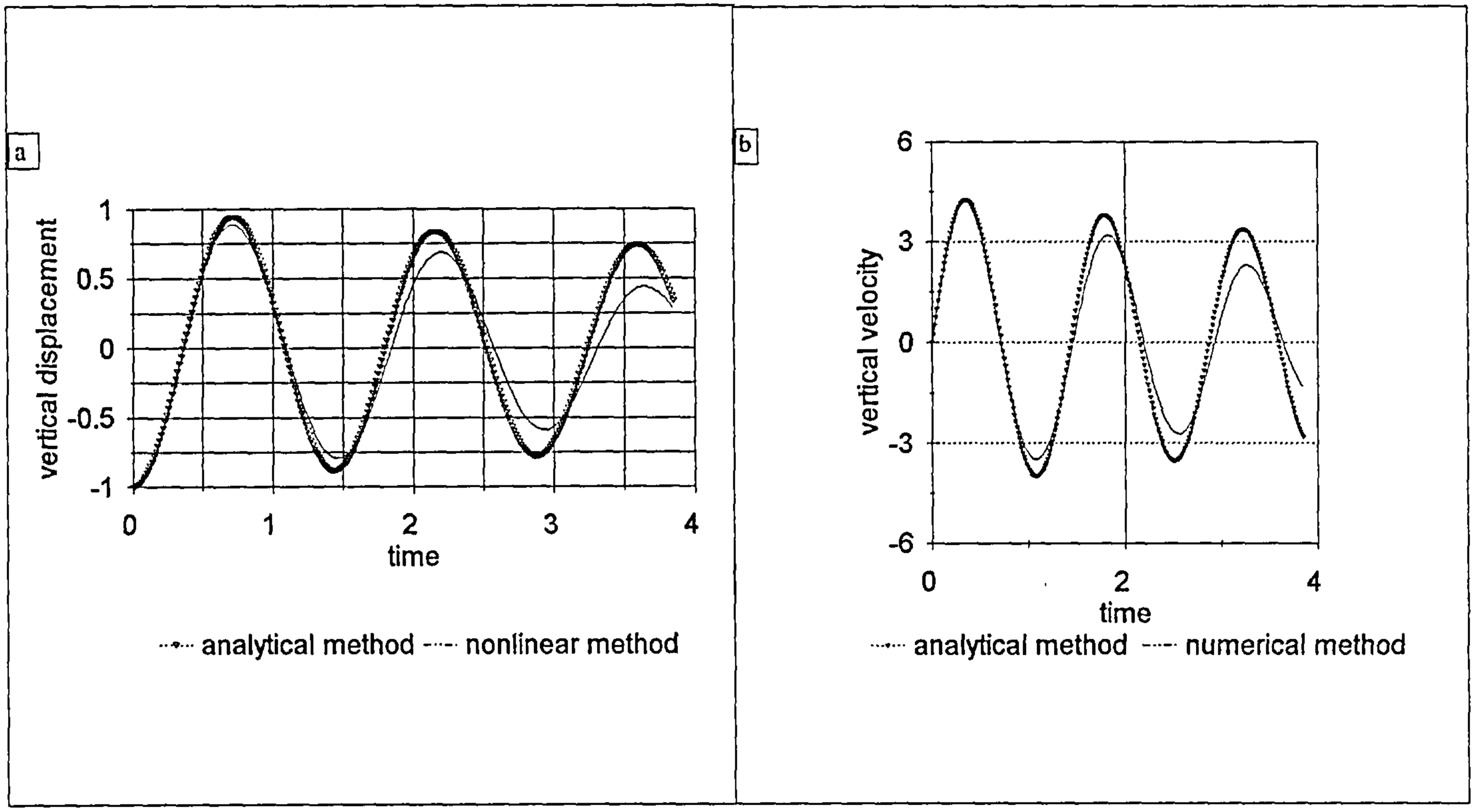

Fig. 3.9 Vertical motion of a cylinder initially displaced to (0,-4a) from (0,-3a) its equilibrium position. Mb=1.0 and R=1/15.

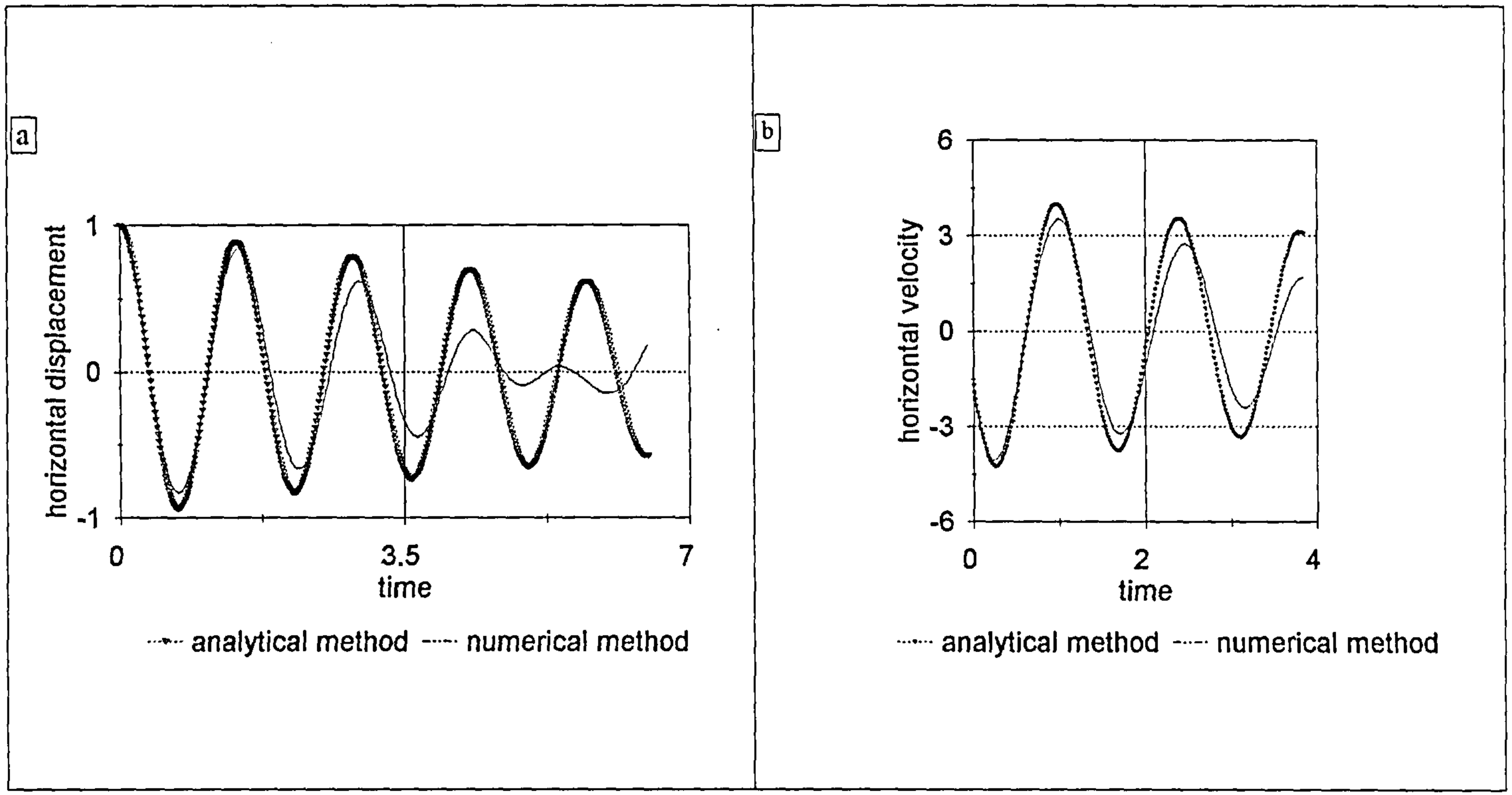

Fig. 3.10 Horizontal motion of a cylinder initially displaced to (a,-3a) from (0,-3a) its equilibrium. Mb=1.0 and R=1/15.

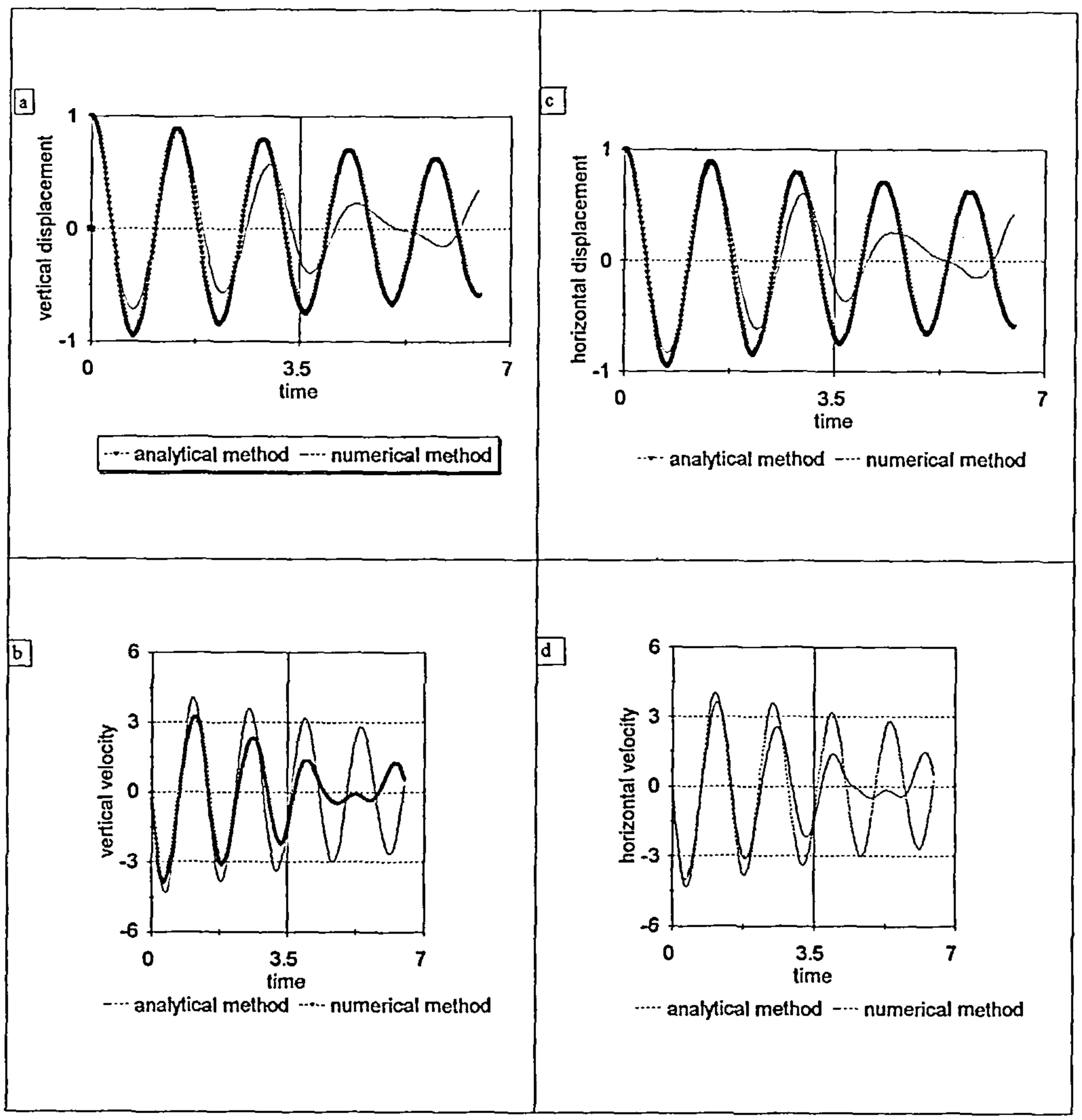

Fig. 3.11 Oblique motion of a cylinder initially displaced to (a,-2a) from its equilibrium position (0,-3a). Mb=1.0 and R=1/15.

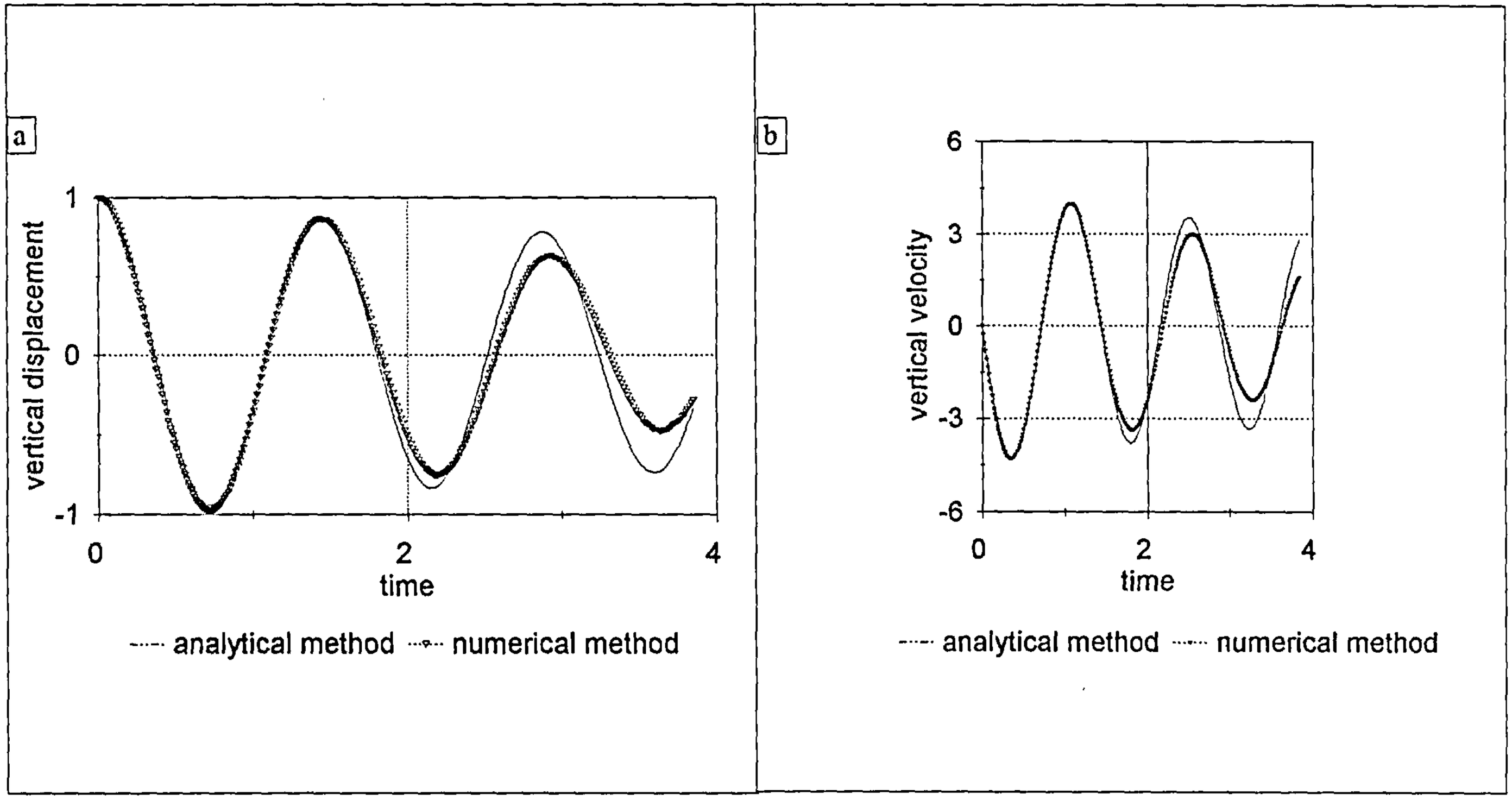

Fig. 3.12 Vertical motion of a cylinder initially displaced to (0,-2a) from (0,-3a) its equilibrium position. Mb=1.0 and R=1/15.

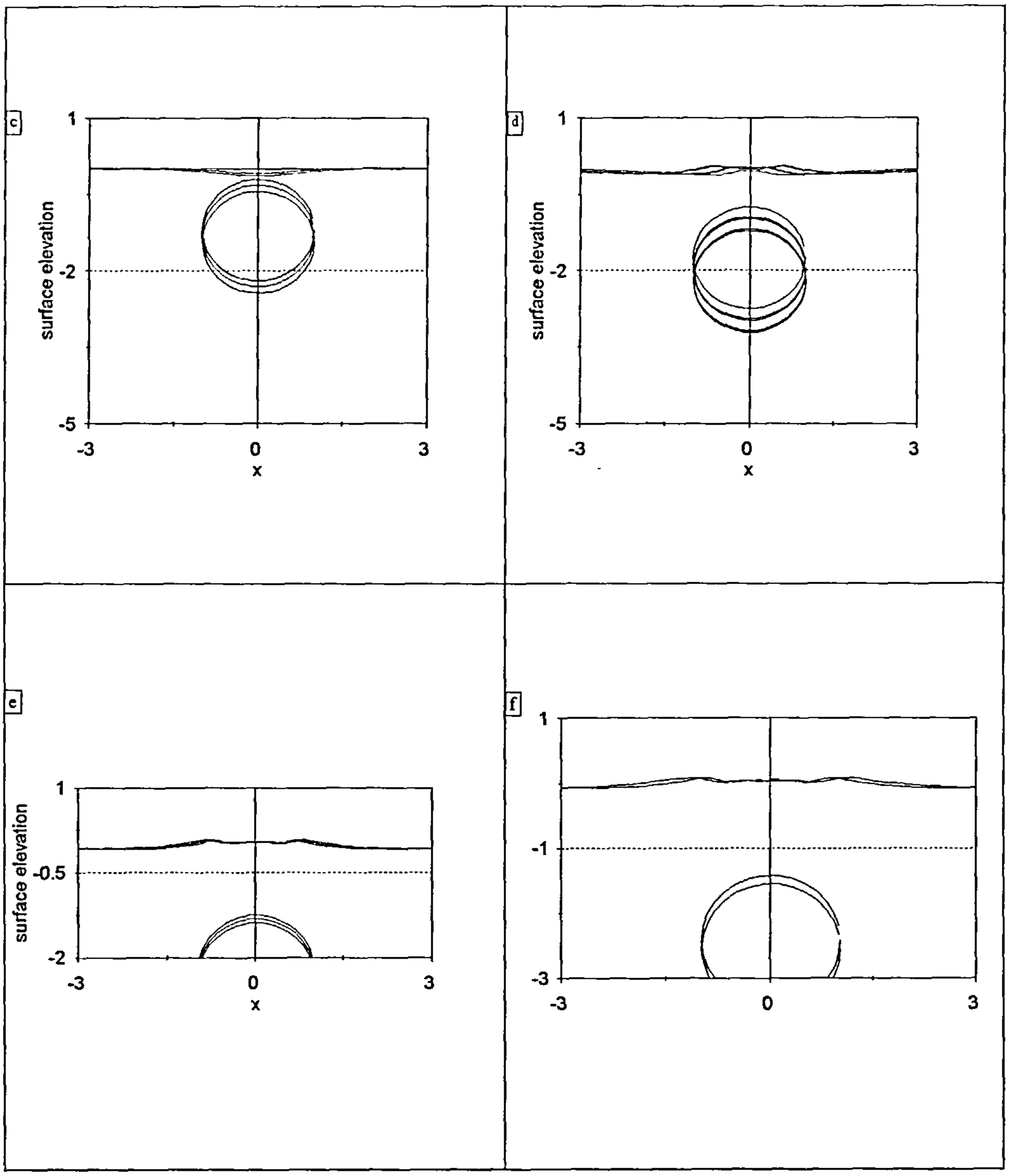

Fig. 3.13 Free-surface elevation and cylinder position due to the vertical motion of a cylinder initially displaced to (0,-1.2a) from its equilibrium position (0,-2.2a). Mb=1.0 and R=1/30.

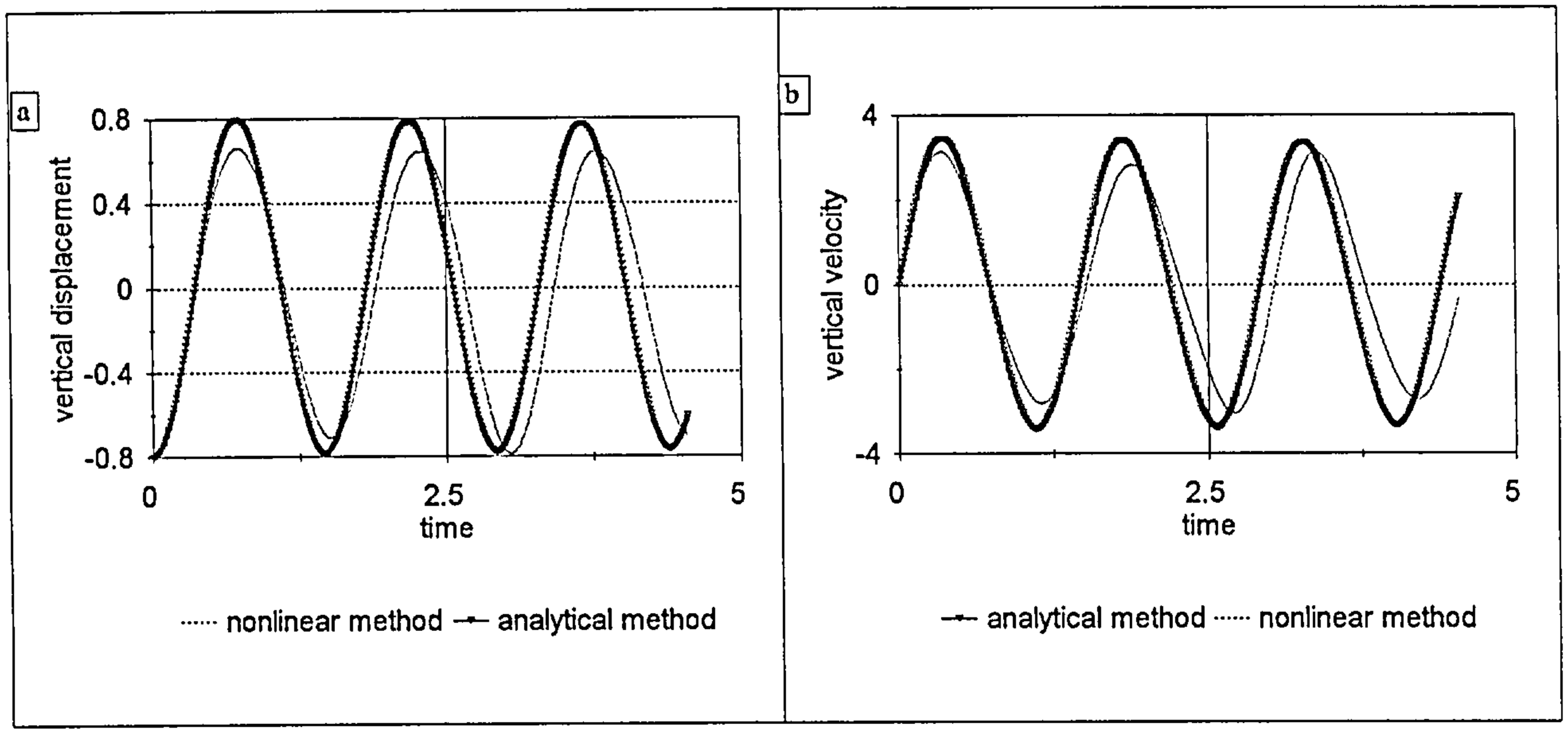

Fig3.14(i) Vertical motion of a cylinder initially displaced to (0,-3a) from (0,-2.2a) its equilibrium position. Mb=1 and R=1/30.

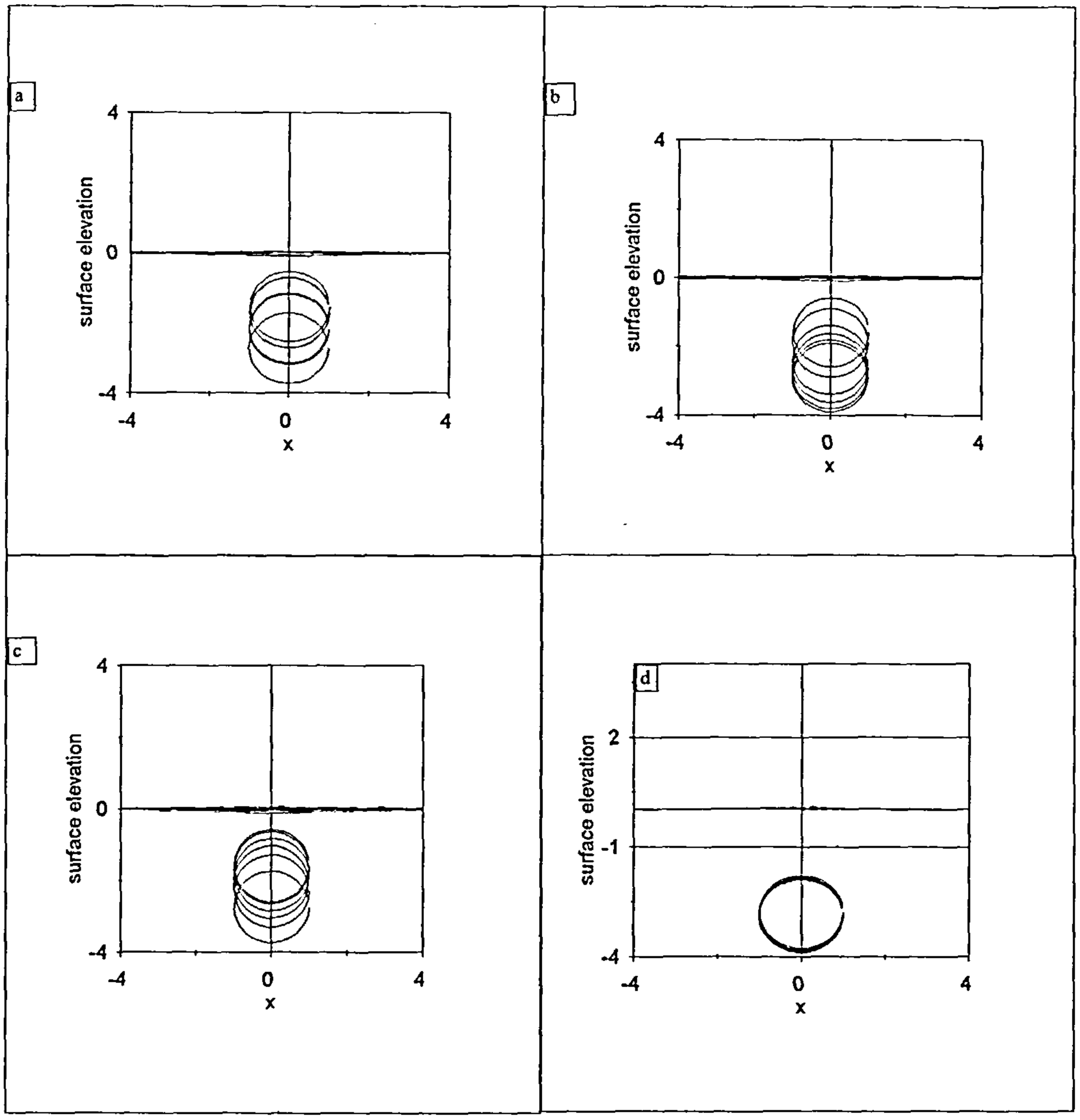

Fig. 3.14(ii) Free-surface elevation and cylinder position due to the transient motion of a cylinder initially displaced to (0,-3a) from (0,-2.2a) its equilibrium position below the surface. Mb=1 and R=1/30.

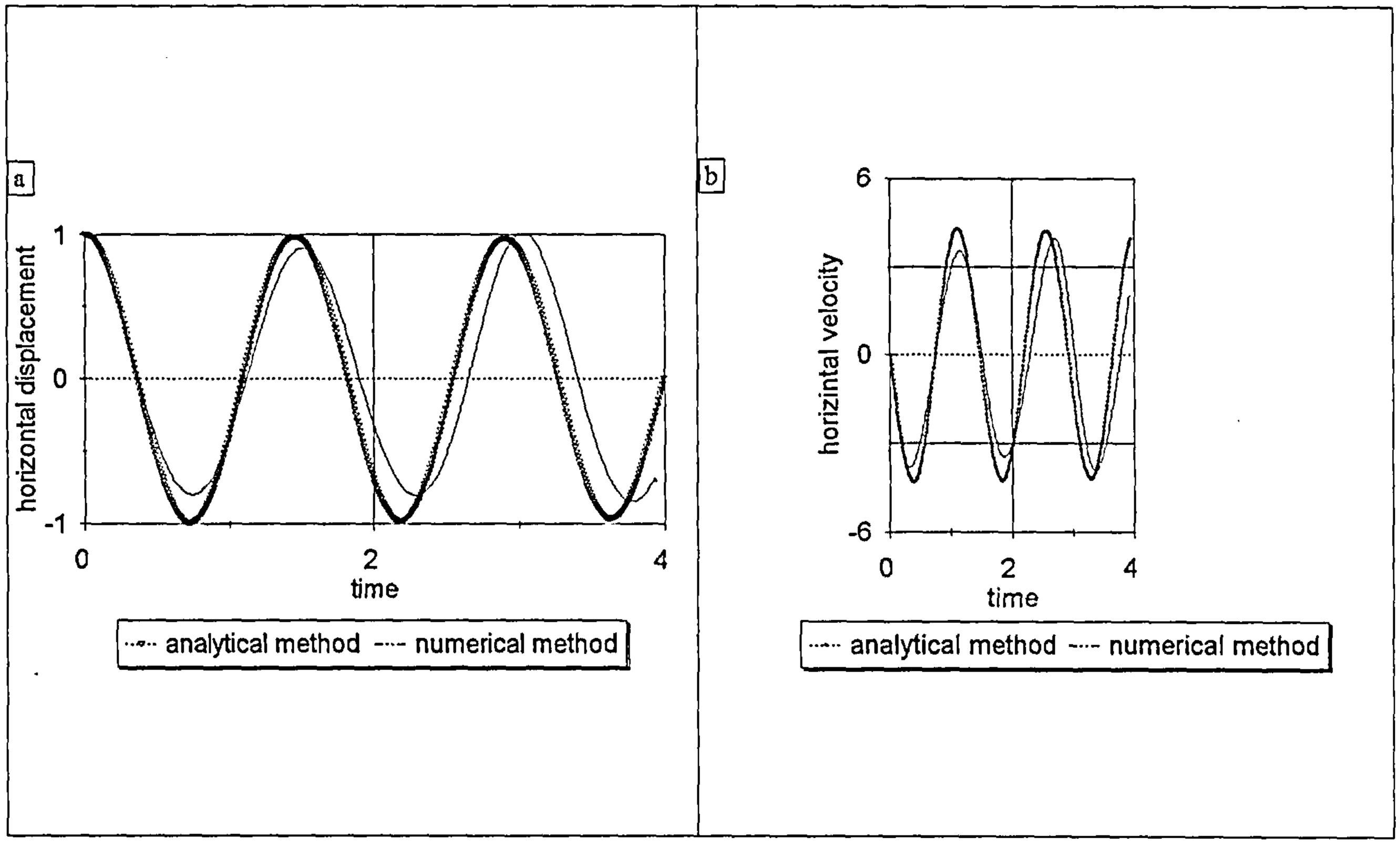

Fig. 3.15 Horizontal motion of a cylinder initially displaced to (a,-2.2a) from its equilibrium position (0,-2.2a). Mb=1.0 and R=1/30.

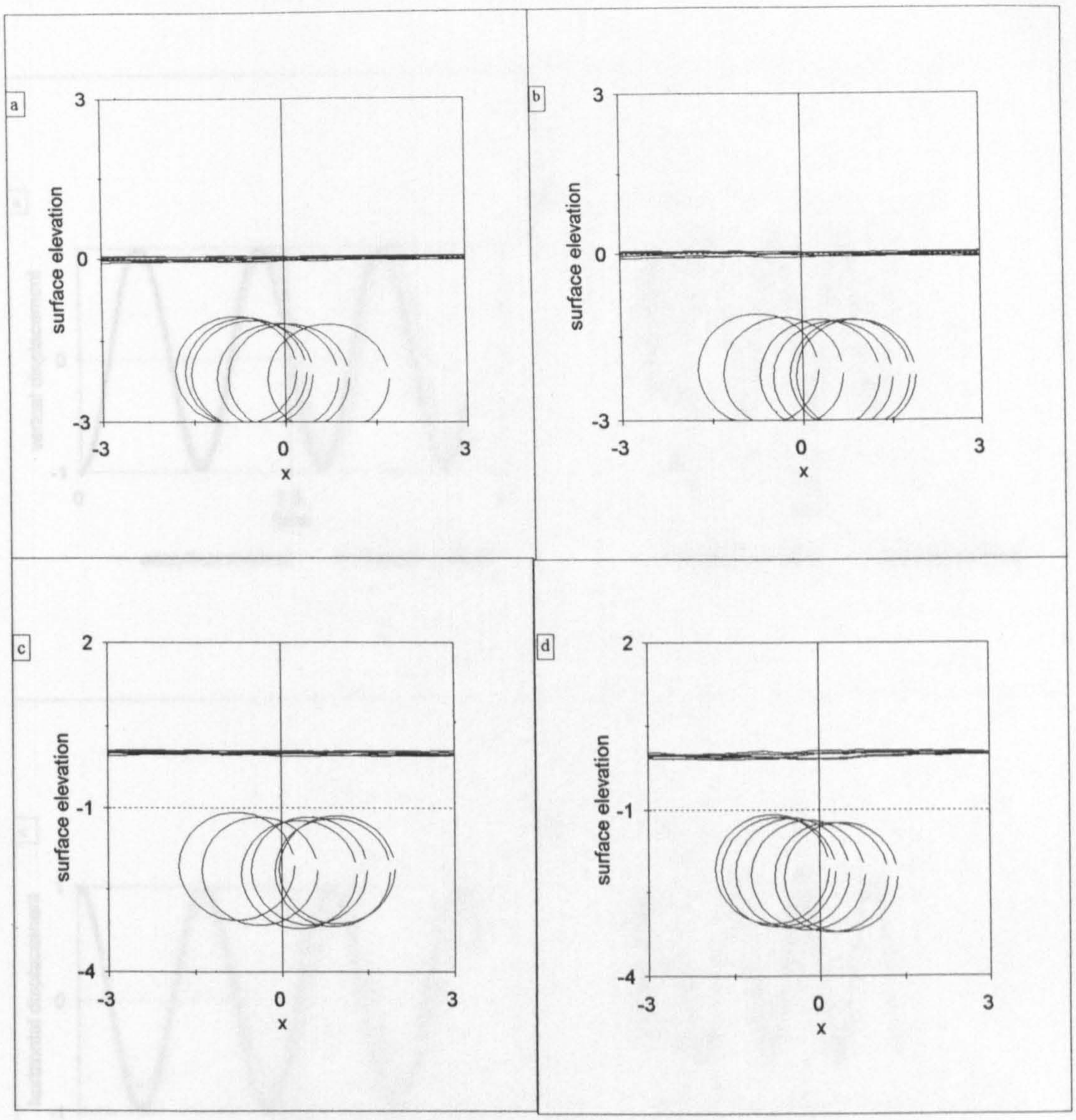

Fig. 3.16 Free-surface elevations due to the transient motion of a cylinder initially displaced to (a,-2.2a) from (0,-2.2a) its equilibrium position below the surface. Mb=1.0 and R=1/30.

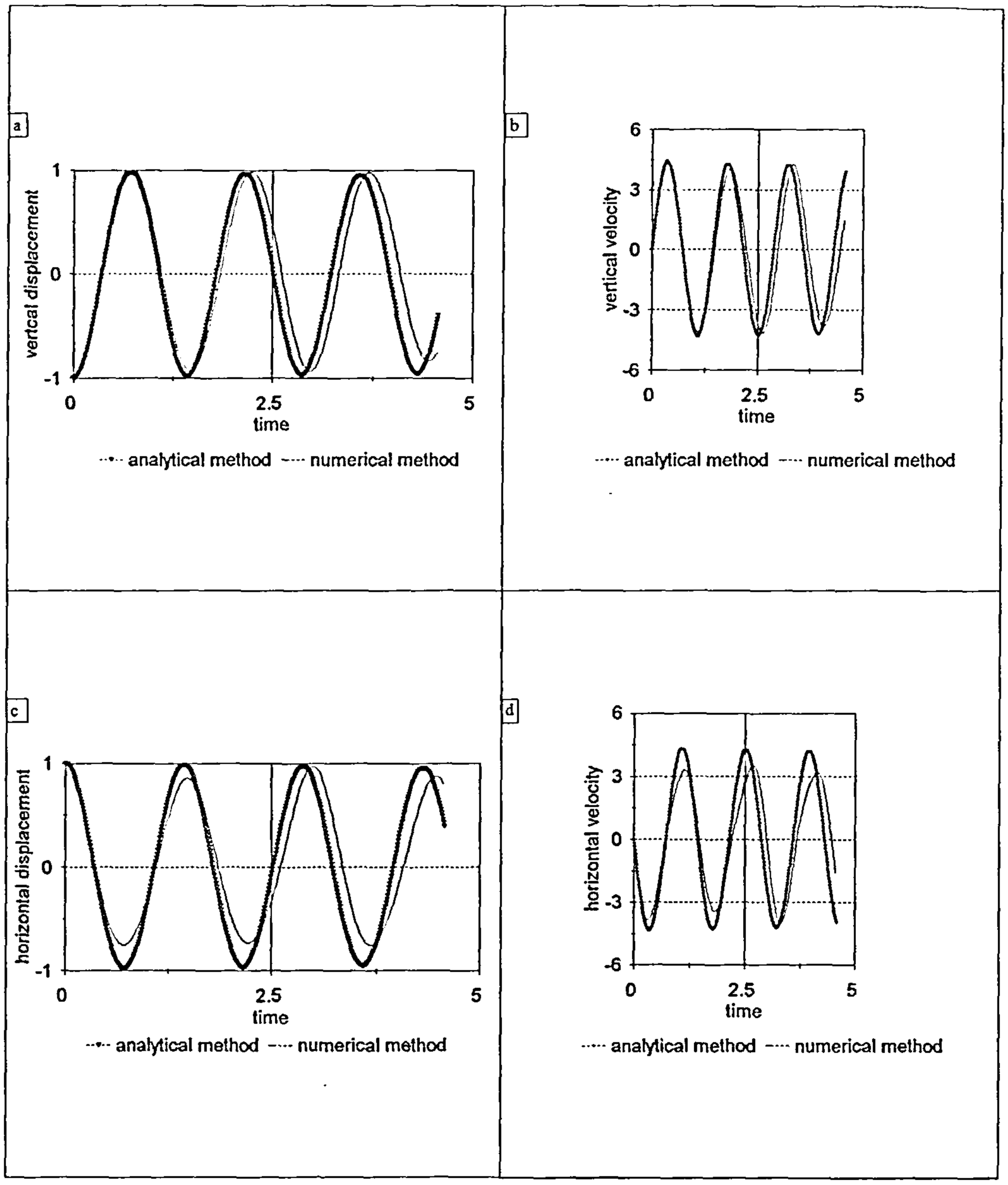

Fig. 3.17 Oblique motion of a cylinder initially displaced to (a,-4a) from (0,-3a) its equilibrium position. Mb=1.0 and R=1/30.

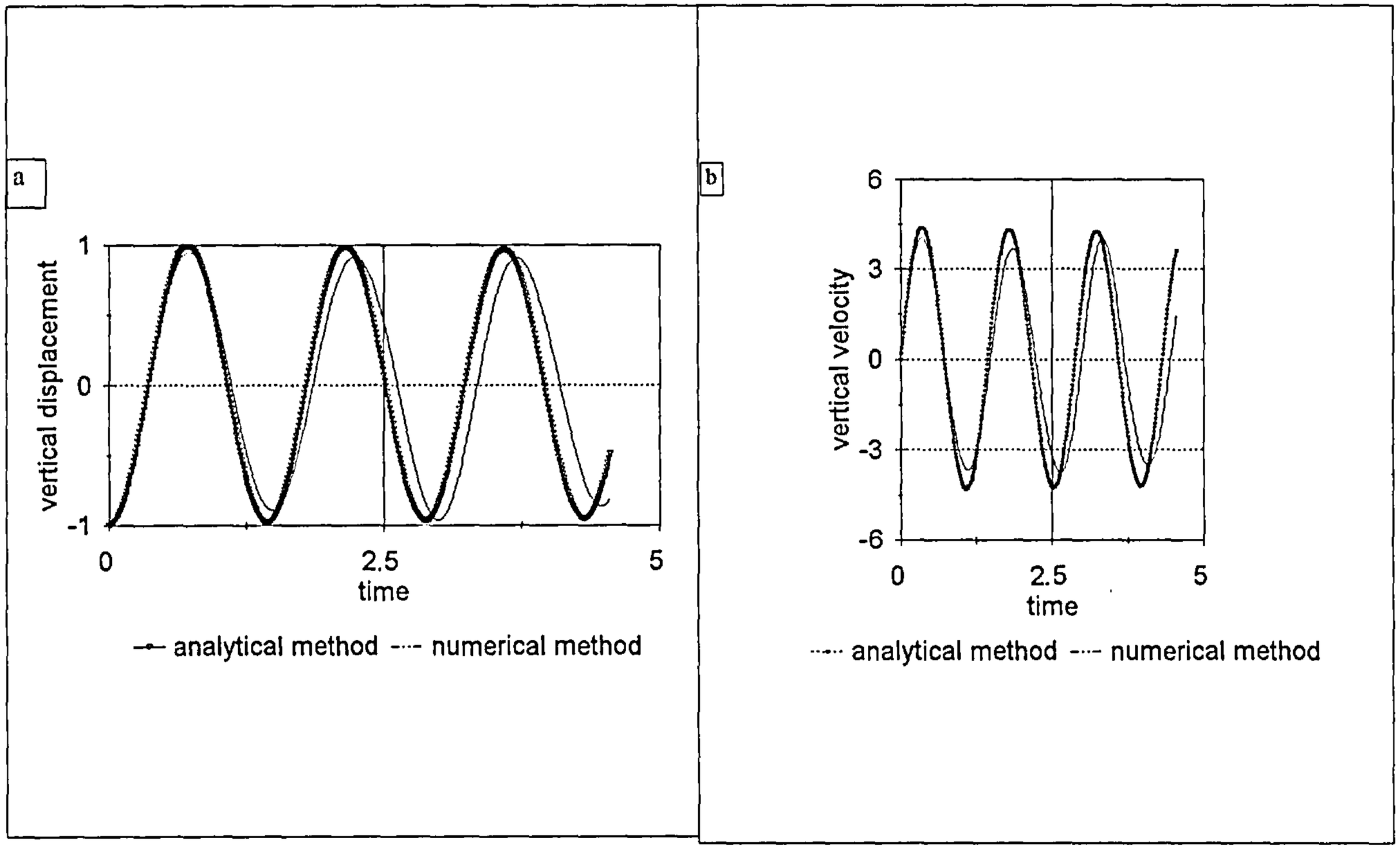

Fig. 3.18 vertical motion of a cylinder initially displaced to (0,-4a) from (0,-3a) its equilibrium position below the surface. Mb=1.0 and R=1/30.

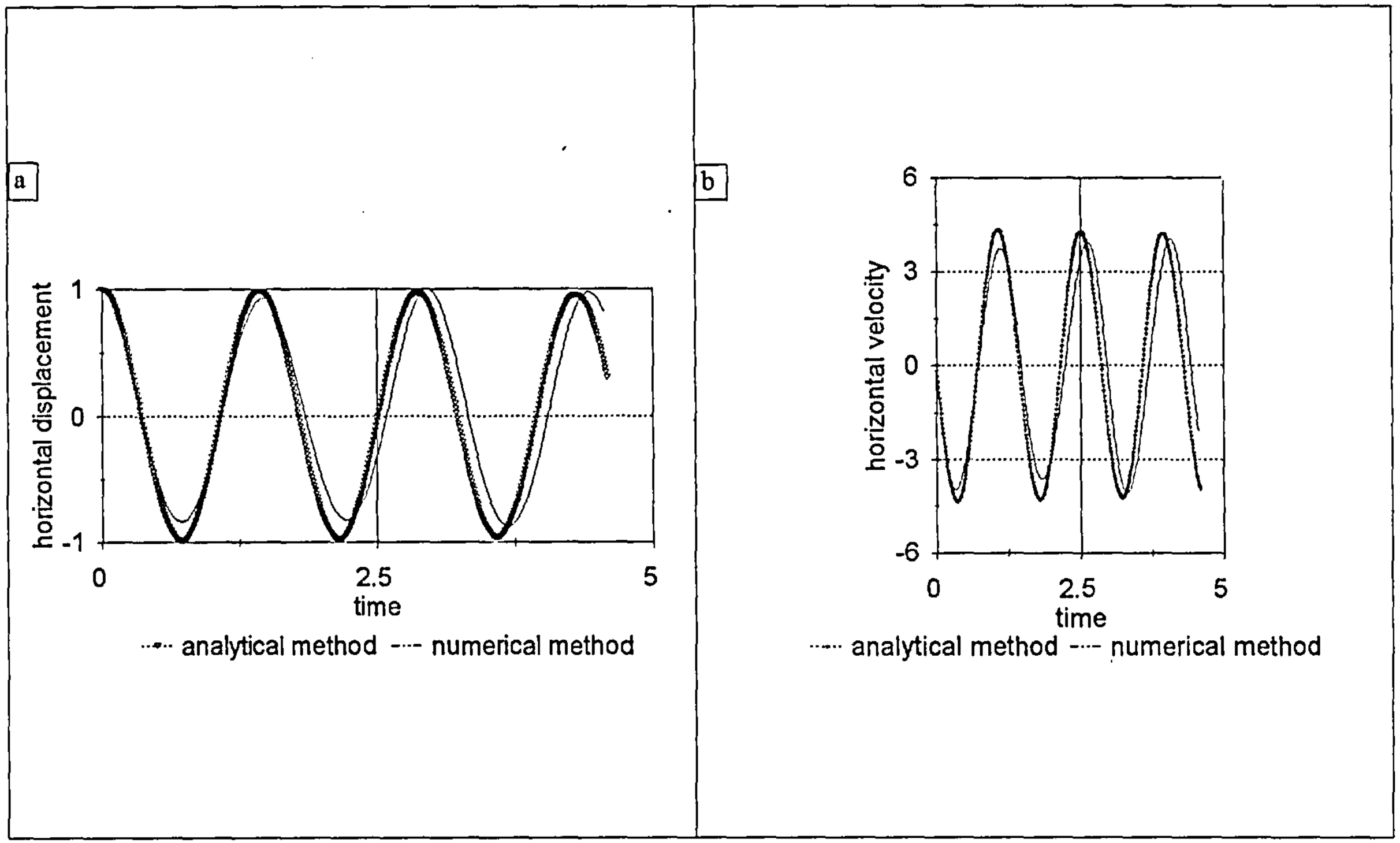

Fig. 3.19 Horizontal motion of a cylinder initially displaced to (a,-3a) from (0,-3a) its equilibrium position below the surface. Mb=1.0 and R=1/30.

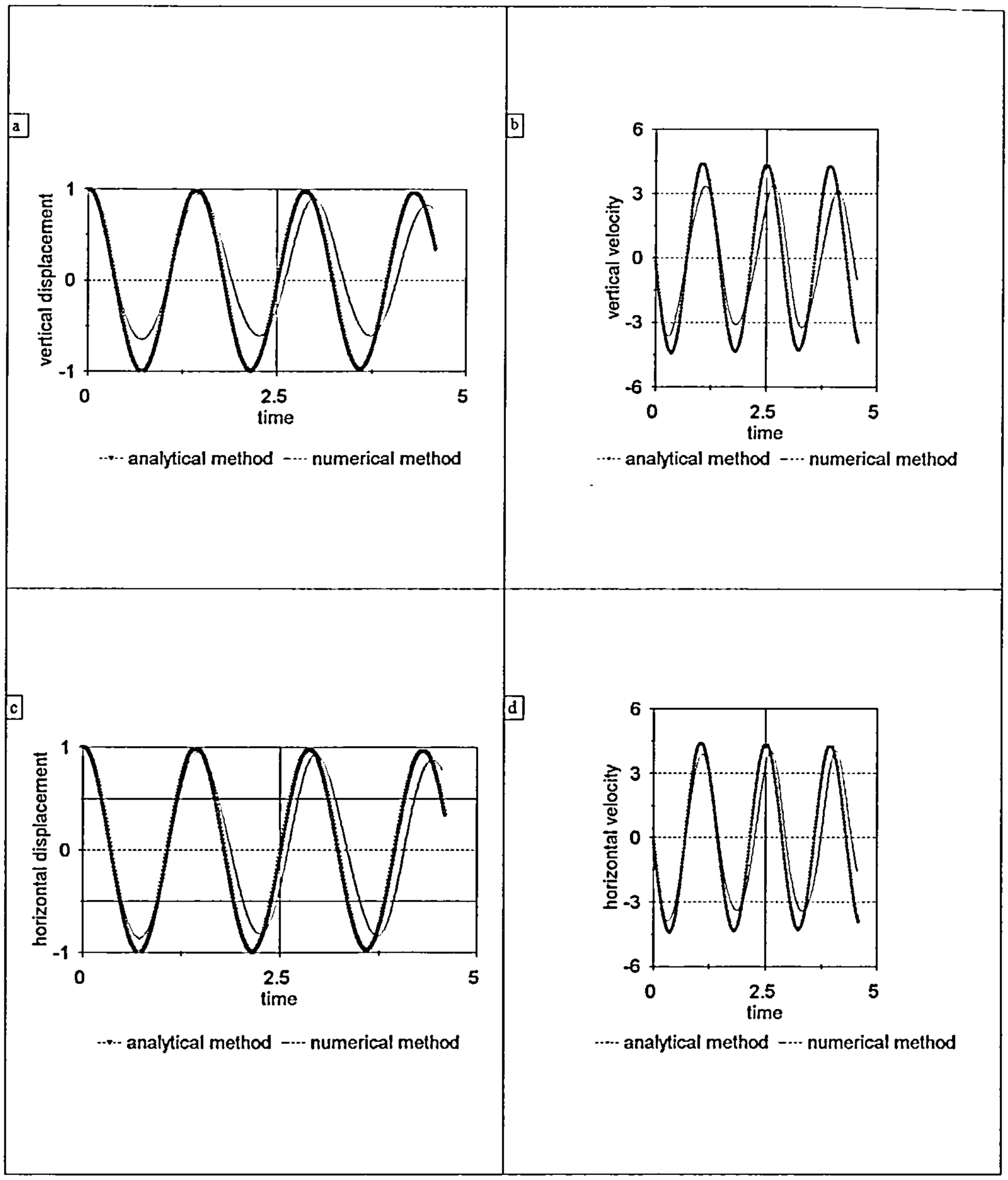

Fig. 3.20 Oblique motion of a cylinder initially displaced to (a,-2a) from (0,-3a) its equilibrium position below the surface. Mb=1.0 and R=1/30.

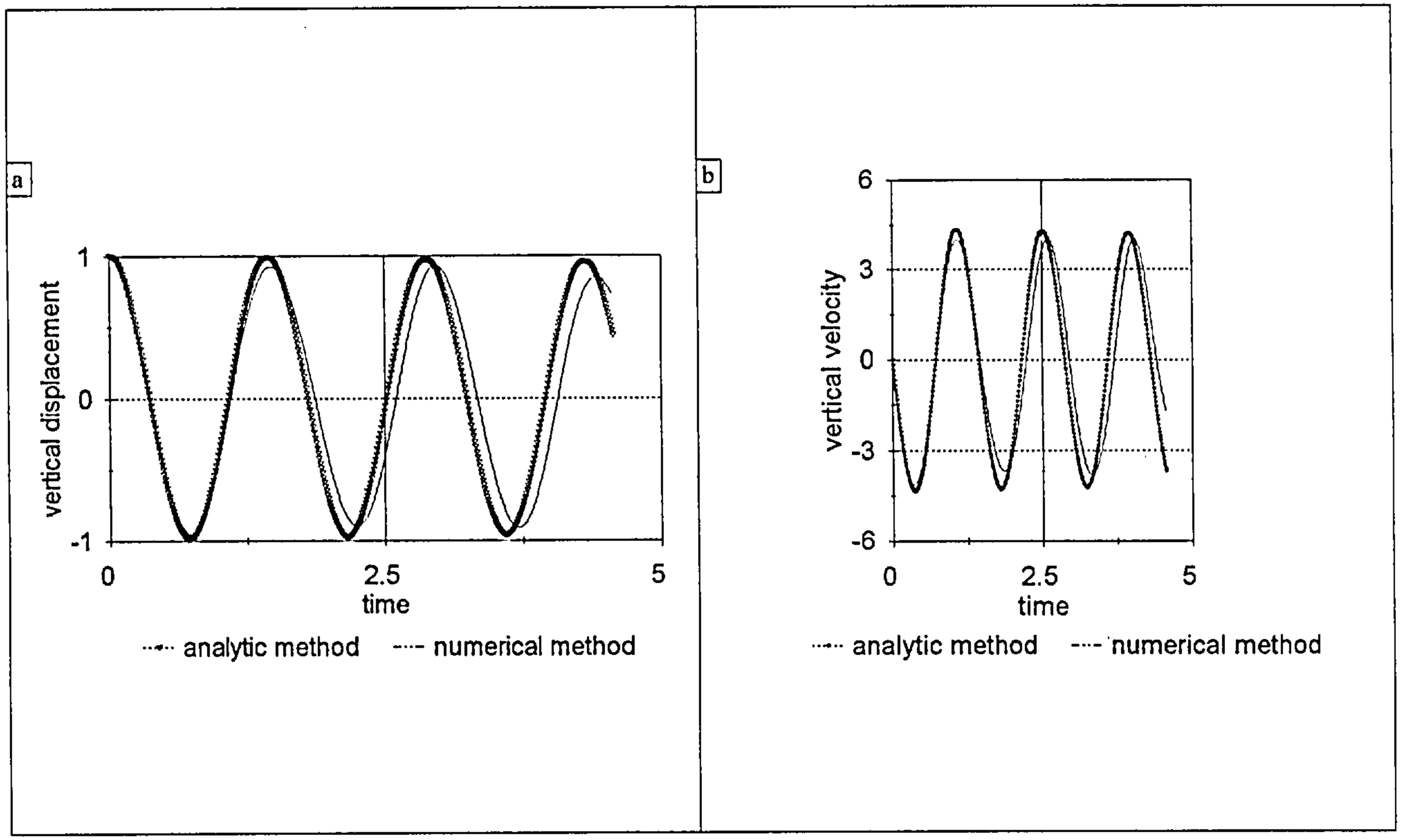

Fig. 3.21 vertical motion of a cylinder initially displaced to (0,-2a) from (0,-3a) its equilibrium position below the surface. Mb=1.0 and R=1/30.

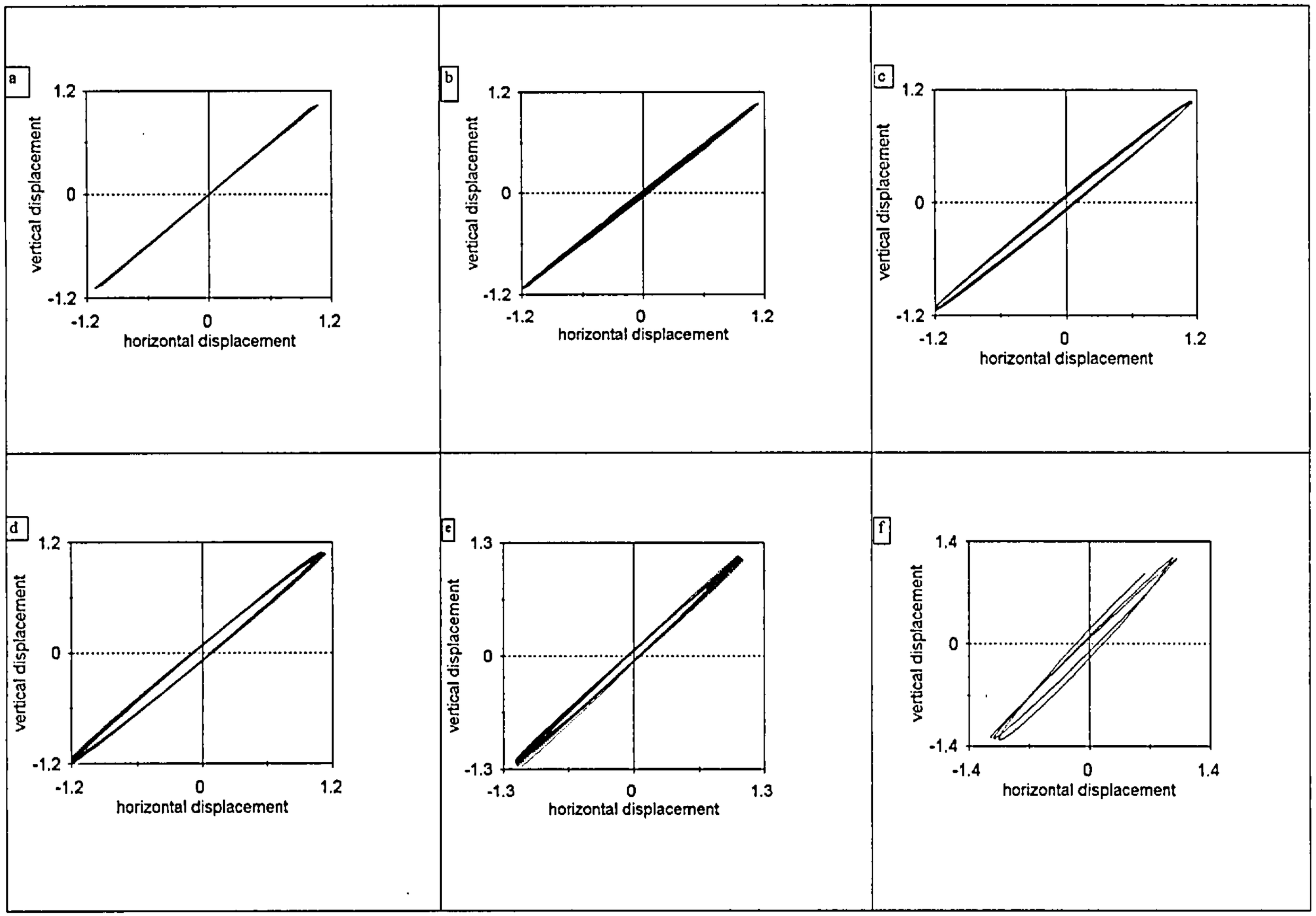

Fig. 3.22 Undamped motion of a cylinder initially displaced to(a,-1.2a) from (0,-2.2a) its equilibrium position using the analytic method. Mb=1 and R=1/15.

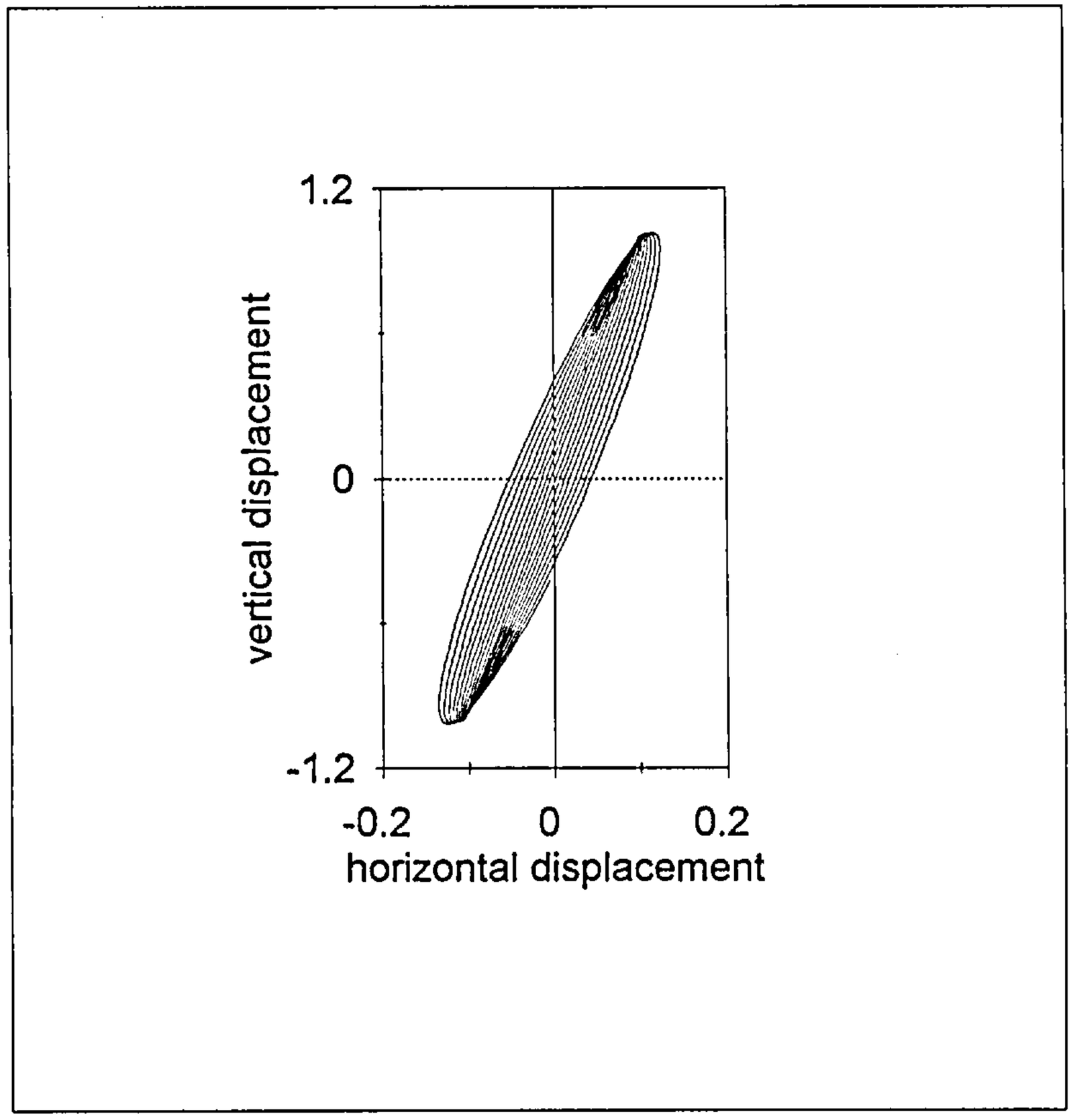

Fig. 3.23 Undamped motion of a cylinder initially displaced to (0.1a,-1.2a) from (0,-2.2a) its equilibrium position below the surface using the analytic method. Mb=1.0 and R=1/15.

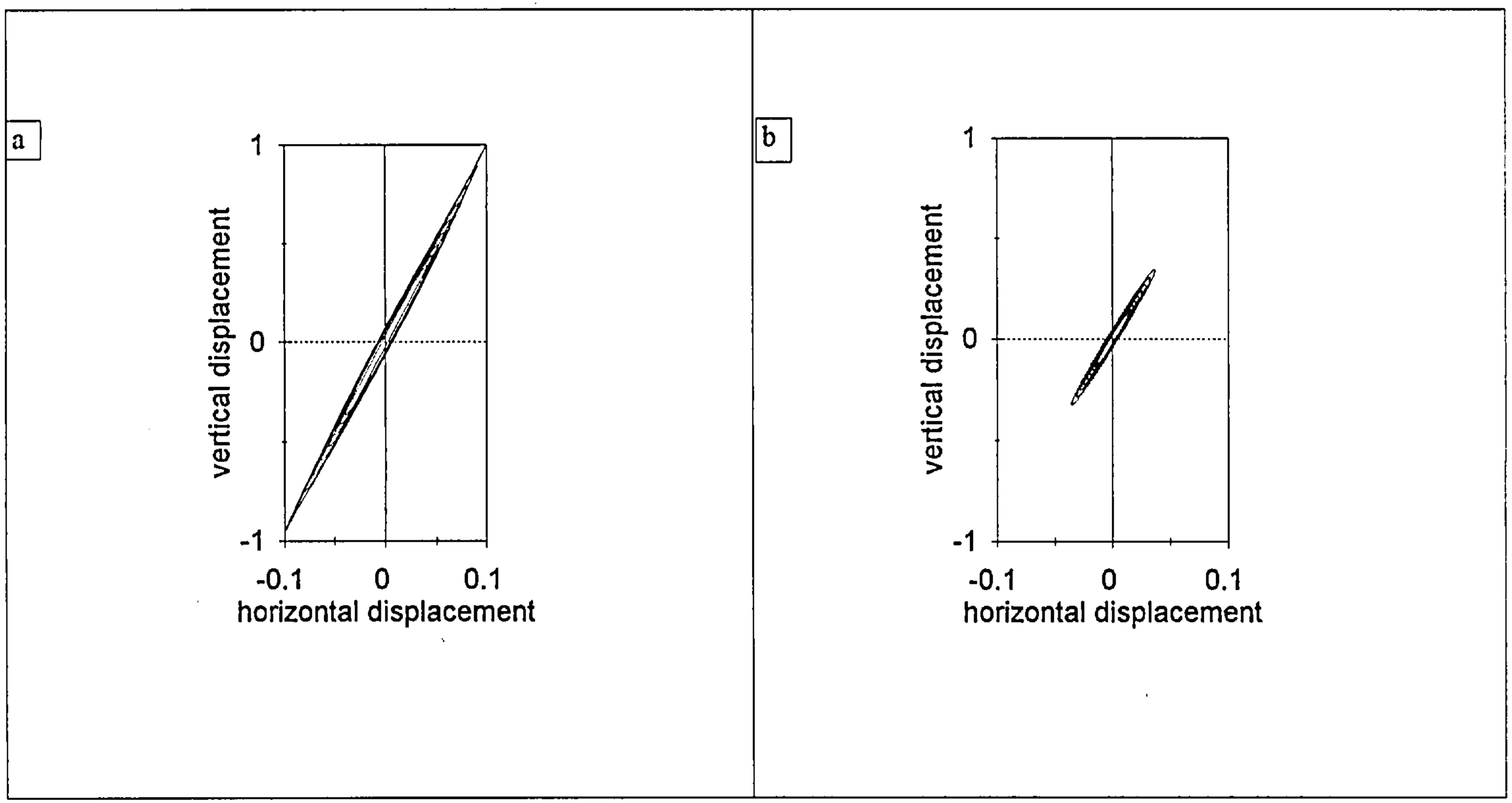

Fig. 3.24 Damped motion of a cylinder initially displaced to (0.1a,-1.2a) from (0,-2.2a) its equilibrium position using the analytical method. Mb=1.0 and R=1/15.

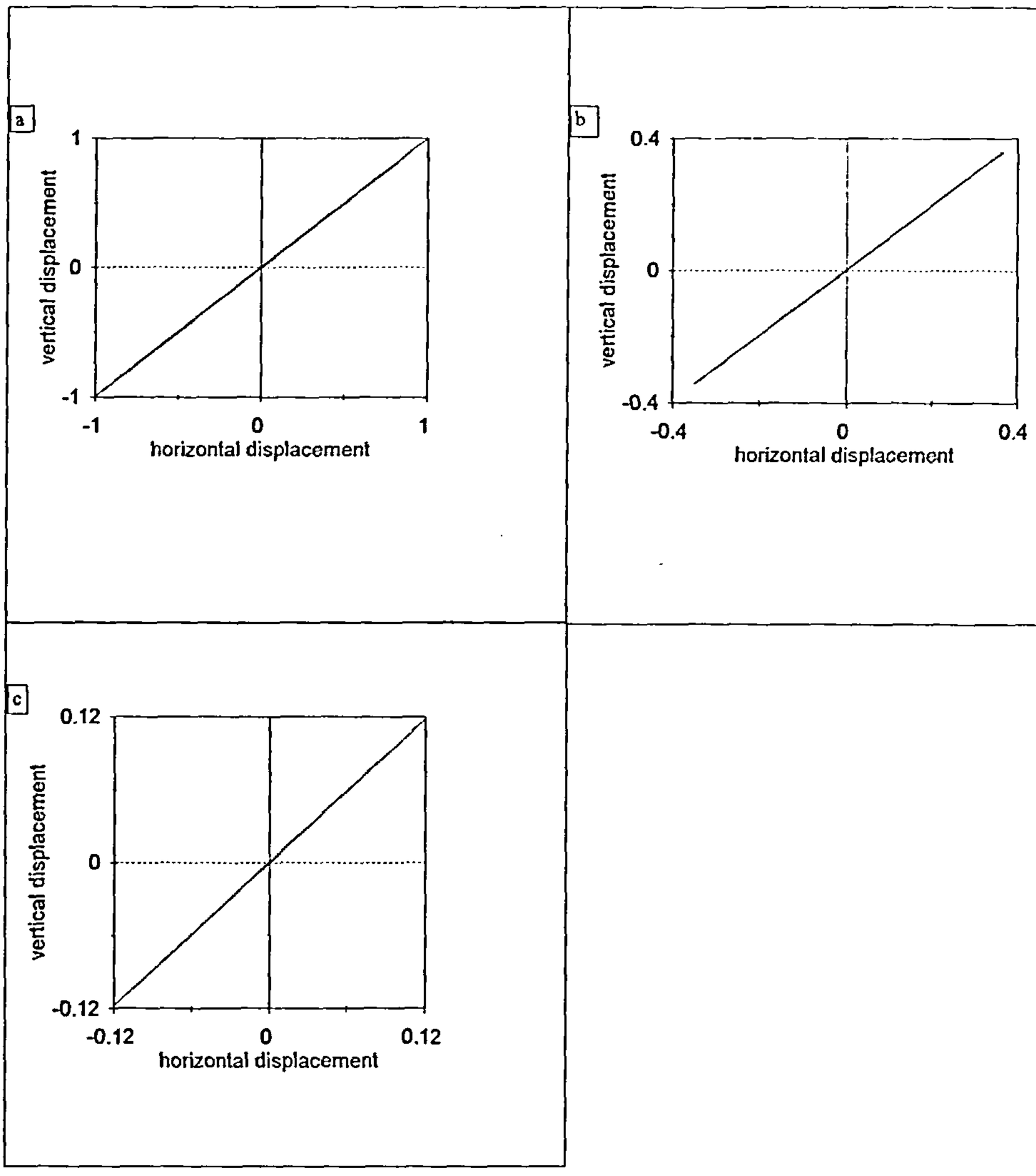

Fig. 3.25 Damped motion of a cylinder initially displaced to (a,-1.2a) from its equilibrium position (0,-2.2a) below the surface using the analytical method. Mb=1.0 and R=1/15.

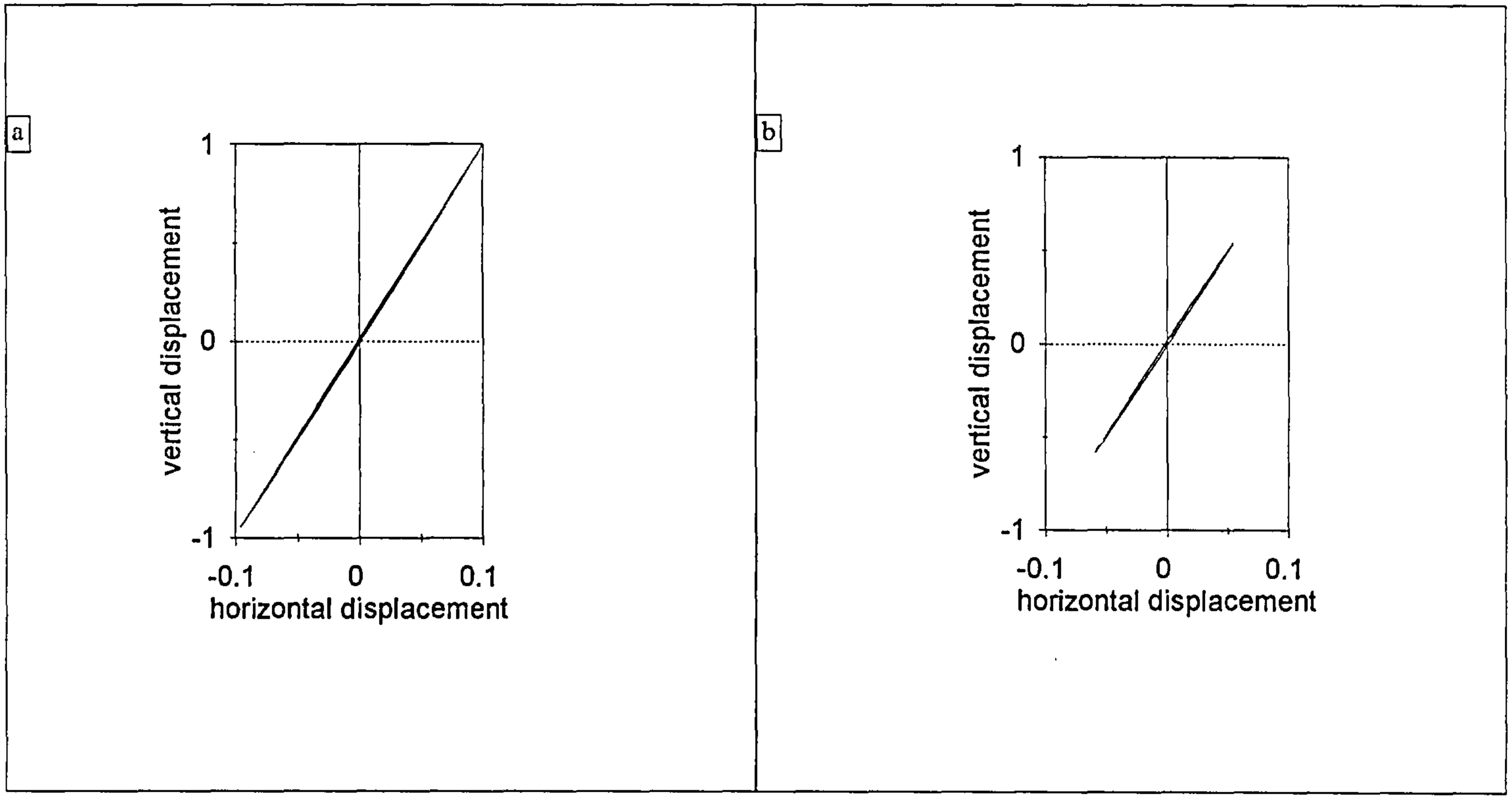

Fig. 3.26 Damped motion of a cylinder initially displaced to (0.1a,-2a) from (0,-3a) its equilibrium position below the surface using the analytic method. Mb=1.0 and R=1/15.

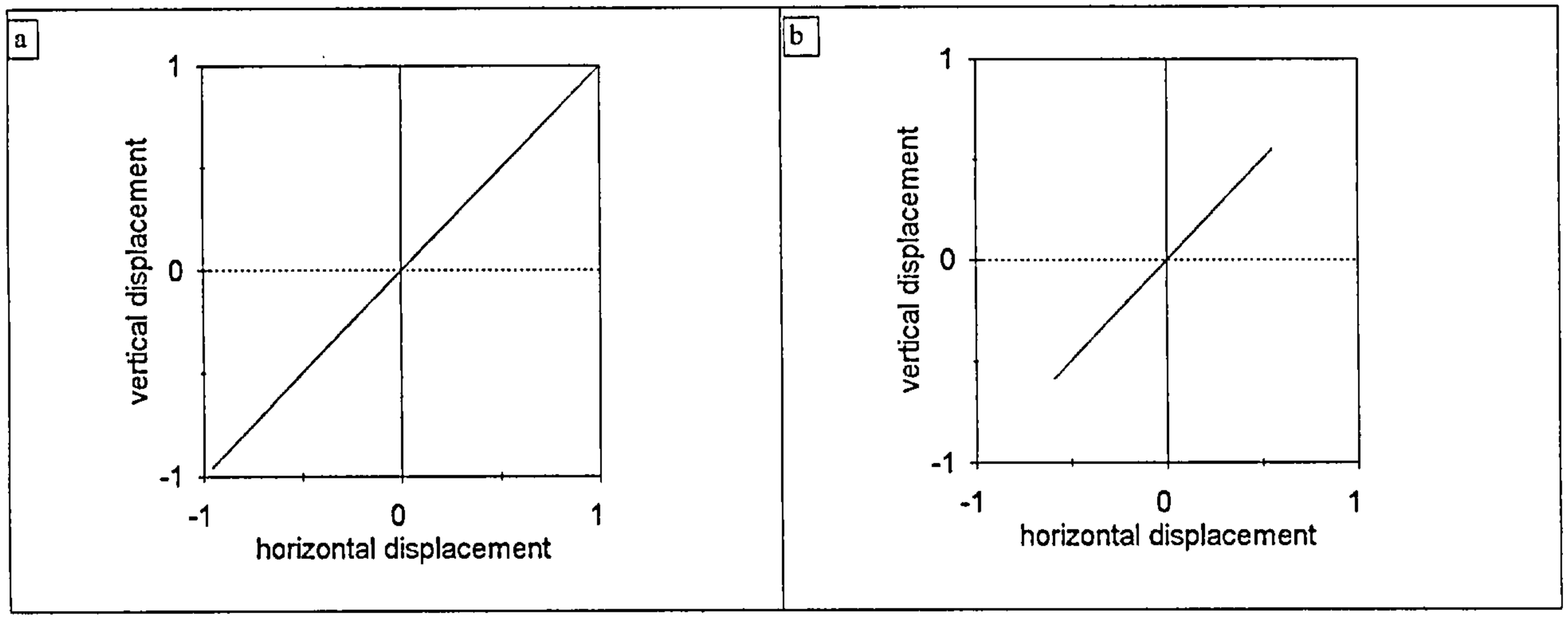

Fig. 3.27 Damped motion of a cylinder initially displaced to (a,-2a) from (0,-3a) its equilibrium position below the surface using the analytic method. Mb=1.0 and R=1/15.

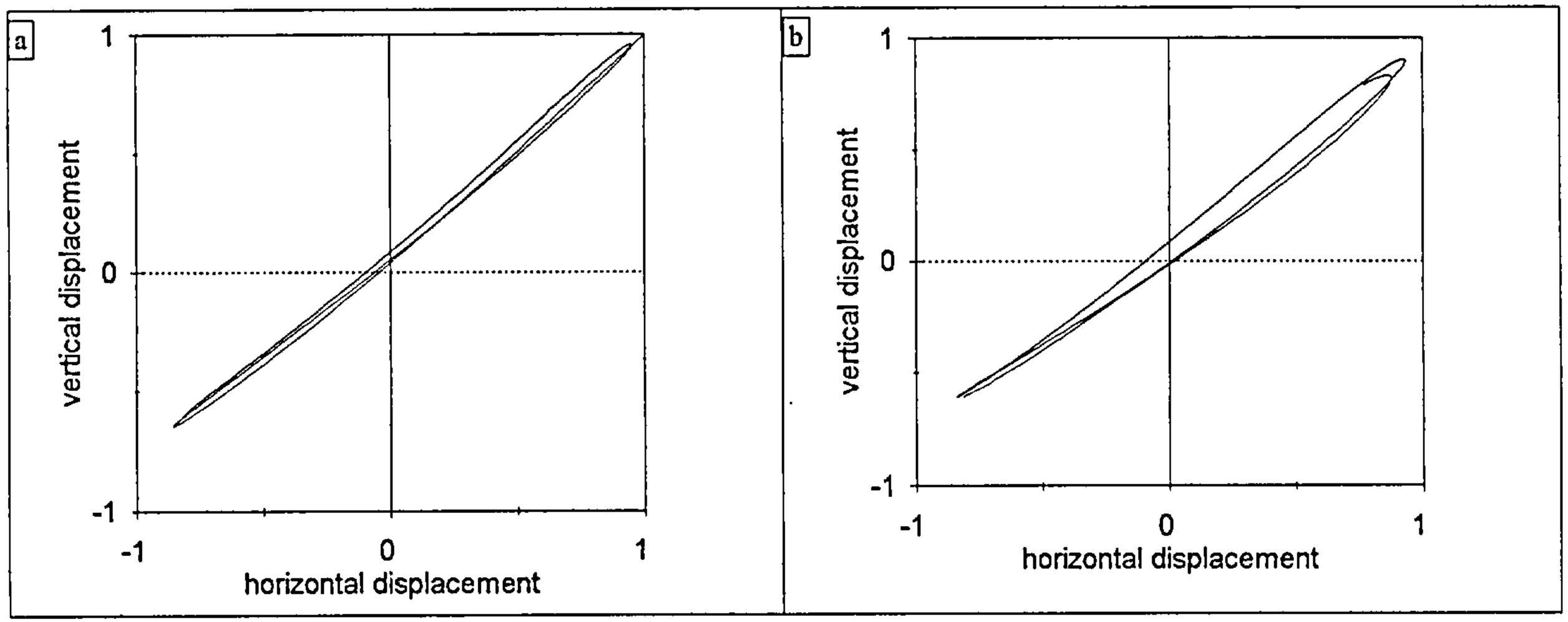

Fig. 3.28 Motion of a cylinder initially displaced to (a,-2a) from (0,-3a) its equilibrium position below the surface using the nonlinear method. Mb=1.0 and R=1/15.

Chapter 4

Small-time asymptotic solution

4.1 Introduction

In a series of papers, Havelock (1909-1949) introduced the problem of the impulsively started motion of a cylinder, with constant velocity or constant acceleration. The solution of the linear, but time-dependent, free surface/body interaction contains explicit memory terms resulting from radiated waves. This work was later on extended to cover nonlinear problems, for example the problem of a submerged dipole based on nonlinear theory was done by Tuck (1965) as a continuation of Havelock's work to second order in the expansion of the free surface boundary condition with wave steepness as the parameter.

In a separate approach, Tyvand & Miloh (1995) applied a method of small-time expansions, valid only for a short time. We consider this approach here, together with the numerical scheme for the fully nonlinear initial boundary value problem, studied earlier analytically by Peregrine (1972), and numerically by Vinje & Brevig (1981), and Greenhow and Lin (1983) . Work of Brevig et al (1981), Greenhow (1987), Telste (1986), Hepworth (1991) and Greenhow (1994) is extended and improved with a view to compare the results obtained through this method with the results of the small time asymptotic method.

The discussions that follow are concerned with the behaviour of the unsteady free surface caused by the forced motion of a cylinder in vertical, horizontal and sideways directions. The results obtained using the small time expansion method of Tyvand & Miloh, are verified by the results of the fully nonlinear numerical scheme of Brevig et al (1981). A range of surface elevations for cylinders of different sizes and different Froude numbers are shown for the two methods. The time duration and Froude numbers for which the two methods agree are highlighted, giving useful information on how small time has to be in the small time expansion method. Beyond this time significant differences appear; indeed the small time expansion method ultimately becomes topologically impossible, whereas the nonlinear numerical method may be continued until the free surface breaks, a physical phenomenon first explained by Greenhow (1987), and photographed by Greenhow & Lin (1983).

4.2 The method of Tyvand & Miloh (1995)

In developing the small-time asymtotic method, Tyvand and Miloh consider a solid circular cylinder of radius a submerged in an inviscid fluid of infinite depth. This section describes their work, and is here included for completeness. Initially the cylinder is at rest and is located at a distance d below the free surface of the fluid. We obtain the surface elevations ζ using the formulae of Tyvand & Miloh, and compare them with those of the nonlinear numerical method. The dimensionless time and cylinder radius are given as $T = \frac{U}{d}t$ and $\epsilon = \frac{a}{d}$ respectively. ρU^2 is the unit of dimensionless pressure.

Based on the assumptions of the potential theory, the continuity equation

implies that the fluid motion is governed by Laplace's equation

$$\nabla^2\Phi = 0 \qquad (1)$$

where Φ is the dimensionless velocity potential. The dimensionless boundary conditions are prescribed as

$$\frac{D}{Dt}(y_p - \zeta(x_p, t)) = 0 \qquad (2)$$

or

$$\frac{\partial\zeta}{\partial t} + \frac{\partial\Phi}{\partial x_p}\frac{\partial\zeta}{\partial x_p} = \frac{\partial\Phi}{\partial y_p}, \quad y_p = \zeta(x_p, t) \qquad (3)$$

the kinematic condition on the free surface,

$$\frac{\partial\Phi}{\partial t} + \frac{1}{2}(\nabla\Phi)^2 + Fr^{-2}\zeta = 0, \quad y_p = \zeta(x_p, t) \qquad (4)$$

the dynamic boundary condition based on Bernoulli's equation on the free surface,

$$|\nabla\Phi| = 0, \quad r_p \to \infty \qquad (5)$$

on the far field and

$$(\vec{r_p} - \vec{r}).(\nabla\Phi - \dot{\vec{r}}) = 0, \quad |\vec{r_p} - \vec{r}| = \epsilon \qquad (6)$$

on the body surface, where $\vec{r_p} = x_p\mathbf{i} + \mathbf{y_p}\mathbf{j}$ is the position vector of a fluid particle, $\vec{r} = x\mathbf{i}+\mathbf{y}\mathbf{j}$ is the position vector of the centre of the cylinder prescribed by the motion of the cylinder and, $\mathbf{i}$ and $\mathbf{j}$ are unit vectors in x- and y-directions.

Initially(t=0)

$$\zeta(x_p, 0) = 0 \qquad (7)$$

$$\Phi(x_p, 0, 0) = 0 \qquad (8)$$

The hydrodynamic pressure P can be obtained from the Bernoulli's equation.

Thus in conjunction with the dynamic boundary condition

$$P = -(\frac{\partial \Phi}{\partial t} + \frac{1}{2} \mid \nabla \Phi \mid^2 + Fr^{-2} y_p) \qquad (9)$$

The units of dimensionless mass, force and momentum are ρd^2, $\rho d U^2$ and $\rho d^2 U$ respectively.

The equations (4.1)-(4.8) are therefore solved analytically using a small-time expansion technique. The following results are obtained

$$\Phi = H(t)[\Phi_0 + t\Phi_1 + t^2\Phi_2 + t^3\Phi_3 + ...], \quad -\infty < t < \infty, \qquad (10)$$

the velocity potential at the free surface

$$\zeta(x_p, T) = H(t)[\zeta_0(x_p, T) + t\zeta_1(x_p, T) + t^2\zeta_2(x_p, T) + t^3\zeta_3(x_p, T) + ...] \quad (11)$$

the free surface elevation and

$$\vec{r}(x, y) = \vec{r_0}(x_0, y_0) + H(t)[t\vec{r_1}(x_1, y_1) + t^2\vec{r_2}(x_2, y_2) + t^3\vec{r_3}(x_3, y_3) + ...] \quad (12)$$

for the position of the centre of the cylinder, where Φ_n and ζ_n are unknown functions, $H(t)$ is the Heaviside unit step function defined as $H(t) = 0$, $t \leq 0$ and $H(t) = 1$, $t > 0$ and $\vec{r_n}(x_n, y_n) = x_n \mathbf{i} + \mathbf{y_n j}$ (n=0,1,2,3,.....) is the instantaneous position of the cylinder centre. In particular $r_0 = (0, d)$.

The above expansions of the velocity potential give Laplace's equation in the form

$$\nabla^2 \Phi_n = 0, \quad y < 0 \quad and \quad (x_p)^2 + (y - d)^2 > \epsilon^2 \qquad (13)$$

i.e the potental to each order in the initial fluid domain and the corresponding far-field conditions in the form

$$\mid \nabla \Phi_n \mid \rightarrow 0, \quad (x_p)^2 + (y_p)^2 \rightarrow \infty \quad (n = 0, 1, 2, 3, ...) \qquad (14)$$

The total time differential operator

$$\frac{d}{dt} = \frac{\partial}{\partial t} + \frac{\partial \zeta}{\partial t}\frac{\partial}{\partial y_p} \qquad (15)$$

is then applied recursively on equations (4.3) and (4.4) at $t = 0$ (see Tyvand and Miloh(1995) for details of the application of this operator) to give the following dynamic conditions

$$\Phi_0 = 0 \qquad , y_p = 0 \qquad (16)$$

$$\Phi_1 = -\frac{1}{2}\zeta_1^2 \qquad , y_p = 0 \qquad (17)$$

$$\Phi_2 = -\zeta_1(2\zeta_2 + \frac{Fr^-2}{2}) \qquad , y_p = 0 \qquad (18)$$

at the dynamic free surface. The corresponding kinematic conditions are:

$$\zeta_1 = \frac{\partial \Phi_0}{\partial y} \qquad , y_p = 0 \qquad (19)$$

$$\zeta_2 = \frac{1}{2}\frac{\partial \Phi_1}{\partial y_p} \qquad , y_p = 0 \qquad (20)$$

$$\zeta_3 = \frac{1}{3}\frac{\partial \Phi_2}{\partial y_p} + \frac{1}{6}\zeta_1^2\zeta_1''(x_p, T) + \frac{1}{3}\zeta_1(\zeta_1'(x_p, T))^2 \qquad , y_p = 0 \qquad (21)$$

To expand the the exact boundary condition at the body surface the polar coordinates (τ, Θ) are introduced such that $(x_p, y_p - d) = \tau(\sin\Theta, \cos\Theta)$, where $-\pi \leq \Theta < \pi$. Applying the total time differential operator

$$\frac{d}{dt} = \frac{\partial}{\partial t} + \dot{\vec{r}}.\nabla \qquad (22)$$

and substituting the expansion (2.3) for Φ when $t = 0$ produces the required boundary condition at each order, i.e

$$\frac{\partial \Phi_0}{\partial \tau} = \vec{r_1}.\dot{\vec{i_\tau}} \qquad , \tau = \epsilon \qquad (23)$$

the zeroth order,

$$\frac{\partial \Phi_1}{\partial \tau} = 2\vec{r_2}.\dot{\vec{i_\tau}} - \dot{\vec{i_\tau}}.\nabla(r_1.\vec{\nabla}\Phi_0) \quad \tau = \epsilon \qquad (24)$$

the first order,

$$\frac{\partial \Phi_2(Fr)}{\partial \tau} = 0 \quad , \tau = \epsilon \tag{25}$$

the second order and

$$\frac{\partial \Phi_3}{\partial \tau} = -\frac{2}{3}\vec{i_\tau}.\nabla(\vec{r_2}.\nabla\Phi_1) \quad , \tau = \epsilon \tag{26}$$

the third order which has a gravity dependent right-hand side, where

$$\vec{i_\tau} = i\sin\Theta + j\cos\Theta \quad .$$

is the radial unit vector.

The potential is split and given as

$$\Phi_n = \phi_n + \psi_n \qquad (n = 1, 2, 3, ...) \tag{27}$$

where ϕ_n is due to non-homogeneous condition at the free surface with zero normal derivative on the body, and ψ_n is due to non-homogeneous condition on the body and homogeneous at the free surface. The hydrodynamic force is derived from Bernoulli's equation (4.9) by integrating pressure integral

$$\vec{F} = -\epsilon \int_{-\pi}^{\pi} P(\epsilon, \Theta)\vec{i_\tau} d\Theta \tag{28}$$

which gives

$$\vec{F} = \vec{F_{-1}}\delta(t) + (\vec{F_0} + \vec{F_1}t + \vec{F_2}t^2 + ...)H(t) \tag{29}$$

where $\delta(t)$ is Dirac's delta function.

Finally, the bipolar coordinates ξ and θ are introduced in which the transformation equations from Cartesian are

$$x_p = \frac{a\sin\theta}{\cosh\xi + \cos\theta} \quad -\pi < \theta < \pi, 0 < \xi < \xi_0 \tag{30}$$

$$y_p = -\frac{a\sinh\xi}{\cosh\xi + \cos\theta} \quad , -\pi < \theta < \pi, 0 < \xi < \xi_0 \tag{31}$$

where a is a dimensionless length, such that $(x, y) = (0, \pm a)$.

Through bipolar coordinates, the first order elevation, ζ_1, can be expressed as

$$\zeta_1 = 4\cos(\frac{\theta}{2}) \sum_{n=1}^{\infty} (-1)^{n+1} n e^{-n\xi_0} sech(n\xi_0) \sin(n\theta + \alpha) \qquad (32)$$

where θ=$2\arctan(\frac{x_p}{\tanh\xi_0})$, $y_p = 0$ and ξ_0= $arcsech(\epsilon)$.

The second-order free-surface elevation due to the free-surface nonlinearity is expressed as a contribution of the first-order potential, ϕ_1, in the form:

$$\begin{aligned}
\zeta_2^{\phi_1} &= \frac{1}{2}\frac{\partial \phi_1}{\partial y_p} \\
&= \frac{\cos(\frac{\theta^2}{2})}{16\tanh\xi_0} \sum_{n=1}^{\infty}\sum_{m=1}^{\infty} (-1)^{n+m} nm e^{-(n+m)\xi_0} sechn\xi_0 sechm\xi_0 \\
&\quad \sum_{k=-2}^{2} (24 - 9k^2 + k^4) \sum_{q=-1}^{1} q(n + qm + k) \cos((n + qm + k)\theta + (q+1)\alpha) \\
&\quad \tanh(n + mq + k)\xi_0 \quad , y_p = 0
\end{aligned} \qquad (33)$$

The second-order free-surface elevation due to geometric nonlinearity at the cylinder contour is given as a contribution of the first-order potential, ψ_1, and is expressed as:

$$\begin{aligned}
\zeta_2^{\psi_1} &= \frac{1}{2}\frac{\partial \psi_1}{\partial y_p} \\
&= -\sin(\alpha)\frac{cos^2(\frac{\theta}{2})}{\tanh(\xi_0)} \sum_{n=1}^{\infty} (-1)^n n e^{-n\xi_0} sech(n\xi_0((n-1)\sin((n-1)\theta - \alpha) \\
&\quad \tanh(n-1)\xi_0 + 2n\sin(n\theta + \alpha)\tanh(n\xi_0) + (n+1)\sin((n+1)\theta + \alpha) \\
&\quad \tanh(n+1)\xi_0) - \frac{2\cos(\alpha)}{\tanh(\xi_0) + (x_p)^2} \sum_{n=1}^{\infty} (-1)^n n e^{-n\xi_0} sech(n\xi_0) \\
&\quad [\sin(\theta)\sin(n\theta + \alpha) - 2n\cos^2(\frac{\theta}{2})\cos(n\theta + \alpha)]
\end{aligned} \qquad (34)$$

The third-order free-surface elevation due to the leading order gravitational effects is given as a contribution of the second-order potential, Φ_2, and is

expressed as:

$$\zeta_3^{Fr} = -\frac{\cos^2(\frac{\theta}{2})}{3Fr^2\tanh(\xi_0)}\sum_{n=1}^{\infty}\frac{(-1)^n n e^{-n\xi_0}}{\cosh(n\xi_0)}[(n-1)\sin((n-1)\theta+\alpha)\tanh(n-1)\xi_0 + 2n\sin((n\theta+\alpha)\tanh(n\xi_0) + (n+1)\sin((n+1)\theta+\alpha)\tanh(n+1)\xi_0] \quad (35)$$

The total free surface elevation, up to and including the third order elevation, is therefore expressed as:

$$\zeta = \zeta_0 + t\zeta_1 + t^2(\zeta_2^{\phi_1} + \zeta_2^{\psi_1}) + t^3\zeta_3^{Fr} \quad (36)$$

The free-surface elevations are thereby computed using a Fortran program, in double precision, at dimensionless time intervals $\Delta T = 0.1$.

4.3 Small-time asymptotic results compared to those of the nonlinear numerical scheme

Calculations for the unsteady nonlinear free-surface flows due to the forced motion of a circular cylinder impulsively started from rest have been carried out using the small time expansion method and the fully nonlinear numerical scheme. We have considered the forced motion with constant velocity for various cylinder sizes and in each case have varied the Froude number to determine its effect on the motion of the free-surface. The initial submergence depth (d), the velocity (U) and the cylinder radius (ϵ) are chosen arbitrarily.

In Figs. 4.1, 4.7 and 4.10 we show profiles for vertical motion at times $T_1 = 0.1$ to $T_{10} = 1.0$, where $\Delta T = T_n - T_{n-1} = 0.1$, n=1,2,..,10, with $\epsilon = 0.8$ and Froude numbers 0.39, 0.78 and 0.1955 respectively. There is good agreement between the two methods for $T = T_1$ to $T = T_5$ in the case when Fr=0.78 and 0.39. The two solutions continue to be in good agreement for larger values of

time, i.e up to T_8, in the case when $Fr = 0.78$. This behaviour is demonstrated in Fig. 4.7. As the Froude number is reduced, i.e to 0.1955, the two methods only agree for shorter times than for larger Froude numbers. Fig. 4.10 shows agreement for up to $T = T_3$.

Similar behaviour in the comparison of the profiles due to the motion of the cylinder moving obliquely upwards was observed. The comparisons were carried out for the cylinder of the same radius, $\epsilon = 0.8$, and same Froude numbers. For this case the solutions appear to be in good agreement for Fr=0.78 and 0.39 between T_0 and T_5 (see Fig. 4.8 and Fig. 4.2). The results diverge earlier for $Fr = 0.1955$ than for the other two Froude numbers, i.e even at T_3=0.3 there is a visible difference between the two methods (see Fig. 4.11). In this case there is an early breaking of the free surface behind the cylinder as according to the numerical scheme (see Fig.4.2.11(c)). The breaking of the free surface seems purely physical as there is a negative pressure build up, see Figs. 4.1-3 , resulting in a Rayleigh-Taylor instability.This is a similar effect to that observed by Greenhow (1987).

The oblique motion is qualitatively resembled by the horizontal motion for Fr=0.78 and 0.39 between T_0 and T_3. Within the given limits there is good agreement between the two methods. At times greater than 0.3 and less than 0.5 the two methods begin to vary as shown in Fig.4.3(b) and Fig. 4.9(b). Calculations of the numerical scheme break down for values of time greater than 0.6 in this case as well.

In general the small time series expansion method and the fully nonlinear numerical scheme are in good agreement for values of $Fr \geq 0.4$ and $\epsilon = 0.8$. The third-order elevation represents the radiation of wave energy out from

the first-order elevation and hence increasing or decreasing the Froude number will inevitably influence the outcome of the summation of the elevations. This influence tends to worsen the comparison with the numerical scheme when small Froude numbers (see Fig. 4.10) are considered, and improve it when Fr is greater than approximately 0.4. We have shown, in Fig. 4.1, good agreement between the two methods for large values of time, i.e up to T_8.

In order to further understand this problem we look at cylinders of smaller radii. Cylinders of radii $\epsilon < 0.8$ were considered and the two solutions seem generally to be in good agreement in specified ranges of time. In particular we analyse the results with ϵ =0.4 for the same Froude numbers as for ϵ =0.8.

For vertical motion with large Froude numbers see Fig. 4.13. There is very good agreement for times less than 0.6 whereas for greater T the results are simply not comparable. Of interest is the fact that the free-surface elevations for small cylinders produced by the asymptotic method seem to be lying above those of the fully nonlinear scheme contrary to the case of larger cylinders. According to Tyvand & Miloh (1994) the geometric nonlinearity effects dominate over the free surface nonlinearity effects especially for smaller cylinders. Now, since the geometric nonlinearity, at the cylinder contour, gives rise to the upward steady force then the above observations may be justified in the sense that the effect of this force depends on the size of the cylinder.

Results for oblique and horizontal motions were also analysed for the smaller cylinder. The ranges of agreement in terms of time and Froude numbers are similar to those of the vertical motion. In Figs. 4.5, 4.14, 4.17 we show the profiles for the same Froude numbers as for the vertical motion. In Fig. 4.6, 4.15, 4.18 elevations for horizontal motion with the same Froude numbers are

also shown.

Good agreement between the two methods has also been shown for cylinders of radii greater than 0.8 and smaller than 0.4. In particular we show in Fig. 4.19 and Fig. 4.20 the elevations for vertical motions of cylinders of radii 0.95 and 0.2 respectively with Fr=0.78.

We now make some comments about the forces and pressures on the cylinder for one case in each of the directions discussed above at Fr= 0.39. In Fig. 4.1(g) we show total pressure distribution on the cylinder as it is forced to move upwards towards the surface at times indicated in the diagram which correspond to some free/cylinder surface positions. Since the body is moving vertically upwards, where initially pressure is hydrostatic, pressure around the body should decrease. The pressure around the bottom of the cylinder seems to be decreasing at a constant rate, but almost stays the same at the top of the cylinder. This phenomenon is physical as also is shown in the experiments photographed by Greenhow and Lin (1983). Figs. 4.1(h)-(i) show vertical hydrodynamic force on the cylinder as a function of time and distance below the surface respectively. The force decreases as the cylinder nears the surface and eventually the calculations breakdown due to negative pressure on the sides of the body as shown in Fig. 4.1(g). The situation is much more complicated for oblique motion. The pressures at the bottom of the cylinder behave in a similar way as above, but vary for the region at the top of the cylinder. In this case negative pressure develops forward of the cylinder and immediately after $T = 0.7$, i.e at $T = 0.75$, see Fi. 4.2(e). The horizontal force increases steadily up to $T = 1.05$ and then drops whereas the vertical force decreeases and then picks up at the same time as the horizontal force, see Fig. 4.2(f)-

(g). The horizontal forces are as discussed in Hepworth (1991) though our case has stronger free/cylinder surface interactions (d=1.2a). Total pressure distributions and forces are shown in Figs. 4.3(e) and (f)-(g) respectively.

4.4 Conclusion

A fairly complete study has been carried out to evaluate the behaviour of the free-surface due to the motion of a submerged circular cylinder with constant velocity and compare calculations of the small-time expansion method and the fully-nonlinear numerical scheme. The results obtained indicate that for good agreement to be achieved for dimensionless time less than 0.8, we must restrict our calculations to cylinders of radii less than 0.9 and Froude number greater than 0.4. This gives approximate bounds for the validity of the small-time expansion to third-order, i.e as far as Tyvand and Miloh(1994) have taken it. Beyond a certain time, the small-time expansion method becomes inreasingly inaccurate, and ultimately topologically impossible with the free-surface moving inside the cylinder. The numerical scheme is, however, not subject to any such restrictions and remains valid and accurate until the breaking of the free-surface caused by a pressure inversion across it in the cases presented here, or the generation of a breaking wave (see Greenhow (1994)).

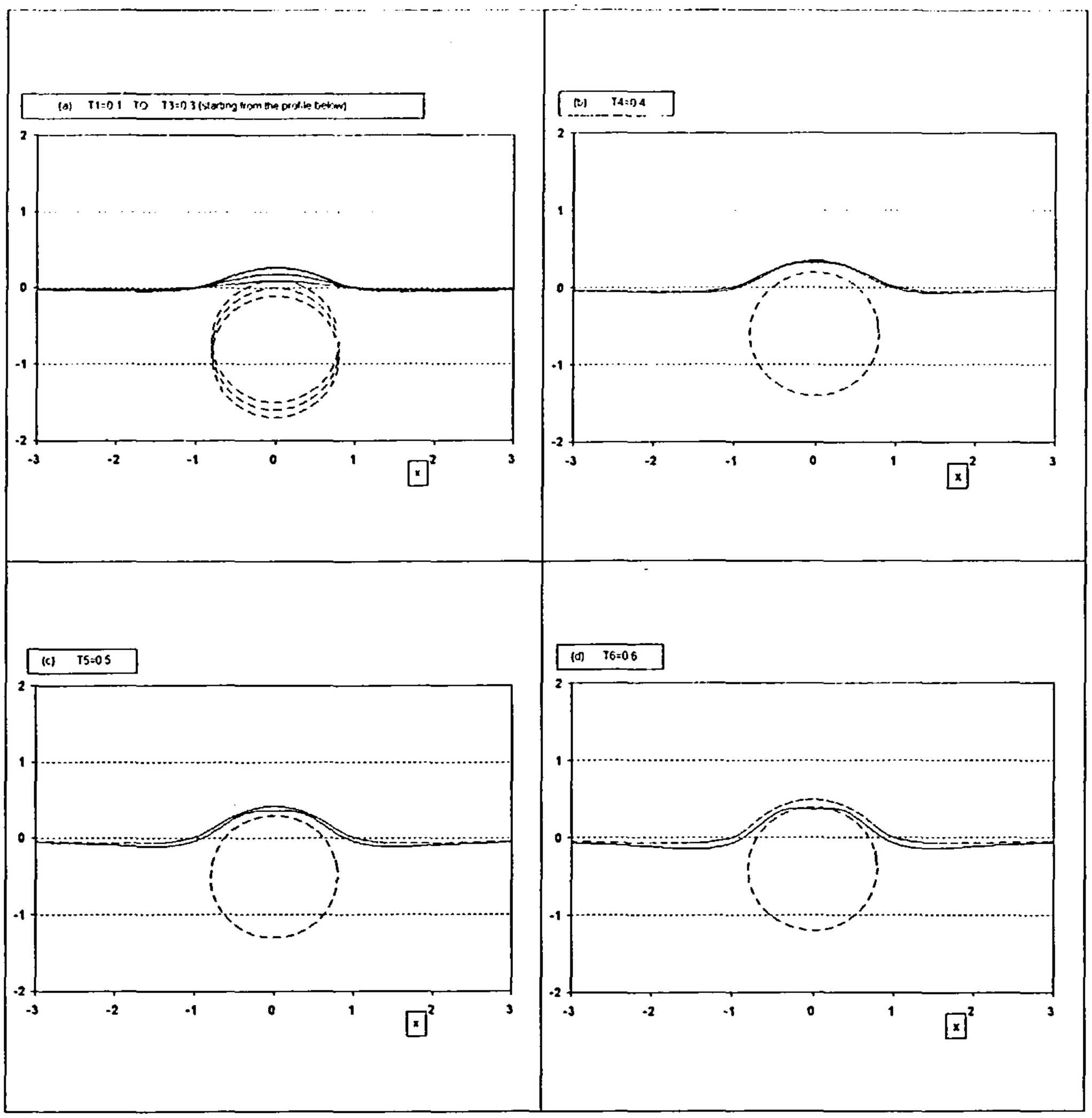

Fig. 4.1 Free-surface elevation and cylinder position due to the vertical and impulsively started motion of a cylinder below the surface. The cylinder radius, time step size and Fr are 0.8, 0.1 and 0.39 respectively. The dotted and solid lines represent the nonlinear and Tyvand & Miloh methods respectively.

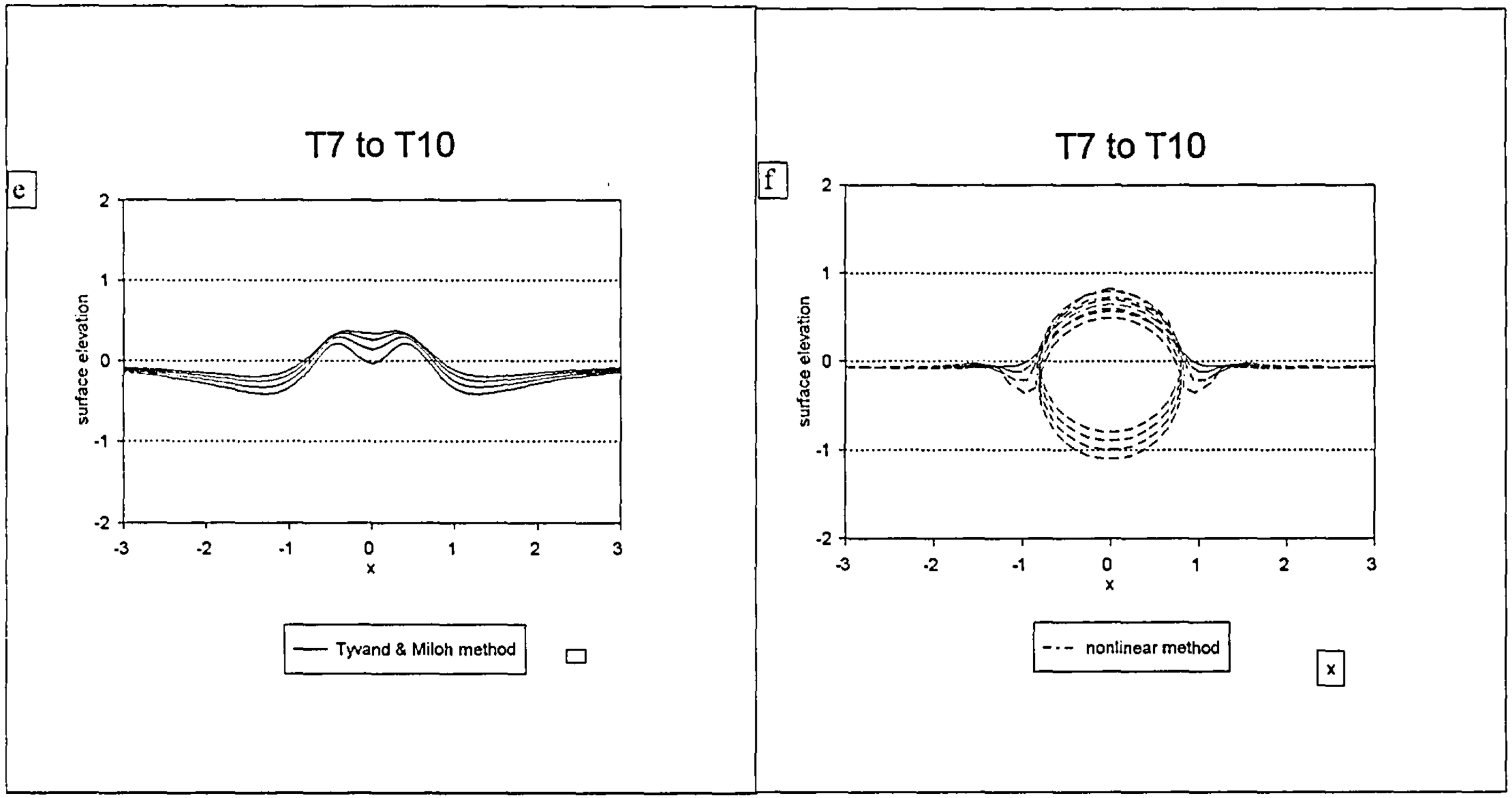
e
T7 to T10
surface elevation
x
Tyvand & Miloh method
f
T7 to T10
surface elevation
x
nonlinear method
x

g

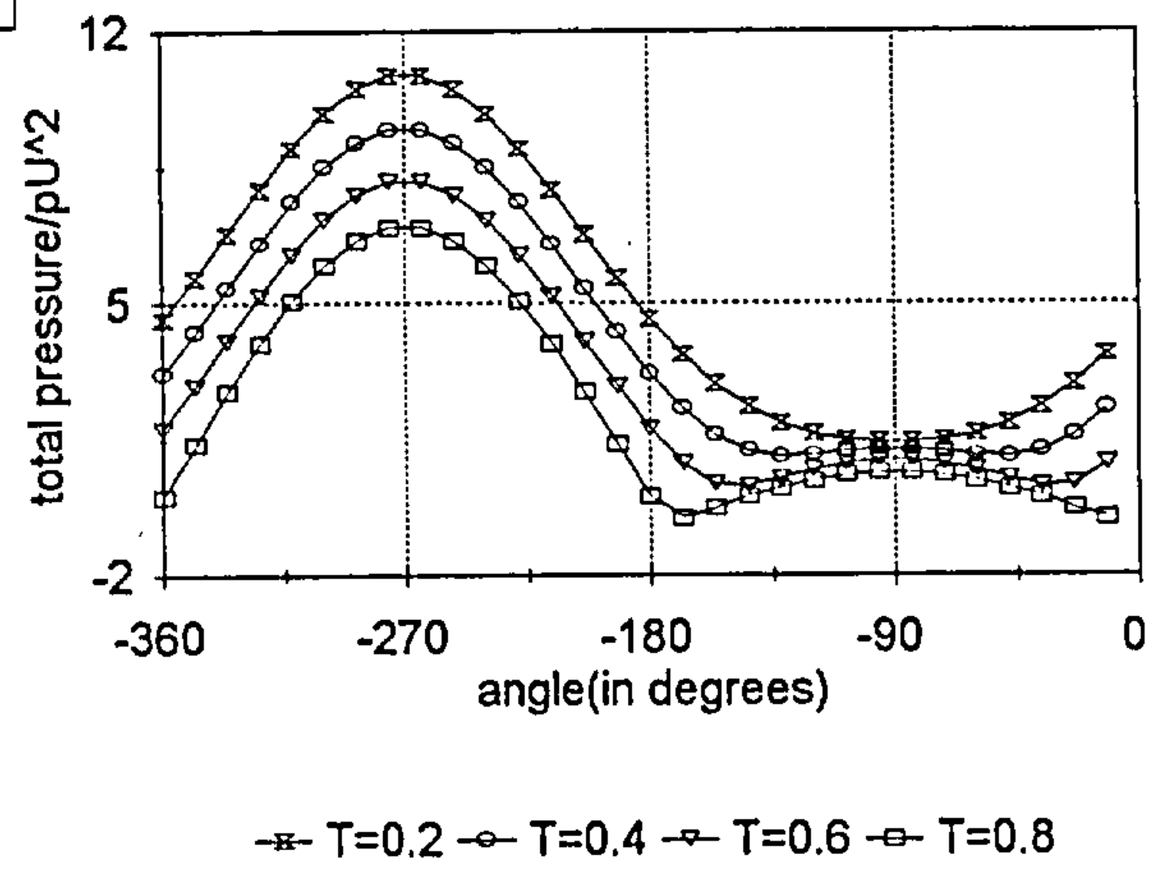
12
5
-2
total pressure/pU^2
-360
-270
-180
-90
0
angle(in degrees)
T=0.2
T=0.4
T=0.6
T=0.8

h

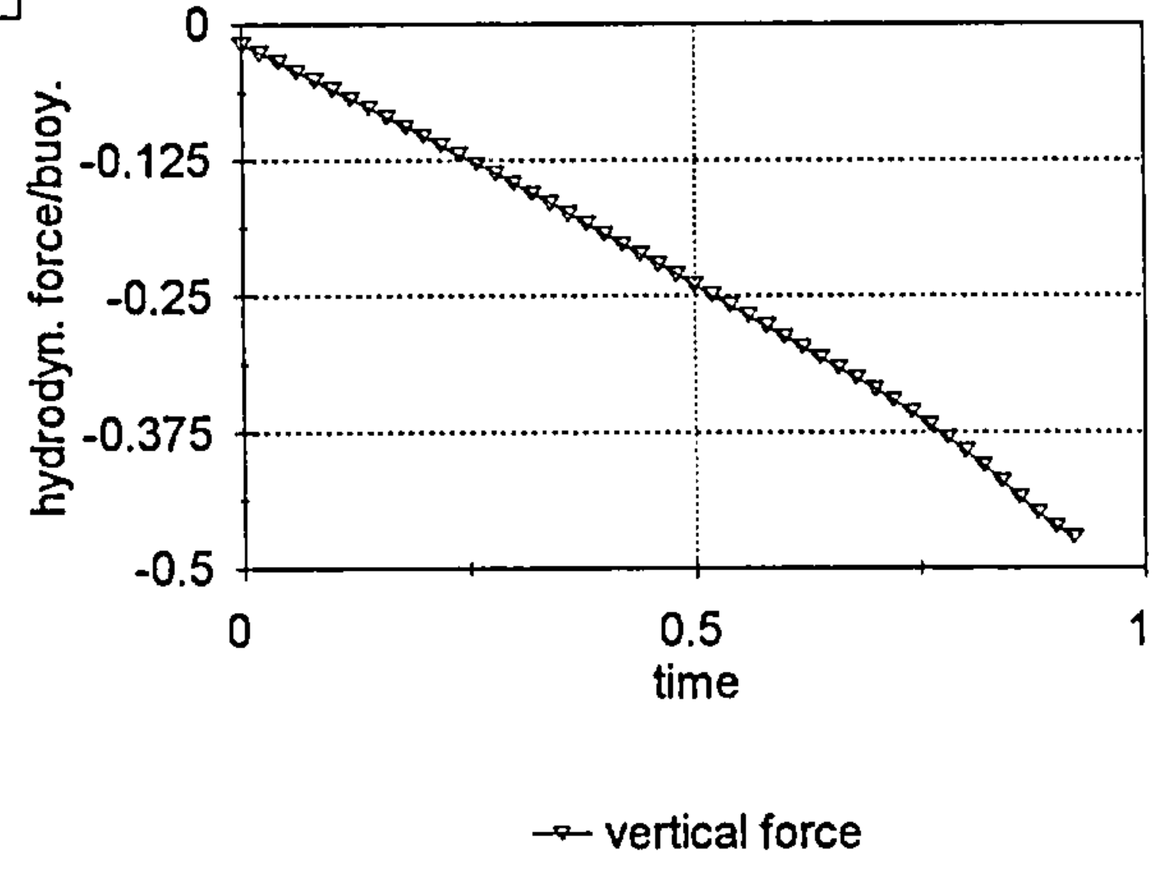
0
-0.125
-0.25
-0.375
-0.5
hydrodyn. force/buoy.
0
0.5
1
time
vertical force

i

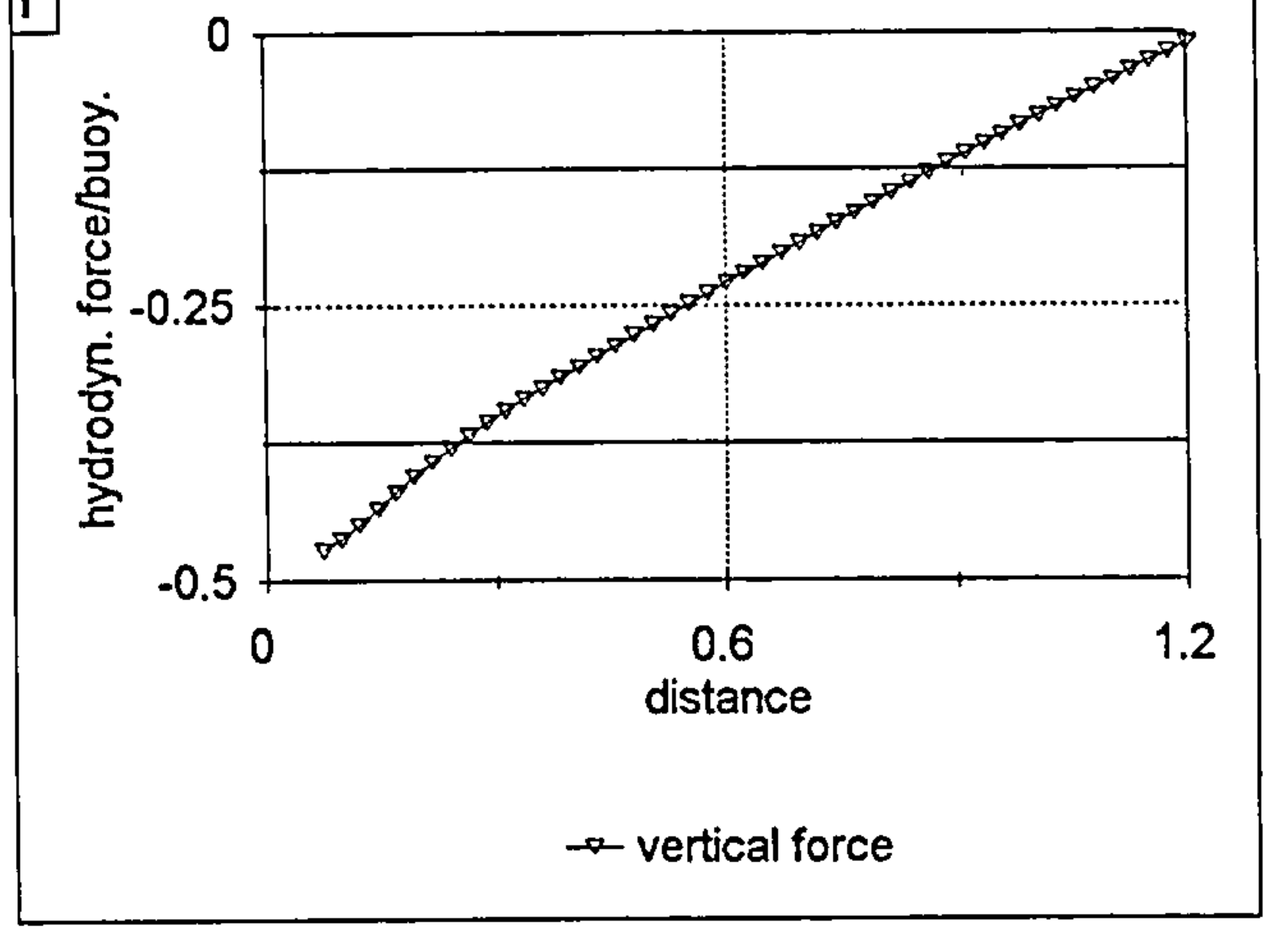
0
-0.25
-0.5
hydrodyn. force/buoy.
0
0.6
1.2
distance
vertical force

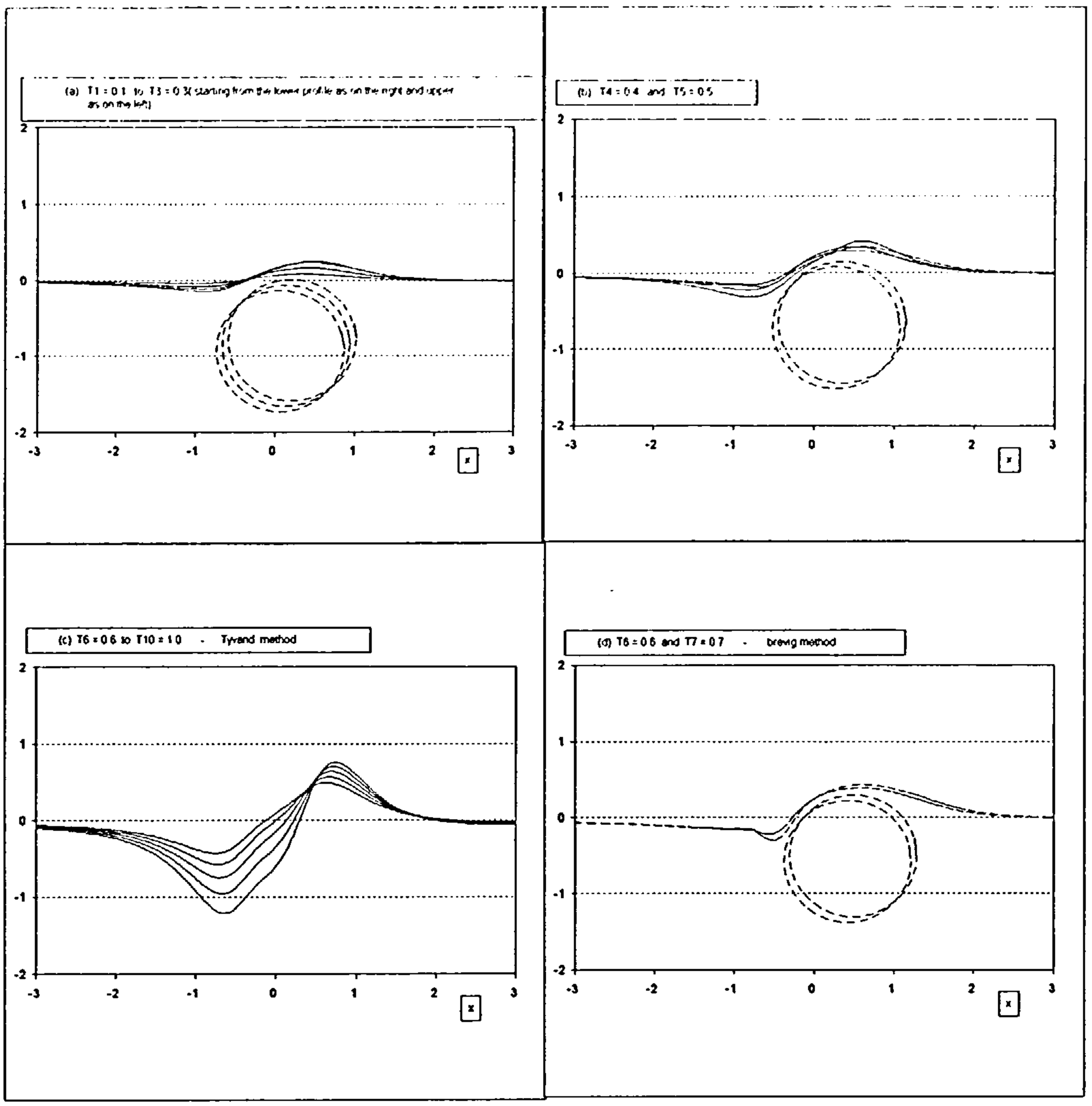

Fig. 4.2 Free-surface elevation and cylinder position due to the oblique and impulsively started motion of a cylinder below the surface. The dimensionless radius of the cylionder, time interval and Fr are 0.8, 0.1 and 0.39 respectively. Solid lines represent Tyvand & Miloh method and dotted lines represent the nonlinear method.

e

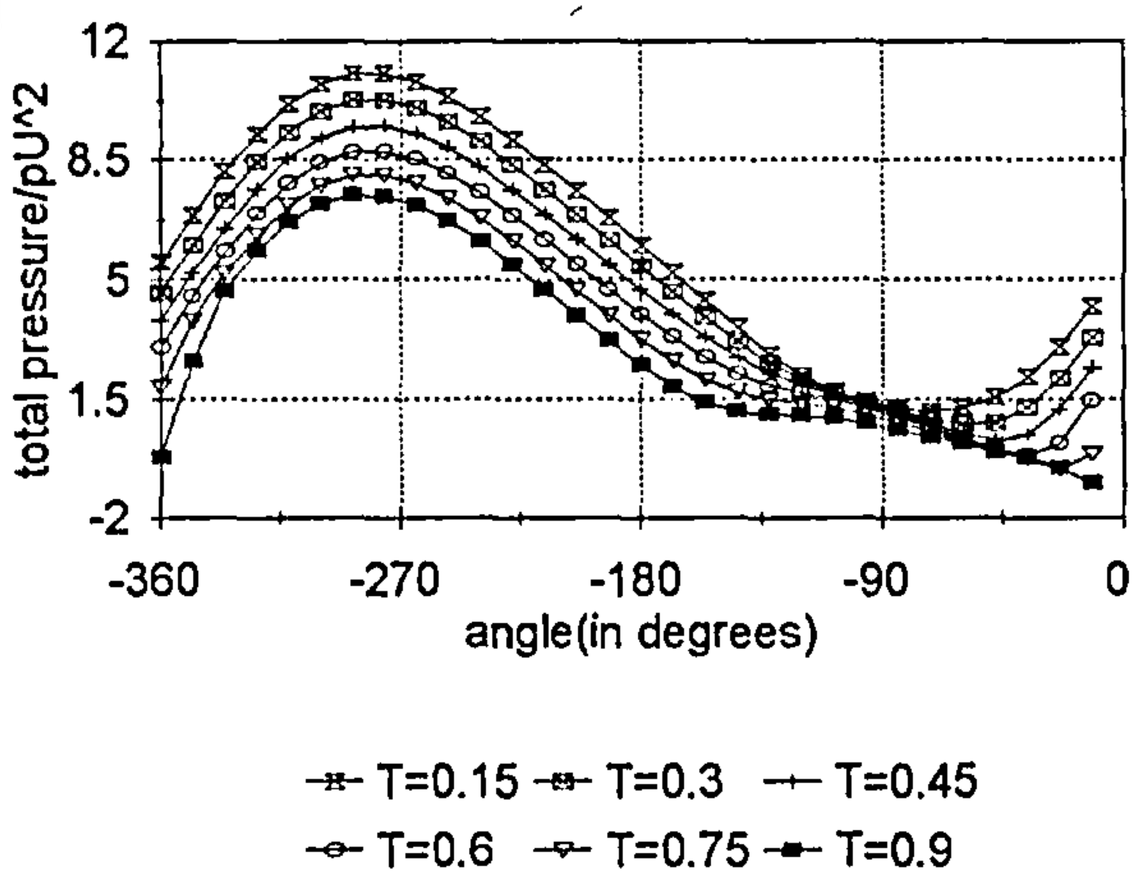
12
8.5
5
1.5
-2
total pressure/pU^2
-360
-270
-180
-90
0
angle(in degrees)
T=0.15
T=0.3
T=0.45
T=0.6
T=0.75
T=0.9

f

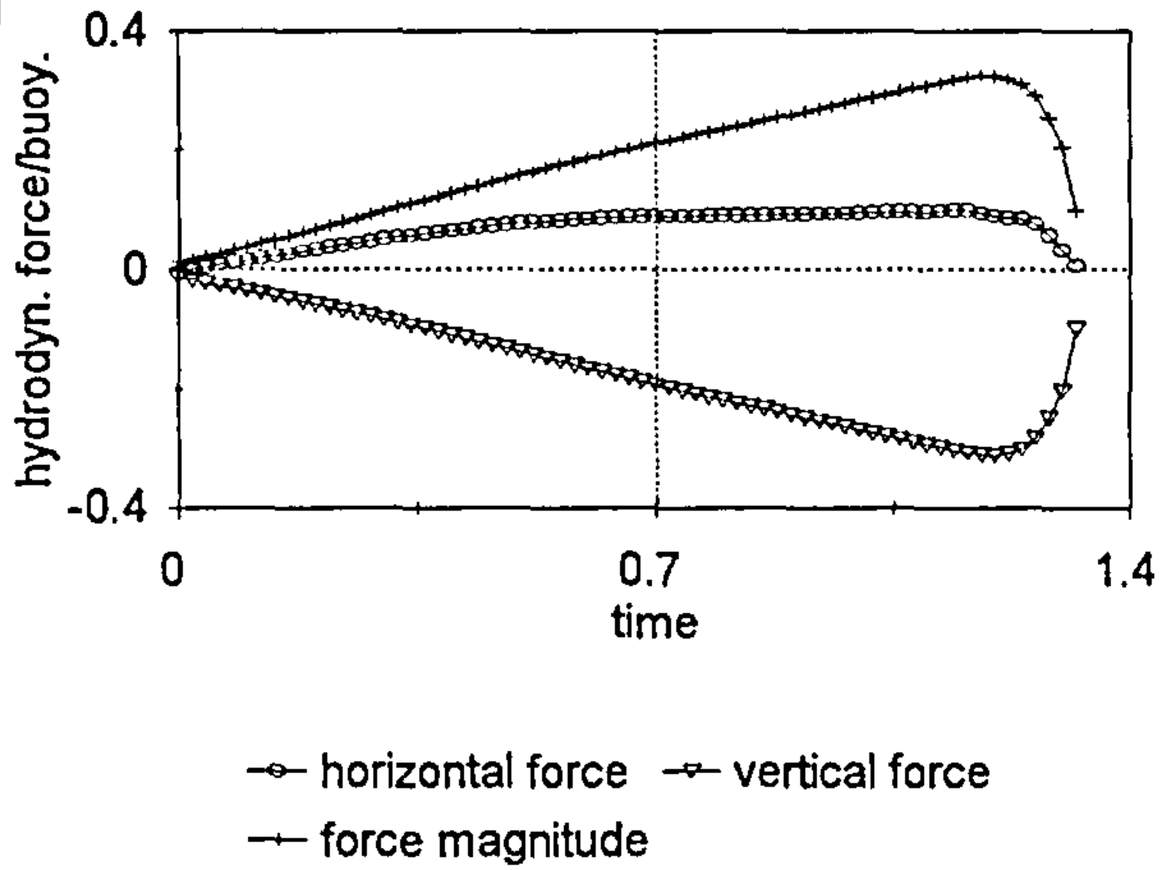
0.4
0
-0.4
hydrodyn. force/buoy.
0
0.7
1.4
time
horizontal force
vertical force
force magnitude

g

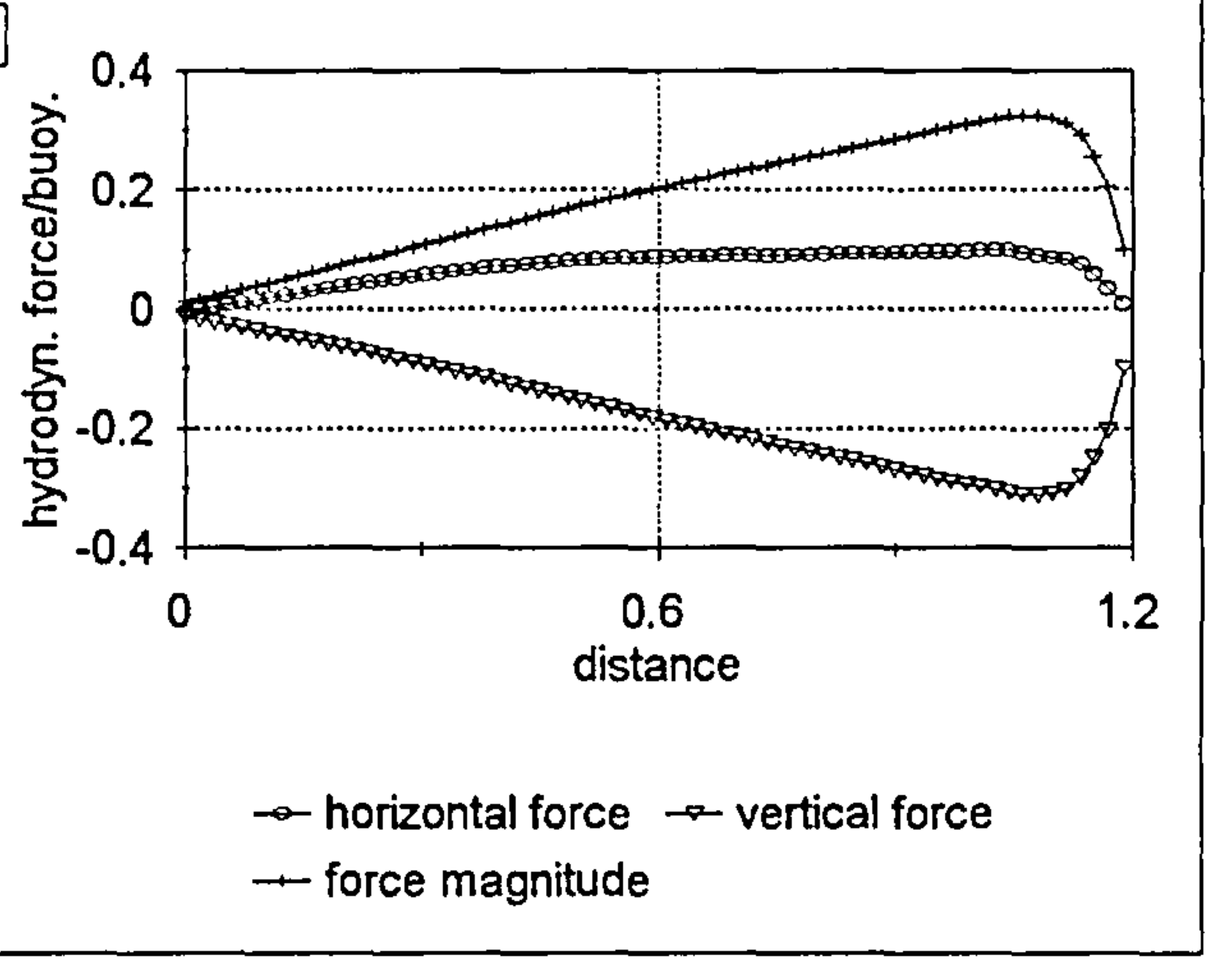
0.4
0.2
0
-0.2
-0.4
hydrodyn. force/buoy.
0
0.6
1.2
distance
horizontal force
vertical force
force magnitude

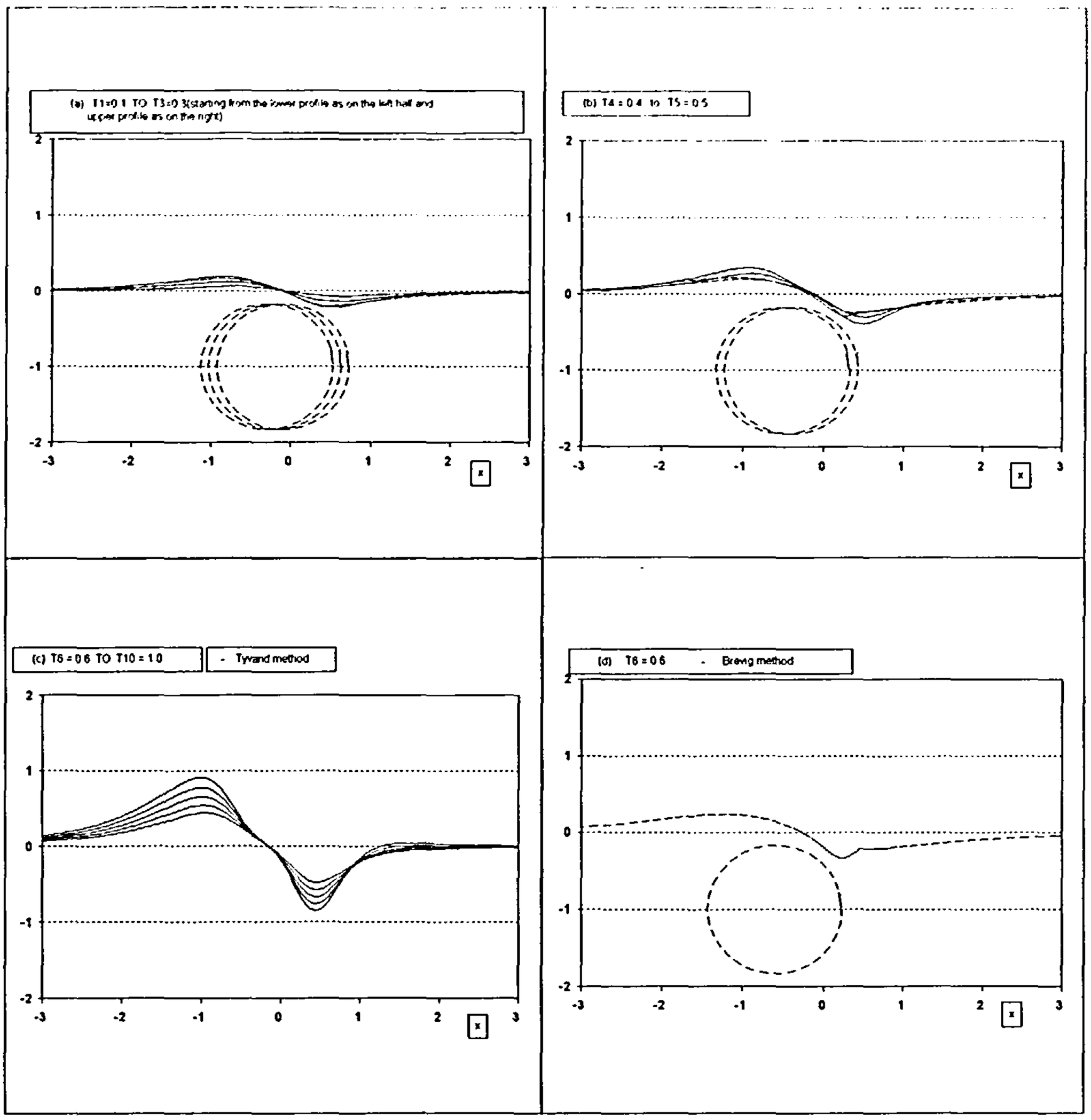

Fig. 4.3 Free-surface elevation and cylinder position due to the horizontal and impulsively started motion of a cylinder below the surface. The dimensionless radius of the cylinder, time interval and Fr are 0.8, 0.1 and 0.39 respectively. The solid and dotted lines represent the Tyvand & Miloh and nonlinear methods respectively.

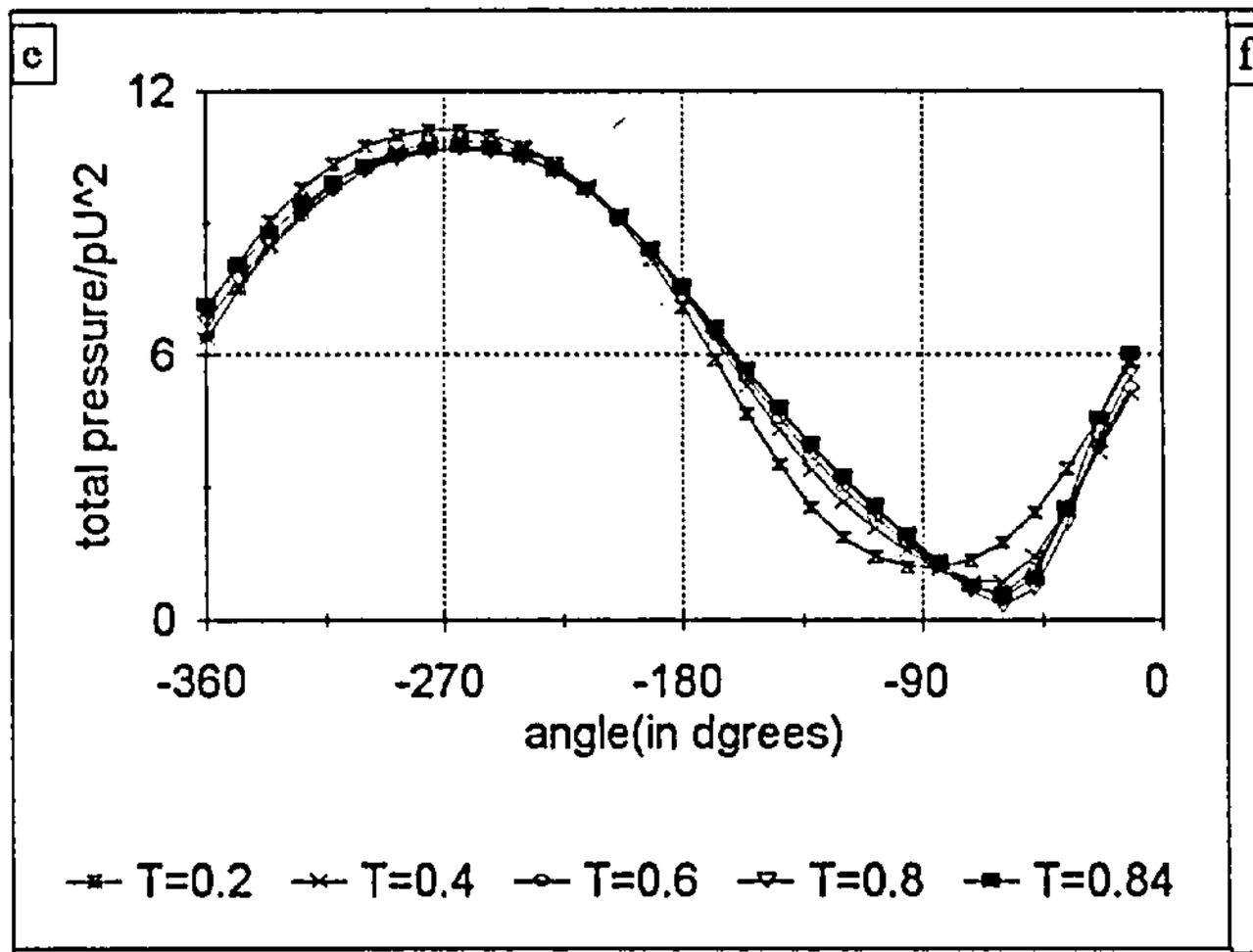
e
12
6
0
total pressure/pU^2
-360
-270
-180
-90
0
angle(in dgrees)
T=0.2
T=0.4
T=0.6
T=0.8
T=0.84

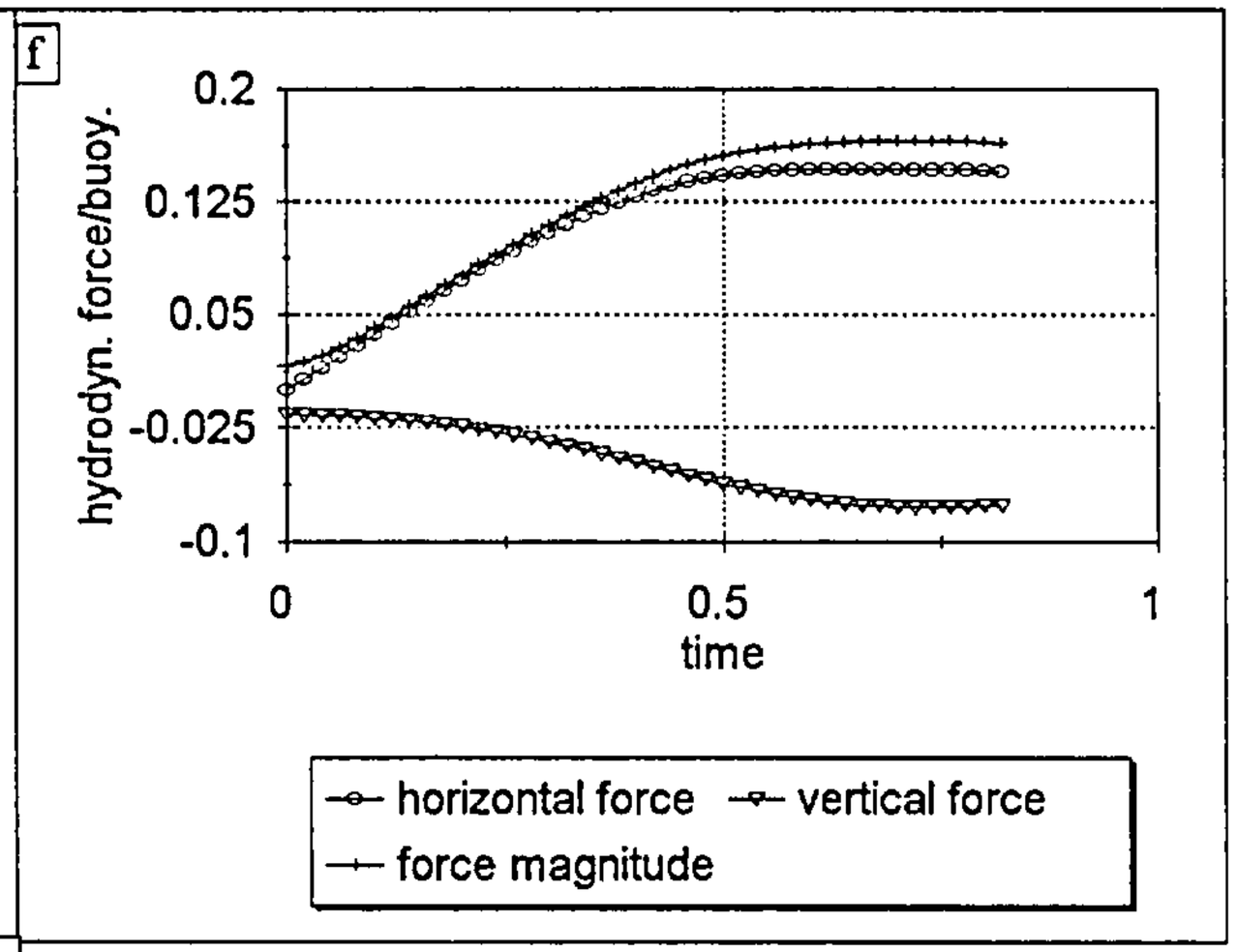
f
0.2
0.125
0.05
-0.025
-0.1
hydrodyn. force/buoy.
0
0.5
1
time
horizontal force
vertical force
force magnitude

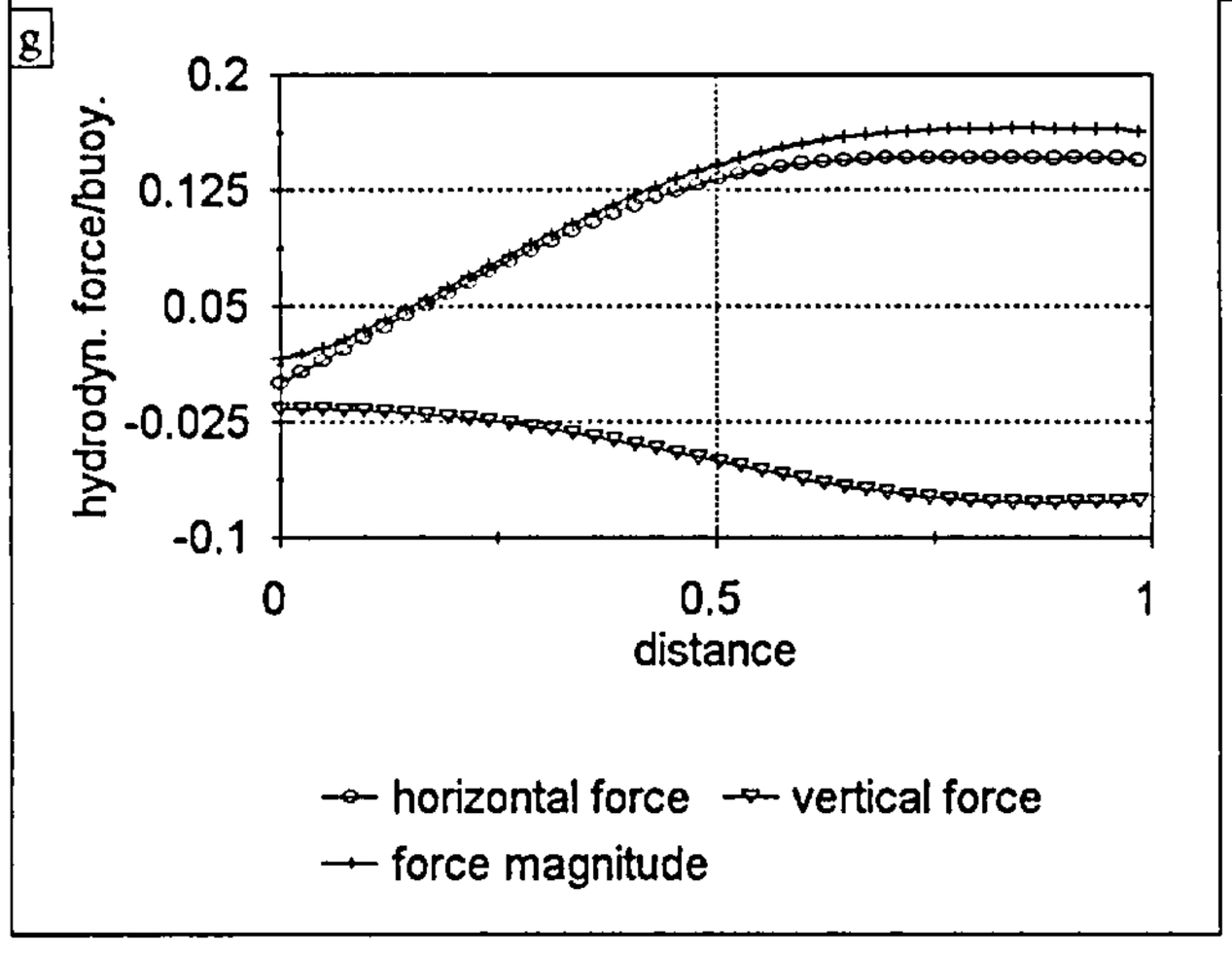
g
0.2
0.125
0.05
-0.025
-0.1
hydrodyn. force/buoy.
0
0.5
1
distance
horizontal force
vertical force
force magnitude

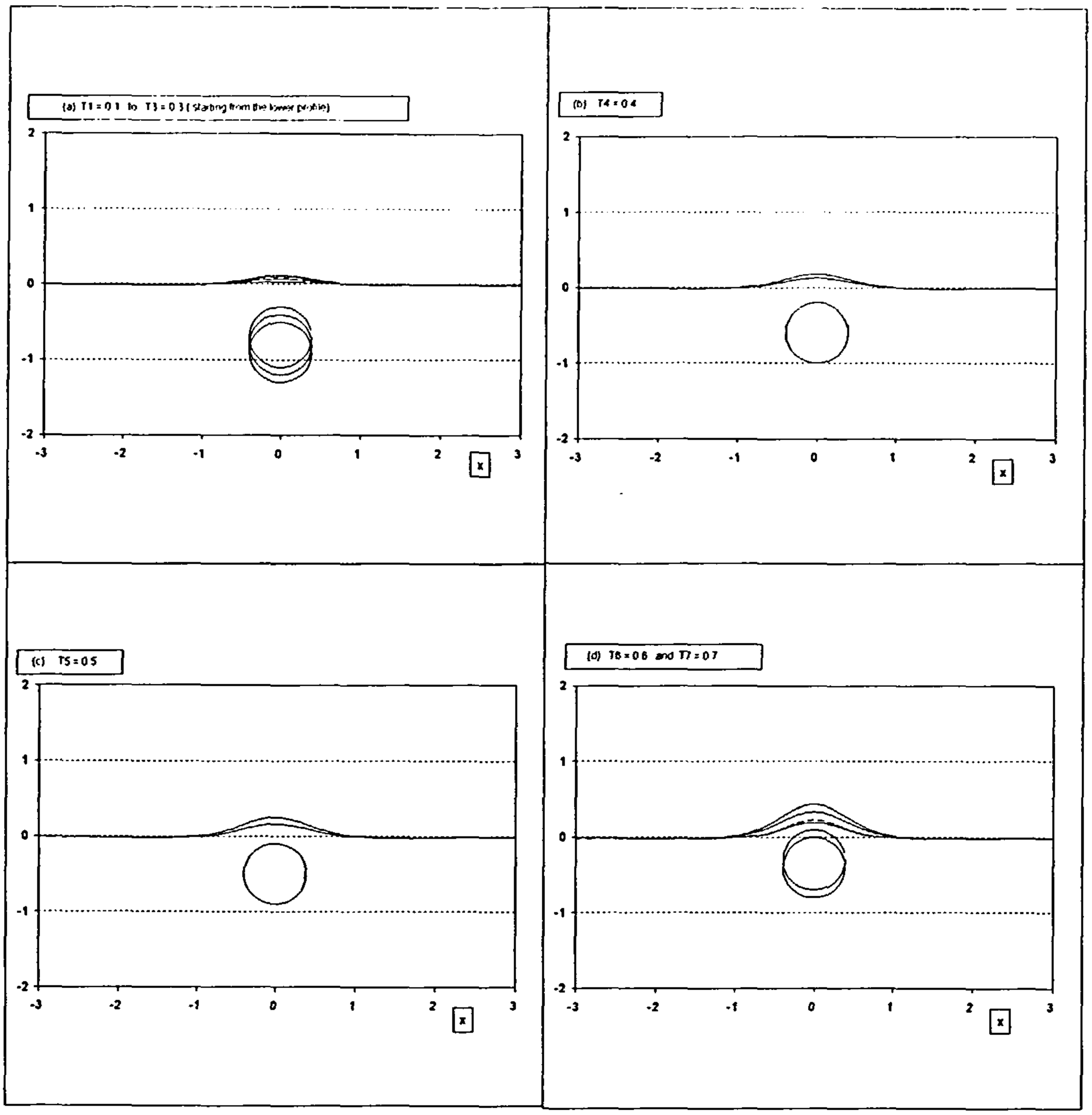

Fig. 4.4 Free-surface elevation and cylinder position due to the vertical and impulsively started motion of a cylinder below the surface. The dimensionless radius of the cylinder, time interval and Fr are 0.4, 0.1 and 0.39. The dotted and solid lines represent respectively the nonlinear and Tyvand & Miloh methods.

e

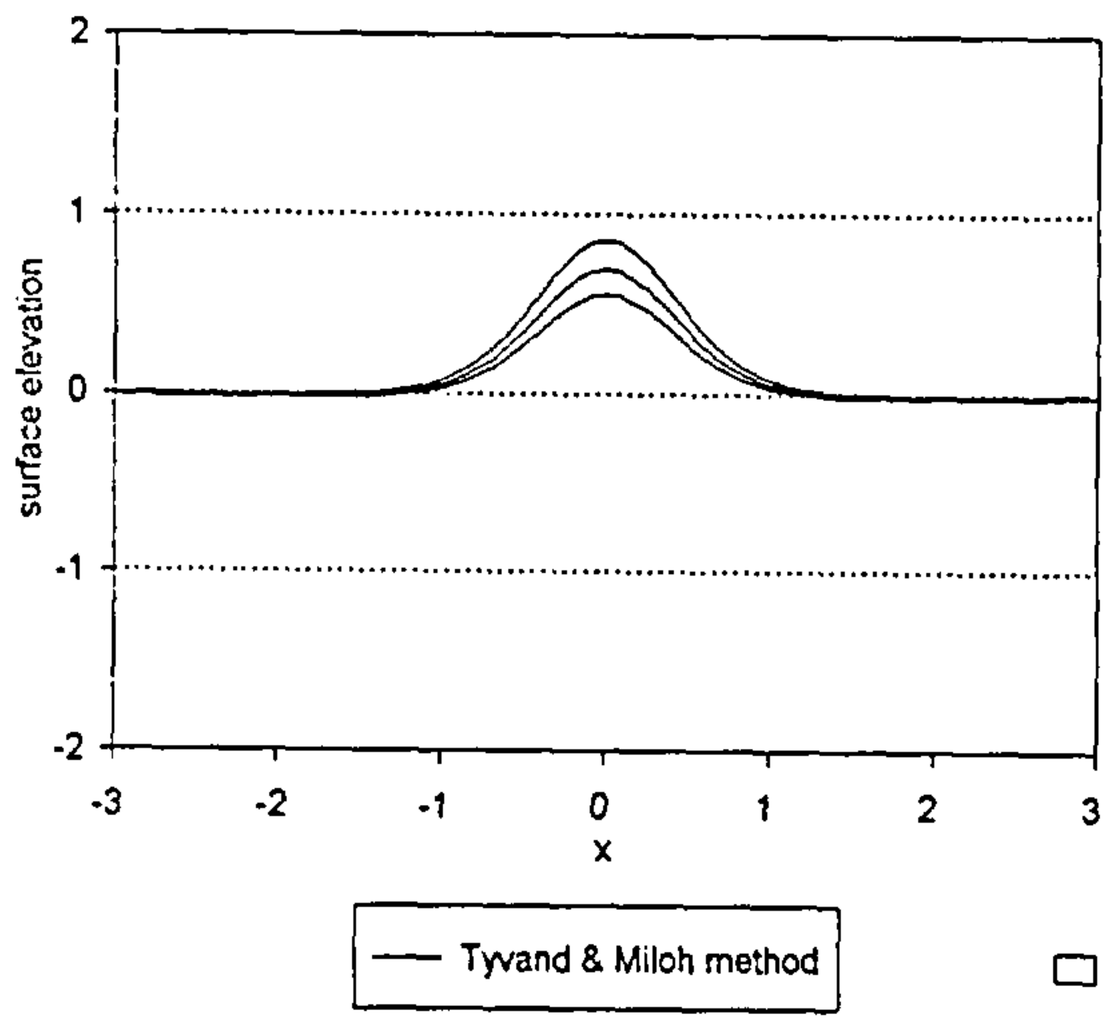
T8 to T10
surface elevation
2
1
0
-1
-2
-3
-2
-1
0
1
2
3
x
Tyvand & Miloh method

f

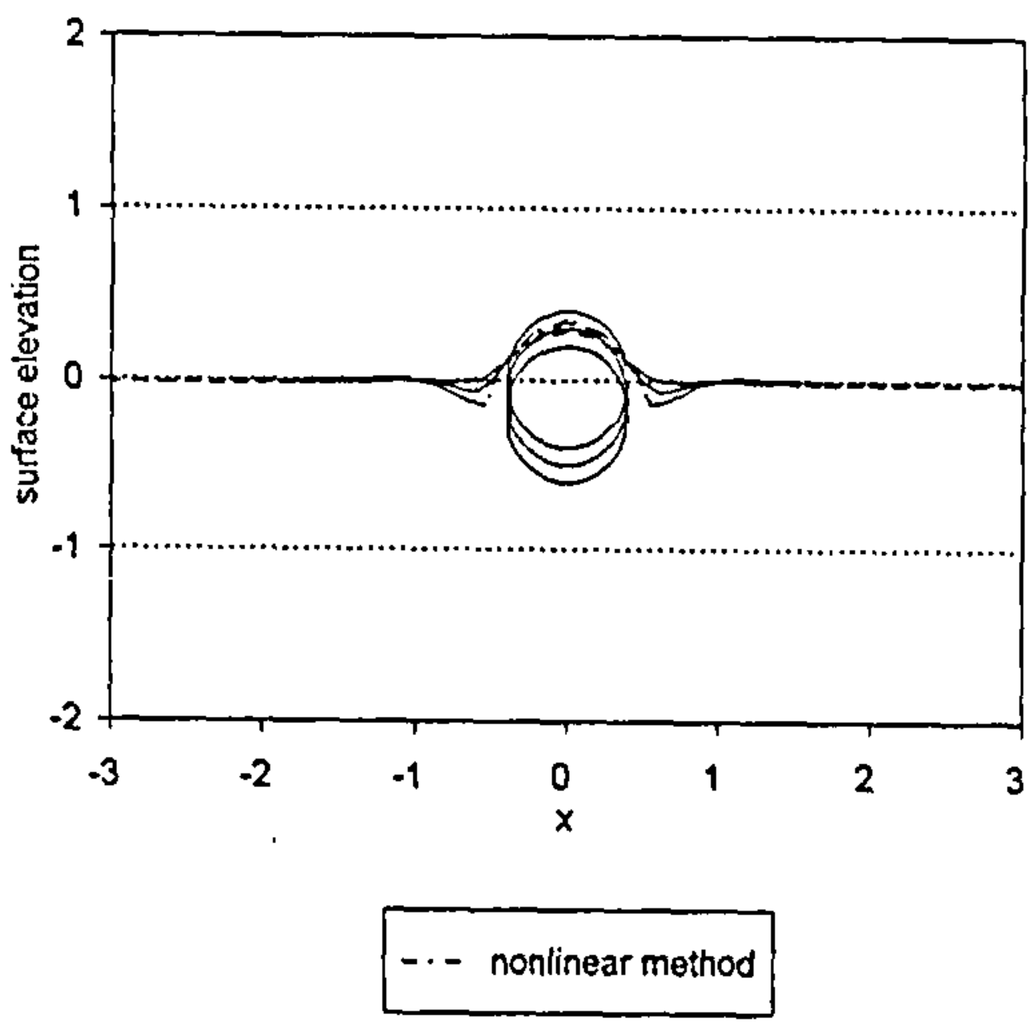
T8 to T10
surface elevation
2
1
0
-1
-2
-3
-2
-1
0
1
2
3
x
nonlinear method

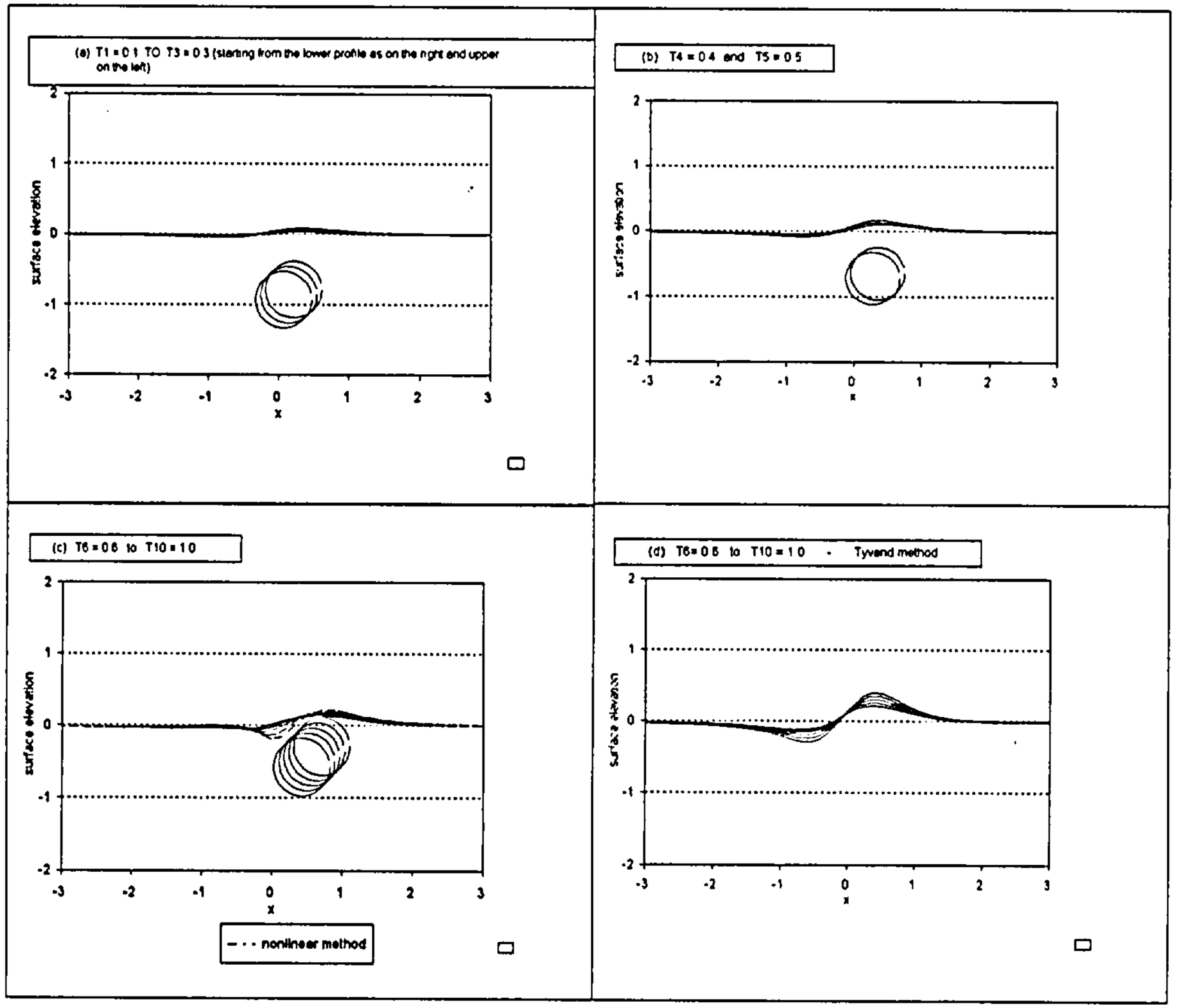

Fig. 4.5 Free-surface elevation and cylinder position due to the oblique and impulsively started motion of a cylinder below the surface. The dimensionless radius of the cylinder, time interval and Fr are 0.4, 0.1 and 0.39 respectively. Dotted and solid lines represent respectively the nonlinear and the Tyvand & Miloh methods.

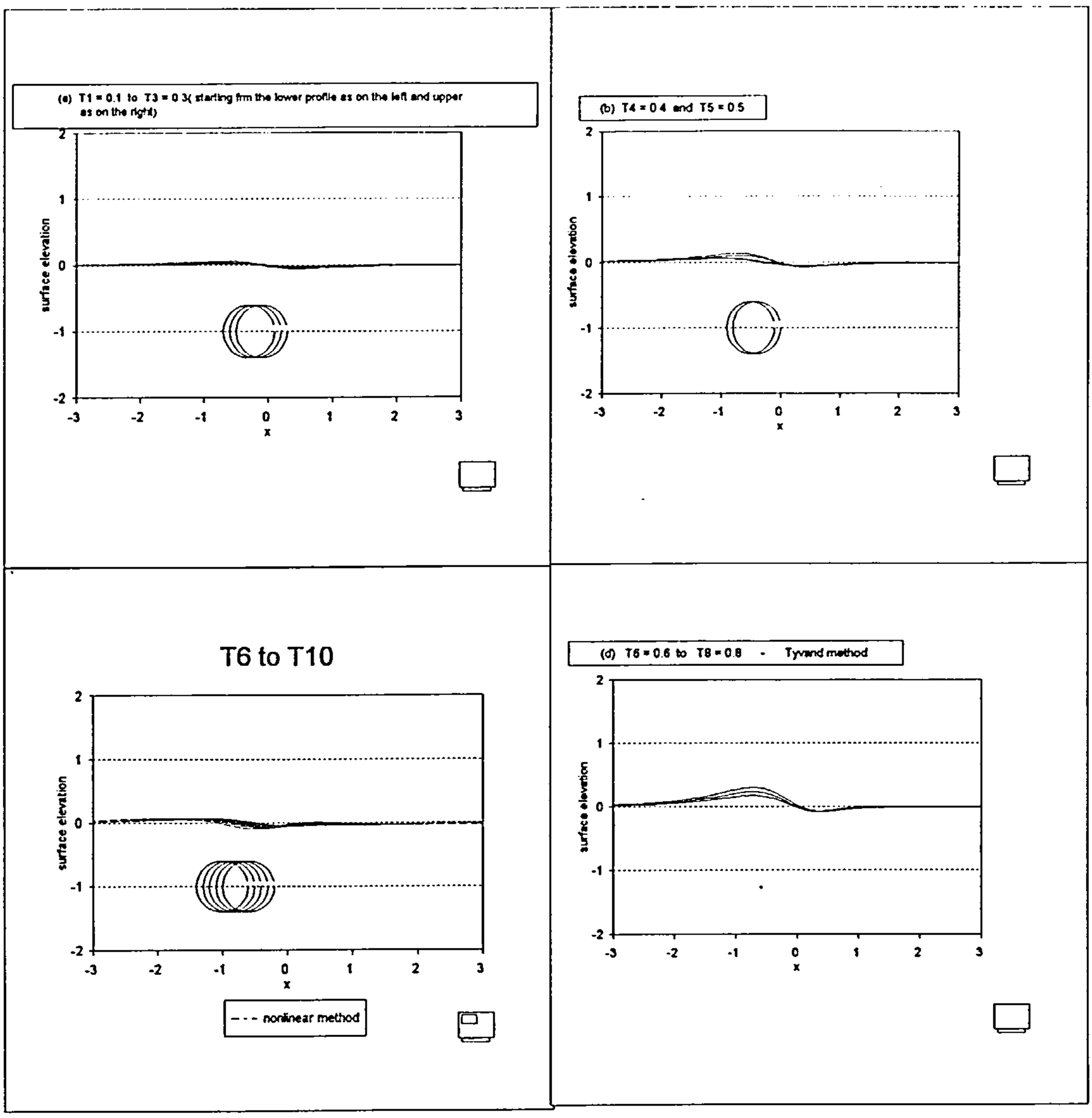

Fig. 4.6 Free-surface elevation and cylinder position due to the horizontal and impulsively started motion of a cylinder below the surface. The dimensionless radius of the cylinder, time interval and Fr are 0.4, 0.1 and 0.39 respectively. The dotted and solid lines represent the nonlinear and Tyvan d & Miloh methods.

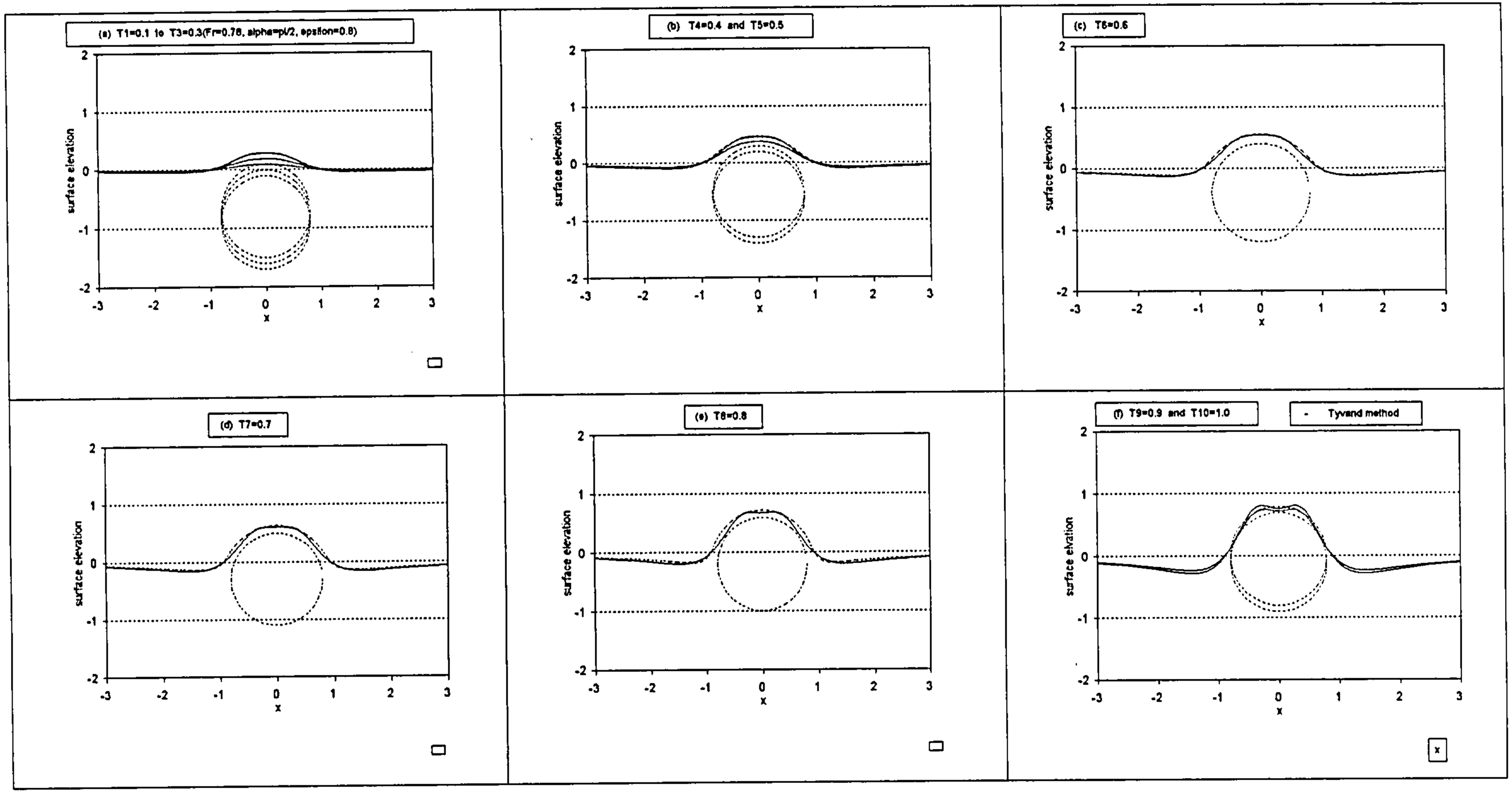

Fig. 4.7 Free-surface and cylinder positions due to the vertical and impulsively started motion of a cylinder below the surface. The dimensionless radius of the cylinder, time and Fr are 0.8, 0.1 and 0.78 respectively. The dotted and solid lines represent respectively the nonlinear and Tyvand & Miloh methods.

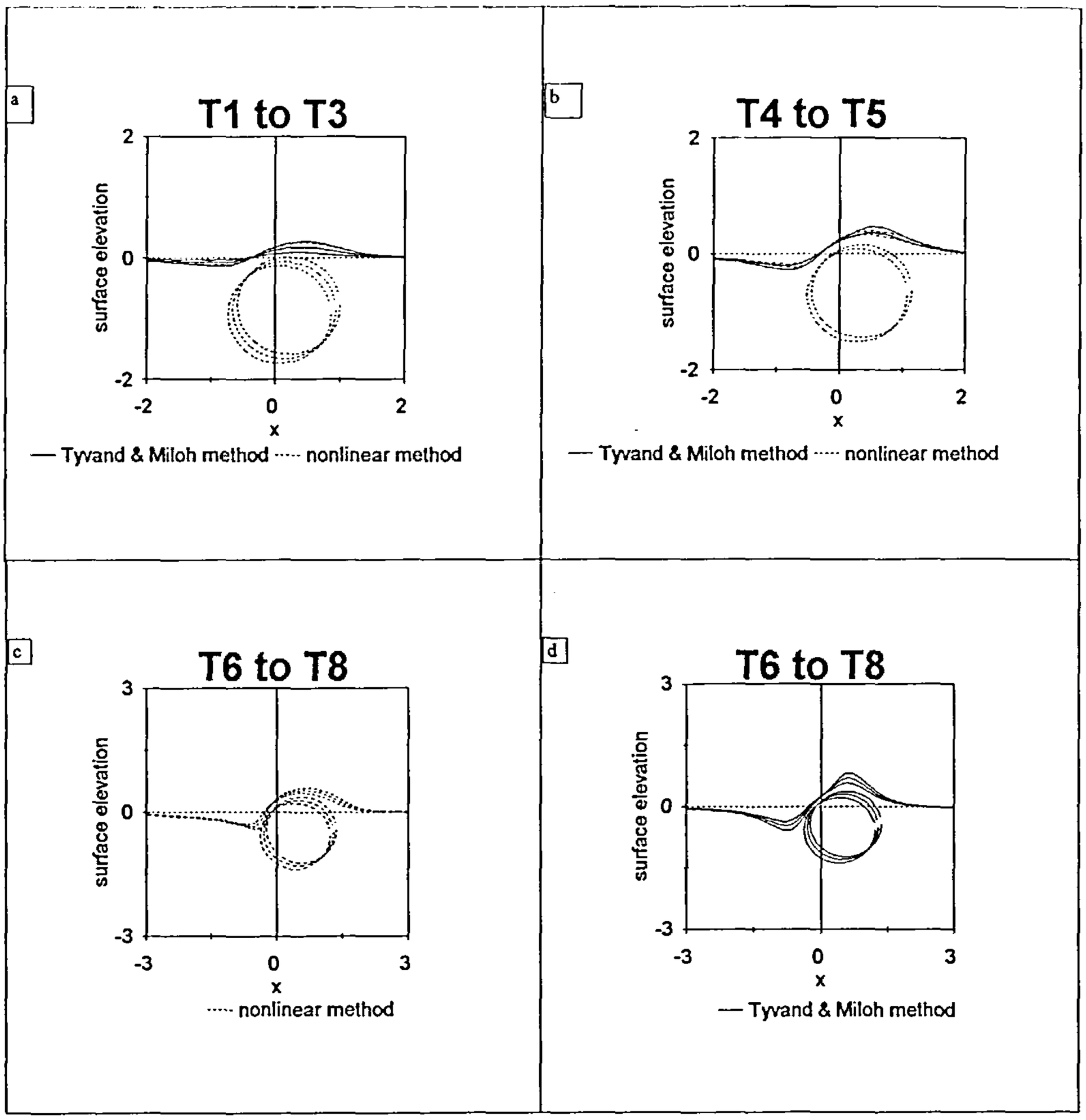

Fig. 4.8 Free-surface elevation and cylinder position due to the oblique motion of a cylinder below the surface. The dimensionless radius of the cylinder, time interval and Fr are 0.8, 0.1 and 0.78 respectively. The dotted and ethods.

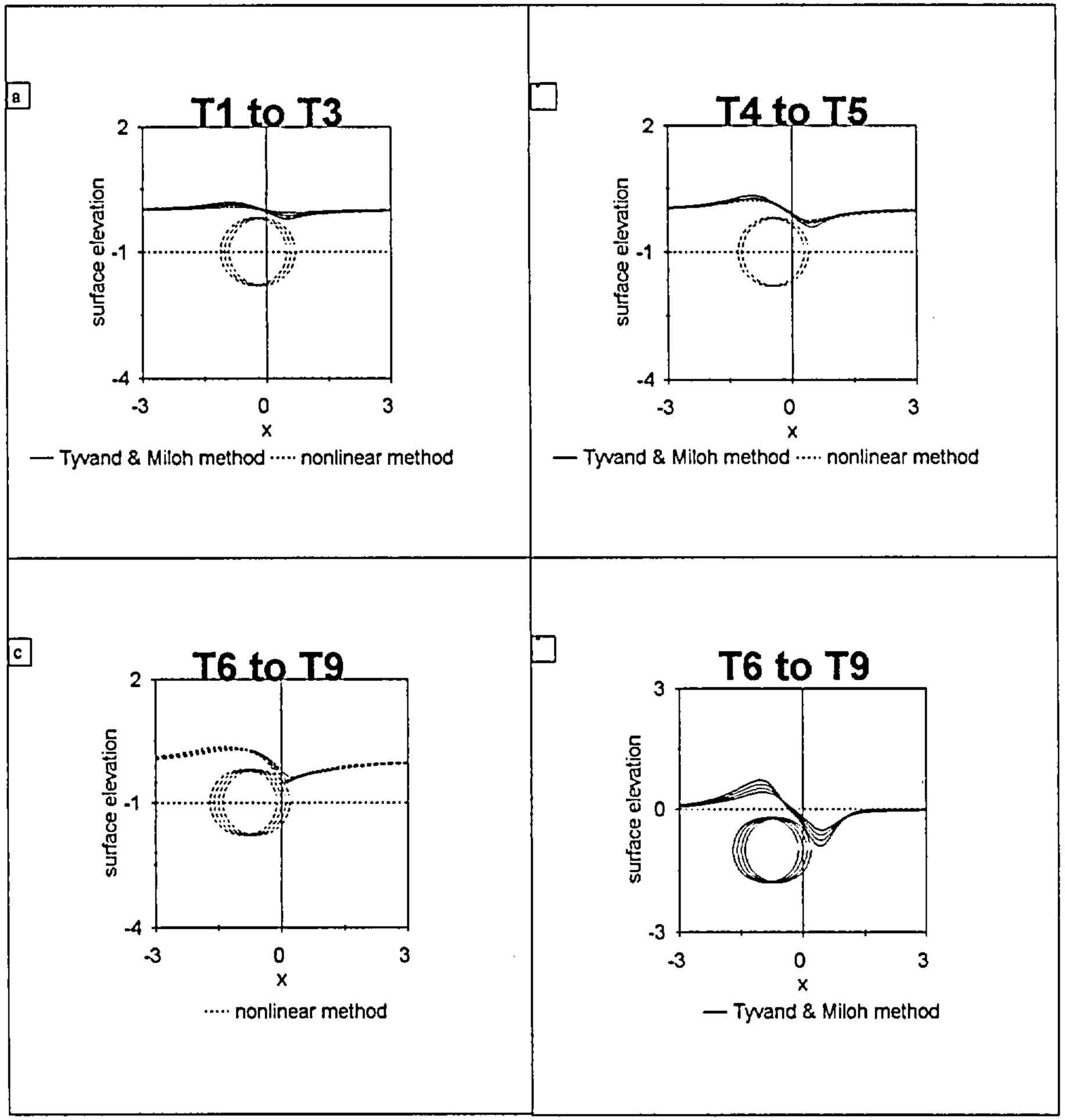

Fig. 4.9 Free-surface elevation for horizontal and impulsively started motion of a cylinder plotted against x the horizontal displacement. The dimensionless radius, time interval and Froude number are 0.8, 0.1 and 0.78 respectively.

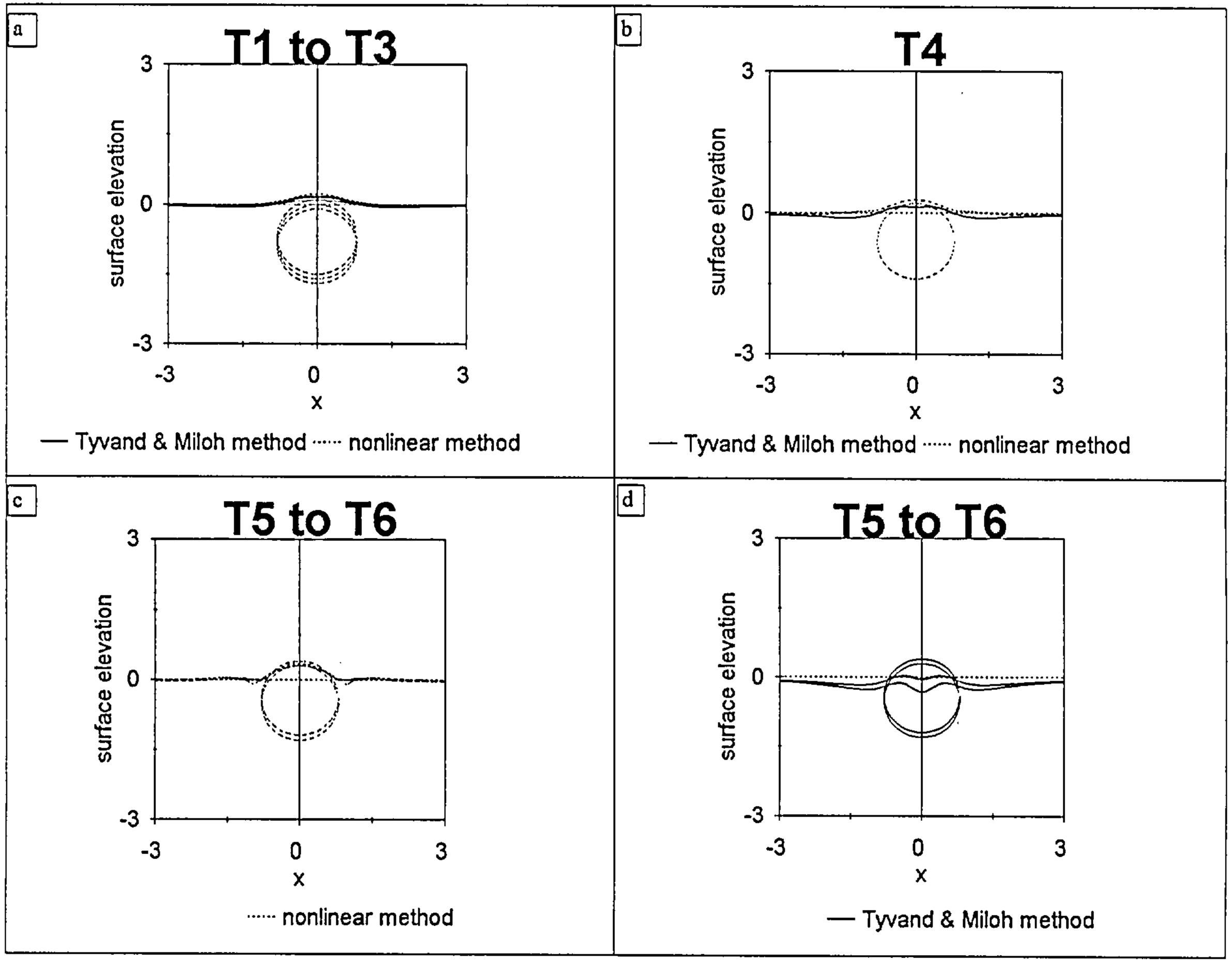

Fig. 4.10 Free-surface elevation and cylinder position due to the vertical and impulsively started motion of a cylinder below the surface. The dimensionless radius of the cylinder, time interval and Fr are 0.8, 0.1 and 0.2 respectively. The dotted and solid lines represent respectively the nonlinear and the Tyvand & Miloh methods.

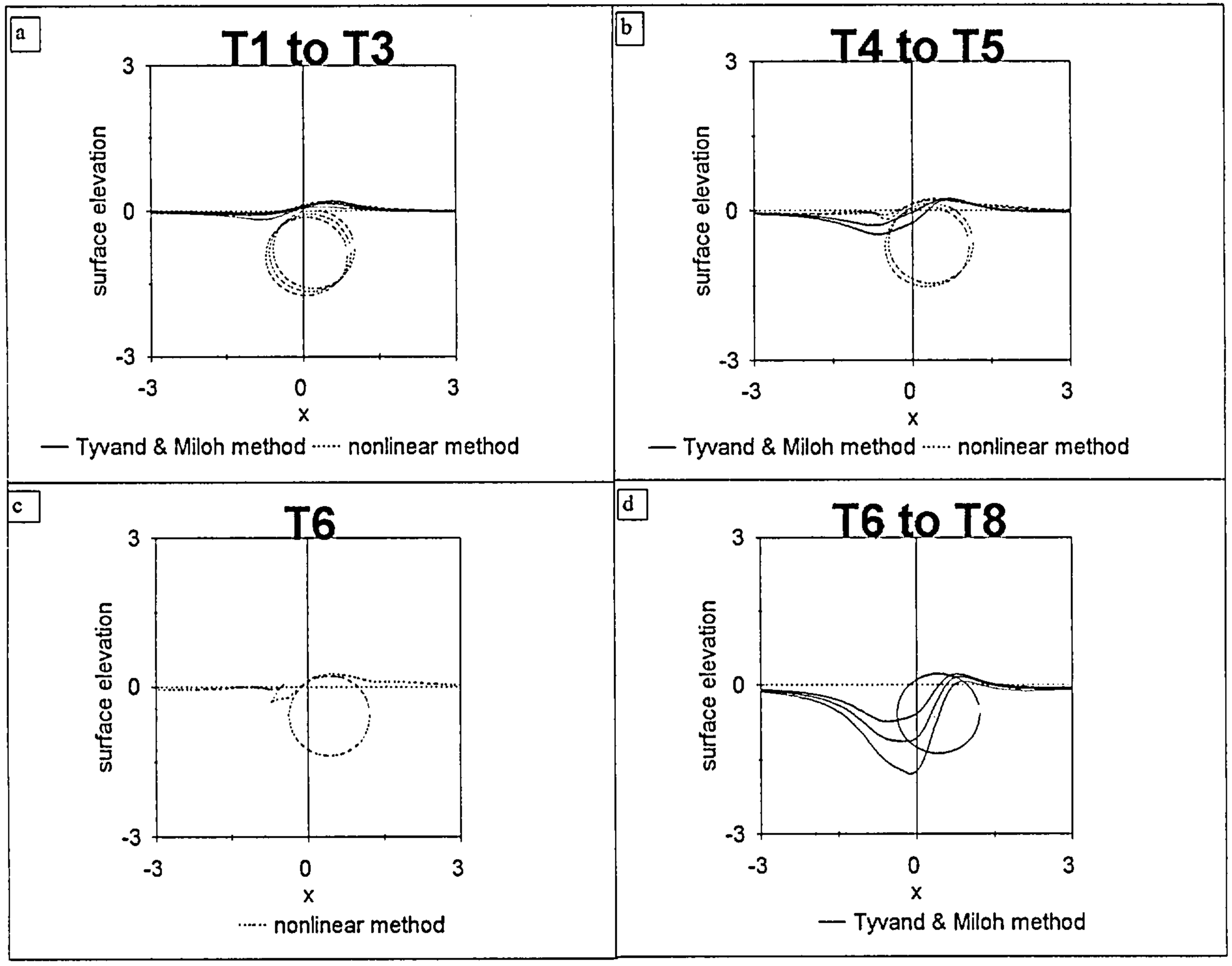

Fig. 4.11 Free-surface elevation for oblique and impulsively started motion of a cylinder plotted against x the horizontal displacement. The dimensionless radius, time interval and Froude number are 0.8, 0.1 and 0.2 respectively.

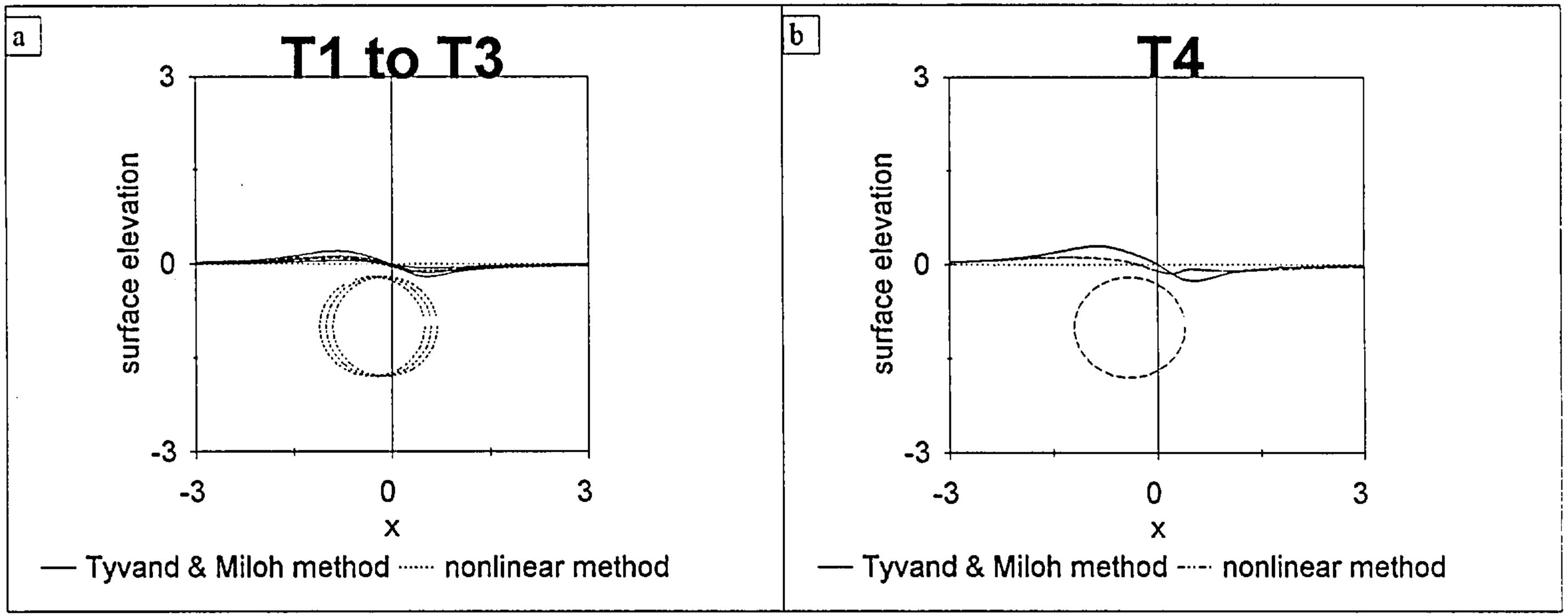

Fig. 4.12 Free-surface elevation for horizontal and impulsively started motion of a cylinder plotted against x the horizontal displacement. The dimensionless radius time interval and Froude number are 0.8, 0.1 and 0.2 respectively.

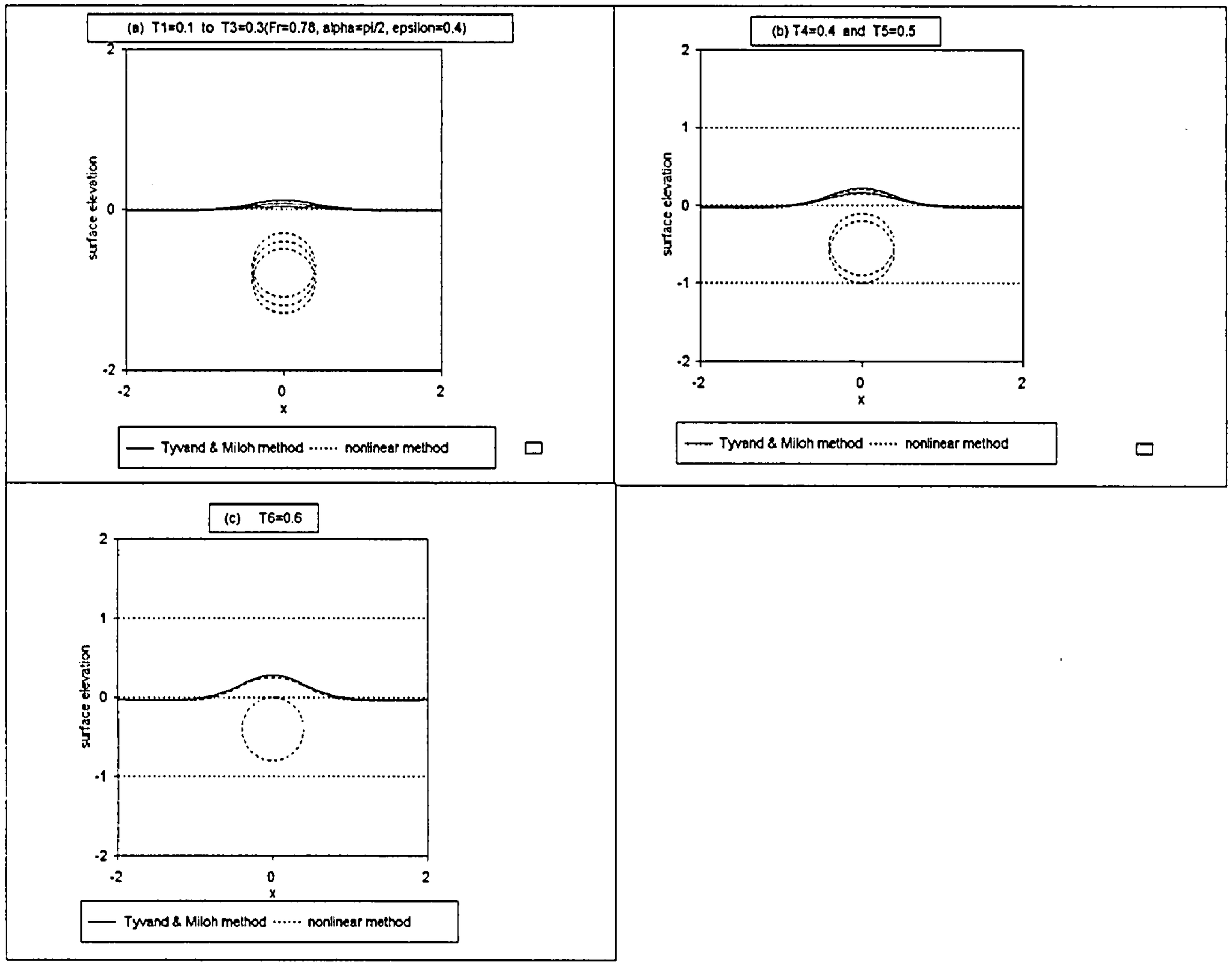

Fig. 4.13 Free-surface elevation and cylinder position due to the vertical and impulsively started motion of a cylinder below the surface. The dimensionless radius of the cylinder, time interval and Fr are 0.4, 0.1 and 0.78 respectively.

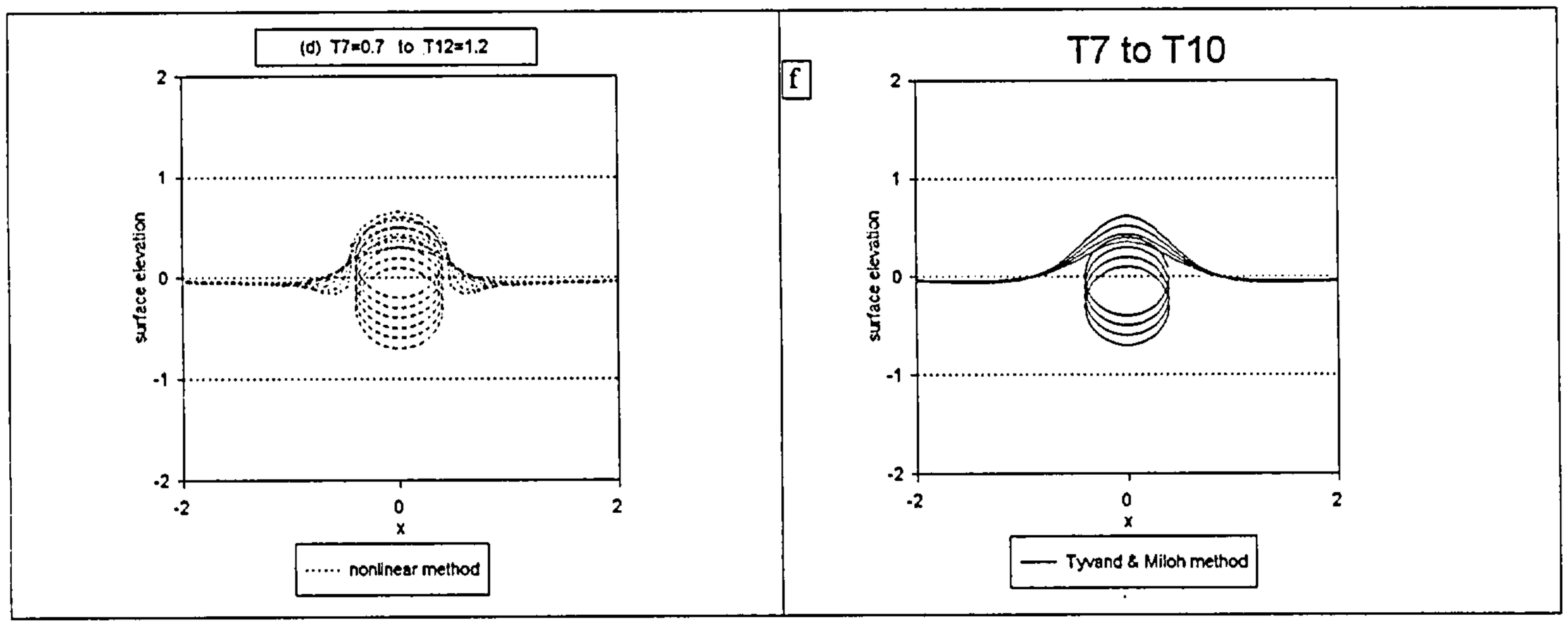
(d) T7=0.7 to T12=1.2
surface elevation
2
1
0
-1
-2
-2
0
2
x
nonlinear method
f
T7 to T10
surface elevation
2
1
0
-1
-2
-2
0
2
x
Tyvand & Miloh method

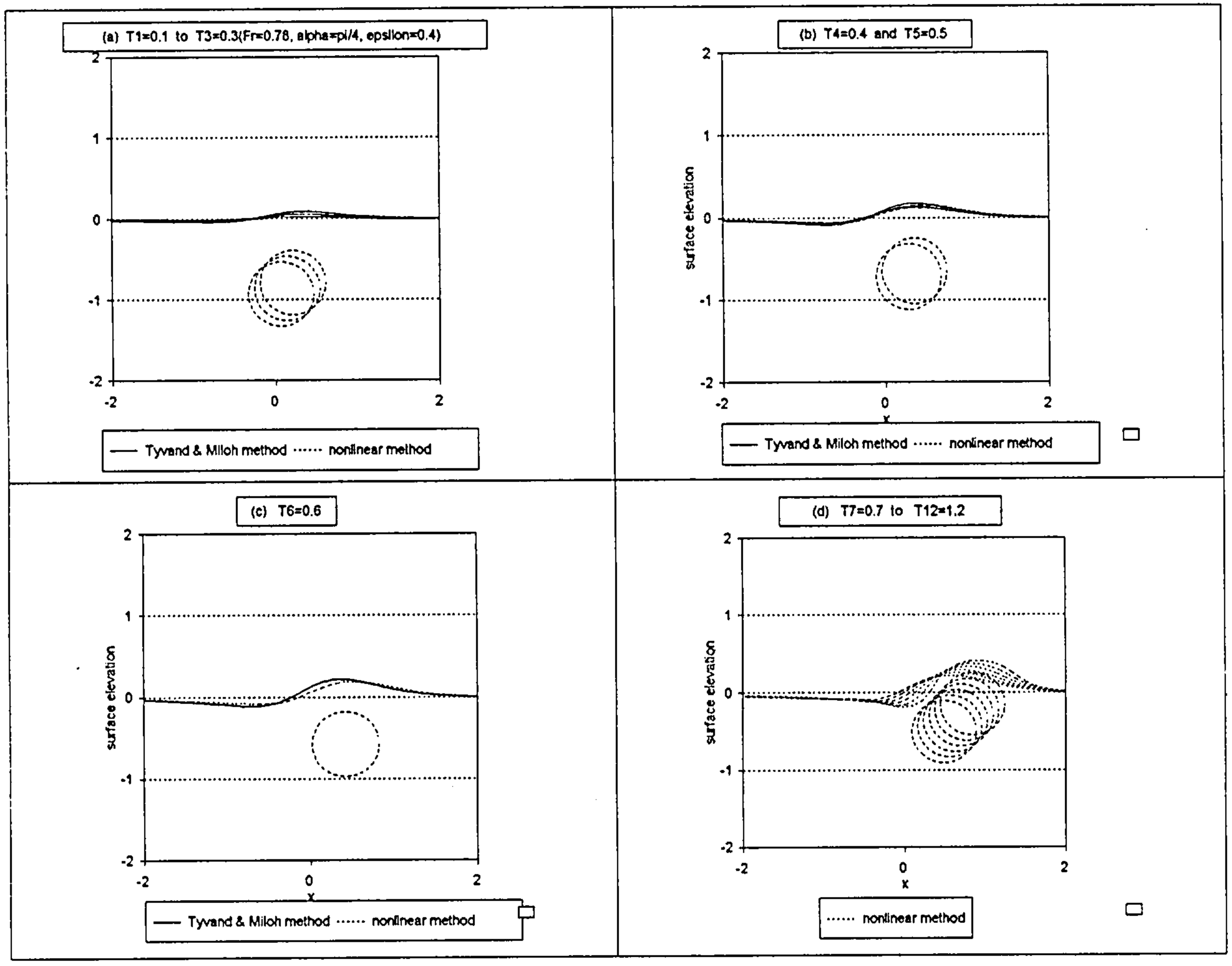

Fig. 4.14 Free-surface elevation due to the oblique and impulsively started motion of a cylinder plotted against x the horizontal displacement. The dimensionless radius, time interval and Fr are 0.4, 0.1 and 0.78 respectively.

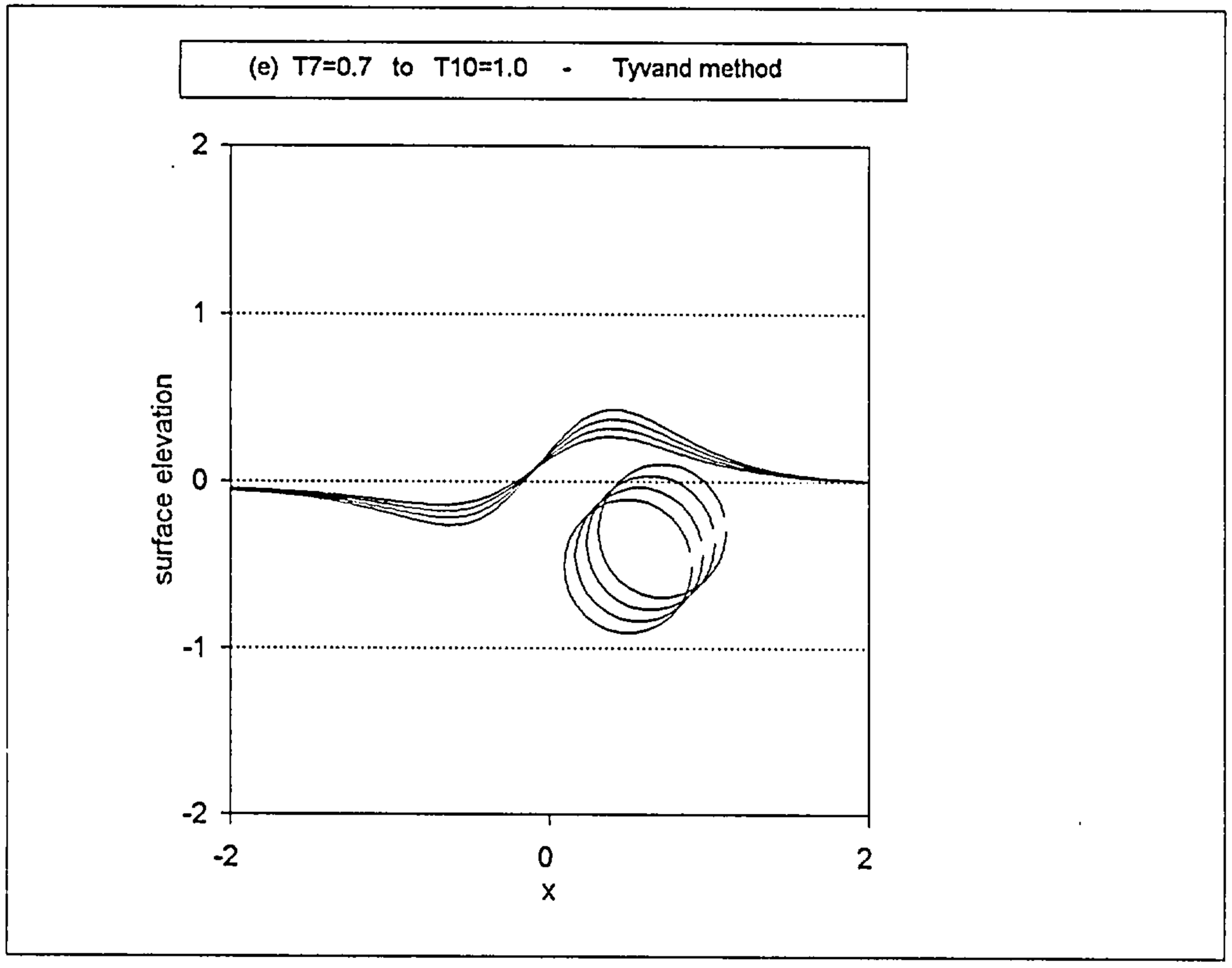
(e) T7=0.7 to T10=1.0 - Tyvand method
surface elevation
2
1
0
-1
-2
-2
0
2
x

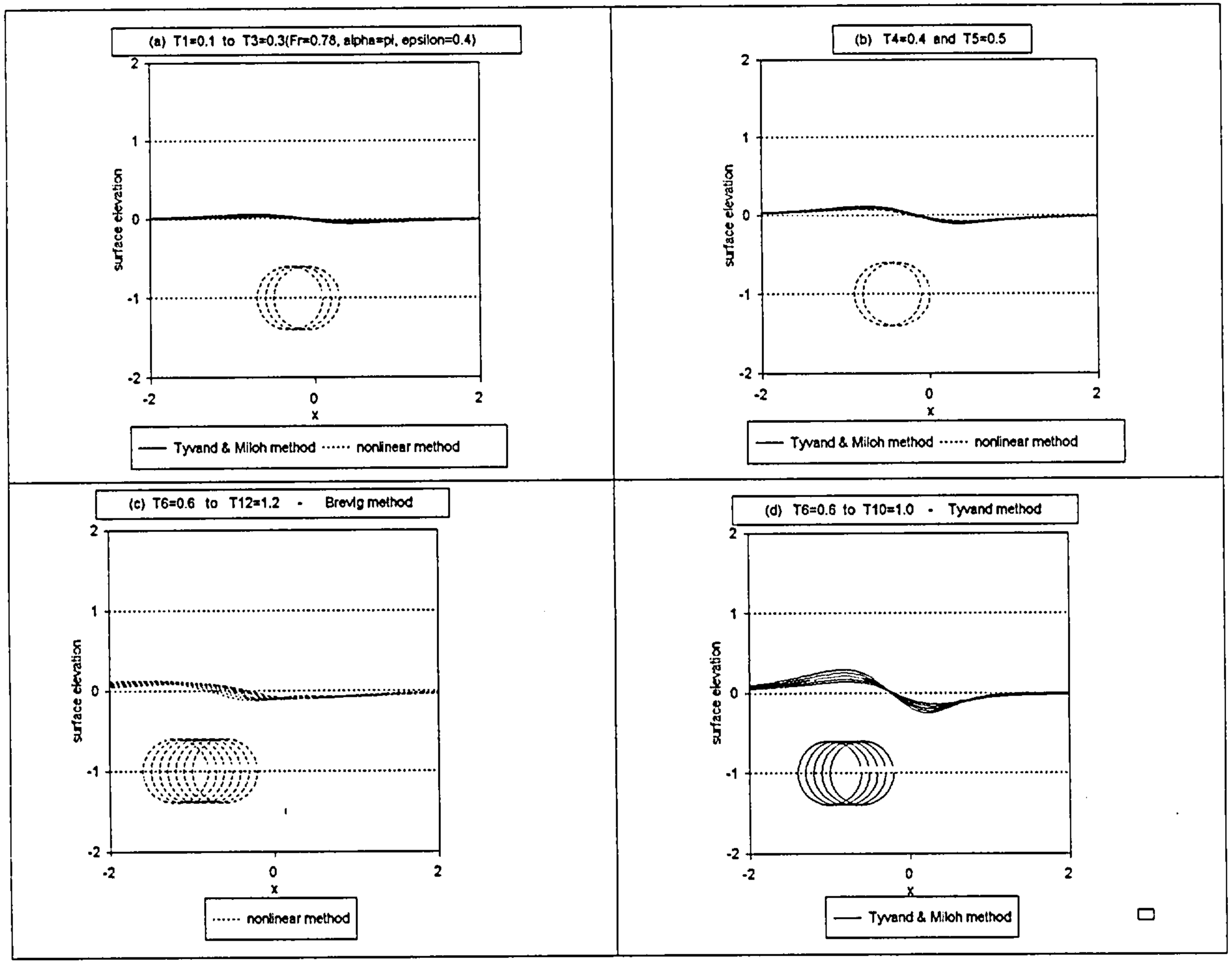

Fig. 4.15 Free-surface elevation due to the horizontal and impulsively started motion of a cylinder plotted against x the horizontal displacement. The dimensionless radius, time interval and Fr are 0.4, 0.1 and 0.78 respectively.

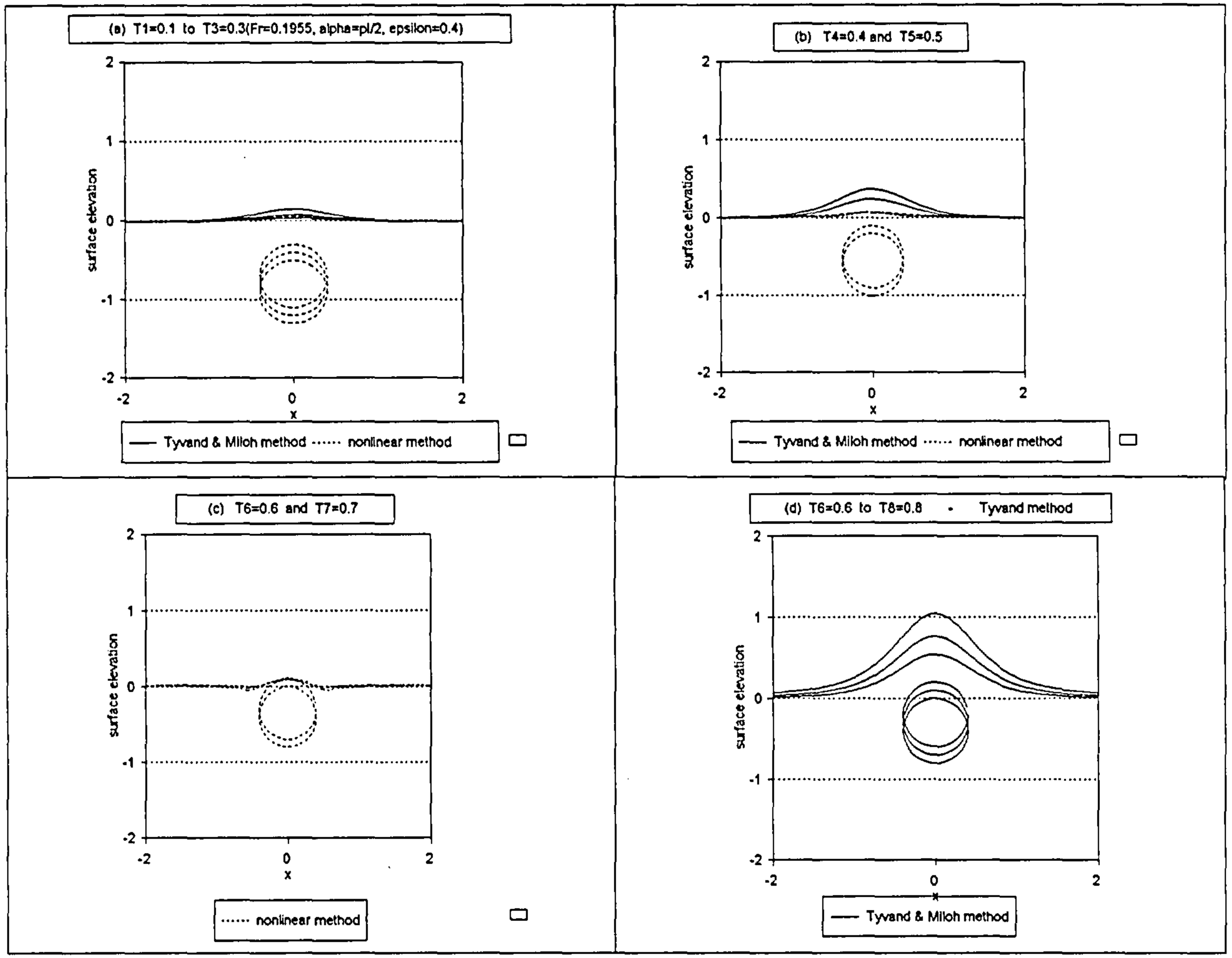

Fig. 4.15 Free-surface elevation due to the vertical and impulsively started motion of a cylinder plotted against x the horizontal displacement. The dimensionless radius, time interval and Fr are 0.4, 0.1 and 0.2.

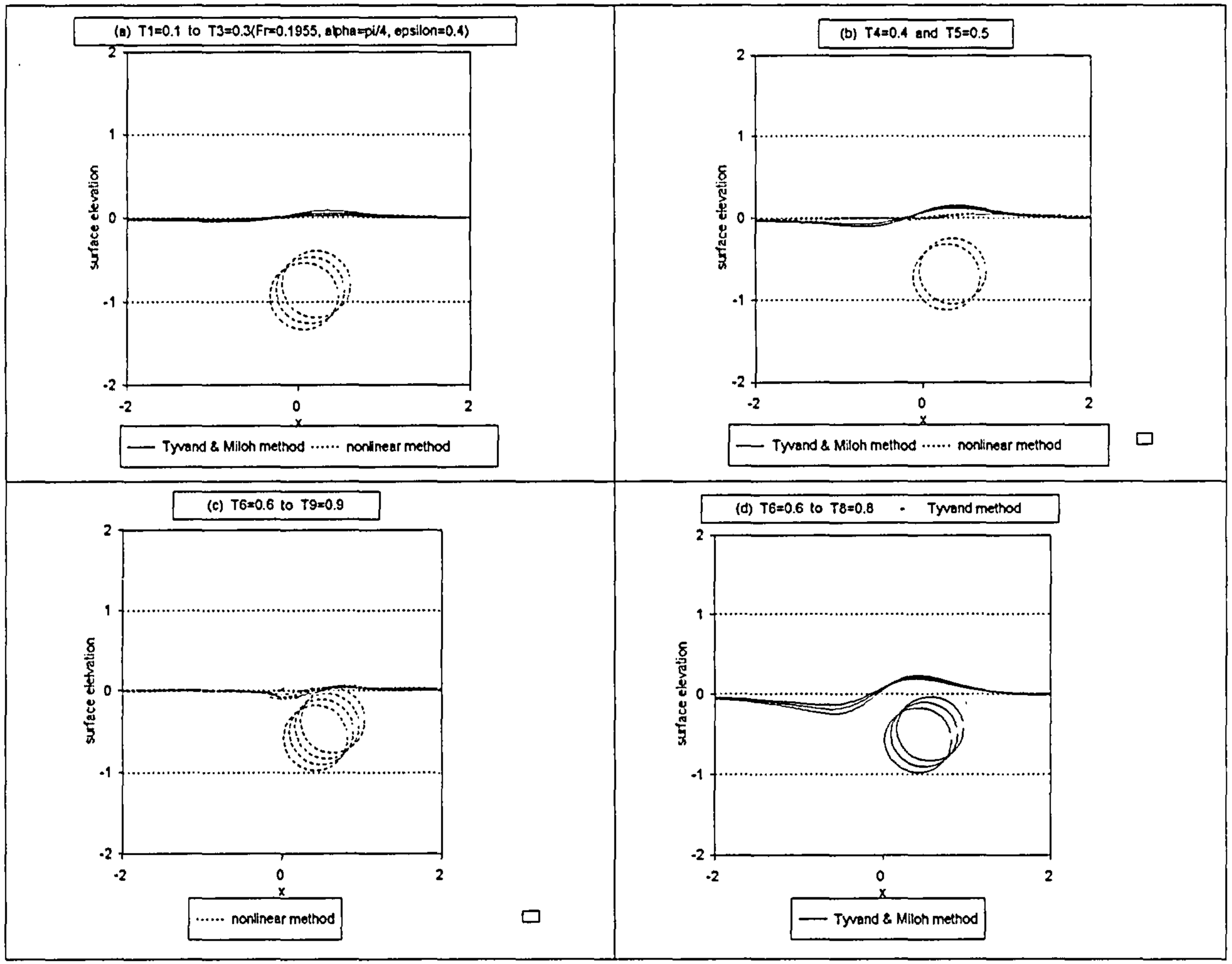

Fig. 4.17 Free-surface elevation and cylinder position due to the oblique and impulsively started motion of a cylinder below the surface. The dimensionless radius of the cylinder, time interval and Fr are 0.4, 0.1 and 0.2 respectively.

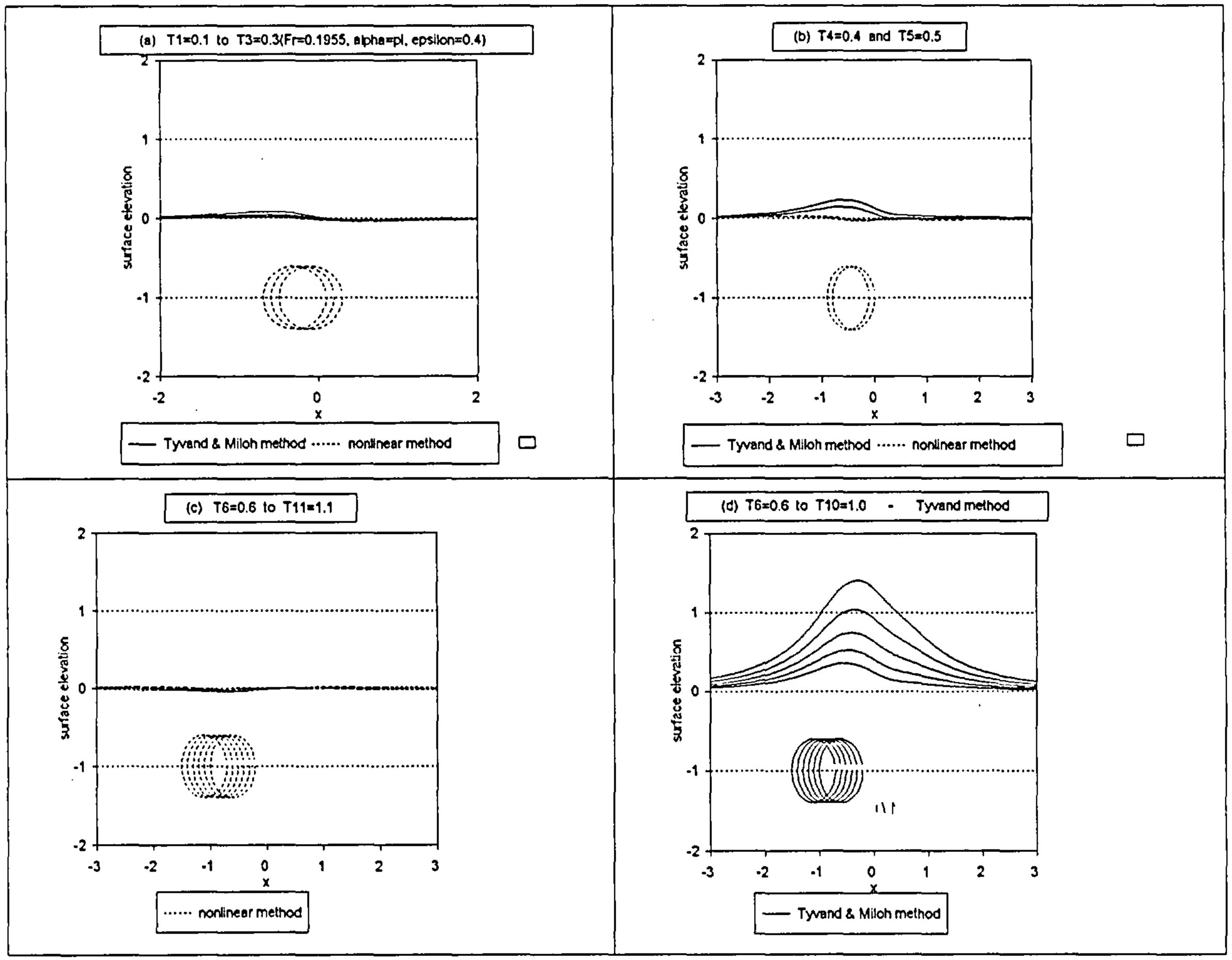

Fig. 4.18 Free-surface elevation and cylinder position due to the horizontal and impulsively started motion of a cylinder below the surface. The dimensionless r-adius of the cylinder, time interval and Fr are 0.4, 0.1 and 0.2 respectively.

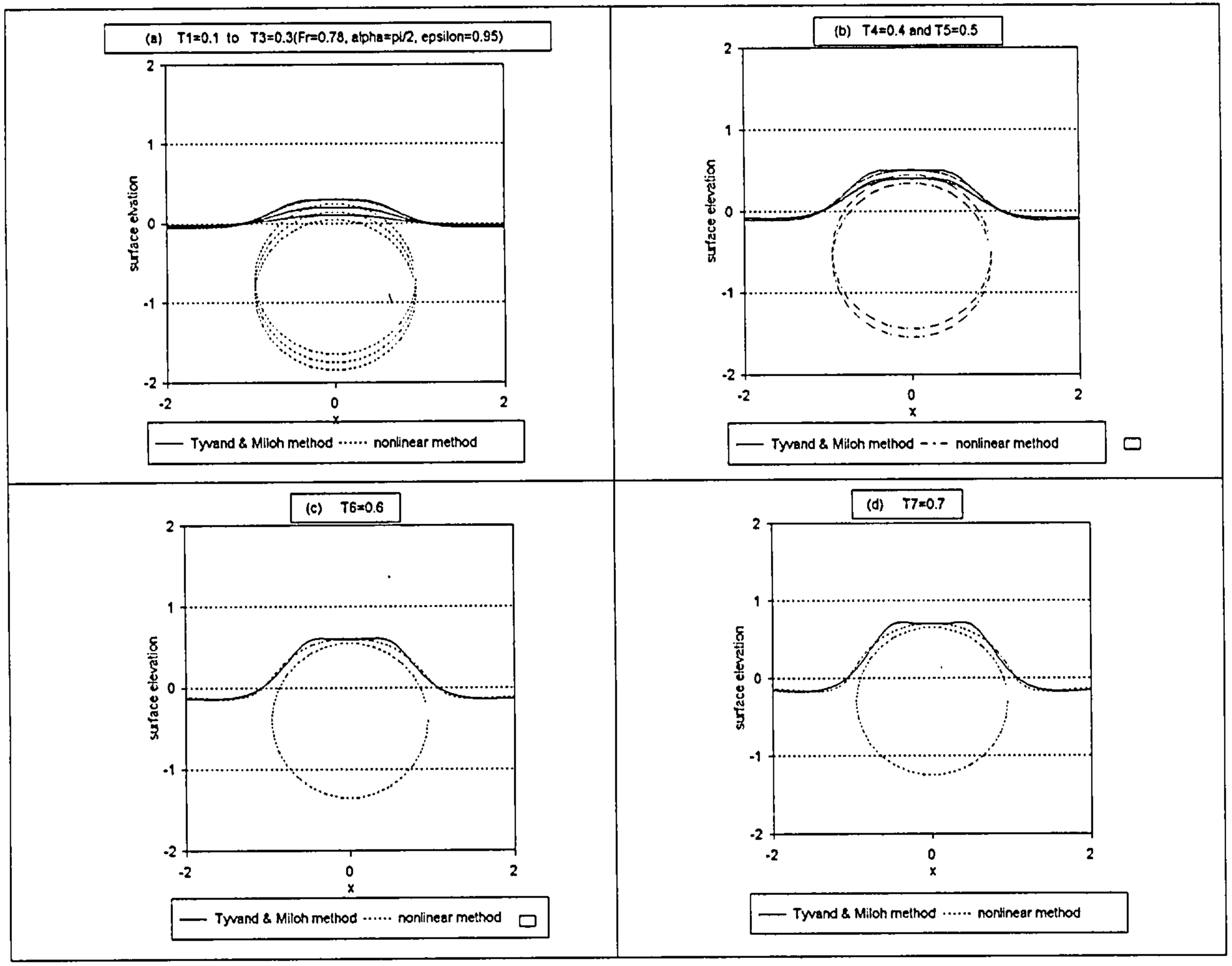

Fig. 4.19 Free-surface elevation and cylinder position due to the vertical and impulsively started motion of a cylinder below the surface. The dimensionless radius of the cylinder, time interval and Fr are 0.95, 0.1 and 0.78 respectively.

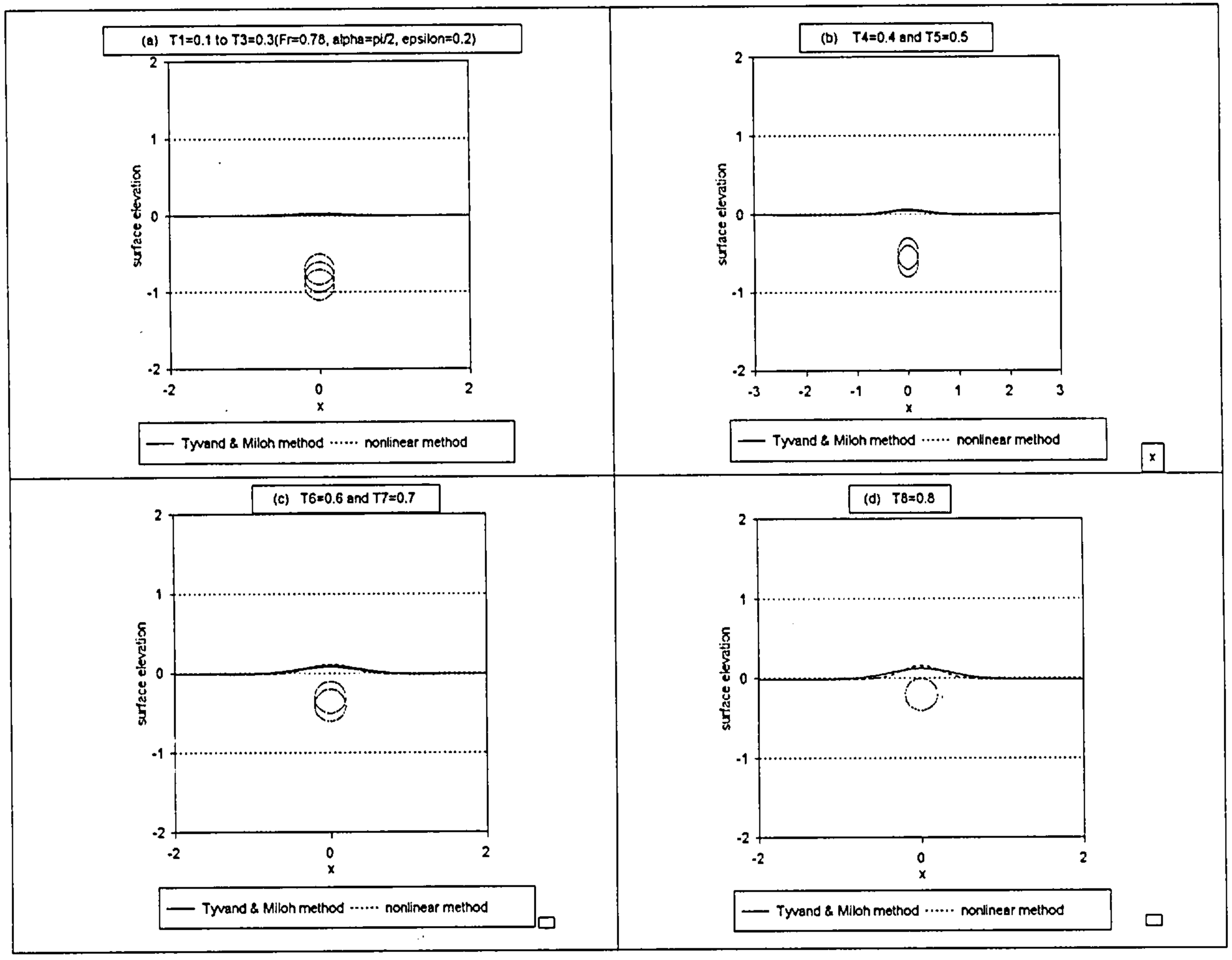

Fig. 4.20 Free-surface elevation and cylinder position due to the vertical and impulsively started motion of a cylinder below the surface. The dimensionless radius, time interval and Fr are 0.2, 0.1 and 0.78 respectively.

Chapter 5

Impulsively-started downward motion

In the preceding chapters, the investigations of the motion of a cylinder below a free surface did not cover the problem of strong interaction between the free surface and the body in the case of downward motion. Greenhow (1987) has used the method of Vinje & Brevig (1981) to simulate flow about a cylinder moving below and entering a free surface. Greenhow's paper discusses the problem of jet formation, cavity formation and the early stages of inflow over the cylinder. For initially half submerged body, he treats the intersection point in a manner discribed by Lin, Newman & Yue (1984), Greenhow & Lin (1985) and Yim (1985).

This chapter extends the results of Greenhow to the case of a cylinder already fully submerged, and gives the implications of this study for the engulfment problem of chapter 6. Tyvand & Miloh (1995) considered the small-time asmpytotic method to calculate flows with strong free/body surface interaction. As their method is not reliable for times greater than $T_{10} = 1.0$, we simply compare our results using the method of Brevig, Greenhow and Vinje (1981) for small times ($T_n < 1.0$). However, as discussed in chapter 3, for the

fully-submerged cylinder there arises a problem of high-frequency waves with short wavelength and small amplitude, as expected from consideration of the related Cauchy-Poisson problem, see Lamb (1932, pp.384-391). These waves, whilst physical, trigger numerical instability causing the numerical scheme to break down. This happens when the cylinder reaches a greater depth than in calculations which break down because of breaking waves. The details of this new feature are discussed below in section 3.

In this chapter it is also shown that the calculations can be continued indefinitely if coarse discretisation of the free surface were effected. Details of the trial run are in section 3 of this chapter. This avoids the high-frequency waves but may lead to incorrect surface elevations. Since the body forces for this case are largely hydrostatic, or given by added mass theory for accelerated motion, our primary interest is the free-surface. This means that coarse discretisation is not acceptable and is therefore not examined in great detail.

5.1 Comparison between Tyvand & Miloh method and the numerical scheme

Assume that a neutrally buoyant circular cylinder is at a distance d below the free surface. The motion is then started impulsively at various Froude numbers using the nonlinear numerical scheme and the Tyvand & Miloh method. In the case of the numerical method, calculations are pursued until the scheme fails due to either breaking waves or high-frequency waves. On the other hand, the small-time asymptotics of Tyvand & Miloh method are carried out only up $T_{10} = 1$, since beyond that time the method is known to be unreliable as noted by the authors.

As in previous chapters all the variables have been non-dimensionalised. In particular the dimensionless variables in this chapter are calculated as in chapter 4 to allow for comparison with the results obtained using the Tyvand & Miloh (1995) method. The lengths are scaled by the initial submergence depth of the cylinder, d; and time, by $\frac{d}{U}$.

Fig. 5.1-3 represent surface deflections for the downward vertical motion (i.e. at angle $\alpha = 270$ lying between the velocity vector and the positive x-axis) which varies depending on Froude number. In chapter 4 we considered cases of cylinder motion when $\alpha = 45, 90, 180$. Comparison tests between the Tyvand & Miloh method, and the fully-nonlinear numerical scheme, of the ensuing free surface response to impulsively started motion of the cylinder were made. In this chapter only calculations with $\epsilon = \frac{a}{d} = 0.8$ are discussed. It suffices to consider only this case since results for the time regions of agreement for various Froude numbers agree with the overall scheme outlined in chapter 4. Also, we note that the vertical cylinder motion, according to Tyvand & Miloh, gives a second-order elevation due to nonlinearity of the free and body surfaces for any given ϵ. This means that the second- order free-surface elevation remains unchanged, except for sign, when motion is vertically downwards or upwards. This implies that an asymmetry between upward and downward motion takes place after a finite time due to the so-called geometric nonlinearity of the cylinder since eventually the surface mound above the cylinder in upward motion is larger than the depth of the surface trough above the same cylinder in the event of downward motion, see Tyvand & Miloh (1995) for details.

In Fig. 5.1 we compare the two methods for a cylinder initially located at $d = 1.25a$ below the free surface and moving at Fr=0.13. For time less

than 0.2, the agreement is very good. When time is equal to 0.2, the depth of the surface trough above the cylinder for the two methods is the same, but noticeable differences begin to emerge over the regions $-1.38 < x < -0.24$ and $0.24 < x < 1.38$. This region increases with time until the surface elevations due to the two methods are completely separated, i.e at $T6 = 0.3$ in Fig. 5.1(f). The numerical scheme calculations are pursued further until they break down. The formation of high-frequency waves is thought to have played a vital role in triggering numerical instability, after which the calculations stop. In exaggerated scales, Fig. 5.1(g), the high-frequency waves are clearly seen in between the left and right wave-fronts.

The agreement is greatly improved when the Froude number is increased. In Fig. 5.2 we demonstrate this with $Fr = 0.38$ and initial depth remaining unchanged. We observe that the two curves completely coincide for times up to and including 0.25. The agreement is still quite good for further time steps of up to $T_8 = 0.4$ even though the regions of separation are easily noticeable as early as $T_7 = 0.35$. Later on the depth of the trough above the cylinder for the nonlinear method is decreasing rapidly, while that due to the Tyvand & Miloh method decreases less rapidly and hence this increases the difference between the two methods. During later times the surface profiles representing the Tyvand & Miloh method are shown in Fig. 5.2(g) and the nonlinear numerical method in Fig. 5.2(h). The numerical calculations have been extended up to the time when they break down because of the trough closing up and outward splashes being formed, see also Fig. 5.3(f). Such splashes are physical but difficult to follow with the discretisation chosen here; in any case the calculations must break down at jet touch down shortly after the last step shown here.

In Fig. 5.3 the free-surface profiles for Fr=0.64 are depicted. The profiles are qualitatively the same as those in Fig. 5.2 except for the region where the two methods disagree. Here for $T_7 = 0.35$ the distance between the curves on the approximate interval $-0.6 \leq x \leq 0.6$ is fairly constant and persists until $T_8 = 0.8$. Thus the qualitative agreement between the two methods is close in this case, both being physically reasonable. This agrees with the previous observations in chapter 4 that the agreement is greatly enhanced by the increase in the Froude number. The widening difference at larger times is as expected, since the Tyvand & Miloh method is for small time only. The accurate nonlinear numerical calculations are continued until the scheme breaks down as before. The breakdown of the calculations is further investigated in the next section.

5.2 Breakdown of the calculations

In this section we discuss the causes of the breakdown in numerical calculations using the Brevig, Lin & Greenhow algorithm. There are two situations of breakdown of calculations observed, both physical, due to a) breaking waves when the motion is started very close to the free surface, $d = 1.25a$ say, and b) formation of high-frequency waves with short wavelength and small amplitude when the motion is started further away from the surface, $d = 1.35a$ say, or with low constant velocity as in the case of $Fr = 0.13$, see Fig. 5.1(g). The later causes effects consistant with those of localised disturbance studied by Cauchy and Poisson(see Lamb 1932, p. 387, for detailed explanation). The analysis presented below seeks to demonstrate that the breaking down of the numerical calculations for motion in specified regions arises from physical ef-

fects and is not purely numerical. An understanding of this kind will inevitably assist in understanding the complexity of the engulfment problem looked at in chapter 6. In other words this analysis sets limits within which the algorithm is efficient; otherwise changes in the numerical treatment (i.e smoothing) could be made to suppress the arising complications of the free surface, leading to more robust, but less accurate, calculations which could be continued for larger times. In this section the lengths are scaled by the radius a of the cylinder; time by $\frac{a}{U}$; and the Froude number, is defined by

$$Fr = \frac{U}{\sqrt{ag}} \qquad (1)$$

Mass is scaled by $\rho\frac{(NBODY)a^2}{2}\sin(\frac{2\pi}{NBODY}) \rightarrow \rho\pi a^2$ as $NBODY \rightarrow \infty$; and pressure by ρU^2.

5.2.1 Examples with breaking waves

Now we consider the impulsively-started motion of a cylinder initially positioned at $d = 1.25a$ below the free surface. The cylinder is forced to move downwards at various Froude numbers and the distance at which calculations breakdown is noted for each run. In the first case the cylinder is forced downwards at $Fr = 0.14$, time step $\Delta T = 0.02$ with 44 points on the body and fine free surface resolution (points are more densely spaced around the origin). The calculations break down immediately after the submergence depth is $d = 1.3a$. The breakdown of the calculations is believed to be caused by failure of the scheme to resolve the free surface accurately enough to avoid triggering numerical instability. We have no reason to believe that the breakdown is physical and hence we pursue this further. This suggests that the time-stepping interval is too large, and this was changed. The time step was then reduced

to $\Delta T = 0.008$. The situation is also greatly improved by a slight increase in velocity of the body while keeping the time step, number of points on the body and free surface, and spacing of the free surface points unchanged. Calculations at $Fr = 0.14$ were extended to at least $d = 1.8a$ before breaking down. Free-surface elevations for later stages of this case are shown in Fig. 5.1(g)-(h). After several other trials of spatial resolutions and time intervals failed to produce better results, the set of initial conditions with fine free-surface gridding, 44 points on the body and $\Delta T = 0.008$ were then assumed standard for similar motions of the cylinder below the surface depending on Froude number. In the computations that follow, the standard initial conditions have been used. We look at the cases when $Fr = 0.43, 0.71, 0.29$ below.

Here we have considered motion at $Fr = 0.43$ while the initial submergence depth has remained unchanged. These calculations break down at submergence depth $d = 2.56a$ compared with $d = 1.8a$ for the previous case. Also, we notice a change in the way the calculations have broken down. In Fig. 5.2(h) a steep wave is clearly seen developing, on both sides of the origin, up to the point when the spilling breaker is fully formed. At this stage a volume of fluid is elevated above the mean water level in the area directly above the body. This is caused by the collision of the left and right inflowing fluid above the cylinder, forcing a volume of fluid to be projected upwards. The behaviour of the free surface of this nature increases the steepness of the wave, with the displaced mound of fluid flattening at the top and hence enhancing the tendency to surface breaking. The jets must arise and be accelerated outwards because of the increasingly high pressure below the flat free surface. At this point a breaking wave is fully developed and there is clearly no possibility

of continuing the calculations; they immediately break down. The reason for this is certainly physical and hence there is no point in trying to continue the calculations. Coarse spacing of the points along the free surface could possibly suppress the problem, but this would result in incorrect surface coordinates being calculated. A similar breaking effect as at $Fr = 0.43$ is observed with runs at $Fr = 0.29, 0.71$. Surface profiles for $Fr = 0.71$ are shown in Fig. 5.3(f). The free surface deflects similarly and a spilling breaker is formed which inevitably leads to the breakdown of the calculations.

The free surface deflections for the motion of the cylinder at $Fr = 0.29$ are shown in Fig. 5.4 with corresponding total pressure distribution and graphs for separate hydrostatic and hydrodynamic pressure distributions around the cylinder. Much of the pressure profiles is as expected, for example total pressure distribution increases with time at every point of the cylinder. This pressure (largely hydrostatic) is greatest at the bottom ($\theta = 270°$) and smallest at the top ($\theta = 90°$) of the cylinder. At later times the pressure at the bottom of the cylinder, on the interval $180° < \theta < 360°$, has increased steadily and symmetrically about $\theta = 270°$ achieving its greatest maximum at time $T = 1.088$, a step before the calculations fail. On the other hand around the top part of the cylinder, pressure has increased steadily but is fairly constant in interval $60° < \theta < 120°$ and is symmetric about $\theta = 90°$. The total pressure distribution is effectively increasing equally on the interval $60° < \theta < 120°$ for more than 30 time steps. The hydrostatic pressure distribution around a circular cylinder is sinusoidal with amplitude $p_2 - p_1$, where p_1 is the hydrostatic pressure at the top of the cylinder and p_2 is the hydrostatic pressure at the bottom of the cylinder. Sinusoidal curves representing hydrostatic pressure

are shown in Fig. 5.4(c)&(f). The tendency of flattening of the total pressure distribution curve, around $\theta = 90^{o}$, is therefore due to hydrodynamic pressure.

Total vertical force, non-dimensionalised by the buoyancy force

$$\frac{NBODY}{2} g a^2 \sin(\frac{2\pi}{NBODY})$$

on the cylinder computed using the numerical scheme is now compared to that obtained by the analytical model using added mass theory in Fig. 5.7. The latter is based on the assumption that the free surface remains wall-like during the motion. The total force, in the case of the numerical scheme, increases slightly at the start of the motion before gradually diminishing and stabilises around 1 at larger times. Vertical force, F(T), according to analytical method is calculated using the equation (2.9) in the form

$$\frac{1}{2}\frac{dM_a}{dY}\dot{Y}^2 + 1 = F(T) \qquad (2)$$

since acceleration is zero. Buoyancy plus the term involving the rate of change of the added mass give us the required vertical force, which is slightily greater than 1 at the start of the motion. This force gradually decreases and tends to 1 at larger times.

The initial increase in vertical force, in the case of the numerical method, is believed to be due to free surface disturbance. At the start of the motion, the cylinder has to do work on the fluid to create surface movements, which therefore retards the motion. Further down the effect of the free surface movements becomes weaker. The hydrodynamic force is also gradually reducing as hydrodynamic pressures are reduced, see Fig. 5.4(k). On the other hand the vertical force according to the analytical method diminishes with depth mo-

tonically because of the depth-dependent added mass. As $Y \to -\infty$, $\frac{dM_a}{dY} \to 0$ and hence $F(T) \to 1$. The force is not expected to increase initially since the model is contructed on the assumption that $\frac{\partial \phi}{\partial Y} = 0$ on $Z = 0$.

The above free-surface profiles indicate that there is a limit for the initial submergence depth at some Froude numbers, for which motion below the surface can be started, and which end when a spilling breaker is formed. It is clear that the motion of the cylinder below a free surface can be started from very close to the surface, say $d = 1.25a$, and continued up to a certain distance, $d = 2.32a$ in the case of $Fr = 0.29$, a distance by which a spilling breaker is fully formed. Greenhow (1988) presents results for water-entry of a horizontal circular cylinder where a surface-piercing code was used. The "*submerged*" cylinder in fact had a slender vertical wall piercing the surface, which has no hydrodynamic effect. The present results show it is therefore possible to extend Greenhow's (1988) calculations up to the distance recorded in the above runs, and perhaps even further, since the method follows the jetting fluid. This is discussed in detail in sections below, where we also establish another limit for initial submergence depth at suitable Fr number for which we again encounter breakdown of calculations due to different behaviour of the free surface.

5.2.2 Examples with high-frequency waves

The motion of the cylinder is started from an initial submergence depth of $d = 1.35a$ at $Fr = 0.29$. At first, fine surface spacing around the region directly above the body, with a standard time step size and number of points on the body and free surface, is used. The calculations broke down at $d = 3.6a$ due to behaviour of the free surface analogous to the physical instability discussed

by Cauchy and Poisson (see Lamb 1932, pp.384-394) in their study of localised disturbance. Fig. 5.5 shows the sequence of physical response of the free surface to this motion.

If a sinusoidal travelling wave is sought, then the free surface equation is

$$\begin{aligned} y &= \eta(x,t) \\ &= A\cos(kx-\omega t) \end{aligned} \qquad (3)$$

where A is the amplitude of the surface elevation, k is the wave number, and ω is the frequency. Linear water wave theory then gives the dispersion relation

$$\omega^2 = gk \qquad (4)$$

where we have assumed deep water.

The cylinder creates localised disturbance of the free surface around the origin, and we therefore have a dispersive system with group velocity which depends on k. Initially the free surface seems to be collapsing behind the cylinder, before it performs a very complicated motion, or rather, responds to the motion of the cylinder in a very complicated way. After a short time there is then a well-developed wavetrain which is approximately sinusoidal locally with a wavenumber $k(X,T)$ and frequency $\omega(X,T)$ which change with X and T. As expected in our case of surface waves on deep water, the wavelength λ increases with X in the outward direction on both sides of the origin. The calculations indicate that the disturbance propagates outwards from the origin in the form of individual waves. A transient wave-front starts from around $x = \pm 0.6a$.

In Figs. 5.5-6 we show waves of long wavelengths and bigger amplitude forward of the wavetrain. The wavetrain actually occurs over a distance of several individual waves, due to dispersion. For a typical group at time $T = 1.76$ we

found $\lambda = 0.19a$ and amplitude A=0.008a for an individual wave immediately behind the wave-front and $\lambda = 0.042a$ and A=0.004a for the wave at the origin. During the later stages of the calculations the wavelengths and wave amplitudes increase. As T increases, the distance between the crests in the region of the wavetrain becomes comparable with, even though smaller than, the length of the wavetrain itself. However, the contributions from the whole region of disturbance are no longer meaningfully in the same phase, and the required fine resolution of the free surface seems to cause numerical instabilities leading to break down of the calculations. Experiments with several surface discretisation and time steps were fruitless as the scheme always failed at approximately the same region of the free-surface and at the same time.

To further understand this problem we have included total pressure distribution profiles calculated at the same times as the surface elevations presented, see Fig. 5.7. In this case the total pressure distribution profiles are qualitatively the same as in Fig. 5.4, even though here the distribution is more hydrostatic than the previous one. This is as expected since the cylinder is now moving at greater depth than in the other case. The total pressure remained positive throughout the calculations. The total vertical force increases at first and then decreases slightly to about 1 during later times (as was the case with the previous case, $d = 1.25a$).

To test further the reliability of these results, the program used by Greenhow(1988) for a partially submerged body was used; calculations were carried out using both codes for motion starting from $d = 1.35a$ at $Fr = 0.29$. The results obtained by the two codes compare very well. The profiles using the code for a submerged cylinder with a vertical wall or spike in the vertical plane

of symmetry (which plays no part in the hydrodynamics), are shown in Fig. 5.8. Development of high-frequency waves responsible for triggering numerical instability is clearly seen in Figs. 5.8(c-d).

Since the instability does not seem to be triggered by the time-stepping procedure, we can conclude that this instability is caused by the spatial resolution (free-surface discretisation) used. A check on initial distribution of points on the waves followed by regridding later on at a finer scale could postpone the breakdown, but is not attempted here. In reality the free surface profiles around the region of disturbance will also involve surface tension, unaccounted for in the present discription of the problem. On the other hand, coarse discretisation of the free surface avoids the problem by simply inhibiting the high-frequency wave formation, but this may lead to incorrect free surface coordinates being computed. An example run was done for motion starting from $d = 1.4a$ below the surface at $Fr = 0.29$, see Fig. 5.9. The calculations showed no signs of numerical instabilty for 400 time steps and could be continued for larger time steps without any foreseable problem. The pressure distribution and total vertical force (both largely hydrostatic) are virtually unaffected by this procedure. This means that at equal distance below the free surface, for the two cases, the pressure distribution and total force are equal.

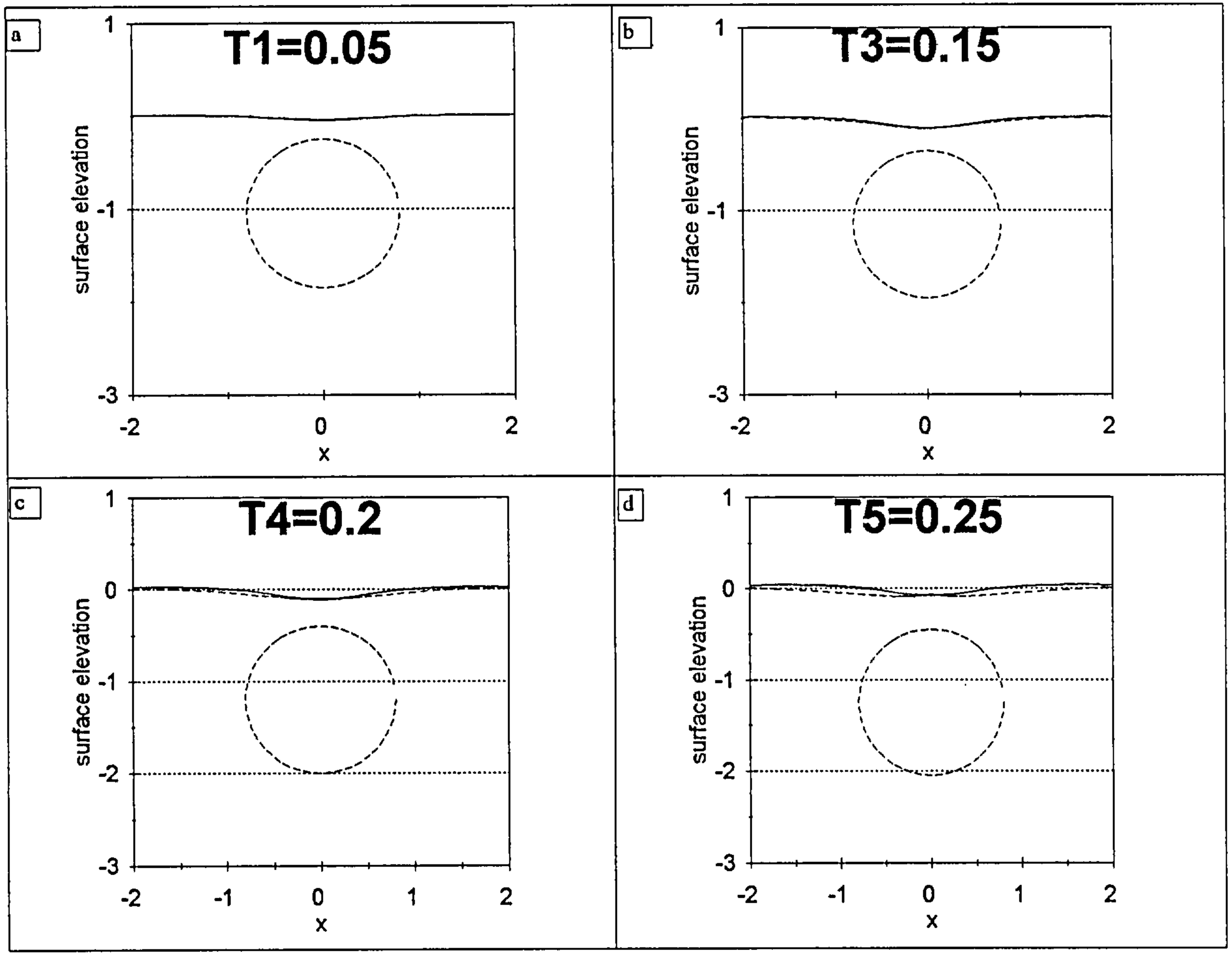

Fig. 5.1 A comparison of the free-surface elevations due to impulsively started motion of a cylinder using the nonlinear (dotted) and Tyvand & Miloh (solid) methods at Fr=0.13 and d=1.25a.

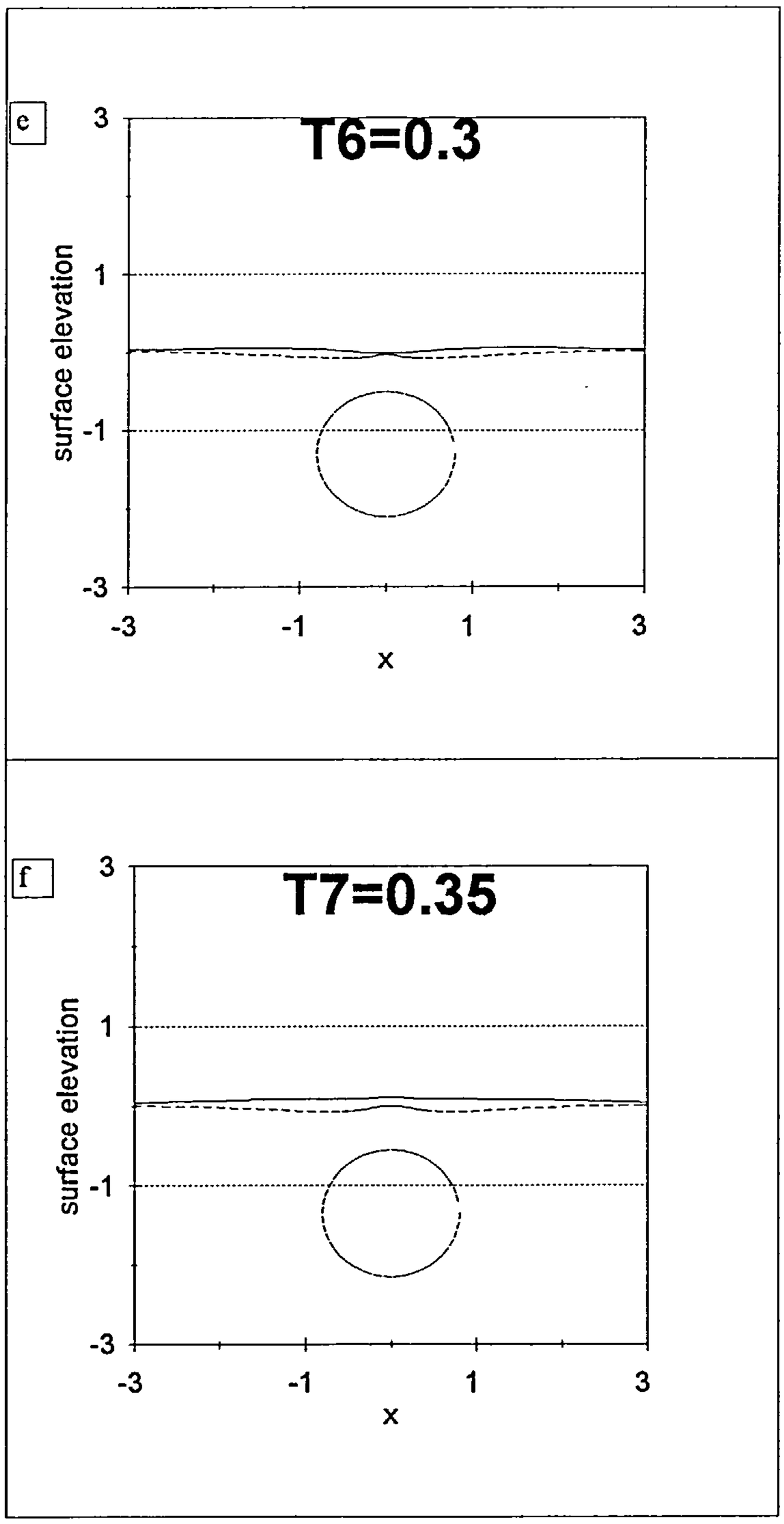

Surface elevations for later stages of the calculations.

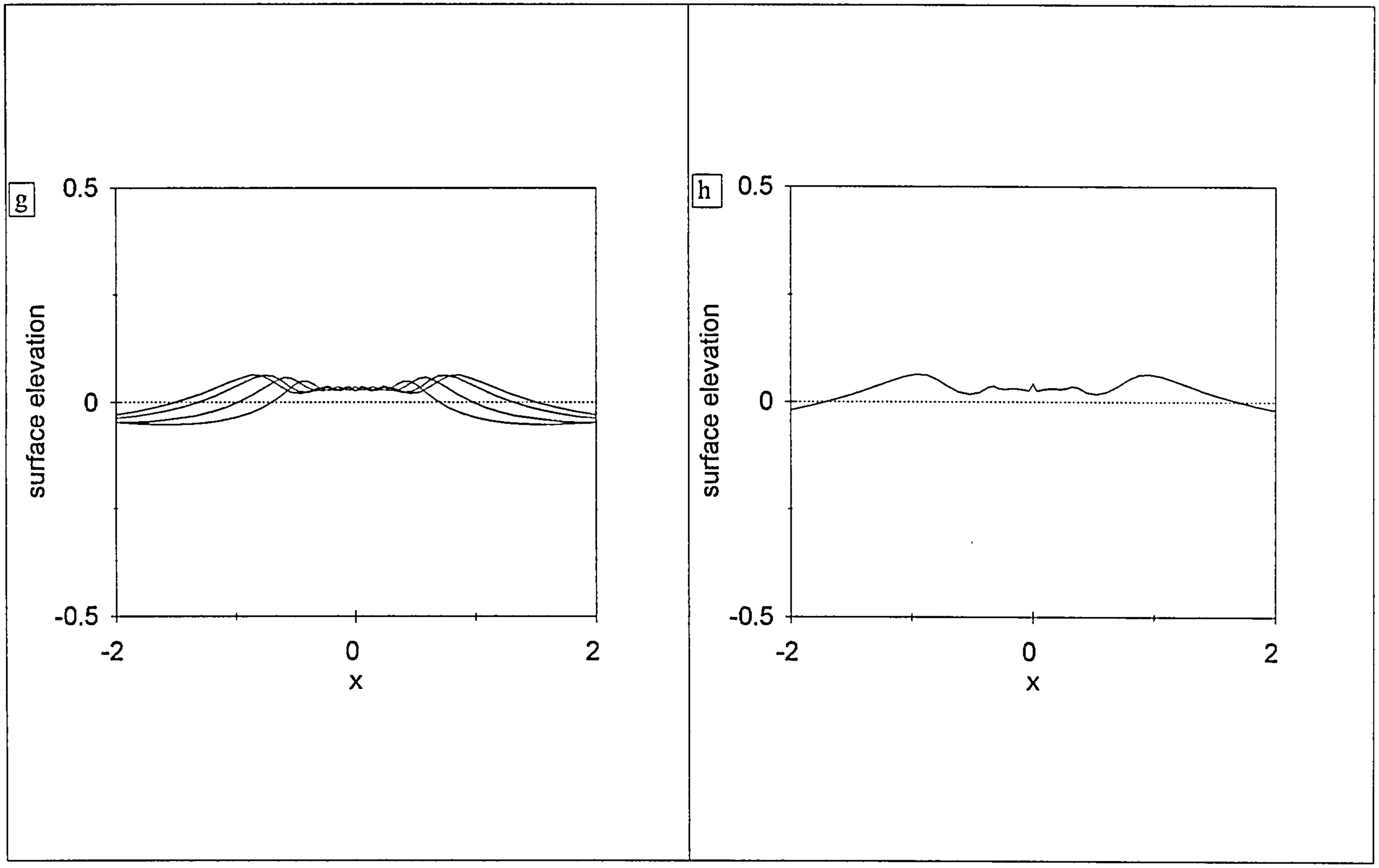

Ccontinuation of the above calculations.

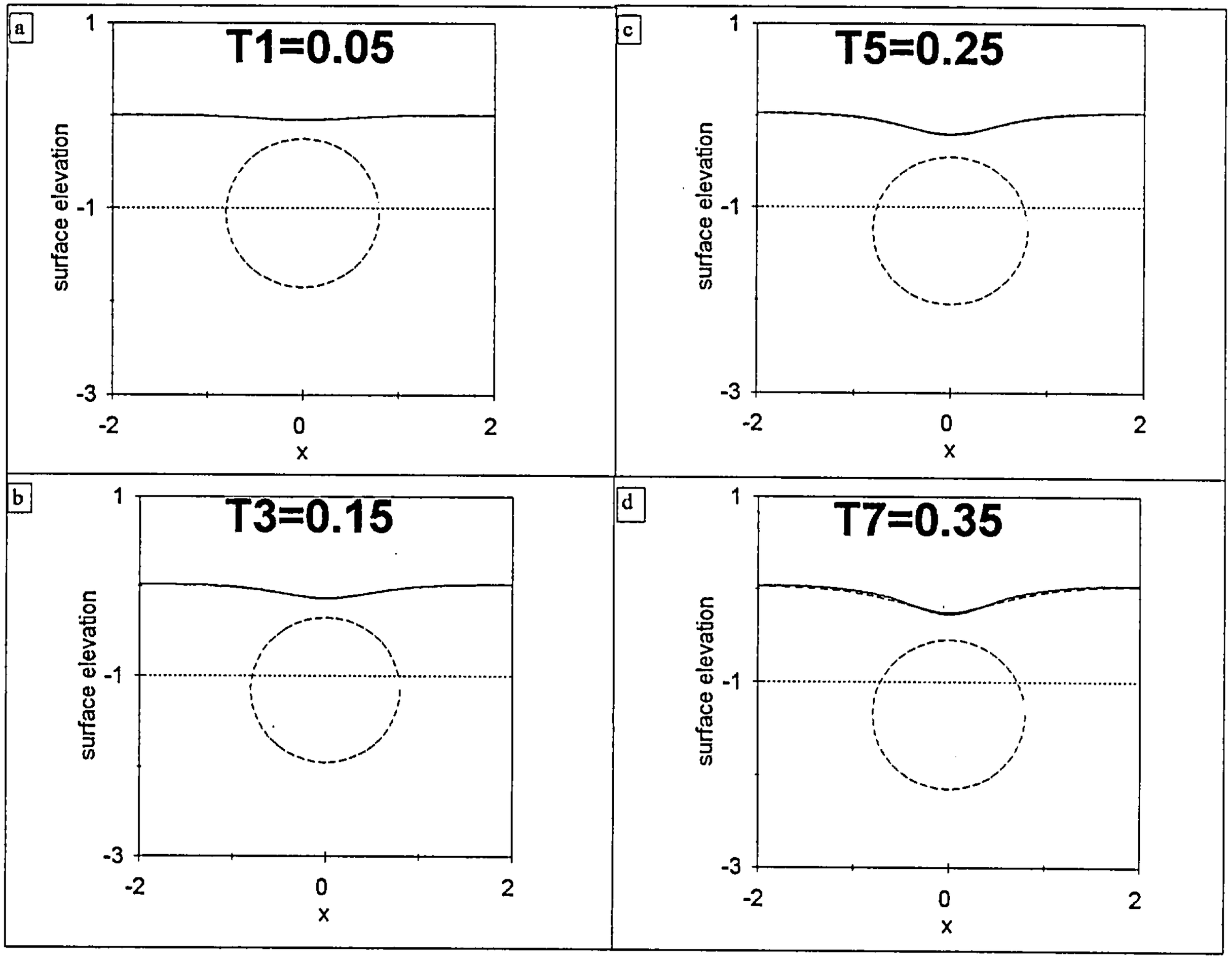

Fig. 5.2 A comparison of the free surface elevations due to an impulsively started motion of a cylinder using the nonlinear and Tyvand & Miloh(Ty & Mh) methods at Fr=0.38 and d=1.25a.

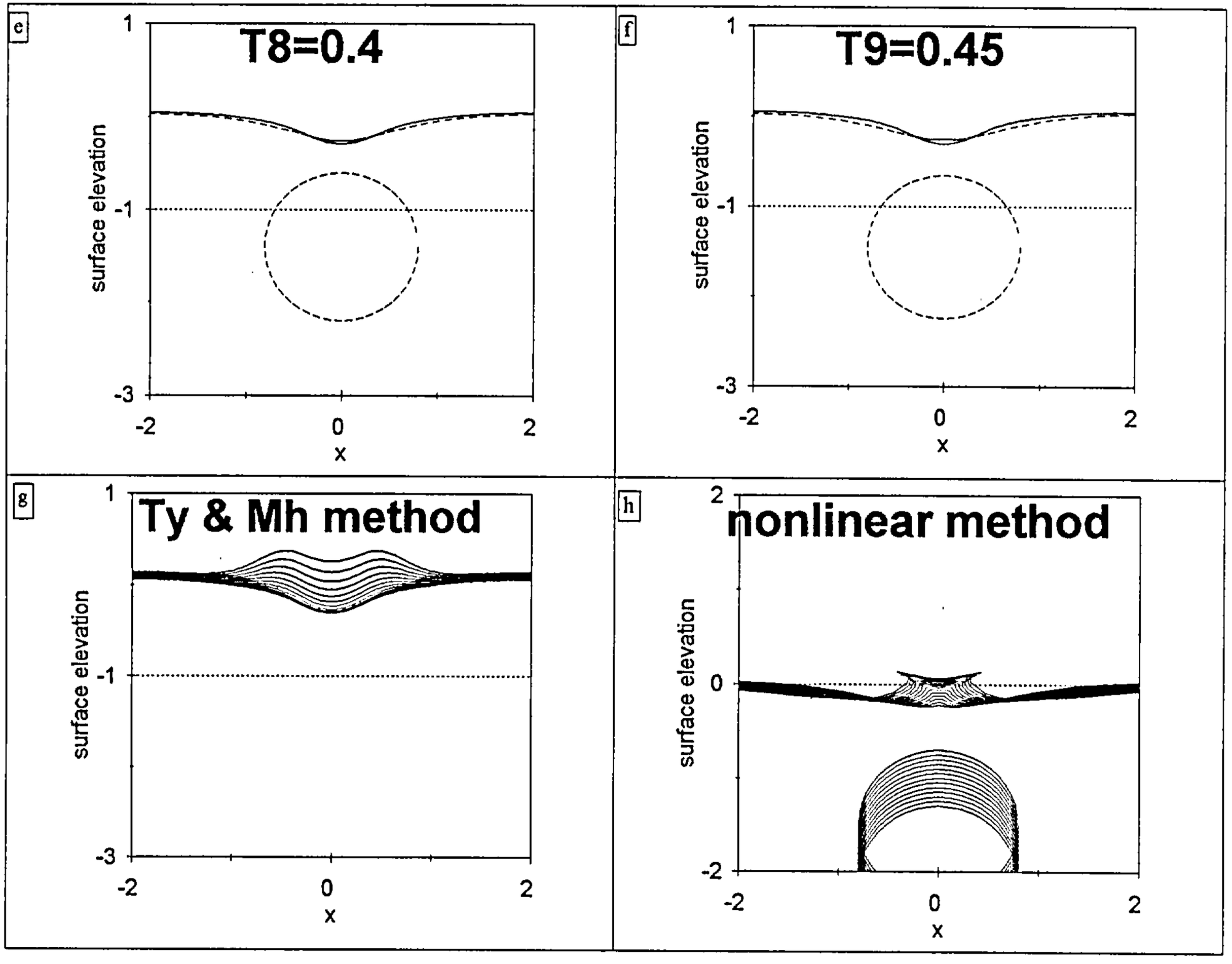

Continuation of the calculations.

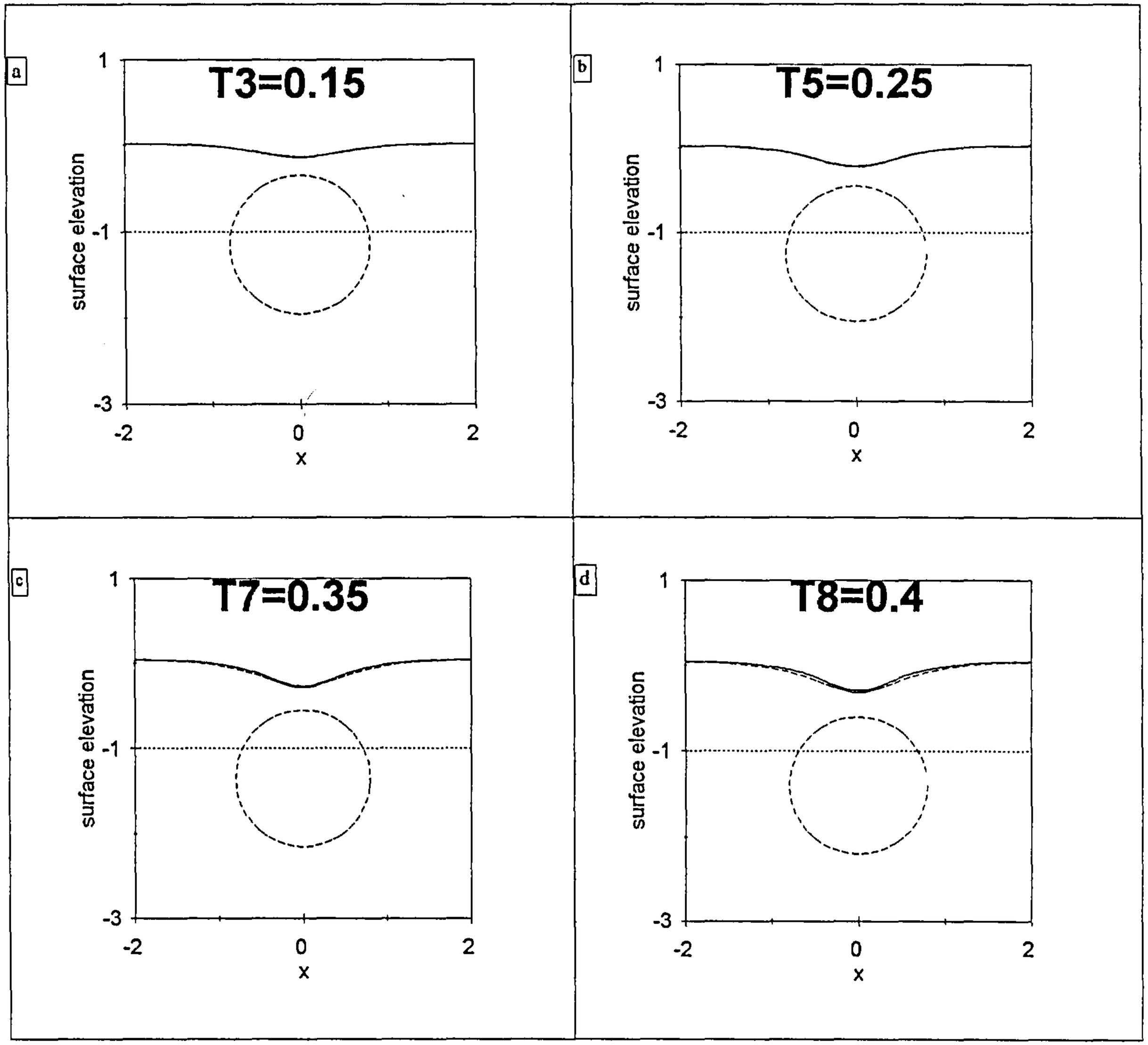

Fig. 5.3 A comparison of the free surface elevations due to an impulsively started motion of a cylinder using the nonlinear and Tyvand & Miloh methods at Fr=0.64 and d=1.25a.

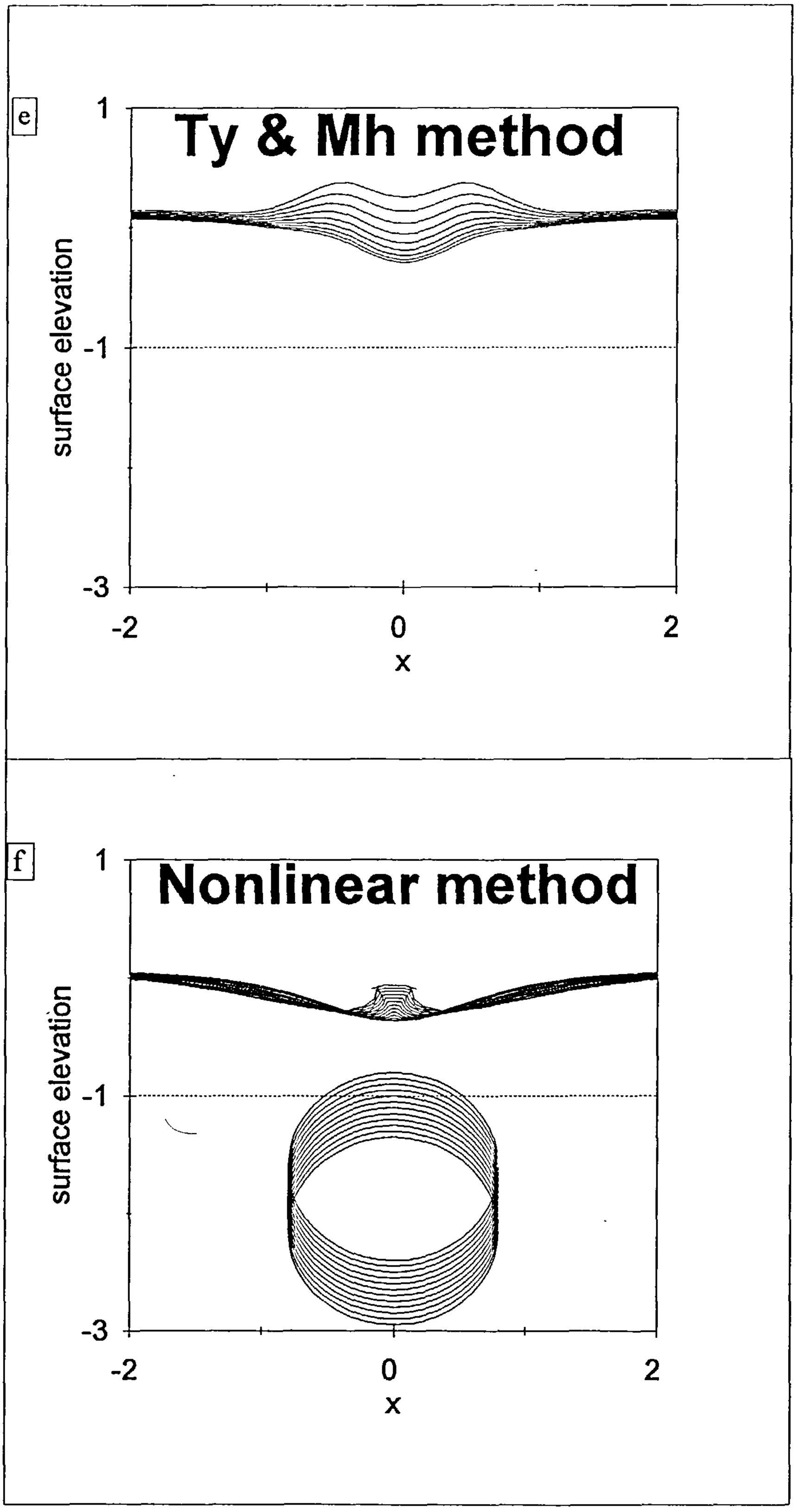

Surface elevations during later stages of the calculations.

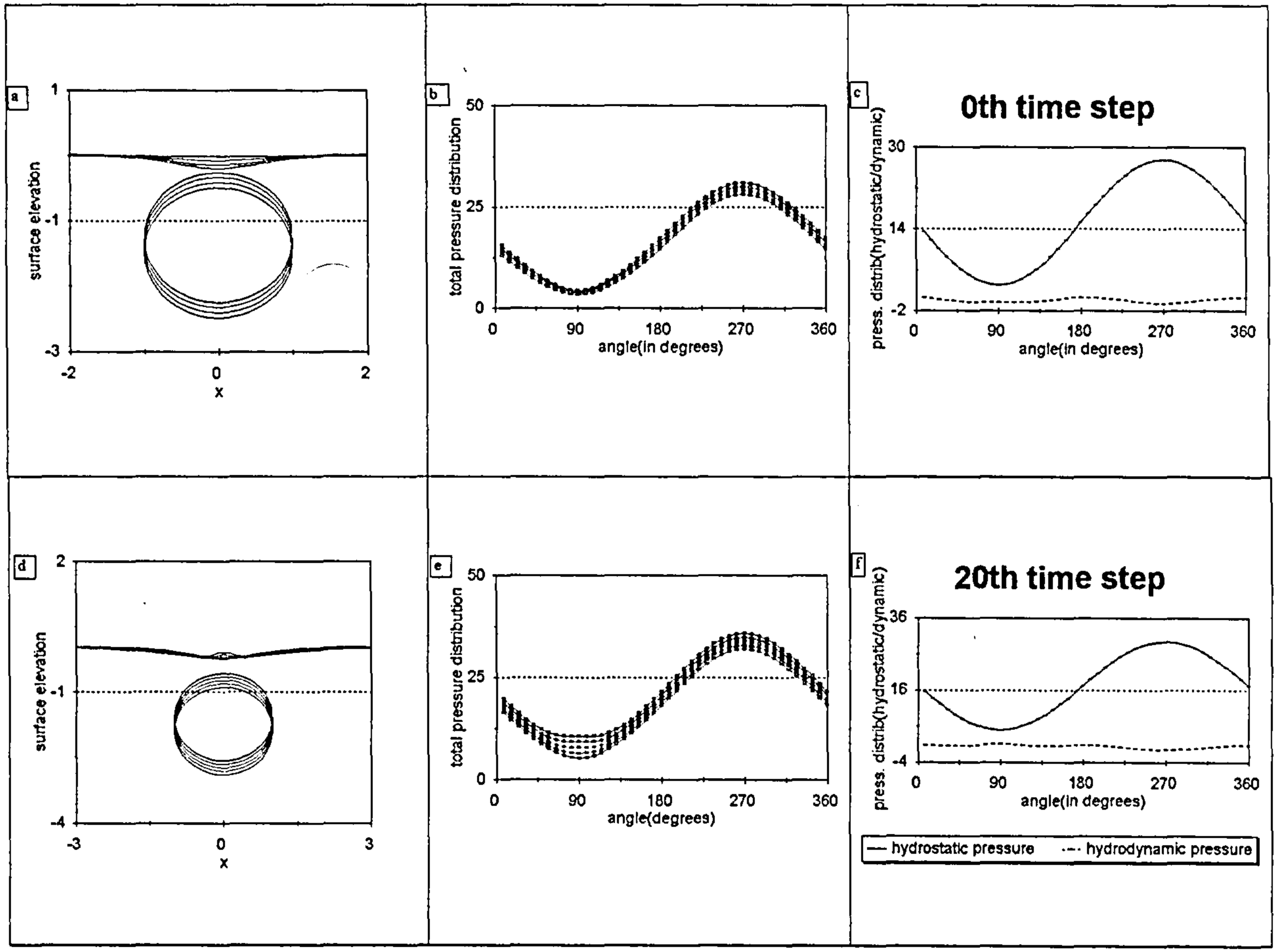

Fig. 5.4 Free-surface elevation and pressure distribution around the cylinder due to an impulsively started motion of a cylinder below the surface at Fr=0.29 and d=1.25a. (a), (d), (g) and (j) represent surface elevations; (b), (e), (h) and (k) represent total pressure distribution corresponding, in time, to adjacent given surface elevations; and (c), (f) and (k) represent hydrostatic, in solid lines, and hydrodynamic, in dotted lines, pressure distributions corresponding to adjacent(0th-first and 20th-last) total pressure distribution lines.

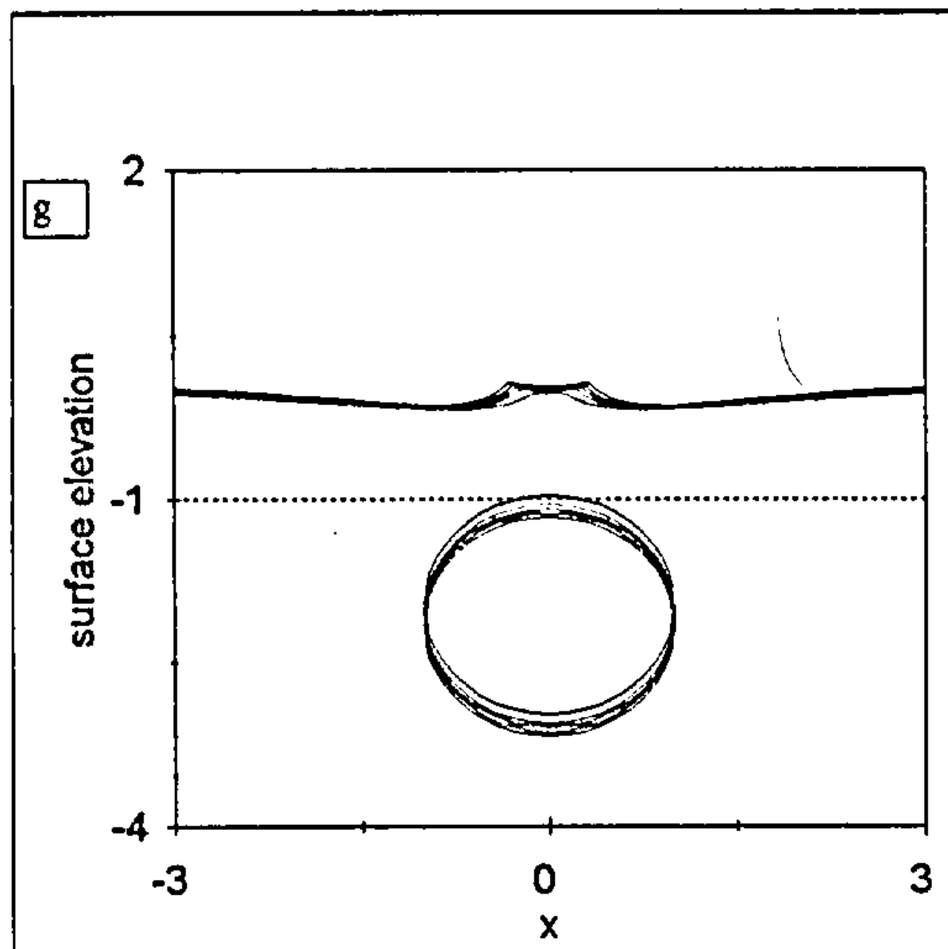
g
surface elevation
2
-1
-4
-3
0
3
x

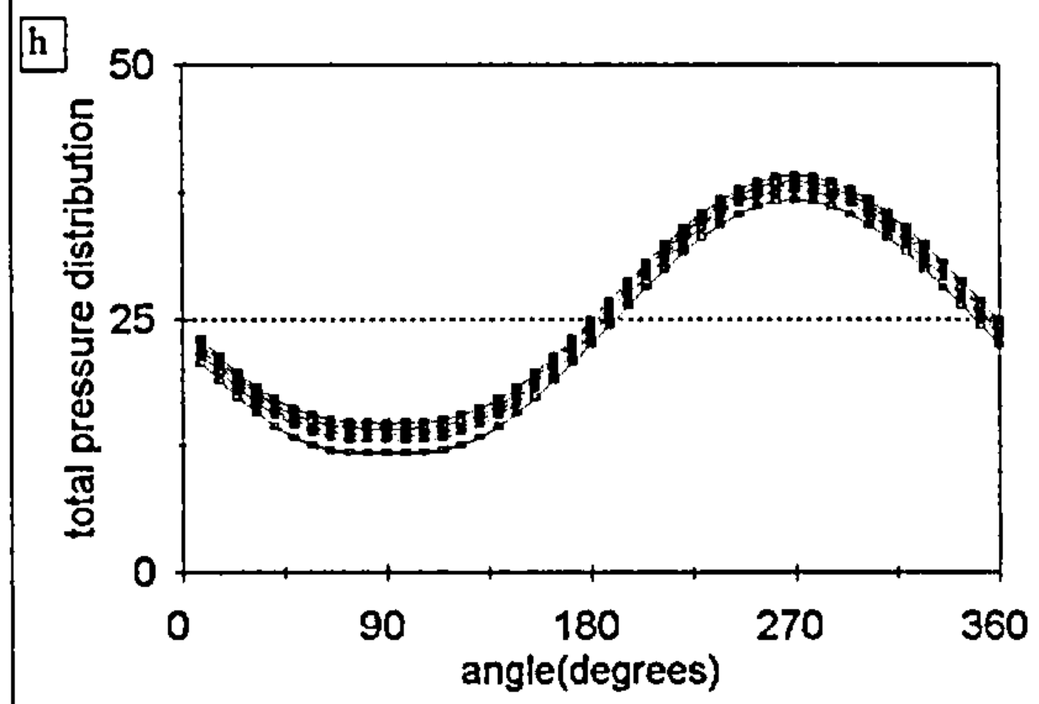
h
total pressure distribution
50
25
0
0
90
180
270
360
angle(degrees)

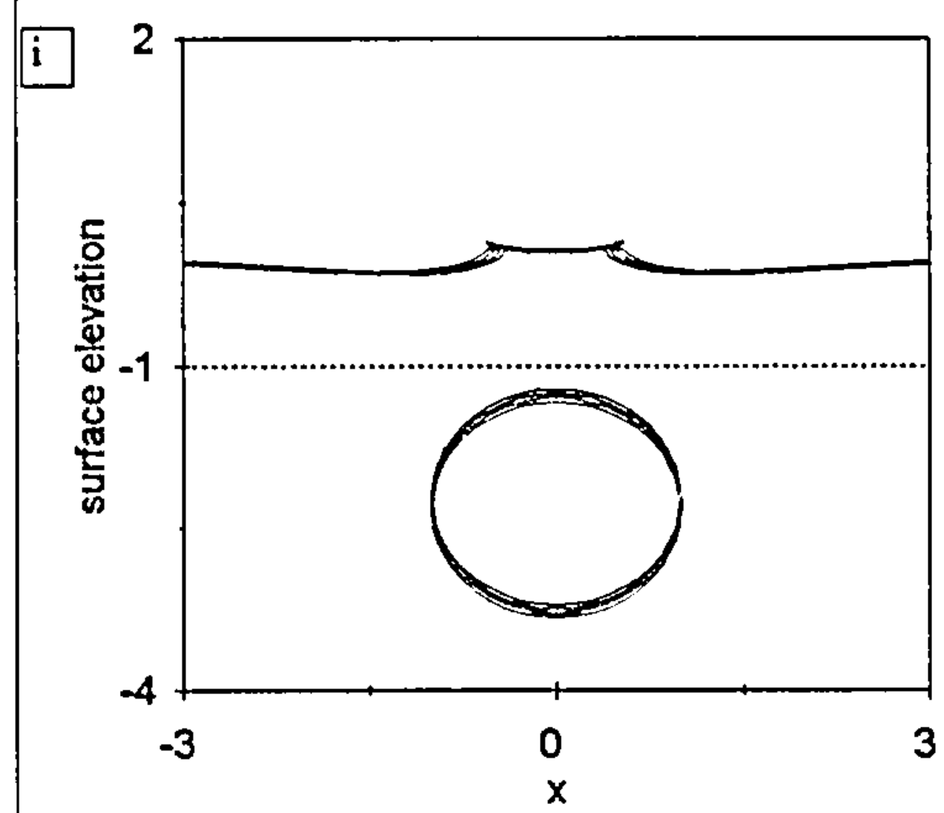
i
surface elevation
2
-1
-4
-3
0
3
x

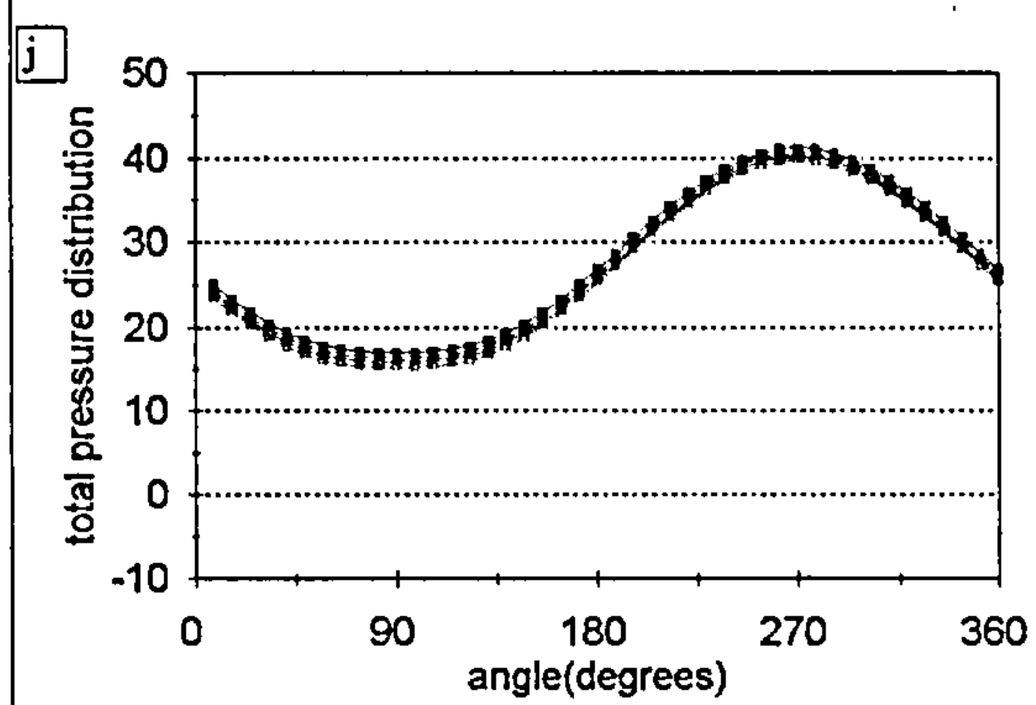
j
total pressure distribution
50
40
30
20
10
0
-10
0
90
180
270
360
angle(degrees)

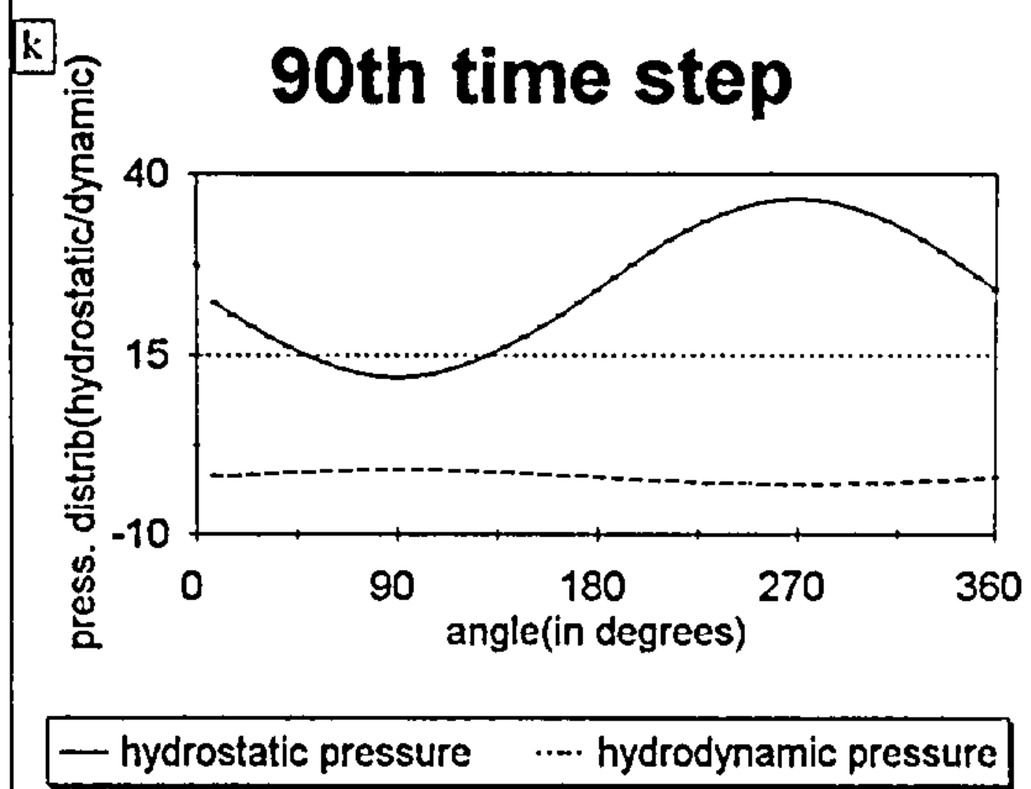
k
90th time step
press. distrib(hydrostatic/dynamic)
40
15
-10
0
90
180
270
360
angle(in degrees)
hydrostatic pressure
hydrodynamic pressure

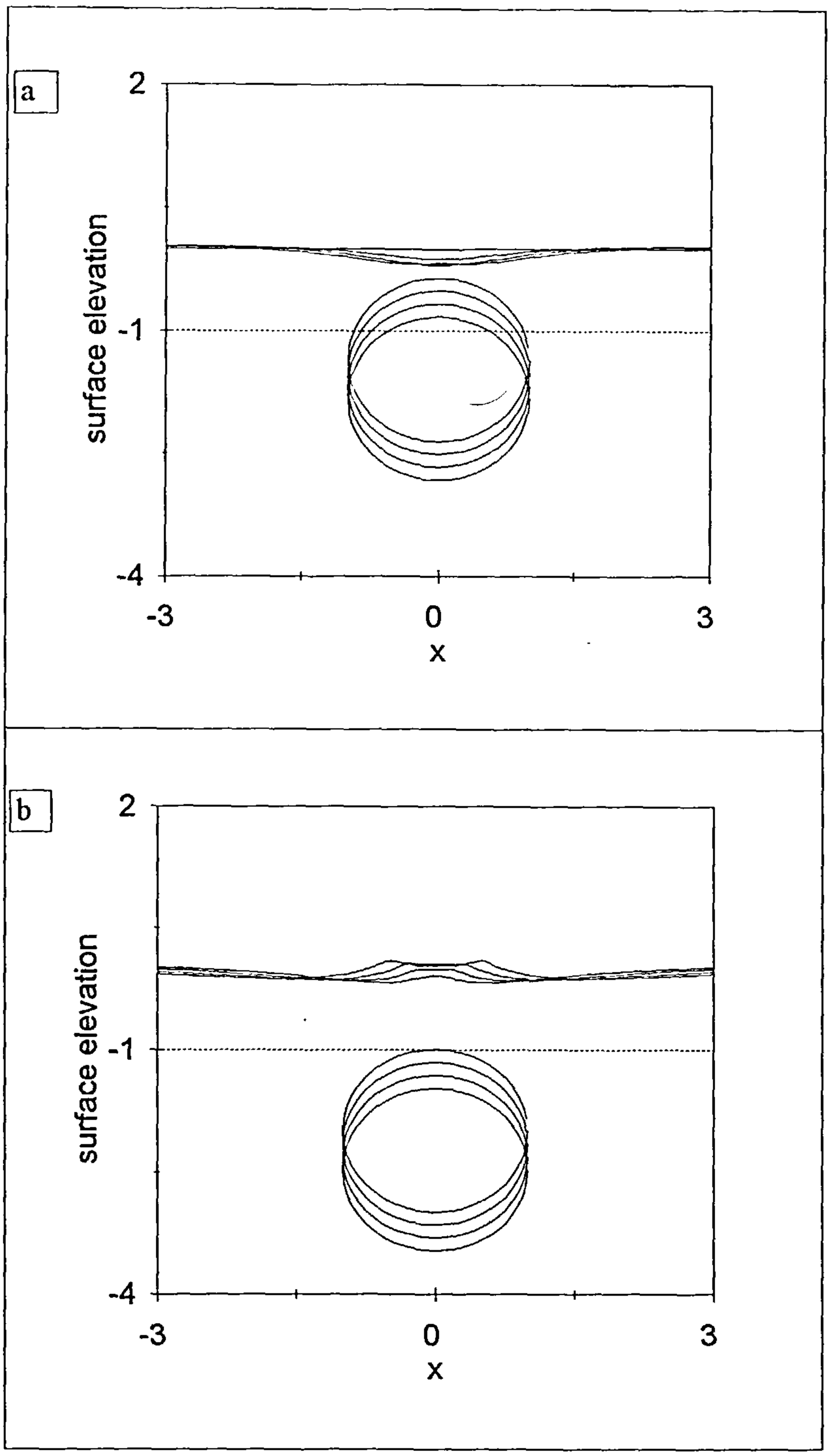

Fig. 5.5 Vertical and forced motion of a cylinder initially located at d=1.35a and movingvertical downwards at Fr=0.29.

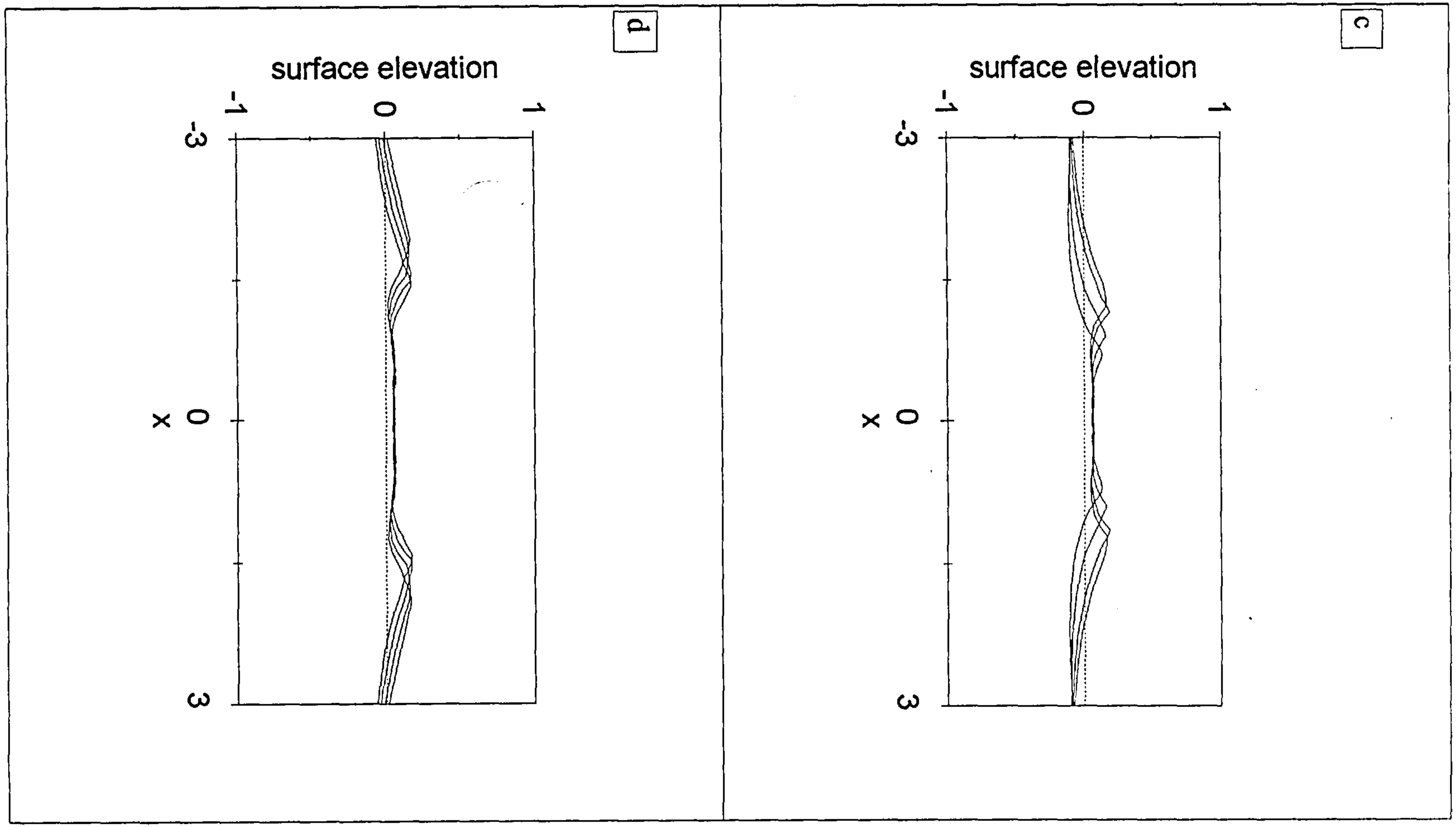
d
surface elevation
-1
0
1
3
x
0
3
c
surface elevation
-1
0
1
3
x
0
3

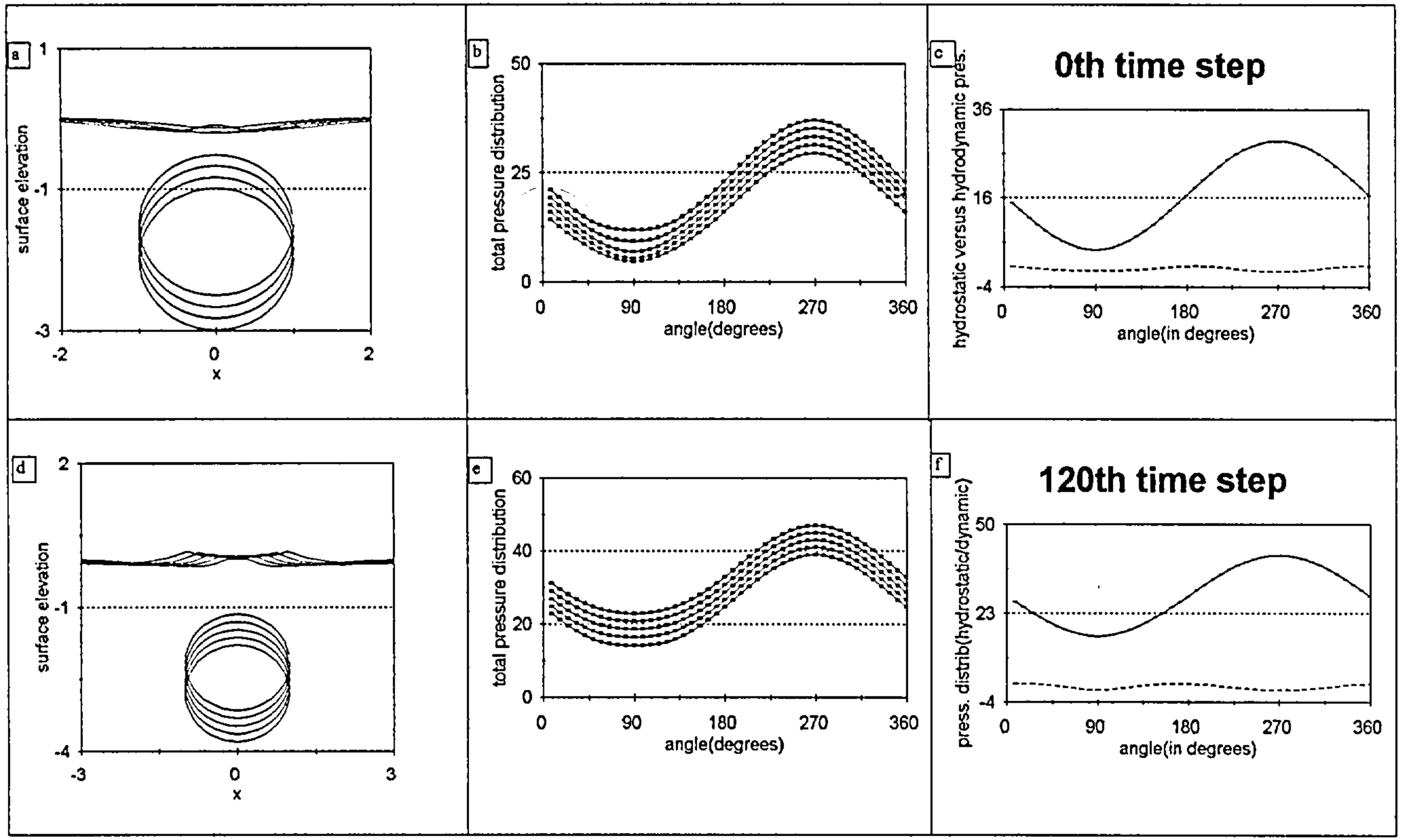

Fig. 5.6 Free-surface elevation and pressure distribution around the cylinder due to the impulsively started motion of a cylinder at Fr=0.29 and d=1.35a. (a), (d), (g) and (j) represent surface elevations; (b), (e), (h) and (k) represent the total pressure distributionat times corresponding to those of the given elevations; and (c), (f), (i) and (l) represent hydrostatic, in solid lines, and hydrodynamic, in dotted lines, pressures at times corresponding to 0th(first) time step up to 300th(last) of the adjacent total pressure and surface elevation lines.

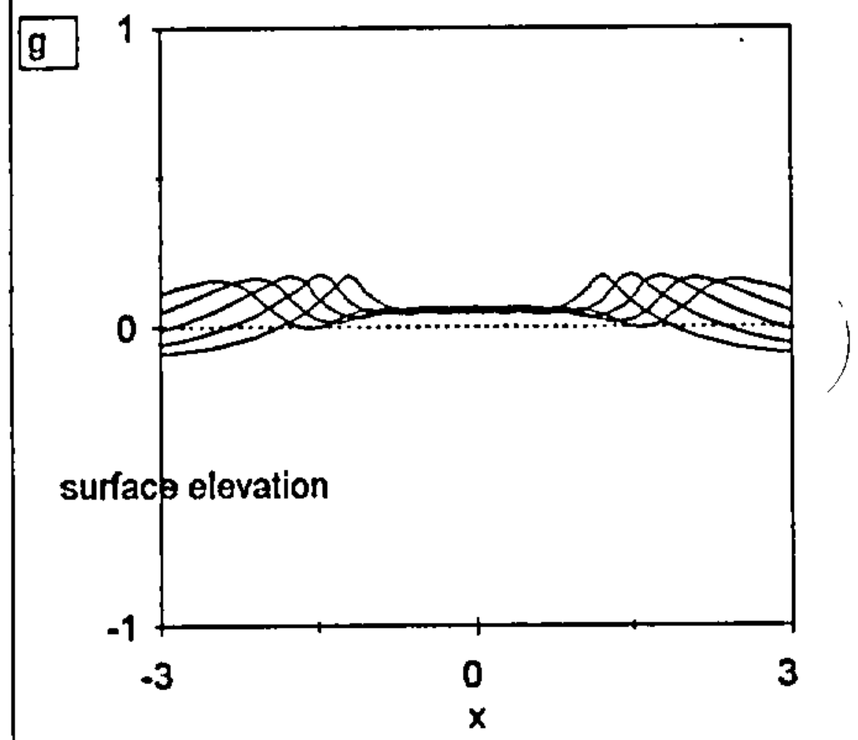
g
1
0
-1
-3
0
3
x
surface elevation

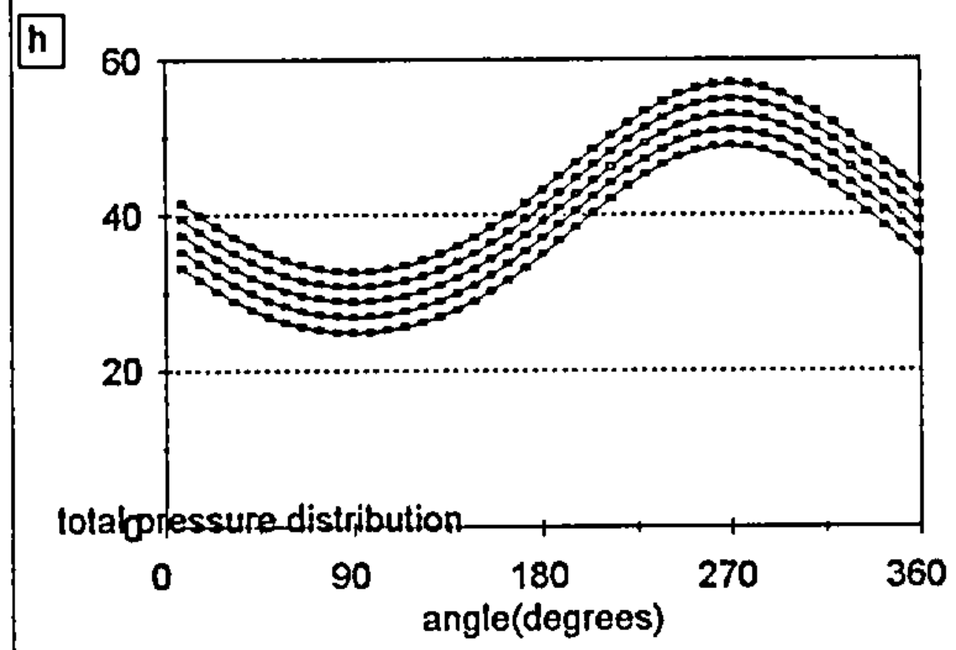
h
60
40
20
0
0
90
180
270
360
angle(degrees)
total pressure distribution

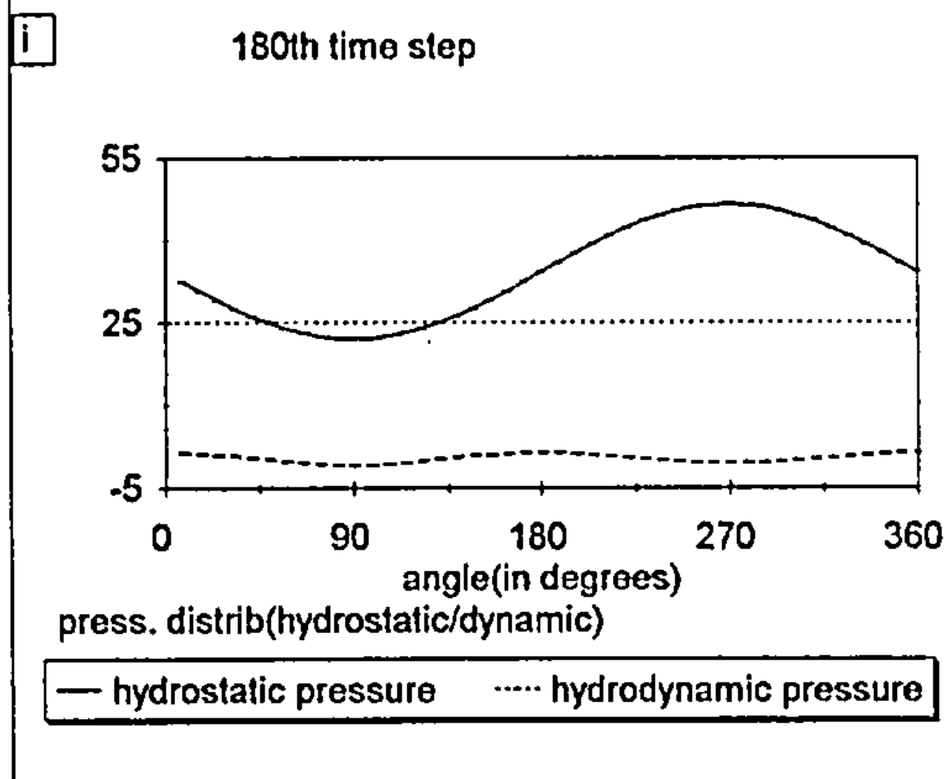
i
180th time step
55
25
-5
0
90
180
270
360
angle(in degrees)
press. distrib(hydrostatic/dynamic)
hydrostatic pressure
hydrodynamic pressure

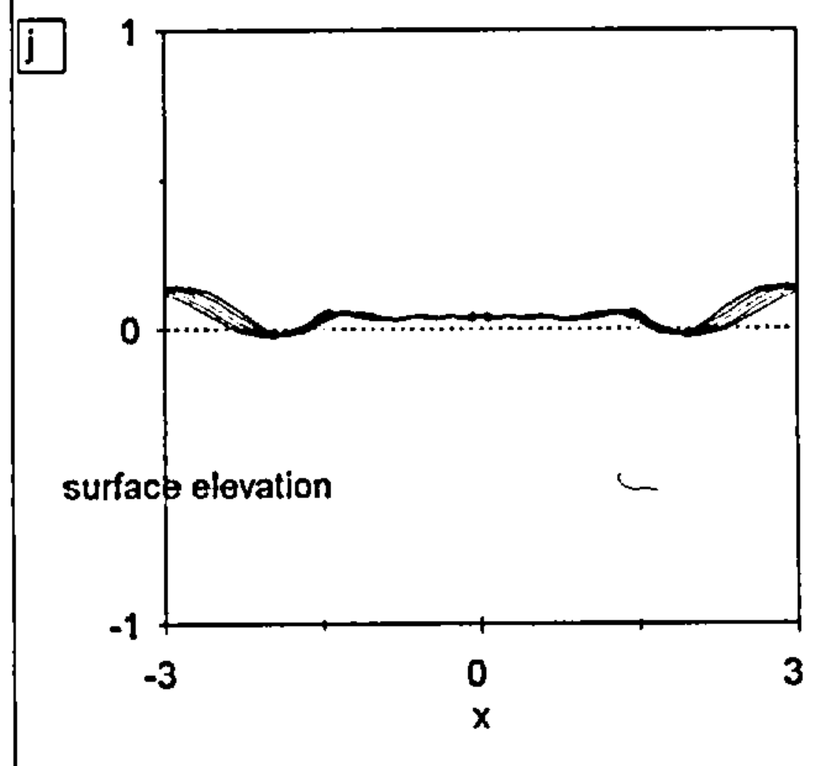
j
1
0
-1
-3
0
3
x
surface elevation

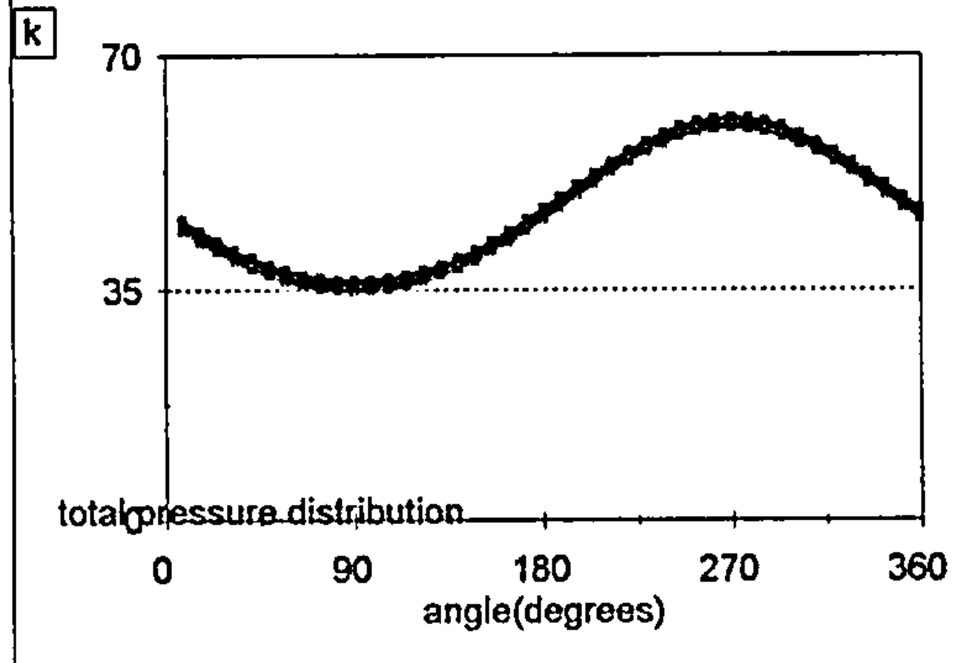
k
70
35
0
0
90
180
270
360
angle(degrees)
total pressure distribution

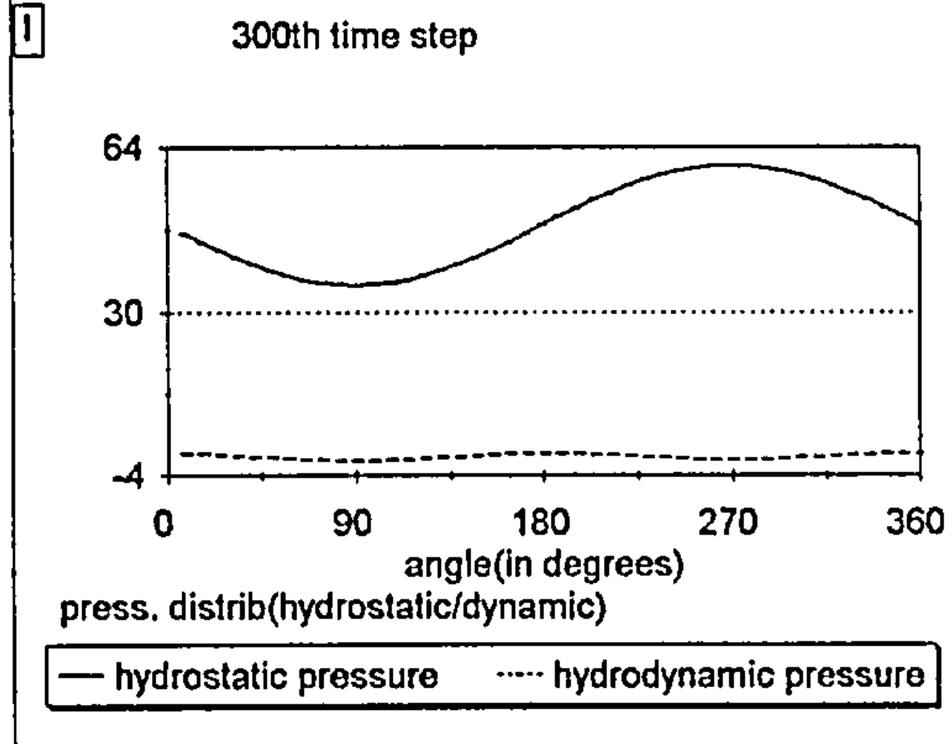
l
300th time step
64
30
-4
0
90
180
270
360
angle(in degrees)
press. distrib(hydrostatic/dynamic)
hydrostatic pressure
hydrodynamic pressure

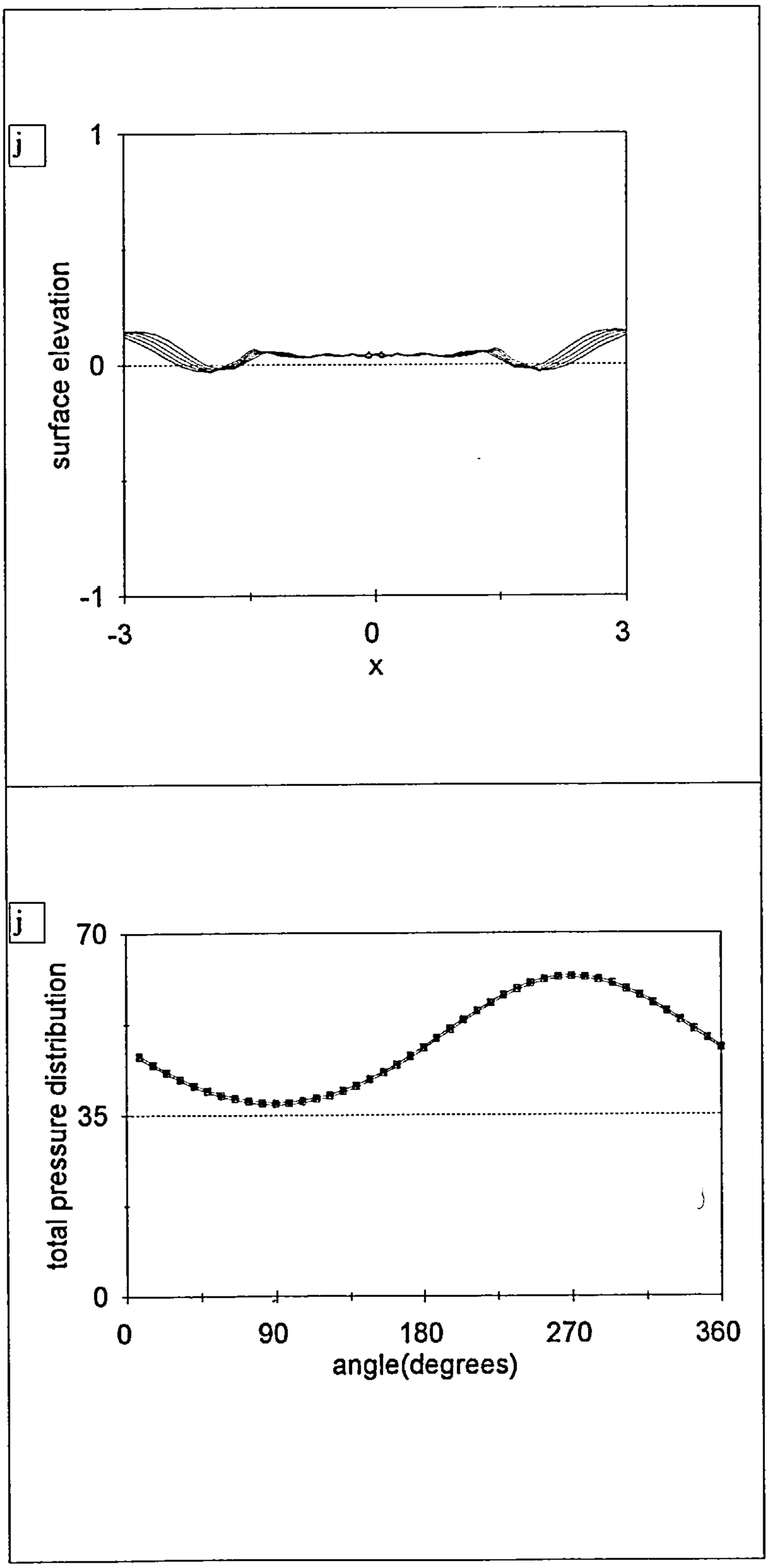
j
1
surface elevation
0
-1
-3
0
3
x
j
70
35
0
total pressure distribution
0
90
180
270
360
angle(degrees)

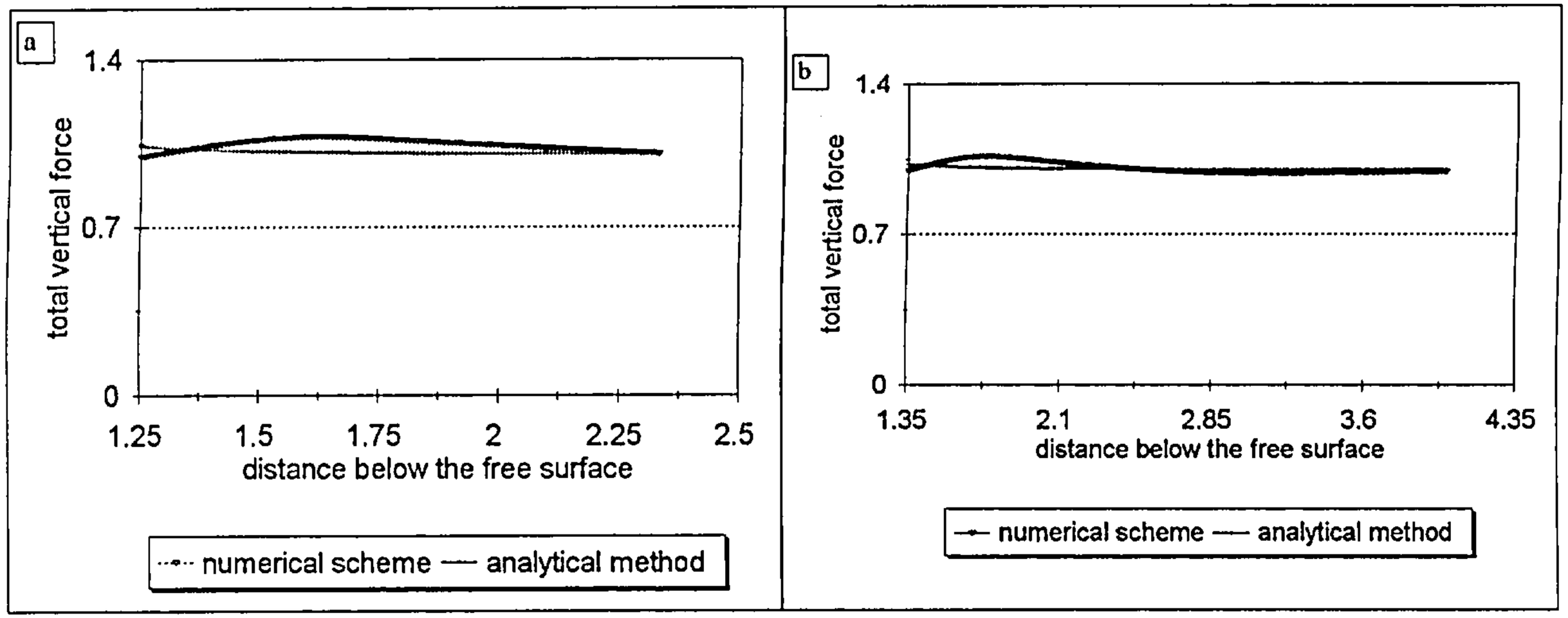

Fig. 5.7 Comparison of the total vertical force acting on the cylinder according to the results of the numerical scheme and those of a simple analytic model at Fr=0.29 and d=1.35a.

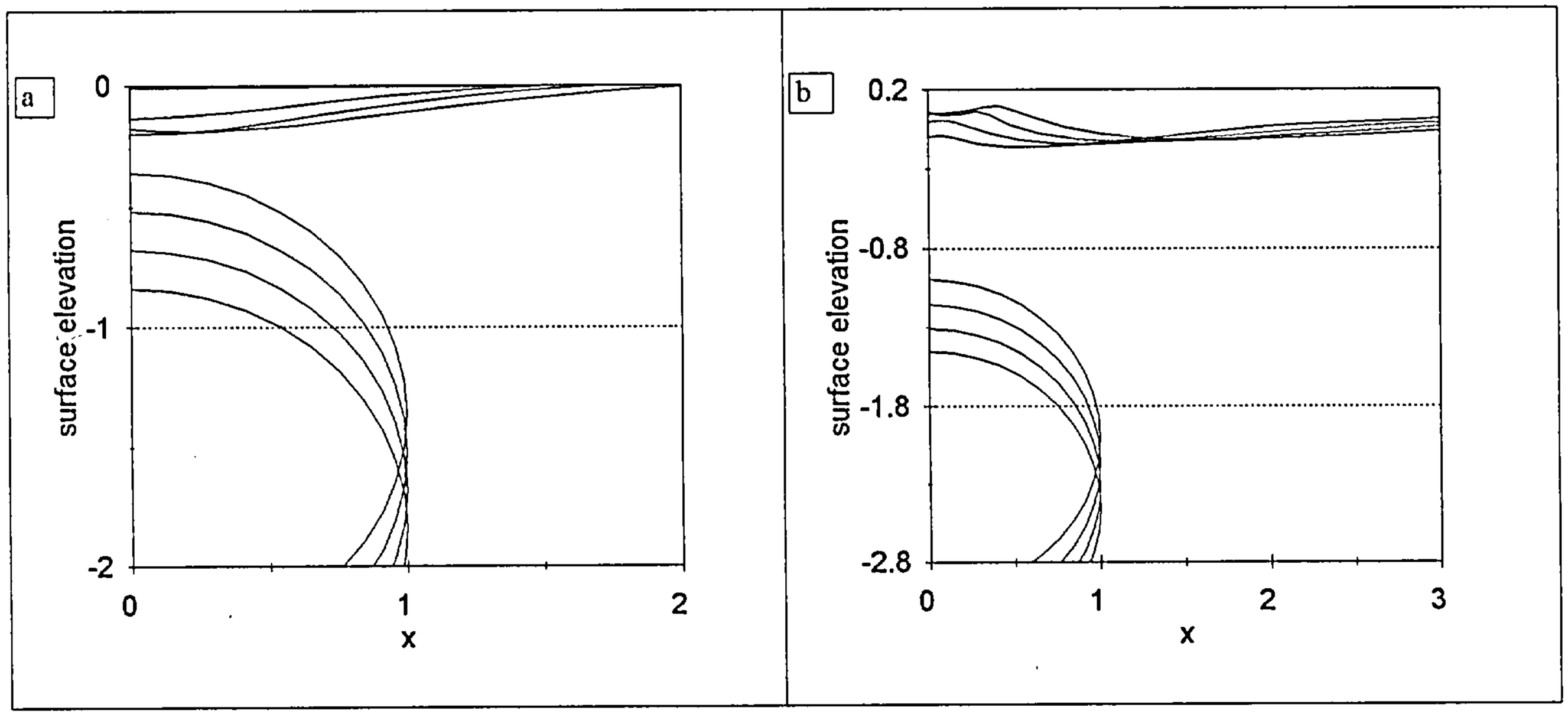

Fig. 5.8 Free-surface elevation due to the forced motion of a cylinder initially located at d=1.35a below the free surface and moving downwards at Fr=0.29. The results are obtained using the program for half-submerged bodies.

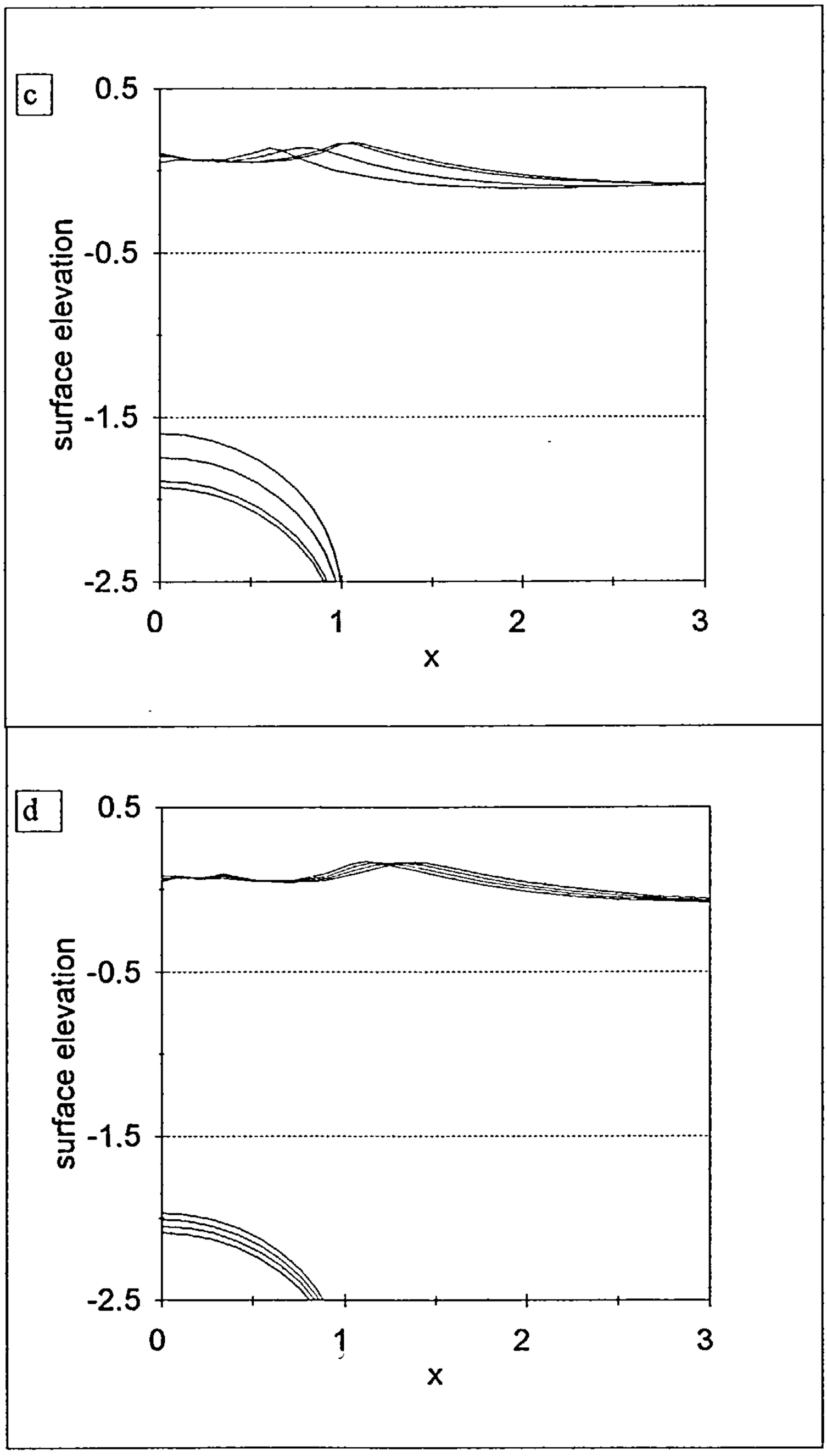
c
0.5
-0.5
-1.5
-2.5
surface elevation
0
1
2
3
x
d
0.5
-0.5
-1.5
-2.5
surface elevation
0
1
2
3
x

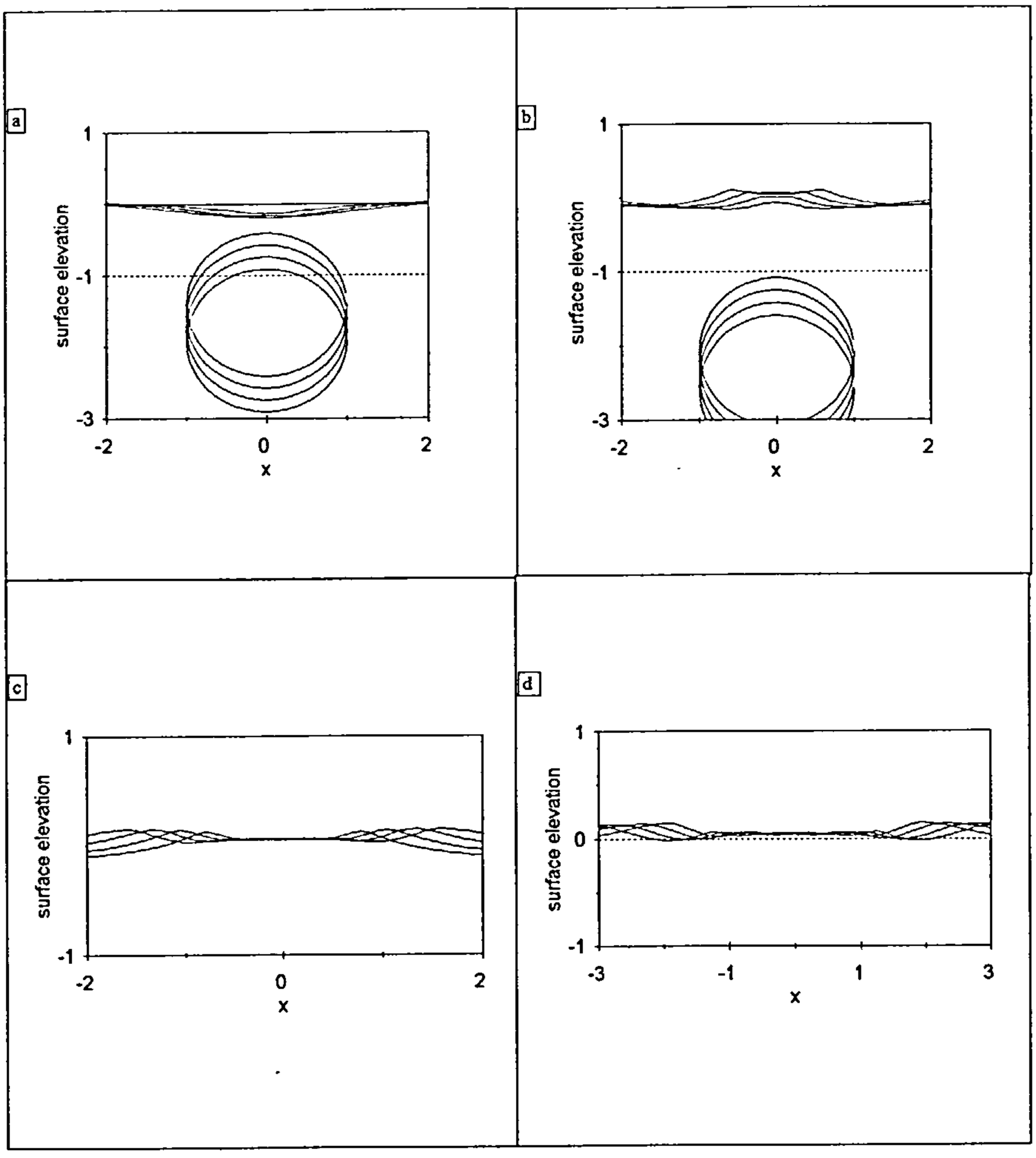

Fig. 5.9 Free-surface elevation due to forced motion of a cylinder initially located at d=1.4a below the free surface and moving downwards at Fr=0.29. Coarse spacing of the free surface points is used.

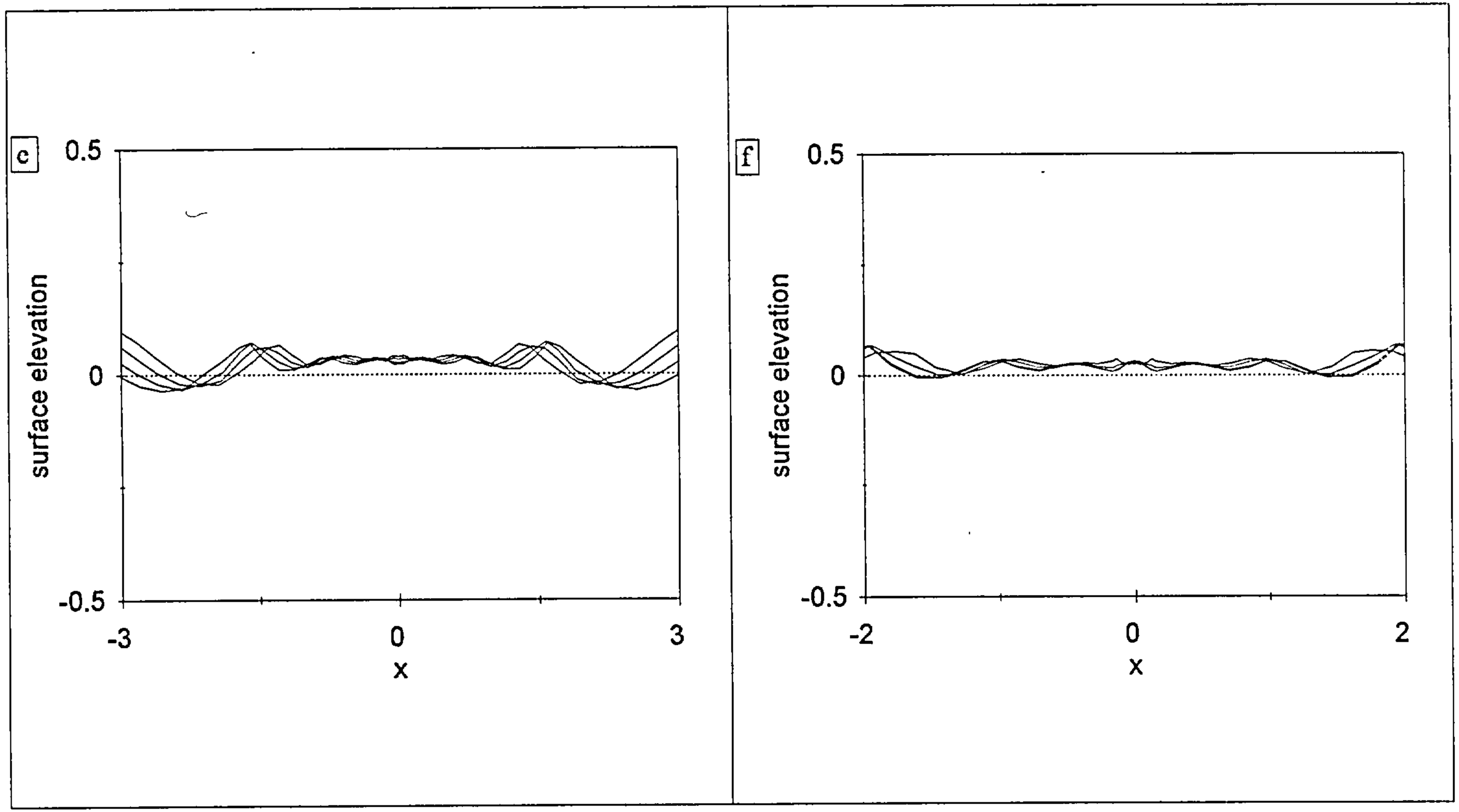

Later stages of the calculations.

Chapter 6

The Engulfment problem

6.1 Introduction

Consider a cylinder partially immersed in water as shown in Fig. 6.1. The objective is to move the cylinder into the water and to be able to follow this motion beyond total submergence. The application of the method of Vinje and Brevig plays a crucial role in this problem. The method has been further developed to handle the dynamics of the intersection point of the free surface and the body by Lin, Newman and Yue (1984), Greenhow and Lin (1985) and Yim (1985). Generally, depending on the initial position of the cylinder and the Froude number, there will be additional problems of resolving splashes when the two inflows (from the right and the left) meet above the submerging cylinder giving rise to jets when the body is moving at high Froude numbers. The surface-piercing problem is firstly discussed and results presented which extend the work of Greenhow (1988).

We consider the free and forced motion of the cylinder as it enters the free surface. The later is investigated for various Froude numbers in accordance with the discussion in chapter 5 and the work by Greenhow (1988). In his work he notes that at low Froude numbers the fluid simply flows in over the

submerging cylinder until the inflows impact on each other causing splashes, which his program is unable to resolve. At high Froude numbers he identifies two significant problems associated with the breakdown of the calculations. Firstly, a jet is formed as the body plunges into water and this problem is solved by slightly altering the program to allow the jet to leave the body. In this study we follow the closure of the free surface over the top of the cylinder in a less complicated case when the motion is started with the cylinder half-submerged in an initially calm water. Photographs of Greenhow and Lin (1983) for high-speed entry of a cylinder, also shown in Faltinsen (1990), confirm the jet formation. The second problem involves the jump in the velocity potential, ϕ, and its directional derivative, $\frac{\partial \phi}{\partial n}$, in the direction of the normal to the body. The second problem causes the contour of integration to collapse into a doubly-connected contour which poses problems, as far as the integral method used to solve this problem is concerned.

In Fig. 6.2(a) we show how the domain of integration looks just before removing the vertical plate along the plane of symmetry. We note that the use of a thin vertical plate is only possible in the case of vertical motion where there is symmetry, and not for oblique motion. The values of the potential on the left and right free surfaces do not match immediately before impact for oblique motion, and its directional derivative does not match even for symmetric vertical entry. This is caused by the fact that the impacting surfaces are moving torwards each other. We seek to continue the calculations beyond this point where the flow domain becomes doubly connected. The calculations obtained by this approach do not exactly describe the process of the impacting inrushing flows, since compressibility effects may be needed. It is concievable

that impact will occur at a point only, rather than across a surface, and the immediate resulting flow is unknown. However, we can take the calculations further by replacing the two intersection points from the body by the average of coordinates representing nearest points in that neighbourhood and velocity potentials. We also put additional points in the region of expected disturbances (above the top of the cylinder for vertical motion and behind the cylinder for oblique motion) for good resolution of jets when they eventually form. Figs. 6.2(b) show what the initially singly-connected flow domain might look like after impact.

In his thesis, Best (1991) alluded to the fact that the jump in the potential and its normal derivative cannot persist after the impact in the case of a toroidal bubble when a jet threads the bubble and impinges upon the far side of it. Zhang, Duncan & Chahine (1993) have also investigated the dynamics of a bubble near a rigid wall, as the re-entrant jet forms in the same way as in Best's description. This phenomenon, also discussed in Best (1992), appears to be very similar to the one of two inflows following a submerging cylinder and finally impacting on each other either on the surface of the cylinder (see also Fig. 6.2(b)) thereby pinching off a bubble connected to the cylinder. Most importantly he proves, theoretically, that the potential on the free-surface other than at the impact point does not change as a result of the impact, and hence the normal derivative of the potential on the bubble can be found without any problems. He shows that the value of the potential is insensitive to impact by proving that for an infinitely small time of impact the pressure elsewhere around the bubble remains unchanged. It is known that the collapse of the contour of integration (flow domain) into a doubly-connected geometry gives

rise to flow with circulation, across the region of impact in this case. Now at the point of impact the potential function is discontinous but may be found by calculating the value of the circulation, Γ, around a closed curve. Integrating the fluid velocity about the closed curve gives the value of the circulation;

$$\Gamma = \int_C u \cdot ds = \phi_1 - \phi_0. \qquad (1)$$

where ϕ_1 and ϕ_0 are potentials on the left and right impact surfaces respectively. Best suggests that in order to continue the calculations after the impact using the integral method we need to reintroduce the branch cut. He argues that " since the surface over which the impact occurs is a point and the value of the integral (6.1) is uniform over this surface there is no vortex sheet created by the impact ". The flow obtained after the impact can then be described by the integral method through re-introduction of a branch cut in the domain so that the contour of integration is once again singly connected. This is explicitly included in the submerged program which we use for further calculations after complete engulfment.

Best also admits that lack of analytic solution for the motion of the free surface for the early stages of the calculations poses problems. However, because of the geometry of the body surface, with high curvature, the fluid velocity is predictably very high in the region of the origin which implies formation of jets of high speed and hence he suggests immediate smoothing of the free surface.

In our case, we exploit the above analysis and will continue the calculations using the integral method of Vinje and Brevig et al. Initially we trace the motion of the half-submerged cylinder using the modified program as explained in chapter 5, see also Greenhow (1988). We note that, the potential on the cylinder was checked and found to be continous. Vertical boundaries

are placed at distances far away from the origin so that the transient motion is undisturbed by waves which would have been reflected by these boundaries. Several free and body surface point distributions are tried for free motion and motion at high or low Froude numbers. The discretisation of best runs are assumed as standards for either free motion or motion at high or low Froude numbers. When the calculations breakdown, after the engulfment phenomenon described earlier, the results of the last reliable time-step are stored, to be used as initial values for the program for completely submerged bodies. At this stage the process of surface smoothing (removing points representing the jets) begins.

Zhao and Faltisen (1994) have recently advanced a numerical scheme dealing with intersection points and the jets that form in that region following the motion of a body entering the free surface and the ensuing free surface motion. They avoid including the jet flow containing fast moving free surface particles with a lot of energy. They call this process " smoothing" and it is applied wherever the jets occur. Most importantly, they have shown that fluid mass, energy and momentum are still approximately conserved when the ejected free surface fluid particles, also known as spray jets, are cut off and an arbitrarily chosen free surface portion cutting off the jets is effected before restarting the calculations. We use this approach in continuing the calculations in situations described below, which we assume are similar to the one described by Zhao and Faltinsen. The smoothing process involves removal of some points of the free surface, and as a result mass and energy may not be exactly conserved. We show below how we have, in fact, smoothed the free surface in a manner that approximately satisfies conservation of fluid mass. A simple hydrostatic

model is compared to our results to ascertain the accuracy of conservation of energy of the system. In general for a body in a conservative field of force the sum of the kinetic energy and potential energies is constant. In the fluid domain Ω the conservation of energy, consisting of kinetic energy only, can be checked by comparing the rate of change of the energy of the system

$$\frac{dE}{dt} = \frac{\rho}{2}\frac{d}{dt}(\int_S \int)\nabla\phi \cdot \nabla\phi dS \qquad (2)$$

to the rate of change of work on the body;

$$\frac{dW}{dt} = -(\int_S \int)\frac{(p - p_0)}{\rho} n_3 dS \qquad (3)$$

where p_0 is the applied pressure at the free surface, n_3 the vertical component of unit normal vector to the body and p is the pressure in the fluid and is obtainable from the Bernoulli's equation (see Newman 1977, page 260-263). For conservation of momentum of the system to be satisfied we demand that the total external force acting on the cylinder should be equal to the rate of change of the cylinder and fluid momentum.

In the calculations that follow, time is scaled by $\sqrt{\frac{g}{a}}$ such that $T = t\sqrt{\frac{g}{a}}$. We then obtain nondimensional velocity as $\dot{Y} = \frac{\dot{y}}{\sqrt{ga}}$ and nondimensional acceleration is $\ddot{Y} = \frac{\ddot{y}}{g}$. The dimensionless Froude number is $Fr = \frac{\dot{y}}{\sqrt{ga}}$. Force is nondimensionalised by buoyancy force as in previous chapters and pressure by ρga. Before complete engulfment the force is nondimensionalised by linearised buoyancy. This means that the buoyancy force is updated for each position of the body until complete submergence when the buoyancy force becomes constant. Linearisation of buoyancy is necessary for continuity purposes since we wish to compare the motion of thye cylinder before and after complete engulfment. The buoyancy force calculated as a function of depth y is given

as

$$Buoyancy = \frac{1}{2}\rho g((NBODY)a^2 \sin(\frac{2\pi}{NBODY}) + ya\sin(\frac{\chi}{2}) - a^2 \arccos(\frac{y}{a})) \quad (4)$$

where, $\chi = 2\arccos(\frac{y}{a})$ is the angle subtended at the centre of the cylinder by the arc of the part of the cylinder not yet under the still water level, see Fig. 6.1.

6.2 Surface-piercing case

We shall consider in this section the water-entry problem of a cylinder which is initally half-submerged in an undisturbed free surface, see Fig. 6.1. Two types of motion of a cylinder entering an initially calm water are investigated. The free motion of a cylinder of specific gravity 1.2, and forced motion of a cylinder at various Froude numbers and directions, give rise to extremely interesting free-surface deflections and body dynamics. The modified program was implemented in Chapter 5 for motion of submerged cylinders and we shall use it here for the initial phases of our calculations (surface-piercing). Firstly, we study the free motion of a cylinder having specific gravity of 1.2, a value that was chosen arbitrarily, but consistent with the sinking required, and not so large that the body dynamics are dominated by gravity acting on the body.

6.2.1 Example of free motion

We use fine point spacing on the free and body surfaces and small nondimensional time steps, $\Delta T = 0.042$. Fig. 6.3 shows surface elevations, total pressure distribution and forces during the initial stages of the entry until the inrushing water reaches the centre (its maximum depth) and collides with the

plane of symmetry resulting in upward movement. After touching the inserted plate introduced on the plane of symmetry, the fluid is repositioned in the next time step before impacting on the plate again slightly above the cylinder. Eventually the calculations break down. Attempts to continue the calculations beyond this point failed, even after many trials with different point distribution on free and body surfaces. When the calculations break down the cylinder centre is located at $d = 1.528a$ implying that the whole body is now under the mean water level. In principle the jet should be able to rise up the thin plate but that does not happen as the scheme breaks down. This is thought to be caused by the zero condition, when viewed in the cylinder's frame of reference, of the vertical and horizontal velocities that the particle at intersection has to satisfy and hence it is unable to rise. This point, at the intersection of the cylinder and the thin vertical plate, can then be understood as a stagnation point which simply has to be removed for the calculations to continue.

The kinematics of the body are shown in Figs. 6.3(e)-(g); displacement-time, velocity-time and acceleration-time graphs for the initial phase. The body accelerates, initially at 0.41g, to maximum speed and maintains that speed for some time before decelerating. Initially the hydrodynamic force increases slightly and is unchanged for a period lasting about $T = 0.4$. It eventually falls steadily to almost a constant value. This seems reasonable, since initially a lot of energy is needed to generate the free-surface flows and is therefore not available to increase the body's kinetic energy. For the last stages before complete engulfment, the velocity of the cylinder is essentially constant, and this persists until the cylinder is well submerged. This zero-acceleration phase is a purely hydrodynamic effect, since, after total submergence, hydro-

static terms and body plus added mass terms would predict accelerated motion downwards of 0.09g. We may conclude that the potential energy lost by the body is predominantly fed into the kinetic and potential energy of the fluid rather than the kinetic of the body itself. It is not known how general this effect might be, but it could be of practical importance, for example to the design of heave compensators on shipboard cranes. The calculations later breakdown after a few time steps as the speed begins to drop.

At this stage the obtained results of the free surface coordinates, velocity potential on the free surface, body position and velocity are stored to be used as initial data in a program for completely submerged bodies. The rest of the initial data is unchanged, except for time step interval which we change depending on the velocities of jets.

6.2.2 Forced motion of a cylinder

The initial phases for the forced vertical motion are qualitatively similar to those discussed above for free motion. For low Froude number, Fr=0.19, the inrushing fluid flows over the cylinder top as it submerges. There is an initial increase in hydrodynamic force up to about the depth d=0.3a and then a slight fall and finally acts upwards as the cylinder submerges, see Fig. 6.4(a) for free/cylinder surface positions and Fig. 6.4(b) for the vertical force. The behaviour of the hydrodynamic force in the cases of Fr=0.46 and 0.31 look quite similar; it acts upwards throughout the inital phases, though remaining remarkably constant for a long time after a rapid increase at the start of the motion. As before, during the last stages of submergence for this phase of these two cases the force increases rapidily, see Fig. 6.5(c) and Fig. 6.6(f). In

Figs. 6.5(a) and 6.6(a)-(c) we show surface elevations up to complete submergence after which the results are stored for use with the program for complete submerged bodies. We also show total pressure distributions for these runs in Figs. 6.5(c) and 6.6(d)-(e).

The situation changes drammatically in the case of oblique motion where we have no plane of symmetry. Here, the term oblique motion refers to the motion of the cylinder restricted to move along a path making an acute angle ι, see Fig. 6.1, with the downward vertical line, here referred to as a 90^o angle or $\iota = 0^o$, emanating from the origin. As explained above the potential and its directional derivative do not match immediately before and after impact rendering the problem more difficult to solve. For vertical motion we placed a thin plate along the line of symmetry in order to be able to pursue further the symmetric motion of the body and fluid. However, this is not applicable here, and we simply force the cylinder through the free-surface, without the plate but with the intersection points constrained to remain on the cylinder. We start with a slight shift from the vertical of $\iota = 30^o$ and consider the motion of the cylinder entering the free-surface at Fr=0.31. The results of the ensuing motion of the cylinder and the free-surface are depicted in Fig. 6.7(a)-(c). The inflow from the right closes in behind the cylinder whereas the one from the left projects forward past the cylinder. At this point the calculations are inevitably going to breakdown as the two inflows eventually impact on each other. These results, as before, are stored for further use with the program for submerged bodies. Total pressure distribution graphs are also shown, see Fig. 6.7(d)-(e).

The upward vertical and horizontal hydrodynamic forces are shown in Fig.

6.7(f). We observe similar behaviour in the pattern of surface deformations for the angle of 45^o at Fr=0.19, 0.31, Fig. 6.8(a)-(c) and 6.9(a)-(b). The forces acting on the body when it is moving at Fr=0.31 are comparable to those for motion at 30-degrees whereas at Fr=0.19 the forces are more oscillatory, see Fig. 6.9(e)(where F_v and F_h represent vertical and horizontal components of the hydrodynamic force on the cylinder). The vertical forces are largely hydrostatic and are shown, by these calculations, to be smaller than the horizontal ones. It is possible that this is due to "sloshing" of fluid from right to left. This somewhat surprising result could be important for marine structures and operations. The case of a 60-degree angle at Fr=0.31 is also considered and resembles the other two cases of oblique motion discussed above, see Fig. 6.10.

The force magnitudes for all the four angles at Fr=0.31 are also compared in Fig. 6.11. At 45 degrees the force magnitude is initially greater than the forces for the other three cases and becomes smaller than the other forces at later time corresponding to an equal distance moved along four different paths. At 90 degrees the force magnitude is smallest at the start of the calculations but picks up after some time to match that of 30- and 60-degree angles for the same distance as above. The distances moved, before breakdown of the calculations, vary with ι and are greater for greater values of ι. The 30- and 60-degree angles seem to represent the average force between that of 90- and 45-degree angles for the same distance moved in all directions. As ι increases beyond the value of 30^o we begin to see negative vertical hydrodynamic forces, see Figs. 6.9(e) and 6.10(g). This downward hydrodynamic effect happens much earlier at high Froude numbers and for large values of ι.

6.3 Motion after complete engulfment

Following the discussions above we shall now implement our findings in following the motion of a cylinder beyond the complete engulfment stage. After carrying out the initial stages of surface-piercing we then proceed to redefine the free-surface at the site of impact. Since, when viewed in the cylinder's frame of reference, the fluid had stagnated around the intersection point and the jet failed to rise up the vertical plate, we had to abandon the "plate" method described above for vertical motion. The removal of the vertical plate, in the case of the symmetric situation, means that the flow domain has re-connected and has become doubly connected, in which case the original integral method is no longer applicable. To solve this problem the results of the last time step of the above run are transfered to the program for the fully-submerged bodies. This implies the introduction of a branch cut needed to transform the doubly connected domain into a singly connected one again. Basing our argument on Best's (1991) thesis, we assume that the potential elsewhere on the free surface remains unchanged at the instant of impact, a fact that is verified by results showing that the potential elsewhere on the free-surface is unaffected. We also are confident that the potential on the body is continuous during the impact stage, as our results revealed that. The rate of change of the potential at the intersection points and a few neighbouring points a number of steps before and up to impact was compared to the change at the same points on the body after impact, showing reasonable agreement. This enables us to restart the calculations with only local changes in the potential and free surface coordinates around the site of impact, as described above.

6.3.1 Continuation of free motion calculations

Because of the steepness of the cavity formed behind the cylinder (see also Fig. 6.3(b)) we decided, arbitrarily, to slightly move upwards the point of stagnation shown in Fig. 6.3(b) to a new position above its original position. The effect of this on the motion of the cylinder should be determined by the behaviour of the forces on the body at the instant of swapping programs (see later). In order to achieve better resolution of the jet, we also added some more points around the region of the cylinder. This was done by simply averaging neighbouring points. We ended up with $N = 129$. The same process is followed in calculating the corresponding potentials. In the case of jet formation we employ the jet removal technique described in section 6.1 to replace the coordinates of points representing tips of the jets. In this way we succeed in minimizing loss in fluid mass. When the jet is removed without replacement, the situation is compensated by the initial dense point distribution around the jet region. This results in slight loss of resolution of the free surface with minimal loss in fluid mass. We later show that these jets are not important as far as the motion of the cylinder is concerned, but they simply have a slight tendency to accelerate or decelerate it.

At later stages when the effect of the jet on the pressure around the cylinder becomes insignificant, the jets are removed and the cavity is widened to allow outward propagation of waves from the centre. This allows the fluid to flow in from regions far away from the vicinity of the cylinder and hence maintain reasonable pressure levels(which are consistent with those before jet removal) throughout the calculations, though good free surface resolution and overall fluid mass conservation might be compromised. Hence, the removal of jets is

purely for numerical reasons, i.e in order to be able to continue the calculations. In order to cope with the speed of the jets the dimensionless time interval is reduced to $\Delta T = 0.007$, one sixth of the original interval. The position and velocity of the cylinder remain as they were at the last step of the previous run.

Fig. 6.12.2 shows the surface elevations and total and hydrodynamic pressure distributions of the first stage of restarted calculations. At first there is a draw down of the fluid particles around the origin creating a small downward jet. This jet does not last long as it immediately reverses and the calculations breakdown at the instant of its re-emergence in an upward direction. At the instant of the jet formation the hydrodynamic pressure at the top of the cylinder increases rapidly and as a result the total pressure also increases. Here we compare the motion of the cylinder obtained by the numerical scheme with that due to a simple hydrostatic model. The latter is a model of a conservative force, and a comparison with the numerical scheme will roughly tell us about the energy conservation of our system. In Fig. 6.12.2(i) we see that our displacement-time curve is quite close to the one of a conservative force. The velocity of the cylinder is now fairly constant because the acceleration of the system is now almost zero but increases, in the negative direction, slightly towards the end of the run, see Figs. 6.12.2(i-k) for velocity-time and acceleration-time graphs. The increase in negative acceleration results from a decrease in total vertical force on the cylinder, as illustrated in Fig. 6.12.12(l), while the pressure on top and bottom of the cylinder is slightly increased. The lines shown as "numerical scheme" refer to motion with nonlinear free-surface and "hydrostatic model" refer to the motion calculated using a simple

hydrostatic model that assumes pressures in the fluid to be simply hydrostatic.

As mentioned above, the cylinder pressures, forces and dynamics are quite insensitive to the complex motion of the free surface, especially the downward jet described above and those to be discussed below. Nevertheless, it is still important to obtain accurate free surface calculations since fast moving jets appear, which, if not properly resolved, can lead to breakdown of the calculations. In our early stages, shown in Fig. 6.12.2(a, b, e, f), the situation is qualitatively similar to the calculations of the collision of two solitary waves calculated by Cooker and Peregrine (1992). In their case the plane of symmetry represented a seawall, whereas in ours, the top of the cylinder might be thought of as giving locally horizontal seabed. However, the two situations are not exactly comparable since, in our case, the problem is considered in the moving reference frame of the cylinder surface which would correspond to a downwards moving seabed for Cooker and Peregrine's situation. At the next stage, after suppressing the jet by replacing that point and the potential by the averages as described above, the calculations broke down after a few steps due to jet formation, two at corners of the base of the trough and one in the centre, see Fig. 6.12.3(b). After this run it became clear that we needed to remove the jets completely as they persistently led to breakdown of the calculations, and an unphysical increase in pressure around the body. This seemed to be due to the numerical scheme becoming unstable as a result of those jets.

Six points, two at the base of the trough, two from the sides of the trough and two at the tips of what looks like "sharp" breakers were removed. The resulting calculations are depicted in Fig. 6.12.4 with a single jet forming up in the middle, see Fig. 6.12.4(b). Cooker and Pregrine's (1991) calcula-

tions also show cavity-like depressions at the the seawall which rapidly "flip through" to give a fast moving upwards jet of the type we see here, see Fig. 6.12.4(b) and (e). These calculations break down also, due to a jet that has re-emerged at the origin. Nevertheless the hydrodynamic pressure around the body does not respond much to this relatively distant jet any longer, see also Figs. 6.12.4(g-h), which show further pressure distributions beyond the instant of jet formation. The body kinematics confirm this observation. We see that the body is now moving with fairly constant velocity but declining slightly due to slight overall upward trend for the acceleration of the body from below -0.05 to slightly above it. Actually, the cylinder periodically accelerates and decelerates slightly over smaller intervals of time. The hydrodynamic pressure on the region above the cylinder is reduced slightly from almost zero to just below zero and increased at the bottom by less than 0.1, see Figs. 6.12.4(c,d,g and h). Thus the total vertical force also is increased positive upwards, see Fig. 6.12.4(l). Nevertheless, this has no significant effect on the overall motion of the system, see also Fig. 6.12.4(i) which shows an approximately constant rate of change of the displacement of the cylinder. The full description of the body kinematics for this run are shown in Fig. 6.12.4(i,j,k); i.e displacement-time, velocity-time and acceleration-time graphs. The computations are continued until the stage when the hydrostatic pressure is clearly dominating, i.e the hydrodynamic pressure is small compared to hydrostatic pressure.

An attempt to remove the middle point and four more points which were part of the previous jet did not help much. The calculations broke down due to similar central jet formation to that of the calculations in Fig. 6.12.4(f). This phenomenon seemed to be due to high pressure which had already accumulated

below the free surface as a result of the inflow following the jet. We stress, however, that these jets have no effect on the already distant cylinder.

Finally the last results are combined with further smoothing attempts aimed at initiating outward wave propagation from the origin. We start the next stage of the smoothing procedure with the point at the tip of the jet not represented in the coordinate system as in the aborted run, but coinciding with the tip of the jet in Fig. 6.12.4(f). To evade the problem mentioned above we preserved the cavity depth created but arbitrarily made it slightly wider so that the jet would behave like a wave and be able to propagate outwards. This was achieved by removing a total of ten points around the region of the jet. The time interval ΔT was also reduced to 0.0014, one thirtieth of the initial interval ($\Delta T = 0.042$) in order to cope with the fast moving jet. Fig. 6.12.5 shows the outcome of the calculations following that smoothing of the free surface around the jet area. Because of the cavity, there seems to be fluid uprush towards the origin in order to fill up the gap created, forcing the jet a further distance upwards. This jet reaches its peak and its height is unchanged for a few time steps before starting to recede. The calculations eventually breakdown because the scheme cannot resolve the fluid particles around the jet area correctly. At this stage pressure distribution around the cylinder seems to be quite stable, increasing hydrostatically as expected as the body is displaced further down, showing that it is increasingly becoming insensitive to free surface disturbances.

Because our interest is to know what happens next to the calculations if the procedure is continued we feel compelled to continue the calculations a little further. The effect of free surface motion on the cylinder motion has

been steadily decreasing to the level for which it can be ignored, but it is still interesting to know how the free surface will continue to behave. The total vertical force for the following calculations will confirm our observation that the cylinder is effectively distant from the free-surface. Also, it does not appear as if tempering with the free-surface particles of jets can distort the overall motion of the free-surface because the pressure throughout the jet is almost zero. Indeed Zhao and Faltisen(1994) also remove jet flows with sucess, giving the overall fluid flow for wedge entry correctly. The sequence of the free surface profiles, before and after effecting the smoothing technique, seem quite believable and the pressures on the body are now quite insensitive to such smoothing. In fact, when you remove the jet before it has fully developed, and the calculations are restarted, a new jet forms at the same or approximately the same place. This process can continue until the jet has developed fully or otherwise we would not make any progress. To continue the computations in time we did not allow the inflows to meet below the jet, as shown in Fig. 6.12.5(c), by substituting that point by the average of the neighbouring points. The results are shown in Fig. 6.12.6.

The calculations for the figures shown in Fig. 6.12.6 break down as soon as the new jets form in front of the inflows below the jet at the centre. Before continuing with the study of the motion of the free surface, we finally show that the effect of the motion of the free surface on the motion of the cylinder is indeed negligible. Firstly, the rate of displacement is constant as is shown in Fig. 6.12.6(e) which also shows a comparison with that of motion due hydrostatic pressures only. Secondly, the acceleration, though not zero, is constant and small, see Fig. 6.12.6(g). Thus the corresponding rate of change

of the cylinder and fluid momentum is also constant, see Fig. 6.12.6(h). This proves the fact that the effect of the free surface disturbances can now be ignored without losing correct body dynamics. We further examine the free surface motion in the calculations that follow.

An attempt with the same number of points on the free surface as before and small alterations, produced results similar to those above. These calculations broke down in a similar way. This happens as the jet height is droping rapidly and is expected to be unstable. Taking the averages to represent the points where new jets have formed for the third time proved fruitful as we were able to continue the calculations for a long time enabling us to observe some of the complex behaviour of the free surface of a disturbed fluid. The mound at the origin is now clearly propagating waves outwards as dipicted in Fig. 6.12.7(a,b) and is flattening quite fast. This, causes some more jets to form and the program again breaks down. Nevertheless, the pressure on the body does not show any response to what is happening on the free surface.

After using the averages technique to represent the points where the jets had formed we managed to continue the calculations for about thirty time steps with $\Delta t = 0.014$ i.e the time intervals had been increased to ten times the ones for the preceding runs and equalled three times the steps of the entry phase. This is done in accordance with the decrease in fluid particle velocities in the region of greatest disturbance, and as a result computation time is reduced. A drawdown at the origin and a "sharp" breaker have formed in Fig. 6.12.8 leading to program stoppage. Fig. 6.12.9 ,10, 11 show further attempts to get the calculations going forward in time with the number of the points reduced to 99, 97 and 93 respectively. The "sharp" breakers we see here are similar to

the ones described earlier on in chapter 5 where the calculations broke down because of breaking waves. The condition of the free surface in, i.e Fig. 6.11 seem to be similar to the one of high-frequency waves discussed in chapter 5. With proper resolution of the free surface in the region of disturbance we may be able to follow these high-frequency waves further but this is outside the objective of this work which aims at solving the engulfment problem.

Lastly, we show the whole life history of the hydrodynamic force on the cylinder from being half-submerged to just after d=2.25a, see Fig. 6.12.12. Beyond that point the hydrodynamic force is fast approaching zero as expected. At the point of swapping the programs we see a good matching of the hydrodynamic forces between d=1.199a and the next stage of the calculations after complete engulfment. However, some problems arise, as mentioned above, due to the formation of jets which result in small errors in the calculation of the forces as the calculations are temporarily adjusted by altering the free surface discretisation.

6.3.2 Summary

The results show significant progress in solving, numerically, the engulfment problem. This has been achieved through the smoothing procedure of the free surface at various stages of the calculations. It was important to show that the calculations could be continued using the above technique without significantly affecting the motion of the body. Admittedly, the initial jet formation had proved difficult to deal with, especially for the reason that it was difficult to follow the motion of the cylinder further than the instant of jet formation. To overcome this problem the smoothing technique proved helpful. Because of

the sudden rise in fluid pressure at the initial phases of the calculations, the results obtained after the jet has formed become inaccurate. For that reason we removed the jet before restarting the calculations. This was done in such a way that the fluid mass was reasonably conserved. The energy carried by jets is lost when jets are completely cut off. This energy is contained in very small volumes of fluid and consequentially loss of it does not result in significant energy loss for the whole system.

At later stages the formation of jets does not necessarily result in inaccurate calculations subsequently, mainly because the free/cylinder surface interaction is no longer strong. In that case the calculations are allowed to go beyond jet formation for as long as the scheme can still handle accuratetly the free surface points. The next calculations are then restarted after the jet has formed, depending on suitability of the initial data. What remains to be shown is what the motion would look like if the specific gravity of the cylinder were increased or reduced. The motion could also have been started with the cylinder just touching the free surface or a little bit submerged. These cases could be examined in a similar way to that presented here. Finally, with the conservation of fluid mass, energy and momentum approximately satisfied we have been able to follow the motion of the cylinder entering the free surface and beyond. The overall motion of the cylinder was shown to be little affected by the details of the free surface disturbance even when the cylinder/free surface interaction was still great. In the next section we consider the forced motion of the cylinder which is initially half-submerged, as in this case. The motion of the cylinder at different Froude numbers will be investigated and the effect of the motion of the fluid is also followed.

6.3.3 Continuation of forced motion after complete engulfment

In this subsection we continue with the calculations of the forced motion for the values of ι considered above. The forced motion of the cylinder is investigated for the following situations;

(a) vertical motion for $\iota = 0^o$ at Fr=0.19, 0.31 and 0.46

(b) oblique motion for $\iota = 30^o$ at Fr=0.31

(c) oblique motion for $\iota = 45^o$ at Fr=0.19 and 0.31

(d) oblique motion for $\iota = 60^o$ at Fr=0.31.

For vertical motion we simply have to move the point in the centre as the inflows impact in a similar way as described above for free motion and the calculations are restarted. As already mentioned above the situation is different for oblique motion. Here, we simply remove two intersection points to create a smoothed boundary around the neighbourhood of the impact site by averaging *nearest points to replace the one directly above the top of the cylinder.* Additional points are then put in the regions of high and low curvature for high resolution of jets.

We now consider the vertical motion of a cylinder moving at Fr=0.19 immediately after complete engulfment, see Fig. 6.13.1. The scheme fails when the body is at a distance $d = 1.22a$ below the free surface. This case is very similar to the one studied above in the sense that we have slow motion in both cases. The initial calculations break down in a similar way as above. The ensuing motion in this case of either the free surface or the body, after altering the boundary conditions, can obviously be compared to that of the free mo-

tion. At low Froude numbers jets on the sides of the body are not well enough developed to be cut off to ensure smooth transition from this initial phase, half-submerged, to the second phase without loss of fluid mass through smoothing. This is not the case when the body entered the fluid at a high speed as then thin jets were formed, see Fig. 6.5. The results of last reliable step were then transfered to the program for totally-submerged bodies after using smoothed free-surface coordinates and corresponding potentials around the impact site. It has to be remembered that, in order to step forwards in time, the distance between the free surface and the cylinder has to be similar to or greater than that between the points on the body. The results of the restarted calculations are shown in Fig. 6.13.1. At the start of the calculations the free surface is reasonably flat before it is visibly drawn down around the origin forming a cavity. The downward moving particles suddenly change direction to upward movement, and at the same time they form waves propagating away from the origin. Fig. 6.13.1(i(e,f)) show fully- developed waves which have formed in the region of disturbance. These look like standing waves, the outward propagating disturbance being strongly reflected by the sudden increase in effective water depth beyond the cylinder. The effect may be similar to radiationless trapped waves in the steady state linear problem, see Ursell (1990). The disturbance around the impact region, eventually, causes a sudden rise in pressure distribution around the top of the cylinder.

An attempt to carry on with the calculations by smoothing of the free surface was not sucessful. A number of trials were made but the calculations broke down each time only after a few time steps. The best results achieved after the initial break down with the program for completely submerged bodies

are shown in Fig. 6.13(ii). Further processing of these results did not produce any meaningful results as the upward jet around the origin continually re-appears, leading to failure of the scheme.

The above difficulties highlight the obvious need to investigate the motion at high Froude numbers. This was done with $Fr = 0.46$ and slightly coarser discretisation of the free surface and body in agreement with previous observations in chapter 5, as well as those discussed in Greenhow(1988). The calculations for initially half-submerged cylinder are then started and the results were discussed in section 1 of this chapter. The scheme fails at $d = 1.38$ in this case, which is a distance equal to $0.16a$ deeper than in the previous calculations, since the increased speed of the body opens up a larger and deeper cavity behind it.

After resolving the free surface around the region of impact and calculation of corresponding potentials, the calculations were restarted. The results of the free-surface behaviour and pressure distributions around the body before and at the time of the breakdown of the calculations are shown in Fig. 6.13.2. As in the previous cases, there is initial draw down of the fluid at the centre and a break down of the calculations, due to the upward jet which has just formed. To proceed with the calculations a few points clustered around the centre were removed and an average was used for the centre coordinate. This led to two downward jets at the corners of the base of the trough leading to very high pressures around the body. At the next stage the computations are taken at the step when the jets appeared and we removed them. These were disrupted by the formation of the "sharp" breakers which at this stage are fully developed as seen in Fig. 6.13.2(ii). Fig. 6.13.2(iii) shows our calculations after removing

the "sharp" breakers again and using the averaging technique to represent the corners at the base of the trough shown in Fig. 6.13.2(ii)(a-b). We see that the free surface has started moving upwards around the centre and possibly an upward jet will form if these calculations are continued, see Fig. 6.13.2(iii)(a)-(b). The formation of jets poses problems encountered previously in the the case of the free motion of the cylinder.

For the motion of the cylinder at Fr=0.31 we found no new features other than those which have already been discussed for the motion at Fr=0.46. However, the calculations were done and recorded as shown in Fig. 6.13.3. For the motion at Fr=0.31 and 0.46 there is qualitative resemblance of our free surfaces to those of Cooker and Peregrine (1991) as mentioned before in the case of free motion (see also Figs.6.13.2(i(e, f, i, j) and 6.13.2(ii(a-b)).

The hydrodynamic forces on the cylinder for the three cases considered are compared in Fig. 6.13.4. As in the case of free motion there is smooth change in forces at the stage of swapping programs, but there are some small disturbances later on as the jets begin to form. The forces show similar behaviour for all Froude numbers. High Froude number results in low hydrodynamic forces and vice versa, and these forces tend to zero as the depth of submergence increases as expected.

We now look at the case of oblique motion for all the cases considered above. Firstly, the calculations at $\iota = 30^o$ at Fr=0.31 are continued as described above. The resulting free surface deformations and cylinder positions are shown in Fig. 6.14(i(a-d)). The pressures are also shown, see Fig. 6.14(i(e-f)). These calculations break down because of the jets forming behind the cylinder which are smoothed to give the results in Fig. 6.14(ii), but we have not pursued them

any further.

The calculations at Fr=0.19, 0.31 for $\iota = 45°$ were also carried out. In this case of low speed, Fr=0.19, the free surface stays fairly flat except for the very thin jet caused by the impacting fluid layers, associated with a high pressure region on the cylinder surface immediately below it. We do not claim the calculation of the jet itself is accurate here. In reality the jet will quickly break up under the action of surface tension, but we again note that its details have no significance for the rest of the flow. The calculations are shown in Fig. 6.15.1 with the jets being occasionally removed to allow the calculations to continue. These calculations were stopped after the the re-emergence of the jet from below the free surface. At high speed, Fr=0.31, the situation is similar to that of Fr=0.19 at the start of the calculations, see Fig. 6.15.2(i)-(ii). After the first two initial smoothing stages the flow becomes very unstable causing numerical instabilites which inhibit further progress, see Figs. 6.15.2(iii)-(v). These calculations were then abandoned. The hydrodynamic forces seem to respond to this unstable situation starting from the moment of complete engulfment which makes it hard for us to continue these calculations.

At 60° and Fr=0.31 we obtained encouraging results with a thin jet forming behind the cylinder like in the initial stages of the case of 45-degree angle. However, these calculations do not show any unsteadiness and can be continued without any forceable problems, see Fig. 6.16(i(a-d)) for free surface plots, (e-f) for total pressure traces and (g-h) for hydrodynamic forces.

In general these calcualtions can be continued for as long as we wish by further application of the above method except in a few cases like the one of the angle of 45-degrees at Fr=0.31 which seemed to be unstable right from

the initial complete engulfment stage. However, what is clear is that these calculations resemble those of the free motion case in many respects. The only difference between them is that the formation of jets on the free surface happens in a slightly different manner for symmetrical situation and in a completely different way for oblique motion, but with more or less the same effect on the motion of the body, i.e cutting off the jets reduces the chances of getting unstable numerical results during the initial phases.

6.4 Summary

The problem of engulfment has been numerically solved in the case of the free motion of a horizontal circular cylinder which is initially half-submerged in an undisturbed fluid. Firstly, the problem of a discontinous potential function and its normal derivative at the impact site is solved by giving a value for the potential at that point(s) corresponding to given free surface coordinate(s) and the normal derivative is automatically calculated by the program. Thus a doubly-connected flow domain is once again singly connected with a branch cut and hence the calculations are continued. Secondly, the break down of the calculations in the ensuing motion of the cylinder results from complex free-surface jet motion which in turn causes, in some cases, the breakdown of the scheme. Problems were overcome through smoothing of the free surface whenever the jets occured. Apart from causing breakdown of the calculations, the jets were found to be main agents of, or effects from, sudden slight acceleration or decceleration of the motion of the cylinder at small times. Nevertheless, this had little effect on overall motion of the cylinder.

The calculations for forced vertical motion at low Froude number Fr=0.19

were terminated after we had failed to resolve the free surface correctly, for the program to handle what seems like unstable overdriven standing waves. The forces and pressures seemed to be unaffected. At 45 degrees the body re-emerges from the free surface, but forces and pressures on the body seem to be slightly affected. In the case of the problem at high and medium Froude numbers, we managed to proceed further than in the case of low Froude number. The calculations for vertical motion were stopped prematurely because they are qualitatively the same as those of the free motion. The oblique cases for 30- and 60-degree angles at Fr=0.31 are quite stable and those calculations can be continued without any problems except for continued formation of jets. At 45 degrees, Fr=0.31, the motion of the fluid became unstable causing numerical breakdown and global features such as the cylinder forces to become significantly affected.

The engulfment problem being investigated here avoids the initial stages of interaction between the body and the free surface as this would present us with a difficult problem of calculating accurately the large slamming forces involved during the time of impact. As noted in Greenhow's (1987) work, the numerical calculations can only be guaranteed to be accurate when the deadrise angle is large; the complete slamming, entry and engulfment of the cylinder is therefore made extremely difficult by the large, unstable and fast moving spray jets formed during the slamming phase, see photos in Faltinsen (1990).

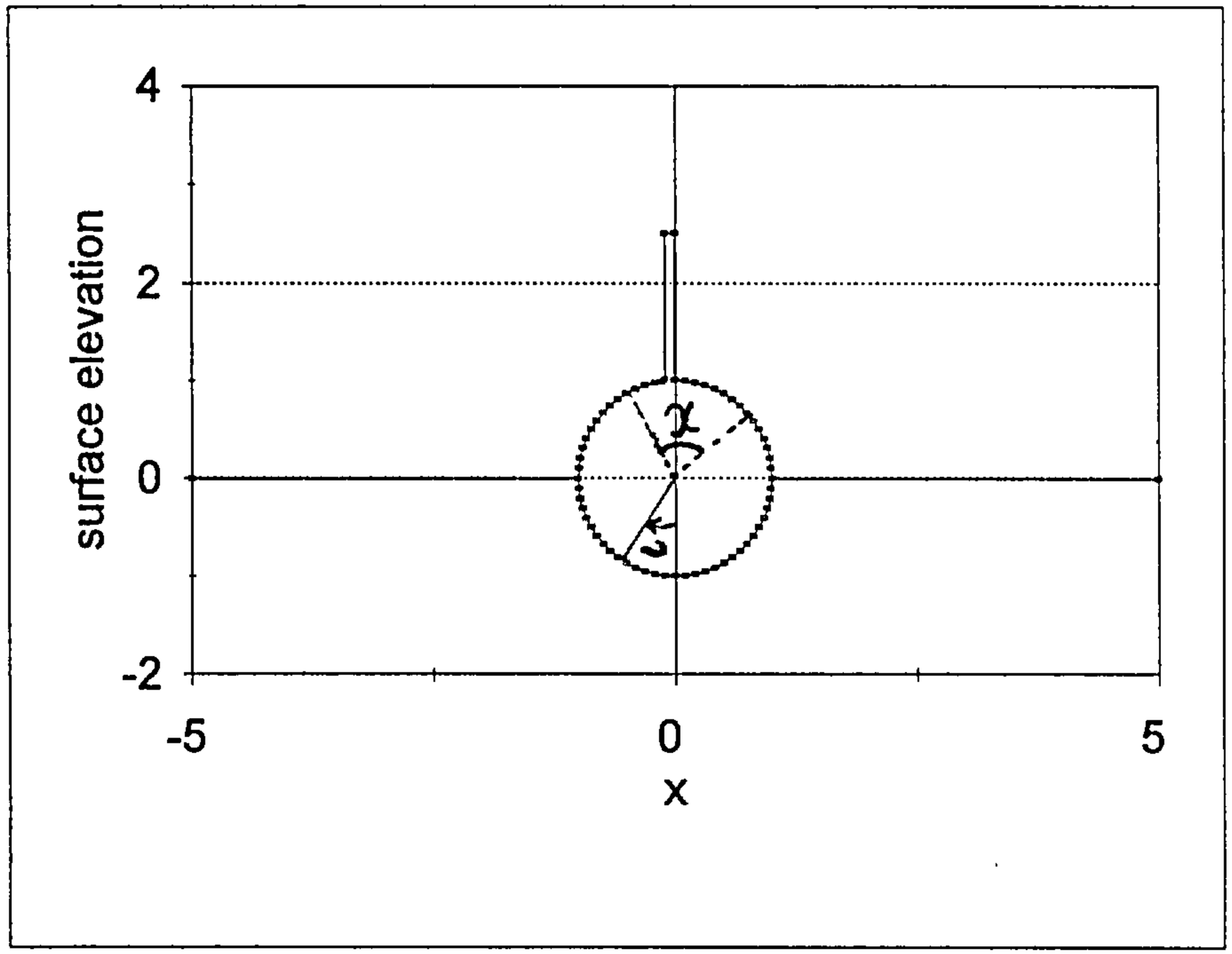

Fig. 6.1 Initial cylinder and free surface positions.

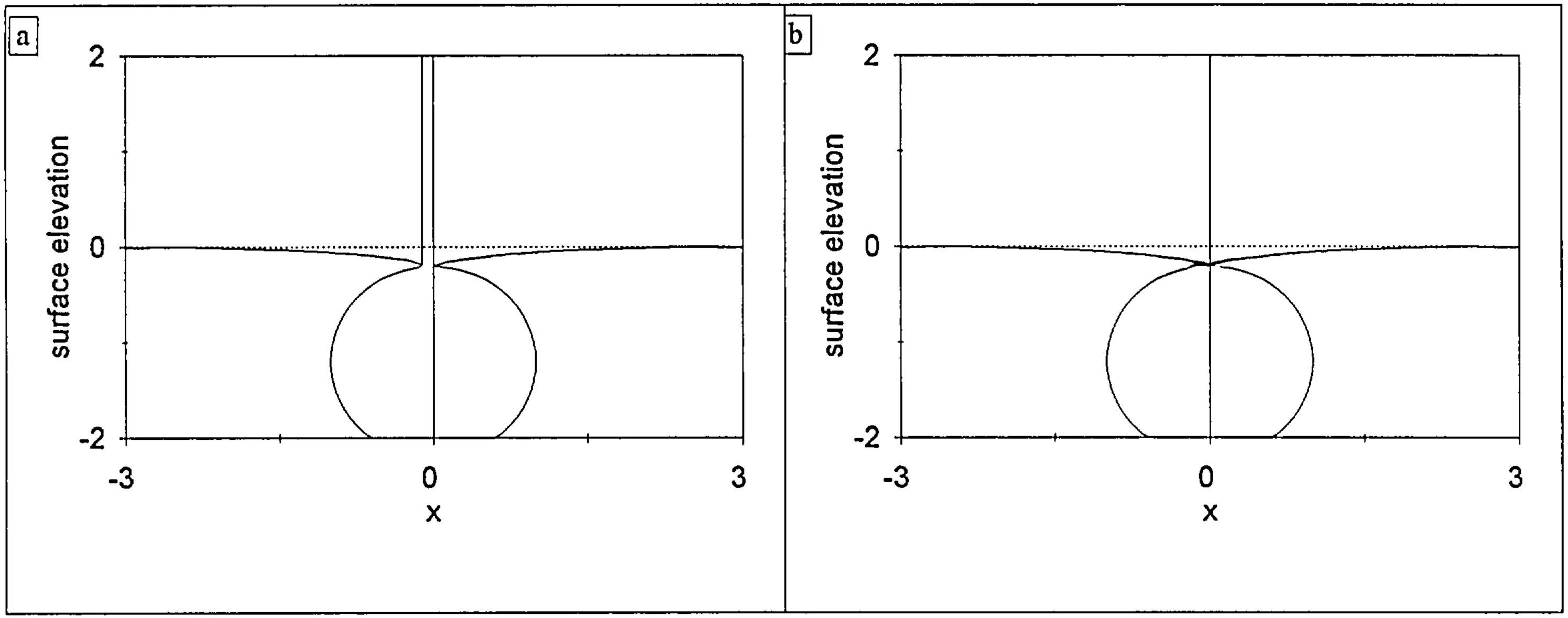

Fig. 6.2 Free-surface elevation and cylinder position at the time of impact of the inflows.

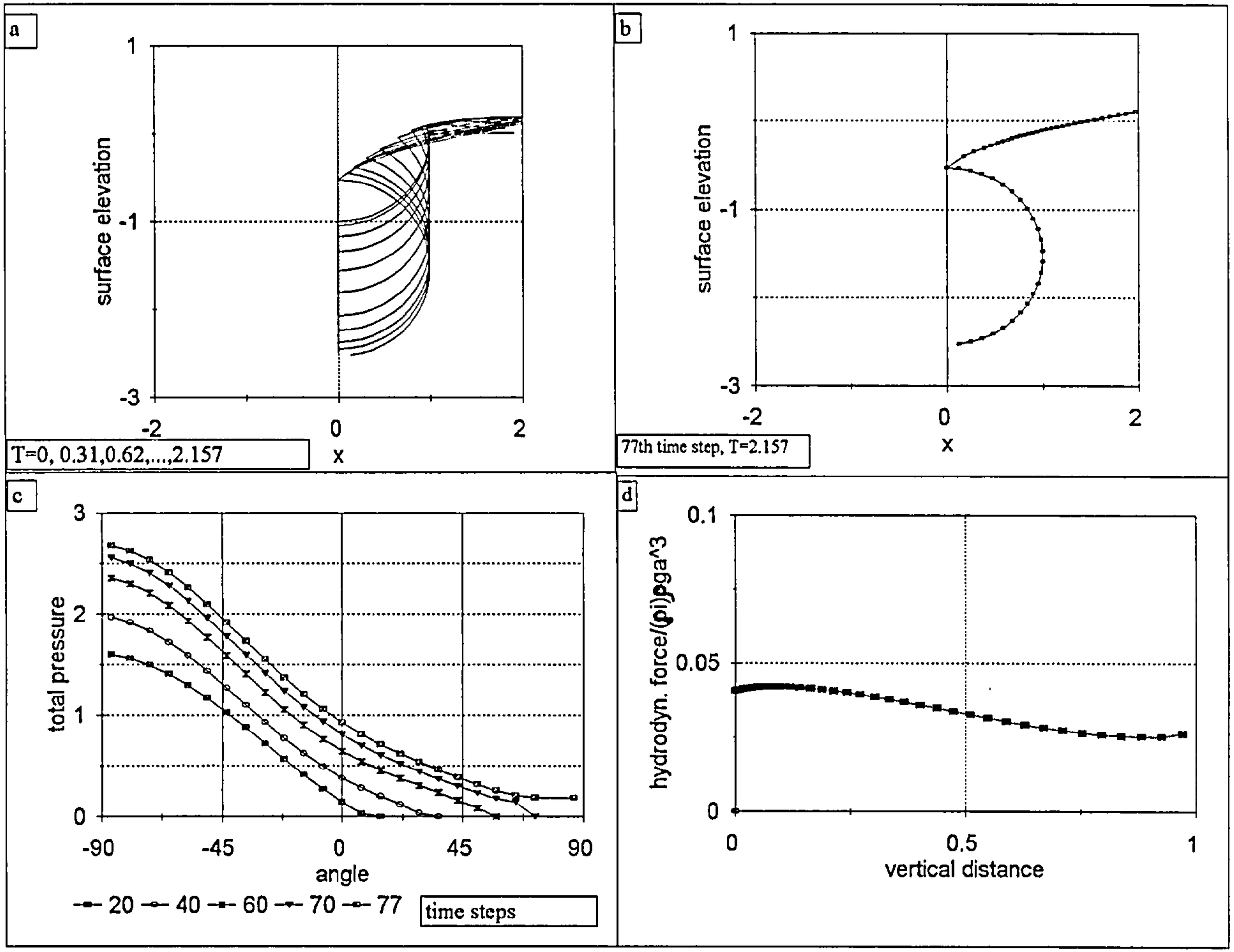

Fig. 6.3 (a)-(b) represent free-surface and cylinder positions, (c) total pressure distribution around the cylinder and (d) vertical force on the cylinder ; due to the free motion of an initially half-submerged cylinder, Mb=1.2.

c

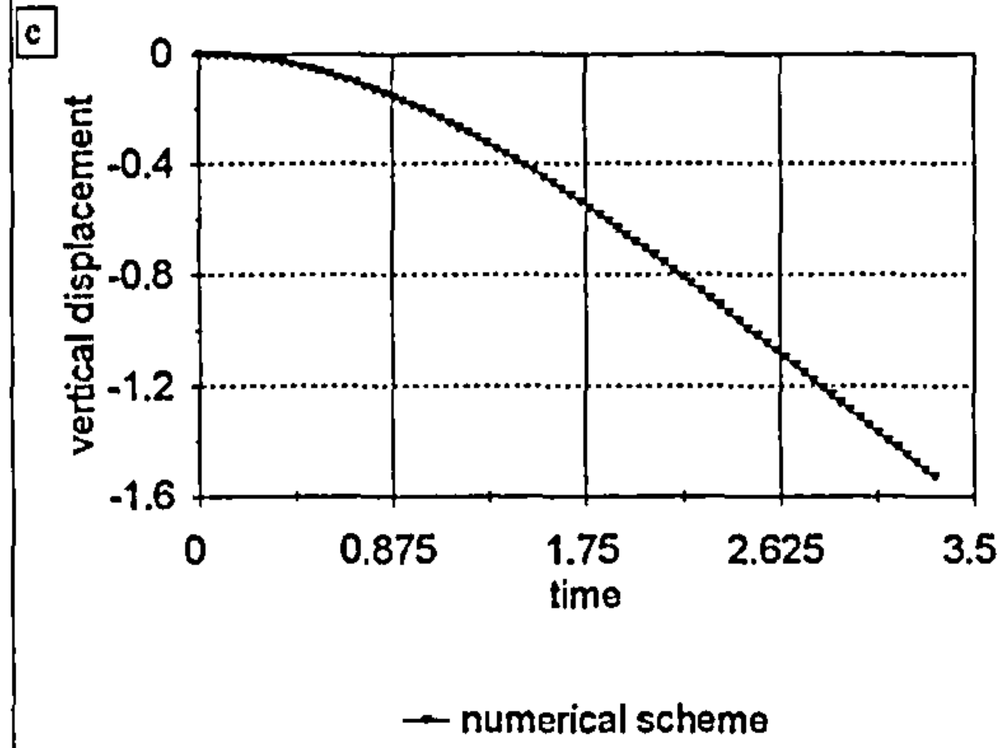
0
-0.4
-0.8
-1.2
-1.6
vertical displacement
0
0.875
1.75
2.625
3.5
time
numerical scheme

f

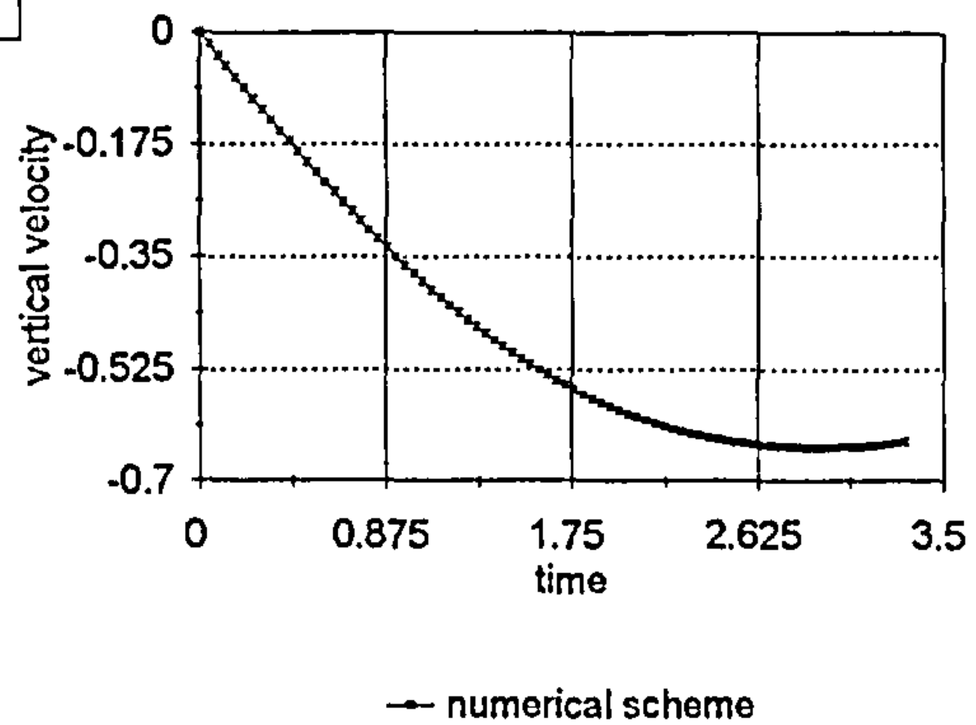
0
-0.175
-0.35
-0.525
-0.7
vertical velocity
0
0.875
1.75
2.625
3.5
time
numerical scheme

g

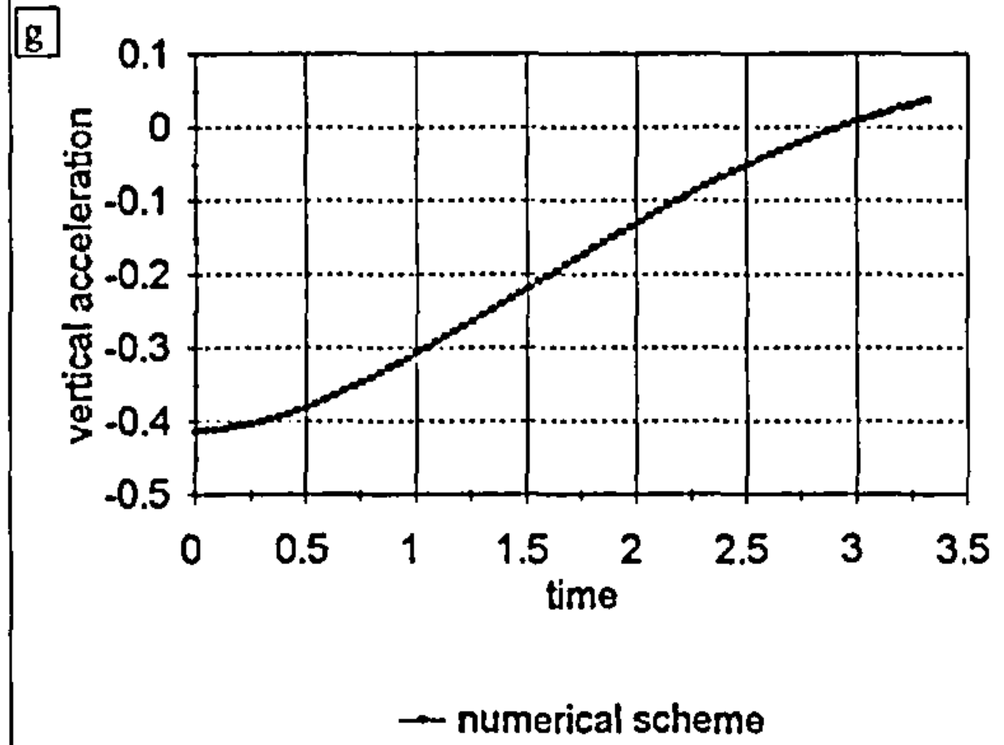
0.1
0
-0.1
-0.2
-0.3
-0.4
-0.5
vertical acceleration
0
0.5
1
1.5
2
2.5
3
3.5
time
numerical scheme

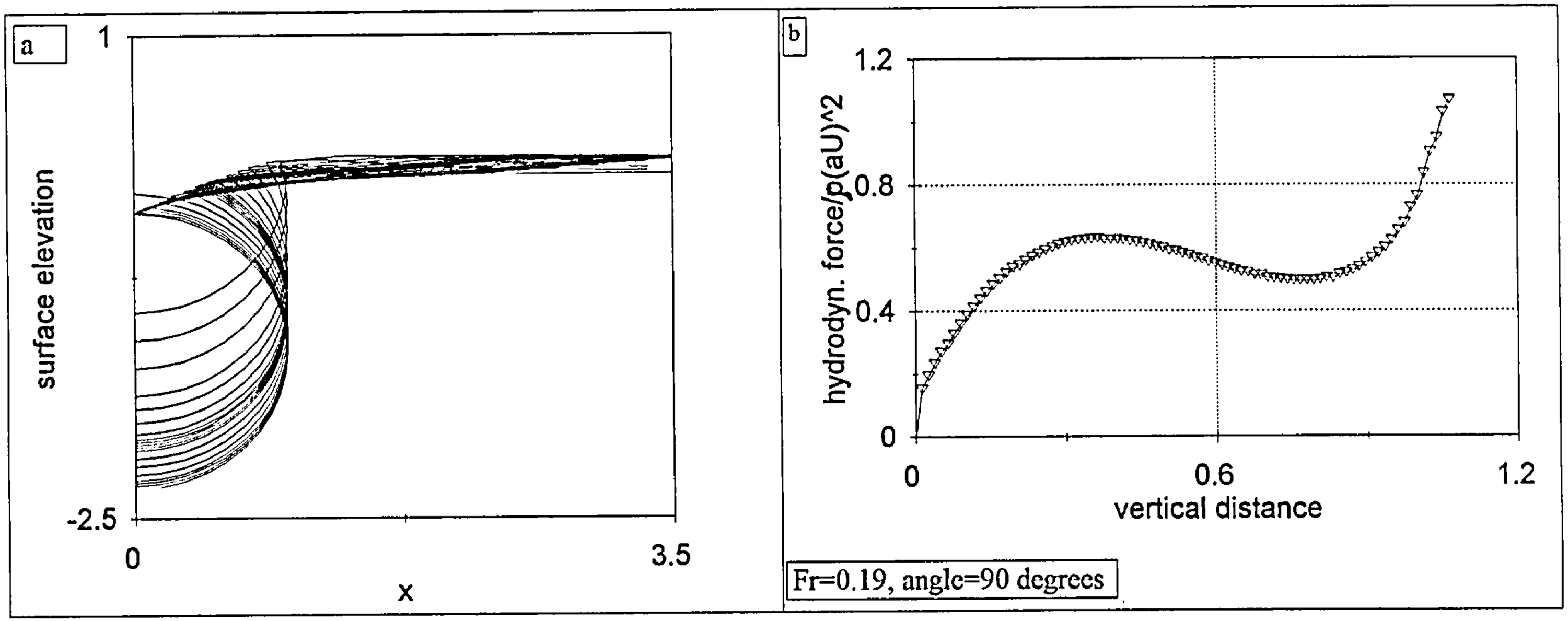

Fig.6.4 (a) Free-surface elevations and cylinder positions, and (b) hydrodynamic force on the cylinder due to an impulsively started motion of an initially half-submerged cylinder, Fr=0.19 and Mb=1.0.

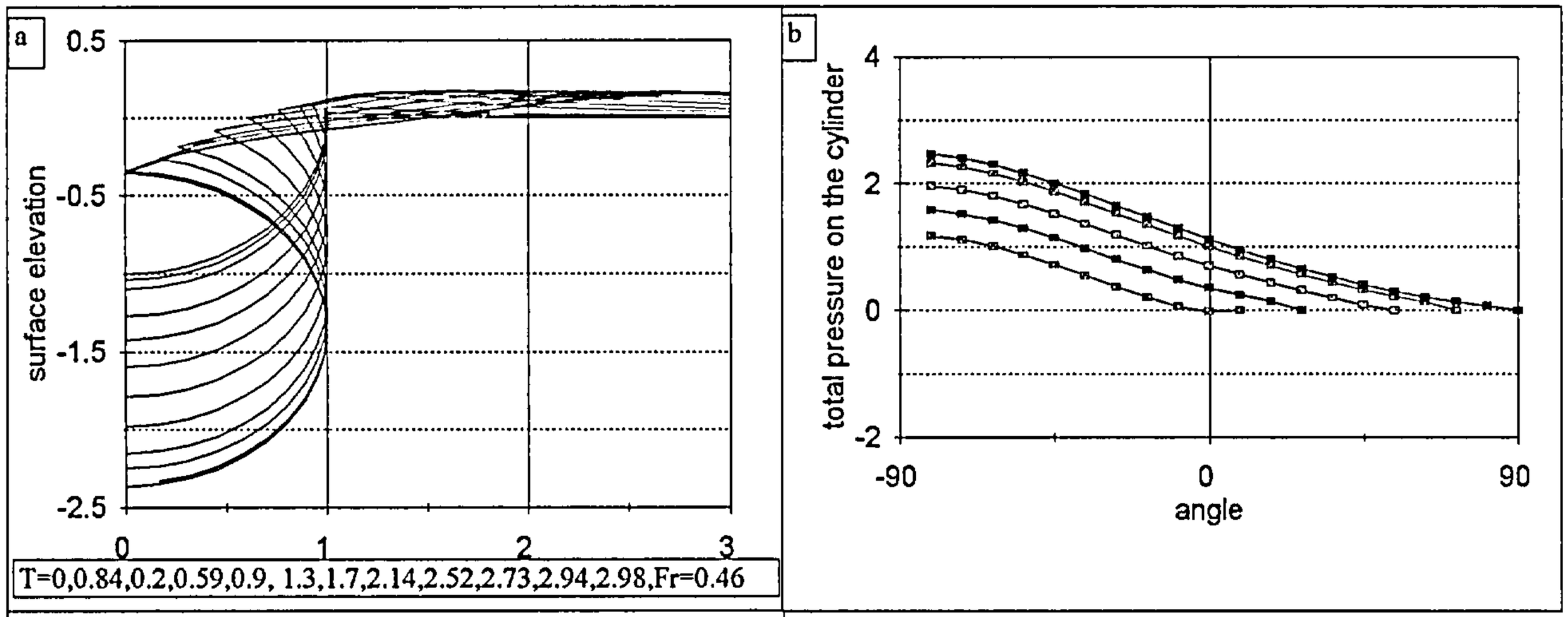

Fig. 6.5 (a) Free-suraface elevations, (b) pressure distribution around the body and [c] hydrodynamic force on the cylinder due to the veretical and impulsively started motion of an initially half-submerged cylinder at Fr=0.46 and Mb=1.0.

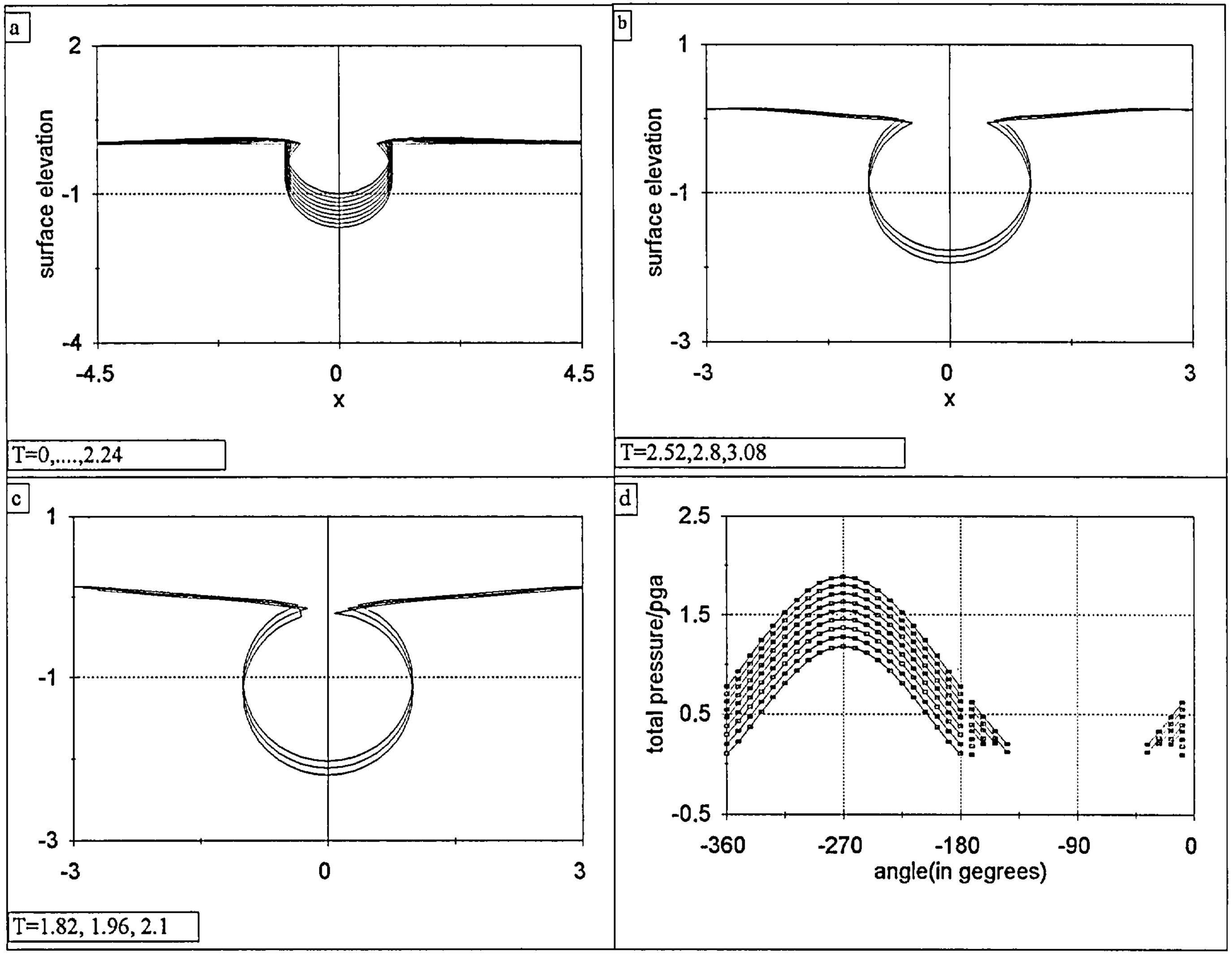

Fig. 6.6 (a)-(c) free-surface and cylinder positions, (d)-(e) pressure distribution around the cylinder and (f) hydrodynamic forces on the cylinder; due to the vertical(90- degrees) and impulsively started motion of an initially half-submerged body moving at Fr=0.31, Mb=1.

c

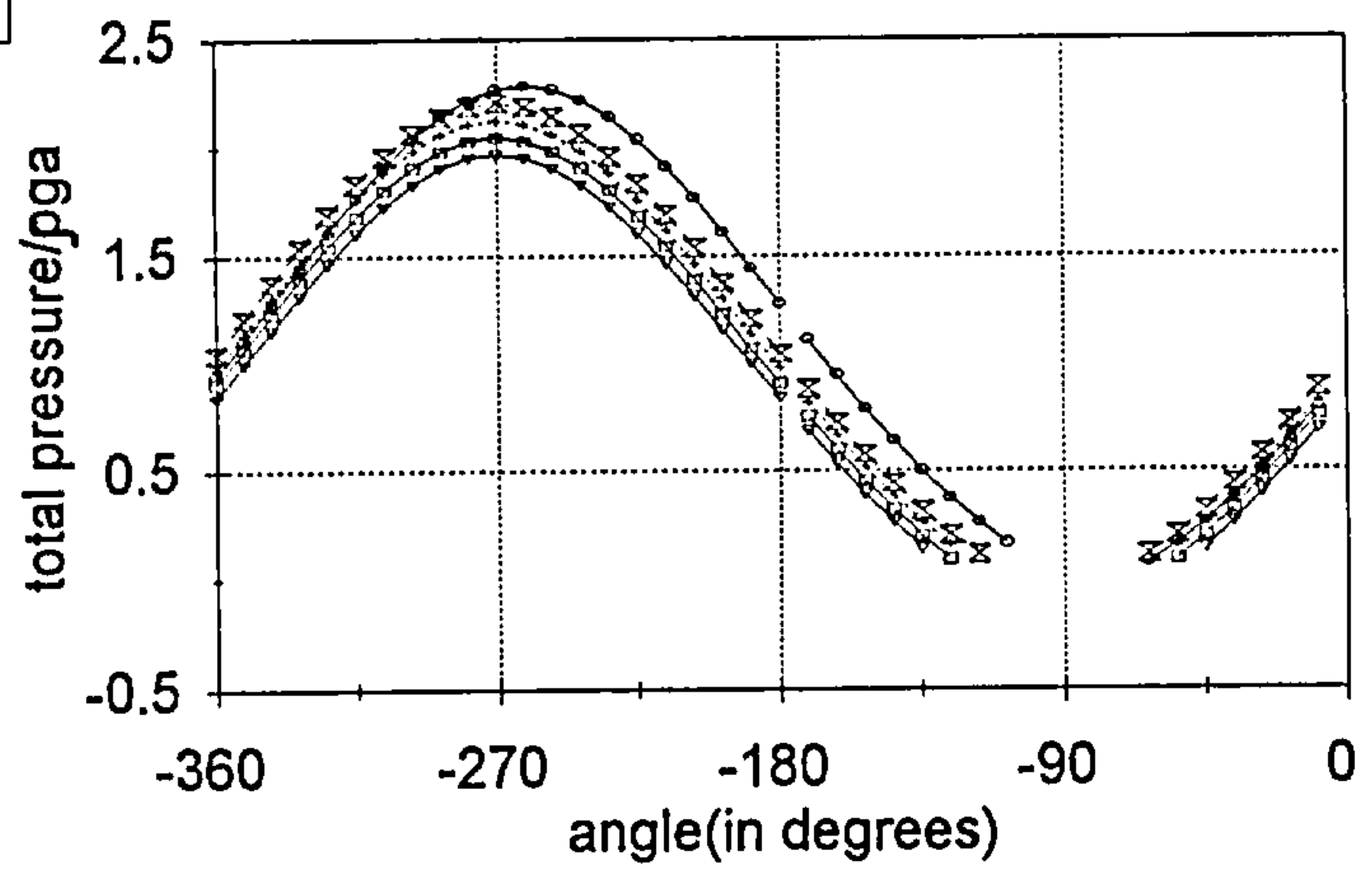

11th 12th 13th 14th 15th

f

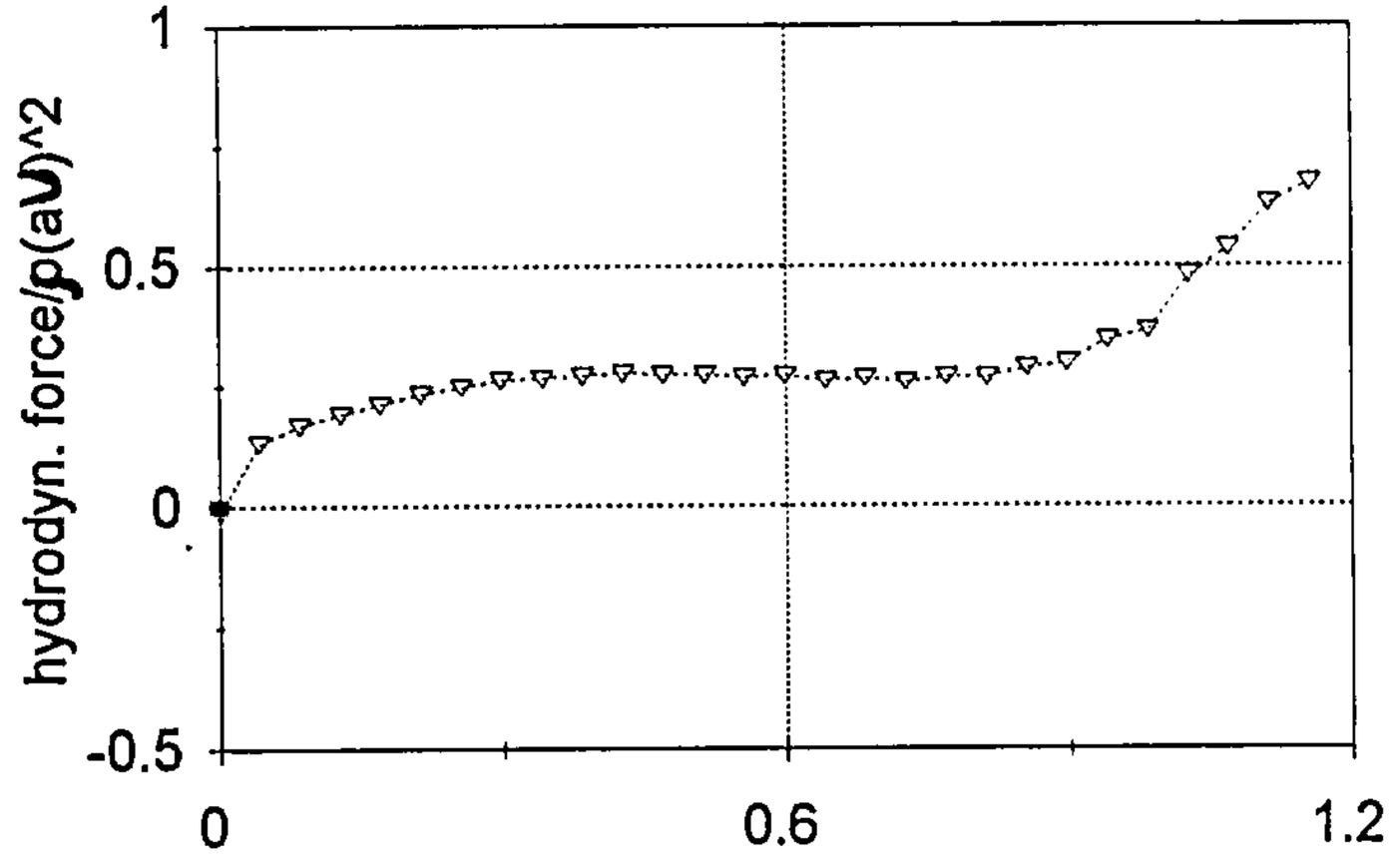

T=0 - 3.922, Fr=0.31, angle=90

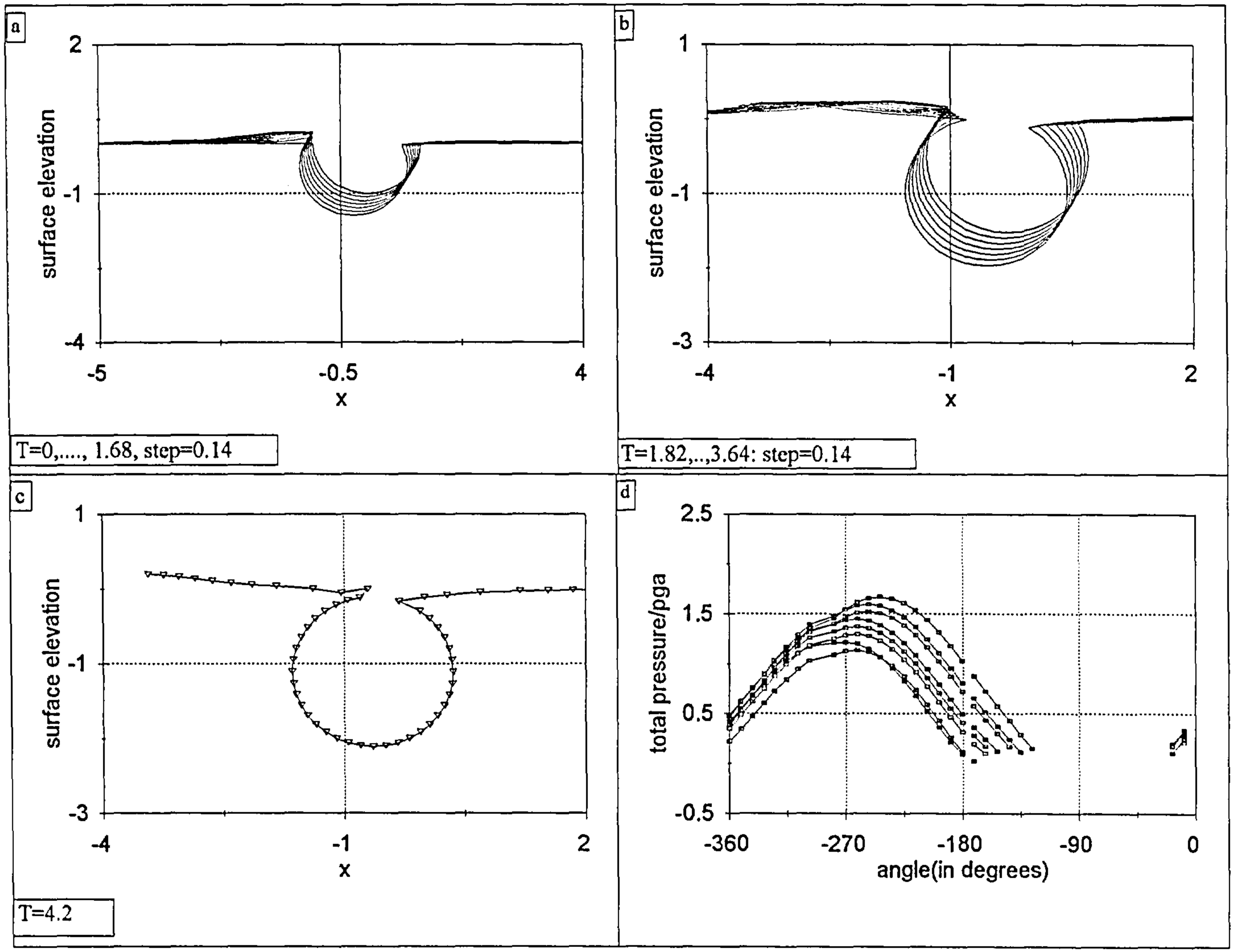

Fig. 6.7 (a)-(c) free-surface and cylinder positions, (d)-(e) pressure distribution around the cylinder and (f) hydrodynamic forces on the cylinder moving obliquely at and angle of 30 degrees at Fr=0.31, Mb=1.0. Initially the cylinder is half-submerged and the motion is started impulsively.

e

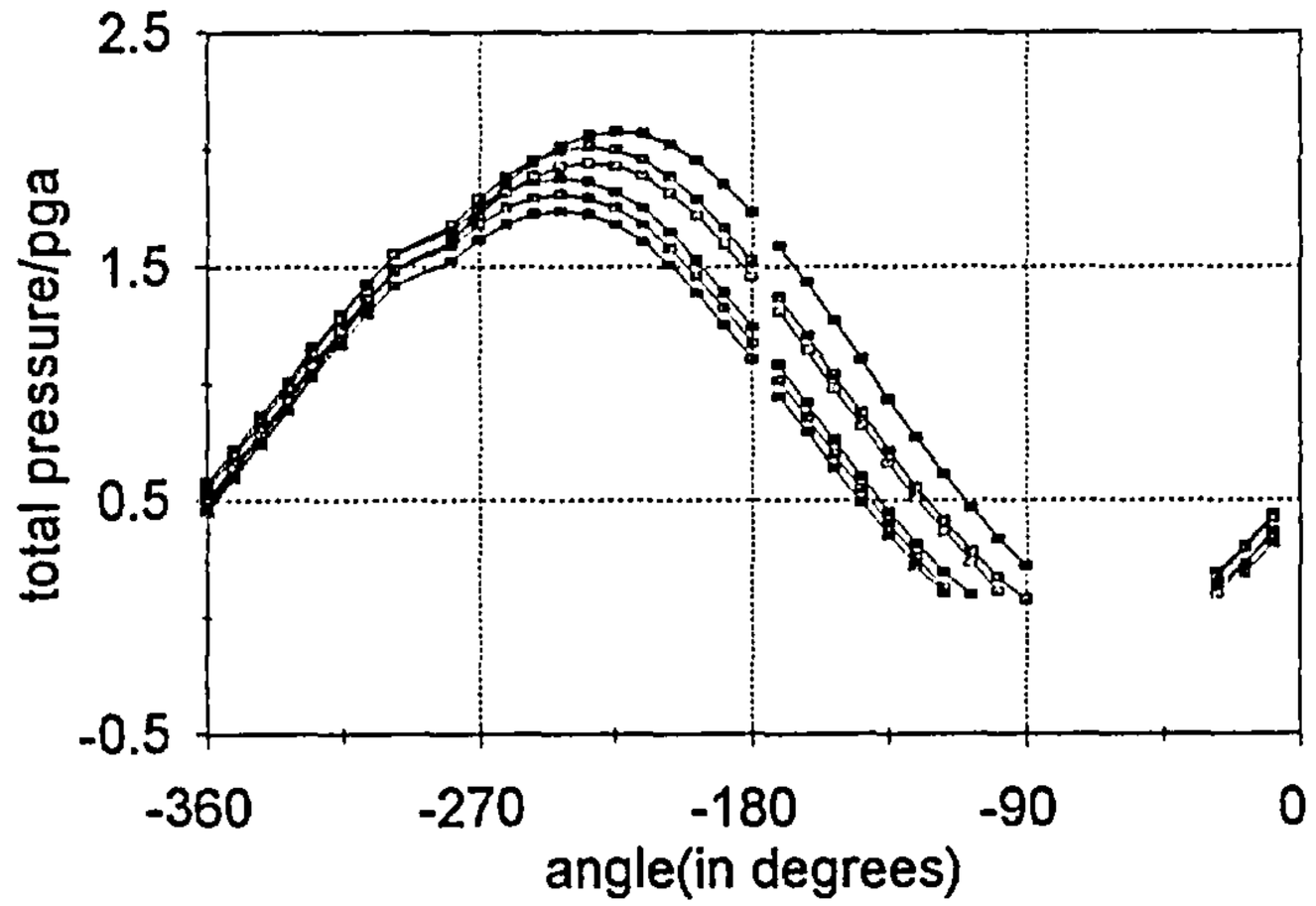
2.5
1.5
0.5
-0.5
total pressure/pga
-360
-270
-180
-90
0
angle(in degrees)

f

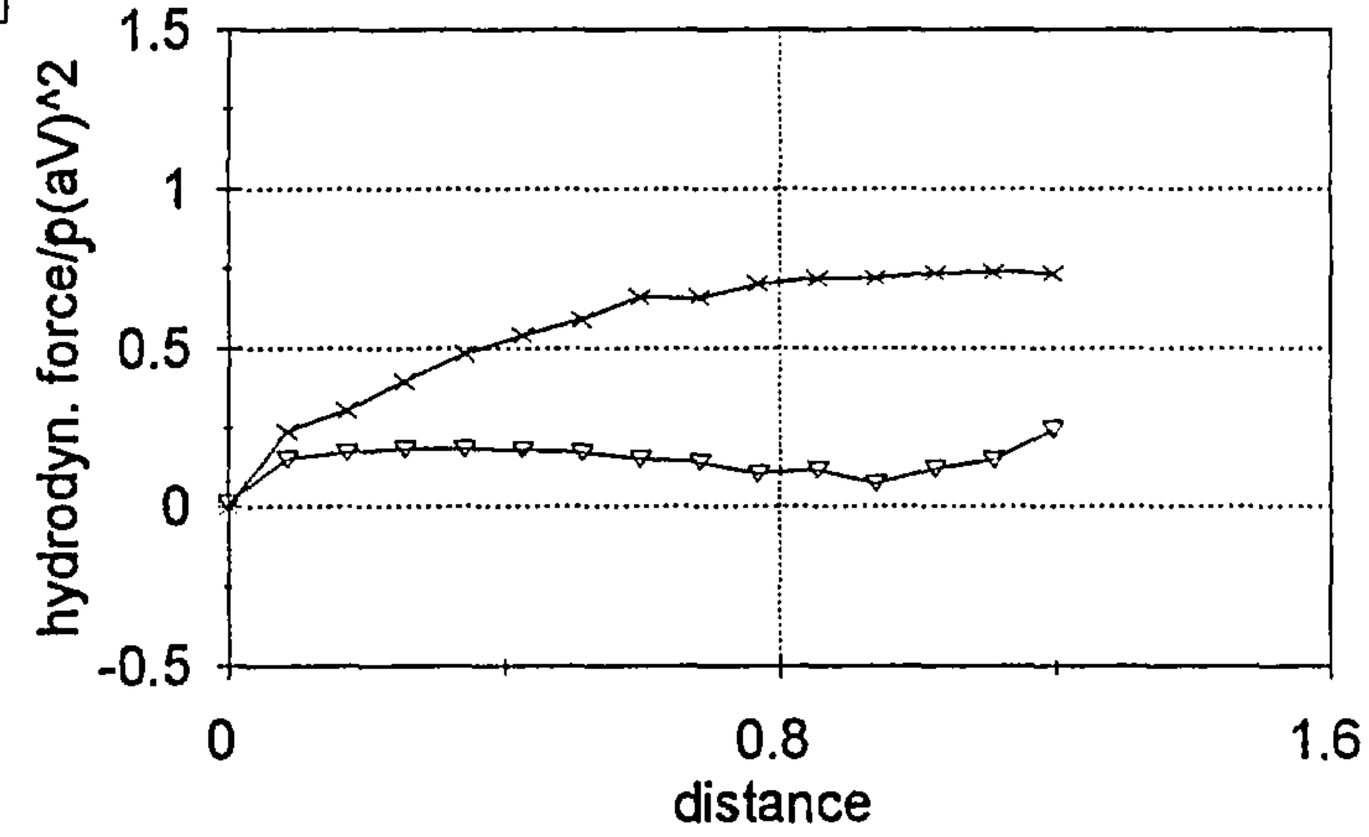
1.5
1
0.5
0
-0.5
hydrodyn. force/p(aV)^2
0
0.8
1.6
distance

Fr=0.31


horizontal force
vertical force

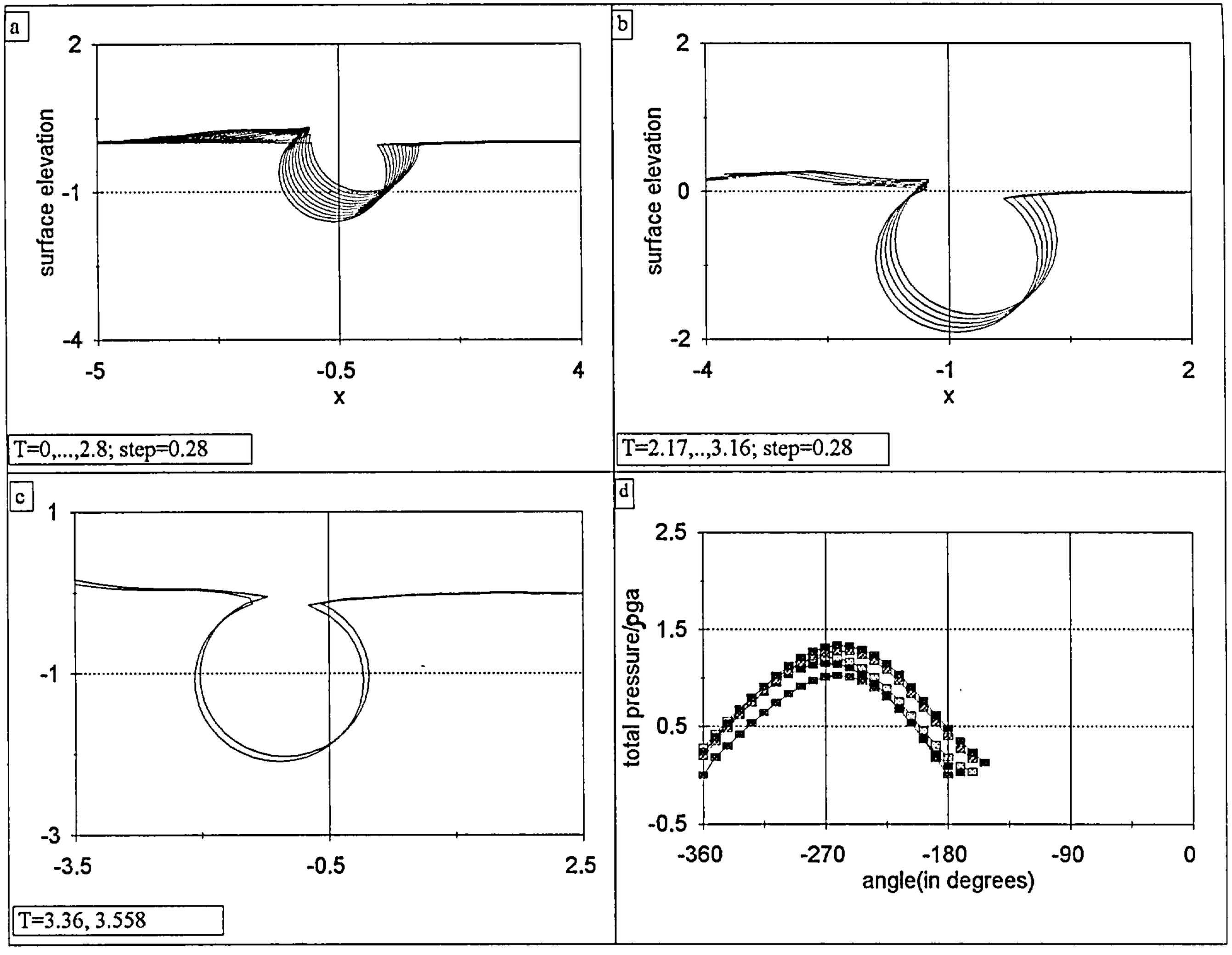

Fig. 6.8 (a)-(c) free-surface and cylinder positions, (d)-(e) pressure distribution around the cylinder and (f) hydrodynamic forces on the cylinder; due to the obique(45- degrees) and impulsively started motion of an initially half-submerged body moving at Fr=0.31,Mb=1.

e

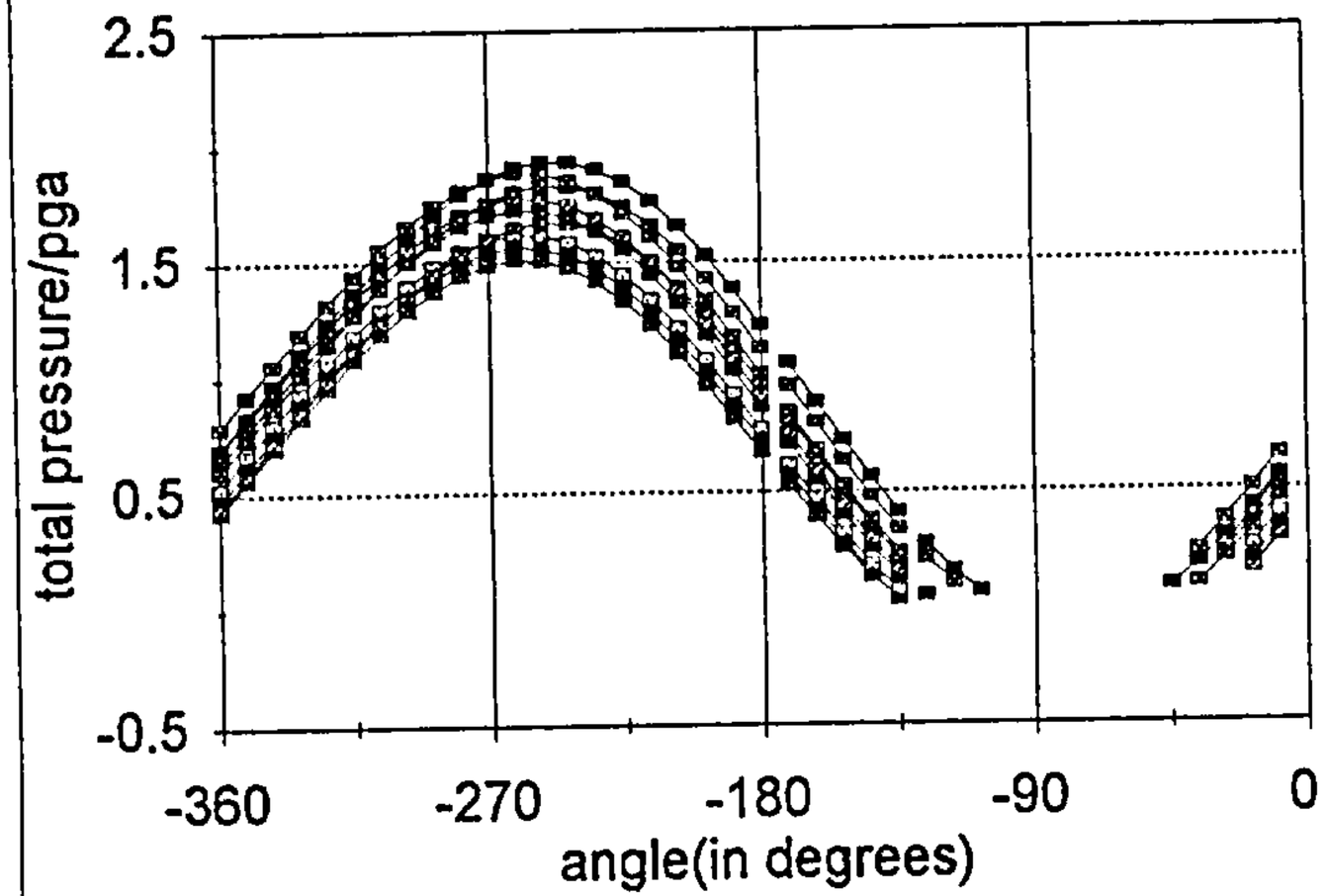
2.5
1.5
0.5
-0.5
total pressure/pga
-360
-270
-180
-90
0
angle(in degrees)

f

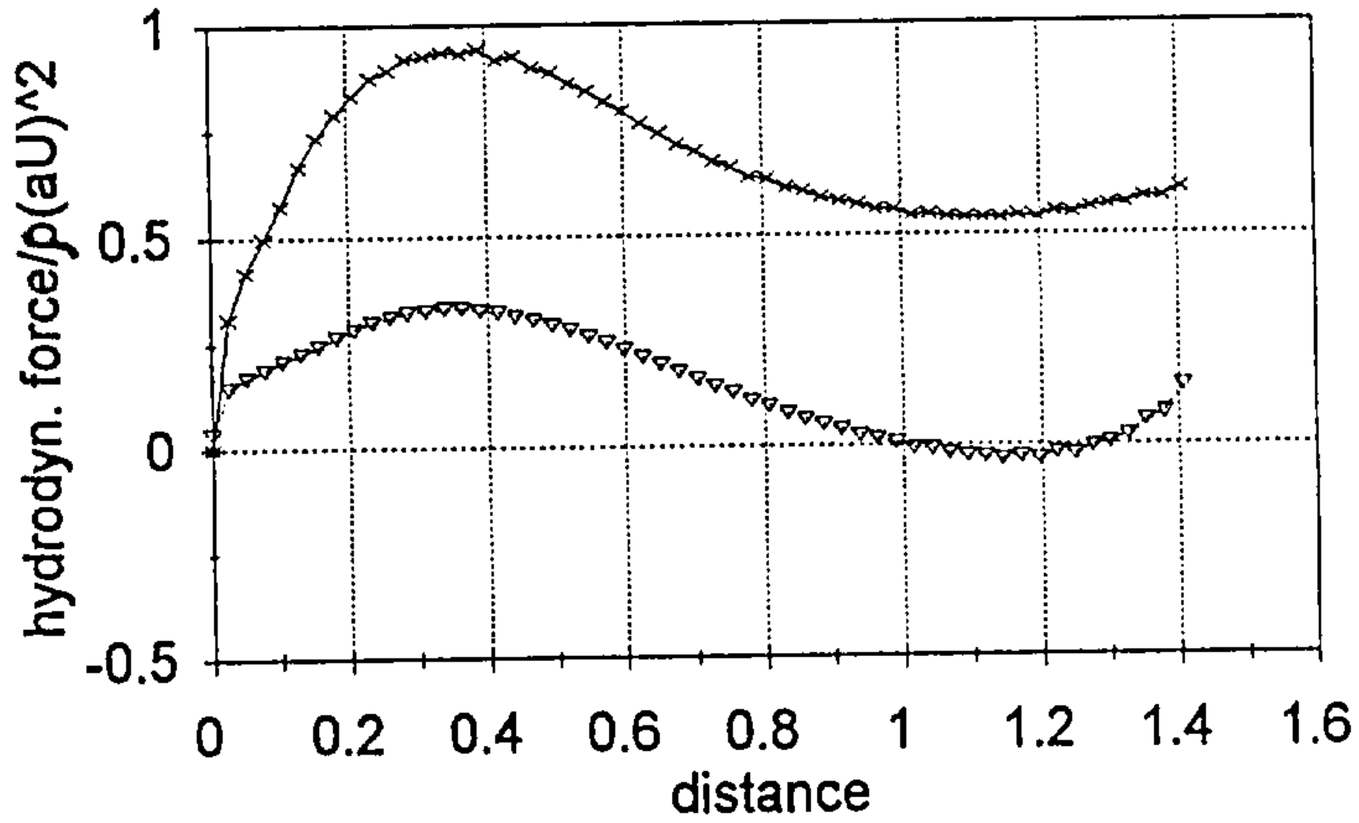
1
0.5
0
-0.5
hydrodyn. force/ρ(aU)^2
0
0.2
0.4
0.6
0.8
1
1.2
1.4
1.6
distance
horizontal force
vertical force

Fr=0.19

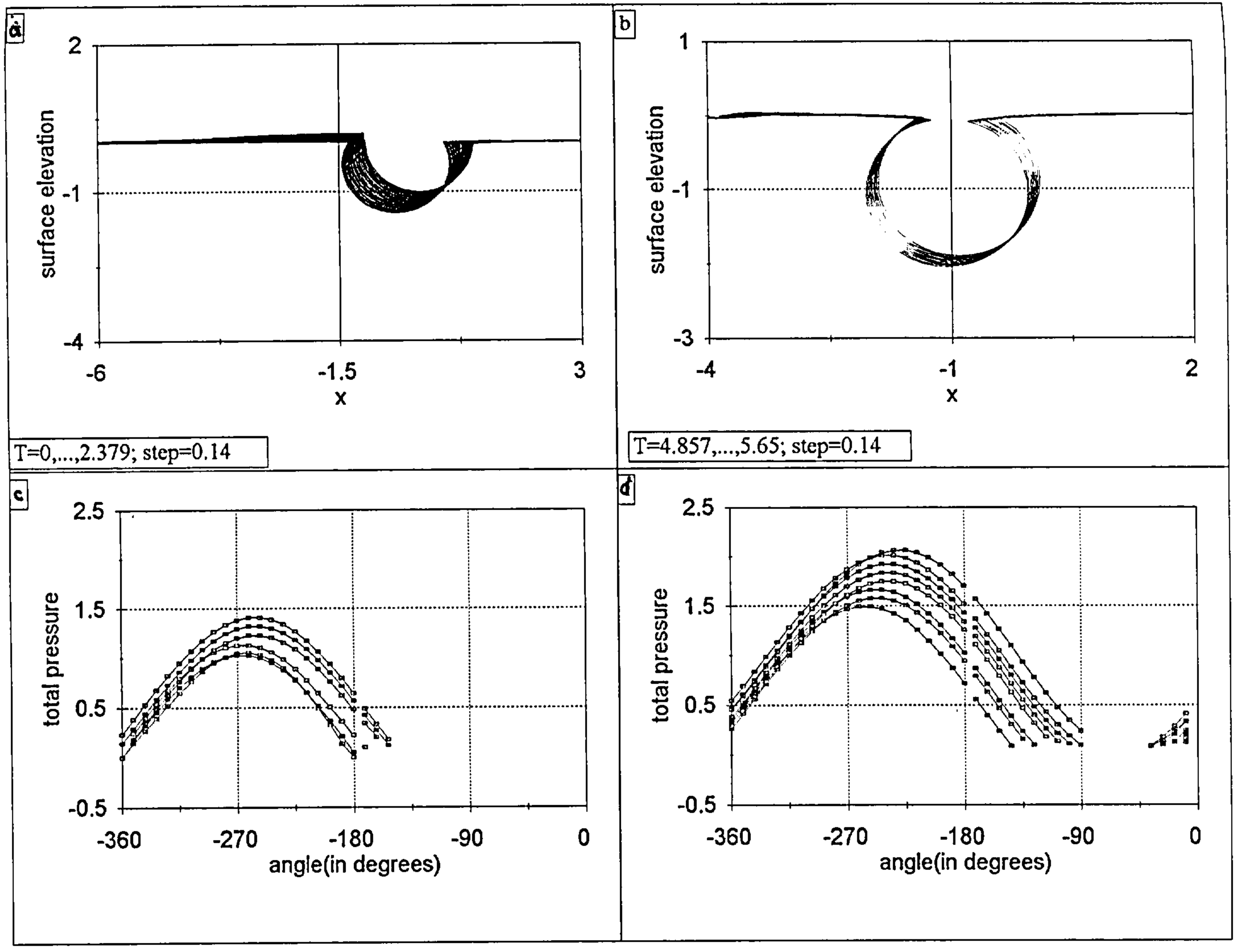

Fig. 6.9 (a)-(b) free-surface and cylinder positions, (c)-(d) pressure distribution around the cylinder and (e) hydrodynamic forces on the cylinder; due to the oblique(45- degrees) and impulsively started motion of an initially half-submerged body moving at Fr=0.19, Mb=1.

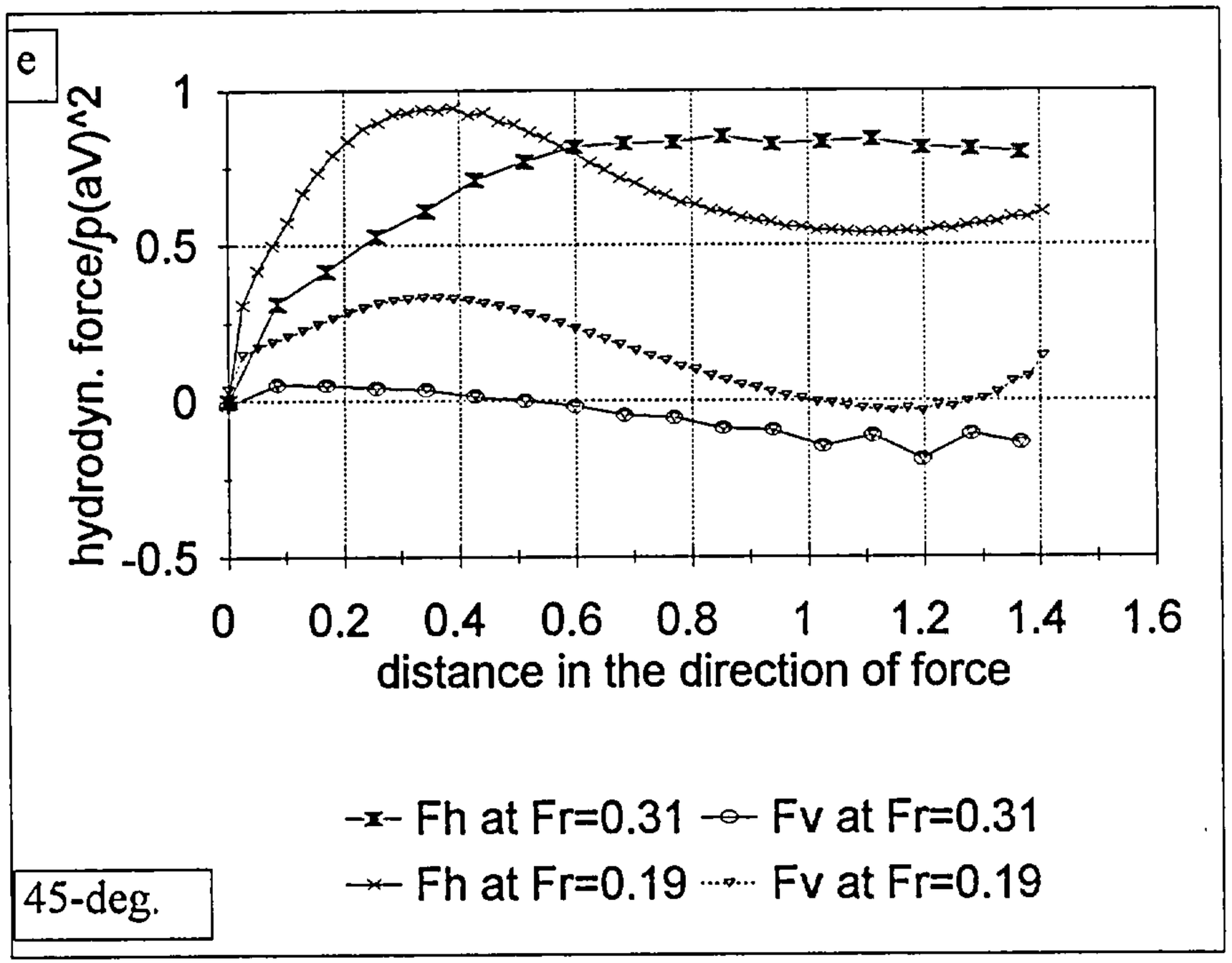
e
hydrodyn. force/ρ(aV)^2
1
0.5
0
-0.5
0
0.2
0.4
0.6
0.8
1
1.2
1.4
1.6
distance in the direction of force
Fh at Fr=0.31
Fv at Fr=0.31
Fh at Fr=0.19
Fv at Fr=0.19
45-deg.

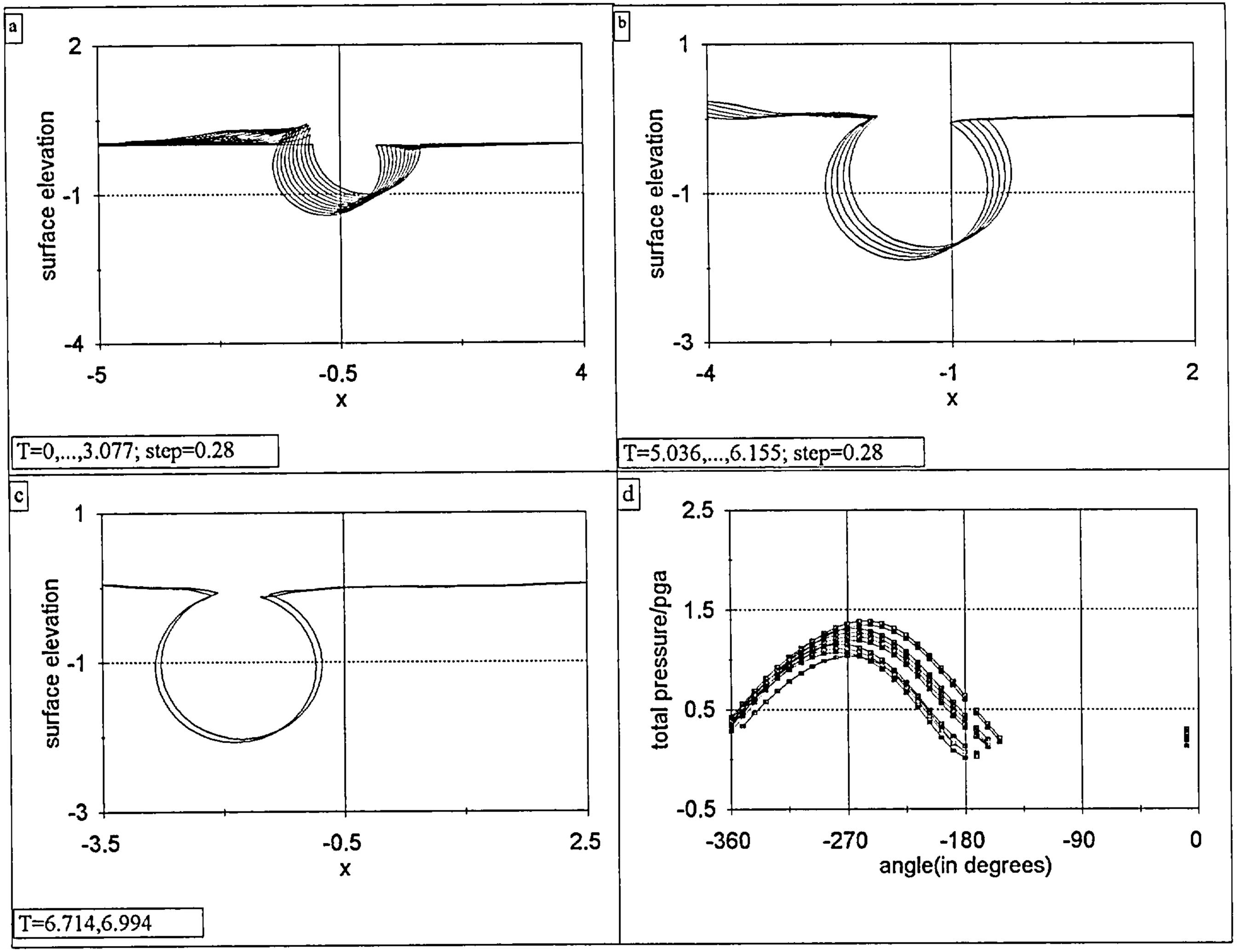

Fig. 6.10 (a)-(c) free-surface and cylinder positions, (d)-(f) pressure distribution around the body and (g) hydrodynamic forces on the body; due to an impulsively started oblique(60 degrees) motion of an initially half-submerged cylinder moving at Fr=0.31, Mb=1.0.

e

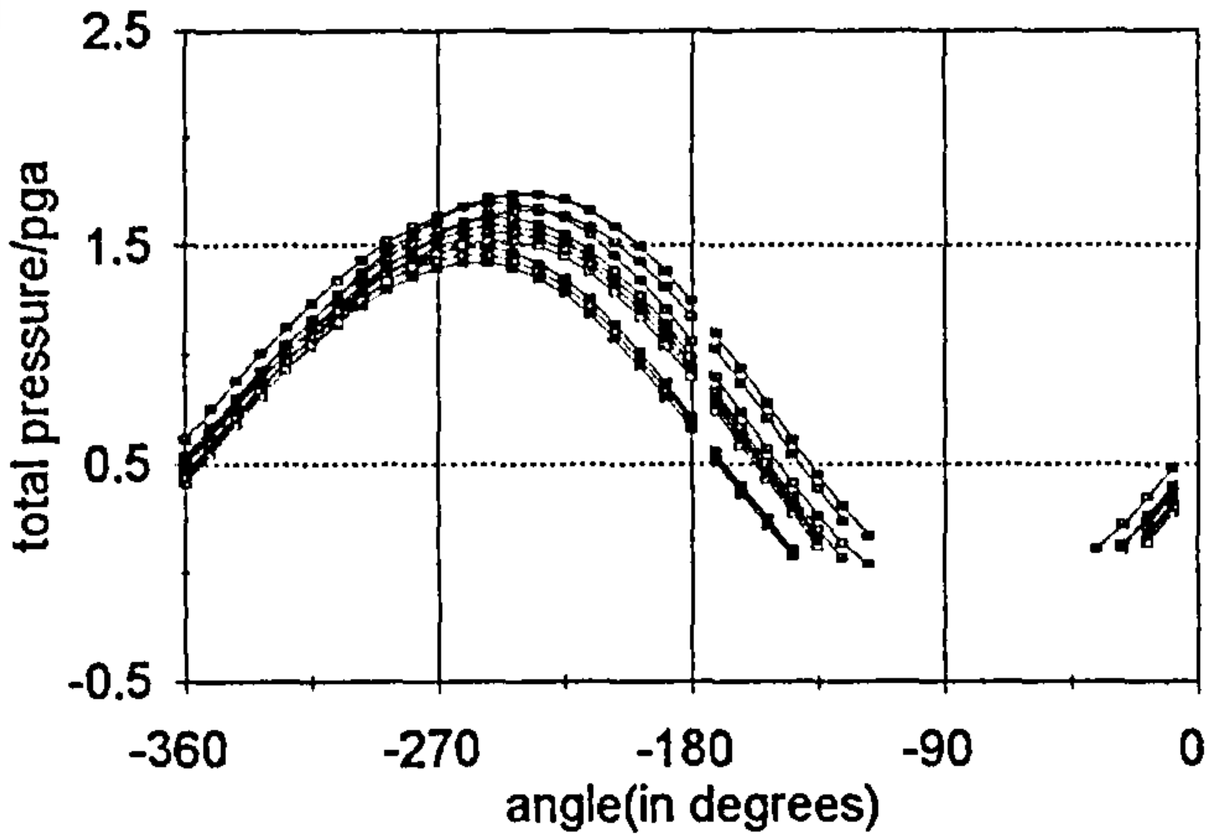
2.5
1.5
0.5
-0.5
total pressure/pga
-360
-270
-180
-90
0
angle(in degrees)

f

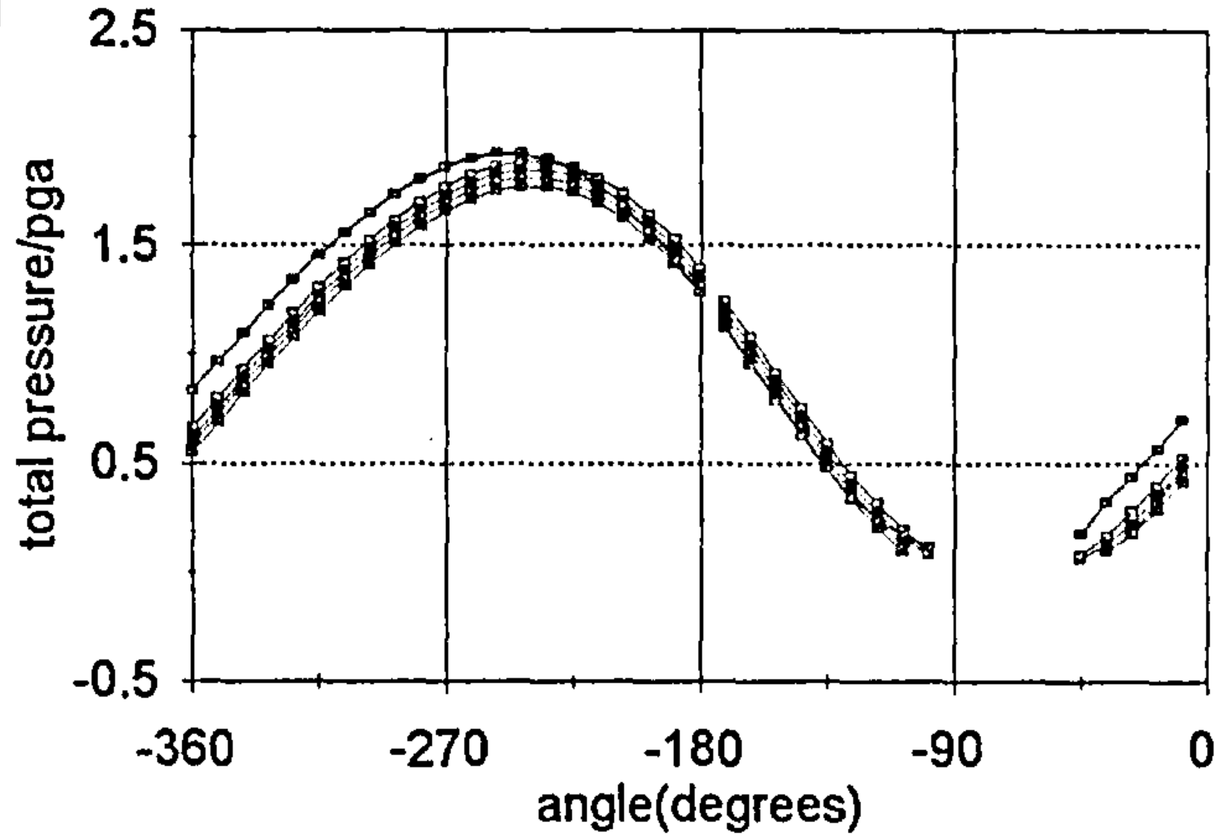
2.5
1.5
0.5
-0.5
total pressure/pga
-360
-270
-180
-90
0
angle(degrees)

g

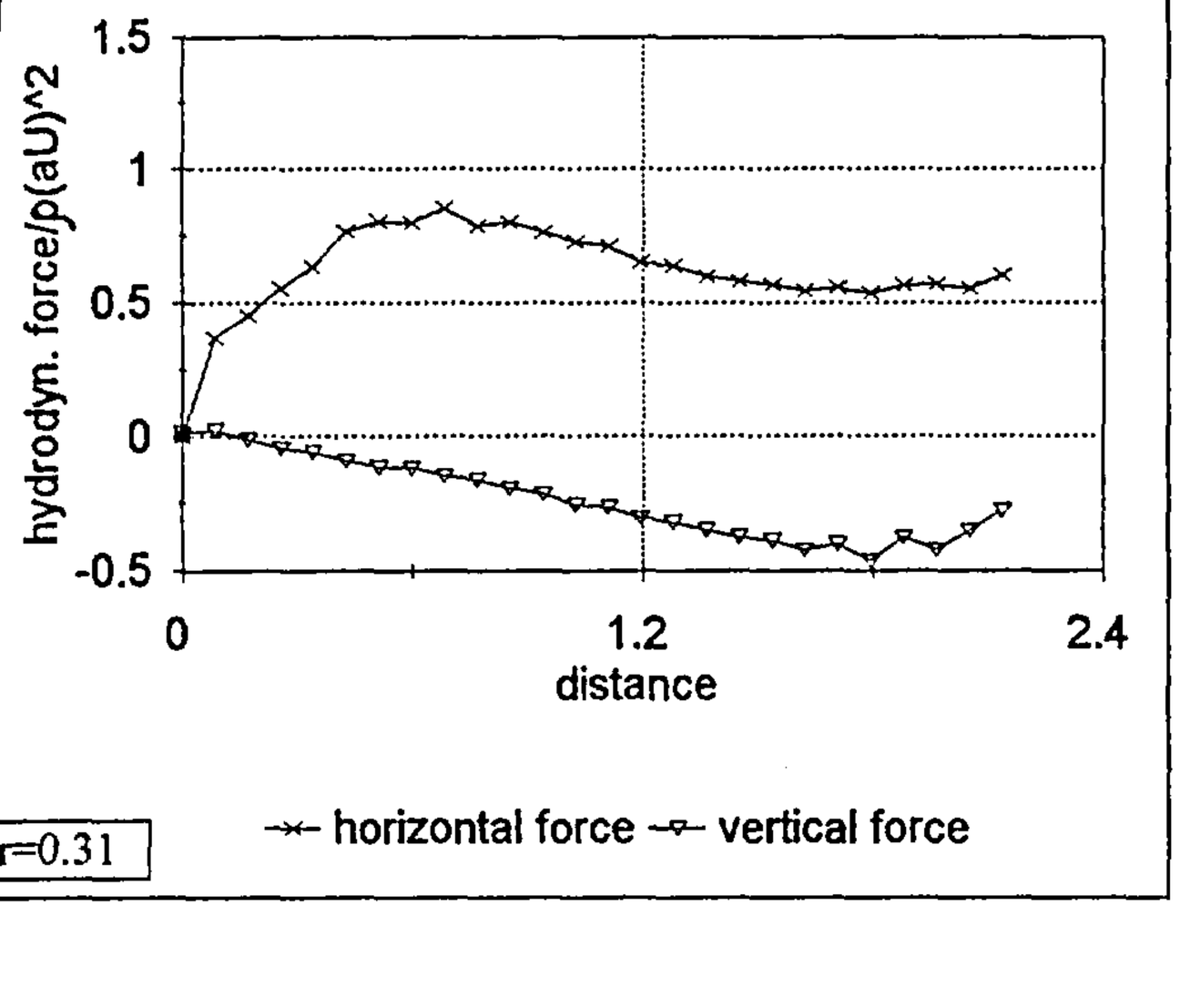
1.5
1
0.5
0
-0.5
hydrodyn. force/ρ(aU)^2
0
1.2
2.4
distance
horizontal force
vertical force

Fr=0.31

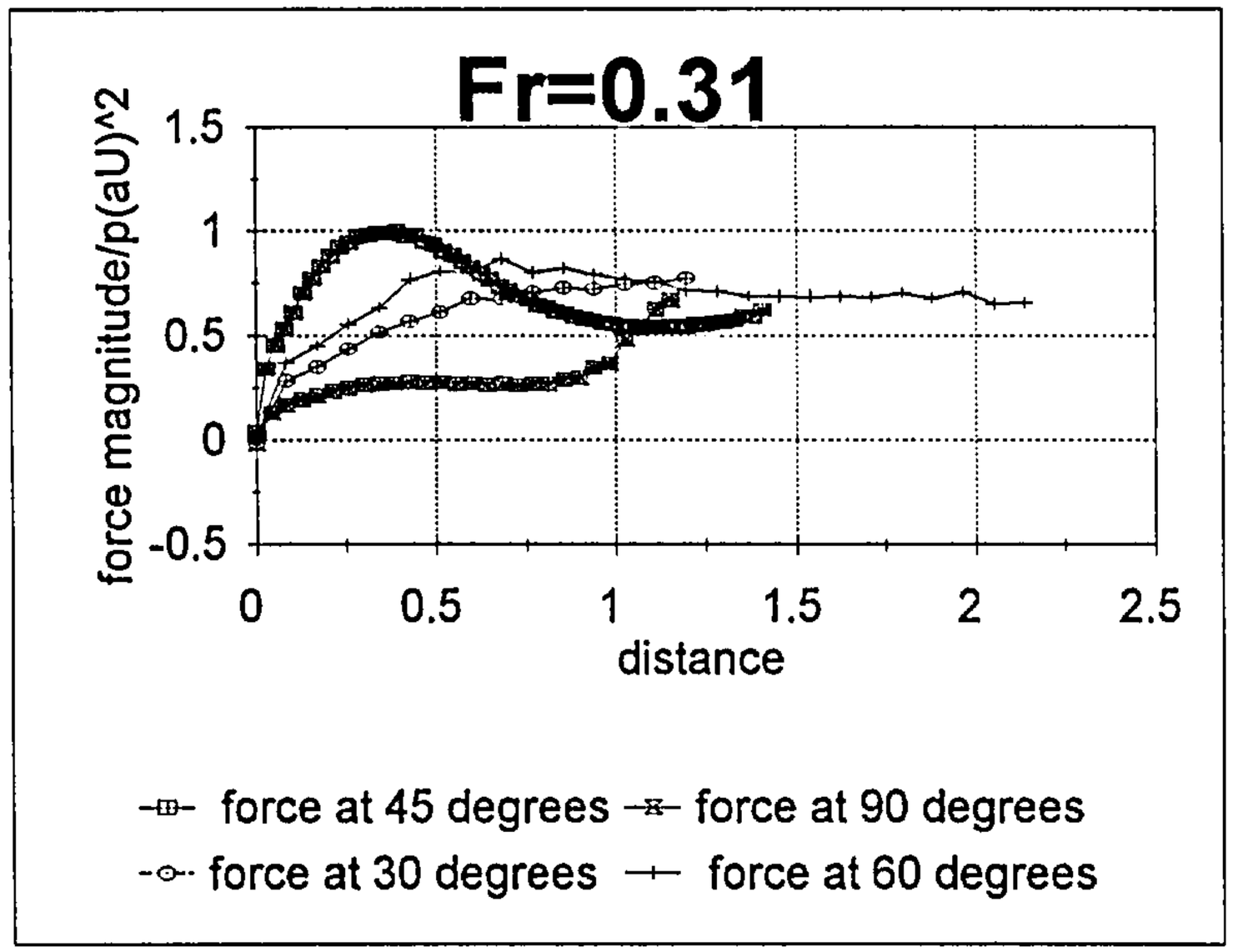

Fig. 6.11 A comparison of force magnitudes for all four angles(30, 45,60 and90)

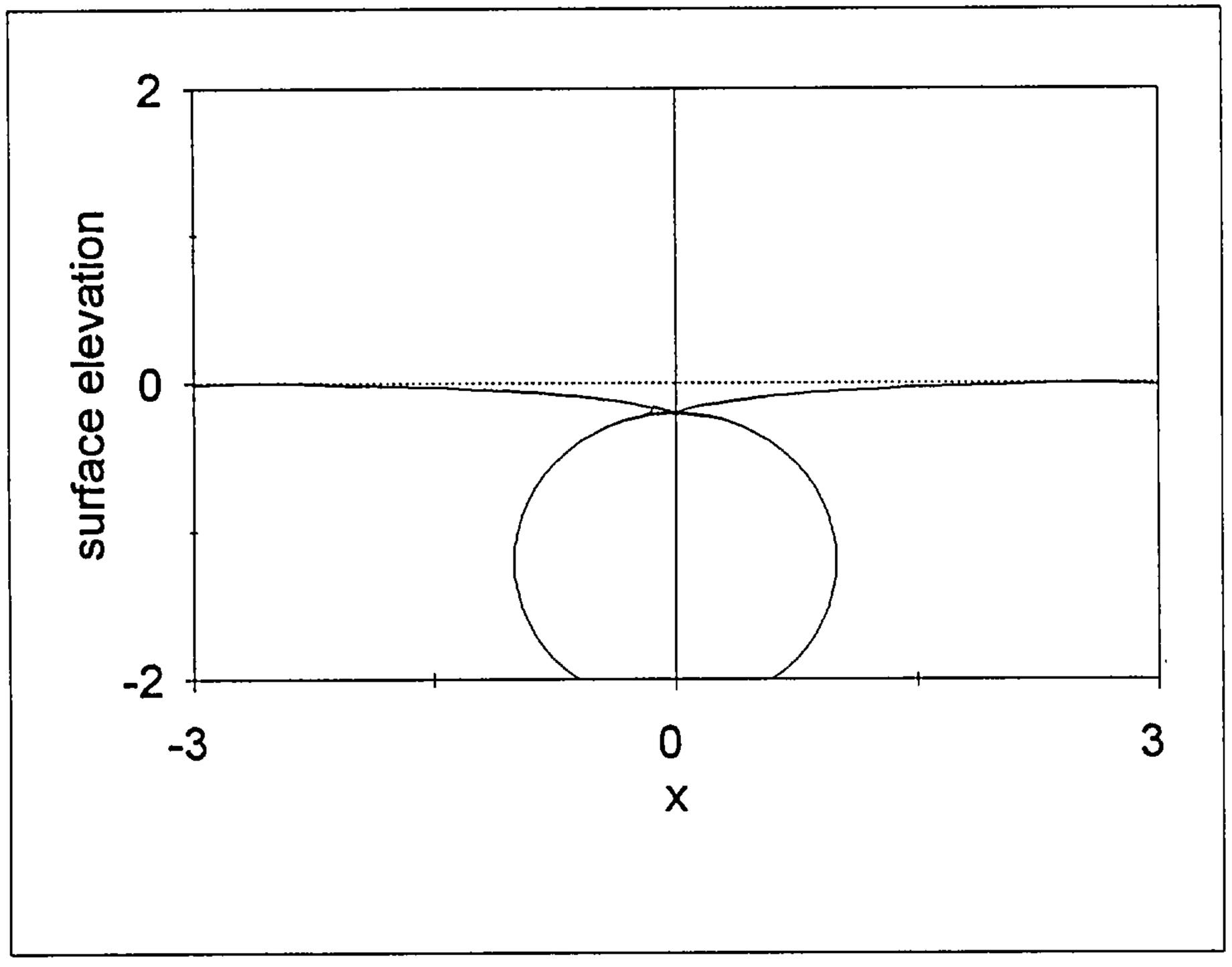

Fig. 6.12.1 A doubly connected fluid-domain.

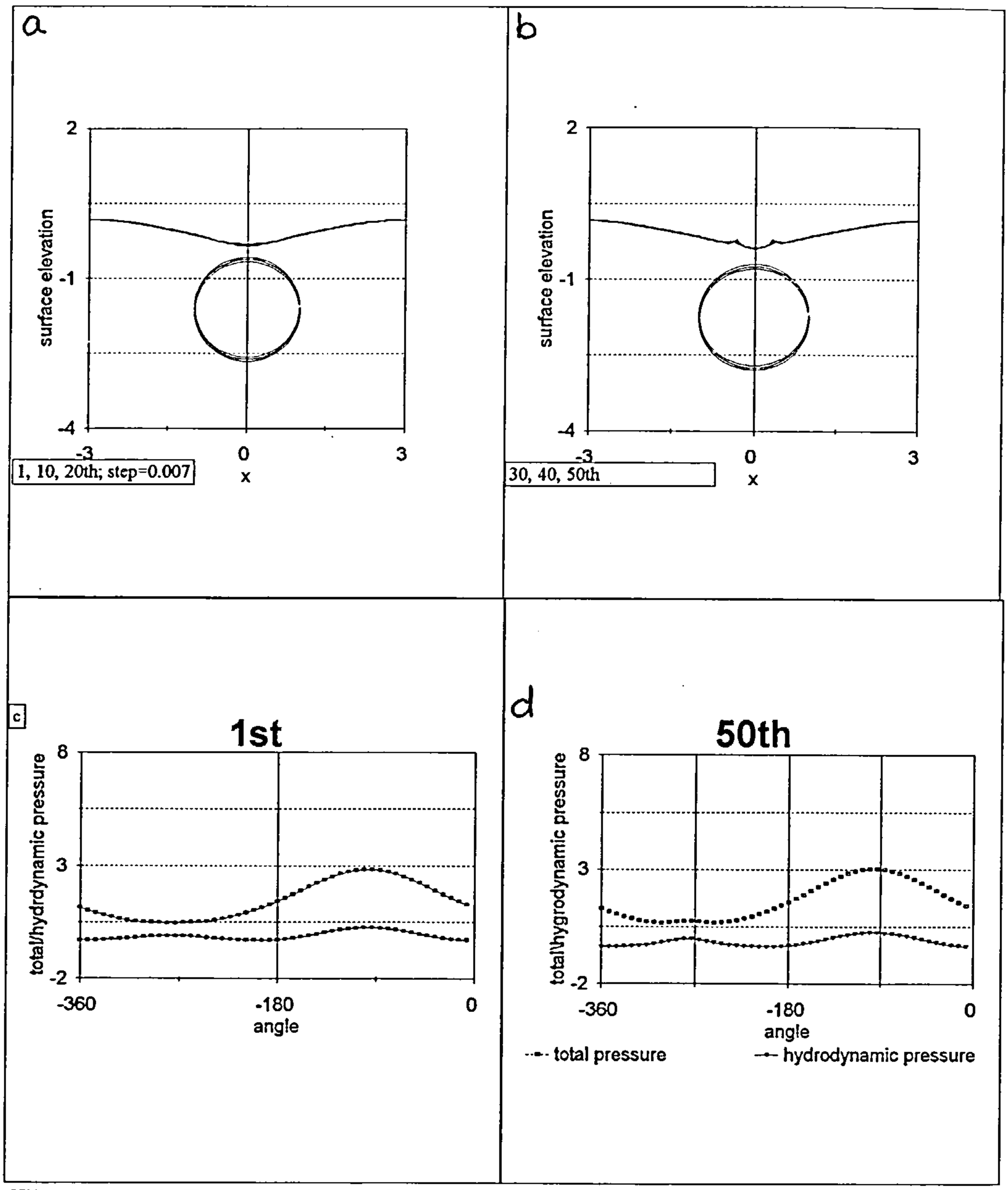

Fig. 6.12.2 Free-surface elevations, pressure distribution and body kinematics immediately after complete submergence of the cylinder. The time step size is reduced to 0.007 and there are now 129 ponits at the free-surface.

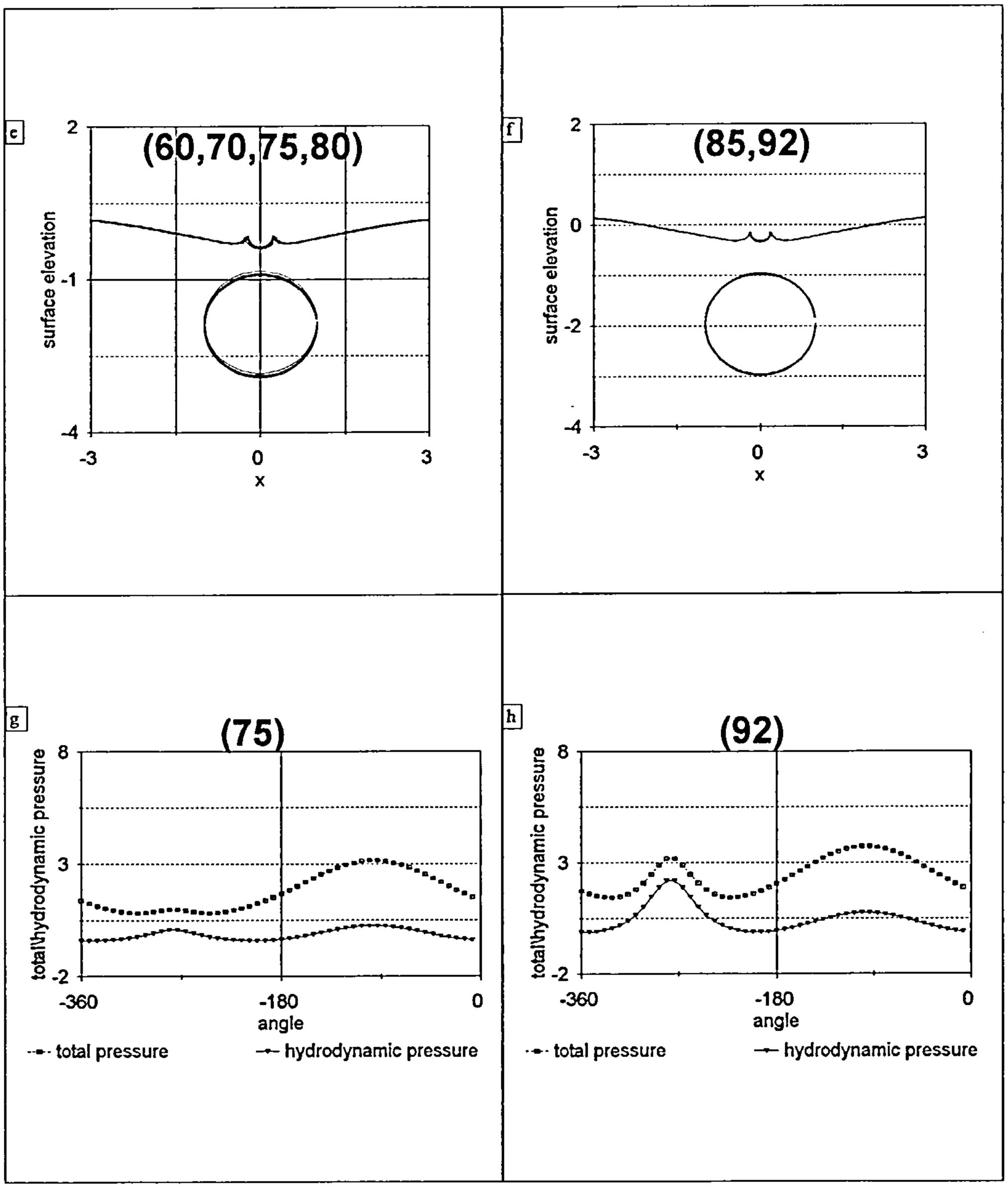
e
(60,70,75,80)
surface elevation
2
-1
-4
-3
0
3
x
f
(85,92)
surface elevation
2
0
-2
-4
-3
0
3
x
g
(75)
total\hydrodynamic pressure
8
3
-2
-360
-180
0
angle
total pressure
hydrodynamic pressure
h
(92)
total\hydrodynamic pressure
8
3
-2
-360
-180
0
angle
total pressure
hydrodynamic pressure

i

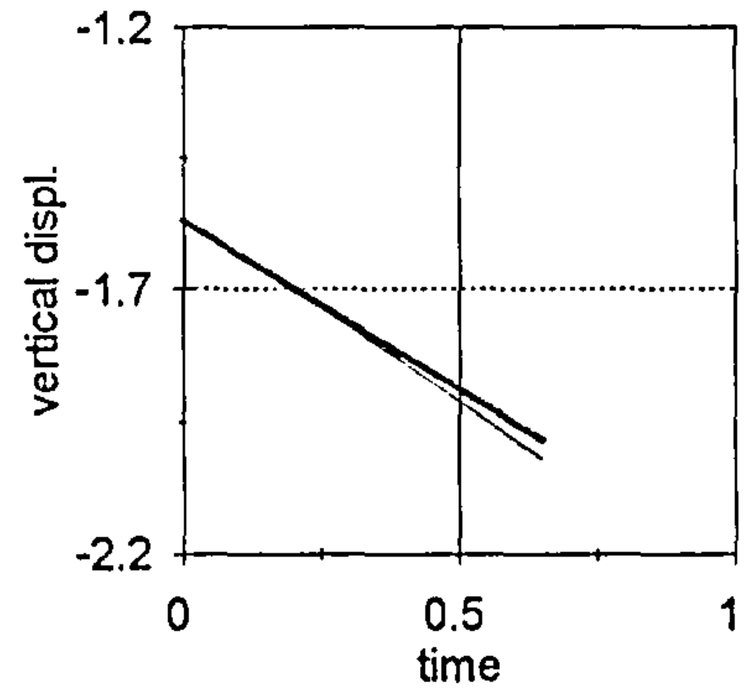

— numerical scheme — hydrostatic model

j

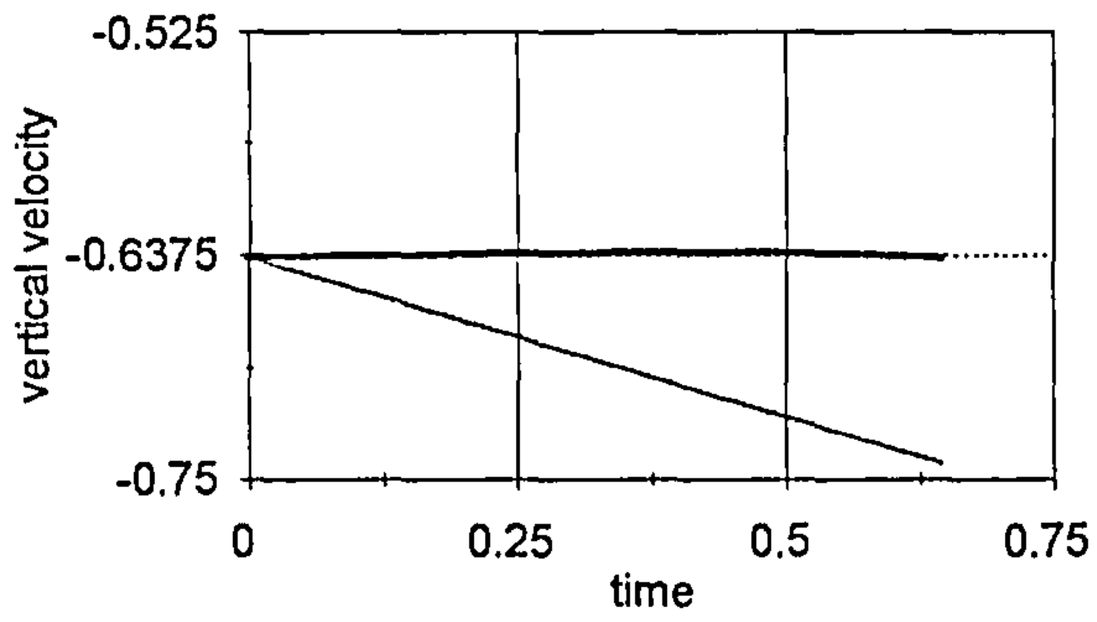

— numerical scheme — hydrostatic model

k

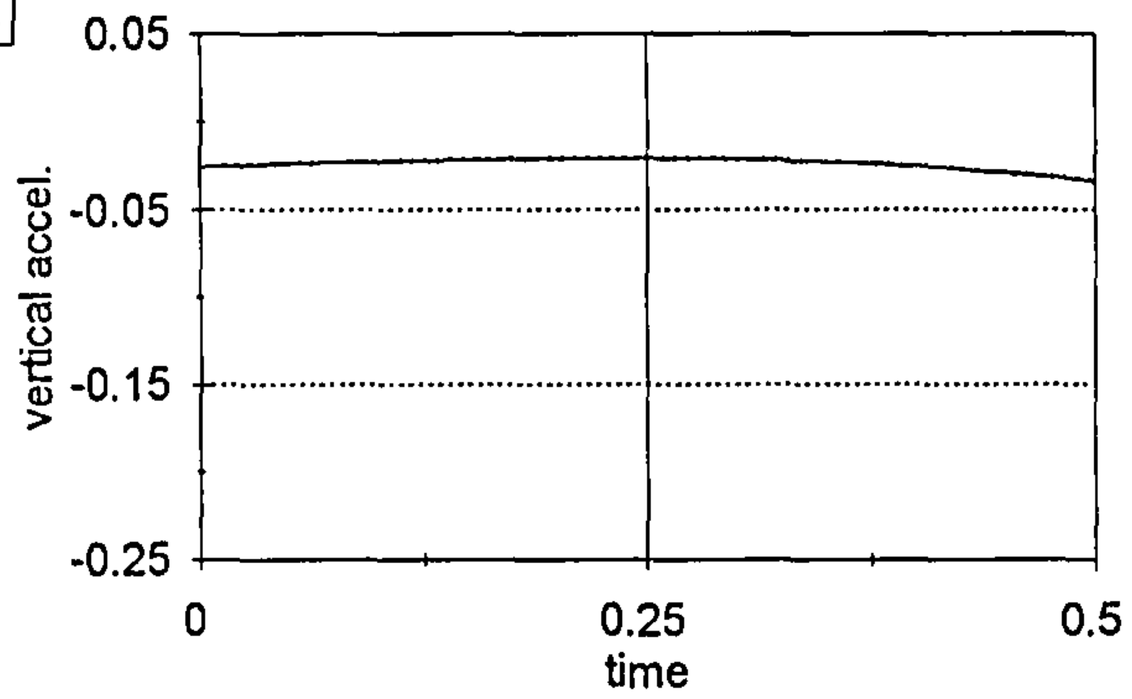

— numerical scheme

l

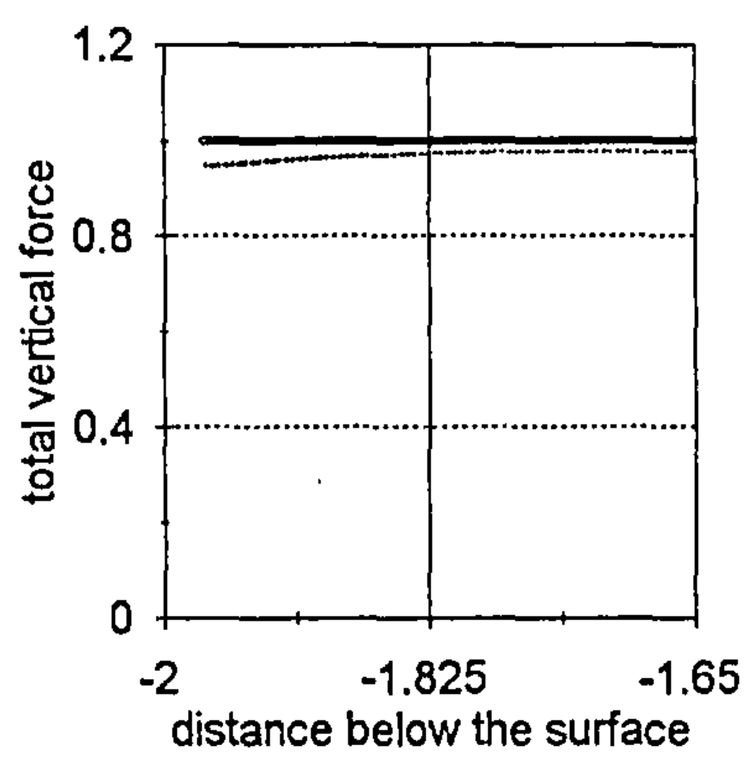

····· numerical scheme -•- hydrostatic model

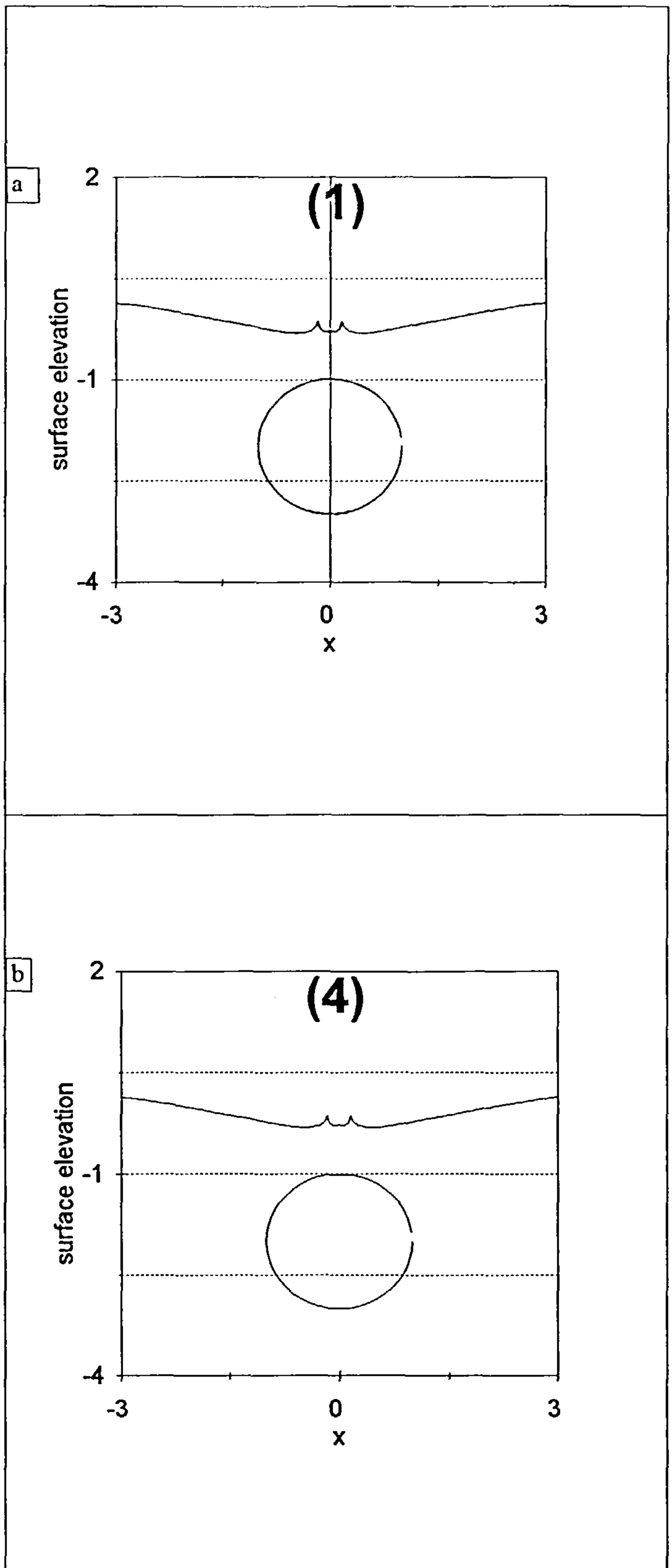

Fig. 6.12.3 Fully developed "sharp" breakers and a jet at the centre.
Time step size=0.007 and free-surface points=129.

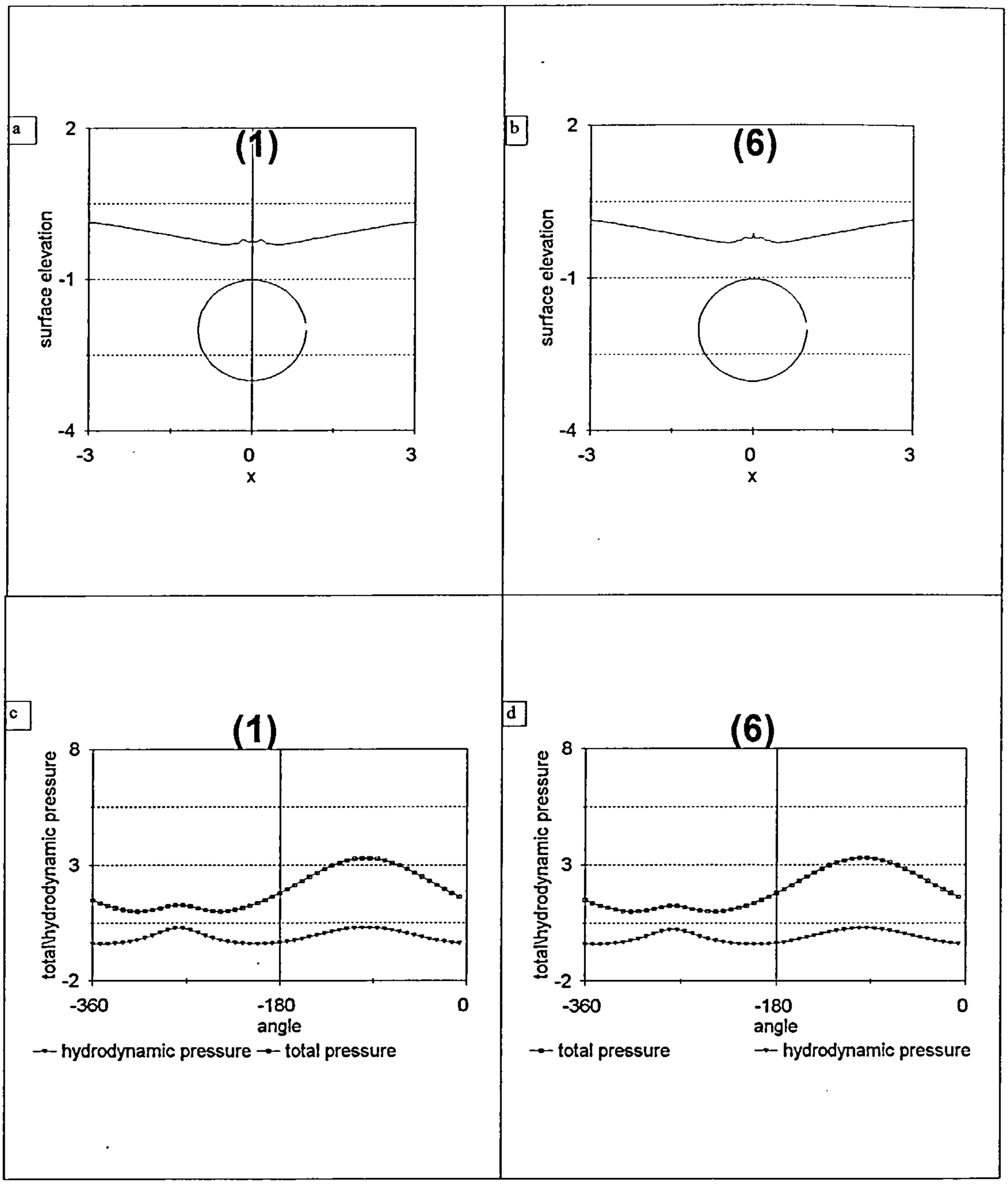

Fig. 6.12.4 Free-surface elevation, pressure distribution and body kinematics. Step size=0.007 and free-surface points =123.

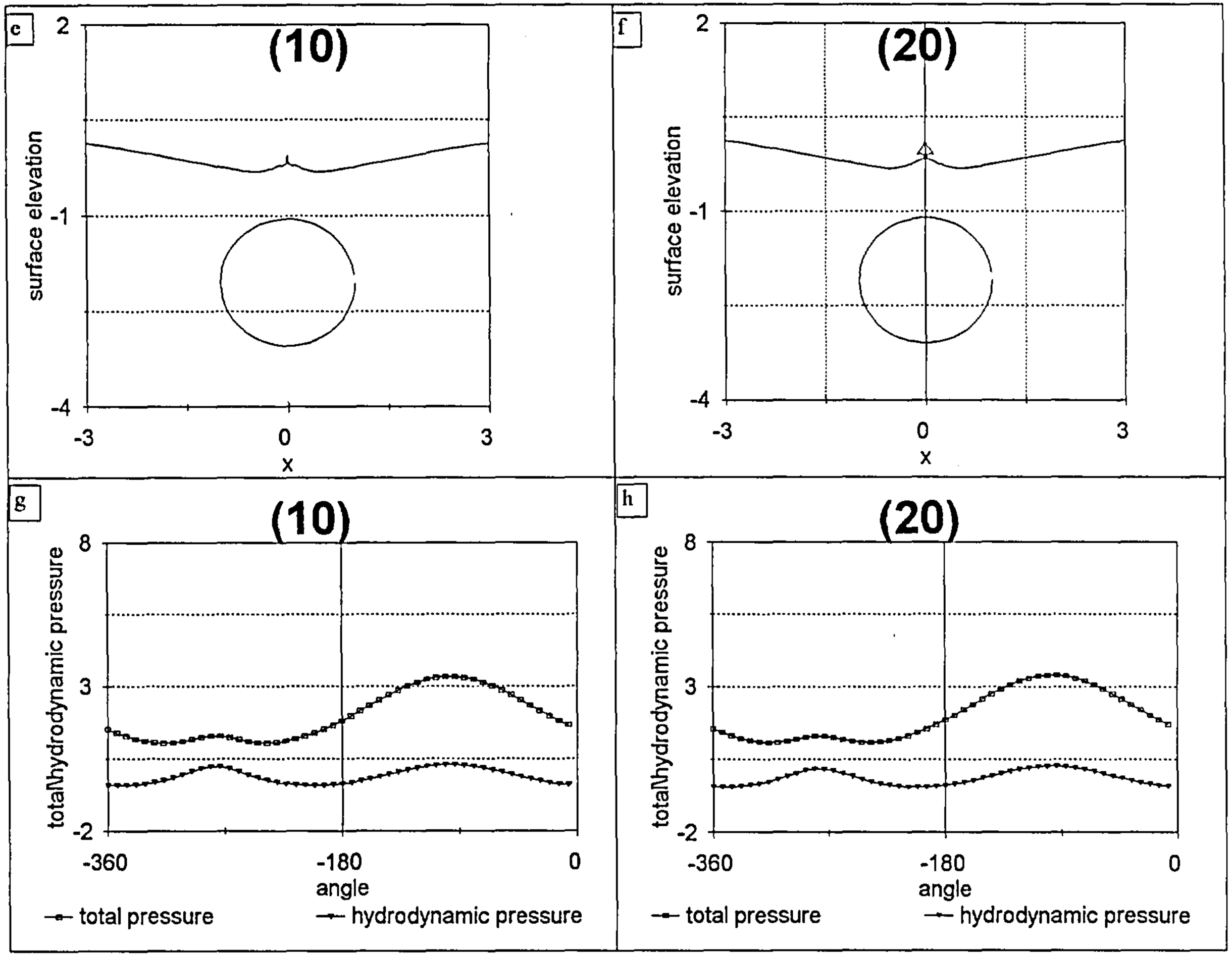
e
(10)
surface elevation
2
-1
-4
-3
0
3
x
f
(20)
surface elevation
2
-1
-4
-3
0
3
x
g
(10)
totalhydrodynamic pressure
8
3
-2
-360
-180
0
angle
total pressure
hydrodynamic pressure
h
(20)
totalhydrodynamic pressure
8
3
-2
-360
-180
0
angle
total pressure
hydrodynamic pressure

i

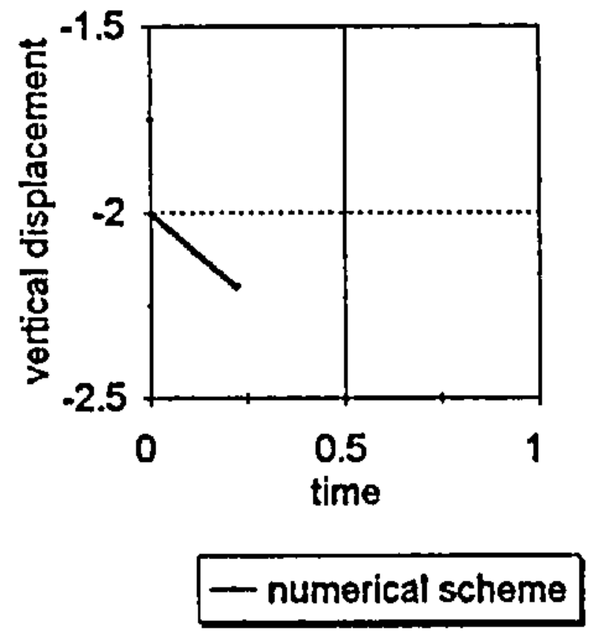
vertical displacement
-1.5
-2
-2.5
0
0.5
1
time
numerical scheme

j

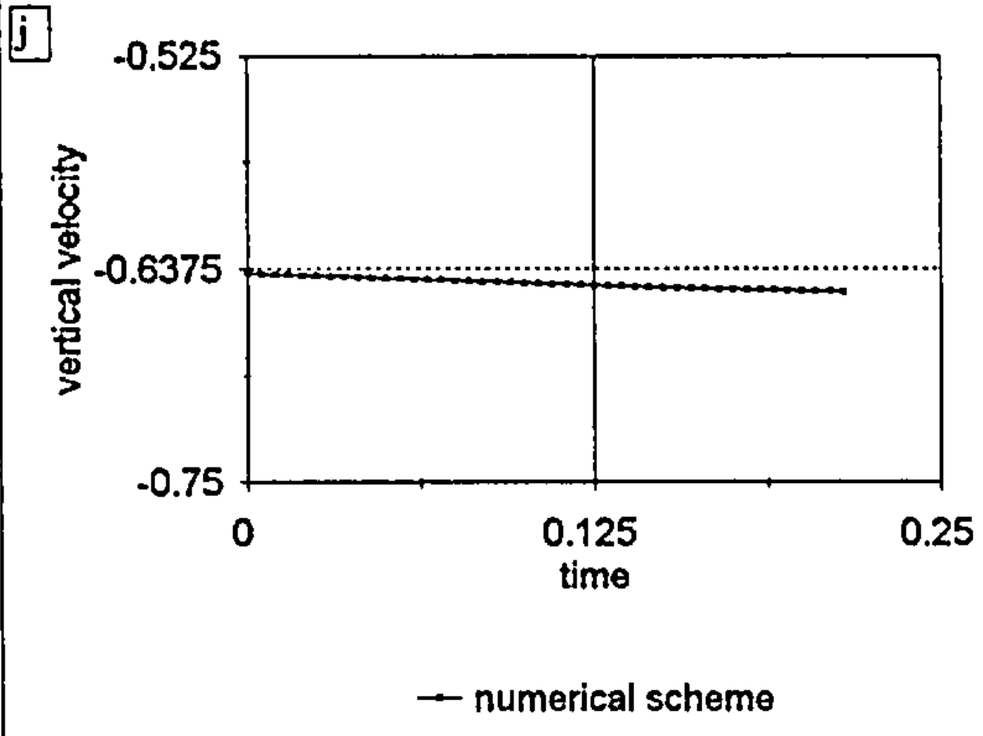
vertical velocity
-0.525
-0.6375
-0.75
0
0.125
0.25
time
numerical scheme

k

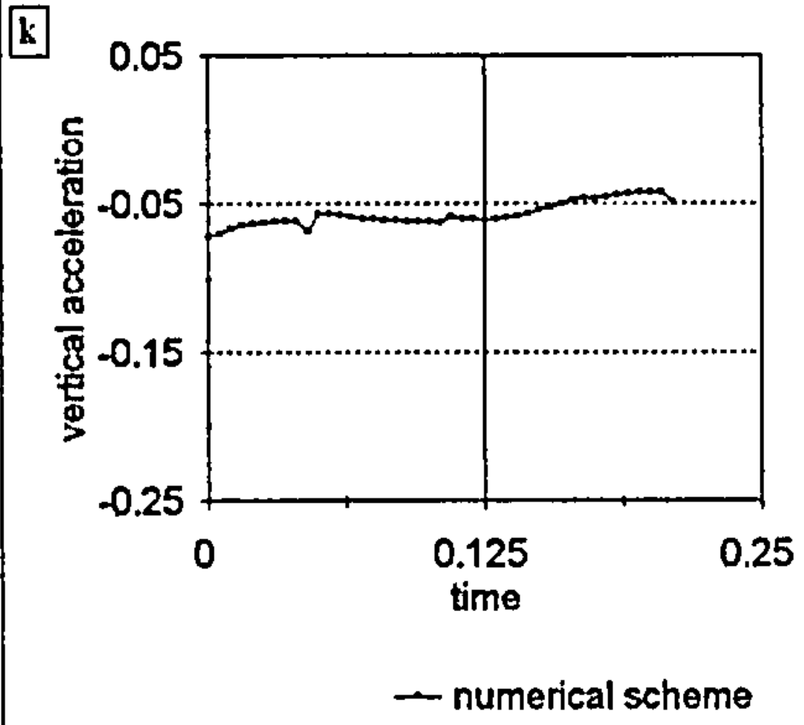
vertical acceleration
0.05
-0.05
-0.15
-0.25
0
0.125
0.25
time
numerical scheme

l

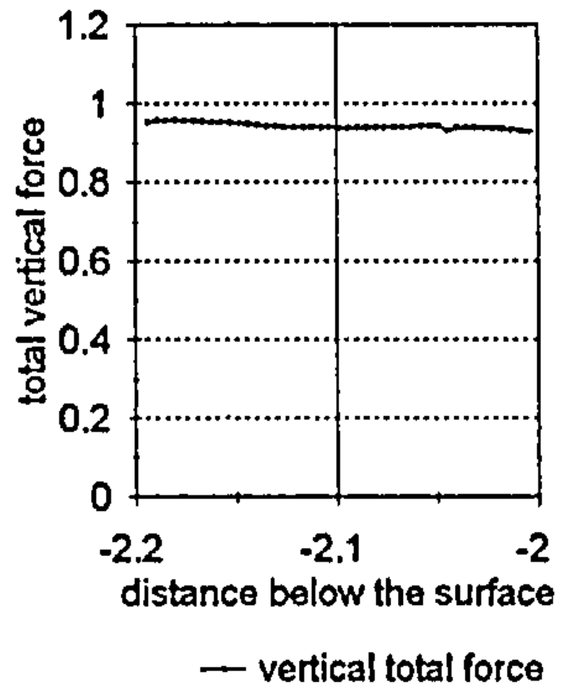
total vertical force
1.2
1
0.8
0.6
0.4
0.2
0
-2.2
-2.1
-2
distance below the surface
vertical total force

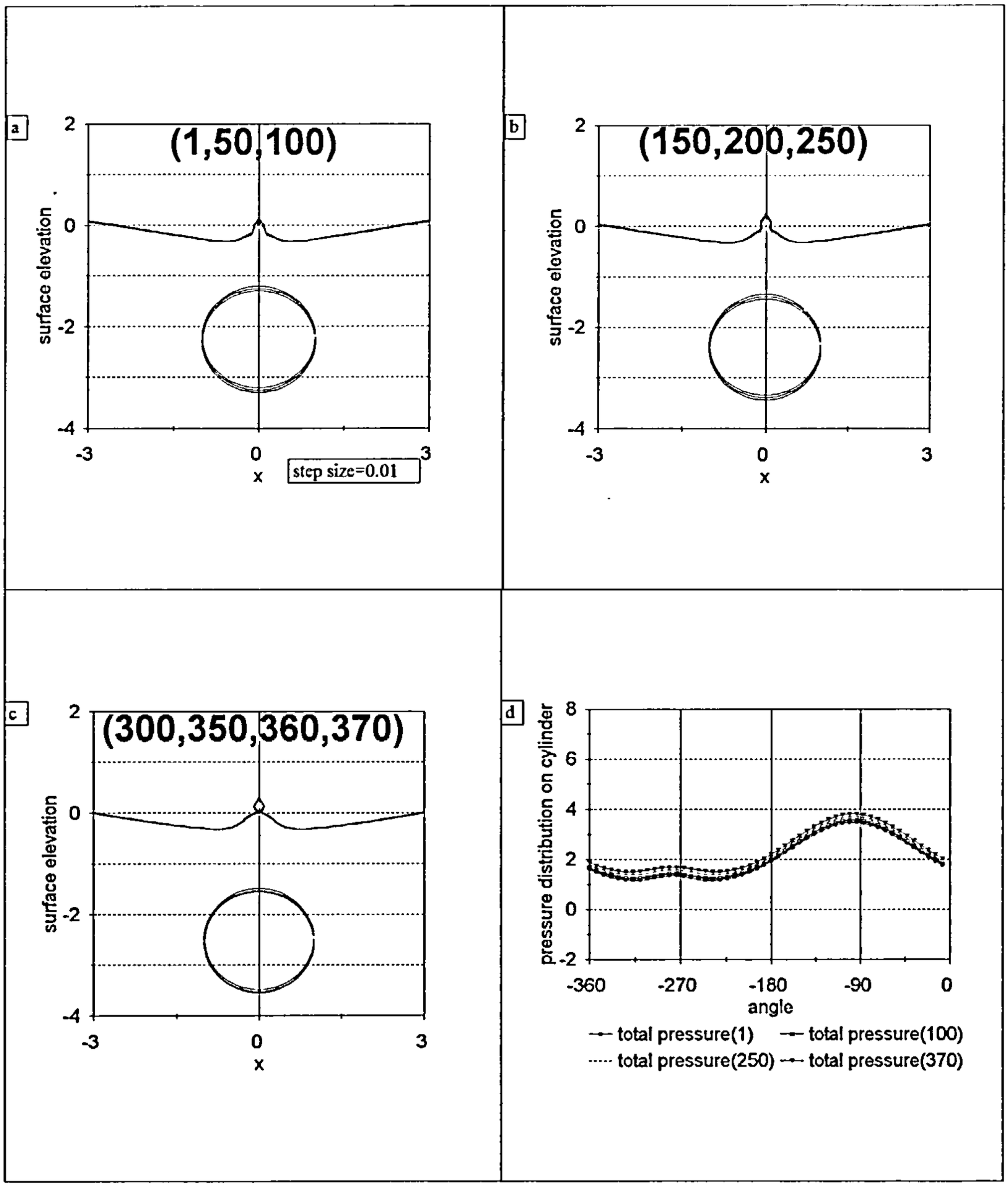

Fig. 6.12.5 A fast developing jet. Pressure distribution corresponding to elevations of indicated time steps is also shown.

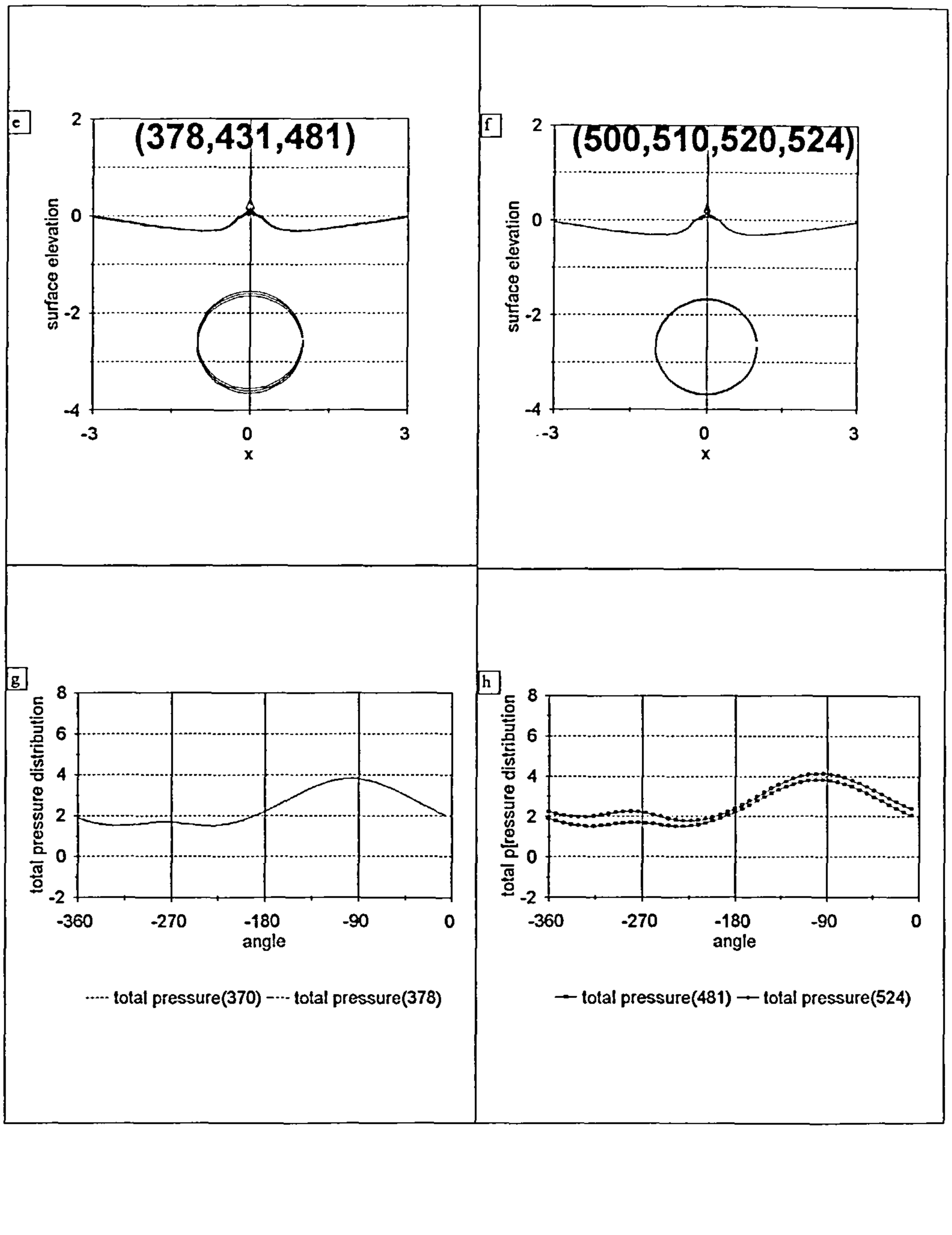
e
(378,431,481)
surface elevation
2
0
-2
-4
-3
0
3
x
f
(500,510,520,524)
surface elevation
2
0
-2
-4
-3
0
3
x
g
total pressure distribution
8
6
4
2
0
-2
-360
-270
-180
-90
0
angle
total pressure(370)
total pressure(378)
h
total p[ressure distribution
8
6
4
2
0
-2
-360
-270
-180
-90
0
angle
total pressure(481)
total pressure(524)

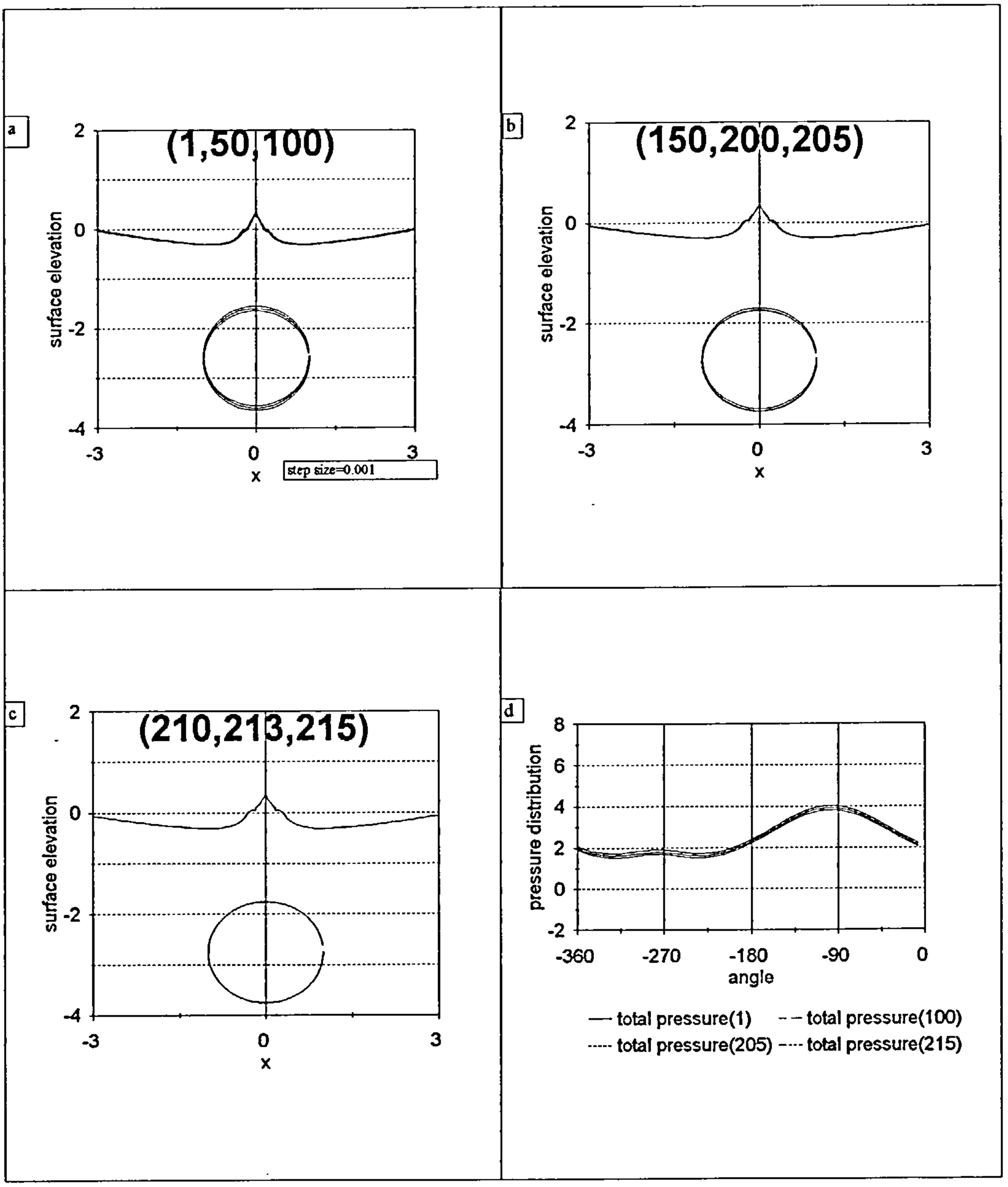

Fig. 6.12.6 Ther jet reaches the peak and the fluid begins to recede. There are now 108 points at the fre-surface and time step size is 0.0014.

c

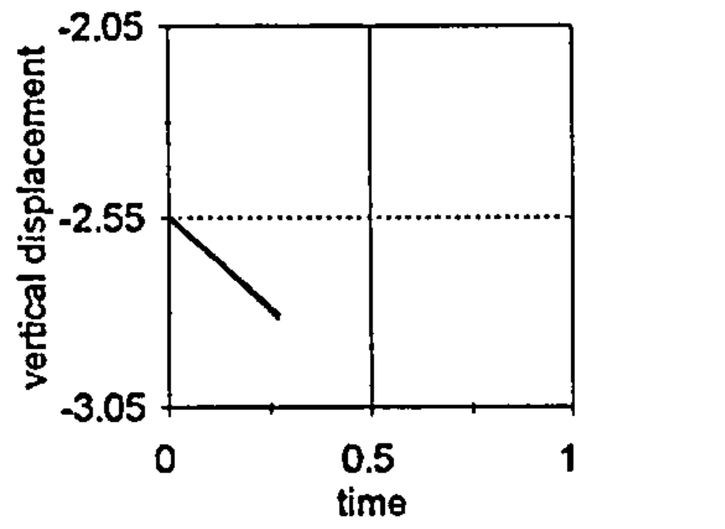

— numerical scheme — hydrostatic model

f

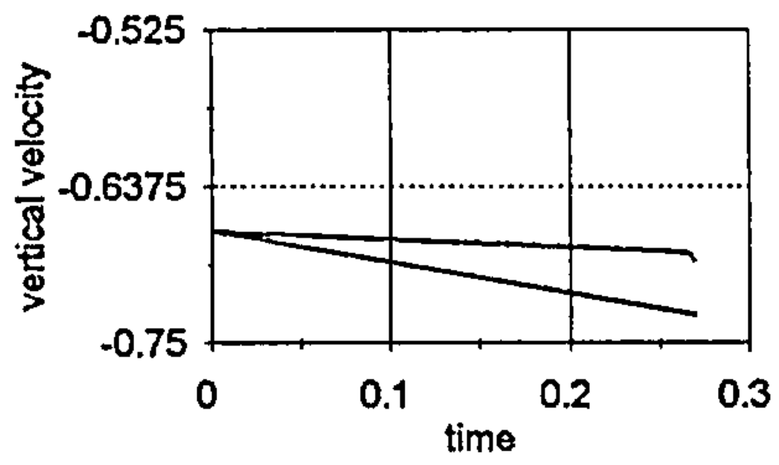

— numerical scheme --- hydrostatic model

g

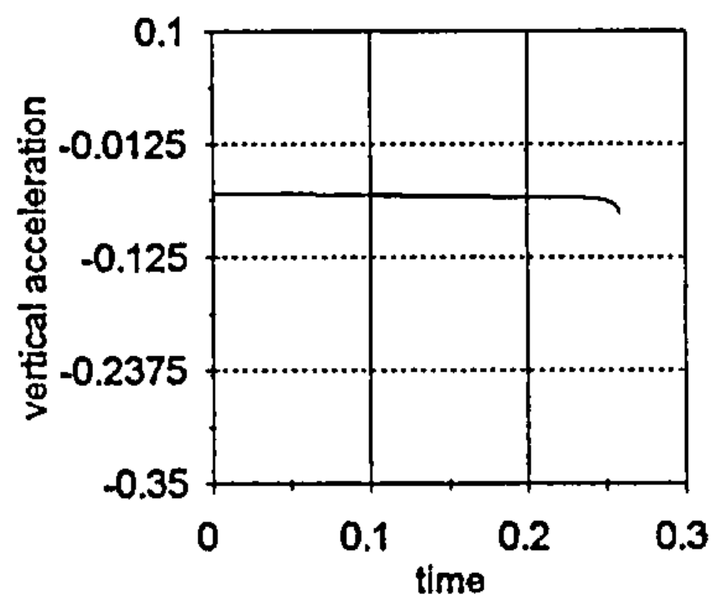

— numerical scheme

h

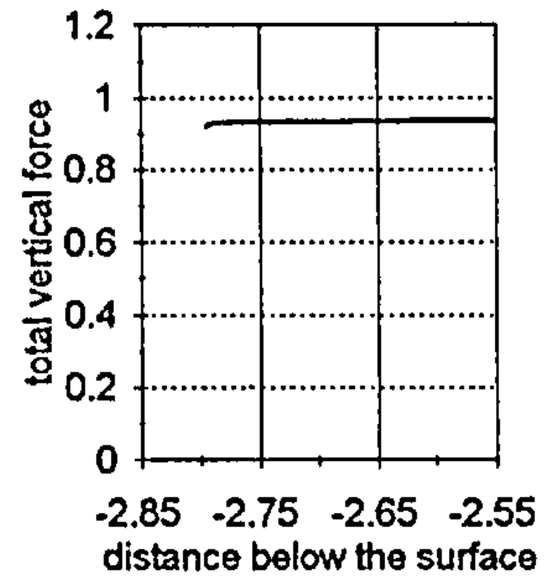

— numerical scheme

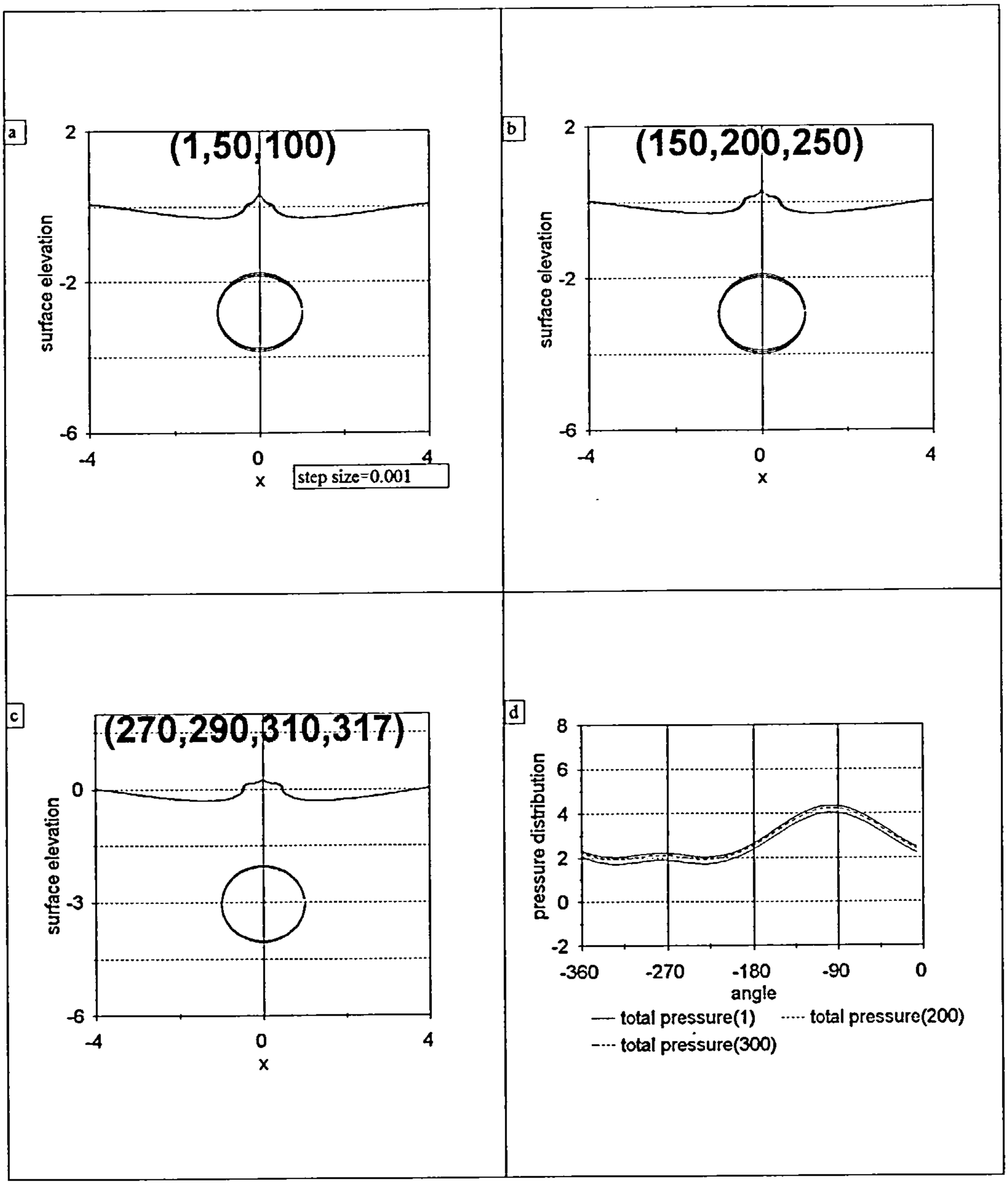

Fig. 6.12.7 The region of the jet is now flattening and waves propagate outwards.

c

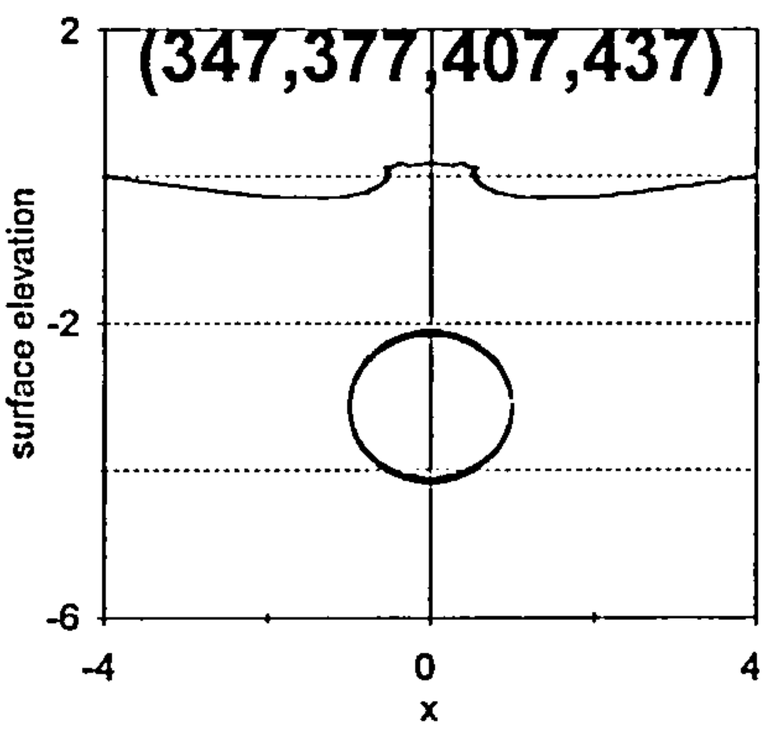
2
(347,377,407,437)
surface elevation
-2
-6
-4
0
4
x

f

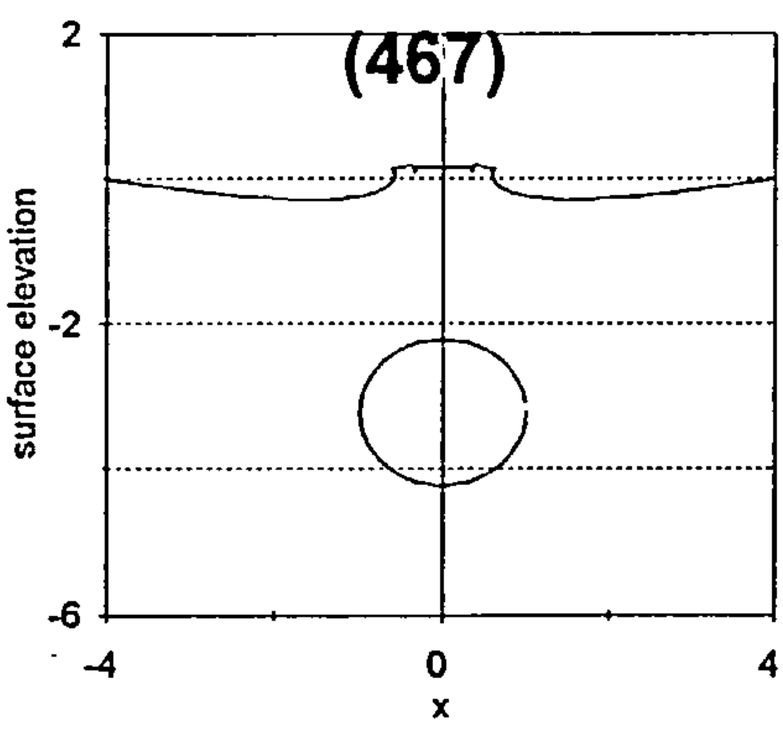
2
(467)
surface elevation
-2
-6
-4
0
4
x

g

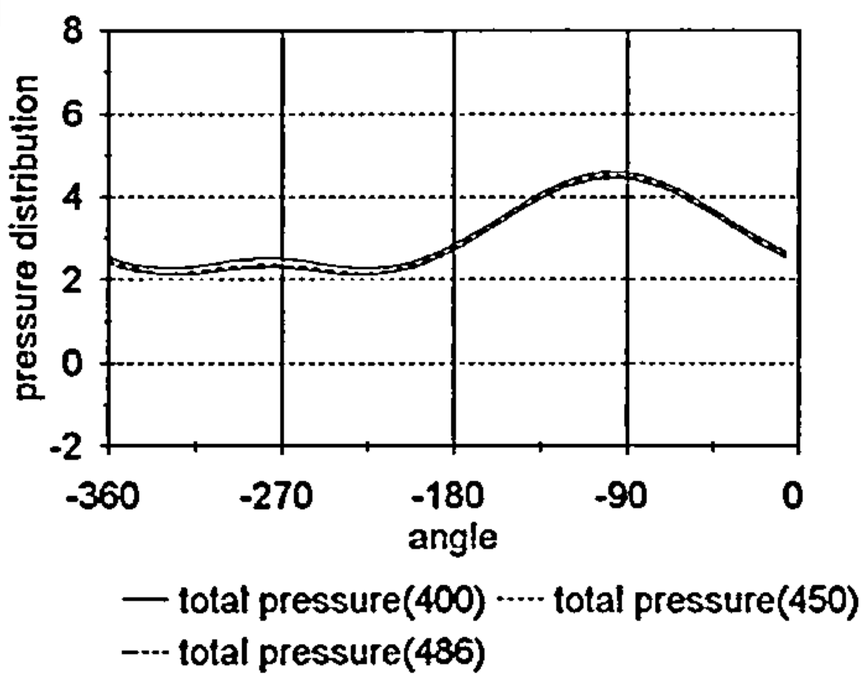
8
6
4
2
0
-2
pressure distribution
-360
-270
-180
-90
0
angle
total pressure(400)
total pressure(450)
total pressure(486)

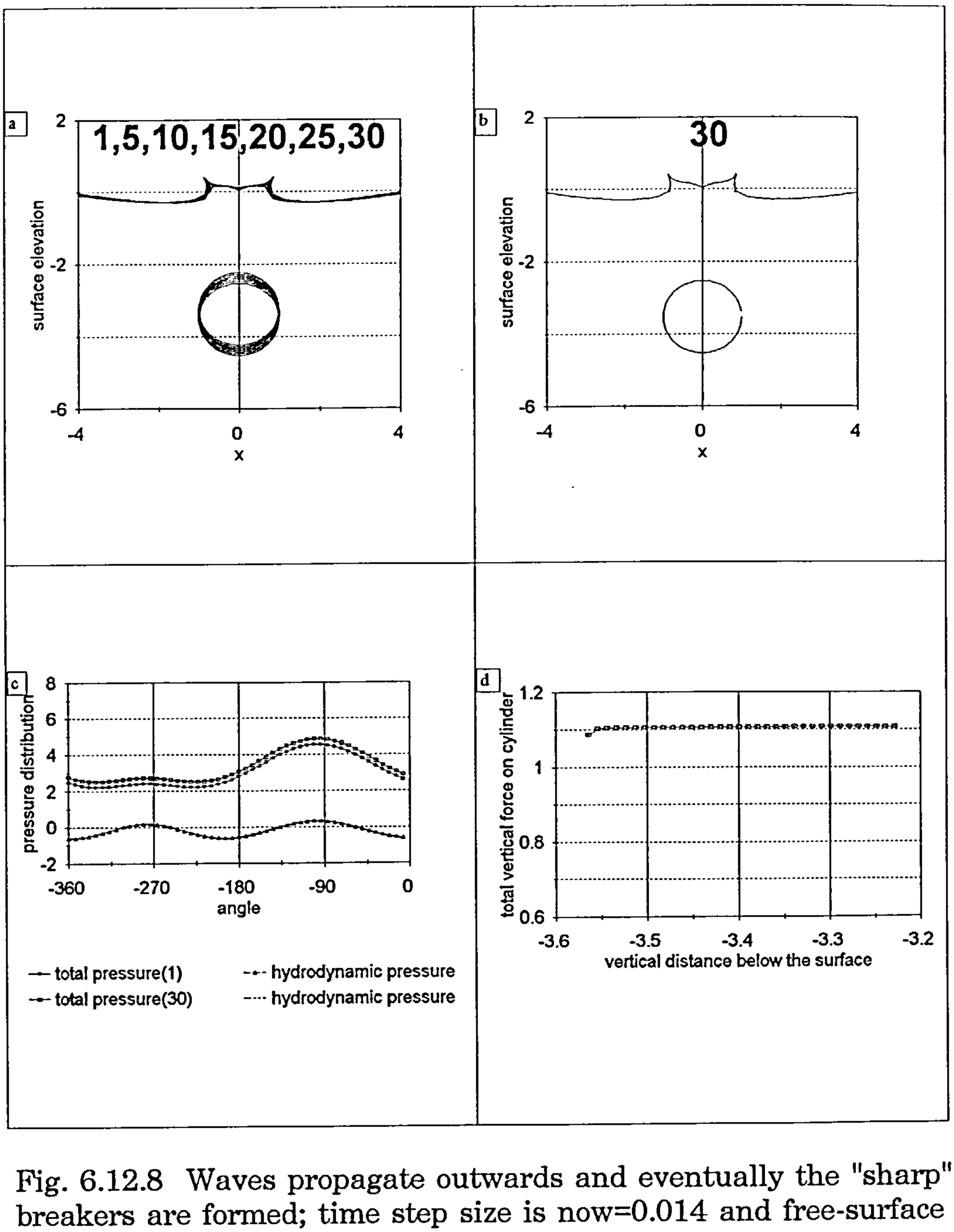

Fig. 6.12.8 Waves propagate outwards and eventually the "sharp" breakers are formed; time step size is now=0.014 and free-surface points=108.

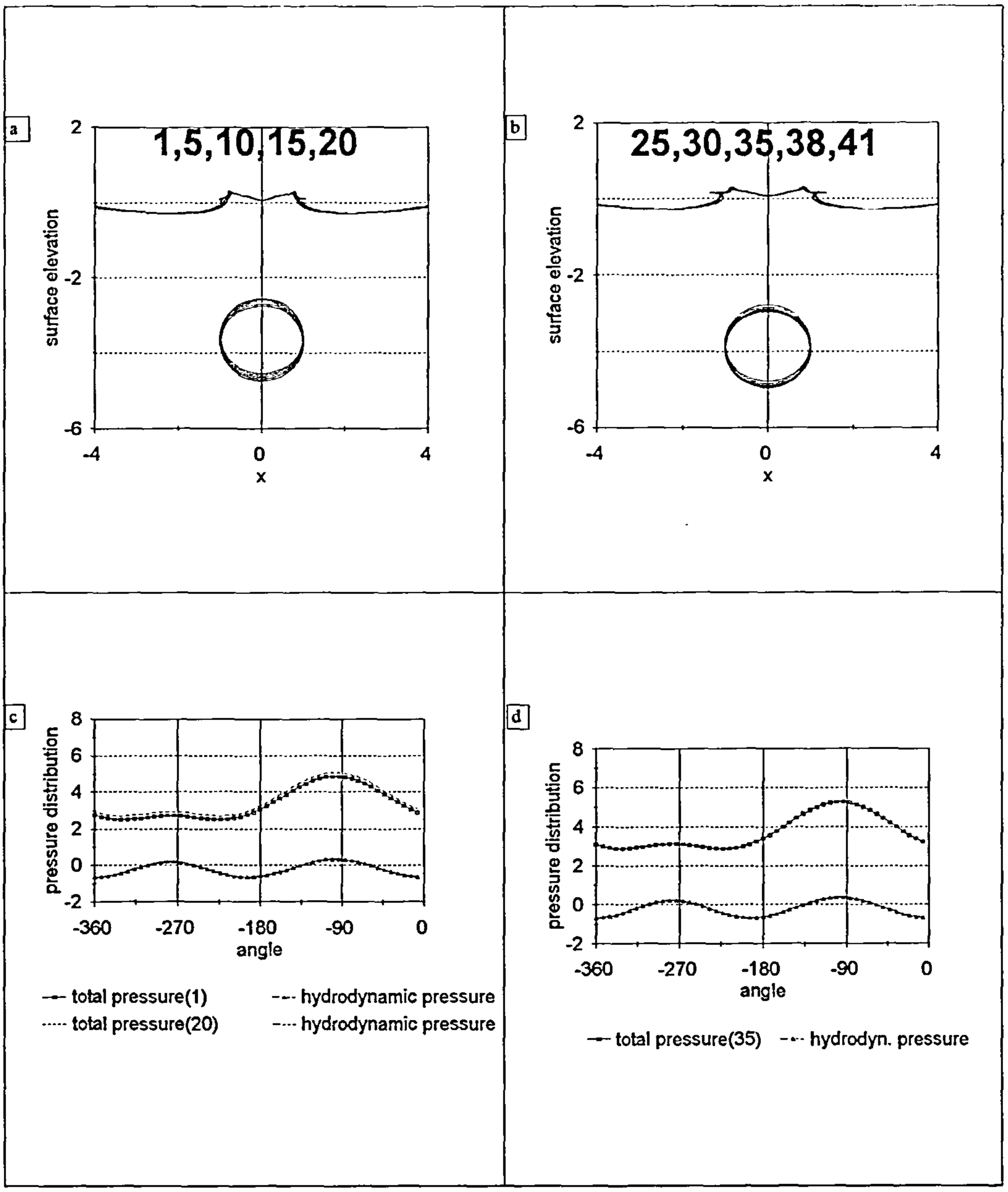

Fig. 6.12.9 Step size=0.014 and free-surface points=99.

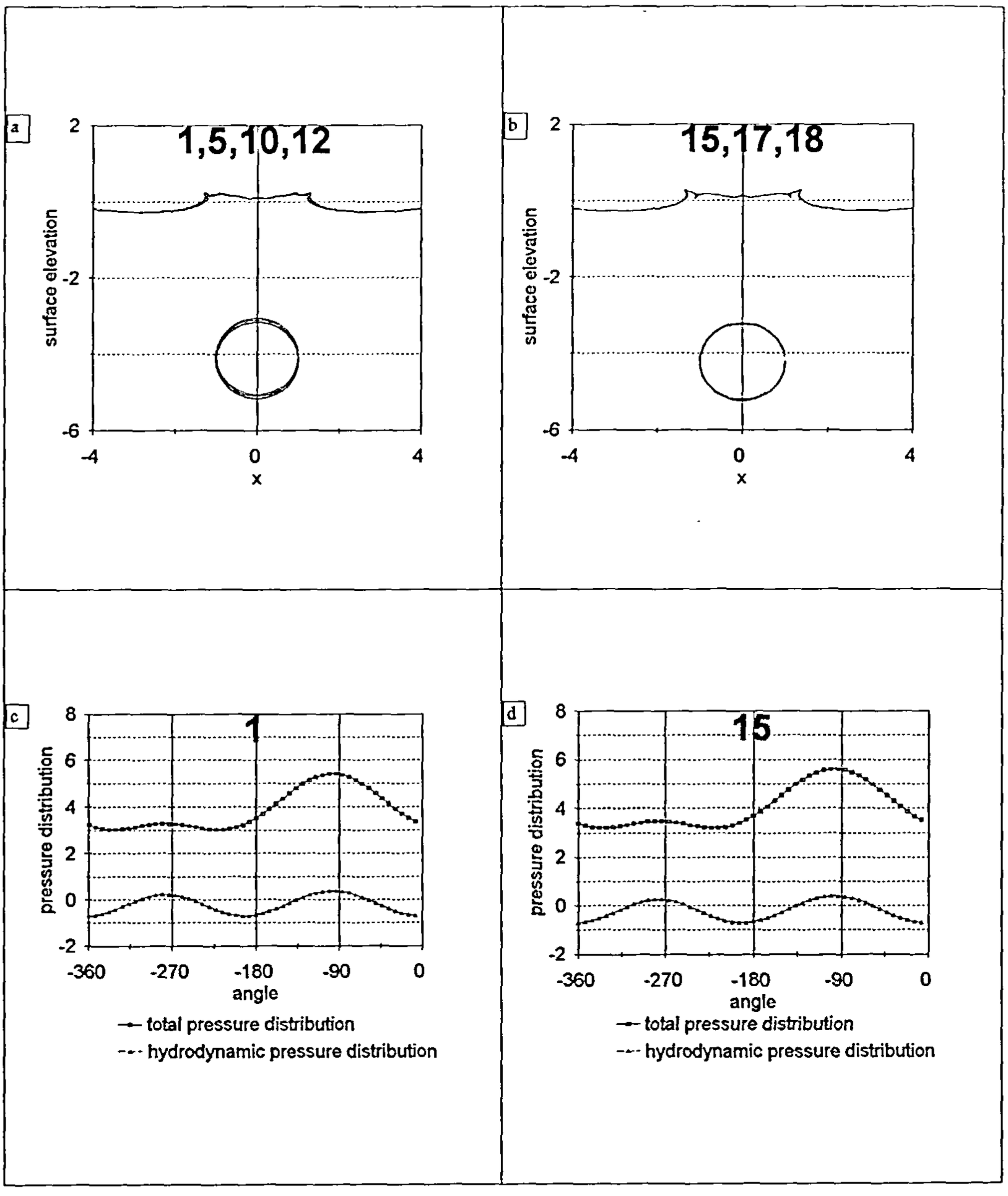

Fig. 6.12.10 Further free-surface deformations with 99 points at the free-surface and step size of 0.014.

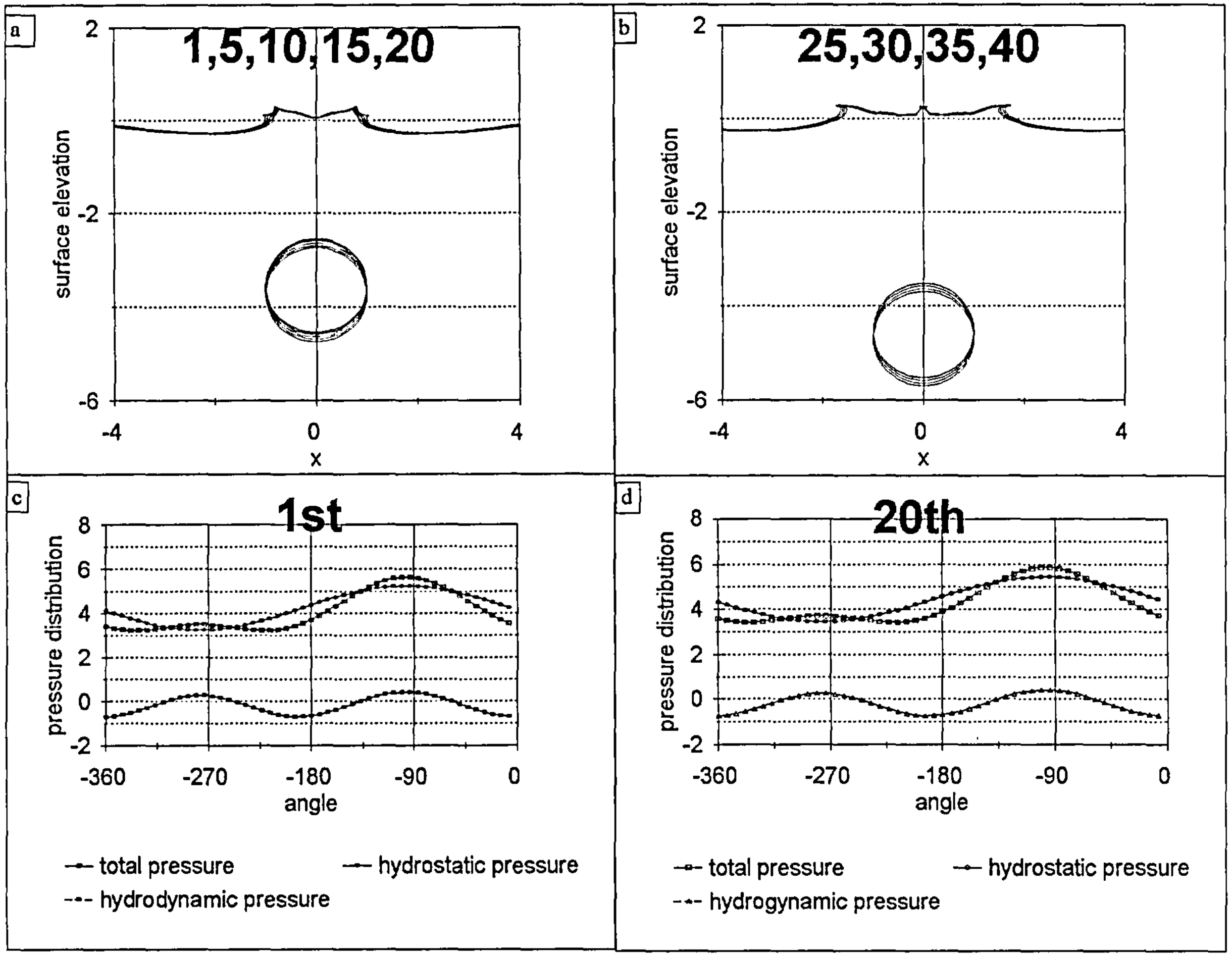

Fig. 6.12.11 Breaking waves. Points at the free-surface are reduced to 93 and step size =0.014.

e

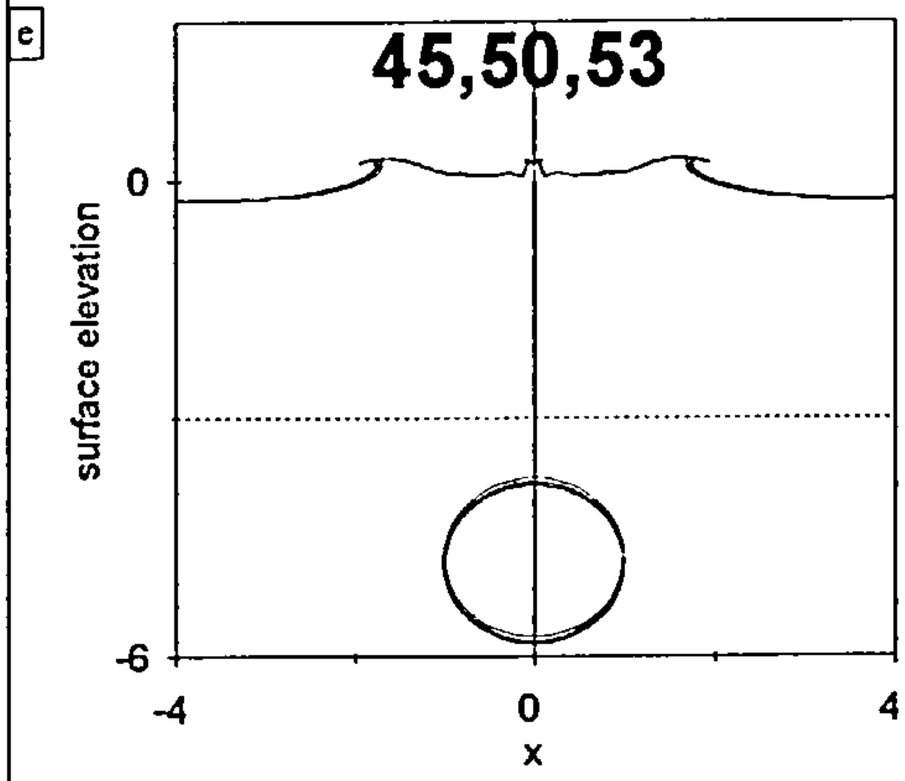
45,50,53
0
-6
surface elevation
-4
0
4
x

f

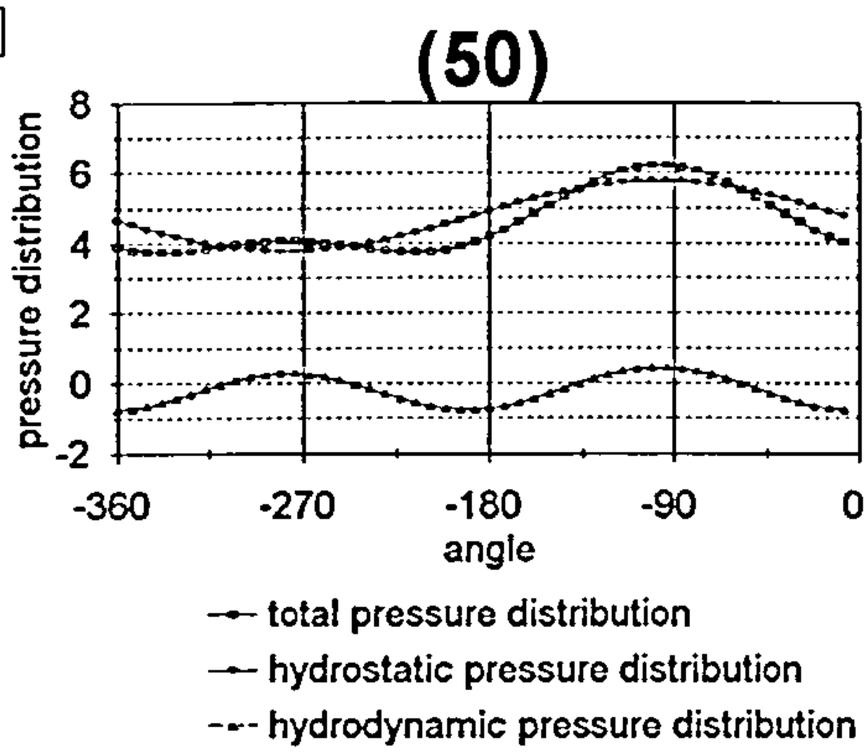
(50)
pressure distribution
8
6
4
2
0
-2
-360
-270
-180
-90
0
angle
total pressure distribution
hydrostatic pressure distribution
hydrodynamic pressure distribution

g

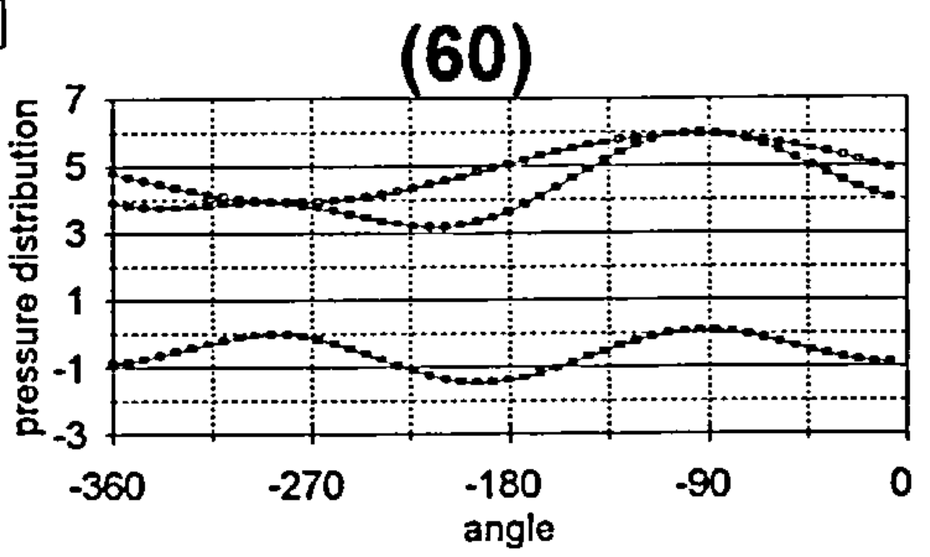
(60)
pressure distribution
7
5
3
1
-1
-3
-360
-270
-180
-90
0
angle
hydrostatic pressure
hydrodynamic pressure
total pressure

h

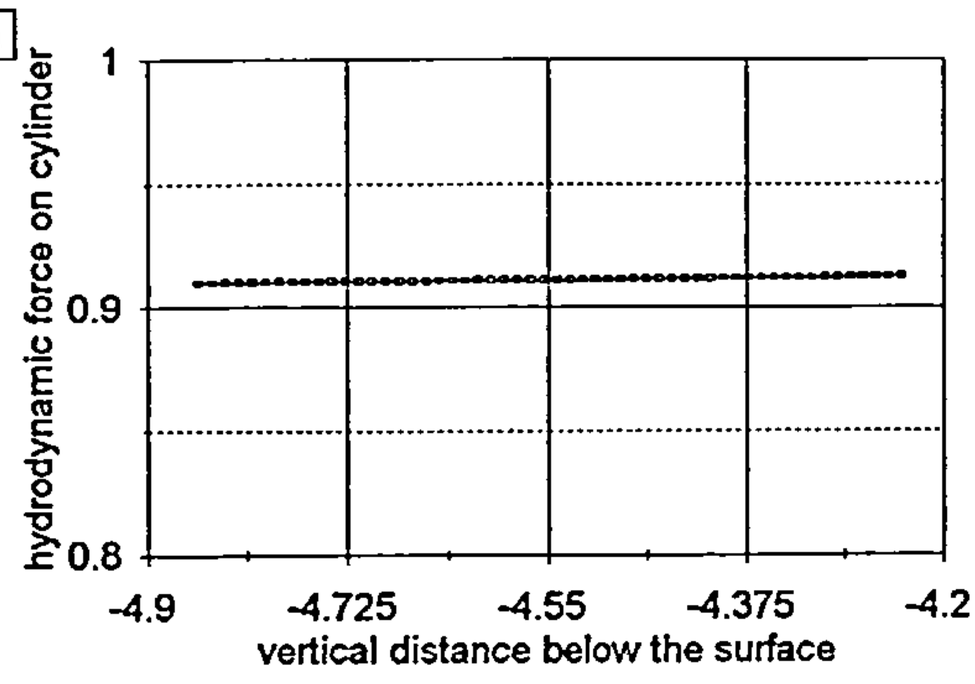
hydrodynamic force on cylinder
1
0.9
0.8
-4.9
-4.725
-4.55
-4.375
-4.2
vertical distance below the surface

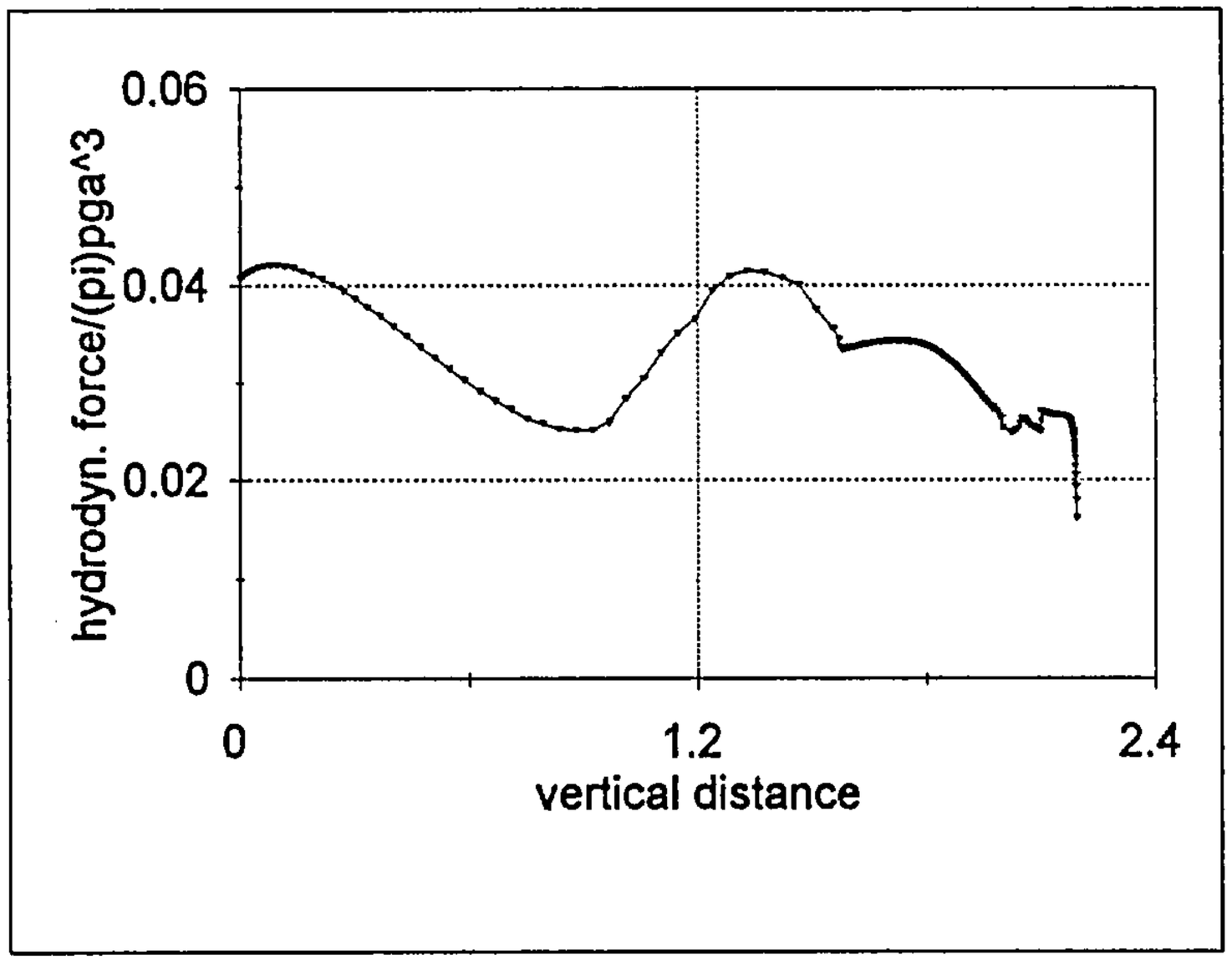

Fig. 6.12.12 Hydrodynamic force on the body due to free motion of the cylinder before and after complete engulfment.

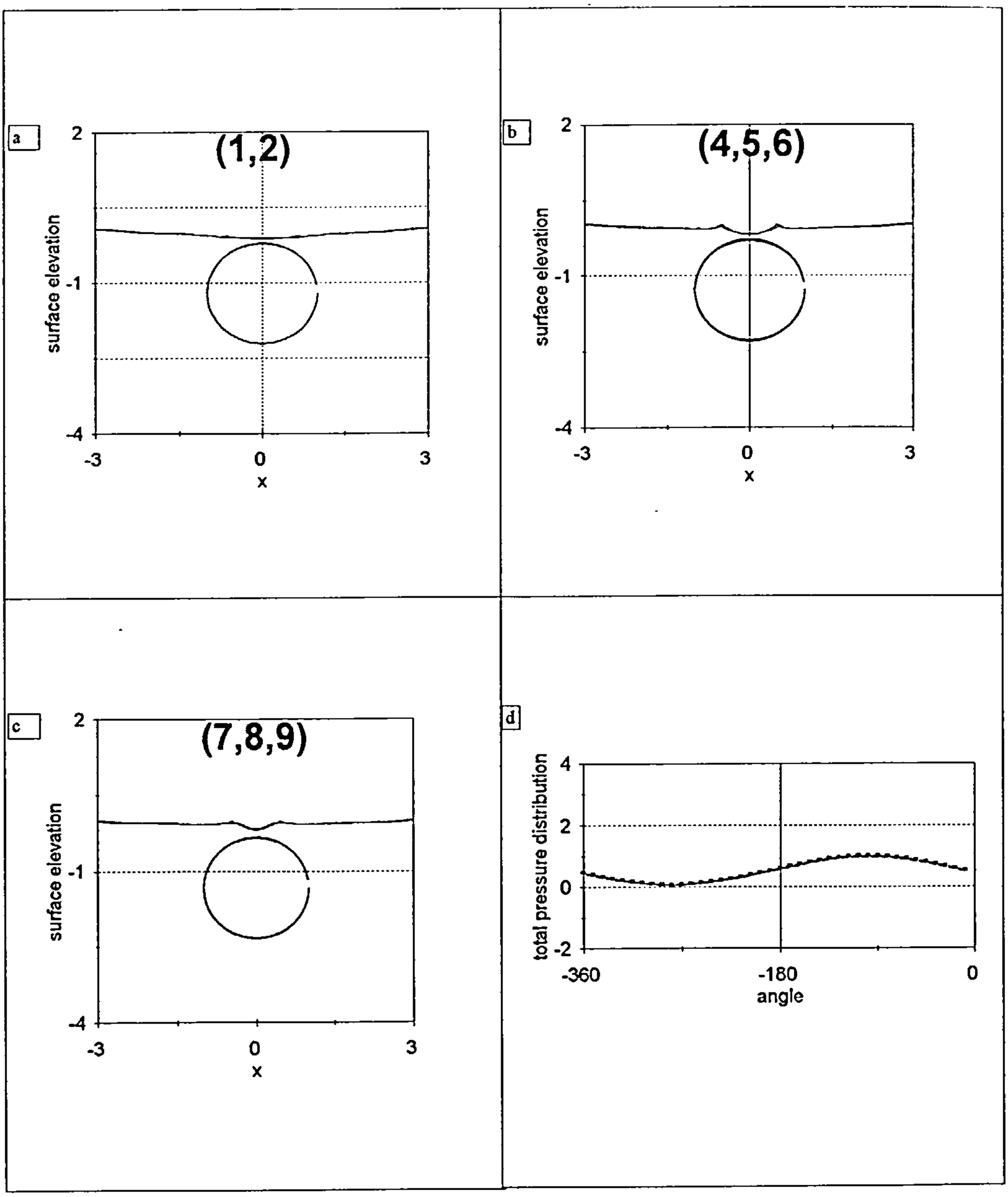

Fig. 6.13.1(i) Free-surface/cylinder positions and pressure distributions due to vertical and impulsively started motion of a cylinder just after complete submergence at Fr=0.19, Mb=1.0.

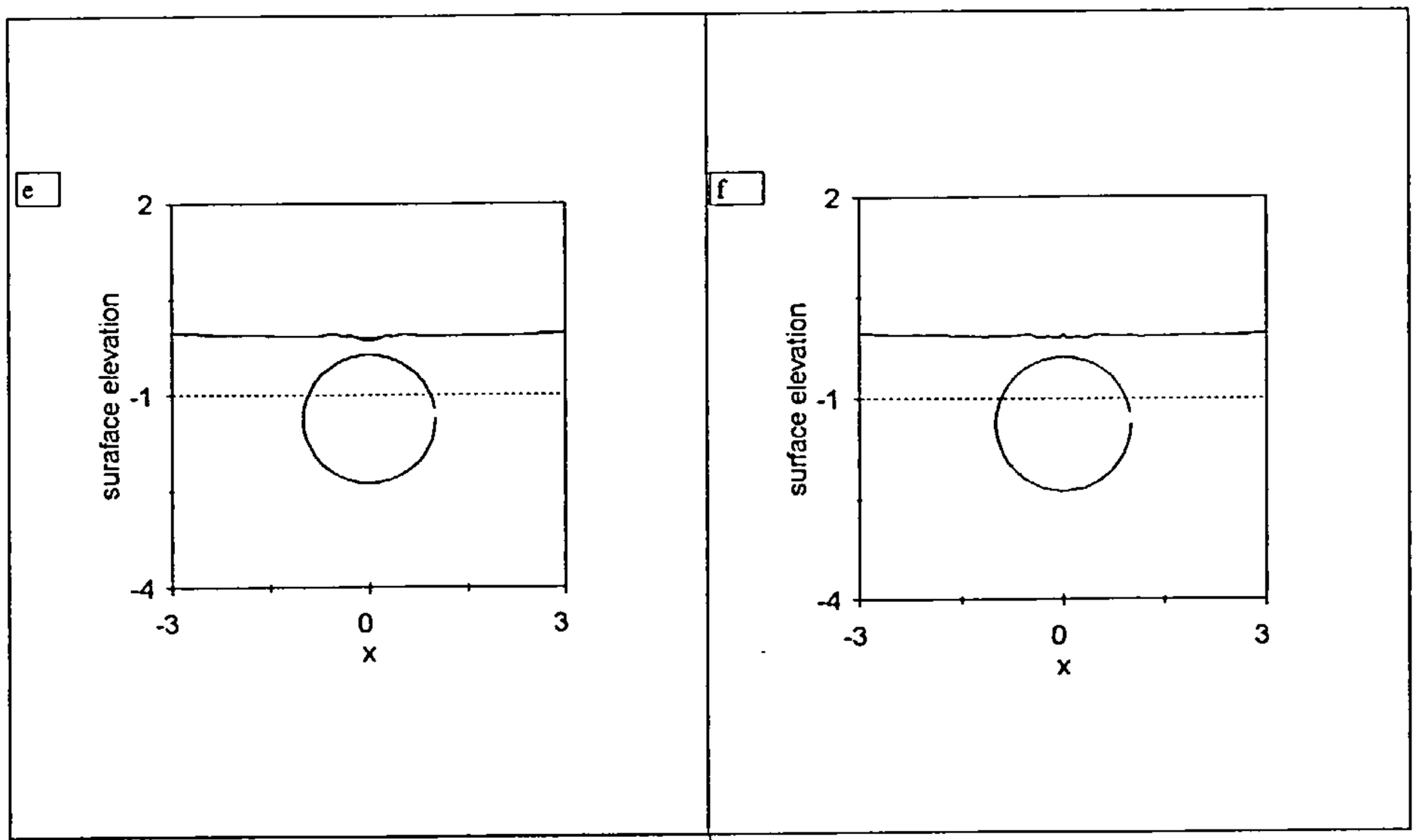
e
2
surface elevation
-1
-4
-3
0
3
x
f
2
surface elevation
-1
-4
-3
0
3
x

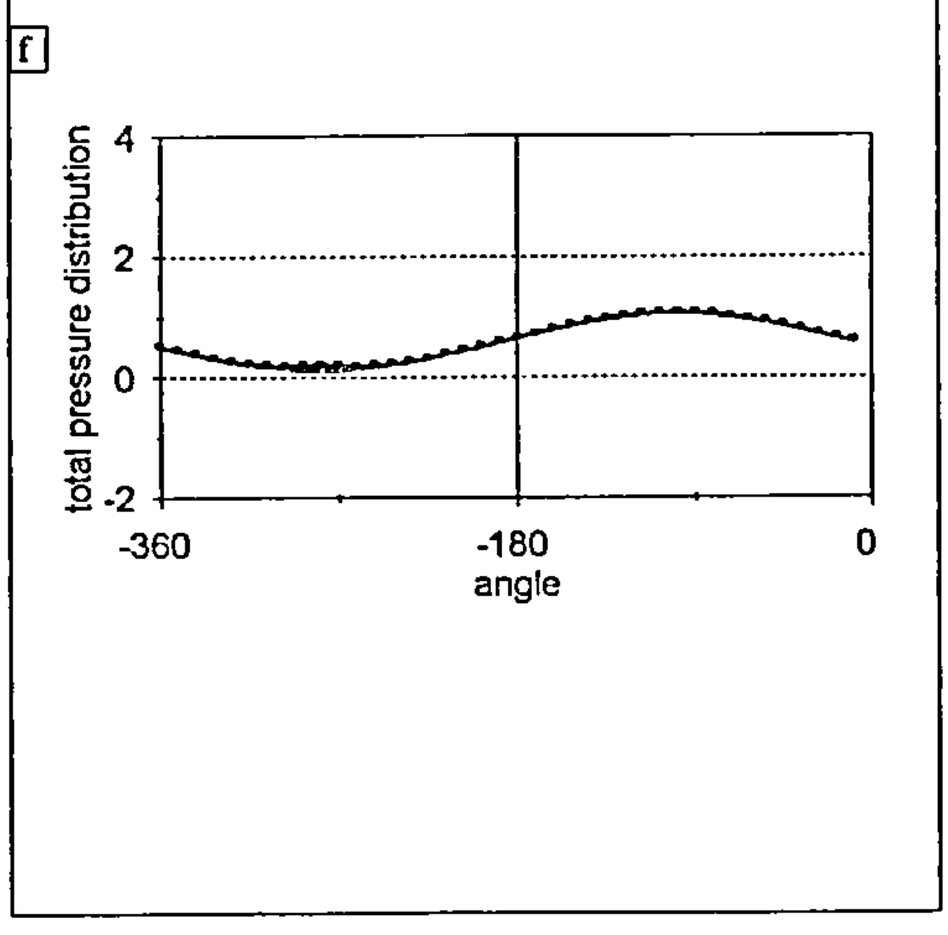
f
total pressure distribution
4
2
0
-2
-360
-180
0
angle

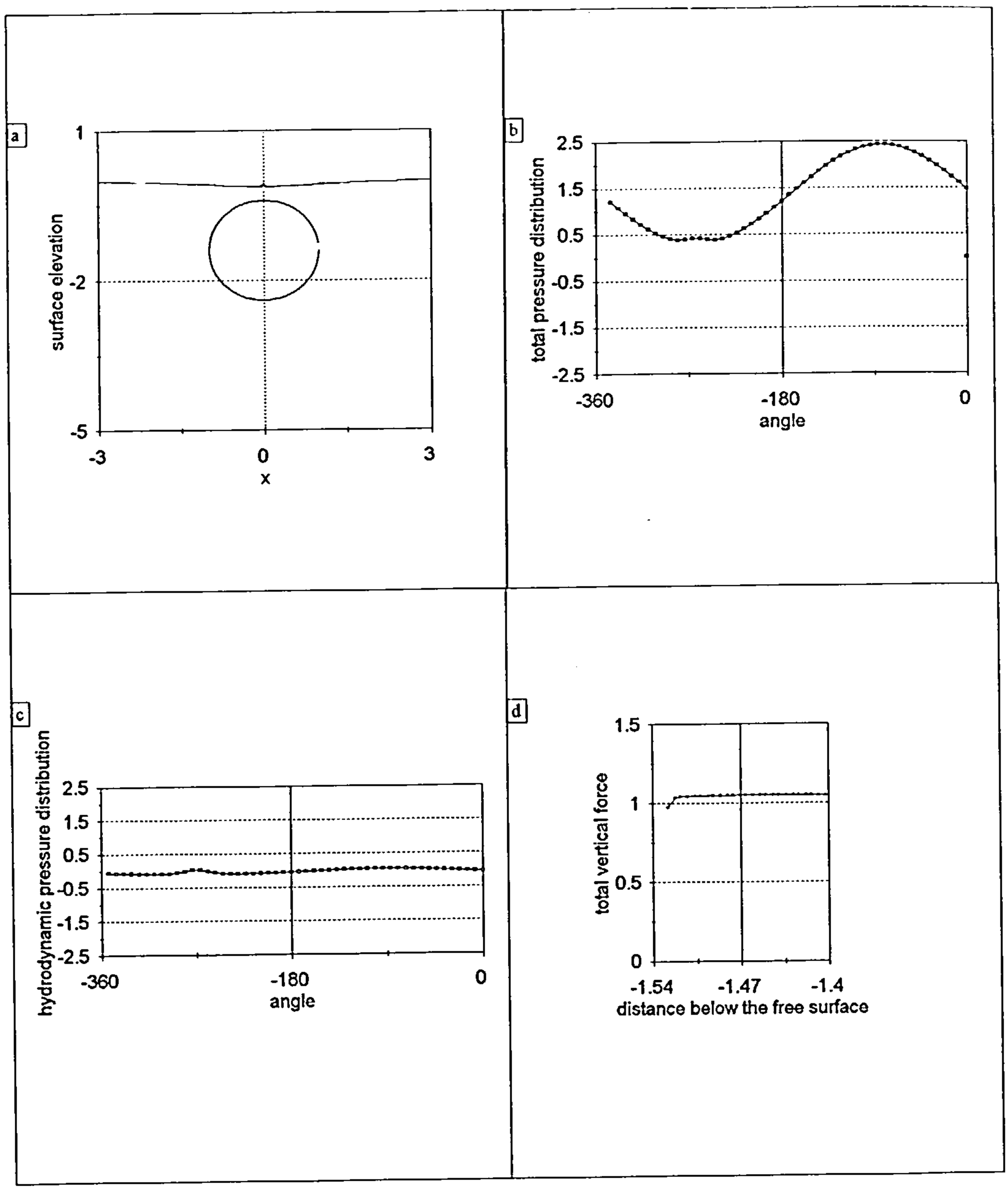

Fig. 6.13.1(ii) A jet has emerged along the line of symmetry.

f

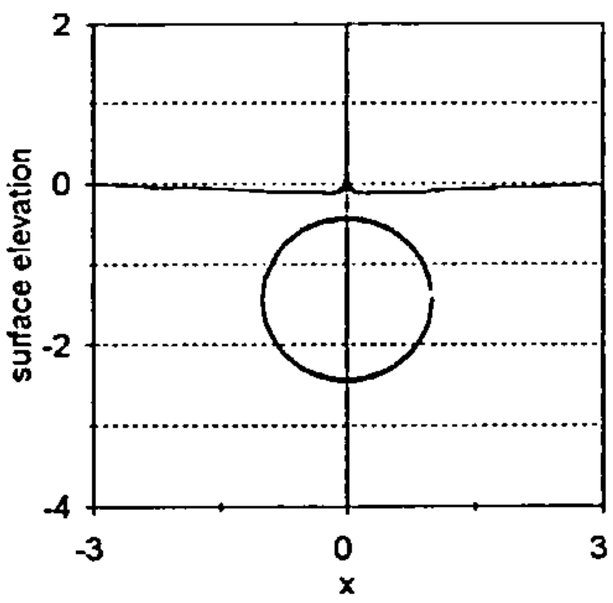
2
0
-2
-4
surface elevation
-3
0
3
x

g

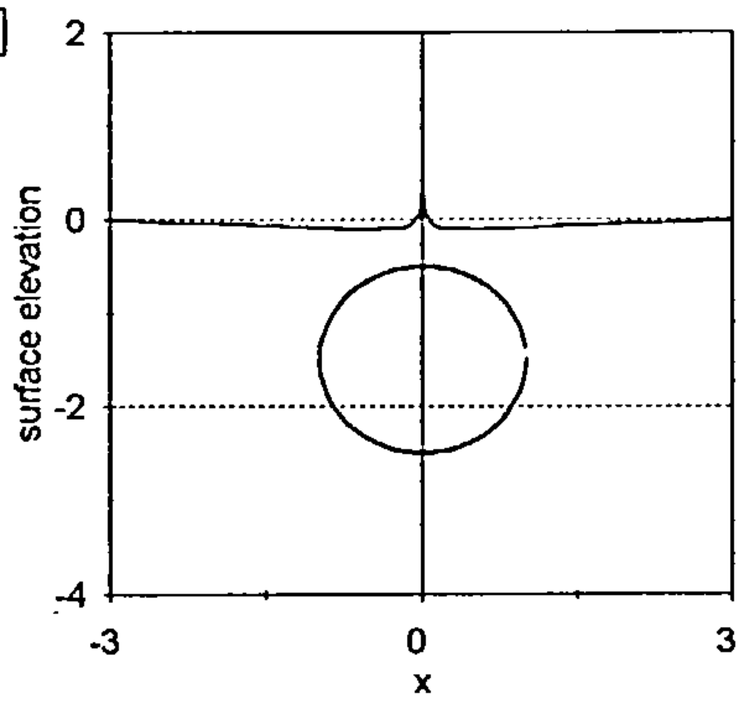
2
0
-2
-4
surface elevation
-3
0
3
x

i

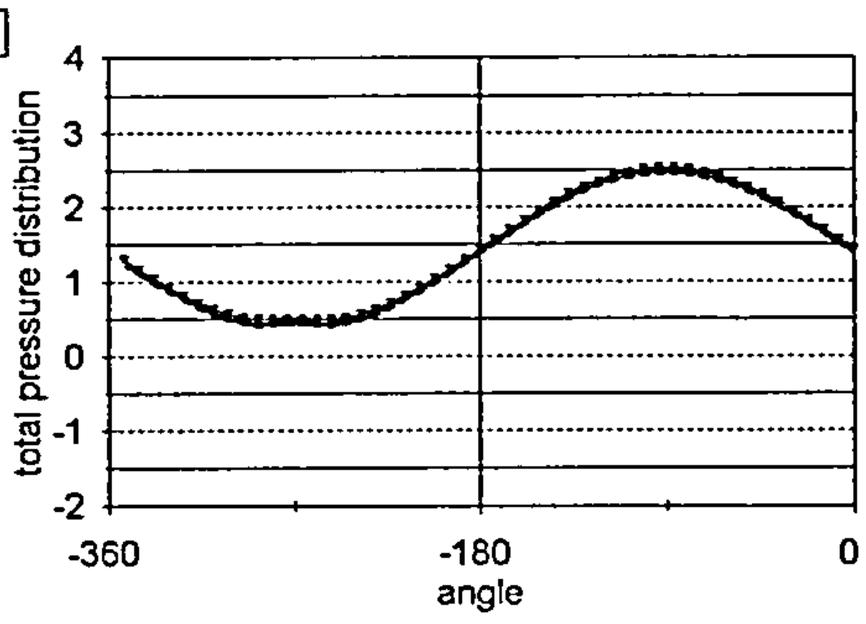
4
3
2
1
0
-1
-2
total pressure distribution
-360
-180
0
angle

j

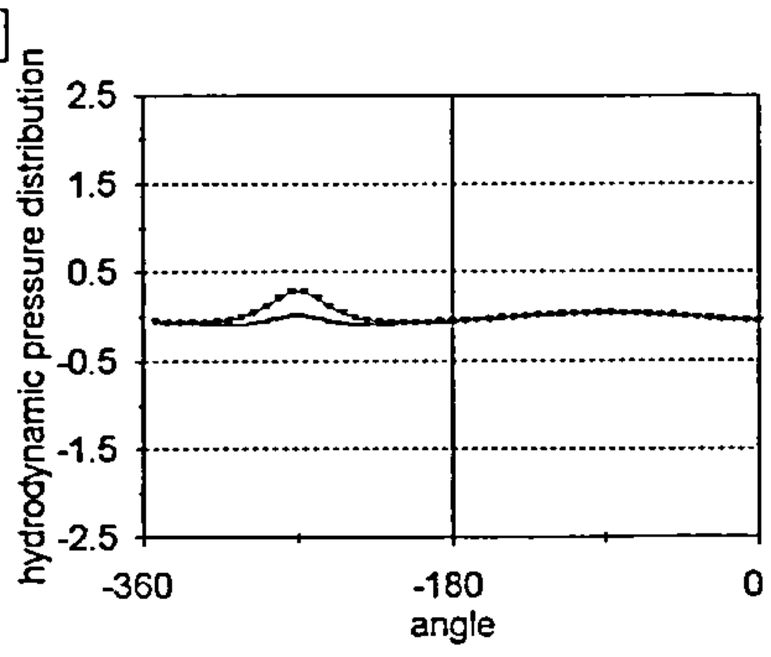
2.5
1.5
0.5
-0.5
-1.5
-2.5
hydrodynamic pressure distribution
-360
-180
0
angle

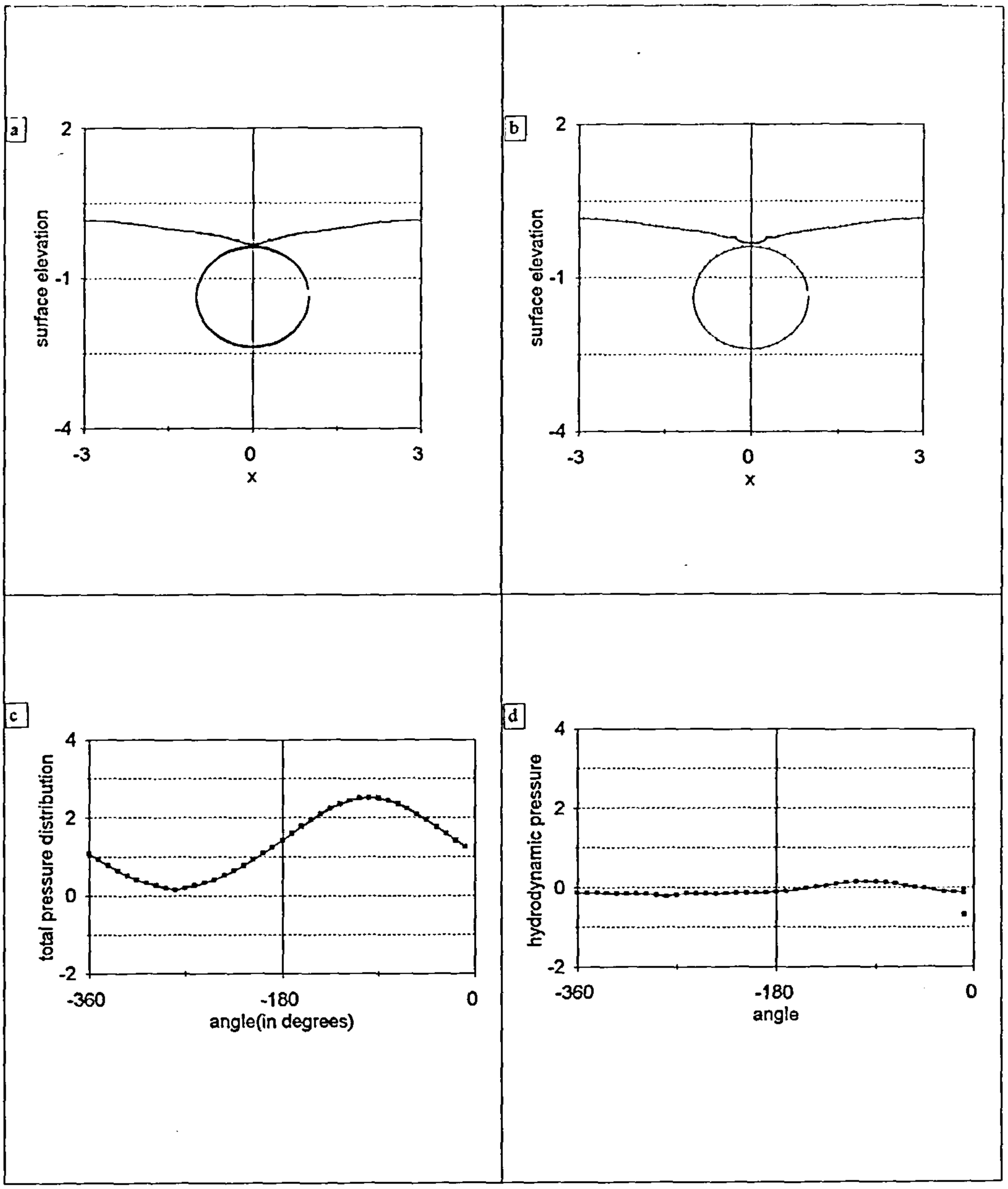

Fig. 6.13.2(i) The number of points at the free-surface is increased to 111 and the time step size is reduced to 0.014 from respectively 90 and 0.042. Fr = 0.46.

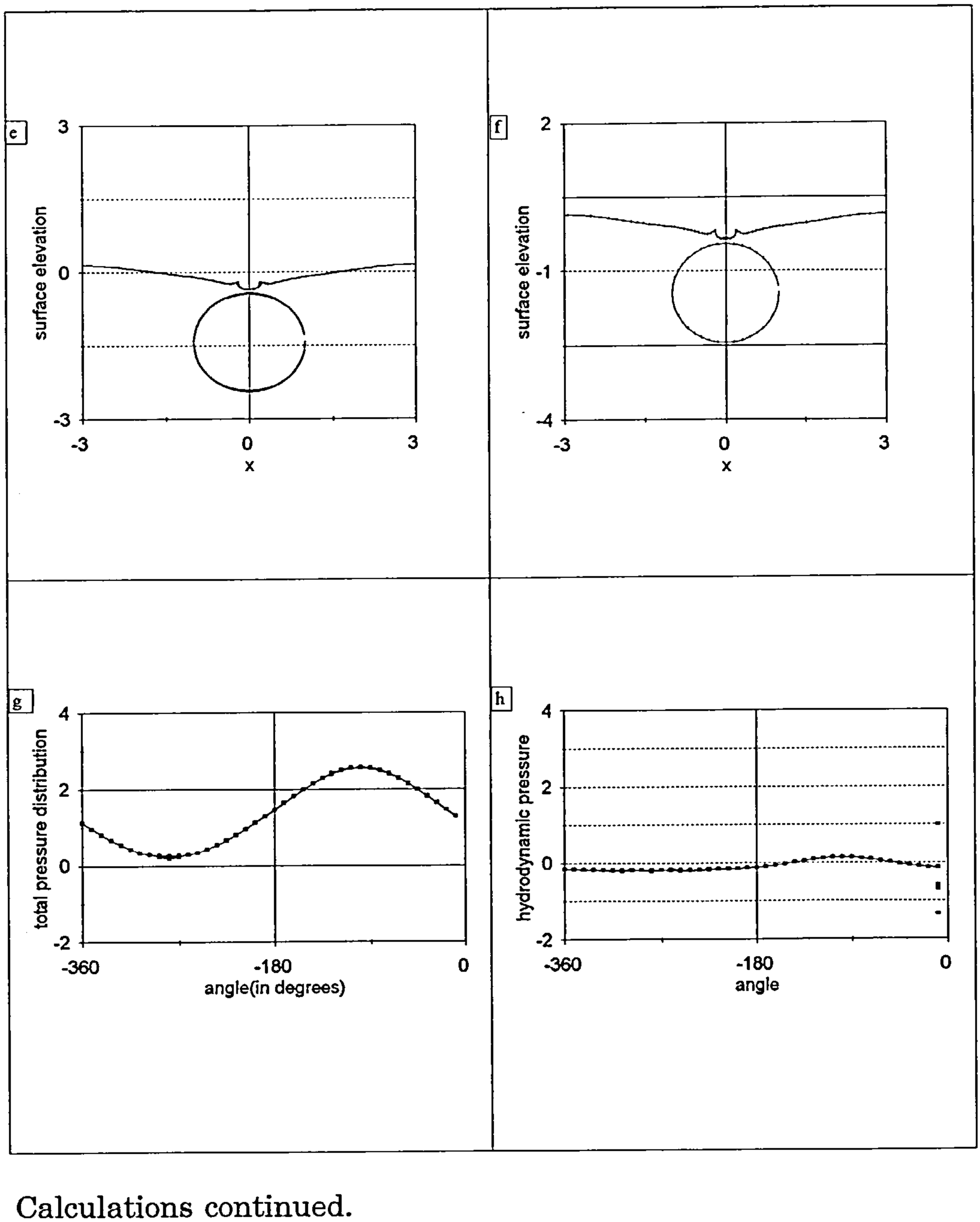

Calculations continued.

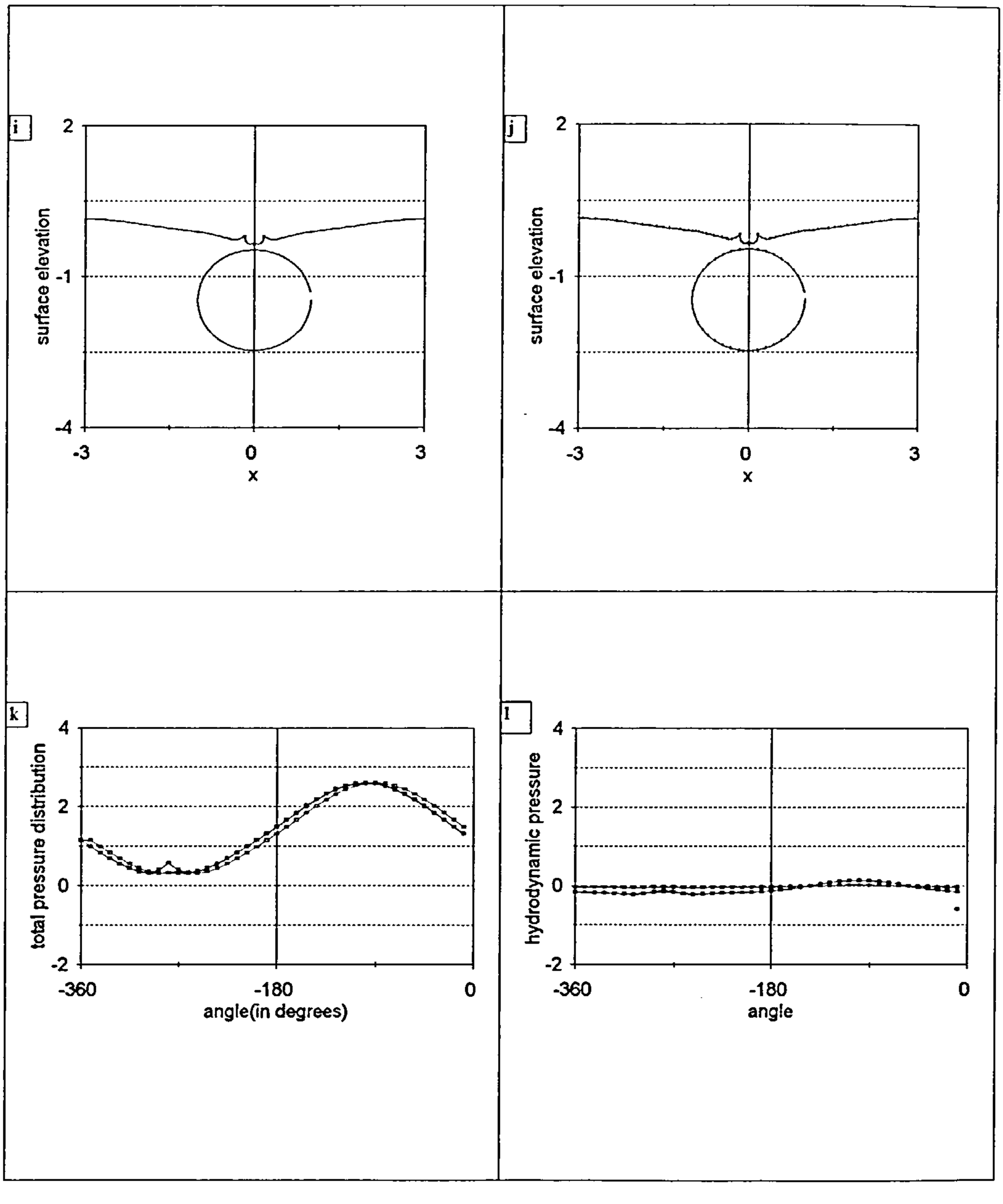

A jet has formed at the centre.

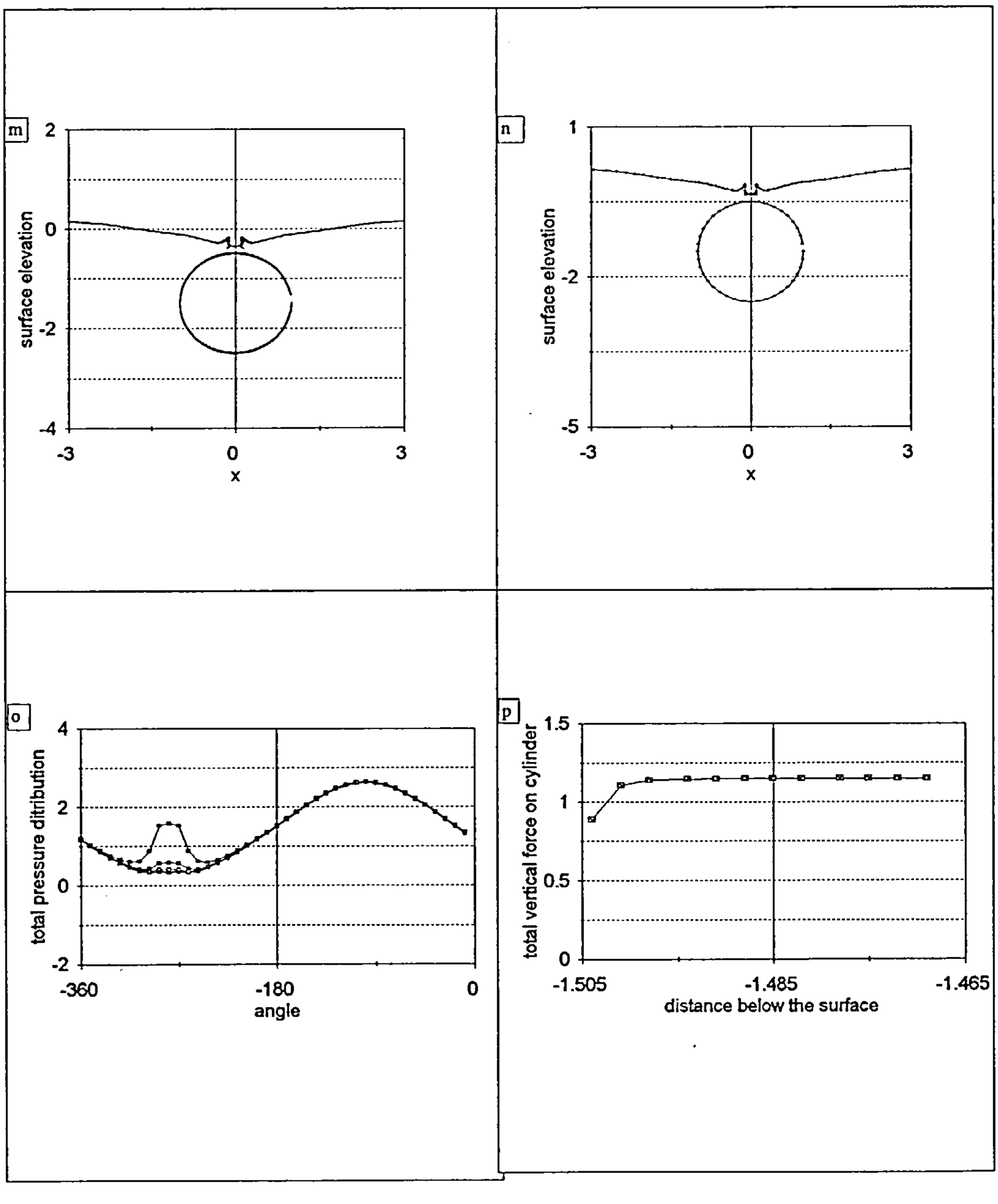

Free-surface elevation and pressure distribution up to the instant of break down of the calculations

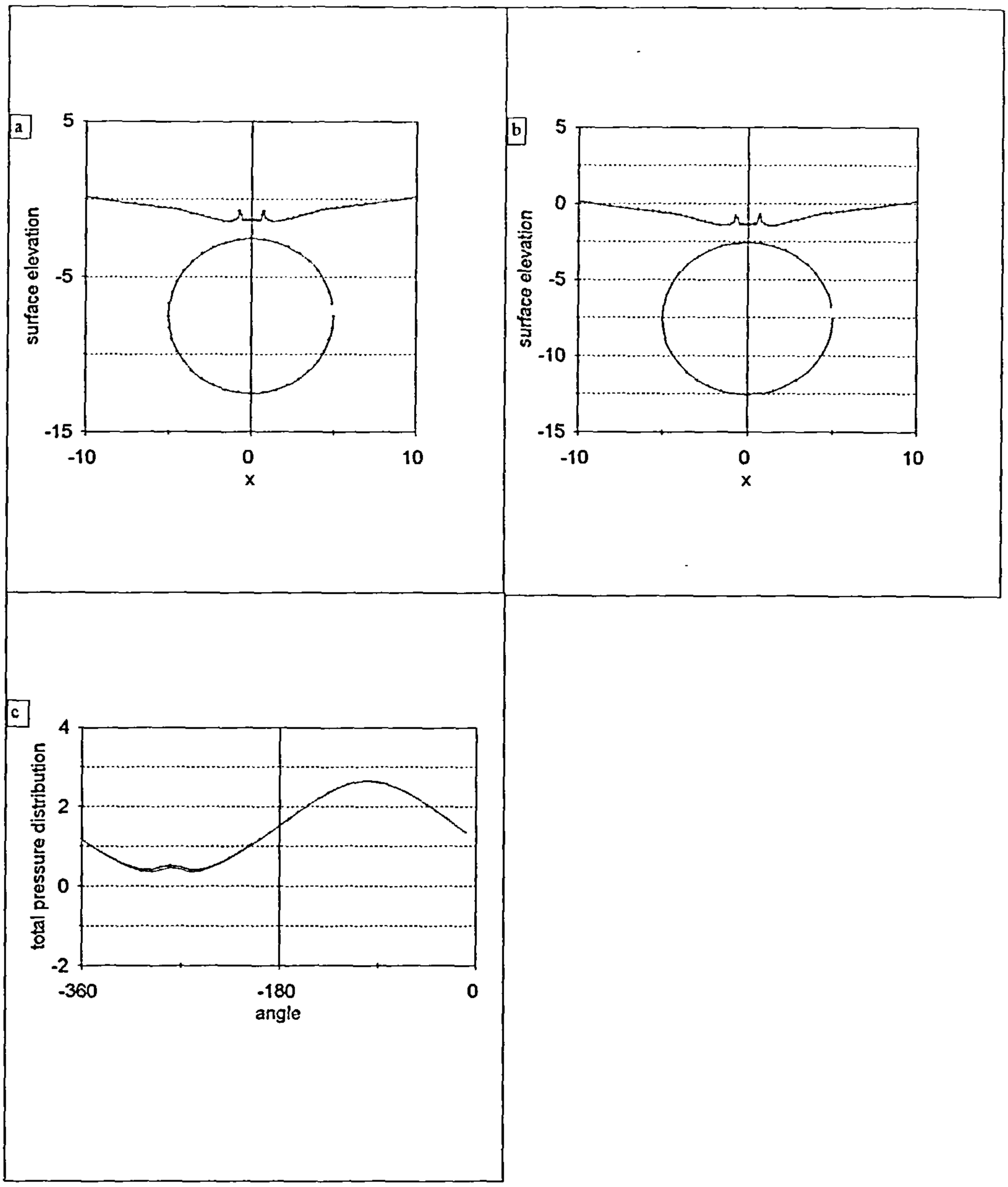

Fig. 6.13.2(ii) Continuation of the calculations with the points on the free-surface equal to 105 and step size equal to 0.014.

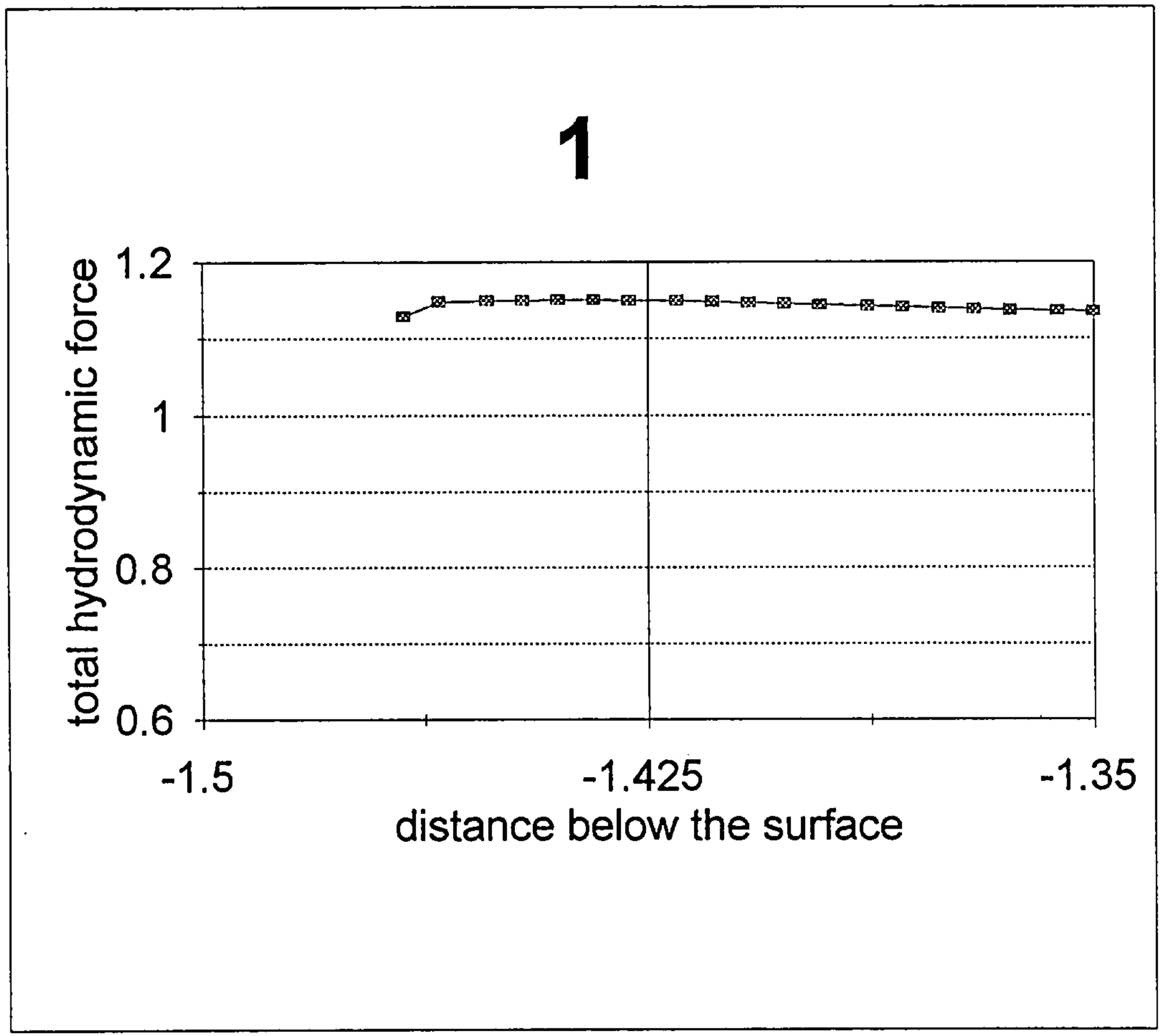

Total vertical force acting on the cylinder as it moves from d=1.344a to d=1.466a.

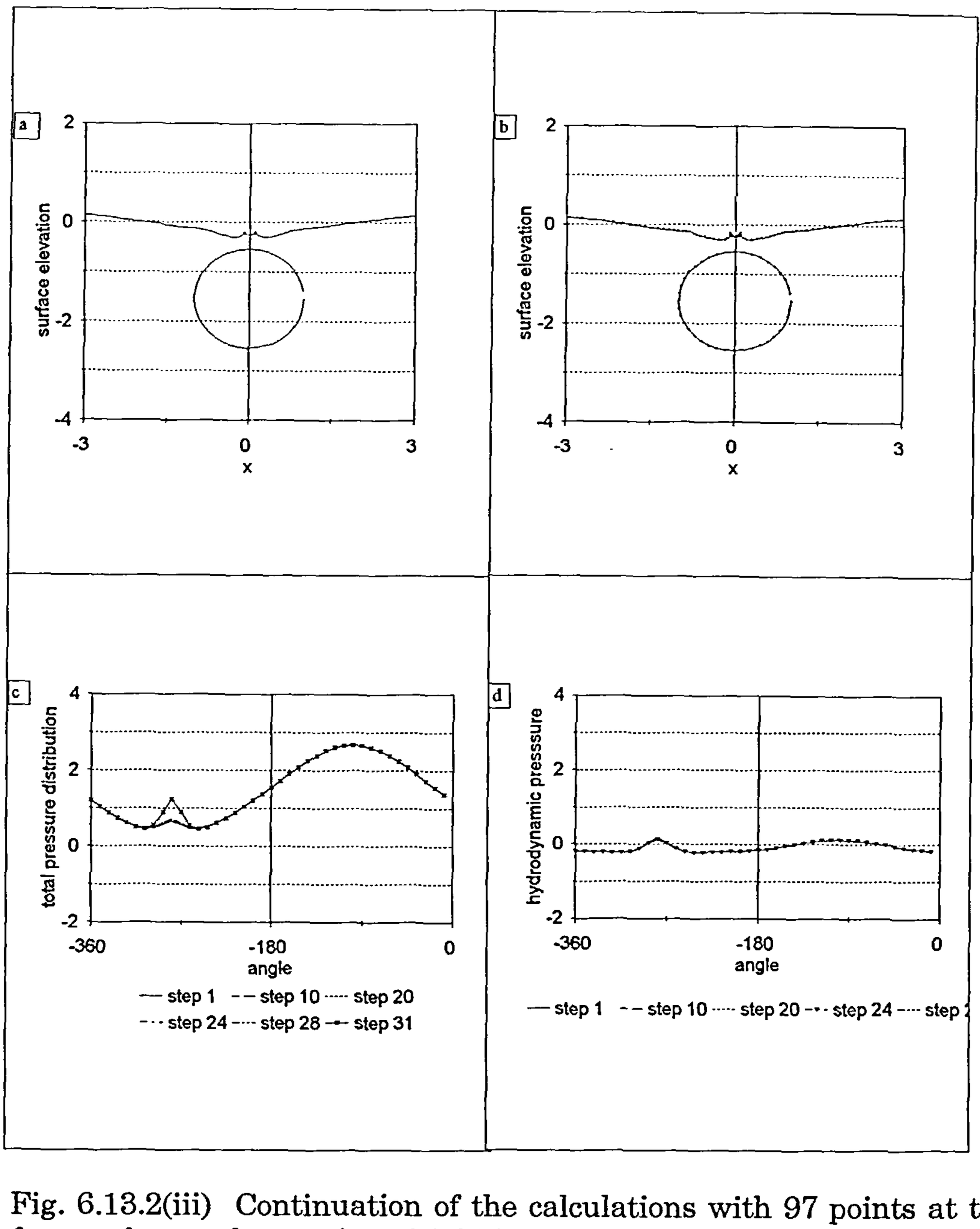

Fig. 6.13.2(iii) Continuation of the calculations with 97 points at the free-surface and step size of 0.014.

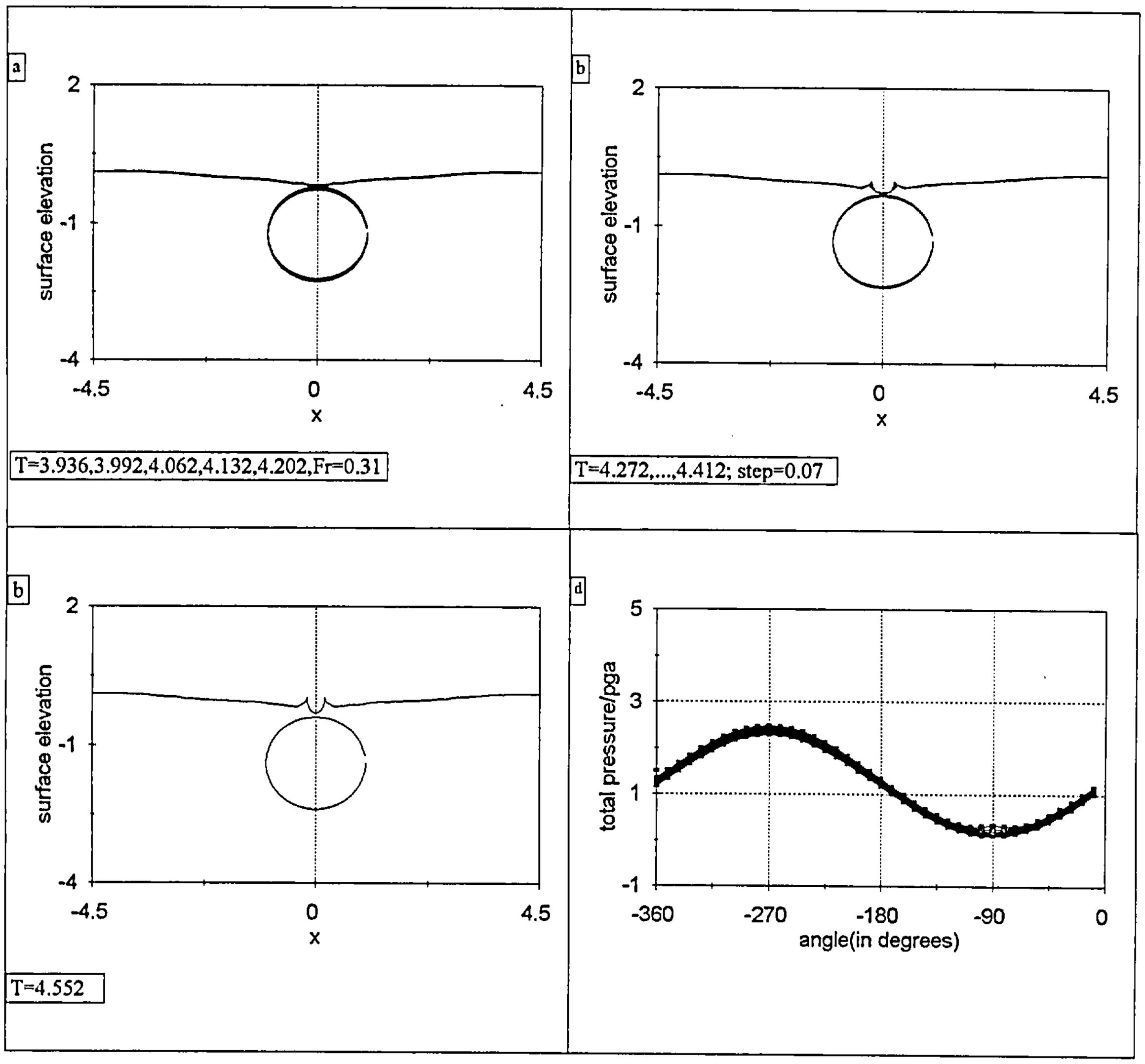

Fig. 6.13.3(i) Continuation of the calculations for vertical and forced motion at Fr=0.31 after complete submergence.

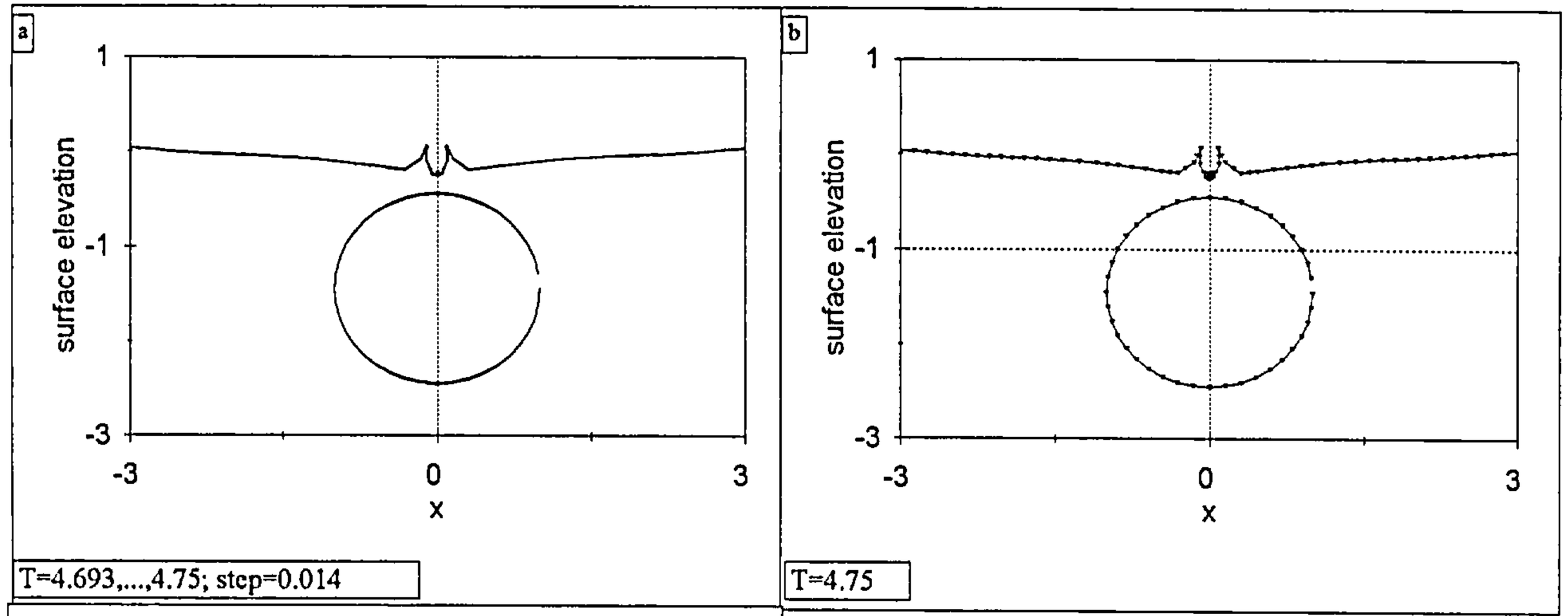

Fig. 6.13.3(ii) A jet is developing at the centre.

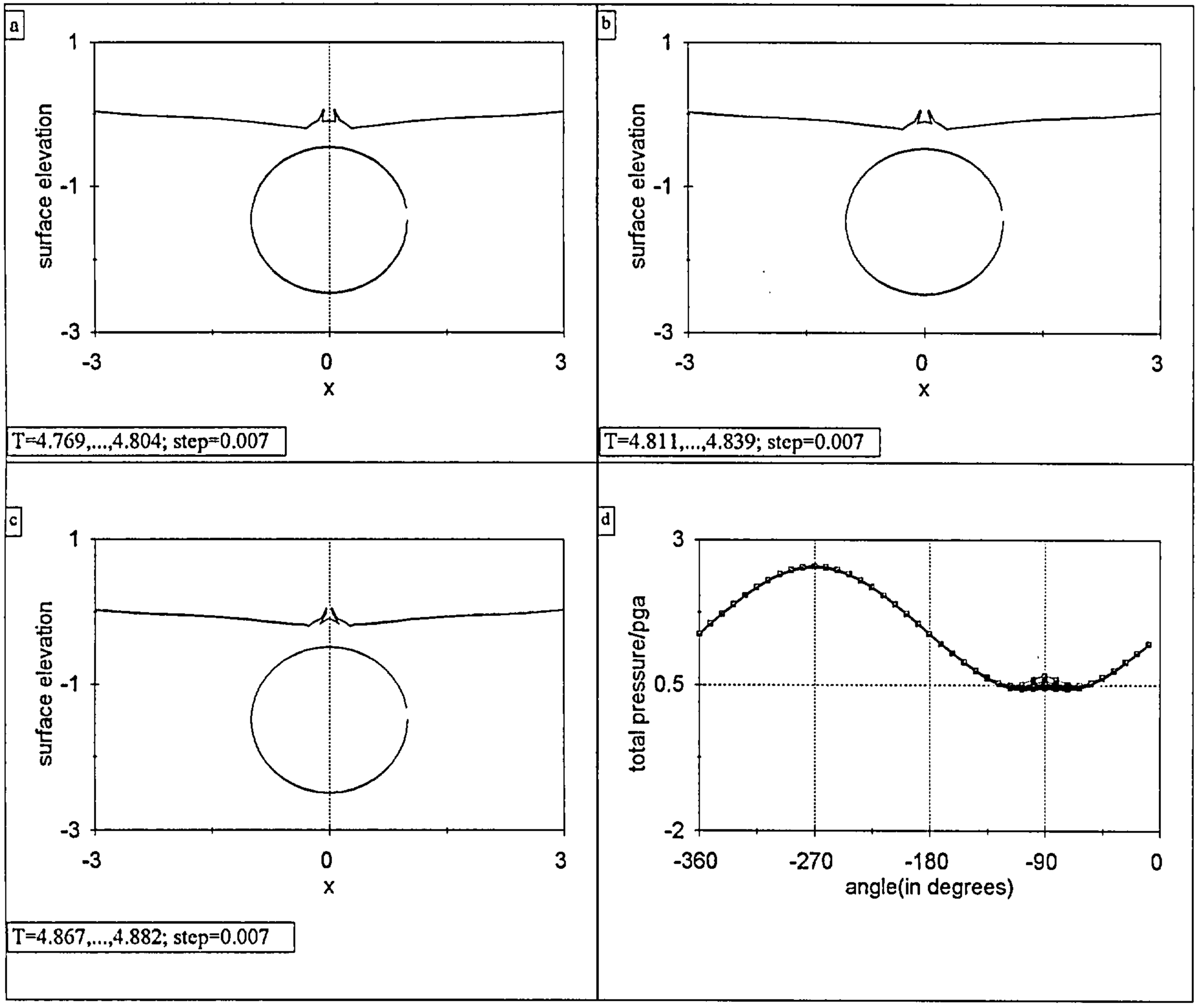

Fig. 6.13.3(iii) Continuation of the above calculations.

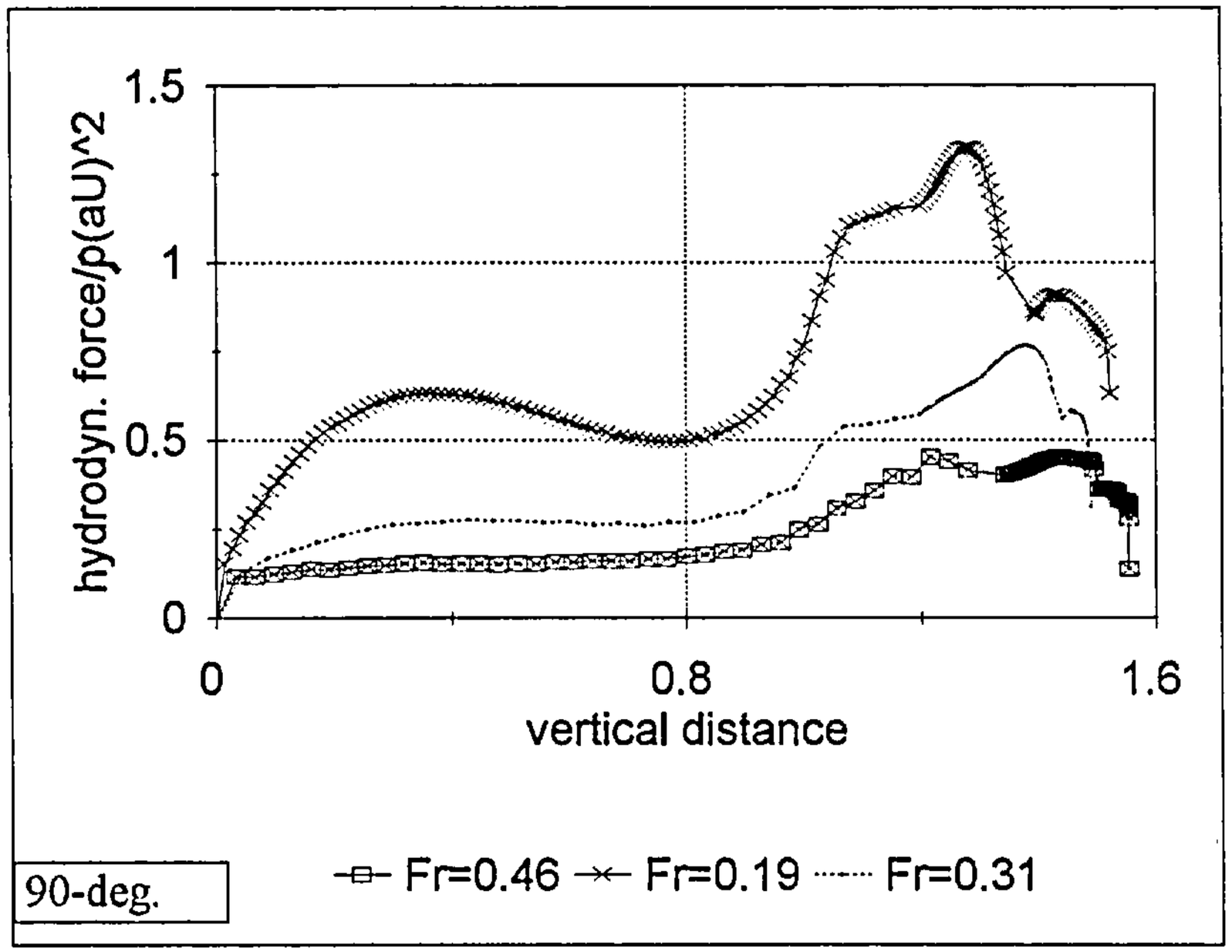

Fig. 6.13.4 Hydrodynamic forces on the body before and after complete engulfment.

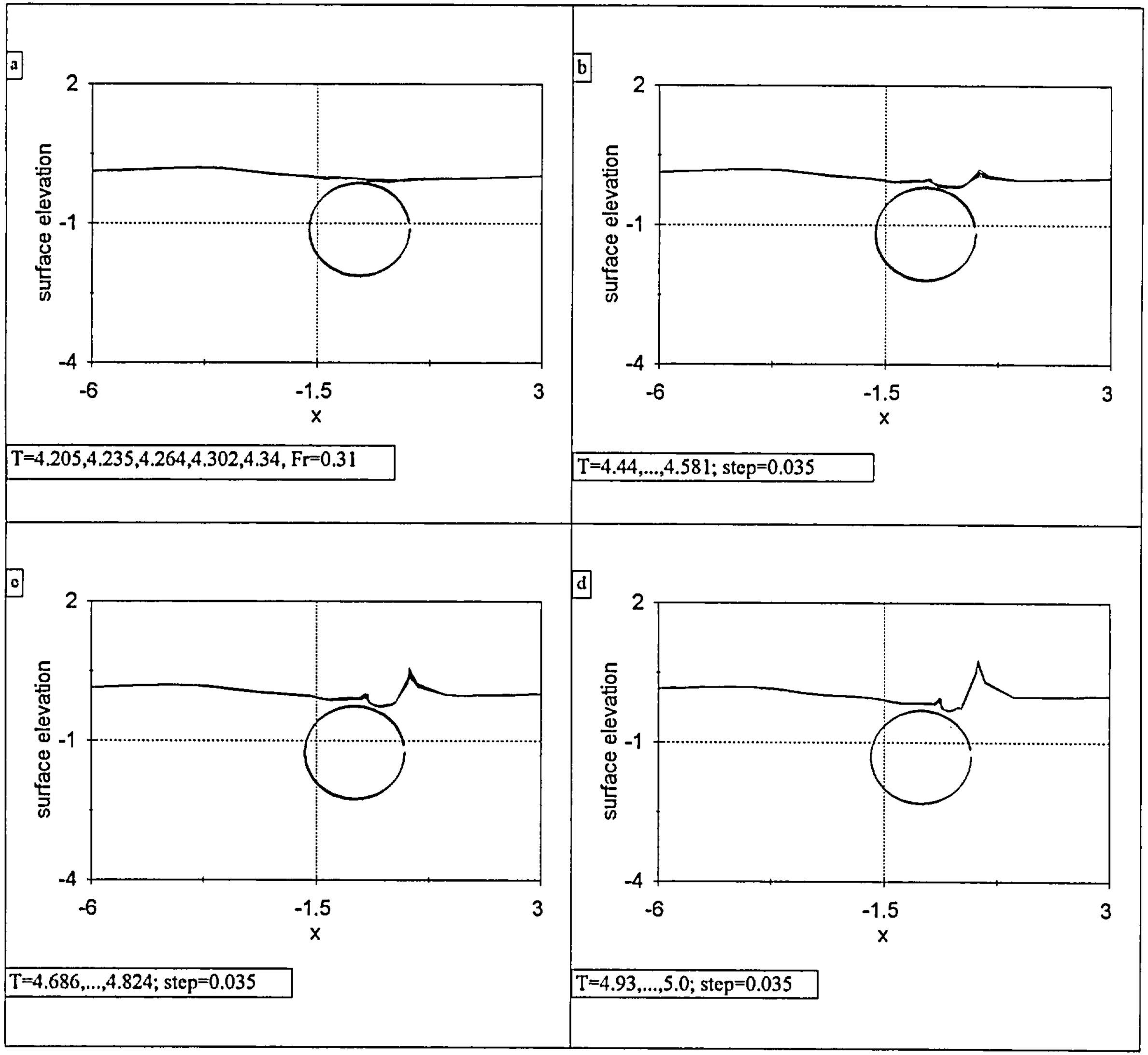

Fig. 6.14(i) Continuation of the calculations after complete submergence for the oblique(30-degrees) and impulsively started motion of a cylinder moving at Fr= 0.31

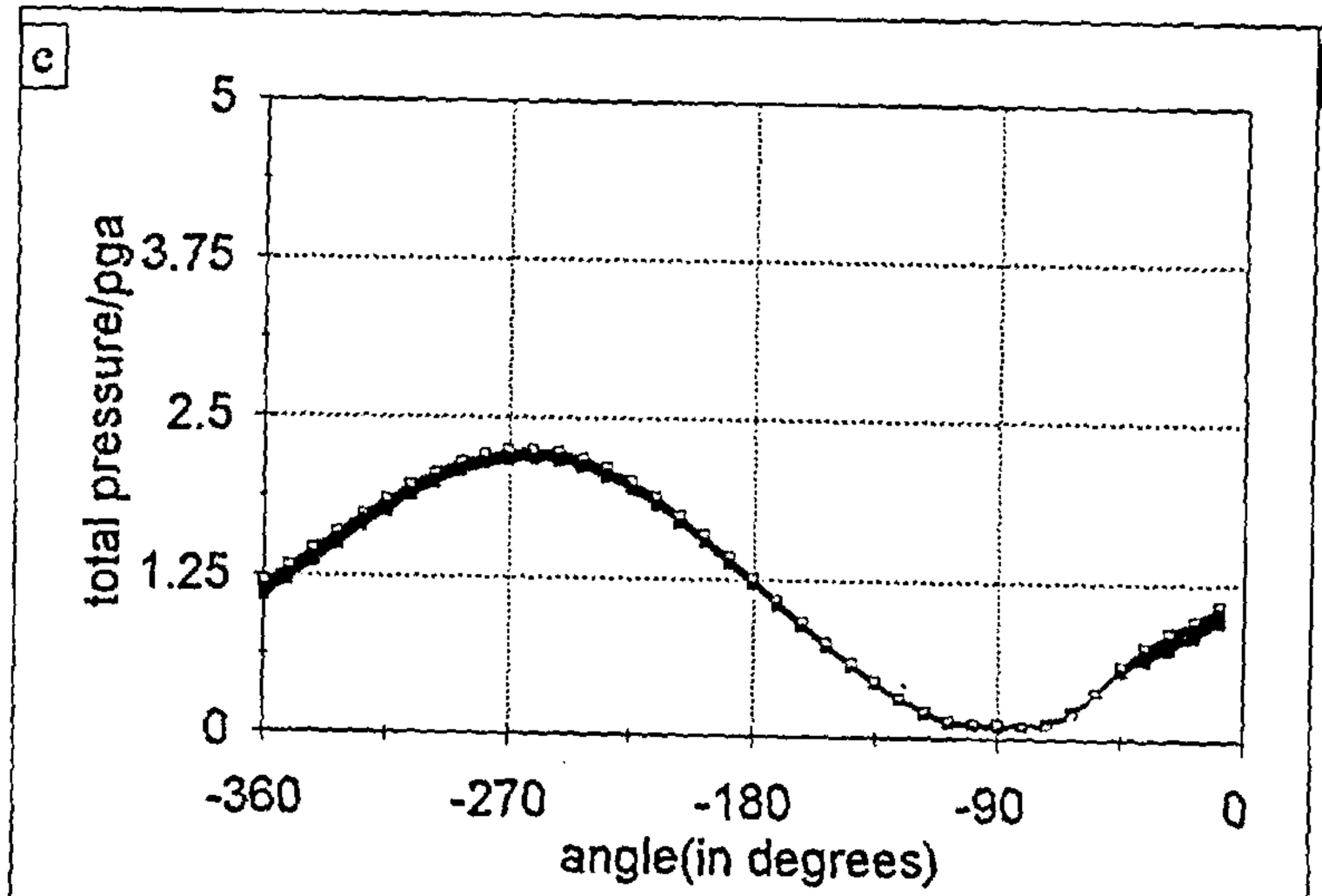
e
5
3.75
2.5
1.25
0
total pressure/pga
-360
-270
-180
-90
0
angle(in degrees)

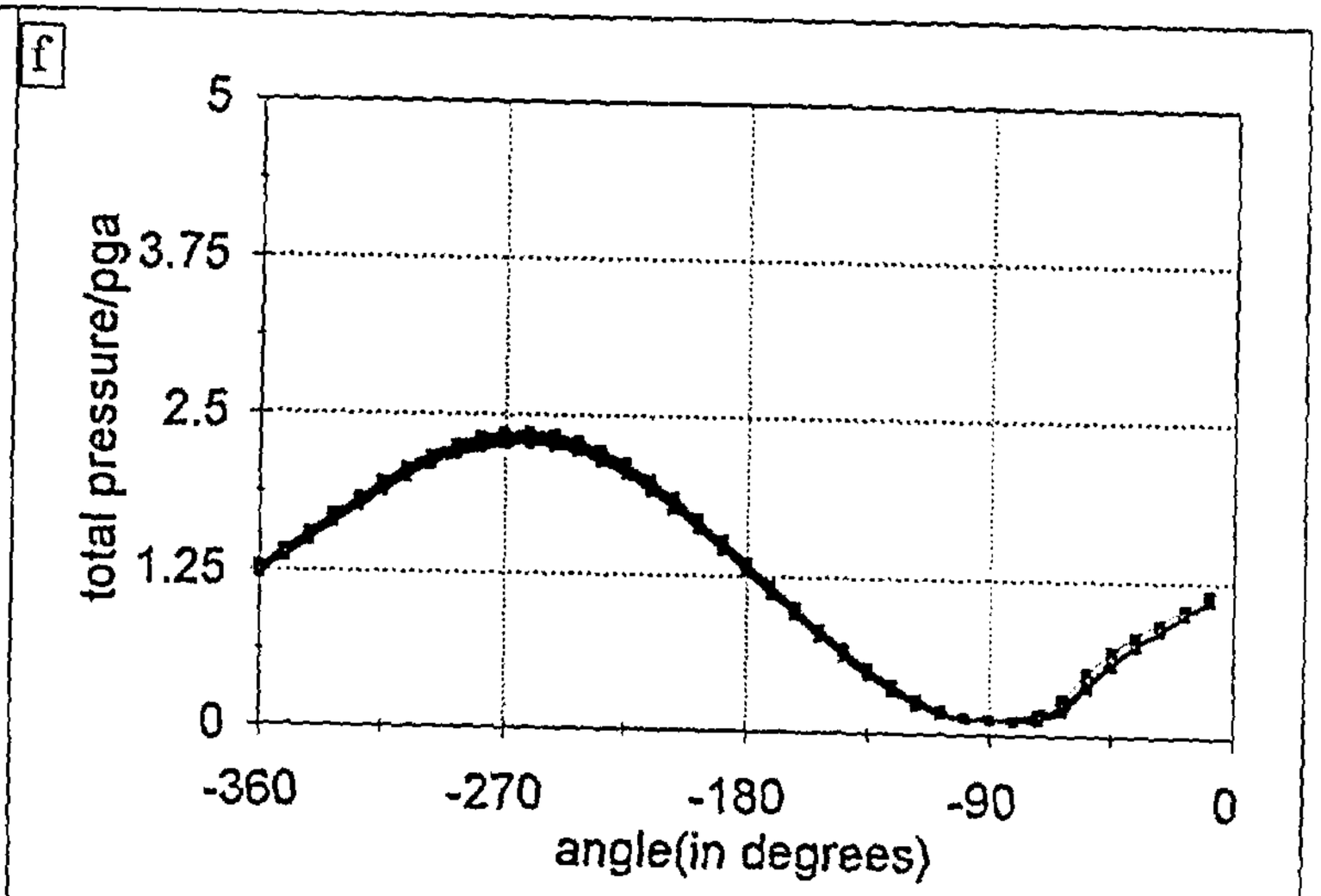
f
5
3.75
2.5
1.25
0
total pressure/pga
-360
-270
-180
-90
0
angle(in degrees)

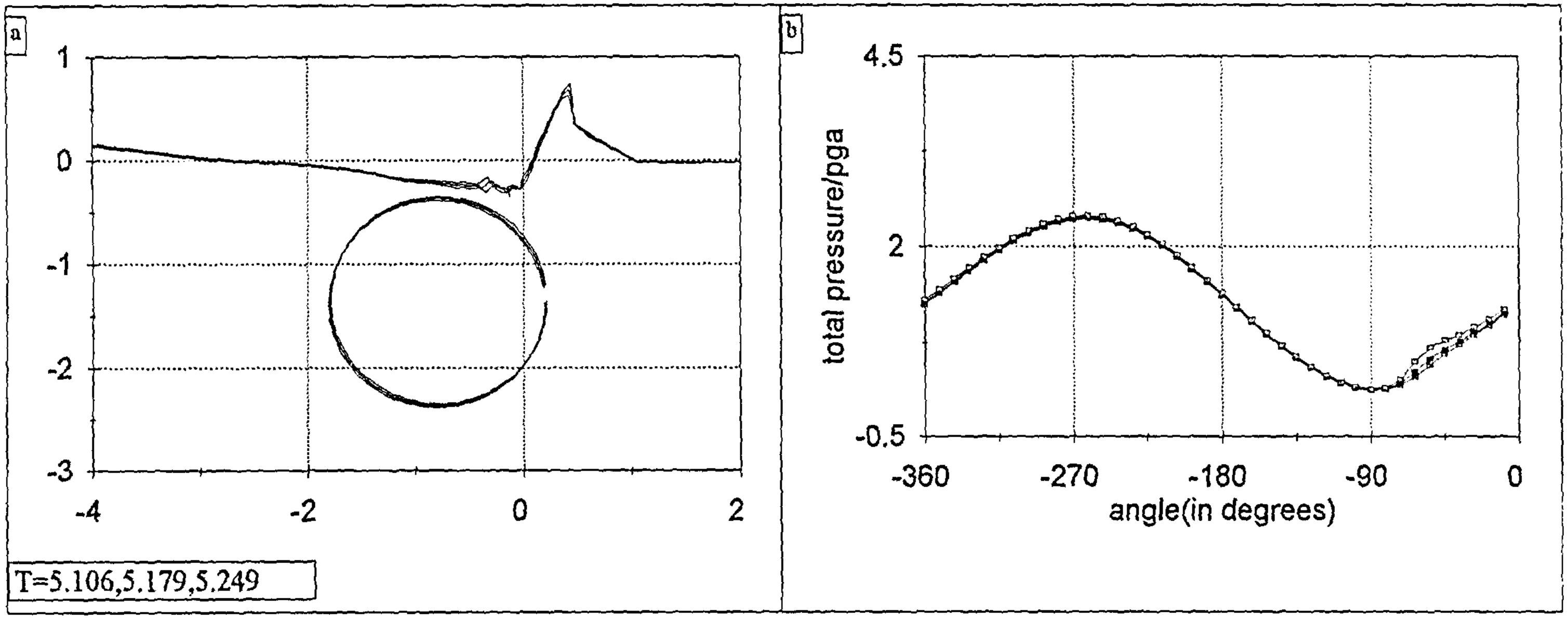

Fig. 6.14(ii) Further results.

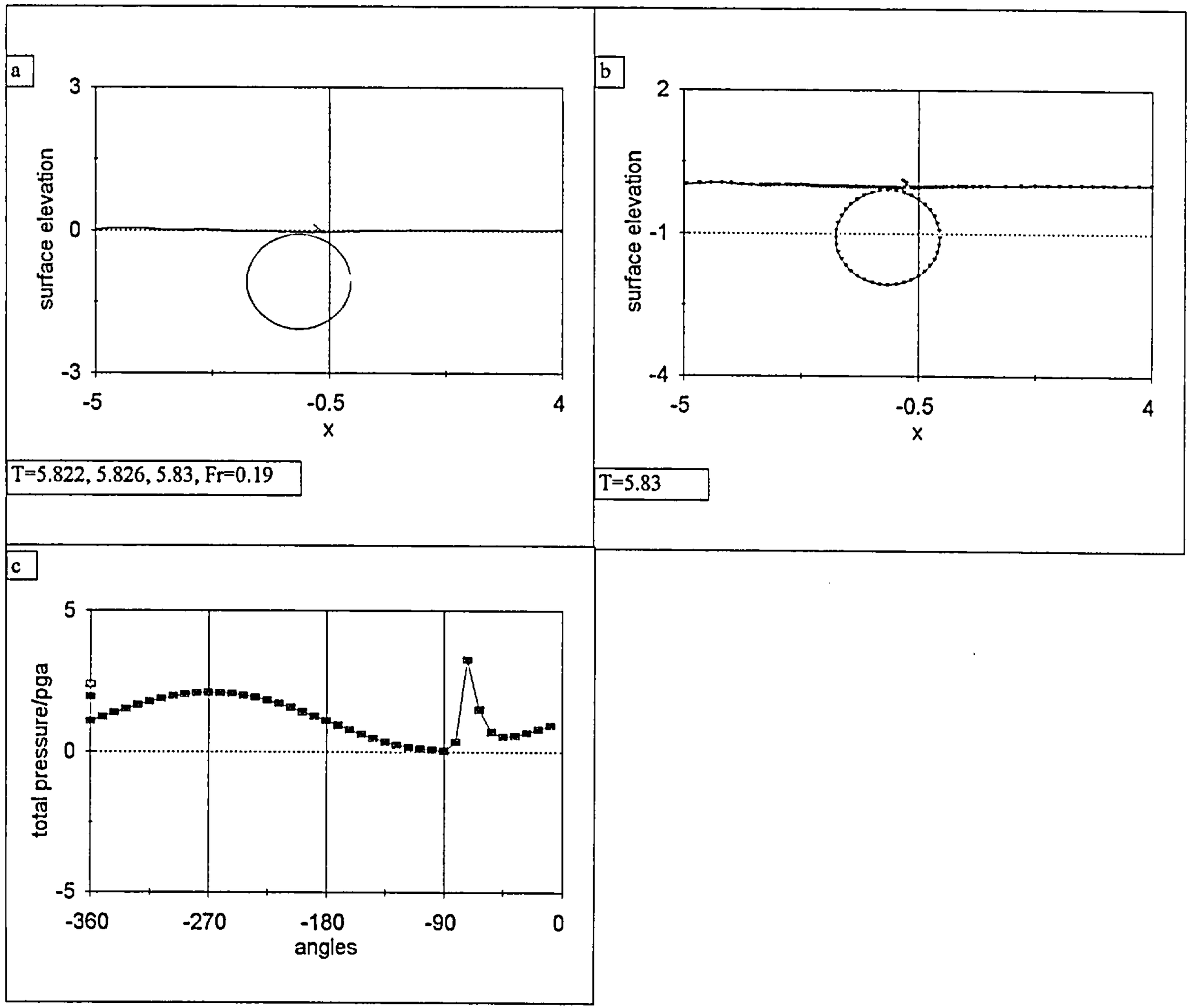

Fig. 6.15.1(i) Further calculations for oblique(45-degrees) and impulsively started motion of a cylinder moving at Fr=0.19, Mb=1.0.

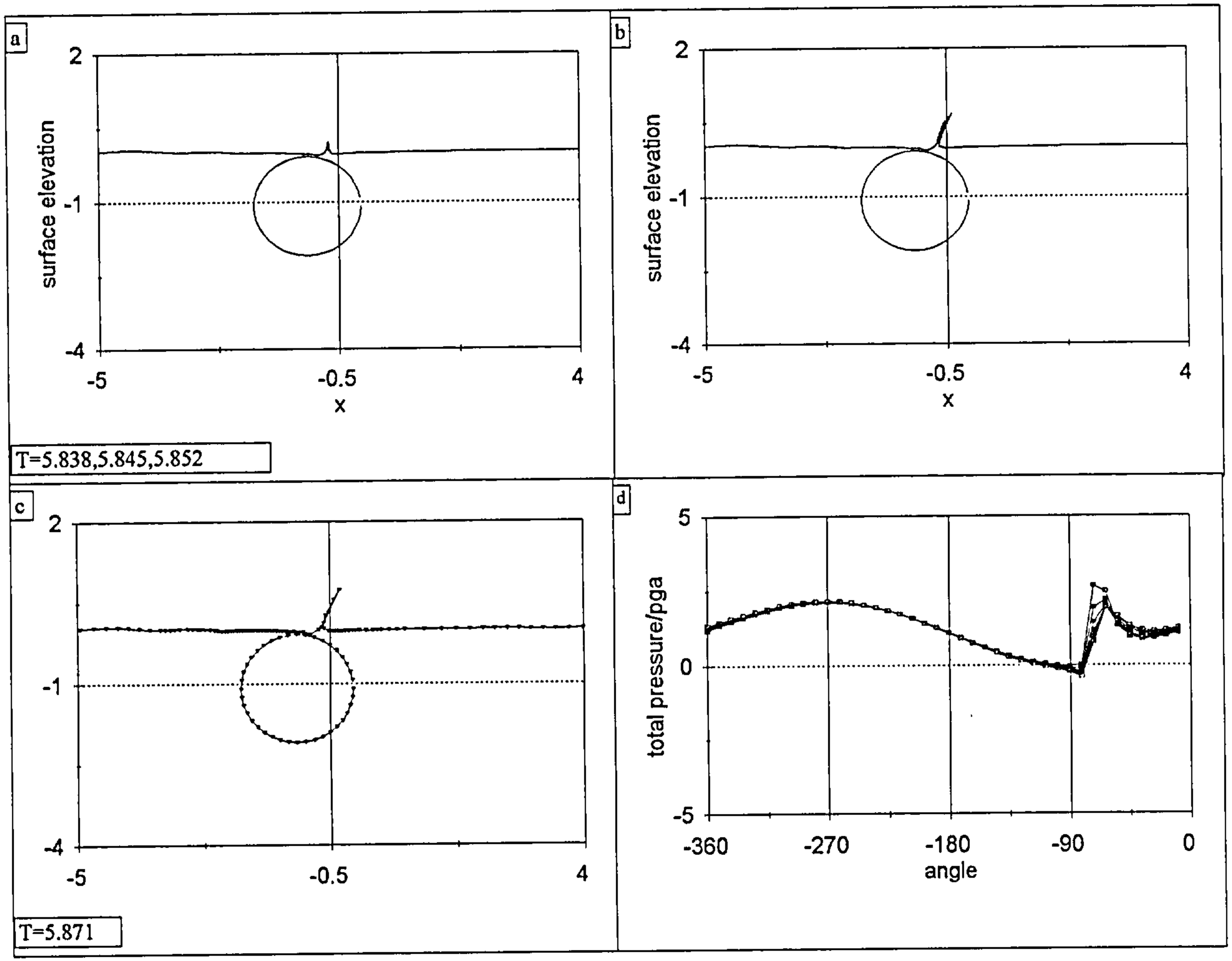

Fig. 6.15.1(ii) Further results with the jet changing direction.

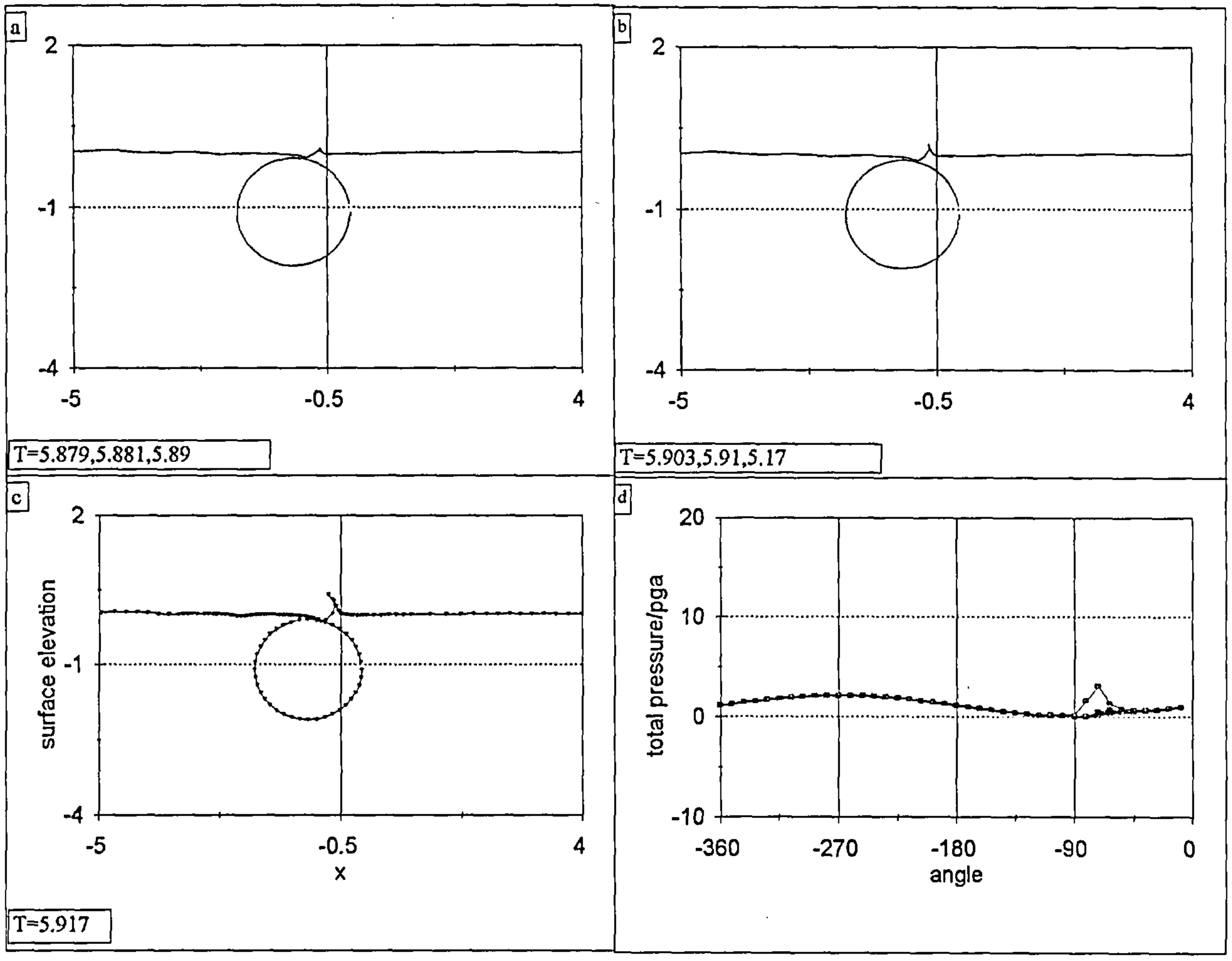

Fig. 6.15.1(iii) Further results.

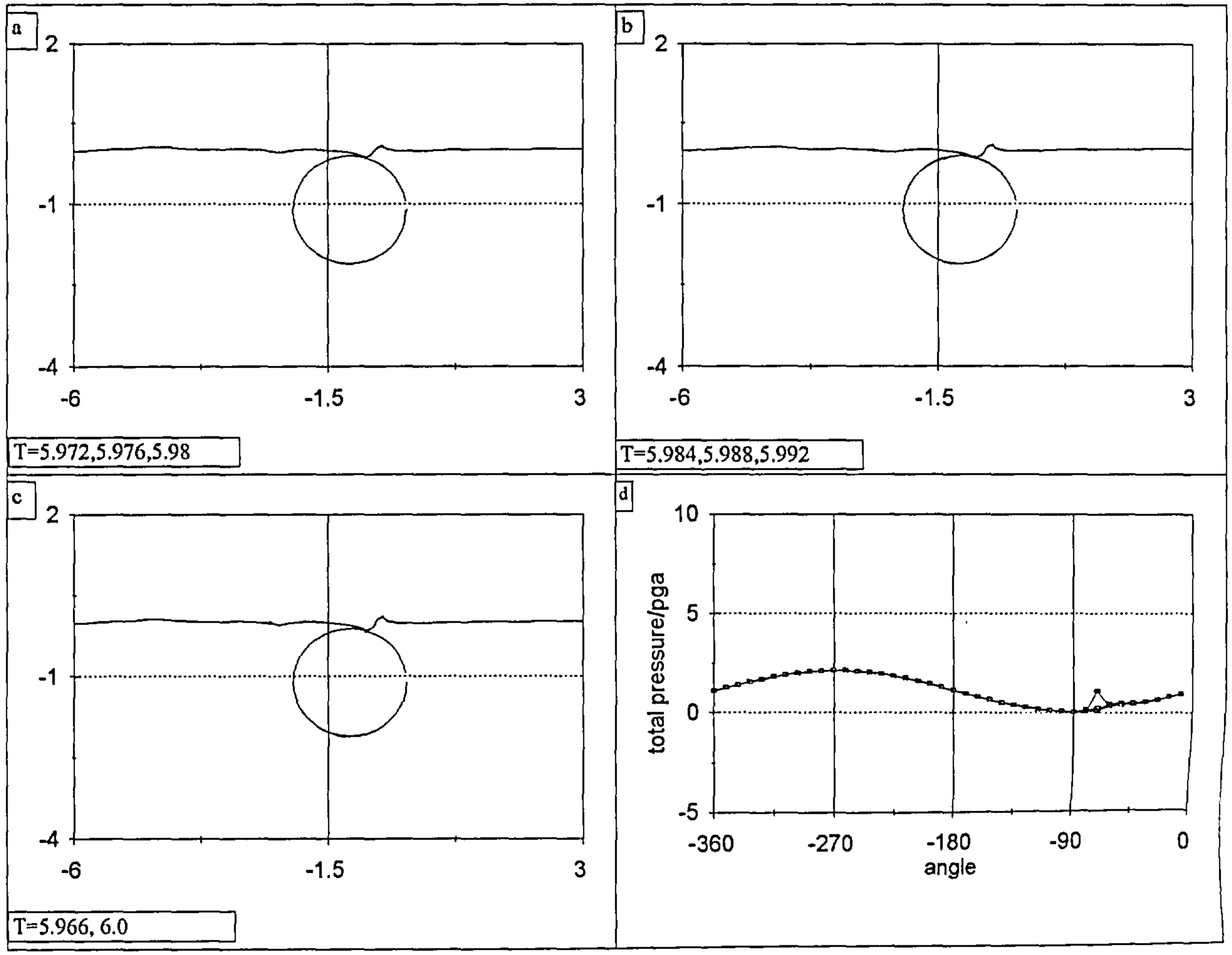

Fig. 6.15.1(iv) Further results.

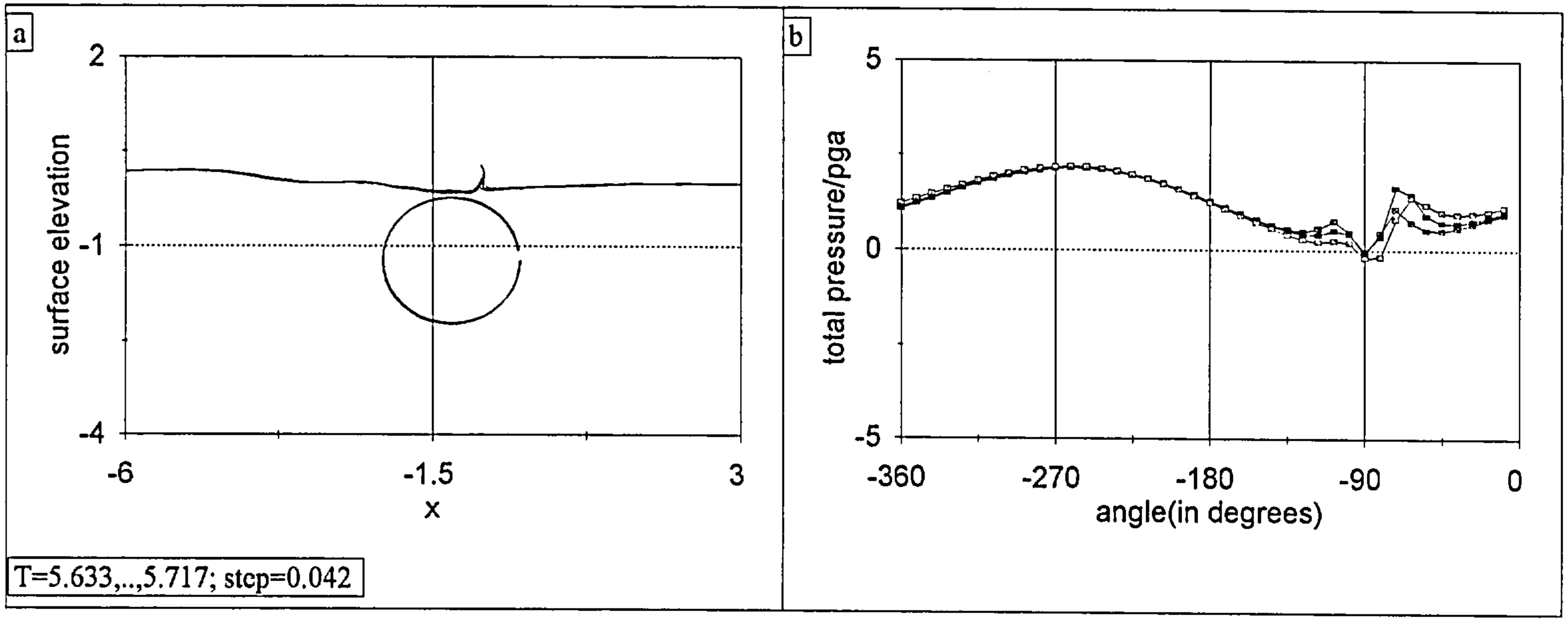

Fig. 6.15.2(i) Further calculations for oblique(45-degreees) and impulsively started motion of a cylinder moving at Fr=0.31, Mb=1.0.

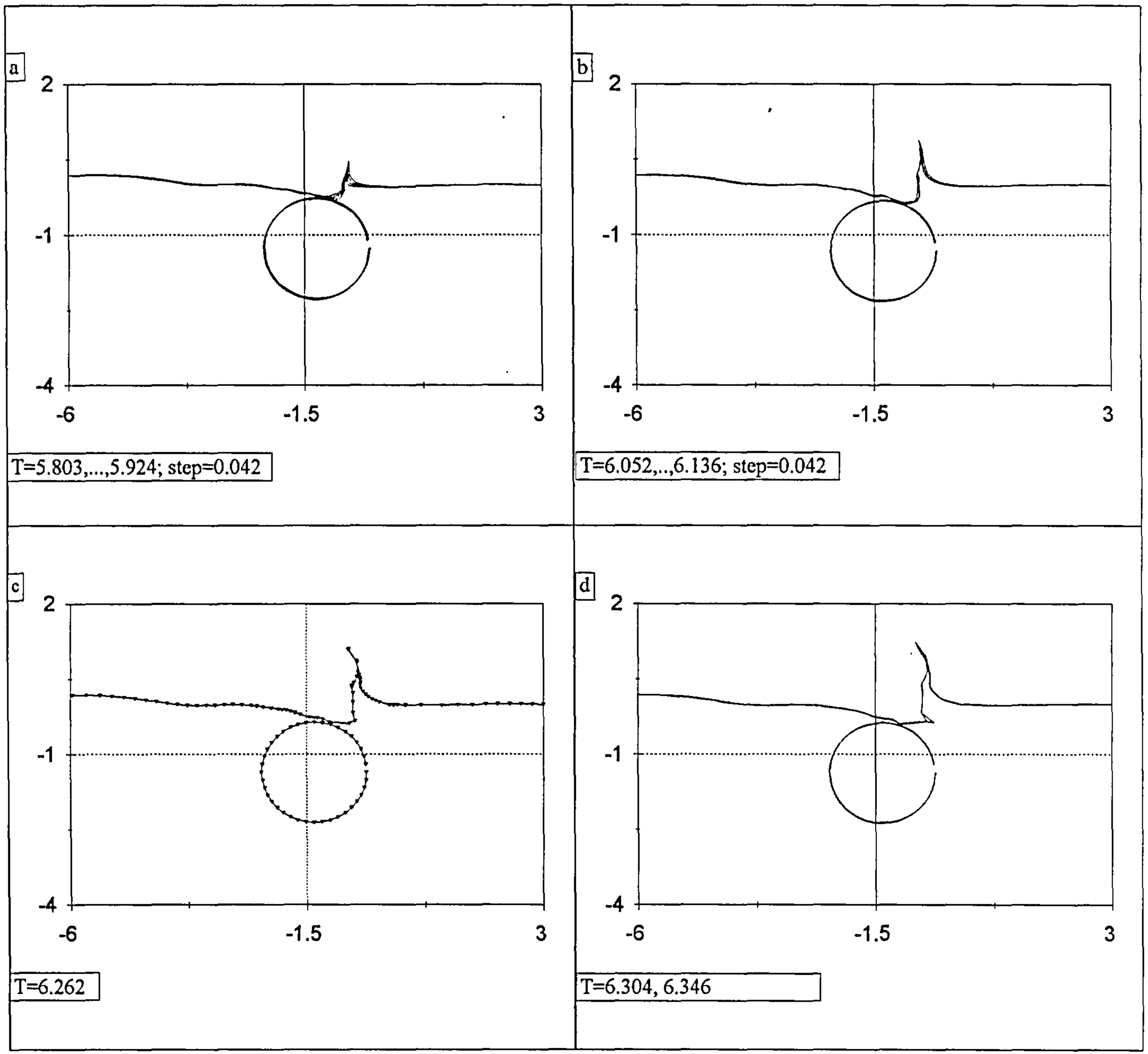

Fig. 6.15.2(ii) Further results.

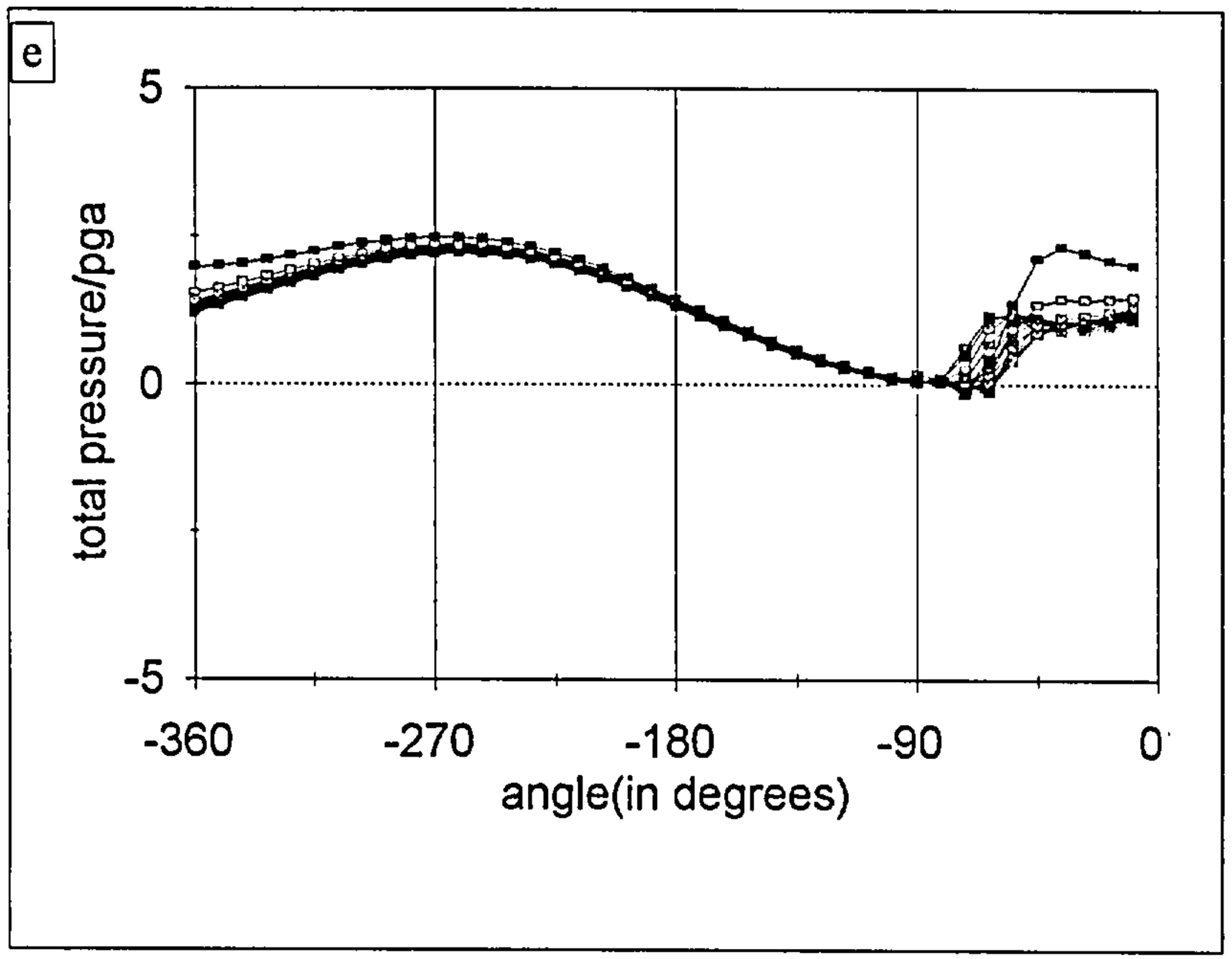
e
5
0
-5
total pressure/pga
-360
-270
-180
-90
0
angle(in degrees)

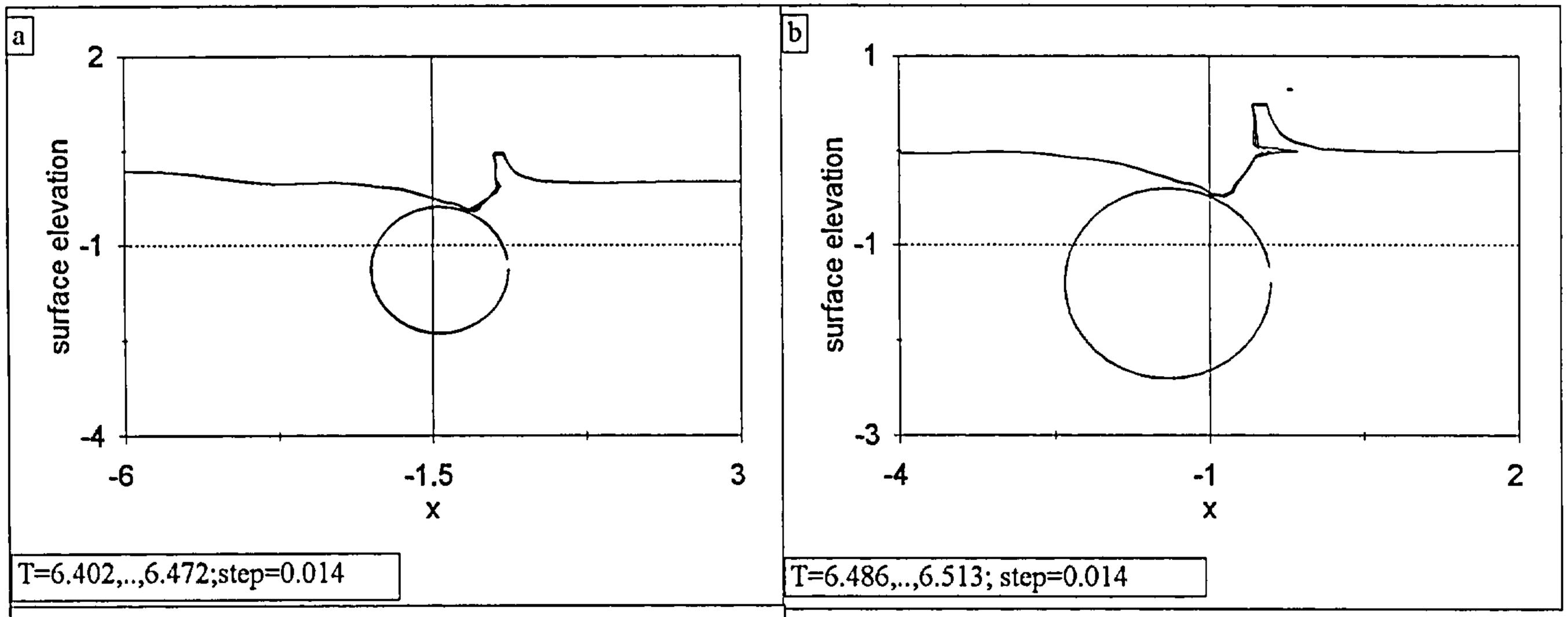

Fig. 6.15.2(iii) Further results.

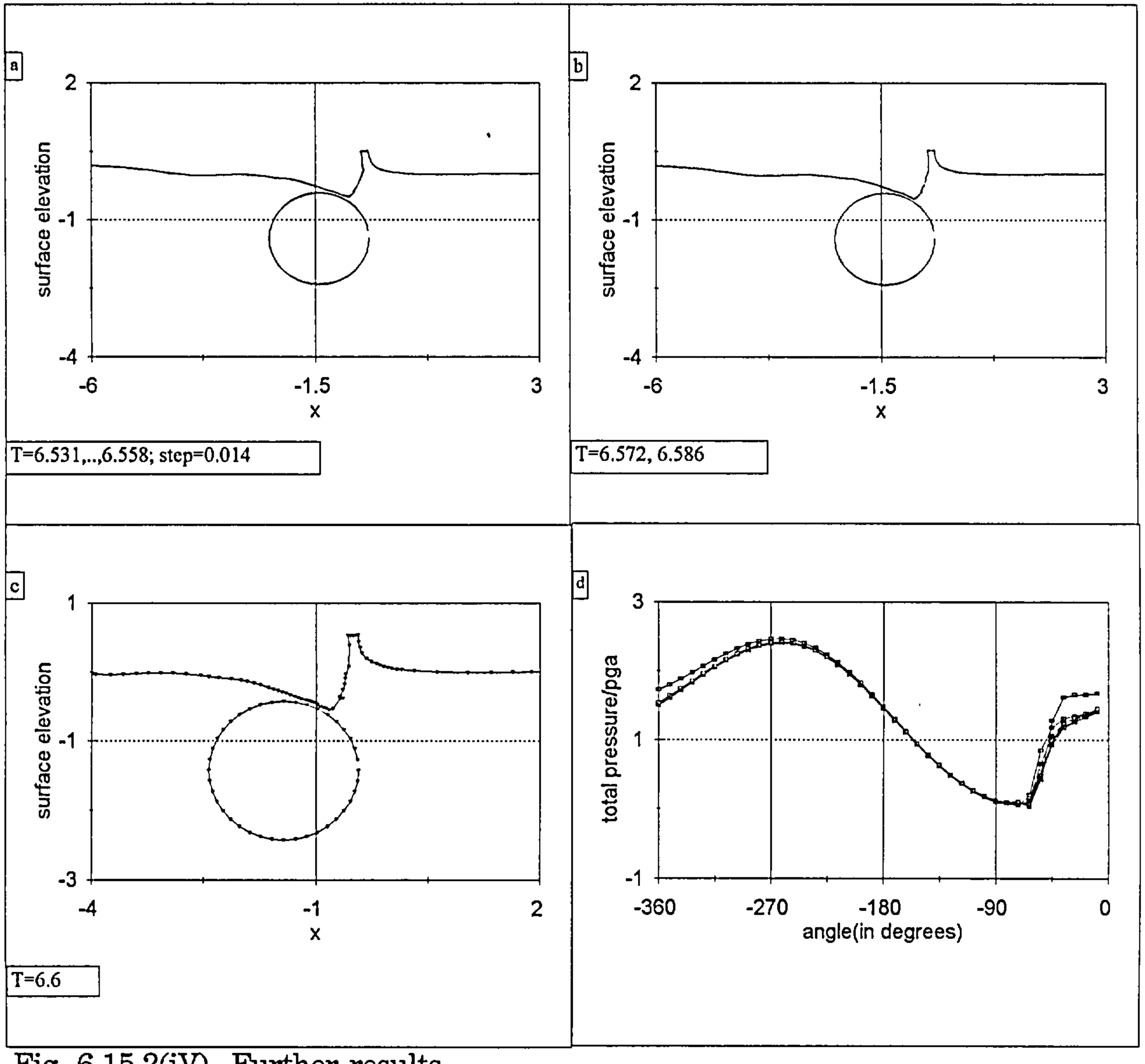

Fig. 6.15.2(iV) Further results.

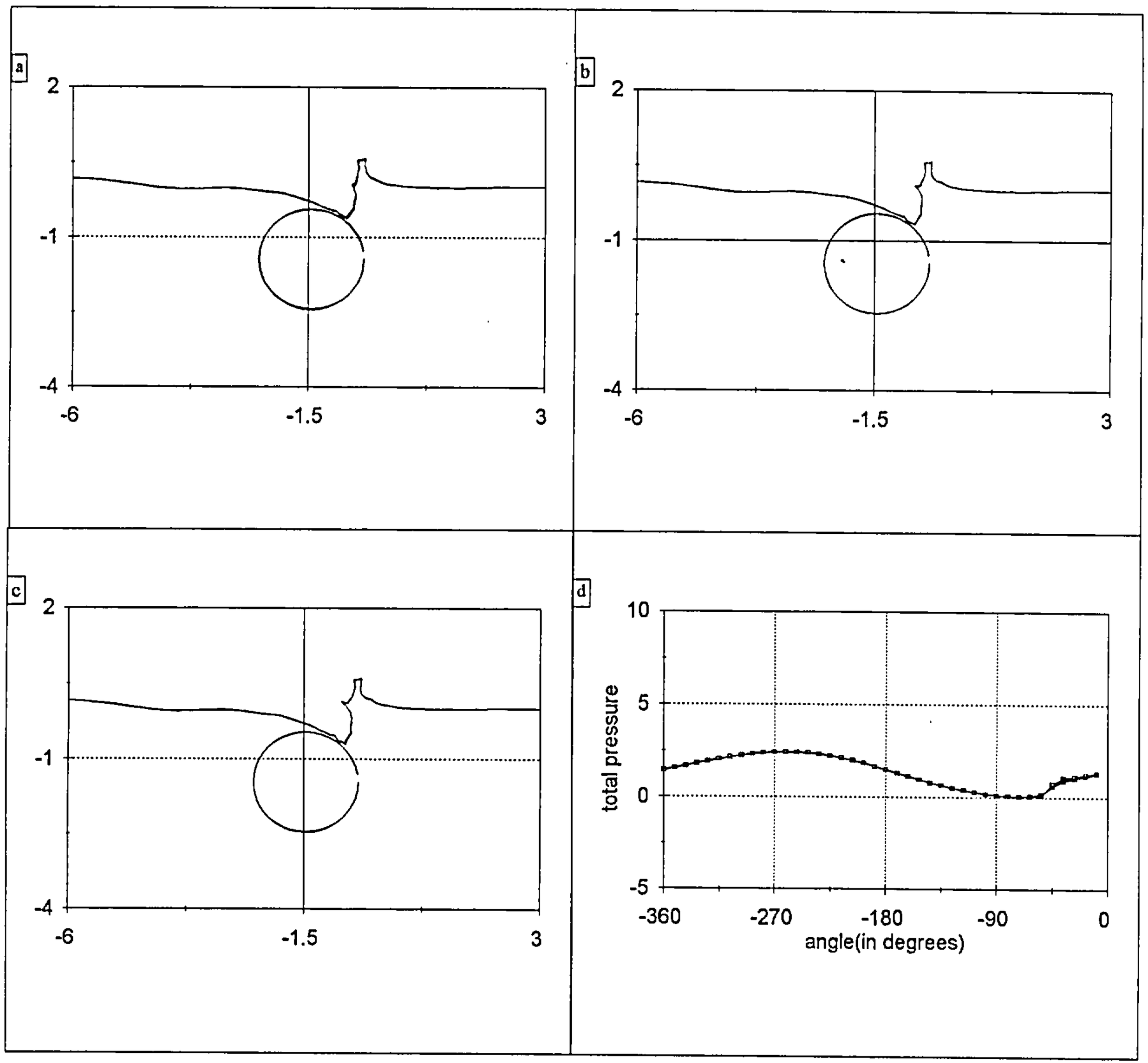

Fig. 6.15.2(v) Further results.

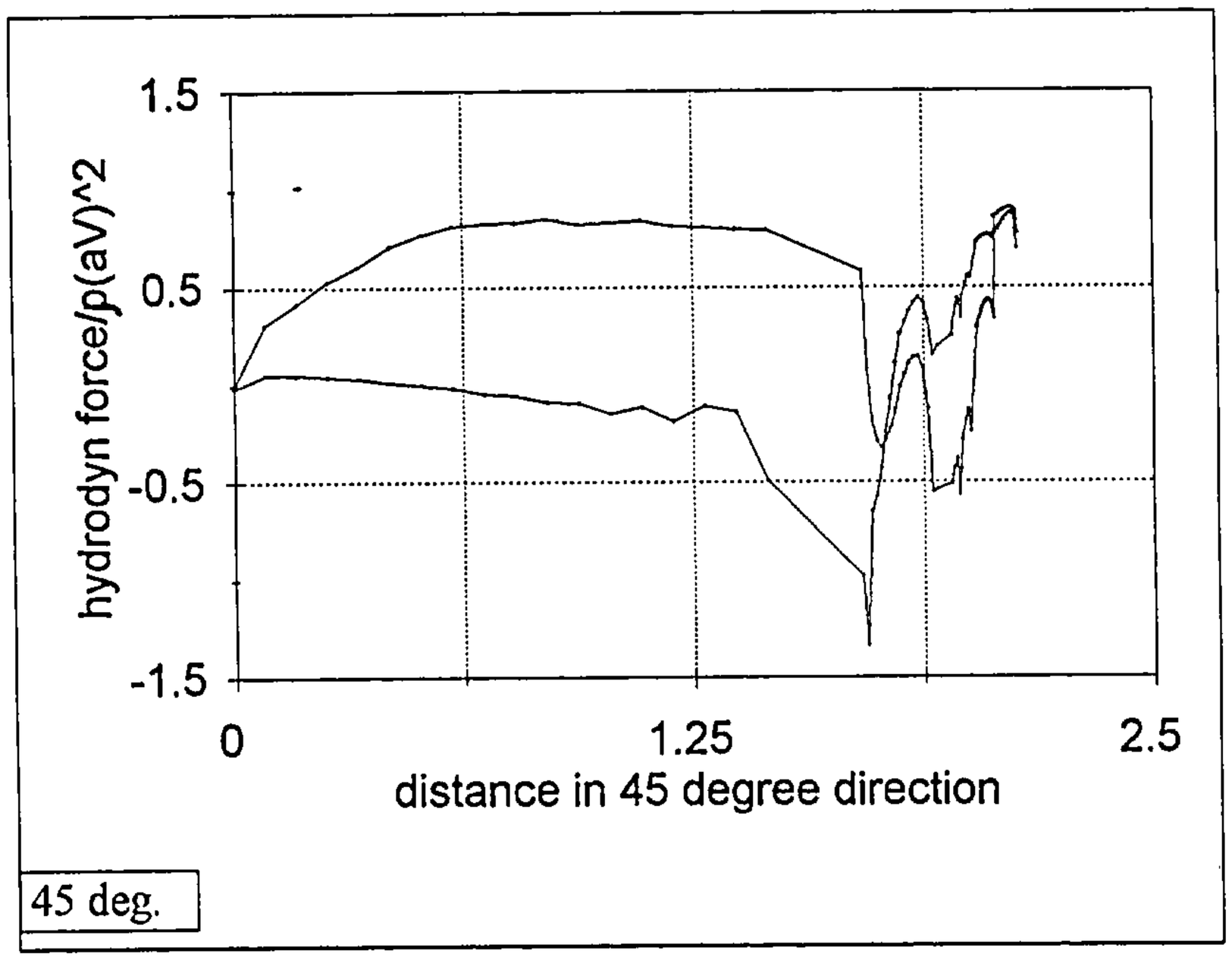

Fig. 6.15.3 Hydrodynamic forces on the body before and after complete engulfment.

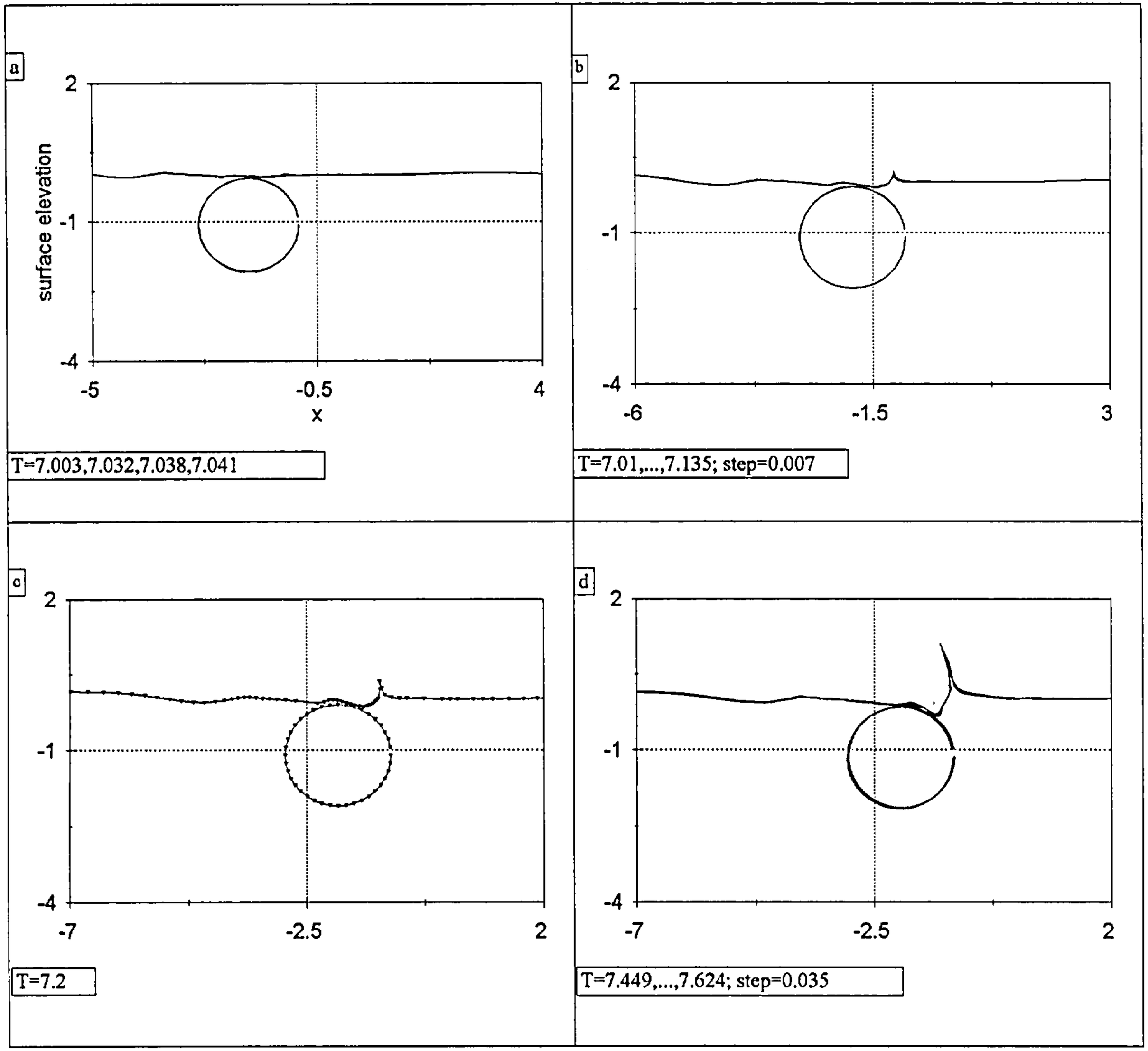

Fig. 6.16(i) Further calculations for oblique(60-degrees) and impulsively started motion of a cylinder moving at Fr=0.31, Mb=1.0.

e

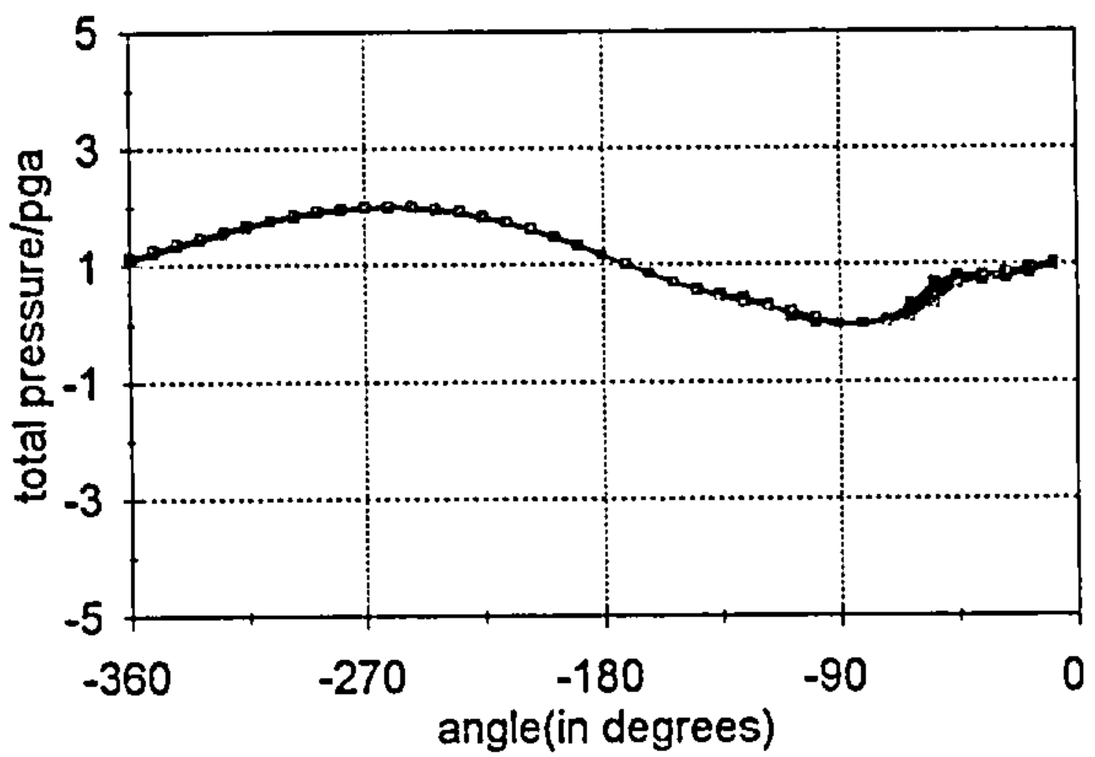

Time=0 to 0.315 at intervals 0.035

f

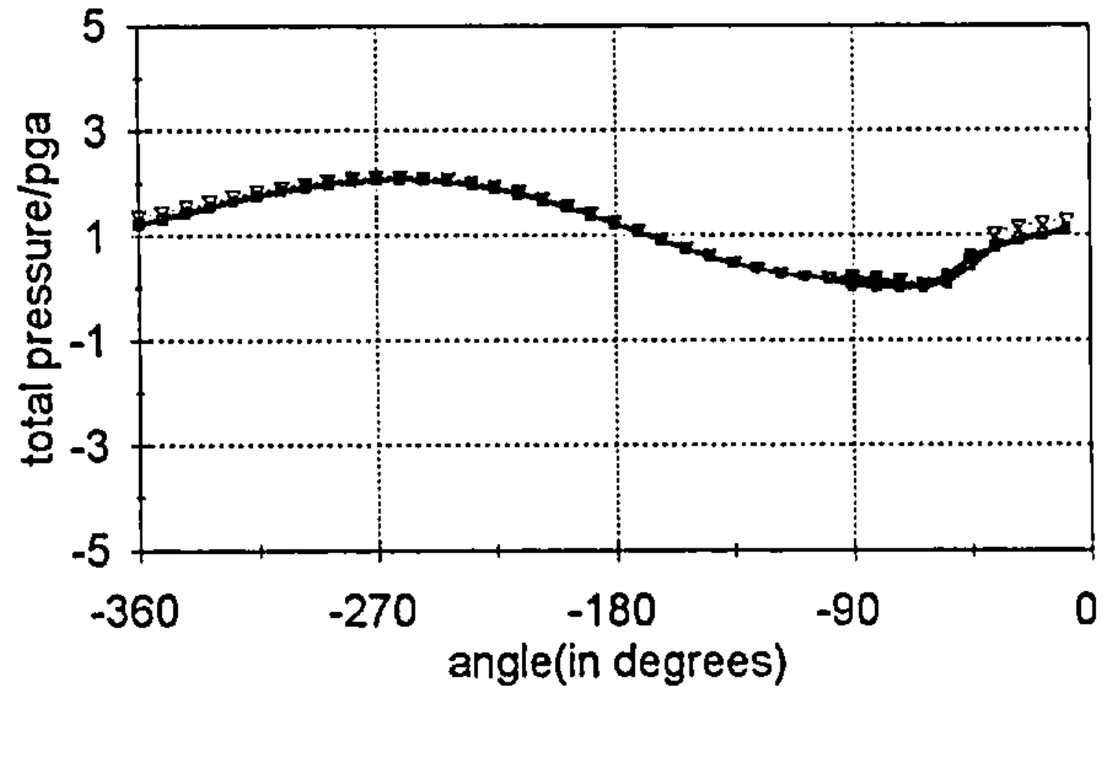

T=0.35 to 0.805 at intervals 0.035

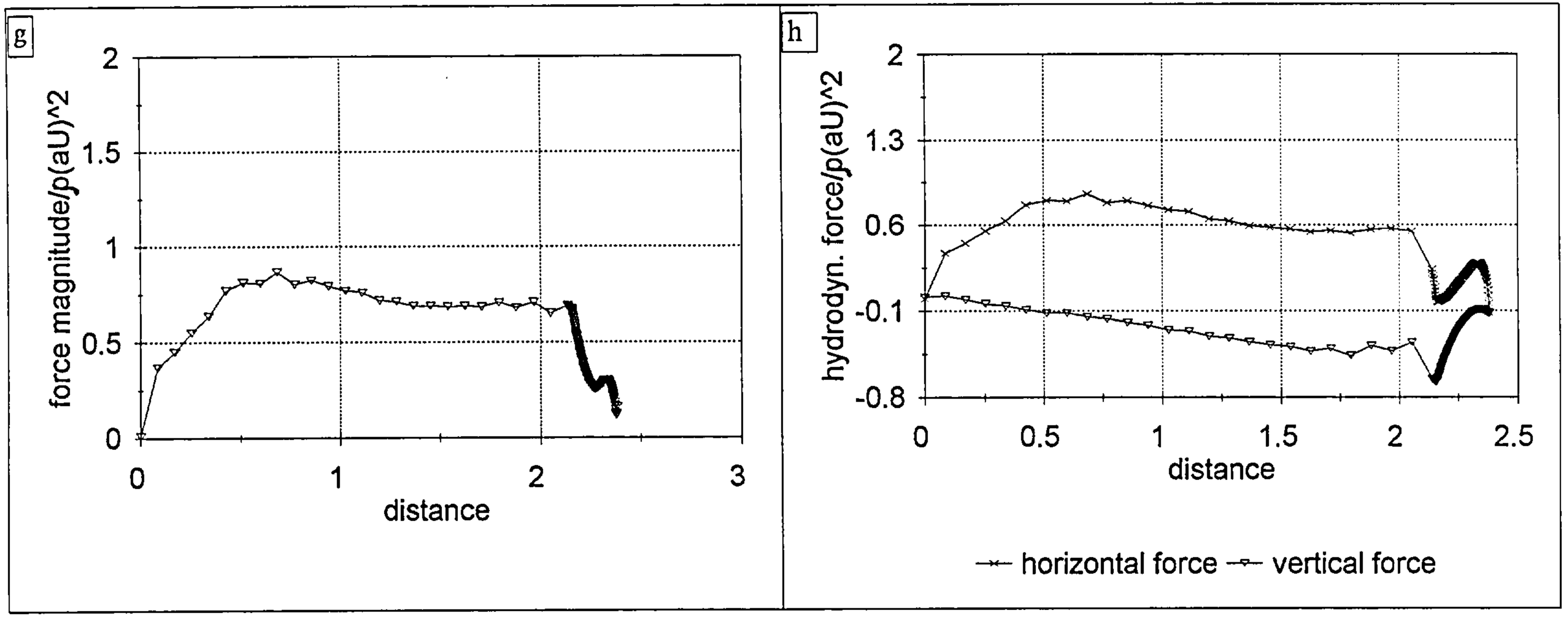
g
force magnitude/p(aU)^2
2
1.5
1
0.5
0
0
1
2
3
distance
h
hydrodyn. force/p(aU)^2
2
1.3
0.6
-0.1
-0.8
0
0.5
1
1.5
2
2.5
distance
horizontal force
vertical force

Chapter 7

Summary of the thesis

A fairly complete study of the hydrodynamics interaction of horizontal circular cylinders with a free-surface has been carried out. We have constructed a numerical model and presented results for the problem of cylinder motions below a free-surface and entering it, assuming that surface tension and viscous effects can be ignored. We use the added mass theory to develop an analytical model, which is then checked for accuracy using the nonlinear method. The fully nonlinear numerical method has also been used extensively to validate the small-time expansion method of Tyvand & Miloh, and is also used to pursue the solution for the engulfment problem. The results are interesting and of varied nature since we have treated more than three interelated problems.

The results of chapter 2, where our analytical methods are compared with the fully nonlinear method, show good agreement in some situations. For the free motion of the cylinder rising to a free-surface, the rigid wall method is in good agreement with the nonlinear method, though the former experiences a slight delay in time. The infinite fluid method is in good agreement at the start of the calculations, but fails to agree with the nonlinear method at the end of the motion. It predicts that the total force on the cylinder increases as

the approaches the free-surface. The constant added mass method is also in good agreement with the numerics until near to the free-surface, where it fails to predict the fall in total force. In the case of the horizontal free motion, we used the numerical method to check whether the predictions of the small-time asymptotic method, i.e that under this kind of motion the path followed by the body, for a small time, is a parabola. The interval of time, within which this happens, was found to be $0 < T < 0.105$. Some interesting features of the free-surface were also observed, for example the thin layer on top of the cylinder as it emerged from the free-surface and the flattening of the mound that builds up behind the sinking cylinder.

For motion of a spring-loaded cylinder moving horizontally, vertically and obliquely, we carried out some comparisons with the numerics for different strengths of the springs. The analytical method is underdamped, and the period of the motion is slightily longer than that of the numerical method, in the case of the larger springs. The two methods became more comparable after halving the springs' strengths. Also, the motion was found to be directionally unstable, with both methods predicting the precession of the direction axis for the oblique motion. On the free-surface we calculated some "sharp" breakers and waves of short wavelength.

The comparison between the small-time asymptotic method and the nonlinear method showed very good agreement for the time interval of $0 < T < 0.3$ for all cases of Fr number and direction of motion. At later stages the motion at high Fr number remains in better agreement than for other cases of small Fr number. Comparing these comparisons for vertical, horizontal and oblique motions we found that the agreement last longer for vertical motion, at

least up to T=0.6 in some cases, than for the other two cases. Beyond T=0.6 the small-time method completely fails to produce any reasonably motion of the free-surface, whereas the numerical method continues to give good prediction of the free-surface movement until breakdown of the calculations with a features also seen on photographs by Greenhow and Lin (1983) in Fig. 6.17.

During the early calculations, we ignored the situations that developed immediately after the breakdown of the calculations. When these were investigated in detail, especially for motion started near the free-surface, we discovered two interesting phenomena of breakdown of the calculations; the formation of "sharp"breakers when the motion is started quite close to the surface, and high-frequency waves when the motion is started slightly further away from the surface. Similar features were seen in the case of the motion of the cylinder after complete engulfment. Forced or free motion of initially half-submerged cylinder ends with the breakdown of the calculations when the fluid domain collapses into a doubly-connected domain. We swap programs, after resolving the problem of the impacted inflows, and continue the calculations beyond complete submergence. When the jets appear they are smoothed and hydrodynamic force and pressure distribution on the cylinder showed no sensitivity to smoothing. These results should serve as the beggining of a rigorous search for theoretical justification of the approach adopted here. Clearly, we lack a theoretical solution for the stage between the collapse of the domain and the next step of the calculations. Nevertheless, the potential on the free-surface and the body away from the impact region seems to be unaffected by the the restarting process of the calculations. The studied motions could also be extended to cover other cases of Fr number for forced motion and cylinders

of different specific gravities for the free motion.

Bibliography

1. Abramowitz M. & Stegun L.A. 1970

Handbook of Mathematical Functions Dover.

2. Barringer I. 1996 Water exit of two-dimensional bodies. B.A.M.C. Loughborough.

3. Bassett A.B. 1888 *A treatise on hydrodynamics*. Reprinted 1961, Dover, New York.

4. Best J.P. 1993 The formation of toroidal bubbles upon the collapse of transient cavities. *J. Fluid Mech.* **251** 79-107.

5. Brevig P. Greenhow M. & Vinje T. 1981 Extreme wave forces on submerged cylinders.

Proc. 2nd BHRA Internat. symp. on Wave and Tidal Energy,

6. Cambridge British Hydraulics Research Assoc., 143-166.

7. Cooker M.J. & Peregrine D.H. 1992 Wave impact pressure and its effect upon bodies lying on the sea bed. *Coastal Engineering*, **18** 205-229.

8. Dean W.R. 1948 On the reflection of surface waves from a submerged circular cylinder. *Proc. Camb. Phil. Soc.* **44** 483-491.

9. Dold J.W. & Peregrine D.H. 1986 An efficient boundary-integral method for steep unsteady water waves. In: K.W. Morton and M.J. Baines (Editors) *Numerical methods for fluid dynamics II*. Oxford Uni-

versity Press 657-679.

10. Evans D.V. Jeffrey D.C. Salter S.H. & Taylor J.R.M. 1979 Submerged cylinder wave energy device: theory and experiment. *Appl. Ocean Res.* **1** 3-12.

11. Faltinsen O. 1990 *Sea loads on Ships and Offshore Structures.* Cambridge University Press.

12. Garabedian P.R. 1953 Oblique water entry of a wedge. *Comm. Pure Appl. Math.* **6** 157-165.

13. Goldstein H. 1980 *Classical Mechanics* Addison Wesley.

14. Greenhow M. 1982 Numerical simulation of standing waves in finite depth. *Adv. Water Resources* **5** 185-189.

15. Greenhow M. and Lin W.M. 1983 Nonlinear free-surface: experiments and theory. Rep. 83-119. MIT, Dept of Ocean Engineering.

16. Greenhow M. 1987 Wedge entry into initially calm water. *Appl. Ocean Res.* **10** 191-198.

17. Greenhow M. & Li Y. 1987 Added masses for circular cylinders near or penetrating fluid boundaries - review, extension and application to water-entry, -exit and slamming. *Ocean Engng*, **14**, 325-348.

18. Greenhow M. 1993 A complex variable method for the floating-body boundary-value problem. *J. Comput. Appl. Maths.* **46** 115-128.

19. Haussling H.J. & Coleman R.M. 1979 Nonlinear water waves generated by an accelerating circular cylinder. *J. Fluid Mech.* **92** 767-781.

20. Havelock T.H. 1936 The forces on a circular cylinder submerged in a uniform stream. *Proc. Roy. Soc. London. Ser. A.* **157** 526-534.

21. Havelock T.H. 1949a The wave resistance of a cylinder started from

rest. *Q. J. Mech. Appl. Maths* **2** 325-334.

22. Havelock T.H. 1949b The wave resistance of a submerged cylinder in accelerated motion. *Q. J. Mech. Appl. Maths* **2** 419-427.

23. Hepworth T. 1991 An investigation of the motion of a submerged cylinder moving below a free surface with constant velocity. 4^{th} year project report, Dep. Math. Statist., Brunel University.

24. Howison S.D. Ockendon J.R & Wilson S.K. 1991 Incompressible water-entry problems at small deadrise angles. *J. Fluid Mech.* **222** 215-230.

25. King A.C. & Needham D.J. 1994 The initial development of a jet caused by fluid, body and free-surface interaction. Part 1. A uniformly accelerating plate. *J. Fluid Mech.* **268** 89-101.

26. Lamb H. 1932 *Hydrodynamics* 6 ed Cambridge University Press.

27. Lin W.M. Newman J.N. & Yue D.K.P 1984 Nonlinear forced motions of floating bodies. In W.C. Webster (Editor) *15^{th} Symp. Naval Hydrodynamics*,
Hamburg (National Academy Press, Washington, DC) 33-49.

28. Longuet-Higgins M.S. & Cokelet E.D. The deformation of steep waves on water. I. A numerical method of computation.
Proc. Roy. Soc. London Ser. A. **350** 1-26.

29. Lui Y. & Yue D.K.P. 1996 On the time dependence of the wave resistance of a body accelerating from rest. *J. Fluid Mech.* **310** 337-363.

30. Milne-Thomson L.M. 1968 *Theoretical hydrodynamics* London Macmillan & Co Ltd.

31. Newman J.N 1977 *Marine Hydrodynamics* MIT Press. Cambridge M.A.

32. Ogilvie F. 1963 First- and second-order forces on a cylinder submerged under a free surface. *J. Fluid Mech.* **16** 451-472.

33. Paterson A.R 1983 *A first course in fluid dynamics* Cambridge University Press.

34. Penney W.G. & Price A.T. 1952 Finite periodic stationary waves in a perfect liquid. *Proc. Roy. Soc. London Ser. A* **244** 254-284.

35. Peregrine D.H. 1972 Flow due to a vertical plate moving in a channel. Unpublished note.

36. Roberts A.J. 1987 Transient free-surface flows generated by a moving vertical plate. *Q.J. Mech. Appl. Math.* **40(1)** 129-158.

37. Sakai T., Husimi Y. & Hatoyama M. 1933 On the resistance experienced by the body moving in an incompressible perfect fluid towards its surface. *Proc. Roy. Soc. Japan* **15** 4.11.

38. Sarpkaya T. & Isaacson M. 1981

Mechanics of wave forces on offshore structures. Van Nostrand Reinhold Company.

39. Srokosz M.A 1981 Breaking effects in standing and reflected waves. *Proc. Conf. Hydrodynamics in Ocean Engineering*, Trondheim, Norway.

40. Telste J.G. 1987 Inviscid flow about a cylinder rising to a free surface. *J. Fluid Mech.* **182** 149-168.

41. Terent'ev A.G. 1991 Nonstationary motion of bodies in a fluid. *Proc. Steklov Inst. Maths* **186** 211-221.

42. Tuck E.O. 1965 The effect of non-linearity on the flow past a submerged cylinder. *J. Fluid Mech.* **22** 401-414.

43. Tyvand P.A. & Miloh T. 1995 Free-surface flow due to impulsive mo-

tion of a submerged circular cylinder. *J. Fluid Mech.* **286** 67-101.

44. Ursell F. 1950 Surface waves on deep water in the presence of a submerged circular cylinder. *Proc. Camb. Phil. Soc.* **46** 141-158.

45. Vinje T. & Brevig P. 1981a Nonlinear, two-dimensional ship motions. Ship Res. Inst. Norway R - 112-81.

46. Vinje T. & Brevig P. 1981b Breaking waves on finite depth water; a numerical study. Ship Res. Inst. Norway R-118-81.

47. Vinje T. 1989 On the small time expansion of nonlinear free surface problems. In J. Grue (Editor)
Proc. 4th Internat. Workshop on Water Waves and Floating Bodies, Ostese, Norway 245-250.

48. Wagner H. 1932 Uber Stoss und Gleitvorgänge an der Oberfläche von Flüssigkeiten. Z. A. M. M. **12**, 193-215. (See also The phenomena of impact and planning on water. N.A.C.A. Translation 1966 1-57)

49. Wu G. X. 1993 Hydrodynamic forces on a submerged circular cylinder undergoing large-amplitude motion. *J. Fluid Mech.* **254** 41-58.

50. Zhao R. & Faltisen O. 1993 Water entry of two-dimensional bodies. *J. Fluid Mech.* **246** 593-612.